

**Analyses of Production and Decay Processes  
of the Higgs Boson and of a New Scalar  
in a Warped Extra Dimension**

Dissertation  
zur Erlangung des Grades  
„Doktor  
der Naturwissenschaften“  
am Fachbereich Physik, Mathematik und Informatik  
der Johannes Gutenberg-Universität  
in Mainz

**Clara Hörner**

geb. in Wiesbaden  
Mainz, den 10.12.2017

Datum der mündlichen Prüfung: 18.05.2018

Dissertation zur Erlangung des Grades „Doktor der Naturwissenschaften“ am Fachbereich  
Physik, Mathematik und Informatik der Johannes Gutenberg-Universität in Mainz (D77)

# Abstract

The thesis investigates production and decay processes of the Higgs boson and of a new scalar in a framework “beyond the Standard Model of particle physics”, which additionally includes a small and warped extra dimension: the Randall-Sundrum (RS) model. The RS model gives a natural explanation for the apparently huge hierarchy between the Planck and the weak energy scales, and for the gauge hierarchy problem arising from the fact that the theoretical prediction of the physical Higgs boson’s mass depends on the scale of very high energies. Furthermore, it offers an appealing framework for investigating questions of the flavor sector of particles, *e.g.* the hierarchies that are observed between the masses of fermions, or suppression mechanisms for flavor changing neutral currents.

In most parts of the thesis, a scenario of the RS model is considered, in which all the particle fields, including the Higgs field, can extend into the bulk, the whole five-dimensional space-time. Whereas this scenario can be regarded as an especially natural realization of the RS model, it is also proven that the predictions for the Higgs processes lie significantly closer to the Standard Model predictions, compared to realizations of the RS model where the Higgs field is localized on a four-dimensional subspace, a brane. In this regard, the tree-level vertices of the Higgs couplings depend in a complicated manner on the shape of the Higgs profile in the extra dimension. Due to the compactified extra dimension, towers of Kaluza-Klein (KK) particles are predicted as heavy copies of the SM particle fields and of possible new, exotic fields, depending on the gauge group implemented in the bulk. These KK particle towers virtually contribute to the rates of loop-induced interactions, and can analytically be summed up by means of five-dimensional propagator functions. In this sense, the fermion propagator function includes, in a complicated manner, the Yukawa couplings induced by the bulk-Higgs field. The fermion, gauge boson, and scalar propagator functions, which are necessary to sum over the contributions of KK towers in the loop-induced Higgs production process through gluon fusion and the Higgs decay into two photons, are developed. In addition, all the direct Higgs couplings to gauge bosons and fermions are computed. With the help of these results, a numerical evaluation of the various Higgs production and decay rates at the LHC is performed, in dependence of the parameter space of the bulk-Higgs RS model. Also, the significant signal strengths for the Higgs decays into two gauge boson final states or fermion final states are compared with the experimental results of ATLAS and CMS.

Furthermore, the implementation of a new, extra scalar field is considered in the RS framework, by what the temporarily reported di-photon anomaly, seen in first 13 TeV data of the LHC, could conveniently be explained. The loop-induced production and decay rates of the new bulk scalar, mediated by KK fermions, are computed, as well as the various decay rates of the scalar at the tree-level. In this way, the temporarily reported excess rate of di-photons by ATLAS and CMS can be reproduced for very natural choices of parameters, whereat exclusion bounds, derived from 8 TeV searches of the LHC, are accounted for. Also, a possible implementation of Higgs portal couplings to the new scalar sector is discussed. Even though the di-photon excess was confirmed to be the result of a statistical fluctuation, the evaluations of the RS model with a new scalar sector can be of value in future analyses in cases of similar excesses. Besides, the RS framework with a new scalar sector might offer a natural explanation mechanism for the mass differences between the SM fermions. This is a crucial ingredient of the RS model, and is investigated, in some parts, in the last section of the thesis.

Altogether, the thesis provides a comprehensive set of computations and analyses of scalar sectors in the theoretical framework of the RS model.

# Zusammenfassung

Die Arbeit untersucht die Berechnung und Auswertung von Produktions- und Zerfallsprozessen des Higgs-Bosons sowie eines neuen, zusätzlichen Skalars im Randall-Sundrum Modell (RS-Modell). Das RS-Modell erweitert das Standard-Modell der Teilchenphysik um eine kleine und gekrümmte, fünfte Raumdimension und kann auf natürliche Weise erklären, wie die scheinbar riesige Hierarchie zwischen der Planck-Skala und der Skala der elektroschwachen Wechselwirkung zustande kommt. Es liefert damit einen Beitrag zur Lösung des Eichhierarchieproblems, das sich aus der UV-Sensitivität der theoretisch berechneten physikalischen Higgsmasse ergibt. Des Weiteren kann das RS-Modell auf attraktive Weise Erklärungsansätze für weitere Fragestellungen des “Flavor”-Sektors der Elementarteilchen anbieten, wie etwa für die bestehenden Massenhierarchien von Fermionen oder die Unterdrückungsmechanismen von neutralen Strömen, die Teilchen-“Flavor”-Veränderungen (flavour-changing-neutral-currents) induzieren.

Vorrangig wird in dieser Arbeit bei den Analysen und Berechnungen von einem Szenario des RS-Modells ausgegangen, in dem neben allen Teilchenfeldern auch das Higgsfeld sich in den vollen fünfdimensionalen Raum, den “bulk”, ausbreiten kann. Während dieses Szenario bereits eine besonders natürliche Realisation des RS-Modells darstellt, wird weiterhin gezeigt, dass die damit gewonnenen Vorhersagen für Higgs-Prozesse deutlich näher an denen des Standard-Modells der Teilchenphysik liegen im Vergleich zu Szenarien in denen das Higgs-Feld auf einer “brane” am Rand der Extradimension lokalisiert ist. Bei der hier gewählten Vorgehensweise hängen jedoch die “Tree-Level-Vertices” von Higgs-Kopplungen in komplizierter Weise von der Profildfunktion des Higgsfeldes in der Extradimension ab. Aufgrund der kompaktifizierten Extradimension werden Türme von Kaluza-Klein-Teilchen (KK-Teilchen) als schwere Kopien der Standard-Modell-Teilchen sowie möglicher neuer exotischer Teilchen vorhergesagt, je nachdem welche Eichsymmetrie im “bulk” des jeweiligen Modellansatzes realisiert ist. Diese KK-Teilchen-Türme tragen als virtuelle Teilchen zu den Raten von schleifeninduzierten Wechselwirkungen bei und können in analytischer Form mittels fünfdimensionaler Propagatorfunktionen aufsummiert werden. Die Propagatorfunktion der Fermionen ist hier im Vergleich zu den “brane”-Higgsmodellen komplexer, weil diese zusätzlich von den Yukawa-Kopplungen, die von einem “bulk”-Higgsfeld induziert werden, abhängen. Die Propagatorfunktionen der Fermionen, Eichbosonen und Skalare werden berechnet. Sie werden benötigt, um die Beiträge von KK-Türmen in den schleifeninduzierten Higgsprozessen der Gluon-Fusion sowie des Higgszerfalls in zwei Photonen aufzusummieren. Außerdem werden die direkten Higgskopplungen an Eichbosonen und an Fermionen berechnet. Mit Hilfe der gewonnenen Resultate werden dann die verschiedenen am LHC gemessenen Higgsproduktions- und Higgszerfallsraten numerisch in Abhängigkeit vom Parameterraum des “bulk”-Higgs-RS-Modells ausgewertet. Ebenso werden die wichtigsten Vorhersagen für Signalstärken von Higgszerfällen in Endzustände, die aus zwei Eichbosonen oder zwei Fermionen bestehen, mit den experimentellen Resultaten von ATLAS und CMS verglichen.

Im zweiten Teil der Arbeit werden außerdem Produktions- und Zerfallsprozesse eines zusätzlichen neuen in das RS-Modell eingeführten skalaren Feldes untersucht. Dies bietet einen Ansatz zur Erklärung der anfänglich am LHC gemessenen Anomalie von Photonenpaaren in dessen ersten 13 TeV-Daten. Berechnet werden die schleifeninduzierten Produktions- und Zerfallsraten des neuen “bulk”-Skalars, die durch KK Fermionen übermittelt werden, sowie ergänzend die verschiedenen “Tree-Level”-Zerfallsraten des Skalars. Hiermit können die genannten zweitweise veröffentlichten Daten von ATLAS und CMS über den Di-Photonen-Exzess für sehr natürliche

Parameterwerte modelltheoretisch reproduziert werden. Dabei werden Ausschlussgrenzen für Modell-Parameter von früheren 8 TeV-Messungen berücksichtigt. Außerdem wird eine mögliche Einbeziehung von Higgs-“Portal”-Kopplungen an den neuen skalaren Sektor diskutiert. Auch wenn inzwischen dieser Di-Photon-Exzess als statistische Fluktuation bestätigt worden ist, so können die in dieser Arbeit erfolgten Auswertungen dennoch von Wert in zukünftigen Analysen beim Auftreten ähnlicher Anomalien sein. Außerdem kann ein analoger Modellansatz eines “bulk”-Skalars einen natürlichen Erklärungsmechanismus für die beobachteten Massendifferenzen der Fermionen des Standard-Modells liefern. Dies kann als ein bedeutendes Merkmal des RS-Modells angesehen werden und wird im letzten Teil der Arbeit behandelt.

Insgesamt liefert die Arbeit damit eine zusammenfassende Darstellung von Berechnungen, Auswertungen und theoretischen Analysen skalarer Sektoren im Rahmen des RS-Modells.

# Contents

Preface . . . . .	1
<b>1 Theoretical Particle Physics</b>	<b>5</b>
1.1 The Standard Model of particle physics . . . . .	5
1.1.1 Some theoretical aspects of the Standard Model . . . . .	8
1.1.2 Lagrangian of the Standard Model . . . . .	13
1.1.3 Electroweak parameters by Peskin and Takeuchi . . . . .	18
1.2 Open questions of the Standard Model . . . . .	23
1.2.1 Hierarchy problems . . . . .	24
1.2.2 Further questions . . . . .	29
1.2.3 Theories of new physics . . . . .	31
<b>2 The Randall-Sundrum Model</b>	<b>35</b>
2.1 Theories of extra dimensions . . . . .	35
2.1.1 Large extra dimensions . . . . .	36
2.1.2 Universal extra dimensions . . . . .	38
2.1.3 A warped extra dimension - the Randall-Sundrum model . . . . .	43
2.2 The minimal Randall-Sundrum model . . . . .	46
2.2.1 Gauge sector and spontaneous symmetry breaking . . . . .	48
2.2.2 Fermion sector . . . . .	57
2.2.3 Higgs sector on or very close to the IR brane . . . . .	60
2.3 Extension by a custodial bulk gauge symmetry . . . . .	68
2.3.1 Gauge sector and spontaneous symmetry breaking . . . . .	69
2.3.2 Fermion sector . . . . .	73
2.4 Electroweak parameters in the RS scenarios . . . . .	79
<b>3 Five-Dimensional Propagator Functions</b>	<b>85</b>
3.1 Gauge boson propagator . . . . .	85
3.1.1 Gauge-boson propagator for $p_4 \approx 0$ . . . . .	88
3.2 Scalar propagator . . . . .	90
3.3 Fermion propagator . . . . .	92
3.3.1 Fermion propagator for $p_4 \approx 0$ . . . . .	92
3.3.2 Fermion propagator for $v \approx 0$ . . . . .	97

<b>4</b>	<b>Higgs Productions and Decays</b>	<b>101</b>
4.1	Calculations . . . . .	104
4.1.1	Feynman rules . . . . .	107
4.1.2	W boson contribution to the Higgs decay into two photons . . . . .	109
4.1.3	Higgs decay rates into vector bosons . . . . .	113
4.1.4	Higgs production through Higgsstrahlung and vector boson fusion . . . . .	116
4.1.5	Scalar contribution to the Higgs decay into two photons . . . . .	117
4.1.6	Fermion contribution to the Higgs decay into two photons . . . . .	120
4.2	Higgs cross sections and decay rates, and the total Higgs decay width . . . . .	132
4.2.1	Tree-level Higgs decay rates . . . . .	132
4.2.2	Loop-induced Higgs processes . . . . .	134
4.2.3	Total Higgs decay width . . . . .	137
4.3	Signal strengths for the Higgs decays at the LHC . . . . .	138
4.3.1	Outlook on the precision measurements of Higgs couplings . . . . .	146
4.3.2	Intermediate summary . . . . .	148
<b>5</b>	<b>A New, Heavy Bulk Scalar in the RS Model</b>	<b>151</b>
5.1	Di-photon resonance from a warped extra dimension . . . . .	151
5.1.1	Some introductory remarks . . . . .	151
5.1.2	Inclusion of a singlet bulk scalar to the RS model . . . . .	154
5.1.3	S couplings to particles . . . . .	157
5.1.4	Phenomenological evaluations of the various S decay rates . . . . .	163
5.1.5	Higgs “portal” couplings . . . . .	169
5.1.6	Three-body decay rate $S \rightarrow t\bar{t}h$ . . . . .	172
5.1.7	Intermediate summary . . . . .	173
5.2	Localization mechanism of fermions by an $Z_2$ -odd bulk scalar . . . . .	174
5.2.1	Framework with a flat extra dimension . . . . .	177
5.2.2	Analytic solutions for $w_L(t)$ . . . . .	178
5.2.3	Intermediate summary . . . . .	180
<b>6</b>	<b>Summary and Conclusions</b>	<b>181</b>
<b>A</b>	<b>The Randall-Sundrum Model</b>	<b>185</b>
A.1	Notations for the extradimensional coordinate . . . . .	185
<b>B</b>	<b>Five-Dimensional Propagator Functions</b>	<b>187</b>
B.1	System of equations involved in the calculation of the fermion propagator . . . . .	187
<b>C</b>	<b>Higgs Productions and Decays</b>	<b>191</b>
C.1	Feynman parameter integral, and loop form factors of Higgs couplings . . . . .	191
C.2	CP-odd loop-contribution of fermions to Higgs processes . . . . .	194
C.3	Dicing of the RS model parameter sets . . . . .	196
<b>D</b>	<b>A New, Heavy Bulk Scalar in the RS Model</b>	<b>199</b>
D.1	Corrections to the expressions $\Delta^{(\pm)}(\mathbf{c}_f, \beta)$ . . . . .	199
D.2	Solutions for the odd bulk scalar vev $w_L(t)$ . . . . .	200



<b>Bibliography</b>	<b>203</b>
<b>Miscellaneous</b>	<b>224</b>
List of abbreviations . . . . .	224
Acknowledgements . . . . .	225
Curriculum Vitae . . . . .	226



# Preface

*“Quantum theory provides us with a striking illustration of the fact that we can fully understand a connection though we can only speak of it in images and parables.”*

**W. Heisenberg**

*“It doesn’t matter how beautiful your theory is, it doesn’t matter how smart you are. If it doesn’t agree with experiment, it’s wrong.”*

**R. Feynman**

Modern theories, based on the quantum principles, are working at the boundary of human being’s ability of imagination. Nevertheless, the theories should give precise theoretical predictions that can be verified or falsified by experiments. Only by close conjunction of the experimental and theoretical progresses, it is guaranteed to gain new physical knowledge. Several years ago, the Higgs boson was experimentally discovered as the last missing element of the Standard Model (SM) of particle physics. The discovery confirms the efforts and progress achieved over the last 70 years in the field of theoretical particle physics, which are self-consistently described by the SM, over a wide range of energy. Three of the four fundamental forces of nature, describing the strong, the weak and the electromagnetic interactions, are included in the theory. These forces are carried out between the elementary particles of the SM, the fermions, through exchanges of force-mediating particles, the gauge bosons. The Higgs boson is predicted by the mechanism of spontaneous symmetry breaking, which can theoretically explain the origin of the masses of all the elementary particles. The theoretical basis for the SM is formed by quantum field theory, combining the principles of quantum mechanics for the microscopic nature, and the theory of special relativity for processes at high velocities and energies, together with the concept of field theory to describe the fundamental interactions of nature. In this context, the elementary particles appear as the quanta of fundamental fields that can be distinguished by certain characteristics, *e.g.* the spin. The interactions of the quanta are described by the theory of gauge groups. The probability amplitudes for the interactions strengths can be computed to high accuracies within the perturbation theory by Feynman. Increasing experimental precision on measuring the particle scatterings, *e.g.* at the experiments at the European Organization for Nuclear Research (CERN), allows to test the fundamental interactions better and better. The SM, as an effective field theory, can describe nature over a wide but still restricted range of energy. For that reason, phenomena of new and undetected physics could possibly arise at energies shortly above the range of validity of the SM. Very few theoretical quantities depend on the endpoint of the energy range of the SM, which are the eligible candidates for junctions to new theories beyond the SM. Such new theories should be related to open questions of the SM. The most important one in this context is the gauge hierarchy problem, which is induced

in the theoretical calculation of the physical Higgs mass. At the Planck energy scale  $m_{Pl} \sim 10^{19}$  GeV/ $c^2$  at the least, the fourth fundamental force of nature, the gravity, cannot be omitted any longer from the SM; which is at  $10^{16}$  eV of energy above the scale of the SM interactions. The gauge hierarchy problem claims that something new might still be undetected, possibly very close to the energy range of the present experimental searches.

In the first chapter of the thesis, the main ingredients of the SM, and the most significant open questions, and probable approaches of new physics are summarized. In the second chapter, we concentrate on new theories with very small, indiscernible extra spatial dimensions, and primarily on the Randall-Sundrum (RS) model [1], and its various incarnations for the Higgs sector and the bulk gauge symmetry. The RS model explains the gauge hierarchy problem with a five-dimensional space, the bulk, that underlies a strong, negative energy density related to an extreme warping of scales. The apparently strong hierarchy between the Planck scale and the scale of the SM might in fact be related to different localizations of the SM particles in the bulk. The extra dimension, mathematically forming an orbifold, is bounded by two four-dimensional subspaces, the ultra-violet (UV) and infra-red (IR) branes. With the extreme warping of space-time, the high Planck scale at the UV brane corresponds to energies shortly above the SM range at the IR brane. Different incarnations of the model are established that consider either a minimal bulk gauge group for the particle fields, similar to the SM, or an extended bulk gauge group to mediate constraints from electroweak precision tests. Also, whereas the Higgs sector can be localized strictly onto the IR brane, more evolved scenarios consider Higgs field's localizations close to the IR brane, or a Higgs field that is only maximally located at the IR brane, and spread out into the bulk. In this regard, it is most natural to assume that all particle fields extend into the bulk, which intriguingly can explain further theoretical questions, such as the origin of the mass differences between the SM particles, or suppression mechanisms for neutral current interactions. The approaches are related to different bulk-localizations of the particle fields, causing modifications of the SM interactions strengths.

To test the validity of the RS model, precise determinations of the Higgs boson interactions strengths with SM particles that are currently measured, *e.g.* at the Large Hadron Collider (LHC) at the CERN, are of special interest. In the RS model, the tree-level Higgs to particles couplings are modified by overlap integrals over the particles profiles in the extra dimension. Besides, the loop-induced processes receive virtual contributions from Kaluza-Klein (KK) particles, appearing in extra-dimensional theories as infinitely many, heavy copies of the SM fields, and of possible new exotic fields. The amplitudes of loop processes can be parametrized in terms of five-dimensional propagator functions that describe the propagation of KK particle fields through the bulk. We compute the necessary propagator functions for gauge bosons, scalars and fermions in Chapter 3 of the thesis. Then, in Chapter 4, we will derive the predictions for all the Higgs couplings to fermions and gauge bosons in the bulk-Higgs RS scenario with a minimal bulk gauge group. We compute the various production and decay rates for the Higgs boson at the LHC. These are the Higgs production through gluon fusion, vector boson fusion and Higgsstrahlung and the Higgs decays into two photon, fermion or gauge boson final states. We compare our results with previously derived predictions in the brane Higgs and narrow bulk-Higgs scenarios of the RS model [2–5], and the relevant experimental signal strengths for the Higgs decay processes at the LHC [6]. It will be consistently proven that the bulk Higgs RS scenario constitutes to be the most natural framework of the RS model, giving predictions much closer to the SM compared to other RS scenarios, and in better agreement to the experimental

results. As a consequence, the parameter space of the bulk Higgs scenario underlies much less constraints compared with the other Higgs scenarios of the RS model.

In Chapter 5 of the thesis, we consider the RS framework by including an additional new scalar field [7], which has been adapted to the temporary reported di-photon anomaly seen in first 13 TeV data of Run 2 experiments at the LHC [8, 9]. Results derived for the Higgs processes could be further developed to compute the various production and decay processes of the new scalar. Also, possible Higgs “portal”-couplings to the new scalar sector are included. The reported di-photon anomaly could be reproduced in the RS model for very natural choices for the couplings and the KK mass scale. In this context, the RS model with an enlarged bulk gauge group, featuring the extended amount of KK particles that can mediate loop-processes, was especially suitable. Also, the framework with an additional bulk scalar can be considered to explain the theoretical origin of the mass differences of the SM fermions, which will be explored in some parts in the last section of Chapter 5.

Chapter 6 gives a résumé of the thesis’s main conclusions.



# Chapter 1

## Theoretical Particle Physics

### 1.1 The Standard Model of particle physics

The SM of particle physics is able to describe, over a wide range of energy, all the known fundamental forces of nature, *i.e.* the electromagnetic force, the weak force and the strong force that are mediated between the known elementary particles. By depending on 18 parameters only, it shows a remarkable internal, theoretical consistency, and has passed extensive experimental tests. The SM has been developed over a period of about 70 years by collaboration of a multitude of theoretical and experimental scientists. In the following, let us summarize some of the steps of the development of the SM, largely taken from [10]. In the first third of the 20th century, dramatic experimental discoveries and theoretical breakthroughs were achieved, which established the theories of quantum mechanics and relativity (e.g. [11–18]). Around the year 1930, Dirac formulated the theory of quantum electrodynamics (QED) to describe the interactions of photons with matter (e.g. [19–22]). Fermi included the beta decay to the theory, and incorporated the neutrino particle that was postulated before by Pauli [23]. Furthermore, Yukawa postulated that the strong interactions between nucleons were transmitted by a massive particle [24]. The muon particle, as a heavy copy of the electron, was discovered, and Klein anticipated that gauge theories form the root cause of beta decay [25]. About ten years later, the computational rules of QED and the concept of renormalization were developed by Feynman, Schwinger and Tomonaga (e.g. [26–35]), which could explain the properties of the anomalous magnetic moment of the electron and the Lamb shift. Several meson and baryon particles were experimentally detected around 1950, providing the need for new quantum numbers, such as the strangeness introduced by Gell-Mann. In addition, neutrinos were detected, as well as the violation of parity in weak interactions by Lee and Yang, and Wu and Telegi [36–38]. The W boson was postulated to mediate the weak interactions, based on work performed by Yang and Mills [39]. Then, around the 1960s, a “zoo” of strongly interacting particles was classified by means of the SU(3) symmetry, succeeded by Ne’eman and Gell-Mann [40–42]. Some times later, the quarks were postulated by Gell-Mann and Zweig as the building blocks of the baryonic matter (e.g. [43, 44]). Nambu proposed that the interactions of quarks with each other can be described by an SU(3) Yang-Mills theory [45]. After that, the electroweak sector of the SM was formulated by Glashow, Salam, Ward and Weinberg [46–49]. The Z boson was predicted, as well as the concept of spontaneous symmetry breaking to induce the masses of gauge bosons, based on work performed by Nambu, Goldstone, Higgs, Brout and Englert [50–55].

Deep inelastic scattering experiments hinted at a substructure inside of the protons. Around 1970, a second family of particles was theoretically implemented to explain the absence of flavor changing neutral currents, by Glashow, Iliopoulos and Maiani [56]. Furthermore, 't Hooft could prove that the Glashow-Salam-Ward-Weinberg model of the electroweak interactions is in fact renormalizable [57, 58]. The Adler-Bell-Jackiw anomaly constraints were investigated, requiring the existence of both quarks and leptons. Besides, the colors as the quantum numbers of the quarks were introduced, leading to the formulation of the theory of quantum chromodynamics (QCD) by Gell-Mann, Fritzsche and Leutwyler [59]. In this sense, it was explored that the strong, weak and electromagnetic interactions can be described by Yang-Mills vector exchange theories. Later, particles of the third generation, such as the tau lepton and the bottom quark, were discovered [60], and neutral current interactions were detected at the CERN, confirming previous theoretical postulates [61, 62]. All these achievements led to the final formulation of the SM, and its universal acceptance around the year 1979 as the basis of elementary particle physics. Further experimental confirmations of not yet detected particles followed shortly after, *e.g.* the discoveries of the W and Z bosons [63–66]. Measurements of the width of the Z boson and the radiative structure of the SM were performed at the experiments of the SLAC and the CERN. Finally, the Higgs boson was discovered as the last undetected particle of the SM in the year 2012 [67, 68].

Despite all these successes, the researches in the field of elementary particle physics have not been finished. Being a renormalizable theory, the SM does not necessarily require extensions of new physics. But still, it suffers from several chinks [10]. The confirmation of the Higgs boson has reinforced the gauge hierarchy problem, which will be explained later in more detail. Altogether, it comprises the problem that the perturbative control of the radiative corrections to the Higgs mass is lost at energy scales already close to the experimental reachability. The most popular and far-reaching theories of new physics have been developed with the motivation to solve the gauge hierarchy problem, among which are extra-dimensional models as the RS model [1], theories of supersymmetry, and composite Higgs models. The SM and many of its bottom-up extensions by new physics are effective field theories that are valid on a wide but still restricted range of energy. The new theories predict consequences for present or future collider experiments, whereas merging into the widely confirmed phenomena of the SM in the lower energy range. In this regard, the SM has been forming the theoretical, well-confirmed basis point for any new theory, and new particles and interactions are expected to appear at energy scales slightly above the range of the SM. Einstein's theory of gravity, describing the fourth fundamental force of nature, is completely omitted from the SM, and until today, it has been impossible to find a consistent quantized description of gravity. For that reason, the SM forms a self-consistent model, valid at energies far away from the Planck scale,  $m_{Pl} = \sqrt{\hbar c/G}$ , at which the quantum corrections of gravity would become important, with  $G$  as the gravitational constant. A complete theory of nature should be situated at the Planck scale, instead. Some approaches for such a unified theory, which can describe all the fundamental forces of nature in a unified manner, are given by the concepts of String theory, for example. In principle, the scale of the fundamental theory should be the number on which everything should be scaled on, and where, naturally, all the phenomena of nature should take place. The length scale related to the Planck mass lies at  $l_{Pl} \sim 10^{-33}$  cm. Comparing it to the scales at which the nuclear  $l_N \sim 10^{-13}$  and the weak  $l_F \sim 10^{-16}$  interactions of the SM are mediated, tremendous



differences are encountered, as [10]

$$\frac{l_N}{l_{Pl}} \sim 10^{20} , \quad \frac{l_F}{l_{Pl}} \sim 10^{17} ! \quad (1.1)$$

One may wonder whether such huge hierarchies can be created by nature, or if they rather indicate the incompleteness of the SM and therefore claim for new physics. It is impossible to explore in experiments the energy region close to the Planck scale, and this will stay so for at least the wide next future. To reach those energy regions, artificially created energy densities similar to the Big Bang would be required, and rough estimations demand for hypothetical collider rings with a diameter of our solar system. And since the Planck energy scale is experimentally unreachable, the ambitions of theoretical physicists should focus on more minimal models, as the extended versions of the SM that are valid at energy scales currently attainable, or at least in the next future.

Next to the question about the origin of the different length scales of the interactions, and the suspicious behaviour of the Higgs mass parameters in the UV energy range, there are further big problems of the SM stemming from the field of cosmology. By observing the fluxes of neutrinos produced by cosmic rays or emitted from the sun, oscillations between the three flavours of neutrinos have been detected [69, 70]. These neutrino oscillations indicate that neutrinos are actually massive particles, which are assumed to be strictly massless in the SM. Furthermore, the predominance of baryons over anti-baryons in the universe cannot be sufficiently explained by the SM (e.g. [71]), although in principle it offers a scenario for an asymmetry between matter and antimatter through charge and parity (CP) violation. And then, there is a remarkable missing mass problem in the universe, resulting from a variety of observations that indicate invisible gravitational sources. Models for the structure formation process after the Big Bang necessarily claim for matter that does not interact with radiation, in order to derive the present-day, granular structure of the universe with stars, galaxies and clusters. Altogether, there are many hints for the existence of this non-luminous dark matter, and this kind of matter must be different to the baryonic type of matter consisting of the SM elementary particles. In fact, the expected amount of dark matter in the universe is more than five times as much as the amount of the visible, baryonic matter. Even worse is the dark energy problem, arising from observations of an accelerated expansion rate of the universe [72, 73]. The SM of cosmology, the  $\Lambda$ -Cold-Dark-Matter ( $\Lambda$ -CDM) model, assumes a mass-energy decomposition for the universe, in which 4.9% are baryonic matter consisting of the SM particles, 26.8% are dark matter and 68.3% is dark energy. In this sense, the total mass content consists to 84.5% of dark matter, and the total mass-energy content is given to 95.1% by dark matter and dark energy [74, 75]. However, such questions are not part of the thesis. Instead, we are working in the framework of the RS model [1] that can address the mysterious questions about the different energy scales at which the SM interactions take place, compared to the fundamental Planck energy scale  $m_{Pl}$ . The RS model can provide a dynamical explanation for the gauge hierarchy problem, and further questions arising in the flavor sector of the SM. The basic ingredients of the RS model will be explained in Chapter 2 of the thesis, whereas we will summarize the significant formulas of the SM, and its biggest open questions, in the present chapter.

### 1.1.1 Some theoretical aspects of the Standard Model

The theoretical description of the SM of particle physics is based on the principles of quantum field theory and the implementation of symmetries. In this connection, the principles of quantum mechanics for microscopic processes, and field theory describing the effects of forces and interactions of nature are combined with the theory of special relativity, which accounts for high-energetic processes at high velocities. These processes describe the scattering interactions of elementary particles, which by nature take place in the cosmic space and are made by human hand in collider experiments, as for example at the LHC at the CERN. In the following, we mention several theoretical issues that are included in the quantum field theory, taken from [10, 76–79]. A quantum field theory, which describes elementary particles and their interactions, is defined by the *action*  $S$  that is a time-integral over the Lagrangian function  $L$ . For a local field theory, it can be expressed by the four-integral over a Lagrangian density  $\mathcal{L}$ , depending on one or more fields  $\phi_i(x)$  and their four-derivatives  $\partial_\mu\phi_i(x)$  [79], as

$$S = \int d^4x \mathcal{L}(\phi_i(x), \partial_\mu\phi_i(x)) \quad \Leftrightarrow \quad \partial_\mu \left( \frac{\delta\mathcal{L}}{\delta(\partial_\mu\phi_i)} \right) - \frac{\delta\mathcal{L}}{\delta\phi_i} = 0. \quad (1.2)$$

An extremum principle for the action results in the equations of motion, which determine the dynamics of a physical system. The above mentioned theoretical symmetries of the physical system are implemented in the Lagrangian, and the mathematical formalism for symmetries is the group theory. A group, in this context, is a certain set  $G$ , together with an operation  $\cdot$ , which combines any two of the elements of the group  $a, b$  to form another group element  $c = a \cdot b$ . In this connection, certain axioms of closure and associativity must hold, as well as the existence of identity and inverse elements. The interactions of the SM are described by unitary Lie groups, where the group elements are unitary transformations, acting on the quantum fields  $\phi$ , by [10, 78]

$$\phi' = U\phi, \quad U^\dagger = U^{-1}, \quad \text{where} \quad U = e^{i\varepsilon^A T^A} \stackrel{\varepsilon^A \ll 1}{\approx} 1 + i\varepsilon^A T^A. \quad (1.3)$$

For local transformations, the transformation parameters  $\varepsilon^A$  depend on the space-time coordinates  $x_\mu$ . The hermitian quantities  $T^A$  fulfil the Lie algebra,  $[T^A, T^B] = if^{ABC}T^C$ , of the group, where  $f^{ABC}$  are the structure constants. In the simplest case of abelian groups, the structure constants vanish. When implementing an internal symmetry in the Lagrangian  $\mathcal{L}$ , an invariance is demanded for the Lagrangian under infinitesimal field transformations as

$$\phi_i(x) \rightarrow \phi'_i(x) = \phi_i(x) + \delta\phi_i(x), \quad \text{where} \quad \delta\phi_i(x) = i\varepsilon^A T_{ij}^A \phi_j(x). \quad (1.4)$$

The transformations cause a change

$$\delta\mathcal{L} = \frac{\delta\mathcal{L}}{\delta\phi_i} \delta\phi_i + \frac{\delta\mathcal{L}}{\delta(\partial_\mu\phi_i)} \delta(\partial_\mu\phi_i) \stackrel{!}{=} 0, \quad (1.5)$$

where  $\delta(\partial^\mu\phi_i) \equiv \partial_\mu\phi'_i - \partial_\mu\phi_i = \partial_\mu(\delta\phi_i)$ , which has to vanish in order to maintain the symmetry invariance. From these considerations, a conserved current follows for the quantum field  $\phi$ , by using further the equation of motion in (1.2) [76, 78],

$$0 \stackrel{!}{=} \delta\mathcal{L} = \varepsilon^A \partial_\mu \left[ \frac{\delta\mathcal{L}}{\delta(\partial_\mu\phi_i)} i T_{ij}^A \phi_j \right] \quad \Rightarrow \quad \partial^\mu J_\mu^A = 0, \quad \text{with} \quad J_\mu^A = -i \frac{\delta\mathcal{L}}{\delta(\partial^\mu\phi_i)} T_{ij}^A \phi_j. \quad (1.6)$$

The conserved charges  $Q^A = \int d^3x J_0^A(x)$  are the generators of the symmetry group, and fulfil the commutation relations of the group. In the quantum field theory, the commutation relations classify particle states, and the generators transform the particles into other particles within a given symmetry multiplet. Also, the conserved symmetry currents satisfy the commutation relations. These physical currents describe interactions between the particles. In general, symmetries are connected with certain conservation laws, as is stated by Noether's theorem [76, 78].

Furthermore, the Lorentz group belongs to the special relativity as the group of transformations  $\Lambda_\nu^\mu$ , acting on the Minkowski-space  $\mathbb{R}^{3+1}$ , according to  $\bar{x}^\mu = \Lambda_\nu^\mu x^\nu$ . The elements of the Minkowski-space are the four-vectors,  $x^\mu = (x^0, x^1, x^2, x^3)^T$ , with one time and three space coordinates. The transformations leave the product of two four-vectors,  $x^2 = x^\mu x_\mu = g_{\mu\nu} x^\mu x^\nu = x_0^2 - \vec{x}^2$ , invariant, from which it follows that  $g_{\mu\nu} \Lambda_\rho^\mu \Lambda_\sigma^\nu = g_{\rho\sigma}$ , where the metric tensor is  $g_{\mu\nu} = \text{diag}(1, -1, -1, -1)$  in a certain convention [10, 79]. The generators of the Lorentz group are the tensors  $S^{\mu\nu} = \frac{i}{4}[\gamma^\mu, \gamma^\nu]$ , where the gamma matrices  $\gamma^\mu$  fulfil the algebra  $\{\gamma^\mu, \gamma^\nu\} \equiv \gamma^\mu \gamma^\nu + \gamma^\nu \gamma^\mu = 2g^{\mu\nu}$ . Lorentz transformations can be decomposed into rotations and velocity transformations. The generators  $S^{\mu\nu}$  include the angular momentum operators,  $J_i \equiv \frac{1}{2}\varepsilon_{ijk} S^{jk}$ , and the ‘‘boost’’ (velocity transformation) operators,  $K_i \equiv S^{i0}$ . To fulfil the demands from special relativity, a theory must be invariant under Lorentz transformations. So does the Dirac equation,

$$[i\gamma^\mu \partial_\mu - m_\psi] \psi = 0, \quad (1.7)$$

which is an important free field equation of quantum field theory [76, 79]. It is invariant under the spinor representation of Lorentz transformations, which is  $\Lambda_{\frac{1}{2}} = \exp\left(-\frac{i}{2}\omega_{\mu\nu} S^{\mu\nu}\right)$ . The solutions of the Dirac equation are linear combinations of plane waves, according to

$$\psi(x) = u(p)e^{-ip \cdot x}, \quad \psi(x) = v(p)e^{+ip \cdot x}, \quad (1.8)$$

where the four-momentum is  $p^\mu = (E/c, \vec{p})^T$ , and  $p^2 = m^2 c^2$ . There are positive and negative frequency solutions, where the negative frequency solutions describe antiparticles. In four space-time dimensions, the algebra of the Lorentz group is isomorphic<sup>1</sup> to the product of two special unitary groups,  $SU(2) \times SU(2)$ . For that reason, the spinor fields appear in two varieties. There are the left-handed spinors, transforming under the first  $SU(2)$  group as a spin- $\frac{1}{2}$  representation, and the right-handed spinors, transforming similarly under the second  $SU(2)$  group. They can be represented by the two-component, complex *Weyl* spinors [10],

$$\psi_L \sim (\mathbf{2}, \mathbf{1}), \quad \psi_R \sim (\mathbf{1}, \mathbf{2}). \quad (1.9)$$

Their behaviour under Lorentz transformations can be written in terms of the *Pauli* spin matrices as

$$\psi_{L,R} \rightarrow \Lambda_{L,R} \psi_{L,R} = e^{\frac{i}{2}\vec{\sigma} \cdot (\vec{\omega} \mp i\vec{v})} \psi_{L,R}, \quad \text{with} \quad \sigma_1 = \begin{pmatrix} 0 & 1 \\ 1 & 0 \end{pmatrix}, \quad \sigma_2 = \begin{pmatrix} 0 & -i \\ i & 0 \end{pmatrix}, \quad \sigma_3 = \begin{pmatrix} 1 & 0 \\ 0 & -1 \end{pmatrix}. \quad (1.10)$$

Here,  $\vec{\omega}$  and  $\vec{v}$  are real rotation and boost angles. In the Dirac notation, one can write the full spinor  $\psi$  as a combination of two Weyl spinors, as  $\psi = (\psi_L \ \psi_R)^T$ . With the notation for the

<sup>1</sup>There is a bijective correlation between the mathematical structure of the Lorentz group and the product of two special unitary groups of dimension 2.

Pauli matrices,  $\sigma^\mu \equiv (1, \vec{\sigma})^T$ ,  $\bar{\sigma}^\mu \equiv (1, -\vec{\sigma})^T$ , the Dirac equation for the spinor  $\psi$  from (1.7) can be written as<sup>2</sup> [79]

$$\begin{pmatrix} -m & i\bar{\sigma} \cdot \partial \\ i\bar{\sigma} \cdot \partial & -m \end{pmatrix} \begin{pmatrix} \psi_L \\ \psi_R \end{pmatrix} = \mathbf{0}. \quad (1.11)$$

The Dirac matrices  $\gamma^\mu$  in the Weyl representation have a  $2 \times 2$  block matrix form as

$$\gamma_0 = \begin{pmatrix} 0 & 1 \\ 1 & 0 \end{pmatrix}, \quad \gamma_i = \begin{pmatrix} 0 & -\sigma_i \\ \sigma_i & 0 \end{pmatrix}, \quad \gamma_5 = \begin{pmatrix} 1 & 0 \\ 0 & -1 \end{pmatrix}. \quad (1.12)$$

Then, the gauge principle demands for an invariance under *local* gauge symmetries, for which the transformation parameters  $\varepsilon^A(x)$  in (1.3) explicitly depend on the space-time coordinates  $x_\mu$ . The symmetry invariance is achieved by introducing vector-bosonic gauge fields via the covariant derivatives,  $\mathcal{D}_\mu = \partial_\mu + igA_\mu$ , where  $g$  is a dimensionless coupling constant, and  $A_\mu(x) = \sum_{A=1}^N A_\mu^A(x)T^A$  contains a sum over the gauge boson fields, equalling the number of group generators  $N$  of the symmetry group. The gauge bosons couple to the matter fields by their kinetic terms in the Lagrangian, as  $\bar{\psi}i\gamma^\mu\mathcal{D}_\mu\psi$ . Gauge transformations of the covariant derivatives read  $\mathcal{D}_\mu \rightarrow \mathcal{D}'_\mu = U\mathcal{D}_\mu U^\dagger$ , by which the gauge bosons themselves are transformed as [10, 76]

$$A_\mu \rightarrow A'_\mu = UA_\mu U^\dagger - i\frac{1}{g}U\partial_\mu U^\dagger \approx A_\mu + \delta A_\mu, \quad \delta A_\mu^A \stackrel{\varepsilon^A \ll 1}{\approx} -\frac{1}{g}\partial_\mu \varepsilon^A - f^{ABC}\varepsilon^B A_\mu^C. \quad (1.13)$$

Here, we see that the structure constants  $f^{ABC}$  enter the changes of the gauge bosons  $\delta A_\mu$  that are induced by the gauge transformations. These changes cancel the terms that are induced by the gauge transformations of the matter fields  $\psi$ , when transforming the whole coupling term as  $\bar{\psi}i\gamma^\mu\mathcal{D}_\mu\psi \rightarrow \bar{\psi}U^\dagger U (i\gamma^\mu\mathcal{D}_\mu) U^\dagger U\psi$ . On this way, the whole kinetic term is invariant under the gauge transformations, and a self-interacting theory is obtained. Field strength tensors for the gauge bosons are built by means of the covariant derivatives, as [10, 76]

$$F_{\mu\nu} = -i[D_\mu, D_\nu] = \partial_\mu A_\nu - \partial_\nu A_\mu + ig[A_\mu, A_\nu] = F_{\mu\nu}^A T^A, \quad F_{\mu\nu}^A = \partial_\mu A_\nu^A - \partial_\nu A_\mu^A - gf^{ABC}A_\mu^B A_\nu^C, \quad (1.14)$$

and they covariantly transform, according to  $F_{\mu\nu} \rightarrow UF_{\mu\nu}U^\dagger$ . The Yang-Mills Lagrangian builds the kinetic terms of the gauge fields,  $\mathcal{L}_{\text{kin.boson}} = -\frac{1}{4}F_{\mu\nu}F^{\mu\nu}$ , and is invariant under both Lorentz and gauge transformations. All in all, by putting the demand of local gauge invariance into a theory, a coupling of the matter fields  $\psi$  to the gauge fields  $A_\mu$  is predicted. It causes the interactions between the matter fields through exchanges of gauge bosons, according to the respective gauge groups. This mechanism forms the fundamental, theoretical basis for the interactions between elementary particles.

A difficulty arises when considering bare mass terms for gauge bosons and fermions. A bare gauge boson mass term transforms under the gauge transformations in a non-invariant manner, as

$$-m^2 A_\mu A^\mu \rightarrow -m^2 A'_\mu A'^\mu \approx -m^2 [A_\mu A^\mu + \mathbf{2}\delta\mathbf{A}_\mu \mathbf{A}^\mu], \quad (1.15)$$

and therefore explicitly breaks the demand of gauge invariance of the theory. To maintain the gauge principle, a mechanism of a *spontaneous* gauge symmetry breaking is included. A scalar field is proposed to the theory, whose potential has a non-vanishing, degenerate ground

<sup>2</sup>With the notation for the four-derivatives,  $\partial_\mu = (\partial_t, \nabla)$ ,  $\partial^\mu = (\partial_t, -\nabla)$ .

state of minimal energy. This means that there are several ground states all corresponding to equivalent physical theories, which can be transformed into each other by means of a symmetry transformation. By choosing one particular of these ground states, the vacuum state is no longer invariant under the full, original symmetry group, which has been broken **spontaneously**. Then, a coupling of the gauge bosons and fermions to the non-vanishing ground state of the scalar can give the mass terms, without explicitly violating the gauge invariance [10, 77].

For a general example, taken from [10], one can consider a real scalar field  $\Phi(x)$  with the components  $\varphi_a(x)$ ,  $a = 1, 2, \dots, n$ , following the scalar Lagrangian

$$\mathcal{L} = \frac{1}{2} \partial_\mu \Phi^t(x) \partial^\mu \Phi(x) - \lambda \left[ \Phi^t \Phi - \frac{v^2}{2} \right]^2. \quad (1.16)$$

This Lagrangian is invariant under the transformations  $\Phi \rightarrow \Phi' = R\Phi(x)$ , where  $R = e^{i\vec{\theta} \cdot \vec{T}}$ , and  $R^t R = 1$ , corresponding to the Lie algebra  $SO(N)$  that consists of  $N(N-1)/2$  antisymmetric generators  $T^A$ . According to the Noether theorem, a conserved current,  $J_\mu^A = i\phi^t T^A \overleftrightarrow{\partial}_\mu \Phi$ , corresponds to each generator that fulfils  $\partial^\mu J_\mu^A = 0$  [10]. An infinite number of field configurations,  $\Phi_0 = \frac{1}{\sqrt{2}} e^{i\vec{\theta} \cdot \vec{K}} (0 \dots 0 v)^T$ , minimizes the potential of the scalar, the second term of the Lagrangian in (1.16). The actual vacuum singles out one of these infinite number of states, by breaking the  $SO(N)$  symmetry, but leaving invariant all the rotations in the  $(N-1)$ -dimensional plane perpendicular to that direction.  $\vec{K}$  are the generators of the  $(N-1)$  broken symmetries that form no longer a Lie algebra, whereas  $(N-1)$  angles parametrize the broken rotations. The field can be expanded away from its vacuum configuration as [10]

$$\Phi(x) = \frac{1}{\sqrt{2}} e^{i\frac{\vec{\theta}}{v} \cdot \vec{K}} \begin{pmatrix} 0 \\ \dots \\ 0 \\ v + \rho(x) \end{pmatrix}. \quad (1.17)$$

By inserting this expansion into the Lagrangian, one can derive

$$\mathcal{L} = \frac{1}{2} \partial_\mu \rho \partial^\mu \rho + \frac{1}{2} \left( 1 + \frac{\rho}{v} \right)^2 \partial_\mu \xi^i \partial^\mu \xi_i - \frac{1}{2} m^2 \rho^2 - \frac{\lambda}{4} \rho^4 - v \lambda \rho^3. \quad (1.18)$$

Here, the phases  $\theta_i$  were absorbed into the definitions of the new fields  $\xi_i(x)$ , the massless Nambu-Goldstone (NG) bosons [51, 52]. Their number equals  $(N-1)$ , the number of the broken symmetries. The Lagrangian is invariant under  $(N-1)$  constant shifts,  $\xi_i(x) \rightarrow \xi_i(x) + \tilde{\theta}_i$ , in a one-to-one correspondence to the remaining  $SO(N-1)$  phase symmetry of the ground state. One can write the couplings of the NG bosons in terms of a divergence of the broken currents, as  $\mathcal{L}_{\text{int}} = -\frac{1}{v} J_\mu^i(x) \partial^\mu \xi^i(x)$ , allowing to find that the unbroken  $SO(N-1)$  symmetry is linearly realized on the NG bosons as  $\Xi(x) \rightarrow e^{i\vec{\theta} \cdot \vec{K}} \Xi(x)$ , where  $\Xi_i(x) = \xi_i(x)$ . There is one massive field  $\rho(x)$ , the Higgs boson, which receives a mass  $m = \sqrt{2\lambda}v$ . The number of the degrees of freedom in this process remains constant. From originally  $N$  scalar fields  $\varphi_a(x)$ , there are now  $(N-1)$  massless NG bosons  $\xi_i(x)$  and one massive Higgs field  $\rho(x)$ . In a certain gauge theory, there are the gauge bosons  $A_\mu^A$  that interact with the currents  $J_\mu^A$  according to  $\mathcal{L}_{\text{int}} = g A_\mu^A J^{A\mu}$ . Then, the couplings of the NG bosons to the currents can be exactly cancelled by performing a gauge transformation as  $\delta A_\mu^i = -\frac{1}{g} \partial_\mu \xi^i + f^{ijk} A_\mu^j \xi^k$  [10]. In this sense, the NG bosons can be

absorbed by a redefinition of the gauge fields, and each gauge field that corresponds to a broken gauge symmetry acquires an extra degree of freedom to become massive. The mass terms are generated by the covariant derivative, acting on the scalar field [10],

$$\mathcal{D}_\mu \Phi \ni \left[ \partial_\mu + ig \sum_{A=1}^N A_\mu^A(x) T^A \right] \cdot \begin{pmatrix} 0 \\ \vdots \\ 0 \\ [v + \rho(x)] \end{pmatrix}, \quad (1.19)$$

where here the field is situated in its simplest ground state. So, the gauge bosons, associated to each broken generator, become massive after “eating” the NG bosons, whereas those of the unbroken generators remain massless.

### Perturbative calculations in quantum field theory

On the one hand, the Lagrangians of particle physics consist of the parts that describe free particle states, the kinetic and the mass terms. On the other hand, they also contain the parts that describe particle interactions by the couplings of gauge bosons to the currents of matter fields, governed by a certain coupling constant  $g$ . Whereas the parts of the free particles define the equations of motions via the Euler-Lagrange equations, the parts of the interactions describe non-linear couplings between the free-particle states. According to the small values of the coupling constants  $g$  in the energy range of the SM, the particle interactions can commonly be computed by means of a perturbation theory. Theoretically, the perturbative approach is implemented by an expansion of the Scattering-matrix (S-matrix), relating the initial particle states  $|i\rangle$  at an asymptotic time  $t_i = -\infty$  to the final particles states  $|f\rangle$  at a time  $t_f = \infty$ , according to [77]

$$|f\rangle = \mathbf{S}|i\rangle. \quad (1.20)$$

By considering a description for the time evolution of the state vectors in a quantum mechanical picture, one can derive the Dyson-expansion for the S-matrix

$$\mathbf{S} = \sum_{n=0}^{\infty} \frac{(-i)^n}{n!} \int \dots \int d^4x_1 d^4x_2 \dots d^4x_n T\{\mathcal{H}_I(x_1)\mathcal{H}_I(x_2)\dots\mathcal{H}_I(x_n)\}, \quad (1.21)$$

which contains a time-ordered product  $T$ , and the Hamiltonians  $\mathcal{H}_I = -\mathcal{L}_I$  that describe the particle couplings. The interactions are extracted from the S-matrix over  $\mathbf{S} = \mathbf{1} + i\mathbf{T}$ , and the amplitude

$$\langle p_f \dots | i\mathbf{T} | p_A p_B \rangle = (2\pi)^4 \delta^{(4)}(p_A + p_B - \sum p_f) \cdot i\mathcal{M}(p_A, p_B \rightarrow p_f) \quad (1.22)$$

describes the scattering of two initial particles with the momenta  $p_A$  and  $p_B$  that interact to a final state of particles with the momenta  $p_f$  [79]. The expression  $\mathcal{M}(p_A, p_B \rightarrow p_f)$  can be calculated according to the **Feynman rules**. Physical measurable quantities, such as cross sections and decay rates, depend on the square of this amplitude, and an integration over the phase space accounting for statistical correlations. On that way, statistical predictions can be derived that give the probability for a certain interaction to take place at a scattering experiment. In the experiments, a certain interaction process has to be repeated and measured very many times to get statistical reliable results.

In principle, the S-matrix, given as a sum in (1.21), describes the interactions to all orders of perturbation theory, where the lowest order for  $n = 0$  gives the dominant contribution. Higher orders give smaller and more complicated contributions, since by increasing order of perturbation theory, the interaction Hamiltonians are coupled to each other to increasing numbers, which results in a more complex interaction structure. In this connection, the time-ordered product of operators, connecting different particle states in  $\mathcal{H}_I$  to each other, can be reformulated in terms of a normal-ordered product by the Wick-theorem. According to the Feynman rules, these connections of particle states result in **vertex couplings** and **propagators** to describe the processing of particle interactions. This can be illustrated graphically by means of Feynman diagrams that consist of incoming particles  $A$  and  $B$ , which scatter and couple to each other, described by the vertices. **Virtual** particle states can be produced, having arbitrarily high momenta according to the uncertainty relation of quantum mechanics. The virtual particles propagate in space-time, which is described by the propagators. These result, after further particle couplings described by the vertices, in the outgoing final state particles  $f$ . In the calculations of scattering amplitudes, one has to integrate over the momentum space of all the undetermined momenta of the intermediate, virtual particles, to account for the statistical description of scattering by means of overlapping probability densities. In increasing orders of perturbation theory, such virtual particles are produced in the intermediate states to larger numbers, forming a higher number of loops that mediate the interactions.

The momentum integrations can give divergent results that commonly occur in the perturbation theory of quantum field theory. In this regard, certain “renormalization” procedures have to be applied in order to derive physical, measurable predictions [26–35]. In the calculations, the divergences are absorbed into the bare quantities of a theory, such as masses, charges, and fields. It is an important attribute of a theory if it is in general possible to perform renormalizations at an arbitrary order of perturbation theory. This is true for the theories that predict only a **finite** number of possible divergent substructures in the Feynman diagrams. In this case, similar patterns can be used for the renormalization of the divergent parts for every order of perturbation theory. The theories of the SM are renormalizable in this sense [57, 58]. Instead, in a non-renormalizable theory an infinite number of divergent substructures can be contained in the scattering amplitudes, at a sufficiently high order of perturbation theory. Then, the theory cannot be self-consistent, making it hard to derive physical predictions [76, 78, 79].

### 1.1.2 Lagrangian of the Standard Model

In theory, the SM of particle physics is grounded on the local gauge groups

$$SU(3) \times SU(2) \times U(1) , \quad (1.23)$$

whose correlated gauge bosons

$$G_\mu^A , \quad A = 1, \dots, 8 , \quad W_\mu^a , \quad a = 1, 2, 3 , \quad B_\mu , \quad (1.24)$$

mediate the interactions between the matter fields to guarantee the local gauge invariance. The quantum numbers that are correlated to the gauge groups are the color charge  $c$ , the weak isospin  $T$  and the hypercharge  $Y$ . The matter fields, named  $f$  in the following, can be grouped into different classes, corresponding to their transformation behaviours under the gauge groups.

There are the quarks fields  $q = u, d$ , transforming as color triplets under  $SU(3)$  [40–45, 59], whereas the leptons  $l = \nu, e$  are color singlets [46–49]. All quarks  $q$  and electrically charged leptons  $e$  can be separated into the two different chiralities, according to  $f = P_L f + P_R f = f_L + f_R$ , where the projection operators are  $P_{L,R} = (1 \mp \gamma_5)/2$ . In addition, there are the electrically neutral leptons  $\nu_L$ , the neutrinos, that exist exclusively as left-handed fields in the SM. The different chiralities are important for the transformation behaviour under the gauge group  $SU(2)$  of the weak interaction, which non-trivially acts only on left-handed fermions. For that reason, the left-handed fermions can be grouped into the weak isospin doublets  $Q_L = (u_L, d_L)^T$ , and  $L_L = (\nu_L, e_L)^T$  [46–49]. Instead, the right-handed fermions form the singlets  $u_R, d_R, e_R$ . Interestingly, the fermions come with three generations of fields, which are totally equal in the quantum numbers, but differ strongly in the masses. Altogether, the particle content of the SM reads [10]

$$\begin{aligned}
\underline{\text{quarks}} \quad Q_L &: \begin{pmatrix} u_L \\ d_L \end{pmatrix}_{\frac{1}{3}}, \begin{pmatrix} c_L \\ s_L \end{pmatrix}_{\frac{1}{3}}, \begin{pmatrix} t_L \\ b_L \end{pmatrix}_{\frac{1}{3}}, & u_R &: (u_R)_{\frac{4}{3}}, (c_R)_{\frac{4}{3}}, (t_R)_{\frac{4}{3}}, \\
& & d_R &: (d_R)_{-\frac{2}{3}}, (s_R)_{-\frac{2}{3}}, (b_R)_{-\frac{2}{3}}, \\
\underline{\text{leptons}} \quad L_L &: \begin{pmatrix} \nu_{eL} \\ e_L \end{pmatrix}_{-1}, \begin{pmatrix} \nu_{\mu L} \\ \mu_L \end{pmatrix}_{-1}, \begin{pmatrix} \nu_{\tau L} \\ \tau_L \end{pmatrix}_{-1}, & e_R &: (e_R)_{-2}, (\mu_R)_{-2}, (\tau_R)_{-2},
\end{aligned} \tag{1.25}$$

where the subscripts write the weak hypercharges  $Y$  under the  $U(1)$  gauge group, respectively. The kinetic terms,  $\mathcal{L}_{\text{kin}} = \sum_f \bar{f} i \mathcal{D}^f f$ , contain the couplings of the matter fields to the gauge bosons via the covariant derivatives [10, 76, 79], given for the quark fields

$$\begin{aligned}
\mathcal{D}_\mu Q_L &= \left[ \partial_\mu - i \frac{g_s}{2} \lambda^A G_\mu^A - i \frac{g}{2} \sigma^a W_\mu^a - i \frac{g'}{6} B_\mu \right] Q_L, \\
\mathcal{D}_\mu u_R &= \left[ \partial_\mu - i \frac{g_s}{2} \lambda^A G_\mu^A - i \frac{2g'}{3} B_\mu \right] u_R, \\
\mathcal{D}_\mu d_R &= \left[ \partial_\mu - i \frac{g_s}{2} \lambda^A G_\mu^A + i \frac{g'}{3} B_\mu \right] d_R,
\end{aligned} \tag{1.26}$$

and for the lepton fields

$$\begin{aligned}
\mathcal{D}_\mu L_L &= \left[ \partial_\mu - i \frac{g}{2} \sigma^a W_\mu^a + i \frac{g'}{2} B_\mu \right] L_L, \\
\mathcal{D}_\mu e_R &= [\partial_\mu + i g' B_\mu] e_R,
\end{aligned} \tag{1.27}$$

to maintain the gauge invariance. These covariant derivatives contain the generators  $\sigma^a$  and  $\lambda^A$  of the non-abelian groups  $SU(2)$  and  $SU(3)$ , respectively. Defining the respective field strength tensors

$$\begin{aligned}
G_{\mu\nu}^A &= \partial_\mu^A G_\nu^A - \partial_\nu G_\mu^A - g_s f^{ABC} G_\mu^B G_\nu^C, \\
W_{\mu\nu}^a &= \partial_\mu W_\nu^a - \partial_\nu W_\mu^a - g \epsilon^{abc} W_\mu^b W_\nu^c, \\
B_{\mu\nu} &= \partial_\mu B_\nu - \partial_\nu B_\mu,
\end{aligned} \tag{1.28}$$



the gauge fields fulfil the following kinetic terms

$$\mathcal{L} = -\frac{1}{4} \sum_{A=1}^8 G_{\mu\nu}^A G^{\mu\nu A} - \frac{1}{4} \sum_{a=1}^3 W_{\mu\nu}^a W^{\mu\nu a} - \frac{1}{4} B_{\mu\nu} B^{\mu\nu} . \quad (1.29)$$

The structure constants  $f^{ABC}$ ,  $\epsilon^{abc}$ , of the groups  $SU(3)$  and  $SU(2)$  predict a self-coupling of the respective gauge bosons  $G_\mu^B$  and  $W_\mu^a$ . Until now, the Lagrangian does not contain any mass terms, either for fermions or gauge bosons, as their simple inclusions would explicitly break the electroweak gauge symmetry. For that reason, the SM fields are coupled to a scalar doublet under  $SU(2)$ , the Higgs field, having the hypercharge  $Y = 1$ , and fulfilling the Lagrangian [50–55]

$$\mathcal{L}_{\text{Higgs}} = (D^\mu \Phi)^\dagger (D_\mu \Phi) + \mu^2 \Phi^\dagger \Phi - \lambda (\Phi^\dagger \Phi)^2 . \quad (1.30)$$

For the parameter choices  $\mu^2 > 0$  and  $\lambda > 0$ , the Higgs potential has a degenerate ground state with an amount of  $|\langle 0 | \Phi | 0 \rangle| = v/\sqrt{2} \neq 0$  [10, 76–79]. By writing the Higgs doublet as  $\Phi = (\phi^+, \phi^0)^T$ , with a charged and a neutral component, the non-zero ground state,  $\langle 0 | \Phi | 0 \rangle = e^{i\alpha}/\sqrt{2} (0 \ v)^T$ , is invariant under a global phase rotation in  $\alpha$ . With one particular of these ground states, the electroweak gauge symmetry of the Higgs Lagrangian  $SU(2) \times U(1)$  is spontaneously broken down to the remaining  $U(1)_{\text{em}}$  electromagnetic (em) gauge symmetry. The charges  $Q$  are the quantum numbers of the electromagnetic symmetry, and the relation  $T_3 + \frac{Y}{2} = Q$  holds between the quantum numbers of the groups, where  $T_3$  is the third component of the weak isospin. This relation fixes the quark charges to  $Q_u = 2/3$ ,  $Q_d = -1/3$ , and the lepton charges to  $Q_l = -1$ ,  $Q_\nu = 0$ , respectively. Usually, the Higgs field is expanded around its simplest ground state as

$$\Phi = \frac{1}{\sqrt{2}} \begin{pmatrix} -i\phi^+ \\ v + h + i\phi^3 \end{pmatrix} . \quad (1.31)$$

Via the covariant derivative in the Higgs Lagrangian, the coupling of the gauge bosons to the constant vacuum expectation value (vev)  $v$  in the expanded Higgs field creates the mass terms for the gauge bosons,

$$\begin{aligned} \mathcal{L}_{\text{Higgs}} \ni (D^\mu \Phi)^\dagger (D_\mu \Phi) &= |(\partial_\mu - i\frac{g}{2}\sigma^a W_\mu^a - i\frac{g'}{2}B_\mu)\Phi|^2 \ni \left| \begin{pmatrix} -i\frac{g}{2}\frac{v}{\sqrt{2}}(W_\mu^1 - iW_\mu^2) \\ \frac{v}{\sqrt{2}}(i\frac{g}{2}W_\mu^3 - i\frac{g'}{2}B_\mu) \end{pmatrix} \right|^2 \\ &= \frac{v^2}{4 \cdot 2} \left[ g^2(W^{\mu 1} + iW^{\mu 2}) \cdot (W_\mu^1 - iW_\mu^2) + g^2 W^{\mu 3} W_\mu^3 + g'^2 B^\mu B_\mu - 2gg' W^{\mu 3} B_\mu \right] , \end{aligned} \quad (1.32)$$

by breaking the electroweak gauge symmetry only spontaneously. A redefinition of the electroweak gauge bosons to the mass eigenstates, according to

$$W_\mu^\pm = \frac{1}{\sqrt{2}}(W_\mu^1 \mp iW_\mu^2) , \quad A_\mu = \cos \theta_w B_\mu + \sin \theta_w W_\mu^3 , \quad Z_\mu = -\sin \theta_w B_\mu + \cos \theta_w W_\mu^3 , \quad (1.33)$$

is sensible, which is governed by the weak mixing angle  $\theta_w$ , where  $\sin \theta_w = g'/\sqrt{g^2 + g'^2}$ , and  $\cos \theta_w = g/\sqrt{g^2 + g'^2}$ . In fact, those redefined fields are the measurable gauge bosons. In the mass basis, one obtains the following results for the mass terms

$$\mathcal{L}_{\text{Higgs}} \ni \frac{g^2 v^2}{4} \left( W^{\mu -} W_\mu^+ + \frac{1}{2\cos^2 \theta_w} Z^\mu Z_\mu \right) , \quad (1.34)$$

with the  $W$  and  $Z$  boson masses  $m_W = \frac{vg}{2}$  and  $m_Z = \frac{vg}{2\cos\theta_w}$ , whereas the photon state  $A_\mu$  remains massless. The interactions of the matter fields with the physical gauge bosons are usually described in terms of the following current notation [10, 76–79]

$$\mathcal{L}_{\text{int}} = g(W_\mu^+ J_W^{\mu+} + W_\mu^- J_W^{\mu-} + Z_\mu J_Z^\mu) + eA_\mu J_{\text{em}}^\mu , \quad (1.35)$$

where

$$\begin{aligned} J_W^{\mu+} &= \frac{1}{\sqrt{2}} (\bar{\nu}_L \gamma^\mu e_L + \bar{u}_L \gamma^\mu d_L) , \\ J_W^{\mu-} &= \frac{1}{\sqrt{2}} (\bar{e}_L \gamma^\mu \nu_L + \bar{d}_L \gamma^\mu u_L) , \\ J_Z^\mu &= \frac{1}{\cos\theta_w} \left[ \bar{\nu}_L \gamma^\mu \left( \frac{1}{2} \right) \nu_L + \bar{e}_L \gamma^\mu \left( -\frac{1}{2} + \sin^2\theta_w \right) e_L + \bar{e}_R \gamma^\mu (\sin^2\theta_w) e_R \right. \\ &\quad \left. + \bar{u}_L \gamma^\mu \left( \frac{1}{2} - \frac{2}{3}\sin^2\theta_w \right) u_L + \bar{u}_R \gamma^\mu \left( -\frac{2}{3}\sin^2\theta_w \right) u_R \right. \\ &\quad \left. + \bar{d}_L \gamma^\mu \left( -\frac{1}{2} + \frac{1}{3}\sin^2\theta_w \right) d_L + \bar{d}_R \gamma^\mu \left( \frac{1}{3}\sin^2\theta_w \right) d_R \right] , \\ J_{\text{em}}^\mu &= \bar{e} \gamma^\mu (-1) e + \bar{u} \gamma^\mu \left( +\frac{2}{3} \right) u + \bar{d} \gamma^\mu \left( -\frac{1}{3} \right) d . \end{aligned} \quad (1.36)$$

Each term holds for all three fermion generations, where the fermions are still the gauge eigenstates. Altogether, the kinetic terms for the fermions and gauge bosons show invariances under large global symmetries, as for example under global chiral family-symmetries as [10]

$$U(3) \times U(3) \times U(3) \times U(3) \times U(3) . \quad (1.37)$$

Those symmetries correspond to unitary transformations according to  $L_i \rightarrow L'_i = U_{ij} L_j$ , where  $U$  is a  $3 \times 3$  unitary matrix, and there is one for each set of fermions with the same quantum numbers  $Q_L, L_L, u_R, d_R, e_R$  [76, 78, 79]. This large symmetry structure is broken by the Yukawa interactions, connecting pairs of fermions with the Higgs field,

$$\mathcal{L}_{\text{Yukawa}} = - (\bar{Q}_L^m \Phi \mathbf{Y}_d^{mn} d_R^n + \bar{Q}_L^m (i\sigma_2 \Phi^*) \mathbf{Y}_u^{mn} u_R^n + \bar{L}_L^m \Phi \mathbf{Y}_e^{mn} e_R^n + \text{h.c.}) . \quad (1.38)$$

Again, the fermions of the three generations are grouped into vectors. These terms can create mass terms for the fermions that are compatible to gauge invariance, similar to the masses of the gauge bosons, by a coupling to the vev of the expanded Higgs field. The couplings are induced by arbitrary, complex matrices  $\mathbf{Y}_f^{mn}$ , which generally define a mixing between the different gauge states of the fermions. However, one can perform the following bilinear transformations of the Yukawa matrices [76, 78],

$$\mathbf{Y}_d = \mathbf{U}_d^\dagger \mathbf{M}_d \mathbf{V}_d , \quad \mathbf{Y}_u = \mathbf{U}_u^\dagger \mathbf{M}_u \mathbf{V}_u , \quad \mathbf{Y}_e = \mathbf{U}_e^\dagger \mathbf{M}_e \mathbf{V}_e , \quad (1.39)$$

where  $\mathbf{U}_i, \mathbf{V}_i$  are unitary  $3 \times 3$  matrices, and

$$\mathbf{M}_u = \text{diag}(y_u, y_c, y_t) , \quad \mathbf{M}_d = \text{diag}(y_d, y_s, y_b) , \quad \mathbf{M}_e = \text{diag}(y_e, y_\mu, y_\tau) , \quad (1.40)$$

are real diagonal matrices. After the following field redefinitions,  $L'_L = \mathbf{U}_e L_L$ , and  $e'_R = \mathbf{V}_e e_R$ , the leptonic part of the Yukawa couplings becomes diagonal. The unitary matrices  $\mathbf{V}_u$  and  $\mathbf{V}_d$  can be absorbed by a redefinition of the fields, as  $u'_R = \mathbf{V}_u u_R$  and  $d'_R = \mathbf{V}_d d_R$ , whereas the matrices  $\mathbf{U}_u$  and  $\mathbf{U}_d$  cannot be simultaneously absorbed by field redefinitions. Instead, one can derive

$$\mathcal{L}_{\text{Yukawa}} = - \left[ \bar{Q}'_L{}^m \Phi \mathbf{V}_{\text{CKM}}^{\dagger, mn} \mathbf{M}_d^n d'_R{}^n + \bar{Q}'_L{}^n (i\sigma^2 \Phi^*) \mathbf{M}_u^n u'_R{}^n + \bar{L}'_L{}^n \Phi \mathbf{M}_e^n e'_R{}^n + \text{h.c.} \right] , \quad (1.41)$$

where the up-type quark term is diagonal in the quark states, but the down-type quark term involves the Cabibbo-Kobayashi-Maskawa (CKM) mixing matrix

$$\mathbf{V}_{\text{CKM}} = \mathbf{U}_u^\dagger \mathbf{U}_d . \quad (1.42)$$

This mixing matrix induces a coupling between the quark mass eigenstates in the charged current interactions, according to

$$J_W^{\mu+} = \frac{1}{\sqrt{2}} \left( \bar{u}'_L{}^{m'} \mathbf{V}_{\text{CKM}}^{mn} \gamma^\mu d'_L{}^n \right) , \quad J_W^{\mu-} = \frac{1}{\sqrt{2}} \left( \bar{d}'_L{}^{m'} \mathbf{V}_{\text{CKM}}^{\dagger mn} \gamma^\mu u'_L{}^n \right) . \quad (1.43)$$

Independently from the up-type quark terms, the down-type quark terms can be diagonalized as well. Then, via a coupling to the vev of the Higgs field, one can obtain the mass terms for the fermions, where the fermion masses are defined as

$$m_i = \frac{v}{\sqrt{2}} y_i , \quad (1.44)$$

and  $y_i$  are the elements of the diagonal matrices in (1.40). Originally, the unitary CKM-matrix is determined by 9 free parameters, but each quark field can absorb one phase after a phase rotation, according to  $q_i \rightarrow e^{i\theta} q_i$ , where  $q_i = u_L, u_R, d_L, d_R$ . In addition, a global phase rotation can be performed, so that the number of free parameters can be reduced to 4, which are three real parameters and one complex phase in the ‘‘standard parametrization’’ [80]. In the ‘‘Wolfenstein parametrization’’, there are the four Wolfenstein-parameters used to describe the CKM-matrix as [81]

$$V_{\text{CKM}} = \begin{pmatrix} 1 - \lambda^2/2 & \lambda & A\lambda^3(\rho - i\eta) \\ -\lambda & 1 - \lambda^2/2 & A\lambda^2 \\ A\lambda^3(1 - \rho - i\eta) & -A\lambda^2 & 1 \end{pmatrix} , \quad (1.45)$$

where the expression holds up to the order  $\lambda^3$ , and the Wolfenstein-parameters are of the order one.

The full Lagrangian of the SM is invariant under the combined operation of three discrete symmetries, which are charge conjugation (C-symmetry), parity transformation (P-symmetry) and time-reversal (T-symmetry) [10, 76, 78, 79]. The C-symmetry transforms particle states into their antiparticle states, where for the matter fields applies  $\psi_L \rightarrow \sigma_2 \psi_R^* \equiv \bar{\psi}_L$  and  $\psi_R \rightarrow -\sigma_2 \psi_L^* \equiv -\bar{\psi}_R$ , whereas the P-transformation transforms the chiralities of the matter fields into each other, as  $\psi_L \rightarrow \psi_R$  and  $\psi_R \rightarrow \psi_L$ , and the T-symmetry reverses the time evolution of a considered process. In the SM, violations of the combined CP-transformations are related to the complex phase of the CKM mixing matrix. By performing the transformations  $\psi_L \rightarrow \sigma_2 \psi_L^*$  and  $\psi_R \rightarrow -\sigma_2 \psi_R^*$  in a general Yukawa Lagrangian, one can show that an invariance under

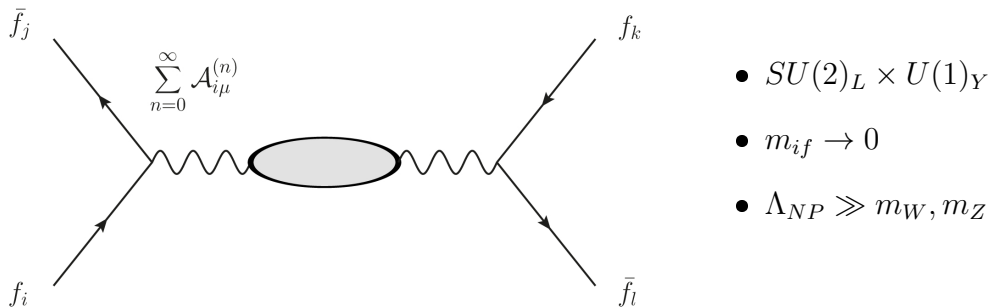


Figure 1.1: Electroweak precision observables test four-fermion interactions at lower energies. Based on the three indicated assumptions on the right-hand side, the significant radiative corrections to these processes, induced by new physics, are the “oblique” corrections, given by vacuum polarizations that affect the gauge boson propagators [82]. These can be parametrized sufficiently in terms of the S, T and U parameters. The sum in the graphic indicates a tower of KK gauge bosons that can mediate the four-fermion interactions in the RS model, which will be explained in Chapter 2 of the thesis.

CP is achieved for the case that the Yukawa couplings are real [10]. Since in the SM the parametrization of the CKM-matrix owns at least one complex phase, there is a source of CP-violation, accordingly. The complex phase is related to the existence of three generations of particles. For two or less generations of particles, the CP-violating phases can be completely absorbed by field redefinitions. The kinetic terms of the SM fields are invariant under CP-transformations. The complex phase of the CKM-matrix constitutes to be the only source for CP violating phenomena in the SM. In this sense, the study of the CP behaviour of particle processes can be a useful tool to test the structure of the SM, and to search for new sources of CP violation, induced by new physics.

Altogether, the full Lagrangian of the SM depends on 18 open parameters, which are the three gauge couplings  $g_s$ ,  $g'$  and  $g$ , corresponding to the three described interactions, the 9 masses of the different fermions or equally their different Yukawa couplings strengths, four parameters of the mixing of the quark states described by the CKM-matrix, and two parameters in the Higgs sector, for example  $\lambda$  and  $\mu$  [10, 76, 78, 79]. These parameters have been experimentally fixed to a great precision resulting in the present consistent formulation of the SM.

### 1.1.3 Electroweak parameters by Peskin and Takeuchi

M. Peskin and T. Takeuchi introduced a suitable formalism for calculating in general the oblique radiative electroweak corrections to four-fermion interactions that are implied by new-physics theories, to confront the predictions with electroweak precision measurements [82–85]. Around that time in the year 1990,  $e^+e^-$ -collider experiments were studied thoroughly, and many suitable electroweak precision observables were introduced to be tested at the experiments. Among these were, for example, decay widths and asymmetries measured at the Z-pole, ratios of cross sections in deep inelastic neutrino scattering experiments, or measurements of atomic parity violation. The predictions from the electroweak theory could be tested to a great precision by means of these observables. And, the nature of the Higgs sector was much more unclear at that

time. It was a challenge to experimentally distinguish between the various proposed models for the mechanism of electroweak symmetry breaking, among which were, for example, also the nowadays excluded Technicolor models. Indirect methods were demanded for comparing the predictions for electroweak precision observables with experimental results. In this context, Peskin and Takeuchi have introduced their three parameters. Nowadays, their formalism is still suitable for testing a large range of new-physics models, and in fact, it provides the most severe tests of the RS model considered in this thesis. In this regard, we now shortly discuss the original derivation of the parameters.

The formalism is grounded on three basic, underlying assumptions that apply to a large range of new-physics models [82]: The first assumption restricts the electroweak gauge group to  $SU(2) \times U(1)$ , and excludes the existence of additional, hypothetical gauge bosons as predicted by some extended models with higher gauge symmetries. The electroweak observables probe the exchanges of electroweak gauge bosons between the light<sup>3</sup> SM fermions, as illustrated in Figure 1.1. The second assumption states that the couplings of new-physics particles to the light SM fermions are suppressed, compared to the couplings to gauge bosons. As a consequence, the “oblique” corrections by vacuum polarizations, which modify the gauge boson propagators in the four-fermion interactions, form the dominant loop corrections, compared to corrections by vertex and box diagrams. The latter scale with the masses of the external, lighter fermions, and it is assumed that  $m_f \rightarrow 0$  as a good approximation. The third assumption states that the intrinsic scale of the new physics, given by the masses of the predicted new particles, is much larger than the masses of the  $W$  and  $Z$  bosons,  $\Lambda_{NP} \gg m_W, m_Z$ . Due to the precise experimental confirmation of the SM in the electroweak energy range, any effects of new physics can only be present at higher energies. In this sense, the Peskin-Takeuchi parameters give a general treatment for radiative corrections induced by vacuum polarizations that are exclusively caused by heavy particles of new physics. The formalism is based on preceding work accomplished by Kennedy and Lynn, who have introduced a general parametrisation for all the radiative corrections to electroweak processes [83, 84]. Peskin and Takeuchi have adapted this former work by applying suitable approximations with regard to the three discussed assumptions.

The matrix elements of the charged and neutral-current interactions, mediated by electroweak gauge bosons, can be formulated in terms of the current notation [82],

$$\begin{aligned} \mathcal{M}_{\text{NC}} &= e^2 Q Q' G_{AA} + \frac{e^2}{s c} [Q(I'_3 - s^2 Q) + (I_3 - s^2 Q)Q'] G_{ZA} + \frac{e^2}{s^2 c^2} (I_3 - s^2 Q)(I'_3 - s^2 Q') G_{ZZ} , \\ \mathcal{M}_{\text{CC}} &= \frac{e^2}{2s^2} I_+ I_- G_{WW} . \end{aligned} \tag{1.46}$$

Here, the functions  $G_{IJ}$  denote the coefficients of the metric tensor  $g^{\mu\nu}$  in the gauge boson propagators, where the remaining terms of the propagators are neglected, according to the assumption  $m_f \rightarrow 0$ . The effects on the propagator coefficients  $G_{IJ}$  of the vacuum-polarization amplitudes  $\Pi_{IJ}$  [82], defined by

$$i g^{\mu\nu} \Pi_{IJ}(q^2) + (q^\mu q^\nu \text{ terms}) \equiv \int d^4x e^{-iqx} \langle J_I^\mu(x) J_J^\nu(0) \rangle , \tag{1.47}$$

---

<sup>3</sup>The top quark was exempted from that consideration, because the lepton collider experiments, at which the electroweak observables were measured, could not produce it directly.

are described by the Dyson equations

$$\begin{aligned} G_{AA} &= D_{AA} + D_{AA} \Pi_{AA} G_{AA} , & G_{ZA} &= D_{ZZ} \Pi_{ZA} G_{AA} , \\ G_{ZZ} &= D_{ZZ} + D_{ZZ} \Pi_{ZZ} G_{ZZ} , & G_{WW} &= D_{WW} + D_{WW} \Pi_{WW} G_{WW} . \end{aligned} \quad (1.48)$$

The Dyson equations can be solved for the propagator coefficients, and by inserting the solutions into the matrix elements in (1.46), the effects of the vacuum polarizations can be included to all orders of magnitude, in principle. Kennedy and Lynn have shown that with a proper redefinition in terms of their “starred” parameters, the matrix elements of the neutral and charged current interactions (1.46) can be re-expressed as [82]

$$\begin{aligned} \mathcal{M}_{\text{NC}} &= e_\star^2 Q \frac{1}{q^2} Q' + \frac{e_\star^2}{s_\star^2 c_\star^2} (I_3 - s_\star^2 Q) \frac{Z_{Z\star}}{q^2 - M_{Z\star}^2} (I'_3 - s_\star^2 Q') , \\ \mathcal{M}_{\text{CC}} &= \frac{e_\star^2}{2s_\star^2} I_+ \frac{Z_{W\star}}{q^2 - M_{W\star}^2} I_- . \end{aligned} \quad (1.49)$$

One recognizes that the forms of these expressions are similar to the forms of the tree-level amplitudes in (1.46), except that all the coupling constants and gauge boson parameters are now replaced by the starred parameters. These starred parameters are the “running”, *i.e.* energy-dependent, couplings  $e_\star^2$ ,  $s_\star^2$ , the “running” masses  $M_{W\star}^2$ ,  $M_{Z\star}^2$ , and “running” wave function renormalization constants  $Z_{W\star}$ ,  $Z_{Z\star}$ , all being functions of the vacuum polarization amplitudes  $\Pi_{IJ}$ . In this sense, the oblique corrections affect the weak-interaction observables only via the starred parameters by Kennedy and Lynn. If restricting on the oblique corrections that are caused solely by heavy new-physics particles, the vacuum polarization functions  $\Pi_{IJ}$  can be expanded around  $q^2 = 0$  of the gauge boson momenta. Neglecting terms of the order of  $q^4$  and higher, one can find [82]

$$\begin{aligned} \Pi_{QQ}^{NP}(q^2) &\approx q^2 \Pi'_{QQ}{}^{NP}(0) , & \Pi_{3Q}^{NP}(q^2) &\approx q^2 \Pi'_{3Q}{}^{NP}(0) , \\ \Pi_{33}^{NP}(q^2) &\approx \Pi_{33}^{NP}(0) + q^2 \Pi'_{33}{}^{NP}(0) , & \Pi_{11}^{NP}(q^2) &\approx \Pi_{11}^{NP}(0) + q^2 \Pi'_{11}{}^{NP}(0) . \end{aligned} \quad (1.50)$$

The first constant terms in the upper two expansions vanish by Ward identities, and then, the expansions depend on 6 parameters, which are  $\Pi'_{QQ}{}^{NP}(0)$ ,  $\Pi'_{3Q}{}^{NP}(0)$ ,  $\Pi_{33}^{NP}(0)$ ,  $\Pi'_{33}{}^{NP}(0)$ ,  $\Pi_{11}^{NP}(0)$ ,  $\Pi'_{11}{}^{NP}(0)$ . Using the expansions for the vacuum polarization amplitudes in the the starred parameters by Kennedy and Lynn, three of the parameters can be fixed by including precisely measured quantities of the weak interaction, like  $\alpha$ ,  $G_F$  and  $\sin \theta_w$ . With the remaining three open parameters, the following three, UV finite, combinations can be determined [82]

$$\begin{aligned} \alpha S &\equiv 4e^2 \left[ \Pi_{33}^{NP}(0) - \Pi'_{3Q}{}^{NP}(0) \right] , \\ \alpha T &\equiv \frac{e^2}{s^2 c^2 m_Z^2} \left[ \Pi_{11}^{NP}(0) - \Pi_{33}^{NP}(0) \right] , \\ \alpha U &\equiv 4e^2 \left[ \Pi'_{11}{}^{NP}(0) - \Pi'_{33}{}^{NP}(0) \right] , \end{aligned} \quad (1.51)$$

where the Peskin-Takeuchi parameters S,T and U are introduced. With these three new weak interaction parameters, the new-physics contributions to processes of the weak interaction can

be parametrized, based on the three assumptions given before. The parameters have different physical significances. The parameter  $S$  is a measure of the total size of the new-physics sector, whereas the parameter  $T$  measures the violation of the custodial iso-spin symmetry induced by the new-physics sector. The parameter  $U$  turns out to be suppressed compared to the first two parameters. As well, the parameter  $U$  is of less significance, because most of the electroweak interaction observables  $x_{\text{expt}}$  depend solely on the parameters  $S$  and  $T$ , according to the linear relation [82]

$$x_{\text{expt}}(S, T) = x_{SM}(m_t, m_h) + a_x S + b_x T . \quad (1.52)$$

In this relation, the first term gives the SM part of the observables, which depends on the Higgs and top quark masses. In this sense, the Peskin-Takeuchi parameters are defined in such a way that for known Higgs boson and top quark masses, they are equal to zero for a pure SM. This allows to test for the existence of new physics by means of experimental results for the parameters, after the Higgs and top quark masses are determined. Experimental results for the various electroweak observables can be displayed in a two-parameter plane in  $S$  and  $T$ , in which each observable is given by a broadened band due to correlated experimental errors. The overlap of different bands has to be determined by a statistical maximum likelihood method, in order to derive the experimental results for  $S$  and  $T$  (and  $U$  in a three parameter analysis) [82]. The current experimental results, determined for these parameters, are [86]

$$\begin{aligned} S_{U_{\text{free}}} &= 0.05 \pm 0.11 , & T_{U_{\text{free}}} &= 0.09 \pm 0.13 , & U &= 0.01 \pm 0.11 , \\ S_{U=0} &= 0.06 \pm 0.09 , & T_{U=0} &= 0.10 \pm 0.07 . \end{aligned} \quad (1.53)$$

They were determined by two different manners, for a floating  $U$  parameter from a three parameter analysis, and with the constraint  $U = 0$ , respectively. One observes that these results are in a good agreement with the SM, whereas, taking into account the large error values, there might still be some space for the existence of new physics, as well.

### Custodial isospin symmetry and the Peskin-Takeuchi parameters

The Higgs Lagrangian of the SM comprises an internal, global symmetry, the custodial symmetry. The Higgs field can be decomposed into 4 real fields  $\phi_i$ ,  $i = 1, \dots, 4$ , and its potential depends on the product  $\Phi^\dagger \Phi$ , and therefore on the square of these four fields [87],

$$\begin{aligned} \mathcal{V}(\Phi^\dagger \Phi) &= \mathcal{V}(\phi_1^2 + \phi_2^2 + \phi_3^2 + \phi_4^2) \\ &\stackrel{\text{ewsb}}{=} \mathcal{V}(\phi_1^2 + \phi_2^2 + \phi_3^2 + h^2 + 2hv + v^2) = \mathcal{V}(\phi^+ \phi^- + \phi^- \phi^+ + \phi_3^2 + h^2 + 2hv + v^2) . \end{aligned} \quad (1.54)$$

This expression is invariant under rotations of the four fields. These rotations can be described by the global symmetry group  $SO(4)$  that is isomorphic to the group product  $SU(2)_L \times SU(2)_R$ , as both fulfil the same Lie algebra. After electroweak symmetry breaking, one of the four fields exhibits a vev, and can be redefined as  $\phi_4 = h+v$ , including the Higgs boson  $h$ . As a consequence, the Higgs potential is invariant under the group  $SO(3)$ , describing rotations of only three scalar fields. The group  $SO(3)$  is isomorphic to the group  $SU(2)_V$ , which is the custodial symmetry, and the diagonal part of the group product  $SU(2)_L \times SU(2)_R$ . The custodial symmetry emerges

also in the parts of the Higgs Lagrangian that couple to the SM particle fields. The easiest example is a Yukawa coupling of the Higgs field to one generation of quark fields, given by

$$\mathcal{L}_{\text{Yuk}} \in y_u Q_L \tilde{\Phi} u_R + y_d Q_L \Phi d_R + \text{h.c.} . \quad (1.55)$$

Assuming that the quarks would have equal masses, so that  $y_u = y_d = y$ , the Yukawa Lagrangian would, in principle, exhibit an invariance under the global symmetry product  $SU(2)_L \times SU(2)_R$ . After electroweak symmetry breaking, the mass terms,

$$\mathcal{L}_{\text{Yuk}} \sim y(\bar{u}_R u_L + \bar{d}_R d_L) + \text{h.c.} , \quad (1.56)$$

remain invariant under the custodial symmetry  $SU(2)_V$  [87]. For that reason, the mass differences between the two fermions in the fermion doublets of the SM cause a violation of the custodial symmetry. This emerges in contributions to the T parameter.

The contributions to the S,T,U parameters that would be induced by a single, new fermion doublet  $(N, E)$  with the masses  $m_N, m_E$  were calculated in the review paper of Peskin and Takeuchi [82]. By evaluating the vacuum-polarization diagram of the new fermion loop created in a virtual gauge boson line, one can find the results [82]

$$S \approx \frac{1}{6\pi} , \quad T \approx \frac{1}{12\pi s^2 c^2} \left( \frac{(\Delta m)^2}{m_Z^2} \right) , \quad U \approx \frac{2}{15\pi} \left( \frac{(\Delta m)^2}{m_N^2} \right) , \quad (1.57)$$

by assuming that  $m_N, m_E \gg m_Z$ , and  $\Delta m \equiv |m_N - m_E| \ll m_N, m_E$ . This result allows to discuss several, significant properties of the S,T, U parameters. One can see that both the parameters T and U scale with the mass difference  $(\Delta m)^2$  of the fermions in the new  $SU(2)$  doublet, but U is suppressed compared to T by a factor  $(m_Z^2/m_N^2)$ . In fact, the parameter U plays a fairly unimportant role. In most models of new physics, it is predicted to vanish, or to have a very small value, at least. All the neutral-current and low-energy observables depend on the parameters S and T only. In contrast, the parameter T is divided through the lighter mass  $m_Z^2$ . The mass splitting  $(\Delta m)^2$  is a measure of the size of the custodial symmetry violation induced by the new fermion doublet. It should be noticed that each extra fermion doublet, putted into the theory, additively contributes to S and T [82]. In this regard, the parameter S is a measure of the total size of the new sector, whereas T is a measure of the total violation of the custodial symmetry that is induced by the new-physics sector [82].

In a more hidden manner, also the mass terms of the gauge bosons of the SM show an invariance under the custodial symmetry [87],

$$\begin{aligned} \mathcal{L}_{\text{Higgs}} \ni D_\mu \langle \Phi \rangle_0 D^\mu \langle \Phi \rangle_0 \in \frac{1}{4} \left[ g^2 [W_\mu^1 W^{\mu 1} + W_\mu^2 W^{\mu 2}] + (g W_{3\mu} - g' B_\mu)^2 \right] \langle \Phi \rangle_0^2 \\ \stackrel{g'=0}{=} \frac{g^2}{4} \langle \Phi \rangle_0^2 [W_{\mu 1} W^{\mu 1} + W_{\mu 2} W^{\mu 2} + W_{\mu 3} W^{\mu 3}] , \end{aligned} \quad (1.58)$$

where  $\langle \Phi \rangle_0^2 = v^2/2$  is the square of the Higgs vev. For  $g' = 0$ , this Lagrangian is invariant under the global custodial symmetry  $SU(2)$ , under which the gauge fields transform as a triplet [87]. One can see that the inclusion of the field  $B_\mu$  breaks the custodial symmetry by the term  $-2gg'W_\mu^3 B^\mu$ . The masses of the W and Z bosons, as given in (1.34), fulfil the ratio at tree level

$$\rho = \frac{m_W^2}{m_Z^2 \cos^2 \theta_w} = 1 . \quad (1.59)$$



Radiative corrections, induced by gauge fields, give small contributions to this ratio, and contribute softly to a violation of the custodial symmetry. The  $\rho$  parameter is linearly correlated with the T parameter, via  $\rho - 1 = \alpha T$  [82]. In this sense, any violation of the custodial symmetry in the Higgs sector results in contributions to the  $\rho$  and T parameters.

## 1.2 Open questions of the Standard Model

The SM of particle physics, relying on the principles of quantum field theory, offers an elaborate theory, which has passed stringent experimental tests. It has proven its ability to give predictions for unexpected phenomena of elementary particle physics that have been confirmed later experimentally. The strong, weak and electromagnetic forces of nature are very successfully described by the model, relying on the group structure  $SU(3) \times SU(2) \times U(1)$ . As stated before, the SM forms an **effective field theory**, which is valid in a specific range of energy up to a certain cut-off  $\Lambda$ . In the hitherto experiments, the electroweak energy range around several hundred  $GeV$  has been explored, which is the energy range where the SM is valid. A quantum field theory with a fundamental energy scale  $M$  can be considered at some energies  $E \ll M$ , and all observable quantities, predicted by the theory, can be expanded in powers of  $E/M$  [88–90]. In general, this expansion can be performed for the whole Lagrangian, as  $\mathcal{L}_\Lambda^{\text{eff}} = \sum_i g_i Q_i$ , which is an infinite sum over all the local operators  $Q_i$ , allowed by the symmetries of the theory, multiplied by coupling constants  $g_i$  that are referred to as Wilson coefficients [88–90]. By a rough analysis of the mass dimensions (for natural units  $\hbar = c = 1$ ), the fundamental action  $S$  of a theory has to be dimensionless. One can write the effective coupling constants  $g_i$  in terms of dimensionless coefficients  $C_i$ , divided by the negative power of the mass dimensions of the fundamental energy scale of the effective couplings,  $-\gamma_i = [g_i]$ , by  $g_i = C_i M^{-\gamma_i}$ . The dimensionless couplings  $C_i$  are assumed to be of order one,  $C_i = \mathcal{O}(1)$ . According to the **naturalness** principle [91–94], only an increase of the symmetries of the theory would legitimate other magnitudes. The most general Lagrangian in four space-time dimensions at an energy scale much below the fundamental scale,  $E \ll \Lambda < M$ , can be written as follows [90]

$$\mathcal{L}_{E \ll \Lambda < M} = \sum_{i=1}^4 \sum_j C_j \Lambda^i Q_j + \sum_k C_k Q_k + \sum_{m=1}^{\infty} \sum_n \frac{C_n}{\Lambda^m} Q_n, \quad (1.60)$$

where  $C_j$ ,  $C_k$  and  $C_n$  are dimensionless coupling constants, whereas  $Q_j$ ,  $Q_k$ ,  $Q_n$  are operators. The first two parts with the operators of mass dimensions  $\leq 4$  give the important contributions, which lead to re-normalizable predictions of the theory. The remaining part with the operators of higher dimensions  $> 4$  gives contributions that are suppressed by powers of the cut-off energy scale  $\Lambda$ . The SM Lagrangian is of mass dimension 4 and forms the middle part of the expansion. This part does not depend on the cut-off energy scale at all. The first term forms the origin of several **hierarchy** problems of the theory, which consist of missing explanations for drastic differences in the magnitudes of theoretical quantities. These hierarchy problems account for the main motivations for new theories beyond the SM. Different choices are sensible for the cut-off energy scale  $\Lambda$ . Since gravity exists undeniably as the forth fundamental force of nature, despite the three forces of the SM, a pure SM would definitely loose its validity at the Planck energy scale  $\Lambda_{\text{Planck}} \sim 10^{19}$  GeV, at which gravity becomes non-negligibly strong in the SM processes.

However, due to several open questions of the SM, and by the spirit of research, one would expect the existence of new physics at energy scales below the Planck scale.

### 1.2.1 Hierarchy problems

It has just been discussed that the different terms in the expanded effective Lagrangian in (1.60) have differing sensitivities on the cut-off energy scale  $\Lambda$ , at which the energy range of validity of a theory is supposed to end. Only the terms of the first part, with the operators of dimension  $< 4$ , come with powers of the cut-off scale, and show a very strong sensitivity on the UV energy range, therefore. For the gauge structure of the SM, only two possibilities are allowed for these terms,

$$\mathcal{L}_{d<4} = C_0\Lambda^4 + C_2\Lambda^2\Phi^\dagger\Phi , \quad (1.61)$$

where  $\Phi$  is the Higgs field. Other terms are not compatible with the demand of gauge invariance. A high cut-off scale as  $\Lambda \sim m_{Pl}$  would cause dramatically high expressions for the terms. We start with a discussion of the second term, which is the most interesting one in our context.

#### The gauge hierarchy problem

The electroweak gauge symmetry of the SM  $SU(2) \times U(1)$  is broken by the vev of the scalar Higgs field. Its magnitude is proportional to the experimentally determined masses of the gauge bosons, as  $m_W \sim v$ ,  $m_Z \sim v$ . From these relations, one would expect that the mass parameter of the Higgs field  $\mu = \sqrt{\lambda}v$  is situated in the energy range of the masses of the electroweak gauge bosons, as well,

$$-\mu^2 \sim -(100 \text{ GeV})^2 . \quad (1.62)$$

The parameter  $\lambda$  of the quartic Higgs self-couplings  $(\Phi^\dagger\Phi)^2$  is naturally predicted to be of order one, because the quartic Higgs self-couplings have a mass dimension 4. However, considering the mass term in the Higgs Lagrangian,  $\mathcal{L} = -\mu^2\Phi^\dagger\Phi$ , and baring in mind the above discussion, one rather finds that

$$-\mu^2 \sim \Lambda^2 , \quad (1.63)$$

since  $\Phi^\dagger\Phi$  is of mass dimension 2. The decomposition in the effective Lagrangian in (1.60) gives thus  $\mathcal{L} = -\mu^2\Phi^\dagger\Phi \equiv C_2\Lambda^2\Phi^\dagger\Phi$ . It has just been discussed that the cut-off  $\Lambda$  can lie in the range of the very high Planck energy scale,  $\Lambda \sim m_{Pl} \sim 10^{19}$  GeV, if considering a pure SM. Then,  $C_2$  is obtained as

$$C_2 \sim \mathcal{O}\left(\frac{\mu^2}{\Lambda^2}\right) \sim \mathcal{O}\left(\frac{10^4}{10^{32-38}}\right) \sim \mathcal{O}(10^{-28..-34}) , \quad (1.64)$$

which is up to 33 orders of magnitude below order one. The definition of *naturalness* puts several demands on the dimensionless coupling  $C_2$ . Following the naturalness criterion by Dirac [91, 92], a natural coupling would just be of  $\mathcal{O}(1)$ . The criterion by t'Hooft is slightly weaker, by claiming that a value  $C_2 \ll 1$  would be allowed only if the limit  $C_2 \rightarrow 0$ , so  $-\mu^2 \rightarrow 0$ , would increase the symmetry of the theory in some way [93]. For example, for vanishing fermion masses, the chiral symmetries and gauge symmetries would be present, explicitly. But, for the case of the Higgs field, there are not any of such symmetry limits that would allow for a very small coupling  $C_2$ . For all these reasons, the theory, in its current incarnation, is considered as highly unnatural, and a strong fine-tuning of  $C_2$  down to a value of  $10^{-28..-34}$  is demanded.

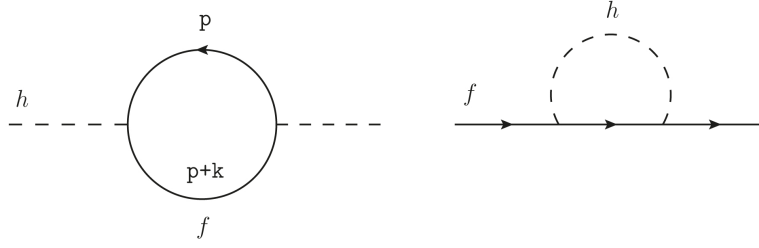


Figure 1.2: Two of the diagrams that form the leading corrections to the bare masses of particles. The bare Higgs mass gets corrected by a fermion (top quark) loop, and the bare fermion mass gets corrected by a loop consisting of a Higgs boson and a fermion line.

This discussion holds for the bare Higgs mass parameter  $\mu$  without encountering loop corrections. In fact,  $\mu^2$  could be much smaller than  $\Lambda^2$ , if the bare scalar mass is of the order  $-\Lambda^2$ , and the value is cancelled to  $-\mu^2$  in a dramatic way by radiative corrections. Nevertheless, a very high amount of parameter tuning would be demanded for such a cancellation, because the one-loop corrections to the Higgs mass diverge strongly. Using the cut-off regularization, where the infinities of loop-integrals are expressed in dependence of a cut-off  $\Lambda_c$ , the amplitude for the vacuum polarization by fermions in the Higgs propagator, as illustrated in Figure 1.2, reads for example

$$\begin{aligned}
 \mathcal{M}_{\delta m_h} &= -i \frac{y_f^2}{2} N_c \int \frac{d^4 p}{(2\pi)^4} \frac{\text{Tr}[(\not{p} + \not{k} + m_f)(\not{p} + m_f)]}{[(p+k)^2 - m_f^2][p^2 - m_f^2]} \\
 &= \frac{y_f^2}{2} N_c \int_0^1 dx \int_0^{\Lambda_c^2} \frac{dp_E^2}{(4\pi)^2} p_E^2 \frac{(-p_E^2 + \Delta_1(x))}{(p_E^2 + \Delta_1(x))^2} \\
 &= \frac{y_f^2}{32\pi^2} N_c \int_0^1 dx \left[ -\Lambda_c^2 + (2\Delta_1(x) + 1) \ln \left( \frac{\Delta_1(x) + \Lambda_c^2}{\Delta_1(x)} \right) + \dots \right],
 \end{aligned} \tag{1.65}$$

where  $y_f$  is the Yukawa coupling,  $N_c$  is the color factor,  $\Lambda_c$  is the cut-off for the momentum integral, and  $\Delta_1(x) = m_f^2 + m_h^2 x(x-1)$ . One can observe that the expression quadratically depends on the cut-off  $\Lambda_c$  in the first term. In this regard, when adding these radiative corrections to the bare Higgs mass, both can quadratically scale with the Planck scale, and one could tune the single contributions in such a way that they exactly cancel to give a result of  $\sim (100 \text{ GeV})^2$ . In this case, one would have to determine parameters over 16 positions in order to achieve the required theoretical description. This is considered as highly unnatural, as well. If, however, the SM would be replaced by some new theory, valid at higher energies, the loops in the Higgs propagator would be quadratically sensitive to the masses of the new particles. On the contrary, the amplitude expression for the vacuum polarization by the Higgs boson in the

fermion propagator, as given in Figure 1.2 on the right-hand side, reads

$$\begin{aligned} \mathcal{M}_{\delta m_f} &= -i \frac{y_f^2}{2} \int \frac{d^4 p}{(2\pi)^4} \frac{\text{Tr}[(\not{p} + \not{k} + m_f)]}{[(p+k)^2 - m_f^2][p^2 - m_h^2]} = \frac{y_f^2}{2} m_f \int_0^1 dx \int_0^{\Lambda_c^2} \frac{dp_E^2}{(4\pi)^2} \frac{p_E^2}{(p_E^2 + \Delta_2(x))^2} \\ &= \frac{y_f^2}{32\pi^2} m_f \int_0^1 dx \ln \left( \frac{\Delta_2(x) + \Lambda_c^2}{\Delta_2(x)} \right) + \dots, \end{aligned} \quad (1.66)$$

where  $\Delta_2(x) = m_h^2(1-x) + m_f^2 x^2$ . One observes that the expression only logarithmically depends on  $\Lambda_c$ , and includes the bare fermion mass  $m_f$ , compared to the corrections to the Higgs propagator. The dependence on  $\Lambda_c$  can be absorbed by a redefinition of the physical fermion mass, and the chiral and gauge symmetries allow for a small, bare fermion mass,  $m_f = y_f v / \sqrt{2}$ . In that way, fine-tuning problems are prevented, in contrast to the Higgs case. This is similarly true for the gauge boson masses. In this sense, the Higgs field seems to play a peculiar role in the SM. Whereas successfully describing the masses of the other particles in the electroweak energy range, it exhibits a strong sensitivity on the UV energy range, as well. The aforementioned points are referred to as the gauge hierarchy problem. After the experimental confirmation of the Higgs boson at the LHC in 2012 in the expected electroweak energy range [67, 68], the gauge hierarchy problem seems to be more pressing than ever.

In this connection, one can also ask about the origin of the huge hierarchy between the electroweak energy scale and the Planck scale of gravity, as

$$\mu^2 = \lambda v^2 = \lambda 4 \frac{m_W^2}{g^2} \sim 10^4 \text{ GeV}^2 \ll \frac{1}{G_{\text{grav}}} \sim M_{Pl}^2 \sim 10^{38} \text{ GeV}^2 ? \quad (1.67)$$

Why are the magnitudes of the strengths of the three SM forces and the gravitational force so much different? The gauge hierarchy problem does not query the consistency of the electroweak theory itself, but it certainly reinforces the question whether new physics could be situated at energies much below the Planck scale. Solutions to the gauge hierarchy problem demand for new theories at energies of several TeV, in order to avoid the fine-tuning problems in the calculation of the Higgs mass.

Furthermore, there are also terms in the expanded Lagrangian in (1.60) that are divided by the cut-off scale to certain powers, with operators of higher mass dimensions, which show a suppressed relation to the UV energy range. Gauge and Lorentz invariance restrain the operators of mass dimension 5, made up of SM fields, to one single term that generates a non-zero Majorana neutrino mass, which violates the lepton number, however [90]. On the contrary, there are many allowed terms made up of dimension 6 operators, which can be tested by precision measurements, excluding a cut-off scale up to  $\Lambda \sim 1 - 10 \text{ TeV}$  [90, 95]. But, slightly above that scale, new physics could be situated, in fact. Based on this motivation, most theories of new physics predict phenomena in this energy range little above the SM. In fact, the LHC experiments at the CERN have been executed to explore this interesting energy area.

### The flavour puzzle

The fermion masses are generated by the Yukawa couplings, which have a natural magnitude of order 1, times the Higgs vev, and a factor of  $\sqrt{2}$ . Even with a detailed experimental confirmation

of the SM, it remains mysterious why the experimentally determined spectrum of quark and lepton masses covers 5 orders of magnitude. From the electron mass at  $\sim 0.5$  MeV to the top quark mass at  $\sim 175$  GeV, the Yukawa couplings show hierarchies up to

$$\frac{m_e}{m_t} \sim \frac{y_e}{y_t} \sim 10^{-6} ! \quad (1.68)$$

Currently, no symmetries or mechanisms are present to explain such hierarchies. Apparently, the gauge forces of the SM do not distinguish between fermions that belong to different generations, because these have the same quantum numbers.

Moreover, it is worth to question why there exist these three generations of quarks and leptons, and what gives rise to the electroweak flavour changing interactions, mediated by a charged W boson and parametrized by the CKM-matrix. Using the parameter  $\lambda \approx 0.23$  of the Wolfenstein parametrization, the hierarchical pattern of the CKM mixing matrix behaves in good approximation as

$$V_{\text{CKM}} \sim \begin{pmatrix} 1 & \lambda & \lambda^3 \\ \lambda & 1 & \lambda^2 \\ \lambda^3 & \lambda^2 & 1 \end{pmatrix} . \quad (1.69)$$

Whereas the mixing between the same generation of quarks is always the largest, and nearly of  $\mathcal{O}(1)$ , the mixing between the first two generations is of the order  $\mathcal{O}(\lambda)$ , and the mixing between the second and third generation is of the order  $\mathcal{O}(\lambda^2)$ . The smallest mixing occurs over two generations, which is of the order  $\mathcal{O}(\lambda^3)$ . The origin of this interesting pattern is not described within the SM. Moreover, flavour changing interactions, mediated by the neutral Z boson, are completely forbidden at tree level in the SM, and suppressed by a partial interference at higher orders, which is called the GIM mechanism [56]. Whereas the leptons of different flavours cannot mix with each other, a neutrino oscillation has been confirmed experimentally [69, 70]. This mixing is described by the PMNS-Matrix [96, 97].

These questions in the fermion sector are part of the still unresolved mysteries of the SM, and demand for explanations.

### The cosmological constant problem

The largest impact of a high cut-off scale,  $\Lambda \sim m_{Pl}$ , is given by the first term in the effective Lagrangian in (1.61),

$$C_0 \Lambda^4 \sim C_0 10^{64 \dots 76} \text{ GeV}^4 , \quad (1.70)$$

which causes the most dramatic hierarchy problem of the theory. The term does not contain any operators, and it effectively describes a shift by  $\Lambda^4$  in the vacuum energy density. This shift is unobservable in particle physics experiments, because theoretical predictions are always related to energy differences between the vacuum and certain excited states, where the absolute vacuum energy density cancels out [79]. But, a vacuum energy gravitationally couples according to the gravitational field theory, where it is part of a source term that predicts the gravitational field. Einstein predicted this source to be the cosmological constant [15], which affects the expansion rate of the universe after the Friedman-le-Maitre model [98]. In fact, an accelerated expansion rate has experimentally been measured via the red-shift of emitted spectral lines in the light from distant galaxies, and the dilation in the light decay of supernova luminosity curves [72, 73].

By means of these observations, a very tiny upper bound on the cosmological constant follows, as [79]

$$\Lambda^4 < 10^{-29} \frac{\text{g}}{\text{cm}^3} \sim (10^{-11} \text{ GeV})^4 \sim 10^{-44} (\text{GeV})^4 . \quad (1.71)$$

With a natural coupling for  $C_0$  of a size  $\mathcal{O}(1)$ , this term lies about 120 magnitudes below the value that is obtained for a Planck-sized cut-off scale, given in 1.70! The impression manifests itself that the SM cannot be the last theoretical statement, and especially in its connection to gravity there is a huge, remaining lack of explanation.

Following the experimentally confirmed accelerated expansion rate of the universe, it is commonly concluded that some kind of dark energy has to cause for a non-vanishing but small cosmological constant, given in (1.71). This dark energy is included in the  $\Lambda$ -CDM model, mentioned before, having an amount of 68.3% of the total energy in the present-day observable universe [74,75]. The nature of the hypothetical dark energy is unknown and subject to current theoretical studies. Some proposals implement new scalar fields in the universe, which also give contributions to the cosmological constant, and by combining those with the vacuum energy derived from quantum field theory, one can reproduce the measured value in (1.71).

Also, there are modified theories of gravity that can explain a **degravitation** of the vacuum energy density if considering cosmological distances [99–103]. In these approaches, Newton's constant  $G$  is promoted to a covariant differential operator,

$$G_\Lambda(\square_g) = \mathcal{G}(\square_g)\mathcal{F}(\square_g) , \quad (1.72)$$

which is acting on the energy-momentum tensor that describes the vacuum energy,

$$G_\Lambda(\square)\langle T_{\alpha\beta}\rangle_v = \mathcal{G}(\kappa/\lambda_c^2)\mathcal{F}(\Lambda/\lambda_c^2)\langle T_{\alpha\beta}\rangle_v , \quad (1.73)$$

where  $\mathcal{G}(\kappa/\lambda_c^2) = \frac{G}{1-\sigma e^{-\kappa/\lambda_c^2}}$ , and  $\mathcal{F}(\Lambda/\lambda_c^2) = \frac{\Lambda/\lambda_c^2}{1+\Lambda/\lambda_c^2}$ . Describing an essentially flat universe, according to cosmological observations, one can follow the assumptions that the vacuum energy can be modelled on macroscopic scales by an almost time-independent, Lorentz-invariant, energy process, as  $\langle T_{\alpha\beta}\rangle_v \simeq T_v \cos(\mathbf{k}_c \cdot \mathbf{x})\eta_{\alpha\beta}$ . Here,  $T_v$  is the average density of the vacuum energy, and  $\mathbf{k}_c = 1/\lambda_c$  is the three-dimensional characteristic wave-vector, with  $k_x = k_y = k_z \sim 1/\lambda_c$ , and  $|\lambda_c| \gg 1$ , due to the homogeneous distribution of the vacuum energy throughout the whole universe. The parameter  $\sqrt{\Lambda} \sim 10^{30}$  m gives the scale where the de-gravitation process sets in, and it is assumed that  $|\sigma| < 1$ , and  $\sqrt{\kappa} \ll \sqrt{\Lambda}$ , to perform a formal series-expansion of  $\mathcal{G}_\kappa$ , for more details see [103]. In this scenario, the differential operator  $G_\Lambda(\square)$  applies instead of Newton's constant for small characteristic wavelengths, whereas for energy processes with a characteristic wavelength much larger than the macroscopic filter scale,  $\lambda_c \gg \sqrt{\Lambda}$ , a strong de-gravitational effect occurs, according to

$$\lim_{\lambda_c \rightarrow +\infty} G_\Lambda(\square)\langle T_{\alpha\beta}\rangle_v = 0 . \quad (1.74)$$

For that reason, the vacuum energy density with a wavelength as large as the visible universe,  $\lambda_c \sim 10^{29}$  m, effectively decouples from the gravitational field. This scenario allows to reproduce the observed accelerated expansion rate of the universe, with the high value for the vacuum energy as predicted by the quantum field theory. In this scenario, the implications for the orbital dynamics of a binary-system and generic n-body systems can be computed by using

post-Newtonian perturbation methods [102, 103]. In this way, the dominant corrections to the general relativistic results can be derived for the predictions of gravitational wave emissions. This could provide intriguing possibilities to test for modified gravity in the context of future measurements of gravitational waves.

## 1.2.2 Further questions

### Unification of the Standard Model's forces and gravity

Theories of new physics have to consider the region of higher energies above the electroweak energy scale. Despite the Planck energy scale at which gravity becomes strong, there are further suggestions for the scale at which new physics could emerge naturally. The electroweak theory provides a unified description of the weak and the electromagnetic forces, and in this sense, it is obvious to ask whether the complete group structure of the SM with the three gauge groups  $SU(3) \times SU(2) \times U(1)$  could actually be described in a unified manner by a single larger symmetry group. The simplest choice for such a larger symmetry group is the group  $SU(5)$  [104], and in this scenario, the couplings  $g_s$ ,  $g$ , and  $g'$  of the SM are connected to the unified coupling  $g_5$  by [79, 105]

$$g_5 = g_3 = g = \sqrt{\frac{5}{3}}g' . \quad (1.75)$$

Within this framework, one can extrapolate the values of the three couplings of the SM forces from the energy scale  $m_Z$  upwards. They come close together at very high energies, around  $\sim 10^{16}$  GeV, though they do not actually meet. Nevertheless, it is remarkable that this energy scale lies already close to the scale where the gravitational attraction of elementary particles becomes comparable to the strengths of their strong, weak and electromagnetic interactions. Maybe, it might be reasonable to hope that the unification of the SM forces is in some way related to a unification of gravity with the three SM forces. However, the minimal unified model with a  $SU(5)$  gauge symmetry, as well as further more extended models, are nowadays excluded, because a proton decay is predicted by these models [106, 107].

Before, it has also been discussed that the naive unification of the principles of quantum field theory, predicting a high value for the vacuum energy, and gravity, describing the expansion rate of the universe with a cosmological constant, leads to the tremendous cosmological constant problem, and to the question about the origin of the dark energy, accounting for the observed accelerated expansion rate of the universe. Moreover, after the successful quantization of the electromagnetic force in connection with the other two microscopic forces of the SM, it has not yet been possible to find a quantized description of the gravitational force for their microscopic interactions. For sure, it is understood that the unification of quantum field theory and gravity cannot be implemented in a straightforward way, and important concepts have still been missing from the current understanding [79]. In this context, another mystery in the relation of elementary particle physics and gravity is the dark matter problem.

### Dark matter

Many astrophysical observations of the cohesion and dynamics of galaxies, and models of the structure formation process of the universe provide indications of invisible gravitational sources.

In spiral galaxies, for example, observations indicate that the rotation velocities of the outer stars remain constant, rather than declining for longer distances away from the centre (e.g. [108]). This could be explained by the existence of a big halo of dark matter around the spiral galaxies, including ten times more matter than the visible matter localized in the centre. A further example is the detection of the “bullet-cluster”, which is the name for two crossing galaxies that consist of stars and gas matter. Using the effect of gravitational lensing, one can determine the mass centres of the two crossing galaxies, and against the expectations, the galaxies seem to cross nearly without collisions. The mass centres are lying in the two centres of the shining stars, rather than in the gas dragging behind, due to its electromagnetic interaction, where one would expect the mass centres for the visible matter to be situated. On the contrary, by assuming high densities of dark matter particles in the galaxies that interact only very weak and by gravitation, one can draw the conclusion that the mass centres are lying in the crowds of the stars, because dark matter clouds can cross nearly without collisions, as observed (e.g. [109, 110]). Moreover, observations of the cohesions in galaxy clusters have shown that the velocity dispersions of the stars, following the virial theorem, indicate a much higher mass emergence than what is observed by the visible matter [111]. Furthermore, the modelling of the structure formation process of the universe after the Big Bang between nucleosynthesis and late matter abundances needs kind of matter that cannot interact with radiation, as the visible matter does. The observed cosmic microwave background gives a relic radiation map of times very shortly after the Big Bang. It shows a remarkable homogeneous black-body radiation spectrum with a temperature of 2.726 K, and temperature anisotropies of millionths degrees [112]. Following this map, one concludes that, at very early times of the universe, the dominant element was radiation, and growing density perturbations have led to the corned structure of the present day universe consisting of galaxies and clusters. Without the inclusion of dark matter, the structure formation process could not have happened, according to simulations (e.g. [113]), because ordinary matter is affected by radiation, and density perturbations would have washed out. Instead, dark matter is needed for having formed the potential wells for the ordinary matter to built structures. Moreover, there is an intriguing connection in this context, the weakly interacting massive particle (WIMP)-miracle: Considering the synthesis of the early, expanding universe, particle creation and annihilation processes must have happened, until approaching a thermal equilibrium state with a constant particle number density, due to a large expansion rate of the universe. Including dark matter particles with a self-annihilation cross section in the range of what is expected for particles that interact weakly, with masses of  $\sim$  GeV - TeV, one determines a present-day dark matter fraction of  $\sim$  25%, coinciding with the expected amount of dark matter that follows from other observations [74, 75]! This remarkable connection indicates that dark matter could plausibly consist of stable, weakly interacting, massive particles, the so called WIMP-particles. Many new-physics theories predict dark matter candidates with the necessary properties and masses, like supersymmetry with the lightest super-symmetric particle, solutions of the strong CP problem of the SM with the axions, and extradimensional models with a KK parity that include a lightest, stable KK particle.

In this regard, many experimental efforts have been made for detecting any dark matter particles. For example, experiments have been searching for the recoil of dark matter particles at nucleons (e.g. [114]), or in particle collisions where dark matter particles could possibly be produced out of SM particles (e.g. [115, 116]). Due to the very weak interaction properties, dark matter particles could only be indirectly detected in the detectors via missing transverse



momentum in the collision plane. Until now, all the measurements confirm the SM and lack any signals of dark matter. So, the simplest dark matter hypotheses may not form the correct answers. More involved models with an elaborated, complete dark sector, which consists of several dark matter particles and dark forces mediated between the dark matter particles, are currently under investigation [116,117]. Last but not least, one should mention that it is commonly accepted to explore new theories beyond the SM, whereas the dark matter conclusions usually assume a one hundred percent validity of Einstein's theory of general relativity. The  $\Lambda$ -CDM model parametrizes the Big Bang cosmological model basing on the input assumption of existing dark matter and dark energy, and it has been argued that, in this way, it might be rendered non-falsifiable. Attempts with modifications of the general relativity might also explain the dark matter problem. Apparently, all the effects of dark matter appear by their gravitational interactions, therefore allowing for solutions that assume deviations from the general relativity on cosmological scales.

The dark matter problem is certainly one of the most pressing open questions of modern basic researches, no matter in which physical field the correct answer is hidden.

### 1.2.3 Theories of new physics

#### Supersymmetry

It has been discussed that several open questions of the SM ask for theoretical extensions and new-physics phenomena at energies as low as several TeV. In this regard, the most popular extension is given by the theory of supersymmetry (SUSY), offering a consistent framework for calculations, in which the low energy SM predictions are safely reproduced. Early work in this context was accomplished, *e.g.* by [118–124]. In the SUSY framework, the Poincaré symmetry group of space-time, consisting of the momentum generators  $P^\mu$  of the translations, and the generators  $M^{\mu\nu}$  of rotations and velocity transformations, generated by the angular momentum  $\mathbf{J}$  and the boosts  $\mathbf{K}$ , is extended by the SUSY transformations, which are generated by the supercharges  $Q_\alpha^A, \bar{Q}_\beta^B$ . These 2-dimensional representations of the Poincaré group are spinors carrying a spin 1/2. In principle, one could consider a higher number of such sets with  $A, B = 1, 2, \dots, N$ . The generators of the SUSY transformations obey respective commutation relations with the generators of the Poincaré symmetry group of space-time [125],

$$[Q_\alpha, P^\mu] = 0, \quad [Q_\alpha, M^{\mu\nu}] = (\sigma^{\mu\nu})_\alpha^\beta Q_\beta, \quad \{Q_\alpha, \bar{Q}_\beta\} = 2P_\mu \sigma_{\alpha\beta}^\mu. \quad (1.76)$$

Therefore, the induced SUSY transformations have to be considered as part of the space-time transformations. In fact, one can show that the result of two SUSY transformations corresponds to a space-time translation. Moreover, the generators  $Q_\alpha$  convert bosonic states into fermionic states, and vice versa. An  $N = 1$  set of SUSY employs two collections of fields, the chiral supermultiplets consisting of one left-handed Weyl spinor and one complex scalar, and the gauge supermultiplets containing the gauge bosons and their spin 1/2 SUSY partner fields [126,127]. The fields and their partner fields are connected by the SUSY transformations. Since the generators of all the internal symmetries (gauge symmetries etc.) commute with  $P^\mu, M^{\mu\nu}$  and  $Q_\alpha$ , the SUSY transformations do not change internal charges, and super-partners have to be charged equally. Moreover, an additional internal symmetry can be implemented, the  $R$ -symmetry, which predicts a conserved supercharge. The SUSY-particles and their partner fields are oppositely

charged under that supercharge. The supercharge has to be conserved in the decay of SUSY-particles, which predicts a decay chain that ends up in the production of a lightest SUSY-particle that cannot decay further. If this lightest SUSY-particle is predicted to be electrically and color neutral, it offers an appealing candidate for a dark matter particle. For that reason, the SUSY theories with a realized  $R$ -symmetry naturally predict the existence of particles that behave like dark matter. Furthermore, the  $R$ -symmetry demands that the number of fermions has to equal the number of bosons, and that the particles within one SUSY multiplet must have equal masses.

When implementing the SM particles into the simplest set of SUSY, the quarks and leptons are chosen as the fermionic components of the chiral supermultiplets. In this way, the squarks and sleptons are added to the SM, as spin zero super-partners [10, 125, 128]. The gauge bosons are part of the gauge super-multiplets, which include the gluinos, the winos and the bino as new spinor super-partners to the theory. In addition, it is necessary to have two scalar Higgs bosons in order to reproduce the Yukawa interactions of the SM. In this case, the Higgsinos are the super-partners, which form a vector-like pair of spinor doublets. A lightest SUSY particle can be realized by a mixture of the Higgsino, sneutrino, and the zino and photino, the partners of the Z boson and the photon after electroweak symmetry breaking.

In fact, a theory that predicts gauge boson and fermion particles with equal masses is in contradiction to all experimental paradigms, and for that reason, the SUSY cannot be implemented as an exact symmetry of nature. Nevertheless, it might be broken spontaneously, which would allow for small differences between the masses of the observed SM particles and their super-partners. By including a mechanism that can describe, in some way, a slight breaking of SUSY, tremendously interesting results can be derived. In a unified theory for the strong and the electroweak interactions of the SM along with SUSY, one can find that the renormalization of the coupling constants is improved in such a way that the three couplings meet with an impressive accuracy at an energy scale close to  $10^{16}$  GeV [79]. In addition, the cosmological constant problem can be softened in such a theory to a discrepancy of 50 orders of magnitude between the determined and predicted size of the vacuum energy (in comparison to 120 orders in a pure SM). And, moreover, the gauge hierarchy problem can be solved in a SUSY theory, because, in every order of perturbation theory, the loop diagrams involving the super-partner fields cancel out the diagrams of the SM counterparts with the slightly differing masses. For example, in addition to the diagram of the top-quark loop correction to the Higgs mass, given in Figure 1.2, one would encounter a similar diagram where sfermions are exchanged, which implies a quadratic divergence similar to that in the formula (1.65). Adding the two amplitudes together, the Higgs mass correction in this scenario would depend on

$$\mathcal{M}_{\delta m_h} \sim [-y_f^2 + y_s^2] \Lambda_{\mathbf{c}}^2 + \dots, \quad (1.77)$$

with  $y_s$  as the Yukawa couplings of the sfermions. For small enough mass differences between the observed quarks and leptons and their scalar super-partners, one can predict a physical Higgs mass of the correct size. If such postulates were true, the scalar super-partners of the SM quarks and leptons should be light enough to be experimentally discovered at present collider experiments. Certainly, this was one of the main motivations for the construction of the LHC experiments.

## Composite Higgs models

A second class of promising new theories for the gauge hierarchy problem assume the Higgs boson to emerge as a bound state of a strongly interacting sector, rather than being an elementary field. In these frameworks, new, asymptotically free gauge interactions become strongly coupled at a scale  $\Lambda \sim \text{few TeV}$ . This scale is dynamically generated by **dimensional transmutation**. Above that scale, no elementary scalars exist, and in that way no hierarchy problem either. In its original form, the so-called **technicolor** theories (e.g. [129, 130]) predict heavy resonances that result from the strongly coupled sector. Unfortunately, the predicted Higgs boson is much heavier than the measured one, and furthermore, the electroweak precision tests of the  $S$  parameter exclude a wide range of these models [82].

Nevertheless, if assuming the Higgs boson to be a pseudo NG boson of the enlarged global symmetry group  $\mathcal{G}$ , these problems can be mitigated [51, 52, 131, 132]. Then, the approximate global symmetry group  $\mathcal{G}$  is broken down to  $\mathcal{H}$  by new, strong gauge interactions. A bare Higgs mass term causing the fine-tuning problem in the SM is forbidden by some symmetry, and the Higgs potential is solely generated by radiative corrections, according to the Coleman-Weinberg formalism [133]. This formalism states that, without a bare Higgs mass term, the physical Higgs mass is generated through radiative corrections, however, resulting in a Higgs potential with a non-vanishing vacuum expectation value. In this scenario, the strong constraints from electroweak precision tests can be avoided. The mass of the composite Higgs boson is not sensitive to virtual effects above the composite scale, similar to the mass of the pion in QCD, which is UV stable whereas being a composite state.

For example, a minimal realization of such a model considers a global symmetry group  $\mathcal{G} = SO(5) \times U(1)_X$ , which is spontaneously broken down to  $\mathcal{H}_1 = SO(4) \times U(1)_X$  at the scale  $f$  [134]. The group  $SO(4)$  is isomorphic to  $SU(2)_L \times SU(2)_R$ , which means that both fulfil the same Lie algebra. The electroweak gauge group of the SM  $SU(2)_L \times U(1)_Y$  can be embedded into the group structure  $SU(2)_L \times SU(2)_R \times U(1)_X$ , and the coset  $SO(5)/SO(4)$  implies  $4 = \dim(\mathcal{G}) - \dim(\mathcal{H}_1)$  real NG bosons forming a complex doublet  $H$  under  $SU(2)_L$ , the composite Higgs boson.

In a more extended framework, one can consider the dynamical symmetry breaking  $\mathcal{G} \rightarrow \mathcal{H}_1$  at the scale  $f$ , and the subgroup  $\mathcal{H}_0 \in \mathcal{G}$  is gauged by external vector bosons. This symmetry breaking implies  $n = \dim(\mathcal{G}) - \dim(\mathcal{H}_1)$  Goldstone bosons, and  $n_0 = \dim(\mathcal{H}_0) - \dim(\mathcal{H})$  of the Goldstone bosons can be absorbed to give a mass for the vector bosons of  $\mathcal{H}_0$  [134, 135]. The unbroken gauge group is  $\mathcal{H} = \mathcal{H}_1 \cap \mathcal{H}_0$ , and the remaining  $n - n_0$  pseudo NG bosons include the Higgs doublet. The SM gauge group  $G_{SM}$  is embedded into the unbroken subgroup  $\mathcal{H}_1$ , and is unbroken at tree level. The SM fields are elementary fields, and are external to the strong sector. Their couplings to the strong sector break the global symmetry  $\mathcal{G}$  explicitly.

The Higgs potential vanishes at the tree level as a consequence of the Goldstone symmetry. The effective Higgs potential is generated at the one-loop order, by exchanges of virtual SM fields, which can break the electroweak symmetry. In this connection, the electroweak scale  $v$  is determined dynamically, and can be smaller than  $f$ . The mass scale of the resonances of the strong sector is given by  $m_\rho \sim g_\rho f$ , with  $1 \lesssim g_\rho \lesssim 4\pi$ . The strong dynamics can be integrated out, and their effects can be parametrized by form factors. The Higgs mass is generated at the one loop order  $m_h \sim g_{SM} v$ , with  $g_{SM} \lesssim 1$ , as a generic SM coupling. In the limit  $\xi = (v/f)^2 \rightarrow 0$ , where  $f \rightarrow \infty$ , the Higgs boson would thus stay light, and all other resonances would become

infinitely heavy [134].

After having mentioned two of the most popular versions of new physics, SUSY and composite Higgs models, the next chapter introduces a third class of promising new theories that include a very small, extra spatial dimension to the SM. The RS model, in particular, as one of these new theories forms the framework for the subsequent parts of the thesis.

# Chapter 2

## The Randall-Sundrum Model

### 2.1 Theories of extra dimensions

Our perception as well as all physical researches indicate that three spatial dimensions and one time dimension exist. Nevertheless, the mathematical use of very small and indiscernible extra dimensions provides a fruitful tool for theoretical approaches in physics. Extradimensional theories were elaborated already 100 years ago, at times at which only two of the four fundamental forces of nature were known, the electromagnetism and gravity. G. Nordström introduced a fourth spatial dimension in his attempt to unify the theory of electromagnetism with his scalar theory of gravity, at times before Einstein's theory of relativity had been published, or much less confirmed. Nordström considered a five-dimensional vector field, in which he combined the electromagnetic vector field with his new scalar gravitational potential. In this way, the electromagnetic field and the hypothetical scalar field of gravity could be understood as unified into one single field. In this regard, our four dimensional space-time was considered as a surface of a higher five-dimensional space-time. Nordström detected that the five-dimensional field equations of his framework could be separated into the electromagnetic field equations, the Maxwell's equations, and the equations of his new, proposed gravitational field [136]. Shortly afterwards, T. Kaluza followed these ideas, and published a unified description for the theory of electromagnetism and Einstein's theory of general relativity [137]. He introduced a five-dimensional metric tensor, in which he included the four-dimensional metric tensor of our space-time, the electromagnetic vector potential and an other scalar field. Furthermore, he used the "cylinder condition", claiming that not any component of the five-dimensional metric tensor should depend on the extra-dimensional coordinate. The shortcomings of Nordström's and Kaluza's theories were that both of them could not provide any mechanism to hide the extra dimension, or to explain the origin of the "cylinder condition". Finally, several years later O. Klein explained how an extra spatial dimension can be escaped of detection and perception [138]. He proposed that an extra dimension could have a "compactified" behaviour, being of a limited length but periodically recurring, similar to a two-dimensional surface that is coiled up to a cylinder, as illustrated in Figure 2.1. When watching the surface from a distance far away, the second dimension can not be perceived any longer, and the surface rather appears like a one-dimensional line. For radii just small enough, compactified extra dimensions could exist but would escape from detections, in principle. This plausible compactification mechanism for extra dimensions from the KK theory has been used in numerous subsequent theories, *e.g.* in the String theory,

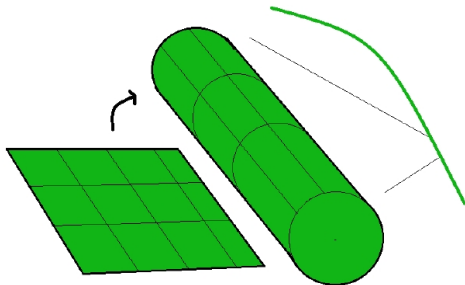


Figure 2.1: Sketch of the idea of a compactified extra dimension. It appears like coiled up on a small radius, and from a distance far away it cannot be perceived any longer, similar to the two dimensional surface of a cylinder coiled up to an apparently one dimensional line.

or the RS model.

### 2.1.1 Large extra dimensions

In the year 1998, a framework was published by N. Arkani-Hamed, S. Dimopoulos and G. Dvali [139] that uses multiple and in principle larger compactified extra spatial dimensions to find a solution to the gauge hierarchy problem, and to explain the weakness of gravity in relation to the other forces of nature. In this Arkani-Hamed-Dimopoulos-Dvali (ADD) model, it is declared that gravity is the only fundamental force of nature that can mediate through the higher-dimensional space-time, the bulk. The other forces, and all the elementary particle fields, are assumed to reside on a four-dimensional subspace, a brane. In this regard, the fundamental, higher dimensional Planck mass  $m_{Pl(4+n)}$ , defining the higher-dimensional gravity constant, forms the fundamental energy scale of the theory. In principle, it can lie as low as the energy range of the SM, around several TeV, which is much below the usual, effective, four-dimensional Planck mass  $m_{Pl} \sim 10^{19}$  GeV. In this way, a gauge hierarchy problem is avoided, and the apparent weakness of gravity can be explained, as only the effective, four-dimensional behaviour of gravity appears weak compared to the other SM forces. The strength of gravity depends on the length distance between two points at which it is measured. For distances  $r \ll R$ , where  $R$  is the compactification radius of the extra dimensions, a sizeable deviation from the known gravity potential is predicted [139],

$$V(r) \sim \frac{m_1 m_2}{M_{Pl(4+n)}^{n+2}} \cdot \frac{1}{r^{n+1}}, \quad (r \ll R), \quad (2.1)$$

as gravity can mediate through the whole extra-dimensional bulk. However, for distances much larger than the extra-dimensional radii  $r \gg R$ , the extra-dimensions cannot be perceived, and the gravitational potential follows the usual  $1/r$ -behaviour in the four space-time dimensions [139],

$$V(r) \sim \frac{m_1 m_2}{M_{Pl(4+n)}^{n+2} R^n} \cdot \frac{1}{r}, \quad (r \gg R). \quad (2.2)$$

n	1	2	3	4	5	6	7
$R$ [cm]	$10^{13}$	$10^{-2}$	$10^{-7}$	$10^{-9.5}$	$10^{-11}$	$10^{-12}$	$10^{-12.71}$

Table 2.1: Sizes of the extra dimensional radii in dependence of the number  $n$  of extra dimensions, as predicted by the ADD model with the formula (2.4), for a higher-dimensional Planck mass of  $m_{Pl(4+n)} \sim 1$  TeV.

By comparing the last equation with Newton's gravitational potential, a relation between the higher dimensional Planck mass  $m_{Pl(4+n)}$  and the four-dimensional Planck mass  $m_{Pl}$  follows

$$M_{Pl}^2 \sim M_{Pl(4+n)}^{2+n} R^n . \quad (2.3)$$

From the four-dimensional point of view, gravity seems to be diluted compared to the three SM forces, and this is connected to the fact that the SM forces cannot propagate through the extra dimensions, compared to gravity. Yet, their strengths should be of comparable sizes, if looking at the higher-dimensional behaviours. The higher-dimensional Planck mass  $m_{Pl(4+n)}$  may lie close to the electroweak energy range, whereas from the effective four-dimensional point of view, the four-dimensional Planck mass  $m_{Pl}$  has the known high value of  $\sim 10^{19}$  GeV. The last formula can be used to determine the sizes of the extra-dimensional radii in dependence of the number  $n$  of extra dimensions and the higher dimensional Planck mass  $m_{Pl(4+n)} \sim m_{EW}$ , as predicted by the model,

$$R \sim 10^{\frac{30}{n}-17} \text{cm} \times \left( \frac{1 \text{ TeV}}{m_{EW}} \right)^{1+\frac{2}{n}} . \quad (2.4)$$

In Table 2.1, the sizes of the extra dimensional radii, obtained from formula (2.4), for a higher dimensional Planck mass of  $m_{Pl(4+n)} \sim m_{EW} \sim 1$  TeV are listed, in dependence of the number  $n$  of extra dimensions.

Clearly, the existence of only one large extra dimension  $n = 1$  is empirically excluded. This case would imply a radius for the extra dimension as  $R \sim 10^{13}$  cm, which is about the size of the solar system, and would imply deviations from the known gravity law over distances of such a size. But, the existence of  $n \geq 2$  extra dimensions implies radii as  $R < 0.1$  mm, and these cases might, in fact, be of interest, as measurements of the gravity law over small distances are searching around this scale for deviations from the  $1/r$  behaviour. From the observations, the case of  $n = 2$  extra dimensions can be excluded for radii down to  $R > 44 \mu\text{m}$  to 95% confidence level (CL), implying a lower bound on the higher dimensional Planck mass as  $m_{Pl(4+n)} > 1.9$  TeV [140]. Also, the existence of extra dimensions could cause signals of missing energy in collider experiments, where hypothetical force-mediating particles of gravity, which couple to the SM particles, could escape into the bulk and carry away energy [139, 141]. Intriguingly, extra dimensions could also enable direct productions of micro black holes at the LHC [142]. But, the strongest constraints result from astrophysical measurements, as for example from measurements of the heat of Neutron Stars. The heat would be increased for existing extra dimensions, because additional decays of the hypothetical gravity force-mediating particles would contribute to the heat energy. The case of  $n = 2$  extra dimensions is excluded up to a Planck

mass of  $m_{Pl(4+n)} < 1700$  TeV, and one can only reach  $m_{Pl(4+n)} \sim \text{TeV}$  for a number  $n \geq 4$  of extra dimensions [143].

Possible shortcomings of the ADD model are that, whereas solving the gauge hierarchy problem, it introduces a new hierarchy concerning the magnitudes of the unnatural big radii  $R$  of the extra dimensions compared to the higher-dimensional Planck mass. According to the formula (2.4), one could demand  $R \sim 1/m_{\text{EW}}$  to cure this problem, but this would require a large number  $n$  of extra dimensions, accordingly.

### 2.1.2 Universal extra dimensions

Shortly after the publication of the ADD model, the idea of universal extra dimensions was established [144]. In this scenario, several compactified extra dimensions are added to the SM, and in contrast to the ADD model, it is assumed that all particle fields can **universally** propagate into the extra dimensions. In general, particle fields that extend into compactified extra dimensions, and therefore live in a higher-dimensional space-time, imply very interesting physical consequences. For one extra dimension, compactified on a simple circle  $S^1$ , the periodicity condition

$$x_5 \equiv x_5 + 2\pi R \quad (2.5)$$

applies. According to this condition, every five-dimensional particle field, as the simplest example of a five-dimensional scalar field  $\Phi(x_M)$  with a mass  $M$ , can be expanded into an infinite Fourier series, as

$$\Phi(x_\mu, x_5) = \sum_{n=-\infty}^{\infty} \chi_n^\phi(x_5) \phi_n(x_\mu) . \quad (2.6)$$

Every mode in the expansion consists of a four-dimensional KK particle field and a profile function that describes the dependence on the extra dimension. A more convenient compactification in the sense of particle physics is the  $S^1/Z_2$  orbifold compactification. In this connection, the physical domain runs from  $x_5 = 0$  to  $x_5 = \pi R$ , and a discrete symmetry is imposed, the  $Z_2$ -symmetry, by identifying  $x_5 \leftrightarrow -x_5$  in addition to the periodicity condition. This is illustrated in Figure 2.2. The endpoints do not transform under the  $Z_2$ -symmetry, and are called the fixed points of the orbifold [145]. At these fixed points, four-dimensional subspaces, so-called branes, can be localized. If considering the action of a five-dimensional scalar field [145],

$$S_{5D} = \int d^5x \left[ (\partial^M \Phi)(\partial_M \Phi) - M^2 \Phi \Phi \right] , \quad (2.7)$$

one can substitute the KK Fourier tower of the five-dimensional scalar, and integrate over the fifth dimension. One **requires** that for every four-dimensional Fourier mode  $\phi_n(x_\mu)$  in the expansion, the action for a four-dimensional scalar applies [145],

$$S_{5D} \stackrel{!}{=} \int d^4x \sum_{n=1}^{\infty} \left[ \partial^\mu \phi_n \partial_\mu \phi_n - m_n^2 \phi_n^2 \right] . \quad (2.8)$$

so that the single modes describe distinct, four-dimensional, scalar particles, the KK particles. The requirement results in conditions that are imposed on the profile functions  $\chi_n^\phi(x_5)$ :



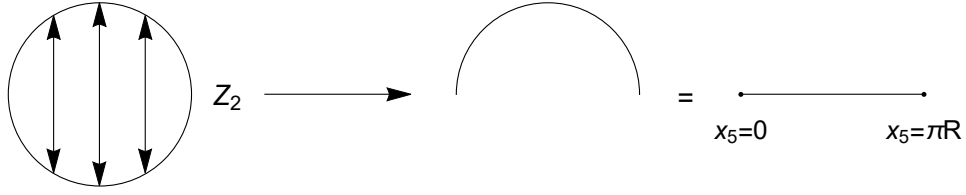


Figure 2.2: Sketch of the  $S^1/Z_2$  orbifold compactification of an extra dimension [145]. The physical domain runs from  $x_5 = 0$  to  $x_5 = \pi R$ , by identifying  $x_5 \leftrightarrow -x_5$ , apart from the discrete  $Z_2$ -symmetry that is imposed. The endpoints of the orbifold are the fixed points and do not transform under  $Z_2$ .

1) The five-dimensional action has to be invariant under the  $Z_2$ -symmetry. For that reason, the field  $\Phi(x_\mu, x_5)$  has to follow an intrinsic parity transformation

$$\Phi(x_\mu, -x_5) = P\Phi(x_\mu, x_5) , \quad P = \pm 1 , \quad (2.9)$$

so that the field has to be even (+) or odd (-) under the  $Z_2$ -symmetry. An odd field has to fulfil Dirichlet boundary conditions at the branes, which can be translated into boundary conditions for the profiles as

$$\chi_n^\phi(x_i) \stackrel{!}{=} 0 , \quad x_i = 0, \pi R . \quad (2.10)$$

An even field has to fulfil Neuman or mixed-type boundary conditions at the branes, as

$$\partial_{x_5}\chi_n^\phi(x_5)|_{x_5=0,\pi R} \stackrel{!}{=} 0 , \quad \text{or at least} \quad \partial_{x_5}\chi_n^\phi(x_5)|_{x_5=0,\pi R} \stackrel{!}{=} \xi\chi_n^\phi(x_i) , \quad x_i = 0, \pi R . \quad (2.11)$$

2) The profiles  $\chi_n^\phi(x_5)$  have to form a complete set of functions on the extra dimension, fulfilling an orthonormality condition,

$$\frac{1}{2\pi R} \int_{-\pi R}^{\pi R} dx_5 \chi_m^\phi(x_5)\chi_n^\phi(x_5) = \delta_{mn} , \quad (2.12)$$

which results from a matching of the five-dimensional kinetic terms of the action to the four-dimensional kinetic terms of scalars.

3) In addition, the mass terms have to match to those of four-dimensional scalars, requiring an equation of motion for the profiles

$$\partial_{x_5}^2\chi_n^\phi(x_5) - M^2\chi_n^\phi(x_5) = -m_n^2\chi_n^\phi(x_5) . \quad (2.13)$$

Detections of KK particles could provide measurable signals for the existence of a compactified extra dimension in particle scattering processes. With the help of the three kinds of conditions, one can determine the KK spectrum that is dictated by the KK profiles. The general solution to the differential equation in (2.13) reads

$$\chi_n^\phi(x_5) = C_1 e^{i\sqrt{m_n^2 - M^2}x_5} + C_2 e^{-i\sqrt{m_n^2 - M^2}x_5} , \quad (2.14)$$

where the periodicity condition implies that

$$\begin{aligned} e^{\pm i\sqrt{m_n^2 - M^2} x_5} &\stackrel{!}{=} e^{\pm i\sqrt{m_n^2 - M^2} (x_5 + 2\pi R)} \\ \Leftrightarrow e^{i\sqrt{m_n^2 - M^2} 2\pi R} &\stackrel{!}{=} 1, \quad \Rightarrow \quad \sqrt{m_n^2 - M^2} = \frac{n}{R}. \end{aligned} \quad (2.15)$$

Therefore, the single KK modes have the masses

$$m_n^2 = M^2 + \frac{n^2}{R^2}, \quad (2.16)$$

where the lightest mode for  $n = 0$  has a mass  $M$ , whereas the higher modes have heavier masses, ascending with multiples of  $n/R$ . Also, one can see that  $m_n < M$  is not possible. The  $Z_2$ -symmetry demands further that

$$\chi_n^\phi(-x_5) = \pm 1 \cdot \chi_n^\phi(x_5), \quad \Rightarrow \quad C_2 = \pm C_1, \quad (2.17)$$

depending on the parity of the profiles  $\chi_n^\phi(x_5)$ . One can write the KK decomposition in terms of profiles that are even (+) and odd (-) under the  $Z_2$ -symmetry, for what it follows from the previous steps that  $\chi_n^{\phi^+}(x_5) = 2C_1 \cos\left(\frac{n}{R}x_5\right)$ , and  $\chi_n^{\phi^-}(x_5) = 2iC_1 \sin\left(\frac{n}{R}x_5\right)$ . With the identification for the four-dimensional fields,  $\phi_n^\pm(x_\mu) \equiv \frac{1(i)}{\sqrt{2}} [\phi_n(x_\mu) \pm \phi_{-n}(x_\mu)]$ , and by respecting the normalization condition in (2.12), giving  $C_1 = 1/\sqrt{2}$ , one can find then

$$\Phi(x_\mu, x_5) = \frac{1}{\sqrt{2\pi R}} \phi_0(x_\mu) + \sum_{n=1}^{\infty} \frac{1}{\sqrt{\pi R}} \left[ \phi_n^+(x_\mu) \cos\left(\frac{nx_5}{R}\right) + \phi_n^-(x_\mu) \sin\left(\frac{nx_5}{R}\right) \right], \quad (2.18)$$

where

$$\begin{aligned} \phi_n^-(x_\mu) &= 0, \quad \text{if } P_\Phi = +1, \quad \text{or} \\ \phi_n^+(x_\mu) &= 0, \quad \text{if } P_\Phi = -1, \quad (\text{including } \phi_0(x_\mu)). \end{aligned} \quad (2.19)$$

The KK decomposition on an  $S^1/Z_2$  orbifold is reduced by a factor 2 compared to the decomposition on a simple circle, given in (2.6). Further, it projects out the zero mode for a field that is odd under the  $Z_2$  parity. The KK decompositions illustrate that an infinite tower of new fields with separate masses is predicted for five-dimensional fields. The procedure can be generalized to the fields with other spin, in which the four-dimensional KK fields in the expansions are adapted accordingly. In principle, we can consider the described setting as an extension of the SM, where all fermions and gauge bosons are allowed to spread out into the extra dimension, resulting in specific towers of KK particles. The lightest KK modes, the zero modes, form the equivalents to the SM particle fields, and moreover, there can be additional, five-dimensional, particle fields, as long as these fields are odd under the  $Z_2$  symmetry and do not have zero modes. The mass scale  $M_{KK}$  of the lightest, additional KK modes, in addition to the SM fields, in this framework is scaling with the inverse radius of the extra dimension, according to  $M_{KK} \approx R^{-1}$ . In general, the extra dimensions are assumed to be compactified on radii much larger than the Planck length, but smaller than those of the ADD model.

The five-dimensional gauge symmetries predict gauge bosons that can be separated into a four-dimensional vector component and a scalar part,  $A_M = A_\mu + A_5$ . Both parts are separately

expanded in KK decompositions, where the KK particle fields have the respective spins. The scalar parts  $A_5$  have to be odd under the  $Z_2$ -symmetry to avoid the presence of additional, light scalars by the zero modes. Also, the quantity  $F_{\mu 5} = \partial_\mu A_5 - \partial_5 A_\mu$  in the five-dimensional kinetic Lagrangian of the gauge bosons,  $\mathcal{L}_{\text{bosons}} \in \frac{1}{4} F_{MN} F^{MN} = \frac{1}{4} (F_{\mu\nu} F^{\mu\nu} + F_{\mu 5} F^{\mu 5})$ , must own a well-defined  $Z_2$  parity, where  $\partial_\mu$  is even, and  $\partial_5$  is odd. This is fulfilled for  $Z_2$ -even vector components  $A_\mu$  and  $Z_2$ -odd scalar components  $A_5$ , respectively. After electroweak symmetry breaking, the KK modes of the scalar decompositions form the third degrees of freedom of the massive KK gauge bosons of the vector decompositions, as the terms

$$\mathcal{F}_{\mu 5}^2 \ni \partial_\mu A_5 \partial_5 A^\mu \sim \sum_n A_\mu^{(n)} \partial^\mu A_5^{(n)} \partial_{x_5} \chi_n^{A_\mu}(x_5) \quad (2.20)$$

mix the fields  $A_\mu^{(n)}$  and  $A_5^{(n)}$  [145]. This is similar to the non-physical components of the Higgs field in the SM that form the longitudinal polarization states of the massive gauge bosons. Following the mass dimensions for the five-dimensional fields<sup>1</sup>, five-dimensional gauge couplings  $g_5$  have a dimension  $[g_5] = -1/2$ . By considering, for example, a zero-mode gauge boson coupling to two KK fermions,

$$\int d^4x \int_{-\pi R}^{\pi R} dx_5 g_5 \bar{\Psi} \Gamma^M A_M \Psi \ni \int d^4x g_4 \bar{\Psi}^{(m)} \gamma^\mu A_\mu^{(0)} \Psi^{(n)} \delta_{mn} , \quad (2.22)$$

one can define the dimensionless couplings by

$$g_4 \equiv g_5 \chi_0^{A_\mu}(x_5) , \quad (2.23)$$

where the zero-mode profile  $\chi_0^{A_\mu}(x_5) \approx 1/\sqrt{2\pi R}$  is constant in the extra dimension to the lowest approximation. The Kronecker delta  $\delta_{mn}$  in the formula stems from the normalization condition for the fermion profiles, which has been applied. Instead, for a general coupling of KK fermions to a higher-mode KK gauge boson, the expression includes the integral over the extra-dimensional coordinate including the profiles of the coupled KK particles,

$$\mathcal{B}_{kmn} = \int_{-\pi R}^{\pi R} dx_5 \chi_k^\Psi(x_5) \chi_m^{A_\mu}(x_5) \chi_n^\Psi(x_5) . \quad (2.24)$$

In the expression before, this integral has resulted in the normalization condition for the fermion profiles. In general, in extra-dimensional models, the overlap integrals are crucial ingredients of the effective, four-dimensional couplings. These can modify the interactions of the SM equivalents, the zero modes, in an interesting manner. In this way, for example, a GIM mechanism can be achieved to explain the suppressed flavor-changing neutral currents of the SM, or a natural explanation mechanism can be found for the mass splitting of the zero-mode fermions.

A five-dimensional Lie algebra, connected with the commutation relation,

$$\{\Gamma_M, \Gamma_N\} = 2\eta_{MN} , \quad (2.25)$$

<sup>1</sup>In  $d \neq 4$  space-time dimensions, the mass dimensions of the fields are

$$[\Phi] = [A_\mu] = E^{(d-2)/2} , \quad [\Psi] = E^{(d-1)/2} , \quad (2.21)$$

following from the demand that the action has to be dimensionless. So, in five dimensions, the bosons have a mass dimension 3/2, and the fermions have a mass dimension 2.

can only be fulfilled by irreducible four-dimensional representations, in contrast to the SM, where the representations of the four-dimensional Lie algebra can be reduced into two two-dimensional representations. For example, one can choose a representation in terms of the  $4 \times 4$  Dirac matrices,  $\Gamma_\mu = \gamma_\mu$ ,  $\Gamma_5 = -i\gamma_5$  [145]. As a consequence, the left- and right-handed zero-mode fields, implied for a doublet fermion under the five-dimensional  $SU(2)$  symmetry, transform **equally** under  $SU(2)$ , so that vector-like KK fermions are predicted by the theory. The important property of the SM  $SU(2)_L$  gauge transformations, to exclusively act on left-handed particles, is missing generically, and has to be implemented in some way. The chiral fermion content of the SM can be achieved by proposing **two different** fermion fields for the doublets and singlets. The zero-mode chirality parts, which are not compatible to the SM, are projected out by means of the  $Z_2$ -symmetry. In this regard, chiral fermions exist only for the zero modes, and for every KK mode  $n > 1$ , the fermion content is doubled compared to the SM.

The presence of the integrals over the extra-dimensional coordinate when deriving the four-dimensional, effective theory allows for a natural explanation mechanism for the mass differences of the SM fermions. For example, we can consider a five-dimensional fermion field  $\Psi$ , and add a  $Z_2$ -odd bulk mass term, as

$$\mathcal{L} \sim \bar{\Psi} (i\partial_M \Gamma^M + \epsilon(x_5)M) \Psi , \quad (2.26)$$

where  $\epsilon(x_5) = +1$  ( $-1$ ), for  $\pi R > x_5 > 0$ , ( $-\pi R < x_5 < 0$ ) [145]. The five-dimensional mass is just an arbitrary, five-dimensional parameter, for which the  $Z_2$ -odd behaviour is allowed and even necessary because an even mass term would explicitly break the  $Z_2$ -symmetry of the Lagrangian. It could be generated by a coupling of the fermions to the vev of a  $Z_2$ -odd bulk scalar, inducing a spontaneous breaking of the  $Z_2$ -symmetry. Such a mechanism will be investigated in some parts in the last section of the thesis. The odd bulk mass term characterizes the form of the fermion profiles  $\chi_n^f(x_5)$  via the equations of motion,

$$[-\partial_{x_5} + \epsilon(x_5)M] \chi_n^{fL}(x_5) = m_n \chi_n^{fR}(x_5) , \quad [\partial_{x_5} + \epsilon(x_5)M] \chi_n^{fR}(x_5) = m_n \chi_n^{fL}(x_5) . \quad (2.27)$$

We consider  $f$  and  $f'$  as two different fermion fields, where  $f$  is a  $SU(2)_L$  doublet and  $f'$  is a singlet. The zero modes of the right-handed doublet and the left-handed singlet are projected out by means of the  $Z_2$ -symmetry. One can derive the following solutions for the profiles of the zero modes (for  $m_n = 0$ )

$$\chi_0^{fL}(x_5) = N e^{Mx_5} , \quad \chi_0^{f'R}(x_5) = N e^{-M'x_5} . \quad (2.28)$$

Considering a five-dimensional Yukawa Lagrangian that couples to a brane-localized Higgs sector [145],

$$\mathcal{L} \sim \int_{-\pi R}^{\pi R} dx_5 \delta(x_5 - \pi R) h f_L f'_R \lambda_{5D} , \quad (2.29)$$

with a five-dimensional Yukawa coupling  $\lambda_{5D}$ . By integrating over the extra dimension, one can compare the Lagrangian to the four-dimensional form of the SM, given by  $\lambda_{4D} h f_L f'_R$ . A relation follows between the four-dimensional and five-dimensional Yukawa couplings [145]

$$\lambda_{4D} \propto \lambda_{5D} e^{(M-M')\pi R} . \quad (2.30)$$

For natural, five-dimensional parameters, the four-dimensional masses of the two different quarks  $m_{q_1}$  and  $m_{q_2}$  that scale with  $\lambda_{4D}$  can have exponentially large differences in the magnitudes. For example, taking  $\lambda_{5D,q_1} \approx \lambda_{5D,q_2}$  and  $M' \approx -M$  for each quark, and further  $M_{q_1} = -3/(\pi R)$  and  $M_{q_2} = -1/(\pi R)$ , one finds [145]

$$\frac{m_{q_1}}{m_{q_2}} \sim e^{2\Delta M\pi R} \approx \frac{1}{100} . \quad (2.31)$$

This is implied by the overlaps of the zero-mode fermion profiles with the exponential behaviour in the integrals over the extra-dimensional coordinate.

In principle, the general setting for the universal extra dimensions can be implemented for an arbitrary number  $\delta$  of extra dimensions [144]. Experimental tests of particle processes through LHC data, and electroweak precision tests performed at the  $Z$  pole, tests of the magnetic moment of the muon and of flavor changing neutral currents, can give exclusion bounds on the compactification scale  $R$  of the extra dimensions [146, 147]. In the subsequent sections of the thesis, similar tests will be considered in the context of the RS model, which will be introduced in the following.

### 2.1.3 A warped extra dimension - the Randall-Sundrum model

A framework to solve the gauge hierarchy problem by extending the SM with only one small and compactified extra dimension was published by L. Randall and R. Sundrum in the year 1999 [1]. The approach considers the four-dimensional Minkowskian spacetime  $\eta_{\mu\nu}$  together with a compact  $S^1/Z_2$ -orbifold, which can be parametrized by an angular coordinate  $\phi = \frac{x_5}{r_c}$ , where  $\phi \in [-\pi, \pi]$ . The parameter  $r_c$  is the radius of the extra dimension, prior to orbifolding. The lower part of the extra dimension  $[-\pi, 0]$  is physically equivalent to the upper part  $[0, \pi]$ , apart from the  $Z_2$ -symmetry, where the periodic identification in the coordinate  $\phi \equiv \phi + 2\pi r_c$  applies. The four-dimensional space along the fifth dimension is extremely warped by a negative energy density, in contrast to the models presented before. As an effect, a large hierarchy of scales is caused between two objects that are situated at different positions along the extra dimension. To respect the four-dimensional Poincaré-invariance in the four-, the  $x^\mu$ ,-directions, the ansatz for the five-dimensional metric reads [1]

$$ds^2 = G_{MN}dx^M dx^N = e^{-2\sigma(\phi)}\eta_{\mu\nu}dx^\mu dx^\nu + r_c^2 d\phi^2 . \quad (2.32)$$

The orbifold has two fixed points at  $\phi = 0$  and  $\phi = \pi$ , at which four-dimensional subspaces are localized that only extend into the  $x_\mu$ -directions,

$$g_{\mu\nu}^{\text{vis}}(x^\mu) \equiv G_{\mu\nu}(x^\mu, \phi = \pi) , \quad g_{\mu\nu}^{\text{hid}}(x^\mu) \equiv G_{\mu\nu}(x^\mu, \phi = 0) . \quad (2.33)$$

In this original framework, only the gravitational force can extend into the whole five-dimensional space-time, the bulk. The four-dimensional field content of the SM is assumed to be exclusively localized onto the brane at  $\phi = \pi$ , similar to the ADD model. The classical action for this set-up has the form [1]

$$S = \int d^4x \left( \left\{ \int_{-\pi}^{\pi} d\phi \sqrt{-G} [-\Lambda + 2M^3 R] \right\} + \sqrt{-g_{\text{vis}}} [\mathcal{L}_{\text{vis}} - V_{\text{vis}}] + \sqrt{-g_{\text{hid}}} [\mathcal{L}_{\text{hid}} - V_{\text{hid}}] \right) . \quad (2.34)$$

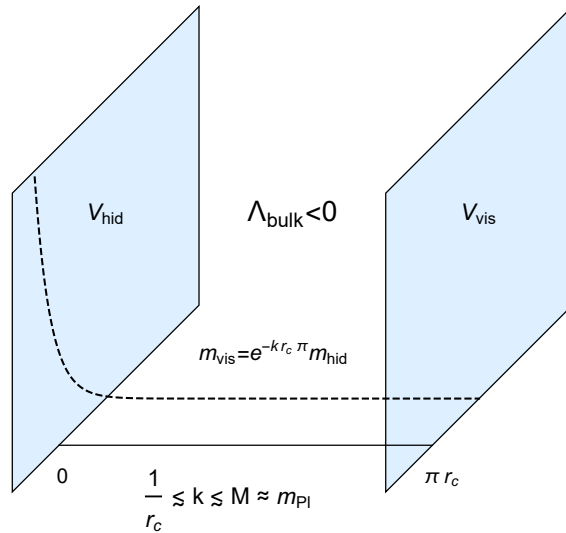


Figure 2.3: Sketch of the RS model. It considers an  $S^1/Z_2$  orbifold that forms a slice of  $\text{AdS}_5$  space with a negative energy density, bounded by two fourdimensional branes. An exponential warping of scales is induced along the extra dimension from  $x_5 = 0$  to  $x_5 = \pi r_c$ , indicated by the dashed curve and the mass relation. The model does not require any large hierarchies between the fundamental parameters  $k$ ,  $r_c$  and  $M$ .

A negative, five-dimensional vacuum energy density  $\Lambda$  resides in the bulk, and constant vacuum energies  $V$  are localized on each of the branes, acting as gravitational sources even in the absence of particle excitations. Here,  $M$  represents the fundamental mass scale of the higher-dimensional theory. The five-dimensional Einstein's equations for this framework read [1]

$$\sqrt{-G} \left( R_{MN} - \frac{1}{2} G_{MN} R \right) = - \frac{1}{4M^3} \left[ \Lambda \sqrt{-G} G_{MN} + V_{\text{vis}} \sqrt{-g_{\text{vis}}} g_{\mu\nu}^{\text{vis}} \delta_M^\mu \delta_N^\nu \delta(\phi - \pi) \right. \\ \left. + V_{\text{hid}} \sqrt{-g_{\text{hid}}} g_{\mu\nu}^{\text{hid}} \delta_M^\mu \delta_N^\nu \delta(\phi) \right] , \quad (2.35)$$

neglecting the brane-localized Lagrangians. By using the five-dimensional metric, one can calculate the Christoffel symbols of the model, and one can determine the Ricci tensor and the Ricci scalar for a local basis on a Riemann manifold. These can be inserted into the Einstein's equations, resulting in the following differential equations

$$\frac{6}{r_c^2} \sigma'(\phi)^2 = - \frac{\Lambda}{4M^3} , \quad \frac{3}{r_c^2} \sigma''(\phi) = \frac{1}{4M^3 r_c} [V_{\text{hid}} \delta(\phi) + V_{\text{vis}} \delta(\phi - \pi)] . \quad (2.36)$$

The first of the two equations gives the solution

$$\sigma(\phi) = r_c |\phi| \sqrt{\frac{-\Lambda}{24M^3}} , \quad (2.37)$$

which is consistent with the orbifold symmetry, and demands a negative sign for  $\Lambda$  in order to obtain a real root. Such a warped space, caused by a negative energy density, is called an

“anti-de Sitter (AdS) space”. By defining the curvature scalar  $k \equiv \sqrt{\frac{-\Lambda}{24M^3}}$ , one derives the following result for the exponential of the warp factor [1]

$$\sigma(\phi) = kr_c|\phi| . \quad (2.38)$$

Then, from the second derivative of the solution,  $\sigma''(\phi) = 2kr_c[\delta(\phi) - \delta(\phi - \pi)]$ , one can obtain the following energy densities on the branes

$$V_{\text{hid}} = -V_{\text{vis}} = 24M^3k , \quad \Lambda = -24M^3k^2 . \quad (2.39)$$

The curvature term in the five-dimensional action determines a relation between the fundamental mass  $M$  and the four-dimensional Planck mass  $m_{Pl}$  after having integrated over the extra dimension. The result is [1]

$$m_{Pl}^2 = M^3r_c \int_{-\pi}^{\pi} d\phi e^{-2kr_c|\phi|} = \frac{M^3}{k} [1 - e^{-2kr_c\pi}] , \quad (2.40)$$

which indicates that  $m_{Pl}$  depends only mildly on the radius  $r_c$  in the limit of a large  $kr_c$ . On the contrary, the scale for the particle fields that exclusively reside on the visible brane at  $\phi = \pi$  has a strong dependence on the choice for  $kr_c$ . In this connection, the action for the Higgs field with a mass parameter  $v_0$  reads

$$S_{\text{vis}} \ni \int d^4x \sqrt{-g_{\text{vis}}} [g_{\text{vis}}^{\mu\nu} D_\mu H^\dagger D_\nu H - \lambda(|H|^2 - v_0^2)^2] , \quad (2.41)$$

where  $g_{\mu\nu}^{\text{vis}} = e^{-2kr_c\pi} \bar{g}_{\mu\nu}$  (whereas  $g_{\text{hid}} = \bar{g}_{\mu\nu}$ ). After a canonical renormalization of the wavefunction,  $H \rightarrow e^{kr_c\pi} H$ , one can find

$$S_{\text{eff}} \ni \int d^4x \sqrt{-\bar{g}} [\bar{g}^{\mu\nu} D_\mu H^\dagger D_\nu H - \lambda(|H|^2 - e^{-2kr_c\pi} v_0^2)^2] . \quad (2.42)$$

By comparing this effective action with the equation before, one derives the intriguing result for the relation between the five-dimensional and the four-dimensional Higgs mass parameters  $v_0$  and  $v$  [1],

$$v \equiv e^{-kr_c\pi} v_0 . \quad (2.43)$$

The relation states that the mass parameters on the visible brane at  $\phi = \pi$  are scaled down by an exponential warp factor  $e^{-kr_c\pi}$ , compared to mass scales on the hidden brane at  $\phi = 0$ . Equivalent relations hold for **any** mass parameters  $m$  on the visible brane,

$$m_{\text{vis}} \equiv e^{-kr_c\pi} m_{\text{hid}} . \quad (2.44)$$

By setting  $e^{kr_c\pi}$  to the order of  $10^{15}$ , TeV scale masses are obtained on the visible brane, which correspond to mass parameters of the order of the Planck mass  $\sim 10^{19}$  GeV on the hidden brane. According to this scaling behaviour, the visible brane is usually denoted as the TeV or infrared (IR) brane, whereas the hidden brane is denoted as the Planck or ultraviolet (UV) brane. Possible gravity force mediating particles, the gravitons, would reside close to the hidden brane, where the high scales hold. Then, the weakness of gravity can be explained by the small

overlap of the graviton wave function in the fifth dimension with the visible brane, where the SM particles are assumed to reside on. The crucial point is that the fundamental scale for the SM particles can **naturally** be of the order of  $\mathcal{O}(TeV)$  on the visible brane. In this relation, also the UV cut-off scale of the theory can be set to this energy range,

$$\Lambda_{IR} = \Lambda_{UV} e^{-kr_c\pi} \sim \text{several TeV} , \quad (2.45)$$

for  $\Lambda_{UV} \sim 10^{16}$  TeV. In this way, the apparently huge hierarchy between the Planck and the electroweak scale is resolved. The weak scale can dynamically be generated by the background metric for a slice of  $AdS_5$  space, according to the formulas (2.40) and (2.43), for a fundamental mass scale  $M \sim m_{Pl}$ . In this sense, the framework is working with natural choices for the parameters, as

$$\frac{1}{r_c} \lesssim k \lesssim M \approx m_{Pl} , \quad kr_c \sim 11 , \quad (2.46)$$

without introducing any larger, new hierarchies, compared to the ADD model [139]. Furthermore, the RS model predicts KK resonances with larger mass differences, whereas in the ADD model the implied KK resonances of gravitons have mass differences of only a few  $eV$ . In this regard, it should be possible to individually detect the single modes of gravitons via their decay products [1]. But, the radius  $r_c$  of the extra dimension has to be stabilized to insure the relation  $e^{kr_c\pi} \approx 10^{15}$ . This can be achieved by the ‘‘Goldberger-Wise mechanism’’ [148, 149] by introducing a scalar field in the bulk. This bulk scalar has quartic interactions that are localized on the branes, and the minimum energy configuration, resulting from this setting, can yield an appropriate compactification scale  $r_c$ .

## 2.2 The minimal Randall-Sundrum model

In the following, we will present a description of the actual frameworks of the RS model that will be investigated in this thesis. In most parts, we will work with the most natural and upgraded version of the RS model, in which all particle fields according to the bulk gauge symmetry, including the Higgs boson, extend into the extra dimension (**bulk-Higgs RS model**). Initially, the Higgs sector was strictly localized onto the IR brane, based on the motivation to solve the gauge hierarchy problem. But, in principle, the setting with a bulk Higgs field can also resolve the gauge hierarchy problem. Though the Higgs field can extend into the whole extra dimension, the Higgs profile is exponentially augmenting from the UV brane to the IR brane, with a maximum positioned onto the IR brane. The derivation of the correct Higgs mass demands for a very slight amount of fine-tuning, such as around 1 in a 1000 [2]. The electroweak symmetry breaking potential is localized onto the IR brane, and we do not consider quartic Higgs interactions in the bulk. For the bulk-Higgs framework, we will consider a minimal implementation for the bulk gauge symmetry. In addition, we will present two alternative versions of the RS model, one with a brane-localized Higgs field (**brane-Higgs RS model**), and another one with an extended gauge symmetry implemented in the bulk (**custodial RS model**).

In this sense, we are working with a version of the SM that is extended by a small and warped extra dimension. The extra dimension has a curled up and microscopic behaviour, and is chosen to be an  $S^1/Z_2$  orbifold that can be parametrized by a dimensionless coordinate  $t \in [\epsilon, 1]$ . The orbifold is bounded by two four-dimensional branes localized at the fixed-points



at  $t = \epsilon = e^{-kr\pi} \approx 10^{-15}$  (UV brane) and  $t = 1$  (IR brane), similar to the framework of the original RS model [1]. The metric of the model reads

$$ds^2 = \frac{\epsilon^2}{t^2} \left( \eta_{\mu\nu} dx^\mu dx^\nu - \frac{1}{M_{KK}^2} dt^2 \right) = e^{-2kr|\phi|} \eta_{\mu\nu} dx^\mu dx^\nu - r^2 d\phi^2 . \quad (2.47)$$

The dimensionless coordinate  $t$  [150–152] is related to the coordinate used in the original publication of the model  $\phi \in [-\pi, \pi]$  by the relation

$$t = \epsilon e^{kr|\phi|} , \quad (2.48)$$

where both the radius  $r$  of the extra dimension and the curvature constant  $k$  are situated close to the Planck scale,  $k \sim 1/r \sim m_{Pl}$ . The transformation properties from the  $\phi$ , or  $x_5$ , coordinates to the  $t$  coordinate are illustrated in Appendix A.1. In this framework, the KK mass scale, the mass scale of the lightest KK resonances, is determined by the relation  $M_{KK} = k\epsilon$ . Usually, one defines the quantity  $L = kr\pi \approx 33-34$  as the “size” of the extra dimension, which is stabilized by the “Goldberger-Wise mechanism” [148]. According to the metric of the framework in (2.47), we observe that the quantity  $L$  dictates a correspondence of the high Planck scale at the UV brane with the TeV scale at the IR brane, which is needed to solve the gauge hierarchy problem [1]. We consider a minimal amount of particle fields which are similar to the SM particle fields, so that we extend the SM gauge group,

$$SU(3)_c \times SU(2)_L \times U(1)_Y , \quad (2.49)$$

to five dimensions [150]. Also, we include a five-dimensional Higgs field, so that all particle fields of the setting can propagate into the extra dimension. The calculations are performed with an effective, four-dimensional description of the RS model that is valid at momenta lower than the warped-down UV cut-off  $\Lambda_{TeV} \sim 10M_{KK}$  [153]. Due to the microscopic, curled up, and periodic behaviour of the extra dimension, we can expand the initial five-dimensional particle fields into the KK decompositions [137, 138]. Every KK mode in the decompositions consists of a four-dimensional particle field together with a profile function that defines the behaviour along the extra dimension. The KK decompositions of the five-dimensional particle fields can be inserted into the original, five-dimensional action of the model, while integrating over the fifth dimension in order to derive an effective four-dimensional action. In this connection, the profile functions of the fields have to fulfil particular normalization conditions, as well as differential equations in dependence of the extra dimensional coordinate (equations of motion), to match the resulting four-dimensional action with the action of the SM.

The original, five-dimensional action reads [2, 154]

$$S = \int d^4x \frac{2\pi r}{L} \int_\epsilon^1 \frac{dt}{t} \frac{\epsilon^4}{t^4} [\mathcal{L}_{\text{gauge}} + \mathcal{L}_{\text{Higgs}} + \mathcal{L}_{\text{ferm}}] , \quad (2.50)$$

with

$$\mathcal{L}_{\text{gauge}} = -\frac{1}{4} G_{MN}^b G^{MNb} - \frac{1}{4} F_{MN}^a F^{MNa} - \frac{1}{4} B_{MN} B^{MN} , \quad (2.51)$$

and<sup>2</sup>

$$\begin{aligned}\mathcal{L}_{\text{Higgs}} &= g^{MN} D_M \Phi^\dagger D_N \Phi - \mu^2 |\Phi|^2 - V_{\text{branes}} , \\ V_{\text{branes}} &= k\epsilon\delta(t - \epsilon) km_{UV} |\Phi|^2 + k\delta(t - 1) \left[ -km_{IR} |\Phi|^2 + \frac{2r}{k} \lambda |\Phi|^4 \right] ,\end{aligned}\tag{2.52}$$

and

$$\mathcal{L}_{\text{ferm}} = \sum_f \bar{f} (i\Gamma^M \nabla_M - M_f) f - [\bar{Q} \mathbf{Y}_d^{5D} \Phi d + \bar{Q} \mathbf{Y}_u^{5D} \epsilon \Phi^\dagger u + \bar{L} \mathbf{Y}_e^{5D} \Phi e + \text{h.c.}] .\tag{2.53}$$

Here,  $\frac{\epsilon^4}{i^4} r = \sqrt{G}$  is the square root of the determinant of the five-dimensional metric, and  $G_{MN}^b$ ,  $b=1, \dots, 8$ ,  $F_{MN}^a$ ,  $a=1, 2, 3$ , and  $B_{MN}$  are the five-dimensional field strength tensors of the groups  $SU(3)_c$ ,  $SU(2)_L$  and  $U(1)_Y$ , respectively. The initial, kinetic terms for the fermions in the action are modified compared to the SM, due to the curved space along the extra dimension [155–157]. In this connection, the Dirac matrices in the curved space  $\Gamma^M = E_A^M \gamma^A$  have to be included that are related to the Dirac matrices in the flat space  $\gamma^A = (\gamma^\mu, i\gamma_5)$  by the fünfbein  $E_A^M = \text{diag}(\frac{t}{\epsilon}, \frac{t}{\epsilon}, \frac{t}{\epsilon}, \frac{t}{\epsilon}, \frac{1}{r})$  [157]. Primarily, the covariant derivative,  $\nabla_M = D_M + \omega_M$ , includes a second term with the spin connection  $\omega_M$ . Nevertheless, this term does not give a contribution to the action in the RS model, because the metric is diagonal [155]. Then, the kinetic terms obtained for the KK fermions are similar to the SM. Also, the kinetic terms for the bulk Higgs field depend on the five-dimensional metric tensor, and therefore on the warp factor of the curved space.

In the following, we begin with a more detailed description of the sectors for the gauge fields and the Higgs field. Then, in the subsequent section, we will give a description for the fermion sector.

### 2.2.1 Gauge sector and spontaneous symmetry breaking

The original parameters in the Higgs potential in (2.52) have the mass dimensions  $[M_{UV}] = [2km_{UV}] = 1$ ,  $[M_{IR}] = [2km_{IR}] = 1$  and  $[\lambda_{IR}] = [\frac{4r}{k}\lambda] = -2$  of the fundamental energy scale, which varies along the extra dimension [2, 154], corresponding to the Planck scale at the UV brane and the warped-down Planck scale, lying around several TeV, at the IR brane. Accordingly, a possible  $|\Phi|^4$ -term on the UV boundary would be suppressed by negative powers of 2 of the Planck scale, and is neglected here. Similarly, such a term in the bulk would be suppressed by an intermediate scale between the Planck and the TeV energy scales. However, the inclusion of such a term would result in a significantly more involved structure of the Higgs sector, and we refrain from including it, similar to the framework discussed in [154]. The mechanism of the spontaneous symmetry breaking of the electroweak symmetry is induced by the IR brane-localized potential, which is forcing the Higgs field to adopt a position-dependent vev  $v(t)$  in the bulk. As usual, one can expand the five-dimensional Higgs field around this vev [2]

$$\Phi(x, t) = \frac{t}{\epsilon\sqrt{r}} \left( \begin{array}{c} -i\varphi^+(x, t) \\ \frac{1}{\sqrt{2}} [v(t) + h(x, t) + i\varphi^3(x, t)] \end{array} \right) ,\tag{2.54}$$

<sup>2</sup>Here, the dimensionless quantities  $m_{UV} = \frac{M_{UV}}{2k}$ ,  $m_{IR} = \frac{M_{IR}}{2k}$  and  $\lambda = \frac{\lambda_{IR} k}{4r}$  are defined from the dimensionful parameters  $M_{UV}$ ,  $M_{IR}$  and  $\lambda_{IR}$ , where  $[M_{UV}] = [M_{IR}] = 1$  and  $[\lambda_{IR}] = -2$ , respectively.

where  $h(x, t)$  is the physical, five-dimensional Higgs scalar. For convenience, we have extracted the factors  $\frac{t}{\epsilon\sqrt{r}}$ , so that the remaining components in the decomposed Higgs field, as the Higgs boson and the vev, have a mass dimension 1. The Lagrangian of the Higgs sector,

$$\begin{aligned} \mathcal{L}_{\text{Higgs}} = & \frac{2\pi r}{L} \left( \int_{\epsilon}^1 \frac{dt}{t} \left[ \frac{\epsilon^2}{t^2} \eta^{\mu\nu} (\partial_{\mu} \Phi^{\dagger}) (\partial_{\nu} \Phi) - M_{KK}^2 \frac{\epsilon^2}{t^2} (\partial_t \Phi^{\dagger}) (\partial_t \Phi) - \mu^2 \epsilon^4 \frac{1}{t^4} |\Phi|^2 \right] \right. \\ & \left. - \delta(t - \epsilon) k^2 m_{UV} |\Phi|^2 + \delta(t - 1^{-}) [M_{KK}^2 \epsilon^2 m_{IR} |\Phi|^2 - 2r \lambda \epsilon^4 |\Phi|^4] \right) , \end{aligned} \quad (2.55)$$

reads, by keeping only the terms for  $[v(t) + h(x, t)]$ , and after a partial integration, as

$$\begin{aligned} \mathcal{L}_{\text{Higgs}} = & \frac{\pi}{L} \left( \int_{\epsilon}^1 \frac{dt}{t} \left[ (\partial^{\mu} h(x, t)) (\partial_{\mu} h(x, t)) - \frac{\mu^2 \epsilon^2}{t^2} [v(t) + h(x, t)]^2 \right. \right. \\ & \left. \left. + t^2 M_{KK}^2 [v(t) + 2h(x, t)] \partial_t \left( \frac{1}{t^3} \partial_t (tv(t)) \right) + t^2 M_{KK}^2 h(x, t) \partial_t \left( \frac{1}{t^3} \partial_t (th(x, t)) \right) \right] \right. \\ & \left. - k^2 m_{UV} [v(\epsilon) + h(x, \epsilon)]^2 + M_{KK}^2 m_{IR} [v(1) + h(1)]^2 - \lambda [v(1) + h(1)]^4 \right. \\ & \left. - M_{KK}^2 \left[ \frac{1}{t^2} (v(t) + 2h(x, t)) \partial_t (tv(t)) + \frac{1}{t^2} h(x, t) \partial_t (th(x, t)) \right]_{\epsilon}^1 \right) . \end{aligned} \quad (2.56)$$

Demanding that the terms that are linear or quadratic in  $h(x, t)$  should cancel on the UV and IR branes yields the boundary conditions [2]

$$\begin{aligned} \partial_t [tv(t)]|_{t=\epsilon} = m_{UV} v(\epsilon) , \quad \partial_t [tv(t)]|_{t=1^{-}} = m_{IR} v(1) - \frac{2\lambda}{M_{KK}^2} v(1)^3 , \\ \partial_t [th(x, t)]|_{t=\epsilon} = m_{UV} h(x, \epsilon) , \quad \partial_t [th(x, t)]|_{t=1^{-}} = m_{IR} h(x, 1) - \frac{6\lambda}{M_{KK}^2} v(1)^2 h(x, 1) . \end{aligned} \quad (2.57)$$

By means of a variational principle with respect to the vev  $v(t)$ , applied onto the Lagrangian, one obtains the following equation of motion for the  $t$ -dependent vev [2, 154, 157–159],

$$\partial_t \left( \frac{1}{t^3} \partial_t [tv(t)] \right) - \frac{\mu^2}{k^2 t^4} v(t) = 0 , \quad \Leftrightarrow \quad (t^2 \partial_t^2 + t \partial_t - \beta^2) \frac{v(t)}{t} , \quad (2.58)$$

introducing now the bulk-Higgs localization parameter  $\beta^2 = 4 + \frac{\mu^2}{k^2}$ . So, in order to determine a formula for the Higgs vev  $v(t)$ , one has to solve its defining differential equation (2.58) subject to the boundary conditions (2.57). The general solution reads [2]

$$v(t) = N_v (t^{1+\beta} - r_v t^{1-\beta}) , \quad (2.59)$$

where

$$r_v = \epsilon^{2\beta} \frac{2 + \beta - m_{UV}}{2 - \beta - m_{UV}} , \quad N_v^2 = \frac{M_{KK}^2}{2\lambda} \frac{(m_{IR} - 2 - \beta) - r_v (m_{IR} - 2 + \beta)}{[1 - r_v]^3} . \quad (2.60)$$

Usually, one assumes that  $\beta$  must be a real and positive number and obeys to the Breitenlohner-Friedman bound  $\mu^2 > -4k^2$  [160]. Moreover, it does not necessarily have to be larger than 2. Unless  $\beta$  is very close to zero, or  $m_{UV}$  is extremely fine-tuned to the value  $(2 - \beta)$ , the coefficient  $r_v \propto \epsilon^{2\beta}$  in (2.60) is extremely small, and can be set to zero for all practical purposes. In this case, we obtain

$$v(t) = v(1) t^{1+\beta}, \quad v(1) = \sqrt{\frac{M_{KK}^2}{2\lambda} (m_{IR} - (2 + \beta))}, \quad (2.61)$$

by dropping terms of the order of  $\epsilon \approx 10^{-15}$  and smaller. The solution predicts the vev to be peaked towards the IR brane. For that reason, the RS model with a bulk-Higgs field can also resolve the gauge hierarchy problem [157, 161]. For varying choices of  $\beta$ , the Higgs vev is plotted in Figure 2.4. We can observe that in the limit of larger values for  $\beta$ , it approaches to an IR brane-localization. Such a brane-localized Higgs scenario will be discussed later. The constant value for the Higgs vev  $v(1)$  on the IR brane should be a real number, and  $\lambda > 0$  is required by vacuum stability, so that an upper bound follows on the parameter  $\beta$ ,

$$0 < \beta < m_{IR} - 2. \quad (2.62)$$

The relation between the parameter  $v(1)$  and the physical value  $v_{SM}$  of the Higgs vev in the SM can be determined, for example, by the mass terms for the W and Z bosons [2],

$$\mathcal{L}_m = \frac{2\pi}{L} \int_{\epsilon}^1 \frac{dt}{t} \frac{v(t)^2 g_5^2}{4} \left[ W_{\mu}^{+}(x, t) W^{-\mu}(x, t) + \frac{1}{2\cos^2\theta_W} Z_{\mu}(x, t) Z^{\mu}(x, t) \right]. \quad (2.63)$$

To the lowest order in  $v^2/M_{KK}^2$ , the five-dimensional gauge coupling is related to the gauge coupling  $g$  of the SM via  $g = g_5/\sqrt{2\pi r}$  [162], and the profiles of the zero-mode W and Z bosons are constant in the extra dimension,  $\chi_0^{[W,Z]}(t) = 1/\sqrt{2\pi} + \dots$ . Then, the relation between the vev parameters follows,

$$v_4^2 \equiv \frac{2\pi}{L} \int_{\epsilon}^1 \frac{dt}{t} v^2(t) = \frac{\pi}{L(1+\beta)} v(1)^2 = M_{KK}^2 \frac{\pi}{L(1+\beta)} \frac{\delta}{2\lambda}, \quad (2.64)$$

where  $\delta \equiv m_{IR} - 2 - \beta$ . The remaining parameter  $v_4$ , which we will write as  $v$  in the following, coincides with the SM parameter  $v_{SM}$  to the lowest order in an expansion in powers of  $v^2/M_{KK}^2$ . The first order correction can be determined from the shift of the Fermi constant in the RS model, which will be given later in (2.221). With this result, one can obtain the following expression for the  $t$ -dependent vev [2]

$$v(t) = v_4 \sqrt{\frac{L(1+\beta)}{\pi}} t^{1+\beta}. \quad (2.65)$$

One can choose the following KK decomposition for the Higgs field

$$h(x, t) = \sum_{n=0}^{\infty} \chi_n^h(t) h^{(n)}(x), \quad (2.66)$$

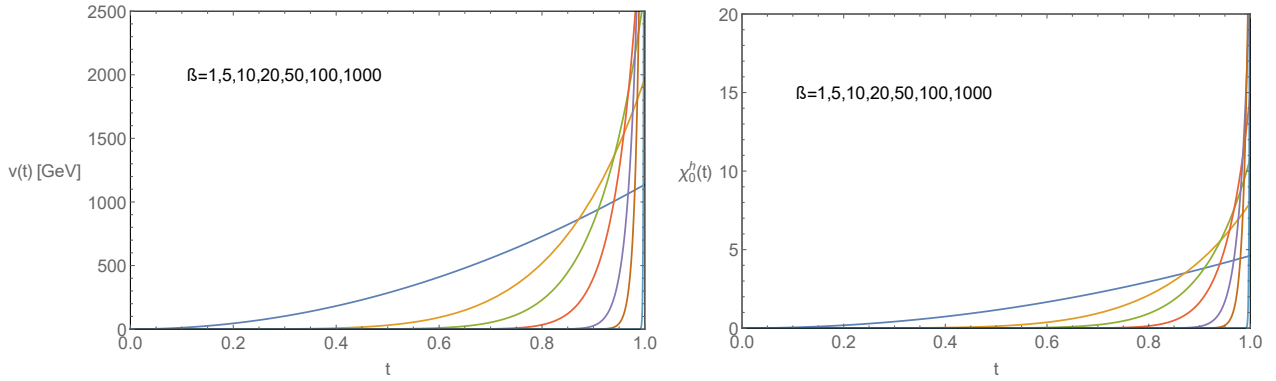


Figure 2.4: Plot of  $v(t)$  and  $\chi_0^h(t)$  for different values of  $\beta$ , and  $L = 33.5$ ,  $M_{KK} = 5$  TeV. For higher values of  $\beta$ , one can observe that the functions approach to an IR brane-localization.

where the zero mode  $h^{(0)}(x)$  corresponds to the Higgs boson of the SM. The profile functions have to obey the normalization conditions

$$\frac{2\pi}{L} \int_{\epsilon}^1 \frac{dt}{t} \chi_m^h(t) \chi_n^h(t) = \delta_{mn} , \quad (2.67)$$

in order to ensure that the kinetic terms of the effective, four-dimensional Lagrangian are canonically normalized. To obtain canonical, four-dimensional mass terms for the KK Higgs bosons, the equations of motion [2, 154, 157–159]

$$\left( \partial_t^2 - \frac{3}{t} \partial_t - \frac{\mu^2}{t^2 k^2} + (x_n^h)^2 \right) [t \chi_n^h(t)] = 0 , \quad \Leftrightarrow \quad (t^2 \partial_t^2 + t \partial_t + t^2 (x_n^h)^2 - \beta^2) \frac{\chi_n^h(t)}{t} = 0 , \quad (2.68)$$

apply further for the KK Higgs profiles. The general solution to the equations of motion reads

$$\chi_n^h(t) = N_n t [J_\beta(x_n t) - r_n Y_\beta(x_n t)] , \quad (2.69)$$

and by applying the UV boundary condition, one finds again that  $r_n \propto \epsilon^{2\beta}$  is negligibly small in most areas of the extra dimension, except of the region  $t \sim \epsilon$ . Including the normalization condition, one can further derive

$$\chi_n^h(t) = \sqrt{\frac{L}{\pi}} \frac{t J_\beta(x_n t)}{\sqrt{J_\beta^2(x_n) - J_{\beta+1}(x_n) J_{\beta-1}(x_n)}} . \quad (2.70)$$

The boundary condition on the IR brane determines an eigenvalue equation for the masses of the scalar KK modes, reading [2]

$$\frac{x_n J_{\beta+1}(x_n)}{J_\beta(x_n)} = 2(m_{IR} - 2 - \beta) = 2\delta , \quad (2.71)$$

where  $\delta = m_{IR} - 2 - \beta$  has been introduced before. The parameter  $\delta$  is important in finding the solution to the gauge hierarchy problem in the bulk-Higgs RS model, since it determines

the amount of the Higgs vev, and the mass of the zero-mode Higgs boson as the lightest Higgs resonance. A little hierarchy problem remains, however, because a natural parameter  $\delta$  of  $\mathcal{O}(1)$  would imply a Higgs vev and zero-mode mass of the order of the KK mass scale  $M_{KK}$ , which cannot be less than a few TeV, empirically. Instead, one has to assume that

$$\delta = m_{IR} - 2 - \beta \ll 1 \quad (2.72)$$

in order to obtain a realistic Higgs vev and zero-mode mass,  $m_h, v \ll M_{KK}$  [2]. With this adaptation, one can expand the relation (2.71) in a power series of  $\delta$ , and finds

$$x_0^2 = \frac{m_h^2}{M_{KK}^2} = 4(1 + \beta)\delta \left[ 1 - \frac{\delta}{2 + \beta} + \frac{2\delta^2}{(2 + \beta)^2(3 + \beta)} + \dots \right]. \quad (2.73)$$

With  $M_{KK} = 2$  TeV, for example, one needs  $(1 + \beta)\delta \approx 10^{-3}$ . In this sense, we see that the enormous amount of a fine-tuning, needed in the SM to compute the physical Higgs mass, is drastically reduced in the bulk-Higgs RS model. For that reason, the model can be considered as a suitable approach of new physics to the gauge hierarchy problem. An approximate solution for the zero-mode Higgs profile, given in (2.70), for  $m_h \ll M_{KK}$ , reads

$$\chi_0^h(t) = t^{1+\beta} \sqrt{\frac{L(1 + \beta)}{\pi}} \left[ 1 + \frac{m_h^2}{4M_{KK}^2} \left( \frac{1}{(2 + \beta)} - \frac{t^2}{(1 + \beta)} \right) \right] + \mathcal{O}\left(\frac{m_h^4}{M_{KK}^4}\right), \quad (2.74)$$

where we have skipped terms with powers of  $\epsilon$ . This approximate solution will be used in the subsequent calculations of the thesis. As a last step, one can relate the parameter  $\lambda$  to the physical value  $\lambda_4$  of the Higgs self coupling. For that purpose, one can consider the four-dimensional, effective Lagrangian for the zero-mode Higgs field to the lowest order in  $v^2/M_{KK}^2$ ,

$$\mathcal{L}_{\text{Higgs}} \ni \frac{1}{2} \partial_\mu h^{(0)}(x) \partial^\mu h^{(0)}(x) - \frac{m_h^2}{2} h^{(0)}(x)^2 - v \frac{4L}{\pi} (1 + \beta)^2 \lambda h^{(0)}(x)^3 - \frac{L}{\pi} (1 + \beta)^2 \lambda h^{(0)}(x)^4, \quad (2.75)$$

which has been obtained by an integration over the extra dimension. By comparing it to the corresponding SM Lagrangian

$$\mathcal{L}_{SM} \ni -\frac{m_h^2}{2} h^2 - v_{SM} \lambda_{SM} h^3 - \frac{\lambda_{SM}}{4} h^4, \quad (2.76)$$

where  $m_h^2 = 2\lambda_{SM} v_{SM}^2$ , one can derive from either of these terms the following relation to the leading order [2]

$$\lambda_{SM} \approx \lambda_4 \approx \frac{4L}{\pi} (1 + \beta)^2 \lambda. \quad (2.77)$$

The relation between  $\lambda_{SM}$  and  $\lambda_4$  receives higher-order corrections in  $v^2/M_{KK}^2$ , depending on which of the three couplings is used to perform the matching [2].

The electroweak gauge fields are described as the gauge eigenstates in the Lagrangian (2.51). As usual, one can perform the following field redefinitions for the mass eigenstates after electroweak symmetry breaking [154]

$$W_M^\pm = \frac{1}{\sqrt{2}} (A_M^1 \mp iA_M^2), \quad A_M = s_W A_M^3 + c_W B_M, \quad Z_M = c_W A_M^3 - s_W B_M, \quad (2.78)$$

where

$$s_w = \frac{g'_5}{\sqrt{g_5^2 + g'^2_5}}, \quad c_w = \frac{g_5}{\sqrt{g_5^2 + g'^2_5}}. \quad (2.79)$$

Here,  $g_5$  and  $g'_5$  are the five-dimensional gauge couplings belonging to the groups  $SU(2)_L$  and  $U(1)_Y$ , respectively. To the leading order, they are related to the four-dimensional gauge couplings of the SM by the relation  $g_5 = \sqrt{2\pi r} g_4$  [162]. We define the five-dimensional gauge boson masses as

$$M_W = \frac{g_5 v}{2}, \quad M_Z = \frac{M_W}{c_w}. \quad (2.80)$$

From the four-dimensional point of view, the five-dimensional gauge bosons can be decomposed into a four-dimensional vector part with the Lorentz index  $\mu$  and a scalar part, where we choose [3, 150]

$$A_M = A_\mu + ktA_t, \quad (2.81)$$

with  $A = W^\pm, A, Z, \mathcal{G}$ . Both parts individually decompose in the KK decompositions. For the vector parts, the decompositions read [3, 150]

$$A_\mu(x, t) = \frac{1}{\sqrt{r}} \sum_{n=0}^{\infty} \chi_n^A(t) A_\mu^{(n)}(x), \quad W_\mu^\pm(x, t) = \frac{1}{\sqrt{r}} \sum_{n=0}^{\infty} \chi_n^W(t) W_\mu^{\pm(n)}(x), \quad (2.82)$$

where similar expansions can be chosen for the Z-bosons and the gluons. In the bulk-Higgs RS model, the decompositions for the scalar parts are included in the definitions of Goldstone bosons and new, physical scalars, as will be presented in the next section. The profile functions of the KK gauge bosons form complete sets of even functions on the orbifold. The normalization conditions,

$$\frac{2\pi}{L} \int_{\epsilon}^1 \frac{dt}{t} \chi_m^{[A]}(t) \chi_n^{[A]}(t) = \delta_{mn}, \quad (2.83)$$

apply, with  $[A] = A, W, Z, \mathcal{G}$ , in order for the action to be compatible to the four-dimensional kinetic terms of the SM fields. To obtain canonical, four-dimensional mass terms, the profiles have to follow the equations of motion [154, 157–159, 163],

$$\left[ \partial_t^2 - \frac{1}{t} \partial_t - \frac{M_{[A]}^2}{2M_{KK}^2} k(1 + \beta)t^{2+2\beta} + (x_n^{[A]})^2 \right] \chi_n^{[A]}(t) = 0, \quad \text{with } [A] = W, Z, \quad (2.84)$$

$$\left[ \partial_t^2 - \frac{1}{t} \partial_t + (x_n^{[A]})^2 \right] \chi_n^{[A]}(t) = 0, \quad \text{with } [A] = A, \mathcal{G},$$

which define the profiles and masses  $m_n^{[A]}$  of the KK gauge bosons. In order to ensure the existence of zero modes, Neumann boundary conditions are chosen for the profiles at the branes [154]

$$\partial_t \chi_n^{[A]}(t) \Big|_{t=\epsilon, 1} = 0, \quad (2.85)$$

with  $[A] = A, W, Z, \mathcal{G}$ . Due to  $U(1)_{\text{em}}$ -gauge invariance, the zero-mode photon has to be massless,  $m_0^A = 0$ , resulting in a constant profile function along the extra dimension [162],

$$\chi_0^A(t) = \frac{1}{\sqrt{2\pi}}. \quad (2.86)$$

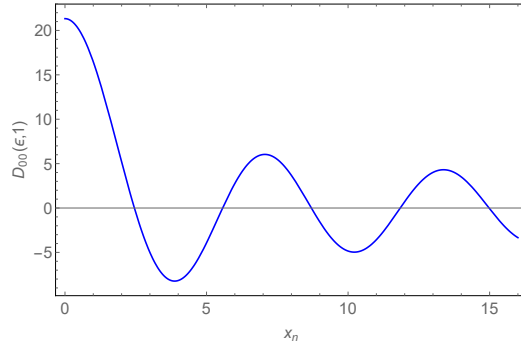


Figure 2.5: Plot of  $D_{00}(\epsilon, 1)$  from (2.90) in dependence of  $x_n = m_n/M_{KK}$ .

This applies also for the case of the zero-mode gluon. Instead, for the zero-mode profiles of the massive gauge bosons, one can solve the equations of motion by applying an expansion in powers of  $m_W^2/M_{KK}^2$ ,

$$\chi_0^W(t) = \frac{1}{\sqrt{2\pi}} \left( 1 + \frac{m_W^2}{M_{KK}^2} \left[ \frac{t^2}{2} \left( \frac{1}{2} - \ln(t) \right) + \frac{Lt^{4+2\beta}}{4+2\beta} - \frac{Lt^2}{2} + \frac{1}{4} - \frac{1}{(4+2\beta)^2} - \frac{1}{4L} + \dots \right] \right), \quad (2.87)$$

where terms of the order of  $\epsilon^2$  and smaller are neglected, and for the Z boson profile, one has to replace  $W \rightarrow Z$ , accordingly. In the profile here, the relation  $m_W^2 = \tilde{m}_W^2$  has been applied that holds to the lowest order between the physical mass of the W boson and the parametric mass  $\tilde{m}_W = \frac{g_5 v}{2\sqrt{2\pi r}}$ , predicted by the IR boundary condition. Higher order corrections to that relation can be derived by determining the W boson profile up to the order  $\mathcal{O}(m_W^2/M_{KK}^4)$ , and by applying the IR boundary condition on that result, where one can find

$$m_W^2 = \tilde{m}_W^2 \left( 1 - \frac{\tilde{m}_W^2}{2M_{KK}^2} \left[ \frac{2L(1+\beta)^2}{(2+\beta)(3+2\beta)} - \frac{(1+\beta)(3+\beta)}{(2+\beta)^2} + \frac{1}{2L} \right] + \dots \right). \quad (2.88)$$

For the Z boson mass, one has to replace  $m_W \rightarrow m_Z$ , and  $\tilde{m}_W \rightarrow \tilde{m}_Z = \frac{\sqrt{(g_5^2 + g_5'^2)v}}{2\sqrt{2\pi r}}$ .

For the higher KK states  $n \geq 1$ , the general solution for the profiles of the gluons or photons, defined by the second equation of (2.84), reads

$$\chi_n^{[A]}(t) = t [C_1 J_1(x_n t) + C_2 Y_1(x_n t)], \quad (2.89)$$

which is a combination of Bessel functions. From the UV boundary conditions, we find that  $C_1 = -C_2 Y_0(\epsilon x_n)/J_0(\epsilon x_n)$ , so that the IR boundary condition gives

$$D_{00}(\epsilon, 1) \equiv Y_0(x_n)J_0(\epsilon x_n) - J_0(x_n)Y_0(\epsilon x_n) \stackrel{!}{=} 0, \quad (2.90)$$

which determines the mass eigenvalues  $x_n = m_n/M_{KK}$  for the KK gluons or photons. The remaining constant  $C_2$ , defined by the normalization condition in (2.83), drops out here. Now, we can numerically solve for the roots of  $D_{00}(\epsilon, 1)$ , and we get:

$$D_{00}(\epsilon, 1) \stackrel{!}{=} 0, \quad \Rightarrow \quad x_n \approx 2.45, 5.57, 8.70, 11.84, \dots \quad (2.91)$$



These roots can also be observed from Figure 2.5, where the course of  $D_{00}(\epsilon, 1)$  is plotted in dependence of  $x_n$ . The lightest KK mass state of the RS model, which is the KK gluon or photon, lies at  $m_1 \approx 2.45 M_{KK}$ , accordingly [162]. This result is valid independently of the Higgs localization in the extra dimension, because the gluon and the photon do not directly couple to the Higgs field, and the differential equation in the second row of (2.84) does not have any dependence on the Higgs field.

The extended scalar sector of the bulk-Higgs RS model has been studied for example in [154, 157, 158, 163], and below we follow the presentation from [154]. In the RS model, one has to enlarge the usual gauge-fixing Lagrangian of the SM in order to remove all the mixing terms between the four-dimensional vector gauge fields and their scalar correspondents. For the W bosons, the following form can be chosen, in this connection,

$$\begin{aligned} \mathcal{L}_{GF} = & -\frac{r}{\xi} \left[ \partial_\mu W^{\mu+} - \xi \left( M_{KK}^2 t \partial_t \left( \frac{W_t^+}{t} \right) + M_W \frac{v(t)}{vr} \varphi^+ \right) \right] \\ & \cdot \left[ \partial_\mu W^{\mu-} - \xi \left( M_{KK}^2 t \partial_t \left( \frac{W_t^-}{t} \right) + M_W \frac{v(t)}{vr} \pi^- \right) \right]. \end{aligned} \quad (2.92)$$

The terms for the photons, Z bosons and  $\varphi^3$  [154] are skipped here, as these terms are not explicitly needed in this thesis. The Goldstone bosons of the model are defined as those linear combinations of scalar fields that are multiplied by the gauge parameter  $\xi$ ,

$$G^\pm = M_{KK}^2 t \partial_t \left( \frac{W_t^\pm}{t} \right) + M_W \frac{v(t)}{vr} \varphi^\pm. \quad (2.93)$$

Then, the gauge-fixing Lagrangian adopts a form similar to the SM. By means of a variational principle, one obtains the following equations of motion for the fields  $W_t^\pm$  and  $\varphi^\pm$  [154]

$$\square_4 W_t^\pm + M_W^2 \frac{v(t)^2}{v^2 r} W_t^\pm + M_W \frac{v(t)^2}{v^2 r} \partial_t \left( \frac{v}{v(t)} \varphi^\pm \right) - \xi \partial_t G^\pm = 0, \quad (2.94)$$

$$\begin{aligned} \square_4 \varphi^\pm - M_{KK}^2 t \partial_t (t^{-3} \partial_t [t \varphi^\pm]) - M_W M_{KK}^2 \frac{v}{v(t)} t \partial_t \left( \frac{v(t)^2}{v^2 t} W_t^\pm \right) + \epsilon^2 t^{-2} \mu^2 \varphi^\pm \\ + \xi M_W \frac{v(t)}{v} G^\pm = 0. \end{aligned} \quad (2.95)$$

These equations allow to define the new, charged physical scalar fields,

$$\phi^\pm = M_{KK} \left( W_t^\pm + (M_W)^{-1} \partial_t \left[ \frac{v}{v(t)} \varphi^\pm \right] \right), \quad (2.96)$$

following the demand that their mass terms in (2.94) should be independent of the gauge. In order to check the definitions, one can add  $M_{KK}^2 t \partial_t (t^{-1} (2.94))$  to  $M_W \frac{v(t)}{vr} (2.95)$ , and one can use the relation  $\mu^2 = k^2(\beta^2 - 4)$  from equation (2.60). In this way, one derives the equations of motion for the charged Goldstone bosons  $G^\pm$  [154], as

$$\square_4 G^\pm - \xi M_{KK}^2 t \partial_t \left( \frac{\partial_t G^\pm}{t} \right) + \xi M_W^2 \frac{v(t)^2}{v^2 r} G^\pm = 0, \quad (2.97)$$

which can be compared with the equations of motion for the gauge boson profiles in (2.84). One can identify the mass term for the KK modes in (2.84) with minus times the term with the box operator in (2.97). Then, one can observe that the Goldstone bosons and their KK excitations have similar profiles as the gauge bosons, and their masses are related by

$$(m_n^G)^2 = \xi(m_n^W)^2 . \quad (2.98)$$

This confirms that the Gauge-Goldstone equivalence theorem is fulfilled [154]. The equations of motion for the charged physical scalars  $\phi^\pm$  can analogously be derived by adding  $M_{KK}(2.94)$  to  $\frac{M_{KK}}{M_W} \partial_t \left[ \frac{v}{v(t)}(2.95) \right]$ , yielding [154, 157, 158, 163]

$$\square_4 \phi^\pm - M_{KK}^2 \partial_t \left( t^{-1-2\beta} \partial_t \left[ t^{1+2\beta} \phi^\pm \right] \right) + M_W^2 \frac{v(t)^2}{v^2 r} \phi^\pm = 0 . \quad (2.99)$$

We choose the KK decompositions for the charged Goldstone bosons and physical scalars as follows

$$G^\pm(x, t) = \sum_{n=0}^{\infty} m_n^W \frac{1}{\sqrt{r}} \chi_n^{G^\pm}(t) G^{\pm(n)}(x) , \quad \phi^\pm(x, t) = \frac{v}{M_W v(t)} \sum_{n=1}^{\infty} m_n^{\phi^\pm} \chi_n^{\phi^\pm}(t) \phi^{\pm(n)}(x) . \quad (2.100)$$

Similar to the SM, the Goldstone bosons  $G^{\pm(n)}(x)$  form the longitudinal degrees of freedom of the W bosons and their KK excitations. The profiles follow the same equations of motion as the gauge boson profiles in equation (2.84). The equations of motion for the profiles of the physical scalars read

$$\frac{m_n^{(\phi^\pm)^2}}{M_{KK}^2} \chi_n^{\phi^\pm}(t) + t^{1+\beta} \partial_t \left( t^{-1-2\beta} \partial_t \left[ t^\beta \chi_n^{\phi^\pm}(t) \right] \right) - \frac{M_W^2}{M_{KK}^2} \frac{v(t)^2}{v^2 r} \chi_n^{\phi^\pm}(t) = 0 , \quad (2.101)$$

where the boundary conditions [154]

$$\chi_n^{\phi^\pm}(t) \Big|_{t=\epsilon, 1} = 0 \quad (2.102)$$

are chosen to ensure that the decompositions of the scalars do not have zero modes. Such zero modes are excluded empirically. The profiles have to fulfil the normalization conditions

$$\frac{2\pi}{L} \int_\epsilon^1 \frac{dt}{t} \chi_m^{G^\pm}(t) \chi_n^{G^\pm}(t) = \delta_{mn} , \quad \frac{2\pi}{L} \int_\epsilon^1 \frac{dt}{t} \chi_m^{\phi^\pm}(t) \chi_n^{\phi^\pm}(t) = \delta_{mn} , \quad (2.103)$$

in order to derive proper kinetic terms for the four-dimensional scalars  $\phi^{\pm(n)}(x)$  and Goldstone bosons  $G^{\pm(n)}(x)$ . We can invert the KK decompositions for the Goldstone bosons and scalars in equation (2.100) by using the equations of motion to obtain the KK decompositions for the fields  $\varphi^\pm$  and  $W_t^\pm$

$$\begin{aligned} \varphi^\pm &= \sum_{n=0}^{\infty} \left[ \frac{M_W}{m_n^W} \frac{v(t)}{v \sqrt{r}} \chi_n^{G^\pm}(t) G^{\pm(n)}(x) - \frac{M_{KK}}{m_n^{\phi^\pm}} t^{-\beta} \partial_t \left( t^\beta \chi_n^{\phi^\pm}(t) \right) \phi^{\pm(n)}(x) \right] , \\ W_t^\pm &= \sum_{n=0}^{\infty} \left[ -\frac{1}{\sqrt{r} m_n^W} \partial_t \left( \chi_n^{G^\pm}(t) \right) G^{\pm(n)}(x) + \frac{v(t)}{v r M_{KK}} \frac{M_W}{m_n^{\phi^\pm}} \chi_n^{\phi^\pm}(t) \phi^{\pm(n)}(x) \right] . \end{aligned} \quad (2.104)$$

In this sense, a framework with a bulk-Higgs field results in different physical predictions for the scalar field content, compared to a brane-Higgs framework. One combination of the fifth components of the gauge fields  $A_t$  and the Goldstone bosons in the decomposition of the Higgs field  $\varphi_i$  remains physical, and gets an explicit, gauge-independent mass term. In this way, additional physical scalars are predicted in the bulk-Higgs RS model, whose corresponding KK modes are physical fields and do not decouple in the limit of the unitary gauge where  $\xi \rightarrow \infty$  [164]. In addition, a second combination of the  $A_t$ 's and  $\varphi_i$ 's provides the longitudinal degrees of freedom for the vector gauge bosons in the KK towers, and disappears in the unitary gauge, which are the ‘‘unphysical’’ Goldstone bosons. Altogether, taking into account the Z-bosons, photons, and the corresponding scalar fields, three KK towers of physical scalars are predicted, which do not contain zero modes, and four KK towers of Goldstone bosons are predicted, where three of which contain zero modes.

### 2.2.2 Fermion sector

The Lagrangian (2.53) defines the fermion sector of our system, where in the sum the index  $f$  runs over  $f = Q, L, u, d, e$ . Here,  $Q = (U, D)^T$  and  $L = (\mathcal{V}, E)^T$  are doublet fields under  $SU(2)_L$ , and  $u, d, e$  are singlet fields, where each of which are three-component vectors in generation space [154]. The five-dimensional Lie algebra can only be fulfilled by irreducible four-dimensional representations, causing the left-handed and right-handed KK fermions to **identically** transform under the five-dimensional  $SU(2)_L$ -gauge transformations. This is the reason why one includes  $SU(2)_L$  doublet and singlet fields of both left-handed and right-handed chiralities in the model, in contrary to the SM [150, 155, 156]. Only the left-handed doublet fermions and the right-handed singlet fermions have even  $Z_2$ -parities, and have zero modes in the KK decompositions. So, the SM fermion content is guaranteed in the lower energy range. In the following, we use a compact notation, where we collect the left- and right-handed components of the up- and down-type quarks and leptons into the six component vectors [2, 5]

$$\mathcal{F}_A(x, t) = \frac{\sqrt{r}\epsilon^2}{t^2} \begin{pmatrix} F_A(x, t) \\ f_A(x, t) \end{pmatrix}, \quad (2.105)$$

with  $\mathcal{F} = \mathcal{U}, \mathcal{D}, \mathcal{E}$ , and  $A = L, R$ ,  $F = U, D, E$ , and  $f = u, d, e$ . The KK decompositions for the fermions are chosen as follows [2, 5]

$$\begin{aligned} \mathcal{F}_L(x, t) &= \sqrt{\frac{L\epsilon}{2\pi}} \sum_{n=1}^{\infty} \mathcal{F}_L^{(n)}(t) f_L^{(n)}(x) = \sum_{n=1}^{\infty} \begin{pmatrix} \mathbf{C}_n^F(t) a_n^F \\ \mathbf{S}_n^f(t) a_n^f \end{pmatrix} f_L^{(n)}(x), \\ \mathcal{F}_R(x, t) &= \sqrt{\frac{L\epsilon}{2\pi}} \sum_{n=1}^{\infty} \mathcal{F}_R^{(n)}(t) f_R^{(n)}(x) = \sum_{n=1}^{\infty} \begin{pmatrix} \mathbf{S}_n^F(t) a_n^F \\ \mathbf{C}_n^f(t) a_n^f \end{pmatrix} f_R^{(n)}(x). \end{aligned} \quad (2.106)$$

The index  $n$  of the KK decompositions labels the different mass eigenstates in the four-dimensional, effective theory, so that  $n = 1, 2, 3$  refer to the SM quarks and leptons, whereas  $n = 4, \dots, 9$  label the six fermion modes of the first KK level, and so on. The profiles have to follow the normalization conditions [150]

$$\int_{\epsilon}^1 dt \mathcal{F}_A^{(m)\dagger}(t) \mathcal{F}_A^{(n)}(t) = \delta_{mn}, \quad A = L, R, \quad (2.107)$$

in order to obtain four-dimensional kinetic terms for the KK fermions that are compatible to the SM. The functions  $\mathbf{C}_n^{[F,f]}(t)$  and  $\mathbf{S}_n^{[F,f]}(t)$ , with  $F = Q, L$ , and  $f = u, d, e$ , are diagonal,  $3 \times 3$  matrices in the flavour space [150]. The three-component vectors  $a_n^{[F,f]}$  describe the flavour-mixings of the five-dimensional interaction eigenstates into the four-dimensional mass eigenstates, generated by the Yukawa interactions [150]. For the zero-mode fields, with  $n = 1, 2, 3$ , the rescaled vectors  $\hat{a}_n^{[F,f]} \equiv \sqrt{2}a_n^{[F,f]}$  obey to single normalization conditions

$$\hat{a}_n^{[F,f]\dagger} \hat{a}_n^{[F,f]} = 1, \quad (2.108)$$

where the vectors belonging to different  $n$  are orthogonal to each other. In order to obtain canonical, four-dimensional mass terms, the fermion profiles have to fulfil the following equations of motion [2, 5, 150]

$$\begin{aligned} \frac{d}{dt} \mathcal{F}_L^{(n)}(t) &= -x_n \mathcal{F}_R^{(n)}(t) + \mathcal{M}_f(t) \mathcal{F}_L^{(n)}(t), \\ -\frac{d}{dt} \mathcal{F}_R^{(n)}(t) &= -x_n \mathcal{F}_L^{(n)}(t) + \mathcal{M}_f(t) \mathcal{F}_R^{(n)}(t), \end{aligned} \quad (2.109)$$

where  $x_n = m_{f_n}/M_{KK}$  are the mass eigenvalues, and

$$\mathcal{M}_f(t) = \frac{1}{t} \begin{pmatrix} \mathbf{c}_F & \mathbf{0} \\ \mathbf{0} & -\mathbf{c}_f \end{pmatrix} + \frac{v\sqrt{k(1+\beta)}}{\sqrt{2}M_{KK}} t^{1+\beta} \begin{pmatrix} \mathbf{0} & \mathbf{Y}_f^{5D} \\ \mathbf{Y}_f^{5D\dagger} & \mathbf{0} \end{pmatrix} \quad (2.110)$$

is the generalized mass matrix for a scenario with a bulk-Higgs field [2]. At this point, we introduce the matrices  $\mathbf{c}_{F,f}$ , which contain the dimensionless  $c$ -parameters  $c_{F_i} \equiv +M_{F_i}/k$  and  $c_{f_i} \equiv -M_{f_i}/k$ . Without loss of generality, these matrices can be taken to be diagonal [150]. The five-dimensional Yukawa matrices  $\mathbf{Y}_f^{5D}$  have the mass dimension  $-1/2$ . The dimensionless Yukawa matrices  $\mathbf{Y}_f$  are defined by [2]

$$\mathbf{Y}_f \equiv \frac{\sqrt{k(1+\beta)}}{(2+\beta)} \mathbf{Y}_f^{5D}, \quad (2.111)$$

which are assumed to have a non-hierarchical structure in contrast to the SM. Their entries are random complex elements of the same magnitude, bounded by a maximally allowed entry  $y_\star$ , so that

$$|(Y_f)_{ij}| \leq y_\star \quad (2.112)$$

applies. The observed hierarchies in the zero-mode fermion sector are explained by a geometrical realization of the Froggatt-Nielsen mechanism, as it will be explained in the next section [150, 153, 154, 157, 165–167]. In brane-Higgs or very narrow bulk-Higgs scenarios, the upper bound on the entries  $y_\star$  should not be greater than 3, following the demand that the one loop corrections to the Yukawa couplings have to remain perturbative [2, 153, 159]. Instead, for a bulk-Higgs framework with a small  $\beta$  parameter, the bound can be slightly relaxed to higher values [154]. However, there is no firm theoretical reason why  $y_\star$  should take values very close to the perturbativity bound, and in this sense, we choose the values  $y_\star = 1, 2, 3$  in our subsequent numerical analyses. The boundary conditions for the fermion profiles imply that the profiles that correspond to KK decompositions without zero modes vanish on the two branes [2, 5, 150],

$$(\mathbf{0} \quad \mathbf{1}) \mathcal{F}_L^{(n)}(t_i) = 0, \quad (\mathbf{1} \quad \mathbf{0}) \mathcal{F}_R^{(n)}(t_i) = 0, \quad (2.113)$$

for  $t_i = \{\epsilon, 1\}$ . From these conditions and the equations of motion, one can derive the approximate zero-mode fermion profiles, valid up to the order  $v^2/M_{KK}^2$  [155, 156, 168], as follows

$$\begin{aligned} F_L^{(0)}(t) &= \begin{pmatrix} t^{c_{F_i}} F(c_{F_i}) \hat{a}_i^F \\ \frac{v}{M_{KK}} \left[ -\frac{m_{f_0}}{v(1+2c_{f_i})} (t^{1+c_{f_i}} - t^{-c_{f_i}} \epsilon^{1+2c_{f_i}}) F(c_{f_i}) \hat{a}_i^f + t^{2+\beta+c_{F_j}} \frac{\tilde{Y}_{f,ij}^\dagger}{\sqrt{2}} F(c_{F_j}) \hat{a}_j^F \right] \end{pmatrix}, \\ F_R^{(0)}(t) &= \begin{pmatrix} \frac{v}{M_{KK}} \left[ \frac{m_{f_0}}{v(1+2c_{F_i})} (t^{1+c_{F_i}} - t^{-c_{F_i}} \epsilon^{1+2c_{F_i}}) F(c_{F_i}) \hat{a}_i^F - t^{2+\beta+c_{F_j}} \frac{\tilde{Y}_{f,ij}}{\sqrt{2}} F(c_{F_j}) \hat{a}_j^f \right] \\ t^{c_{f_i}} F(c_{f_i}) \hat{a}_i^f \end{pmatrix}, \end{aligned} \quad (2.114)$$

where we have defined the abbreviations

$$F(c_{[F,f]}) = \sqrt{\frac{1+2c_{[F,f]}}{1-\epsilon^{1+2c_{[F,f]}}}}, \quad \tilde{Y}_{f,ij} = \frac{(2+\beta)Y_{f,ij}}{(2+\beta+c_{F_i}+c_{F_j})}. \quad (2.115)$$

$F(c_{[F,f]})$  is usually named the ‘‘zero-mode profile’’ [150, 155, 156]. Using these approximate profiles, the IR boundary conditions determine the following eigenvalue equations

$$m_{f_n} \hat{a}_n^f = \frac{v}{\sqrt{2}} \tilde{\mathbf{Y}}_f^{\dagger \text{eff}} \hat{a}_n^F, \quad m_{f_n} \hat{a}_n^F = \frac{v}{\sqrt{2}} \tilde{\mathbf{Y}}_f^{\text{eff}} \hat{a}_n^f, \quad (2.116)$$

where we define

$$\tilde{\mathbf{Y}}_{f,ij}^{\text{eff}} = F(c_{F_i}) \tilde{Y}_{f,ij} F(c_{F_j}). \quad (2.117)$$

These can be combined to the equalities [150]

$$\left( m_{f_n}^2 \mathbf{1} - \frac{v^2}{2} \tilde{\mathbf{Y}}_f^{\text{eff}} \tilde{\mathbf{Y}}_f^{\text{eff}\dagger} \right) \hat{a}_n^F = 0, \quad \left( m_{f_n}^2 \mathbf{1} - \frac{v^2}{2} \tilde{\mathbf{Y}}_f^{\text{eff}\dagger} \tilde{\mathbf{Y}}_f^{\text{eff}} \right) \hat{a}_n^f = 0. \quad (2.118)$$

To the lowest order, the mass eigenvalues  $m_{f_n}$  are the solutions to the equation

$$\det \left( m_{f_n}^2 \mathbf{1} - \frac{v^2}{2} \tilde{\mathbf{Y}}_f^{\text{eff}} \tilde{\mathbf{Y}}_f^{\text{eff}\dagger} \right) = 0. \quad (2.119)$$

One can see that the  $\hat{a}_n^{[F,f]}$  are the eigenvectors of the matrices  $\tilde{\mathbf{Y}}_f^{\text{eff}} \tilde{\mathbf{Y}}_f^{\text{eff}\dagger}$  and  $\tilde{\mathbf{Y}}_f^{\text{eff}\dagger} \tilde{\mathbf{Y}}_f^{\text{eff}}$  (with  $n = 1, 2, 3$  and  $F = U, D, E$ ;  $f = u, d, e$ ). Moreover, they form the columns of the unitary matrices  $\mathbf{U}_f$  and  $\mathbf{W}_f$  appearing in the singular-value decomposition [150],

$$\tilde{\mathbf{Y}}_f^{\text{eff}} = \mathbf{U}_f \lambda_f \mathbf{W}_f^\dagger, \quad (2.120)$$

where

$$\lambda_u = \frac{\sqrt{2}}{v} \text{diag}(m_u, m_c, m_t), \quad \lambda_d = \frac{\sqrt{2}}{v} \text{diag}(m_d, m_s, m_b), \quad \lambda_e = \frac{\sqrt{2}}{v} \text{diag}(m_e, m_\mu, m_\tau). \quad (2.121)$$

With the help of the redefinitions (2.105), (2.106) and (2.111), the Yukawa interactions of the Higgs boson with up- and down-type quarks and leptons can be written in the form [2, 5]

$$\mathcal{L}_{hff} = - \sum_{f=u,d,e} \sum_{m,n=1}^{\infty} g_{mn}^f h^{(0)}(x) \bar{f}_L^{(m)}(x) f_R^{(n)}(x) + \text{h.c.} , \quad (2.122)$$

where

$$\begin{aligned} g_{mn}^f &= \frac{(2+\beta)}{\sqrt{2}} \int_{\epsilon}^1 dt \sqrt{\frac{\pi}{L(1+\beta)}} \chi_0^h(t) \mathcal{F}_L^{(m)\dagger}(t) \begin{pmatrix} \mathbf{0} & \mathbf{Y}_f \\ \mathbf{Y}_f^\dagger & \mathbf{0} \end{pmatrix} \mathcal{F}_R^{(n)}(t) \\ &= \sqrt{\frac{2\pi}{L(1+\beta)}} \frac{(2+\beta)\pi}{L\epsilon} \int_{\epsilon}^1 dt \chi_0^h(t) \left[ a_m^{F\dagger} \mathbf{C}_m^F(t) \mathbf{Y}_f \mathbf{C}_n^f(t) a_n^f + a_m^{f\dagger} \mathbf{S}_m^f(t) \mathbf{Y}_f^\dagger \mathbf{S}_n^F(t) a_n^F \right] . \end{aligned} \quad (2.123)$$

The function  $\chi_0^h(t)$  denotes the zero-mode Higgs profile along the extra dimension, as given in (2.74). In the calculations of the Higgs processes in this thesis, only KK diagonal Higgs couplings to fermions with  $m = n$  will contribute. In general, even the diagonal Yukawa couplings are complex numbers, in contrast to the SM. A second term is induced in the Lagrangian of the Yukawa interactions [5],

$$\mathcal{L}_{hff}^{\text{diag}} = - \sum_{f=u,d,e} \sum_{n=1}^{\infty} \left[ \text{Re}(g_{nn}^f) h^{(0)}(x) \bar{f}^{(n)}(x) f^{(n)}(x) + i \text{Im}(g_{nn}^f) h^{(0)}(x) \bar{f}^{(n)}(x) \gamma_5 f^{(n)}(x) \right] , \quad (2.124)$$

given by the imaginary part of the Yukawa couplings  $g_{nn}^f$ . This term creates contributions to Higgs processes with an odd behaviour under the CP symmetries that are not present in the SM.

### 2.2.3 Higgs sector on or very close to the IR brane

In this section, we describe the basic ingredients of a framework with a brane-localized Higgs field in the RS model. We consider the five-dimensional Lagrangian [150]

$$\frac{2\pi r}{L} \int_{\epsilon}^1 dt \frac{\epsilon^4}{t^4} (\mathcal{L}_{W,B} + \mathcal{L}_{\text{Higgs}} + \mathcal{L}_{GF} + \mathcal{L}_{FP} + \mathcal{L}_{\text{fermion}}) , \quad (2.125)$$

where the kinetic terms of the gauge bosons are similar as before

$$\mathcal{L}_{W,B} = G^{KM} G^{LN} \left( -\frac{1}{4} W_{KL}^a W_{MN}^a - \frac{1}{4} B_{KL} B_{MN} \right) , \quad (2.126)$$

and the brane-localized Higgs Lagrangian reads

$$\mathcal{L}_{\text{Higgs}} = \frac{k}{2} \delta(t-1) [G^{\mu\nu} (D_\mu \Phi)^\dagger D_\nu \Phi - V(\Phi)] , \quad V(\Phi) = -\mu^2 \Phi^\dagger \Phi + \lambda (\Phi^\dagger \Phi)^2 , \quad (2.127)$$

with the Yukawa terms

$$\mathcal{L}_{\text{Yukawa}} = \frac{k}{2} \delta(t-1) [\bar{Q} \mathbf{Y}_d^{5D} \Phi d + \bar{Q} \mathbf{Y}_u^{5D} \epsilon \Phi^\dagger u + \bar{L} \mathbf{Y}_e^{5D} \Phi e + \text{h.c.}] . \quad (2.128)$$

The Higgs field can be decomposed as

$$\Phi(x) = \frac{1}{\sqrt{2}\epsilon} \begin{pmatrix} -i\sqrt{2}\varphi^+(x) \\ v + h(x) + i\varphi^3(x) \end{pmatrix}, \quad (2.129)$$

where the factor  $\frac{1}{\epsilon}$  is extracted to obtain a canonical kinetic term for the Higgs boson,

$$\mathcal{L}_{\text{Higgs}} = \int_{\epsilon}^1 dt \delta(t-1) \left( \frac{1}{2} \partial^\mu h \partial_\mu h + \frac{\mu^2 \epsilon^2}{2} (v+h)^2 - \frac{\lambda}{4} (v+h)^4 \right). \quad (2.130)$$

Then, the vev is  $v = \frac{\epsilon\mu}{\sqrt{\lambda}} \approx 246$  GeV, and  $\varphi^\pm = (\varphi^1 \mp i\varphi^2)/\sqrt{2}$  is defined as usual. We see that the Higgs mass parameter  $\mu$  can have a high value at the Planck scale, and gets suppressed in the Lagrangian, whereas the parameter  $\lambda$  is of  $\mathcal{O}(1)$ . Then, the covariant derivative, acting on the Higgs field, reads

$$D_\mu \Phi = \frac{1}{\sqrt{2}\epsilon} \begin{pmatrix} -i\sqrt{2} (\partial_\mu \varphi^+ + M_W W_\mu^+) \\ \partial_\mu h + i (\partial_\mu \varphi^3 + M_Z Z_\mu) \end{pmatrix} + \text{terms bi-linear in fields}, \quad (2.131)$$

where the gauge boson masses are defined as before. Again, we can decompose the five-dimensional gauge boson fields as  $A_M = A_\mu + ktA_t$ . In order to remove the terms that mix the vector gauge bosons and the scalar components  $W_t^\pm$ ,  $Z_t$  and  $A_t$ , one has to include the following gauge-fixing Lagrangian [150]

$$\begin{aligned} \mathcal{L}_{GF} = & -\frac{t^4}{2\xi\epsilon^4} \left[ \left( \partial^\mu A_\mu - \xi M_{KK}^2 t \partial_t \left[ \frac{A_t}{t} \right] \right)^2 \right. \\ & + \left( \partial^\mu Z_\mu - \xi \left[ \frac{k\delta(t-1)}{2} M_Z \varphi^3 + M_{KK}^2 t \partial_t \left( \frac{Z_t}{t} \right) \right] \right)^2 \\ & + 2 \left( \partial^\mu W_\mu^+ - \xi \left[ \frac{k\delta(t-1)}{2} M_W \varphi^+ + M_{KK}^2 t \partial_t \left( \frac{W_t^+}{t} \right) \right] \right) \\ & \left. \times \left( \partial^\mu W_\mu^- - \xi \left[ \frac{k\delta(t-1)}{2} M_W \varphi^- + M_{KK}^2 t \partial_t \left( \frac{W_t^-}{t} \right) \right] \right) \right]. \end{aligned} \quad (2.132)$$

For the consistency of the theory, it is important that one can integrate by parts in the action without encountering boundary terms. Otherwise, the Lagrangian would not be hermitian. The  $\delta$ -function terms on the IR brane give rise to discontinuities of some fields at that border of the extra dimension, which jeopardize this feature. To define the model in a proper way [150], the  $\delta$ -functions have to be considered via the limiting procedure

$$\delta(t-1) \equiv \lim_{\theta \rightarrow 0^+} \delta(t-1+\theta). \quad (2.133)$$

In this way, the discontinuities are moved into the bulk, and proper boundary conditions at the branes can be assigned to the fields, consistent with an integration by parts. All calculations are performed at a small but finite  $\theta$ , and, at the end, the limit  $\theta \rightarrow 0^+$  can smoothly be performed,

giving rise to well-defined jump conditions for the fields and their derivatives at the IR brane. This is indicated by the notation  $f(1^-) \equiv \lim_{\theta \rightarrow 0^+} f(1 - \theta)$  for a function that is discontinuous at  $t = 1$ . The KK decompositions for the gauge bosons can be chosen as [150]

$$[A]_{\mu}(x, t) = \frac{1}{\sqrt{r}} \sum_n [A]_{\mu}^{(n)}(x) \chi_n^{[A]}(t), \quad [A]_t(x, t) = -\frac{1}{\sqrt{r}} \sum_n \frac{kt}{m_n^{[A]}} \varphi_{[A]}^{(n)}(x) \partial_t \chi_n^{[A]}(t), \quad (2.134)$$

where  $[A] = A, Z, W^{\pm}$ . Again,  $[A]_{\mu}^{(n)}$  are the four-dimensional mass eigenstates, and the profile functions  $\chi_n^{[A]}(t)$  form complete sets of even functions on the orbifold, fulfilling the normalization condition  $\frac{2\pi}{L} \int_{\epsilon}^1 \frac{dt}{t} \chi_m^{[A]}(t) \chi_n^{[A]}(t) = \delta_{mn}$ , as before. The scalar fields in the decomposition of the Higgs field can be expanded into the same basis of four-dimensional, scalar mass eigenstates as the scalar components of the gauge bosons [150],

$$\varphi^{\pm}(x) = \sum_n \frac{M_W}{\sqrt{r}} \frac{\chi_n^W(1^-)}{m_n^W} \varphi_W^{\pm(n)}(x), \quad \varphi^3(x) = \sum_n \frac{M_Z}{\sqrt{r}} \frac{\chi_n^Z(1^-)}{m_n^Z} \varphi_Z^{(n)}(x). \quad (2.135)$$

The masses of the scalars  $\varphi_{[A]}^{(n)}$  are  $\sqrt{\xi} m_n^{[A]}$  that are related to the masses of the four-dimensional vector fields  $m_n^{[A]}$  by gauge invariance. From the five-dimensional action, the equation of motion for the gauge boson profiles follows as [150, 162, 169]

$$t \partial_t \left( \frac{1}{t} [\partial_t \chi_n^{[A]}(t)] \right) = -\frac{(m_n^{[A]})^2}{M_{KK}^2} \chi_n^{[A]}(t) + \frac{k M_{[A]}^2}{2 M_{KK}^2} \delta(t-1) \chi_n^{[A]}(t), \quad (2.136)$$

where the boundary conditions at the branes read

$$\partial_t \chi_n^{[A]}(0) = 0, \quad \partial_t \chi_n^{[A]}(1^-) = -\frac{M_{[A]}^2}{2\epsilon^2 k} \chi_n^{[A]}(1). \quad (2.137)$$

From these relations, one can derive the mass eigenvalues  $m_n^{[A]}$ . Altogether, the theory with a brane-localized Higgs field contains a tower of massive gauge bosons, accompanied by a tower of massive, unphysical scalars, and one Higgs field with a mass  $m_h = \sqrt{2}\lambda v$  [150]. Similar to the SM, the unphysical scalars provide the third degrees of freedom for every KK gauge boson in the unitary gauge.

One can introduce the four-dimensional gauge coupling  $g$  that is related, at the lowest order, to the five-dimensional gauge coupling by  $g = g_5/\sqrt{2\pi r}$  [162]. The zero-mode photon and gluon fields have flat profiles,  $\chi_0^{[\gamma, g]} = \frac{1}{\sqrt{2\pi}}$ , whereas the profiles of the heavy gauge bosons get corrections that scale with  $v^2/M_{KK}^2$ . To the first order, these profiles read [150]

$$\chi_{[W, Z]}(t) = \frac{1}{\sqrt{2\pi}} \left[ 1 + \frac{m_{[W, Z]}^2}{4M_{KK}^2} \left( 1 - \frac{1}{L} + t^2(1 - 2L - 2\ln t) \right) + \mathcal{O} \left( \frac{m_{[W, Z]}^4}{M_{KK}^4} \right) \right]. \quad (2.138)$$

Again, from the IR boundary condition, one can derive the physical masses of the gauge bosons in dependence of the parametric masses  $\tilde{m}_W^2 = g^2 v^2/4$  and  $\tilde{m}_Z^2 = (g^2 + g'^2)v^2/4$  [150],

$$m_{[W, Z]}^2 = \tilde{m}_{[W, Z]}^2 \left[ 1 - \frac{\tilde{m}_{[W, Z]}^2}{2M_{KK}^2} \left( L - 1 + \frac{1}{2L} \right) + \mathcal{O} \left( \frac{v^4}{M_{KK}^4} \right) \right]. \quad (2.139)$$



From Figure 2.4 before, one can recognize that the vev and the zero-mode Higgs profile become localized close to the IR brane in the limit  $\beta \gg 1$ . In this limit, one can identify  $1/\beta$  with the width of the Higgs profile [2], and the regulator  $\eta$  used in a brane-Higgs scenario. Considering the Yukawa coupling terms, one can derive the matching relations between the vev  $v(t)$  and the Higgs profile  $\chi_0^h(t)$  of the bulk-Higgs scenario and the corresponding distributions  $\delta_v^{1/\beta}(t-1)$  and  $\delta_h^{1/\beta}(t-1)$  in the brane Higgs scenario [2]. For a bulk-Higgs model, the Yukawa coupling terms read, as given before,

$$-\mathcal{L}_Y^{\text{bulk}} = \sum_f \int_\epsilon^1 dt \frac{v(t) + \sum_n h_n(x) \chi_n^h(t)}{\sqrt{2}} \bar{\mathcal{F}}_L(t, x) \frac{1}{\sqrt{r}} \begin{pmatrix} 0 & \mathbf{Y}_{f,\text{bulk}}^{5D} \\ \mathbf{Y}_{f,\text{bulk}}^{5D\dagger} & 0 \end{pmatrix} \mathcal{F}_R(t, x) + \text{h.c.} , \quad (2.140)$$

where the five-dimensional Yukawa matrices  $\mathbf{Y}_{f,\text{bulk}}^{5D}$  have a mass dimension of  $-1/2$ . In a model with a brane-localized Higgs sector, the Yukawa coupling terms read, instead,

$$-\mathcal{L}_Y^{\text{brane}} = \sum_f \int_\epsilon^1 dt \frac{v\delta_v^\eta(t-1) + h(x)\delta_h^\eta(t-1)}{\sqrt{2}} \bar{\mathcal{F}}_L(t, x) \frac{k}{2} \begin{pmatrix} 0 & \mathbf{Y}_f^{5D} \\ \mathbf{Y}_f^{5D\dagger} & 0 \end{pmatrix} \mathcal{F}_R(t, x) + \text{h.c.} , \quad (2.141)$$

using similar redefinitions as in the bulk Higgs model in (2.105), and the KK decompositions for the fermions from (2.106). Here, the five-dimensional Yukawa matrices  $\mathbf{Y}_f^{5D}$  have a mass dimension of  $-1$ . In order to match the two expressions onto each other, one has to rewrite the functions  $v(t)$  and  $\chi_0^h(t)$  in terms of functions of a unit area, which can be mapped onto the normalized distributions  $\delta_v^\eta(t-1)$  and  $\delta_h^\eta(t-1)$  [2],

$$\begin{aligned} v(t) &= v_4 \sqrt{\frac{L}{\pi} \frac{\sqrt{1+\beta}}{2+\beta}} \delta_v^{1/\beta}(t-1) , \\ \chi_0^h(t) &= \sqrt{\frac{L}{\pi} \frac{\sqrt{1+\beta}}{2+\beta}} \left[ 1 + \frac{\beta m_h^2}{4M_{KK}^2(1+\beta)(2+\beta)(4+\beta)} + \dots \right] \delta_h^{1/\beta}(t-1) , \end{aligned} \quad (2.142)$$

with

$$\begin{aligned} \delta_v^{1/\beta}(t-1) &= (2+\beta)t^{1+\beta} , \\ \delta_h^{1/\beta}(t-1) &= (2+\beta)t^{1+\beta} \left[ 1 - \frac{m_h^2}{4M_{KK}^2(1+\beta)} \left( t^2 - \frac{2+\beta}{4+\beta} \right) + \dots \right] . \end{aligned} \quad (2.143)$$

The relations between the Yukawa matrices in the two different scenarios for the Higgs localizations can be determined by considering the bilinear fermion terms of the Yukawa interactions, resulting in [2]

$$\mathbf{Y}_f \equiv \frac{k}{2} \mathbf{Y}_f^{5D} = \frac{\sqrt{k(1+\beta)}}{2+\beta} \mathbf{Y}_{f,\text{bulk}}^{5D} . \quad (2.144)$$

Equally, one could have used the  $h\bar{f}f$ -couplings, where in this case the above relation would receive corrections of  $\mathcal{O}(m_h^2/M_{KK}^2)$ . It would be wrong to conclude that the Yukawa matrices  $\mathbf{Y}_f$  vanish in the limit  $\beta \rightarrow \infty$  [2]. Rather, the dimensionless Yukawa matrices should be considered as fixed quantities that are related to the observed quark masses and mixing angles

of the SM. Then, it follows that the dimensionful Yukawa matrices  $\mathbf{Y}_{f,\text{bulk}}^{5D}$  must scale with  $\sqrt{\beta/k} \approx \sqrt{\mu}/k$  [170]. Since  $\beta = \sqrt{4 + \mu^2/k^2}$  is naturally of  $\mathcal{O}(1)$ , the limit of a very large  $\beta$  is not particularly natural [2]. For large  $\beta$ , one encounters instead

$$\frac{10}{r} \sim k \sim \frac{\mu}{\beta} \quad \text{or} \quad k \ll \mu \sim \frac{M_{IR}}{2}. \quad (2.145)$$

For a large parameter  $\beta$ , the parameter  $k$  is needed either to be significantly smaller than the Planck scale, and yet  $1/r$  should be smaller by an order of magnitude, or one has to assume that  $\mu$  and  $M_{IR}$  lie significantly above the Planck scale. The latter choice would be especially unnatural for the parameter  $M_{IR}$ , which is naturally situated at the warped down Planck scale around several TeV. For that reason, the first possibility appears more plausible. In addition, increasing the parameter  $\beta$  by lowering the curvature parameter  $k$  does not significantly affect the relation  $\lambda_4 \approx \lambda_{IR}\mu^2$  [2].

Nevertheless, the ‘‘narrow bulk-Higgs scenario’’ forms an interesting, intermediate scenario between a bulk-localized and a strictly brane-localized Higgs scenario of the RS model. For example, the fermion loop-contributions in Higgs processes significantly differ between a narrow bulk-Higgs scenario and a brane-Higgs scenario. For the Higgs production through gluon fusion and the Higgs decay into two photons, the results in both scenarios, in good approximation, have equal amounts but an opposite sign [2]. It has been explained that the difference is created by a ‘‘resonance effect’’, where in the narrow bulk-Higgs scenario, very heavy KK modes with masses of the order of the inverse Higgs width  $1/\eta$  give an unsuppressed contribution to the loop amplitudes [2, 5, 151, 152, 171, 172]. Between the results of both scenarios, not any smooth interpolation can be found, as the effective field theory description of the RS model, valid up to the position-dependent UV cut-off

$$\Lambda_{UV}(t) \sim m_{Pl} e^{-\sigma(\phi)} = m_{Pl} \frac{\epsilon}{t} \equiv \frac{\Lambda_{\text{TeV}}}{t}, \quad (2.146)$$

breaks down in the intermediate region. So, with the help of the cut-off, one can distinguish between different scenarios for the Higgs localization. From the four-dimensional point of view, the operators, generated by the Yukawa interactions, have an amount of  $\frac{v|Y_f|}{\Lambda_{\text{TeV}}}$  for a Higgs localization near or on the IR brane. By comparing the amount of the Higgs width  $\eta$  with the size of these operators, one can distinguish between brane-Higgs and bulk-Higgs incarnations in a sense that the high momentum KK modes of the theory can or cannot resolve the shape of the Higgs profile, and do or do not contribute in scattering amplitudes [2]. For the case

$$\eta \ll \frac{v|Y_f|}{\Lambda_{\text{TeV}}}, \quad (2.147)$$

the Higgs profile cannot be resolved by the high momentum modes of the theory. This is even true for a possibly non-zero width of the Higgs profile. Such a scenario is referred to as the brane-Higgs scenario. The relation (2.147) should be considered as a condition on the Higgs width, or regulator  $\eta$ , at a fixed, physical UV cut-off  $\Lambda_{\text{TeV}}$ . In a brane-Higgs scenario, one can perform the limit  $\eta \rightarrow 0$ , which strictly localises the Higgs sector onto the IR brane. In the contrary case, all the momentum KK states can resolve the features of the Higgs profile for a Higgs width as [2]

$$\eta > \frac{v|Y_f|}{\Lambda_{\text{TeV}}}. \quad (2.148)$$

Then, higher momentum modes can give sizeable contributions to amplitudes. Such a scenario is referred to as the bulk-Higgs scenario, and will be considered in most parts of the thesis. And, a third, intermediate scenario can be considered for a narrow Higgs profile, fulfilling [2]

$$\frac{v|Y_f|}{\Lambda_{\text{TeV}}} \ll \eta \ll \frac{v|Y_f|}{M_{KK}}. \quad (2.149)$$

In this case, whereas the lower momentum KK modes cannot resolve the effects caused by the Higgs profile, the very high momentum modes can resolve the Higgs width and may give strong contributions to amplitudes. For that reason, such a framework is different compared to the brane-Higgs scenario, in which none of the KK modes can resolve the Higgs profile. There is no smooth transition region between the two scenarios, because the effective field theory approach is not valid there. The relation (2.149) shows that the limit  $\eta \rightarrow 0$  would put  $\Lambda_{\text{TeV}}$  to infinity, which cannot be allowed in a theory that is not UV complete. In such a case, the solution to the gauge hierarchy problem also would no longer be maintained. Power corrections, as represented by higher-dimensional operators in the effective Lagrangian of the RS model, scale like  $(M_{KK}/\Lambda_{\text{TeV}})^n$  for a brane-Higgs field. On the contrary, they can be enhanced up to  $\mathcal{O}(1)$  in the intermediate region of the scenarios, scaling like  $(M_{KK}/\eta\Lambda_{\text{TeV}})^n$  in this case [2]. Then, the effective field-theory approach breaks down and the analytic control of the theory is lost. For that reason, the narrow bulk-Higgs scenario really forms an independent incarnation of the RS model.

In the brane-Higgs scenario, the equation of motion for the fermion profiles has the same form as in the bulk-Higgs scenario, given in (2.109), except that the mass matrix reads [5]

$$\mathcal{M}_f(t) = \frac{1}{t} \begin{pmatrix} \mathbf{c}_F & 0 \\ 0 & -\mathbf{c}_f \end{pmatrix} + \frac{v}{\sqrt{2}M_{KK}} \delta(t-1) \begin{pmatrix} 0 & \mathbf{Y}_f \\ \mathbf{Y}_f^\dagger & 0 \end{pmatrix}, \quad (2.150)$$

where the bulk mass parameters are again defined by  $c_{[F,f]} \equiv \pm M_{[F,f]}/k$ . For the zero-mode profiles, for which  $x_n \ll 1$ , the  $C$  and  $S$  profiles from the KK decompositions in (2.105) are given by [150]

$$C_n^{[F,f]}(t) \approx \sqrt{\frac{L\epsilon}{\pi}} F(c_{[F,f]}) t^{c_{[F,f]}}, \quad S_n^{[F,f]}(t) \approx \pm x_n \sqrt{\frac{L\epsilon}{\pi}} F(c_{[F,f]}) \frac{(t^{1+c_{[F,f]}} - \epsilon^{1+2c_{[F,f]}} t^{-c_{[F,f]}})}{(1 + 2c_{[F,f]})}, \quad (2.151)$$

that come along with the rescaled vectors from (2.108). In the  $\phi$ -coordinate, the  $S$  profiles are multiplied with  $\text{sgn}(\phi)$  in order to imply the  $Z_2$ -odd behaviour. The profiles coincide with the fermion profiles of the bulk-Higgs scenario, given in (2.114), if skipping the terms that come from the Yukawa interactions. In this connection, the functions  $F(c)$  are the ‘‘zero-mode profiles’’ from (2.115). In the following, we summarize the implications for the masses and mixings of the zero-mode fermions in the minimal RS model with a brane-localized Higgs field, as derived in [150]. On the IR brane, the profiles of the zero-mode fermions read

$$C_n^{[F,f]}(1) = \sqrt{\frac{L\epsilon}{\pi}} F(c_{[F,f]}), \quad S_n^{[F,f]}(1^-) = \pm \sqrt{\frac{L\epsilon}{\pi}} \frac{x_n}{F(c_{[F,f]})}. \quad (2.152)$$

In reference [150], it was shown how the equations of motion can be integrated over an infinitesimal interval around  $|\phi| = \pi$  in the  $\phi$ -notation, leading to the IR boundary conditions for the

profiles  $S$  and  $C$ . Again, by defining  $Y_{f,ij}^{\text{eff}} \equiv F(c_{F_i})Y_{f,ij}F(c_{f_j})$ , and using the zero-mode fermion profiles on the IR brane, these IR boundary conditions can be recast to the following eigenvalue equations [150]

$$\frac{\sqrt{2}m_n}{v}\hat{a}_n^F = \mathbf{Y}_f^{\text{eff}}\hat{a}_n^f, \quad \frac{\sqrt{2}m_n}{v}\hat{a}_n^f = \mathbf{Y}_f^{\text{eff}\dagger}\hat{a}_n^F, \quad (2.153)$$

that define the mass eigenvalues  $m_n$  as the solutions to the equation

$$\det \left[ m_n^2 \mathbf{1} - \frac{v^2}{2} \mathbf{Y}_f^{\text{eff}} \mathbf{Y}_f^{\text{eff}\dagger} \right] = 0. \quad (2.154)$$

The vectors  $\hat{a}_n^F$  and  $\hat{a}_n^f$  are the eigenvectors of the matrices  $\mathbf{Y}_f^{\text{eff}} \mathbf{Y}_f^{\text{eff}\dagger}$  and  $\mathbf{Y}_f^{\text{eff}\dagger} \mathbf{Y}_f^{\text{eff}}$ , and they form the columns of the unitary matrices  $\mathbf{U}_f$  and  $\mathbf{W}_f$  appearing in the singular-value decomposition,  $\mathbf{Y}_f^{\text{eff}} = \mathbf{U}_f \lambda_f \mathbf{W}_f^\dagger$ , similar to the bulk-Higgs case. For the up- and down-type quarks, these include the matrices [150]

$$\lambda_u = \frac{\sqrt{2}}{v} \text{diag}(m_u, m_c, m_t), \quad \lambda_d = \frac{\sqrt{2}}{v} \text{diag}(m_d, m_s, m_b). \quad (2.155)$$

Again, the relations between the original, five-dimensional fields and the SM mass eigenstates involve the matrices  $\mathbf{U}_f$  and  $\mathbf{W}_f$ , and in this connection, the CKM mixing matrix is given by  $\mathbf{V}_{\text{CKM}} = \mathbf{U}_u^\dagger \mathbf{U}_d$ . These relations were presented before for the bulk-Higgs scenario, including the rescaled Yukawa matrices  $\tilde{\mathbf{Y}}_f$  in this case.

The hierarchies between up- and down-type quark masses can be reproduced, in a very natural way, by assuming a hierarchical structure for the zero-mode profiles as

$$|F(c_{A_1})| < |F(c_{A_2})| < |F(c_{A_3})|. \quad (2.156)$$

In the RS model, in fact, such a hierarchy can be derived for very small differences between the bulk mass parameters  $c_{A_i}$ , due to the behaviour of the zero-mode profile  $F(c)$  [150]. In case of  $-1/2 < c < 1/2$ , the zero-mode profile can be approximated by  $F(c) \approx \sqrt{1+2c}$ , whereas for  $-3/2 < c < -1/2$  it has an exponentially small behaviour as  $F(c) \approx -\sqrt{-1-2c} \epsilon^{-c-1/2}$ . With the hierarchical structure of the profiles, the hierarchies between fermion masses and mixings result without further assumption from the Frogatt-Nielsen mechanism [173]. The products of the masses of up- and down-type quarks are given by [150]

$$\begin{aligned} m_u m_c m_t &= \frac{v^3}{2\sqrt{2}} |\det(\mathbf{Y}_u)| \prod_{i=1,2,3} |F(c_{Q_i}) F(c_{u_i})|, \\ m_d m_s m_b &= \frac{v^3}{2\sqrt{2}} |\det(\mathbf{Y}_d)| \prod_{i=1,2,3} |F(c_{Q_i}) F(c_{d_i})|. \end{aligned} \quad (2.157)$$

Due to  $|F(c_{A_i})| < |F(c_{A_{i+1}})|$ , one can consistently evaluate all the eigenvalues to leading order in hierarchies, and obtains [150]

$$\begin{aligned} m_u &= \frac{v}{\sqrt{2}} \frac{|\det(\mathbf{Y}_u)|}{|(M_u)_{11}|} |F(c_{Q_1}) F(c_{u_1})|, & m_d &= \frac{v}{\sqrt{2}} \frac{|\det(\mathbf{Y}_d)|}{|(M_d)_{11}|} |F(c_{Q_1}) F(c_{d_1})|, \\ m_c &= \frac{v}{\sqrt{2}} \frac{|(M_u)_{11}|}{|(Y_u)_{33}|} |F(c_{Q_2}) F(c_{u_2})|, & m_s &= \frac{v}{\sqrt{2}} \frac{|(M_d)_{11}|}{|(Y_d)_{33}|} |F(c_{Q_2}) F(c_{d_2})|, \\ m_t &= \frac{v}{\sqrt{2}} |(Y_u)_{33}| |F(c_{Q_3}) F(c_{u_3})|, & m_b &= \frac{v}{\sqrt{2}} |(Y_d)_{33}| |F(c_{Q_3}) F(c_{d_3})|. \end{aligned} \quad (2.158)$$

Here,  $(M_q)_{ij}$  denotes the minor of  $\mathbf{Y}_q$ , which is the determinant of the square matrix formed by removing the  $i^{\text{th}}$  row and  $j^{\text{th}}$  column from  $\mathbf{Y}_q$ . So, simply explained, the different four-dimensional fermion masses are effectively induced by overlaps of the zero-mode profiles  $F(c)$ , as

$$m_{q_i} \sim |F(c_{Q_i})F(c_{q_i})|, \quad (2.159)$$

and the observed quark mass hierarchies can be reproduced for  $\mathcal{O}(1)$  differing c-parameters. Furthermore, to the leading order, the elements of the matrices  $\mathbf{U}_q$  and  $\mathbf{W}_q$  can be evaluated as [150]

$$(U_q)_{ij} = (u_q)_{ij} \begin{cases} \frac{F(c_{Q_i})}{F(c_{Q_j})}, & i \leq j \\ \frac{F(c_{Q_j})}{F(c_{Q_i})}, & i > j \end{cases}, \quad (W_q)_{ij} = (w_q)_{ij} e^{i\phi_j} \begin{cases} \frac{F(c_{q_i})}{F(c_{q_j})}, & i \leq j \\ \frac{F(c_{q_j})}{F(c_{q_i})}, & i > j \end{cases}, \quad (2.160)$$

and the coefficient matrices  $\mathbf{u}_q$  and  $\mathbf{w}_q$  read [150]

$$\mathbf{u}_q = \begin{pmatrix} 1 & \frac{(M_q)_{21}}{(M_q)_{11}} & \frac{(Y_q)_{13}}{(Y_q)_{33}} \\ -\frac{(M_q)_{21}^*}{(M_q)_{11}^*} & 1 & \frac{(Y_q)_{23}}{(Y_q)_{33}} \\ \frac{(M_q)_{31}^*}{(M_q)_{11}^*} & -\frac{(Y_q)_{23}^*}{(Y_q)_{33}^*} & 1 \end{pmatrix}, \quad \mathbf{w}_q = \begin{pmatrix} 1 & \frac{(M_q)_{12}^*}{(M_q)_{11}^*} & \frac{(Y_q)_{31}^*}{(Y_q)_{33}^*} \\ -\frac{(M_q)_{12}}{(M_q)_{11}} & 1 & \frac{(Y_q)_{32}^*}{(Y_q)_{33}^*} \\ \frac{(M_q)_{13}}{(M_q)_{11}} & -\frac{(Y_q)_{32}}{(Y_q)_{33}} & 1 \end{pmatrix}. \quad (2.161)$$

The phase factors  $e^{i\phi_j}$  entering  $\mathbf{W}_q$  are given by

$$e^{i\phi_j} = \text{sgn} [F(c_{Q_j})F(c_{q_j})] e^{-i(\rho_j - \rho_{j+1})}, \quad (2.162)$$

$$\rho_1 = \arg(\det(\mathbf{Y}_q)), \quad \rho_2 = \arg((M_q)_{11}), \quad \rho_3 = \arg((Y_q)_{33}),$$

and  $\rho_4 = 0$ . To the leading order, the matrices  $\mathbf{U}_q$ , and therefore also the CKM mixing matrix, do not depend on the right-handed profiles  $F(c_{q_i})$  [167]. The Wolfenstein parameters of the CKM matrix are given by

$$\lambda = \frac{|V_{us}|}{\sqrt{|V_{ud}|^2 + |V_{us}|^2}}, \quad A = \frac{1}{\lambda} \left| \frac{V_{cb}}{V_{us}} \right|, \quad \bar{\rho} - i\bar{\eta} = -\frac{V_{ud}^* V_{ub}}{V_{cd}^* V_{cb}}, \quad (2.163)$$

and can be derived as follows [150]

$$\lambda = \frac{|F(c_{Q_1})|}{|F(c_{Q_2})|} \left| \frac{(M_d)_{21}}{(M_d)_{11}} - \frac{(M_u)_{21}}{(M_u)_{11}} \right|, \quad A = \frac{|F(c_{Q_2})|^3}{|F(c_{Q_1})|^2 |F(c_{Q_3})|} \left| \frac{\frac{(Y_d)_{23}}{(Y_d)_{33}} - \frac{(Y_u)_{23}}{(Y_u)_{33}}}{\left[ \frac{(M_d)_{21}}{(M_d)_{11}} - \frac{(M_u)_{21}}{(M_u)_{11}} \right]^2} \right|,$$

$$\bar{\rho} - i\bar{\eta} = \frac{(Y_d)_{33}(M_u)_{31} - (Y_d)_{23}(M_u)_{21} + (Y_d)_{13}(M_u)_{11}}{(Y_d)_{33}(M_u)_{11} \left[ \frac{(Y_d)_{23}}{(Y_d)_{33}} - \frac{(Y_u)_{23}}{(Y_u)_{33}} \right] \left[ \frac{(M_d)_{21}}{(M_d)_{11}} - \frac{(M_u)_{21}}{(M_u)_{11}} \right]}. \quad (2.164)$$

The zero-mode quark profiles, induced by the different bulk mass parameters, can be expressed in dependence of the quark masses, the Yukawa matrices and the Wolfenstein parameters, and one chosen profile, for which one can choose, for example,  $F(c_{u_3})$  as given in Appendix C.3 [150].

Then, the hierarchical structure between the profiles, induced by the  $c$ -parameters [167], is implied for the left-handed profiles as [150]

$$\frac{|F(c_{Q_1})|}{|F(c_{Q_2})|} \sim \lambda, \quad \frac{|F(c_{Q_2})|}{|F(c_{Q_3})|} \sim \lambda^2, \quad \frac{|F(c_{Q_1})|}{|F(c_{Q_3})|} \sim \lambda^3. \quad (2.165)$$

The values for the right-handed profiles are fixed by the observed quark-mass hierarchies [150]

$$\begin{aligned} \frac{|F(c_{u_1})|}{|F(c_{u_3})|} &\sim \frac{m_u}{m_t} \frac{1}{\lambda^3}, & \frac{|F(c_{u_2})|}{|F(c_{u_3})|} &\sim \frac{m_c}{m_t} \frac{1}{\lambda^2}, \\ \frac{|F(c_{d_1})|}{|F(c_{u_3})|} &\sim \frac{m_d}{m_t} \frac{1}{\lambda^3}, & \frac{|F(c_{d_2})|}{|F(c_{u_3})|} &\sim \frac{m_s}{m_t} \frac{1}{\lambda^2}, & \frac{|F(c_{d_3})|}{|F(c_{u_3})|} &\sim \frac{m_b}{m_t}. \end{aligned} \quad (2.166)$$

With these results, the structure for the flavor mixing matrices  $\mathbf{U}_q$  and  $\mathbf{W}_q$  can be deduced, which naturally imply hierarchies for the entries of the CKM mixing matrix like<sup>3</sup> [150]

$$\mathbf{U}_{u,d} \sim \mathbf{V}_{\text{CKM}} \sim \begin{pmatrix} 1 & \lambda & \lambda^3 \\ \lambda & 1 & \lambda^2 \\ \lambda^3 & \lambda^2 & 1 \end{pmatrix} \sim \begin{pmatrix} 1 & 0.23 & 0.01 \\ 0.23 & 1 & 0.05 \\ 0.01 & 0.05 & 1 \end{pmatrix}. \quad (2.167)$$

So, in the RS model, especially the left-handed fermion profiles show a natural hierarchical behaviour for different  $c$ -parameters. This can be used to explain, in a very natural way, the origin of the different fermion masses by overlaps of different fermion profiles. Similarly, hierarchical entries are induced for the CKM mixing matrix [167, 168].

## 2.3 Extension by a custodial bulk gauge symmetry

In this section, we describe the framework of the RS model, in which an extended bulk gauge symmetry is implemented to maintain a custodial symmetry on the IR brane, the custodial model [151, 174–176]. This model can allow for much smaller KK masses implied by reduced constraints from electroweak precision tests, and therefore it has been of particular interest for phenomenological searches, *e.g.* at the LHC [2, 4]. As mentioned before, also the implementation of a Higgs field in the bulk allows for reduced constraints on the KK mass scale in a setting with a minimal bulk gauge symmetry [154]. In this sense, the bulk-Higgs framework and the custodial model are the two phenomenologically most interesting versions of the RS model.

In the minimal RS model, the effective Lagrangian, equivalent to (1.58), includes the couplings of the zero-mode  $W_\mu^{3(0)}$ -boson to the  $B_\mu^{(0)}$ -boson, and further to the full KK tower of  $B_\mu^{(n)}$ -bosons in addition to the SM,

$$\begin{aligned} \mathcal{L}_{\text{kin.Higgs}} \ni & \int_\epsilon^1 dt \delta(t-1) \frac{1}{4r} \sum_{m,n} [g_5^2 (W_\mu^{1(m)} W^{\mu 1(n)} + W_\mu^{2(m)} W^{\mu 2(n)}) \\ & + (g_5^2 W_\mu^{3(m)} W^{\mu 3(n)} - 2g_5 g_5' W_\mu^{3(m)} B^{\mu(n)} + g_5'^2 B_\mu^{(m)} B^{\mu(n)})]. \end{aligned} \quad (2.168)$$

<sup>3</sup>In reference [150], the default values for the quark masses and CKM parameters are collected that were used to obtain these estimates.

According to the discussion in Subsection 1.1.3, the coupling of the zero-mode  $W_\mu^{i(0)}$ -bosons to the tower of  $W_\mu^{i(n)}$  in the Lagrangian is symmetric in the three different  $W^i$ -fields, and maintains the custodial symmetry. On the contrary, the couplings of the zero-mode  $W_\mu^{3(0)}$ -boson to the tower of  $B_\mu^{(n)}$ -bosons is violating the custodial symmetry in a much stronger manner compared to the SM [145]. The  $\rho$ -parameter, related to the ratio of the charged and neutral current interactions, receives strong contributions.

In this connection, contributions are caused by the KK gauge boson states in the oblique electroweak corrections to effective four-fermion interactions. In contrast to the SM, the S and T parameters already get contributions at tree level by the contributions to the five-dimensional gauge boson propagators, to the gauge boson masses and to different observables like  $G_F$ ,  $\alpha$ ,  $\rho$ , as well as the weak mixing angle [82, 154]. Due to the enlarged custodial symmetry violation, especially the corrections to the T parameter demand for a high value of the  $M_{KK}$  mass scale [150, 177]. The calculations of the S, T, U parameters at tree level, in the minimal RS model with a brane Higgs and a bulk Higgs and the custodial RS model, and the bounds implied on the KK mass scale  $M_{KK}$ , will be presented at the end of this chapter.

### 2.3.1 Gauge sector and spontaneous symmetry breaking

The request to avoid the strong violation of the custodial symmetry, as it arises in the minimal RS model, gave reason to create the custodial RS model, in which a bulk gauge group as [151, 174–176]

$$SU(2)_L \times SU(2)_R \times U(1)_X \times P_{LR} , \quad (2.169)$$

is implemented, whereof  $P_{LR}$  is a discrete symmetry [176]. We consider this model with a Higgs sector localized onto the IR brane [151],

$$\mathcal{L}_{\text{gauge}} = \frac{2\pi r}{L} \int_\epsilon^1 \frac{dt}{t} \frac{\epsilon^4}{t^4} (\mathcal{L}_{L,R,X} + \mathcal{L}_{\text{Higgs}} + \mathcal{L}_{\text{GF}}) . \quad (2.170)$$

The kinetic terms of the gauge fields are

$$\mathcal{L}_{L,R,X} = G^{KM} G^{LN} \left( -\frac{1}{4} L_{KL}^a L_{MN}^a - \frac{1}{4} R_{KL}^a R_{MN}^a - \frac{1}{4} X_{KL} X_{MN} \right) , \quad (2.171)$$

and  $G^{MN}$  is the five-dimensional metric tensor. As always, the five-dimensional gauge bosons can be decomposed into a vector component and a scalar component,  $A_M = A_\mu + ktA_t$ , where both components individually decompose into the KK expansions of four-dimensional vector bosons and scalars. The IR brane-localized Higgs Lagrangian [151],

$$\mathcal{L}_{\text{Higgs}} = \frac{k}{2} \delta(t-1) \left[ \frac{G^{\mu\nu}}{2} \text{Tr} [(D_\mu \Phi)^\dagger (D_\nu \Phi)] - V(\Phi) \right] , \quad (2.172)$$

considers a Higgs bi-doublet, transforming as  $(\mathbf{2}, \mathbf{2})_0$  under  $SU(2)_L \times SU(2)_R$ . The  $SU(2)_L$  gauge transformations act on the bi-doublet from the left-hand side, whereas the  $SU(2)_R$ -transformations act from the right-hand side. Therefore, the covariant derivative reads

$$D_\mu \Phi = \partial_\mu \Phi - ig_{L5} L_\mu^a T_L^a \Phi + ig_{R5} \Phi R_\mu^a T_R^a , \quad (2.173)$$

with  $T_{L,R}^a = \sigma^a/2$ , and where  $g_{L5}$ ,  $g_{R5}$  are the five-dimensional gauge couplings, belonging to the groups  $SU(2)_L$  and  $SU(2)_R$ , respectively. In this model, the Higgs bi-doublet induces a spontaneous gauge symmetry breaking on the IR brane, as [151]

$$SU(2)_L \times SU(2)_R \xrightarrow{\text{IR}} SU(2)_V , \quad (2.174)$$

where a custodial symmetry  $SU(2)_V$  is maintained explicitly. After the symmetry breaking, the Higgs bi-doublet can be decomposed around the vev  $v \approx 246$  GeV as [151]

$$\Phi(x) = \frac{1}{\sqrt{2}\epsilon} \begin{pmatrix} v + h(x) - i\varphi^3(x) & -i\sqrt{2}\varphi^+(x) \\ -i\sqrt{2}\varphi^-(x) & v + h(x) + i\varphi^3(x) \end{pmatrix} , \quad (2.175)$$

with the scalar fields  $\varphi^\pm = (\varphi^1 \mp i\varphi^2)/\sqrt{2}$ . Similar to the SM, one can redefine the charged gauge bosons as

$$L_\mu^\pm = \frac{1}{\sqrt{2}} (L_\mu^1 \mp iL_\mu^2) , \quad R_\mu^\pm = \frac{1}{\sqrt{2}} (R_\mu^1 \mp iR_\mu^2) . \quad (2.176)$$

Furthermore, by redefining new fields as

$$\begin{pmatrix} \tilde{A}_M \\ V_M \end{pmatrix} = \frac{1}{\sqrt{g_L^2 + g_R^2}} \begin{pmatrix} g_L & -g_R \\ g_R & g_L \end{pmatrix} \begin{pmatrix} L_M \\ R_M \end{pmatrix} , \quad (2.177)$$

where  $g_a = g_{a5}/\sqrt{2\pi r}$ , one can find that there is one five-dimensional mass term for the gauge boson  $\tilde{A}_\mu$  that adopts the following form on the IR brane [151]

$$\mathcal{L}_{\text{mass}} = \delta(t-1) \frac{(g_{L5}^2 + g_{R5}^2)v^2}{8} \tilde{A}_\mu^a \tilde{A}^{\mu,a} \equiv \delta(t-1) \frac{1}{2} M_{\tilde{A}}^2 \tilde{A}_\mu^a \tilde{A}^{\mu,a} , \quad (2.178)$$

whereas the field  $V_M$  remains massless. With only one five-dimensional mass parameter for the massive gauge bosons,  $M_{\tilde{A}}$ , the mass Lagrangian on the IR brane remains invariant under the global custodial symmetry transformations  $SU(2)_V$ . In order to obtain the SM field content in the zero modes, the custodial symmetry has to be broken by the  $U(1)$ -gauge bosons that are part of the definition of the  $Z$  boson and photon fields. In the custodial model, the  $B_\mu^Y$  bosons are defined on the UV brane, at the other boundary of the extra dimension. In this connection, the symmetry breaking

$$SU(2)_R \times U(1)_X \xrightarrow{\text{UV}} U(1)_Y \quad (2.179)$$

is induced on the UV brane, where a breaking as  $SU(2)_R \rightarrow U(1)_R$  can be achieved by means of odd orbifold boundary conditions, and a spontaneous symmetry breaking as  $U(1)_R \times U(1)_X \rightarrow U(1)_Y$  appears via a vev. Then, one can define the following new fields

$$\begin{pmatrix} Z'_M \\ B_M^Y \end{pmatrix} = \frac{1}{\sqrt{g_R^2 + g_X^2}} \begin{pmatrix} g_R & -g_X \\ g_X & g_R \end{pmatrix} \begin{pmatrix} R_M^3 \\ X_M \end{pmatrix} , \quad (2.180)$$

including the gauge boson  $B_M^Y$  of the group  $U(1)_Y$ . In this connection, the hypercharge gauge coupling is  $g_Y = \frac{g_R g_X}{\sqrt{g_R^2 + g_X^2}}$ . After that, one can obtain the neutral, electroweak gauge bosons in a way similar to the SM, by

$$\begin{pmatrix} Z_M \\ A_M \end{pmatrix} = \frac{1}{\sqrt{g_L^2 + g_Y^2}} \begin{pmatrix} g_L & -g_Y \\ g_Y & g_L \end{pmatrix} \begin{pmatrix} L_M^3 \\ B_M^Y \end{pmatrix} , \quad (2.181)$$



$\partial_t L_\mu^\pm(x, t)  _{t=\epsilon} = 0$	$L_t^\pm(x, 0) = 0$	$\partial_t \tilde{A}_\mu^\pm(x, t)  _{t=1^-} = -(2M_{KK}\epsilon)^{-1} M_A^2 \tilde{A}_\mu^\pm(x, 1)$	$\tilde{A}_t^\pm(x, 1) = 0$
$R_\mu^\pm(x, 0) = 0$	$R_t^\pm(x, 0) = 0$	$\partial_t V_\mu^\pm(x, t)  _{t=1} = 0$	$V_t^\pm(x, 1) = 0$
$\partial_t Z_\mu(x, t)  _{t=\epsilon} = 0$	$Z_t(x, 0) = 0$	$\partial_t \tilde{Z}_\mu(x, t)  _{t=1^-} = -(2M_{KK}\epsilon)^{-1} M_A^2 \tilde{Z}_\mu(x, 1)$	$\tilde{Z}_t(x, 1) = 0$
$Z'_\mu(x, 0) = 0$	$Z'_t(x, 0) = 0$	$\partial_t Z_\mu^H(x, t)  _{t=1} = 0$	$Z_t^H(x, 1) = 0$
$\partial_t A_\mu(x, t)  _{t=\epsilon} = 0$	$A_t(x, 0) = 0$	$\partial_t A_\mu(x, t)  _{t=1} = 0$	$A_t(x, 1) = 0$

Table 2.2: Boundary conditions for the gauge bosons at the UV and IR branes [151].

and one can define

$$\sin \theta_w = \frac{g_Y}{\sqrt{g_L^2 + g_Y^2}}, \quad \cos \theta_w = \frac{g_L}{\sqrt{g_L^2 + g_Y^2}}. \quad (2.182)$$

In addition, the fields  $V_M^3$  and  $X_M$  can be rotated to the photon field  $A_M$  and a state  $Z_M^H$  as

$$\begin{pmatrix} Z_M^H \\ A_M \end{pmatrix} = \frac{1}{g_{LRX}^2} \begin{pmatrix} g_L g_R & -g_X \sqrt{g_L^2 + g_R^2} \\ g_X \sqrt{g_L^2 + g_R^2} & g_L g_R \end{pmatrix} \begin{pmatrix} V_M^3 \\ X_M \end{pmatrix}, \quad (2.183)$$

where  $g_{LRX}^2 = \sqrt{g_L^2 g_R^2 + g_L^2 g_X^2 + g_R^2 g_X^2}$ . Furthermore, the field  $\tilde{Z}_M \equiv \tilde{A}_M^3$  is defined as a linear combination of  $Z_M$  and  $Z'_M$ . The boundary conditions for the five-dimensional gauge fields at the two branes are summarized in Table 2.2. They are chosen in such a way that the correct particle spectrum of the SM is obtained for the zero modes. By means of these boundary conditions, one can distinguish between two basis sets of fields, the UV and IR bases. In these basis sets, the respective boundary conditions adopt easy expressions. Instead, a transformation of the conditions into the respective other basis set results in relations that mix the different fields, instead. The transformations between the two basis sets are given by the following rotations [151]

$$\begin{aligned} \begin{pmatrix} \tilde{Z}_M \\ Z_M^H \end{pmatrix} &= \mathbf{R}_Z \begin{pmatrix} Z_M \\ Z'_M \end{pmatrix}, & \mathbf{R}_Z &\equiv \begin{pmatrix} c_Z & -s_Z \\ s_Z & c_Z \end{pmatrix}, \\ \begin{pmatrix} \tilde{A}_M^\pm \\ V_M^\pm \end{pmatrix} &= \mathbf{R}_W \begin{pmatrix} L_M^\pm \\ R_M^\pm \end{pmatrix}, & \mathbf{R}_W &\equiv \begin{pmatrix} c_W & -s_W \\ s_W & c_W \end{pmatrix}, \end{aligned} \quad (2.184)$$

along with the angles

$$\begin{aligned} s_Z \equiv \sin \theta_Z &= \frac{g_R^2}{\sqrt{(g_L^2 + g_R^2)(g_R^2 + g_X^2)}} = \frac{g_Y/g_X}{\sqrt{g_L^2 + g_R^2}}, & s_W \equiv \sin \theta_W &= \frac{g_R}{\sqrt{g_L^2 + g_R^2}}, \\ c_W \equiv \cos \theta_Z &= \frac{g_{LRX}^2}{\sqrt{(g_L^2 + g_R^2)(g_R^2 + g_X^2)}} = \sqrt{\frac{g_L^2 + g_Y^2}{g_L^2 + g_R^2}}, & c_W \equiv \cos \theta_W &= \frac{g_L}{\sqrt{g_L^2 + g_R^2}}. \end{aligned} \quad (2.185)$$

In order to perform the KK decompositions for the gauge fields in the custodial model, one can introduce the vectors

$$\vec{Z}_M = \begin{pmatrix} \tilde{Z}_M \\ Z_M^H \end{pmatrix}, \quad \vec{W}_M^\pm = \begin{pmatrix} \tilde{A}_M^\pm \\ V_M^\pm \end{pmatrix}, \quad (2.186)$$

combining the fields that get mixed by the UV boundary conditions. To work with profiles that obey definite Neumann- (+) or Dirichlet- (-) boundary conditions at the UV brane, the rotation matrices are included into the KK decompositions [151],

$$\begin{aligned}
A_\mu(x, t) &= \frac{1}{\sqrt{r}} \sum_n \chi_n^A(t) A_\mu^{(n)}(x) , & A_t(x, t) &= -\frac{1}{\sqrt{r}} \sum_n \frac{kt}{m_n^A} \partial_t \chi_n^A(t) \varphi_A^{(n)}(x) , \\
\vec{Z}_\mu(x, t) &= \frac{\mathbf{R}_Z}{\sqrt{r}} \sum_n \vec{\chi}_n^Z(t) Z_\mu^{(n)}(x) , & \vec{Z}_t(x, t) &= -\frac{\mathbf{R}_Z}{\sqrt{r}} \sum_n \frac{kt}{m_n^Z} \partial_t \vec{\chi}_n^Z(t) \varphi_Z^{(n)}(x) , \\
\vec{W}_\mu^\pm(x, t) &= \frac{\mathbf{R}_W}{\sqrt{r}} \sum_n \vec{\chi}_n^W(t) W_\mu^{\pm(n)}(x) , & \vec{W}_t^\pm(x, t) &= -\frac{\mathbf{R}_W}{\sqrt{r}} \sum_n \frac{kt}{m_n^W} \partial_t \vec{\chi}_n^W(t) \varphi_W^{\pm(n)}(x) ,
\end{aligned} \tag{2.187}$$

where  $\vec{\chi}_n^Z(t) = (\chi_n^Z(t), \chi_n^{Z'}(t))^T$ , and  $\vec{\chi}_n^W(t) = (\chi_n^L(t), \chi_n^R(t))^T$ . The boundary conditions for the profiles can be deduced from the conditions presented in Table 2.2. The normalization conditions for the vectors apply

$$\frac{2\pi}{L} \int_\epsilon^1 \frac{dt}{t} \vec{\chi}_m^{[A]}(t)^T \vec{\chi}_n^{[A]}(t) = \delta_{mn} , \quad [A] = W, Z , \tag{2.188}$$

in order to obtain the correct mass terms for the KK modes. The photon profiles obey the standard normalization condition. Likewise to the brane-Higgs scenario, presented before, one can expand the four-dimensional Goldstone bosons  $\vec{\varphi}^3(x)$  and  $\vec{\varphi}^\pm(x)$  in a basis of mass eigenstates, and define a gauge-fixing Lagrangian in order to remove the mixing terms between the Goldstone bosons, the scalar parts of the gauge bosons and the vector components of the gauge bosons [151]. These parts are skipped here. By inserting the KK decompositions into the five-dimensional action, one can derive the following equations of motion for the gauge boson profiles [151]

$$-t \partial_t \left[ \frac{1}{t} \partial_t \mathbf{R}_{[A]} \vec{\chi}^{[A]}(t) \right] = \frac{(m_n^{[A]})^2}{M_{KK}^2} \mathbf{R}_{[A]} \vec{\chi}_n^{[A]}(t) - \delta(t-1) \frac{L}{2\pi r} \frac{M_{[A]}^2}{M_{KK}^2} \mathbf{P}_{(+)} \mathbf{R}_{[A]} \vec{\chi}^{[A]}(t) , \tag{2.189}$$

where  $\mathbf{P}_{(+)} = \text{diag}(1, 0)$ , and  $[A] = Z, W, A$ , with  $M_Z = M_W = M_{\tilde{A}}$ , and  $M_A = 0$ , in order to obtain proper kinetic terms for the KK modes. The appropriate boundary conditions at the IR brane read<sup>4</sup>

$$\mathbf{R}_{[A]} \partial_t \vec{\chi}_n^{[A]}(t) |_{t=1} = -\frac{L}{2\pi r} \frac{M_{\tilde{A}}^2}{M_{KK}^2} \mathbf{P}_{(+)} \mathbf{R}_{[A]} \vec{\chi}^{[A]}(t) , \tag{2.190}$$

where for the photon profile the right-hand side is equal to zero. At the UV brane, the boundary conditions read

$$(\mathbf{P}_{(+)} \partial_t + \mathbf{P}_{(-)}) \vec{\chi}_n^{[A]}(t) = (0 \ 0)^T , \tag{2.191}$$

with  $\mathbf{P}_{(-)} = \text{diag}(0, 1)$ . One can see that both for the W and Z bosons, the equations of motions and the IR boundary conditions are governed by the same five-dimensional mass parameter  $M_{\tilde{A}}$ . For that reason, when calculating the oblique corrections, parametrized by the Peskin-Takeuchi parameters, the leading corrections in the zero-mode masses and profiles, and the

<sup>4</sup>These conditions can be derived, *e.g.* by using the  $\phi$ -coordinate and by integrating the equations of motion over an infinitesimal interval around  $|\phi| = \pi$  [151].

five-dimensional propagators, are equal, and cancel each other out. As a consequence, small new-physics corrections are induced to these parameters. Using an expansion in powers of  $v^2/M_{KK}^2$ , one can determine the zero-mode gauge boson profiles as

$$\begin{aligned}\bar{\chi}_0^Z(t) &= \left( \frac{1}{\sqrt{2\pi}} - \frac{m_Z^2}{2\sqrt{2\pi}M_{KK}^2} \left[ t^2 \left( L + \log(t) - \frac{1}{2} \right) - \frac{1}{2} + \frac{1}{2L} \right] \right. \\ &\quad \left. + \frac{Lt^2 m_Z^2}{2\sqrt{2\pi}M_{KK}^2} \frac{\sin\theta_Z}{\cos\theta_Z} \right) + \mathcal{O}\left(\frac{v^4}{M_{KK}^4}\right), \\ \bar{\chi}_0^W(t) &= \left( \frac{1}{\sqrt{2\pi}} - \frac{m_W^2}{2\sqrt{2\pi}M_{KK}^2} \left[ t^2 \left( L + \log(t) - \frac{1}{2} \right) - \frac{1}{2} + \frac{1}{2L} \right] \right. \\ &\quad \left. + \frac{Lt^2 m_W^2}{2\sqrt{2\pi}M_{KK}^2} \frac{\sin\theta_W}{\cos\theta_W} \right) + \mathcal{O}\left(\frac{v^4}{M_{KK}^4}\right).\end{aligned}\tag{2.192}$$

The first rows of the IR boundary conditions determine the analytic expressions for the masses of the zero-mode W and Z bosons. To the first order, one can determine [151]

$$\begin{aligned}m_{[A]}^2 &= \tilde{m}_{[A]}^2 \left[ 1 - \frac{m_{\bar{A}}^2}{2M_{KK}^2} L + \frac{\tilde{m}_{[A]}^2}{2M_{KK}^2} \left( 1 - \frac{1}{2L} \right) \right] + \mathcal{O}\left(\frac{v^4}{M_{KK}^4}\right), \\ &= \tilde{m}_{[A]}^2 \left[ 1 - \frac{\tilde{m}_{[A]}^2}{2M_{KK}^2} \left( \frac{L}{\cos^2\theta_{[A]}} - 1 + \frac{1}{2L} \right) \right] + \mathcal{O}\left(\frac{v^4}{M_{KK}^4}\right),\end{aligned}\tag{2.193}$$

where  $[A] = W, Z$ , and the parametric masses are  $m_{\bar{A}} = M_{\bar{A}}/\sqrt{2\pi r}$ , and  $\tilde{m}_W = g_L v/2 = \cos\theta_W m_{\bar{A}}$ , and  $\tilde{m}_Z = \sqrt{g_L^2 + g_Y^2} v/2 = \cos\theta_Z m_{\bar{A}}$ . As stated before, one can observe that the  $L$ -enhanced correction terms in the formulas for the masses of the W and Z bosons scale with the squared of the **same** parametric mass  $m_{\bar{A}}^2$ . This is due to the restored custodial symmetry on the IR brane, which creates the first equal terms in the mass formulas. The second correction terms are different, but of smaller magnitudes compared to the first ones. The origin of these terms are the differing mixing angles of the rotation matrices  $\mathbf{R}_{[A]}$ , arising from the fact that the custodial symmetry is violated on the UV brane. As a consequence, the  $L$  and  $R$  gauge boson fields get mixed by the IR boundary conditions, creating the smaller, differing contributions to the  $W$  and  $Z$  boson masses. Altogether, the dominant equal terms cancel each other out in the calculation of the  $\rho$  and  $T$  parameters, and provide the custodial protection mechanism, which will allow for smaller  $M_{KK}$  masses as a consequence, as we will show in the last section of this chapter. On the contrary, in the minimal RS model, there are two different parametric masses  $\tilde{m}_W$  and  $\tilde{m}_Z$  in the IR boundary conditions and the mass relations, which generate large,  $L$ -enhanced contributions to the  $\rho$  and  $T$  parameters.

### 2.3.2 Fermion sector

To implement also a custodial protection mechanism for the  $Zb_L\bar{b}_L$ -vertex, a discrete symmetry, the  $P_{LR}$ -symmetry, is imposed, which interchanges between the two  $SU(2)$  groups [166, 176]. As a consequence, the left-handed bottom quark has to be part of a  $SU(2)_L \times SU(2)_R$ -bi-doublet with the isospin quantum numbers  $T_L^3 = -T_R^3 = -1/2$  [151]. In this way, the quantum numbers of the other fields are fixed uniquely. The charges of the groups  $U(1)_{\text{em}}$  and  $U(1)_X$  are connected by the relations  $Y = -T_R^3 + Q_X$  and  $Q = T_L^3 + Y$ . Moreover, the right-handed down-type quarks have to be embedded in a  $SU(2)_R$ -triplet in order to get an  $U(1)_X$ -invariant Yukawa coupling.

The same representations under  $SU(2)_L \times SU(2)_R$  are chosen for all three quark generations. Then, the multiplet structure follows for the quark fields with an even  $Z_2$ -parity [151, 166]:

$$\begin{aligned}
Q_L &\equiv \begin{pmatrix} u_L^{(+)} \frac{2}{3} & \lambda_L^{(-)} \frac{5}{3} \\ d_L^{(+)} -\frac{1}{3} & u_L'^{(-)} \frac{2}{3} \end{pmatrix}_{\frac{2}{3}}, & u_R^c &\equiv \left( u_R^{c(+)} \frac{2}{3} \right)_{\frac{2}{3}}, \\
\mathcal{T}_R &\equiv \mathcal{T}_{1R} \oplus \mathcal{T}_{2R} \equiv \begin{pmatrix} \Lambda_R'^{(-)} \frac{5}{3} \\ U_R'^{(-)} \frac{2}{3} \\ D_R'^{(-)} -\frac{1}{3} \end{pmatrix}_{\frac{2}{3}} \oplus \left( D_R^{(+)} -\frac{1}{3} \quad U_R^{(-)} \frac{2}{3} \quad \Lambda_R^{(-)} \frac{5}{3} \right)_{\frac{2}{3}}.
\end{aligned} \tag{2.194}$$

Also, there is a second set of multiplets comprising the components of the fields of the opposite chirality. Altogether, there are 15 different quark fields in the up-type quark sector and 9 in the down-type quark sector. The boundary conditions at the two branes are chosen in such a way that there are three light modes in each sector to be identified with the SM quarks. In addition, there are 9 new and exotic fermion fields with an electric charge of  $5/3$ , which do not have zero modes. The superscripts specify the type of the UV boundary conditions that apply for the respective fields. Whereas the fields with a (+) sign obey mixed boundary conditions that allow for a light zero mode, their corresponding  $Z_2$ -odd parts fulfil Dirichlet boundary conditions and do not have zero modes. On the contrary, the fields with a (-) sign correspond to heavy, exotic fermions with no counterparts in the SM, fulfilling Dirichlet boundary conditions for the  $Z_2$ -even fields to avoid the presence of zero modes. These fields are new compared to the minimal RS model. The KK expansions consist of groups of 15 and 9 modes of similar masses in the up- and down-type quark sectors, respectively. Furthermore, there is an additional KK tower with heavy, exotic fermion fields, with 9 excitations of similar masses for each KK level.

For the implementation of the lepton sector, we will distinguish between two different realizations. The first possibility is to consider a lepton sector similar to the quark sector (**custodial model I**), with a multiplet structure as [3]

$$\begin{aligned}
\xi_{1L} &= \begin{pmatrix} \nu_L^{(+)} 0 & \psi_L^{(-)} 1 \\ e_L^{(+)} -1 & \nu_L'^{(-)} 0 \end{pmatrix}_0, & \xi_{2R} &= \left( \nu_R^{c(+)} 0 \right)_0, \\
\xi_{3R} &= \mathcal{T}_{3R} \oplus \mathcal{T}_{4R} = \begin{pmatrix} \Psi_R'^{(-)} 1 \\ N_R'^{(-)} 0 \\ E_R'^{(-)} -1 \end{pmatrix} \oplus \left( E_R^{(+)} -1 \quad N_R^{(-)} 0 \quad \Psi_R^{(-)} 1 \right)_0.
\end{aligned} \tag{2.195}$$

In this set, there are fifteen different lepton states in the neutrino sector, and nine in the charged-lepton sector. According to the boundary conditions, there are three light modes for each sector that can be identified with the SM neutrinos and charged leptons. In addition, there are 9 new and exotic lepton states with an electric charge  $Q_\psi = +1$  without zero modes. For every KK mode, there are fifteen and nine modes in the neutrino and charged-lepton sectors, and in addition, there is a KK tower of exotic lepton states having nine excitations for every KK mode.

As a second possibility, one can consider a more minimal lepton sector (**custodial model II**). In this realization, the left-handed neutrino and the electron are combined in an  $SU(2)_L$

doublet, similar to the SM, and the right-handed electron along with a new, exotic, neutral particle  $N_R$  are combined in an additional  $SU(2)_R$  doublet,

$$L_L = \begin{pmatrix} \nu_L^{(+)} & 0 \\ e_L^{(+)} & -1 \end{pmatrix}_{-\frac{1}{2}}, \quad L_R^c = \begin{pmatrix} e_R^{c(+)} & -1 \\ N_R^{(-)} & 0 \end{pmatrix}_{-\frac{1}{2}}. \quad (2.196)$$

so that these states transform as  $(\mathbf{2}, \mathbf{1})$  and  $(\mathbf{1}, \mathbf{2})$  under the extended gauge group, respectively [3]. The electric charges and the weak isospins are indicated by the subscripts. The boundary conditions at the branes are chosen in such a way that the zero modes of the fields  $\nu_L^{(+)}$ ,  $e_L^{(+)}$  and  $e_R^{c(+)}$  correspond to the light leptons of the SM, without having a right-handed neutrino, whereas the additional, new lepton field  $N_R^{(-)}$  has no zero mode. The zero modes of the charged leptons get a mass by electroweak symmetry breaking, induced by the Yukawa interactions [3],

$$\mathcal{L}_Y = \frac{v}{\sqrt{2}} \int_{\epsilon}^1 dt \delta(t-1) \epsilon^3 \frac{2}{k} (\mathbf{Y}_e)_{ij} (\bar{L}_L^i \Phi \epsilon L_R^j + \bar{L}_R^i \Phi \epsilon L_L^j) + \text{h.c.}, \quad (2.197)$$

where  $\epsilon = i\sigma^2$ . The mass of the zero-mode neutrino can be explained by means of higher-dimensional operators, similar to the SM. Per KK level, there are 6 lepton states and 6 neutrino states, respectively.

In general, the fermion content of the minimal RS model can be obtained by omitting the exotic fermion fields that carry a superscript  $(-)$ . In the following, we present the KK decompositions for the quark fields. An analogous discussion holds for the leptons of the custodial model I, and the decompositions for the custodial model II can be implemented in a similar way. Similar to the gauge boson sector, an one to one correspondence to the quark fields of the minimal RS model can be achieved by introducing the following vector notation [151]

$$\vec{U} = \begin{pmatrix} u \\ u' \end{pmatrix}, \quad \vec{u} = \begin{pmatrix} u^c \\ U' \\ U \end{pmatrix}, \quad \vec{D} = d, \quad \vec{d} = \begin{pmatrix} D \\ D' \end{pmatrix}, \quad \vec{\Lambda} = \lambda, \quad \vec{\lambda} = \begin{pmatrix} \Lambda' \\ \Lambda \end{pmatrix}. \quad (2.198)$$

Then, we can also use a combined notation by including the respective doublet and singlet fields into the larger vectors

$$\mathcal{F}_A(x, t) = \frac{\sqrt{r}\epsilon^2}{t^2} \begin{pmatrix} \vec{F}_A(x, t) \\ \vec{f}_A(x, t) \end{pmatrix}, \quad (2.199)$$

where  $A=L,R$ , and  $\vec{F} = \vec{U}, \vec{D}, \vec{\Lambda}$  and  $\vec{f} = \vec{u}, \vec{d}, \vec{\lambda}$ . The Lagrangian that is bilinear in the fields reads [151, 155, 156, 170, 178]

$$\frac{2\pi}{L\epsilon} \int_{\epsilon}^1 dt \sum_f \left( \bar{\mathcal{F}} \left[ i\partial - M_{KK} \left( \frac{\mathbf{c}_f}{t} + \frac{1}{2} \overleftrightarrow{\partial}_t \gamma_5 \right) \right] \mathcal{F} - \frac{v}{\sqrt{2}} \delta(t-1) \left[ \bar{\mathcal{F}}_L \begin{pmatrix} \mathbf{0} & \mathbf{Y}_{\vec{f}} \\ \mathbf{Y}_{\vec{f}}^\dagger & \mathbf{0} \end{pmatrix} \mathcal{F}_R + \text{h.c.} \right] \right), \quad (2.200)$$

where  $\overleftrightarrow{\partial}_t \equiv \overrightarrow{\partial}_t - \overleftarrow{\partial}_t$ , including the Yukawa matrices

$$\mathbf{Y}_{\vec{u}} \equiv \begin{pmatrix} \mathbf{Y}_u & \frac{1}{\sqrt{2}} \mathbf{Y}_d & \frac{1}{\sqrt{2}} \mathbf{Y}_d \\ \mathbf{Y}_u & -\frac{1}{\sqrt{2}} \mathbf{Y}_d & -\frac{1}{\sqrt{2}} \mathbf{Y}_d \end{pmatrix}, \quad \mathbf{Y}_{\vec{d}} \equiv \mathbf{Y}_{\vec{\lambda}} \equiv (\mathbf{Y}_d \ \mathbf{Y}_d), \quad (2.201)$$

and the bulk mass matrices

$$\begin{aligned}\mathbf{c}_{\bar{u}} &= \text{diag}(\mathbf{c}_Q, \mathbf{c}_Q, -\mathbf{c}_{u^c}, -\mathbf{c}_{\mathcal{T}_1}, -\mathbf{c}_{\mathcal{T}_2}) , \\ \mathbf{c}_{\bar{d}} &= \text{diag}(\mathbf{c}_Q, -\mathbf{c}_{\mathcal{T}_2}, -\mathbf{c}_{\mathcal{T}_1}) , \quad \mathbf{c}_{\bar{\lambda}} = \text{diag}(\mathbf{c}_Q, -\mathbf{c}_{\mathcal{T}_2}, -\mathbf{c}_{\mathcal{T}_1}) .\end{aligned}\tag{2.202}$$

Each of the entries in these abbreviations forms a  $3 \times 3$  matrix itself. The dimensionless, four-dimensional Yukawa matrices were obtained from the dimensionful, five-dimensional Yukawa matrices by  $\mathbf{Y}_q^{5D} \equiv \frac{2\mathbf{Y}_q}{k}$ . In this setting, the Yukawa couplings to the Higgs field include the  $Z_2$ -even and -odd fermion fields<sup>5</sup> [170]. The diagonal bulk mass matrices  $\mathbf{c}_A$  are obtained from the five-dimensional bulk masses  $\mathbf{M}_q$  of the multiplets  $Q, u^c, \mathcal{T}_1, \mathcal{T}_2$ , where  $\mathbf{c}_Q \equiv +\mathbf{M}_Q/k$  and  $\mathbf{c}_A \equiv -\mathbf{M}_A/k$ , and  $A = u^c, \mathcal{T}_1, \mathcal{T}_2$ .

As before, the KK decompositions can be chosen as

$$\mathcal{F}_A(x, t) = \sqrt{\frac{L\epsilon}{2\pi}} \sum_{n=1}^{\infty} \mathcal{F}_A^{(n)}(t) f_A^{(n)}(x) ,\tag{2.203}$$

where  $A=L,R$ ,  $F = U, D, \Lambda$  + leptons and  $f = u, d, \lambda$  + leptons. There are three light zero modes, and 15 heavy states per KK level for the up-type quarks, three light modes and 9 heavy states per KK level for the down-type quarks, as well as 9 heavy states per KK level for the exotic quarks without any light modes. Therefore,  $n = 1, 2, 3$  label the first three light modes, the zero modes that are the SM equivalents, whereas  $n \geq 3$  label the modes of the higher KK levels. For the profiles, we have the following vectors [151]

$$\begin{aligned}\mathcal{U}_L(t) &= \left( \mathbf{C}_n^{Q(+)}(t) \mathbf{a}_n^u , \mathbf{C}_n^{Q(-)}(t) \mathbf{a}_n^{u'} , \mathbf{S}_n^{u^c(+)}(t) \mathbf{a}_n^{u^c} , \mathbf{S}_n^{\mathcal{T}_1(-)}(t) \mathbf{a}_n^{U'} , \mathbf{S}_n^{\mathcal{T}_2(-)}(t) \mathbf{a}_n^U \right)^T , \\ \mathcal{U}_R(t) &= \left( \mathbf{S}_n^{Q(+)}(t) \mathbf{a}_n^u , \mathbf{S}_n^{Q(-)}(t) \mathbf{a}_n^{u'} , \mathbf{C}_n^{u^c(+)}(t) \mathbf{a}_n^{u^c} , \mathbf{C}_n^{\mathcal{T}_1(-)}(t) \mathbf{a}_n^{U'} , \mathbf{C}_n^{\mathcal{T}_2(-)}(t) \mathbf{a}_n^U \right)^T ,\end{aligned}\tag{2.204}$$

$$\begin{aligned}\mathcal{D}_L(t) &= \left( \mathbf{C}_n^{Q(+)}(t) \mathbf{a}_n^d , \mathbf{S}_n^{\mathcal{T}_2(+)}(t) \mathbf{a}_n^D , \mathbf{S}_n^{\mathcal{T}_1(-)}(t) \mathbf{a}_n^{D'} \right)^T , \\ \mathcal{D}_R(t) &= \left( \mathbf{S}_n^{Q(+)}(t) \mathbf{a}_n^d , \mathbf{C}_n^{\mathcal{T}_2(+)}(t) \mathbf{a}_n^D , \mathbf{C}_n^{\mathcal{T}_1(-)}(t) \mathbf{a}_n^{D'} \right)^T ,\end{aligned}\tag{2.205}$$

$$\begin{aligned}\Lambda_L(t) &= \left( \mathbf{C}_n^{Q(-)}(t) \mathbf{a}_n^\lambda , \mathbf{S}_n^{\mathcal{T}_1(-)}(t) \mathbf{a}_n^{\Lambda'} , \mathbf{S}_n^{\mathcal{T}_2(-)}(t) \mathbf{a}_n^\Lambda \right)^T , \\ \Lambda_R(t) &= \left( \mathbf{S}_n^{Q(-)}(t) \mathbf{a}_n^\lambda , \mathbf{C}_n^{\mathcal{T}_1(-)}(t) \mathbf{a}_n^{\Lambda'} , \mathbf{C}_n^{\mathcal{T}_2(-)}(t) \mathbf{a}_n^\Lambda \right)^T ,\end{aligned}\tag{2.206}$$

including  $\mathbf{C}_n^A(t)$  and  $\mathbf{S}_n^A(t)$ , with  $A = Q, u^c, \mathcal{T}_1, \mathcal{T}_2$  as diagonal  $3 \times 3$  matrices, containing the even and odd profiles that get multiplied by the three-vectors  $\mathbf{a}_n^A$ , with  $A = u, u', u^c, U', U, d, D', D, \lambda, \Lambda', \Lambda$ , to encode the flavor structure [151]. As before, the superscripts ( $\pm$ ) indicate the type

<sup>5</sup>For a brane-localized Higgs sector, one can generalize the Yukawa couplings in such a way that the  $Z_2$ -even and -odd fermion fields separately couple to the Higgs field, requiring the replacements  $\mathbf{Y}_{\bar{q}} \rightarrow \mathbf{Y}_{\bar{q}}^C$  and  $\mathbf{Y}_{\bar{q}}^\dagger \rightarrow \mathbf{Y}_{\bar{q}}^{S\dagger}$ . Then, the superscripts in  $\mathbf{Y}_{\bar{q}}^{[C,S]}$  denote the fields to which the Higgs field couples to [151].

of the UV boundary conditions that the profiles fulfil. For every respective KK mode, there are the normalization conditions

$$\int_{\epsilon}^1 dt \mathcal{F}_A^{(m)\dagger}(t) \mathcal{F}_A^{(n)}(t) = \delta_{mn} , \quad (2.207)$$

and the equations of motion read

$$\frac{d}{dt} \mathcal{F}_L^{(n)}(t) = -x_n \mathcal{F}_R^{(n)}(t) + \mathcal{M}_{\bar{f}}(t) \mathcal{F}_L^{(n)}(t) , \quad -\frac{d}{dt} \mathcal{F}_R^{(n)}(t) = -x_n \mathcal{F}_L^{(n)}(t) + \mathcal{M}_{\bar{f}}(t) \mathcal{F}_R^{(n)}(t) , \quad (2.208)$$

including the mass matrix [151]

$$\mathcal{M}_{\bar{f}}(t) = \frac{\mathbf{c}_{\bar{f}}}{t} + \frac{v\delta(t-1)}{\sqrt{2}M_{KK}} \begin{pmatrix} \mathbf{0} & \mathbf{Y}_{\bar{f}} \\ \mathbf{Y}_{\bar{f}}^\dagger & \mathbf{0} \end{pmatrix} . \quad (2.209)$$

The explicit solutions for the profiles with a (+)-sign,  $\mathbf{C}_n^{A(+)}(t)$  and  $\mathbf{S}_n^{A(+)}(t)$ , associated with the bulk mass parameters  $\mathbf{c}_A$ , are similar to the profiles in the minimal RS model [150, 155, 156]. The (-)-profiles  $\mathbf{C}_n^{A(-)}(t)$  and  $\mathbf{S}_n^{A(-)}(t)$  can be derived in a similar manner [151]. The boundary conditions have been summarized before. The Dirichlet condition  $\mathbf{S}_n^{A(+)}(\epsilon) = 0$  holds for the  $Z_2$ -odd part of the fields with a superscript (+), whereas the fields with a superscript (-) fulfil Dirichlet boundary conditions for the  $Z_2$ -even fields, as  $\mathbf{C}_n^{A(-)}(\epsilon) = 0$ . In the presence of a regularized Higgs profile, the IR boundary conditions are of Dirichlet type for all fields, as  $\mathbf{S}_n^{A(\pm)}(1^-) = 0$ .<sup>6</sup> For the fields with  $n = 1, 2, 3$ , the  $C_n^{(\pm)}(t)$  and  $S_n^{(\pm)}(t)$  profiles can be determined in good approximation, up to the order of  $v^2/M_{KK}^2$ , as [150, 151]

$$\begin{aligned} C_n^{(+)} &\approx \sqrt{\frac{L\epsilon}{\pi}} F(c) t^c , & S_n^{(+)}(t) &\approx \pm \sqrt{\frac{L\epsilon}{\pi}} x_n F(c) \frac{t^{1+c} - \epsilon^{1+2c} t^{-c}}{1+2c} , \\ C_n^{(-)}(t) &\approx -\sqrt{\frac{L\epsilon}{\pi}} x_n F(-c) \frac{t^{1-c} - \epsilon^{1-2c} t^c}{1-2c} , & S_n^{(-)}(t) &\approx \pm \sqrt{\frac{L\epsilon}{\pi}} F(-c) t^{-c} , \end{aligned} \quad (2.210)$$

using the rescaled vectors from (2.108) in the KK decompositions. The overall +-signs of the S-profiles hold for the bi-doublet associated to  $\mathbf{c}_Q$ , whereas the --sign applies for the fields associated to  $\mathbf{c}_A$ , with  $A = u^c, \mathcal{T}_1, \mathcal{T}_2$ . The function  $F(c)$  is the usual zero-mode profile [155, 156]. The S-profiles are multiplied with a  $\text{sgn}(\phi)$  in the  $\phi$ -notation in order to have the  $Z_2$ -odd behaviour. One can observe that the profiles  $C_n^{(+)}(t)$  and  $S_n^{(-)}(t)$  are of  $\mathcal{O}(1)$ , whereas the profiles  $C_n^{(-)}(t)$  and  $S_n^{(+)}(t)$  are of  $\mathcal{O}(v/M_{KK})$ . This is crucial in partially shielding the  $Z b_L \bar{b}_L$  and  $Z d_L^i \bar{d}_L^j$  vertices from corrections that stem from a mixing of zero-mode quarks with their KK excitations [151], which is one of the crucial features of the model.

<sup>6</sup>The presence of IR brane-localized terms that originate from the Yukawa couplings dictates the boundary behaviour of the fields, and causes both the  $Z_2$ -even and -odd profiles to become discontinuous at the IR brane with  $\mathbf{C}_n^{[F,f]}(1) \neq \mathbf{C}_n^{[F,f]}(1^-)$  and  $\mathbf{S}_n^{[F,f]}(1) = 0$ , but  $\mathbf{S}_n^{[F,f]}(1^-) \neq 0$  [151, 179]. To find the correct IR boundary conditions requires a proper regularization of the  $\delta$ -functions. One possibility is to see the  $\delta$ -function as the limit of a sequence of regularized functions  $\delta^\eta$  with support on the interval  $x \in [-\eta, 0]$ , such that  $\lim_{\eta \rightarrow 0^+} \int_{-\infty}^{+\infty} dx \delta^\eta(x) f(x) = f(0)$ , for all test functions  $f(x)$ , *i.e.* smooth functions having compact support [151].

In Chapter 5, we will present the calculation of the decay of a new, heavy bulk scalar into a pair of photons. In this calculation, it is necessary to know the multiplet structure of the fields under the SM electroweak gauge group  $SU(2)_L \times U(1)_Y$ . In this regard, the fields can be distinguished by means of the different bulk mass parameters [7]. For the quark fields, there are two  $SU(2)_L$  doublets

$$\mathbf{c}_Q : \begin{pmatrix} u_L^{(+)} \\ d_L^{(+)} \end{pmatrix}_{\frac{1}{6}}, \quad \begin{pmatrix} \lambda_L^{(-)} \\ u_L'^{(-)} \end{pmatrix}_{\frac{7}{6}}, \quad (2.211)$$

one triplet,

$$\mathbf{c}_{\mathcal{T}_1} : \begin{pmatrix} \Lambda_R'^{(-)} \\ U_R'^{(-)} \\ D_R'^{(-)} \end{pmatrix}_{\frac{2}{3}}, \quad (2.212)$$

as well as four singlets,

$$\mathbf{c}_u : \left( u_R^{c(+)} \right)_{\frac{2}{3}}, \quad \mathbf{c}_{\mathcal{T}_2} : \left( D_R^{(+)} \right)_{-\frac{1}{3}}, \quad \left( U_R^{(-)} \right)_{\frac{2}{3}}, \quad \left( \Lambda_R^{(-)} \right)_{\frac{5}{3}}. \quad (2.213)$$

In the custodial model I, there are two  $SU(2)_L$  doublets,

$$\mathbf{c}_L : \begin{pmatrix} \nu_L^{(+)} \\ e_L^{(+)} \end{pmatrix}_{-\frac{1}{2}}, \quad \begin{pmatrix} \psi_L^{(-)} \\ \nu_L'^{(-)} \end{pmatrix}_{\frac{1}{2}}, \quad (2.214)$$

and one triplet,

$$\mathbf{c}_{\mathcal{T}_3} : \begin{pmatrix} \Psi_R'^{(-)} \\ N_R'^{(-)} \\ E_R'^{(-)} \end{pmatrix}_0. \quad (2.215)$$

Furthermore, there are four singlets,

$$\mathbf{c}_\nu : \left( \nu_R^{c(+)} \right)_0, \quad \mathbf{c}_{\mathcal{T}_4} : \left( E_R^{(+)} \right)_{-1}, \quad \left( N_R^{(-)} \right)_0, \quad \left( \Psi_R^{(-)} \right)_1. \quad (2.216)$$

Instead, in the custodial model II, there are one  $SU(2)_L$  doublet,

$$\mathbf{c}_L : \begin{pmatrix} \nu_L^{(+)} \\ e_L^{(+)} \end{pmatrix}_{-\frac{1}{2}}, \quad (2.217)$$

and two singlets

$$\mathbf{c}_e : \left( e_R^{c(+)} \right)_{-1}, \quad \left( N_R'^{(-)} \right)_0. \quad (2.218)$$



## 2.4 Electroweak parameters in the RS scenarios

Varying exclusion bounds apply for the parameter spaces of the different RS scenarios that are considered in this thesis, which are the bulk-Higgs RS model, the brane-Higgs RS model with a minimal bulk gauge symmetry, and the custodial RS model. In this connection, the most significant constraints stem from electroweak precision tests of the four fermion interactions at lower energies. In Subsection 1.1.3, we have described that the oblique electroweak corrections, induced by heavier new particles, to low energy four fermion interactions can be parametrized by means of the S,T,U parameters [82]. The tree-level predictions for the parameters can be computed in the different RS scenarios to be compared to the experimentally derived results. In principle, it is not sufficient to solely restrain on the oblique corrections when describing the new-physics effects on the four fermion interactions that are implied in the RS model. The fermion to gauge boson vertices underlie non-universal modifications from the SM due to the varying fermion profiles. But, considering a selected subset of the most precisely measured observables, one can still parametrize the electroweak corrections in terms of the S, T and U parameters, in good approximation [154]. In the following, we will shortly recapitulate the calculations of the parameters, and the bounds implied on the  $M_{KK}$  mass scale, in three different RS scenarios. Previously, this was already performed, *e.g.* in the references [2, 150, 151, 154, 174, 177]. Further tests of the various scenarios in the context of the electroweak precision observables and flavour physics were performed, *e.g.* in [180–187]. The relevant vacuum polarization functions of the oblique corrections depend on six open parameters in the applied approximation, as illustrated in equation (1.50). Rather than directly calculating the vacuum polarization functions, one can choose the three S,T,U parameters, and the parameter  $\tilde{v}$  together with the five-dimensional gauge couplings  $g_5$  and  $g'_5$ , which can be determined in terms of six precisely known electroweak observables. For the observables, one can take  $G_F$ ,  $m_Z$ ,  $m_W$  (or equivalently  $s_W^2$ ),  $\alpha$  (or equivalently  $s_0^2$ ),  $s_\star^2$  and  $\rho_\star$  [2, 154]. In the following, we will specify the definitions of these observables in the three RS scenarios, the minimal model with a brane Higgs (**mm**), the minimal model with a bulk Higgs (**mmbH**) and the custodial model with a brane Higgs (**cm**).

By the fact that the photon has a flat profile along the extra dimension, the fine-structure constant  $\alpha$  can be defined as

$$\alpha = \frac{e_5^2}{2\pi r 4\pi} , \quad (2.219)$$

which explicitly reads in the different models

$$\alpha_{\text{mm}} = \frac{g^2 g'^2}{4\pi(g^2 + g'^2)} , \quad \alpha_{\text{mmbH}} = \frac{g_5^2 g_5'^2}{2\pi r 4\pi(g_5^2 + g_5'^2)} , \quad \alpha_{\text{cm}} = \frac{g_L^2 g_Y^2}{4\pi(g_L^2 + g_Y^2)} . \quad (2.220)$$

To derive the relations between the RS model parameter  $v$  and the Higgs vev in the SM  $v_{SM} \approx 246$  GeV, one can determine the corrections to the Fermi constant  $G_F$  in the RS scenarios by constructing the effective four-fermion interaction that mediates the muon decay. The RS model corrections to this decay process arise due to the modified interactions of the zero-mode W boson with light fermions, and further because the infinite tower of KK W bosons is virtually exchanged instead of just the SM W boson. These effects can be sufficiently parametrized in terms of the five-dimensional W boson propagator functions in the respective scenarios, evaluated at zero four-momentum. These propagator functions are calculated in the next chapter of the

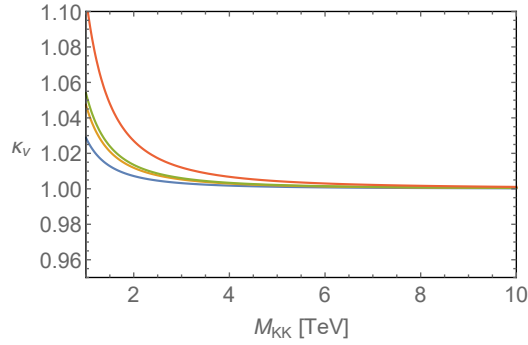


Figure 2.6: In this plot, the relation  $\kappa_v = \frac{v}{v_{SM}}$  between the Higgs vev in the RS model  $v$  and the SM  $v_{SM} \approx 246$  GeV is plotted in dependence of the KK mass scale, in the bulk-Higgs model for  $\beta = 1, 10$  (blue and yellow curves), in the minimal model (green curve), and the custodial model (orange curve).

thesis in Section 3.1.1. In the different RS scenarios, one can derive for the leading corrections

$$\frac{G_F}{\sqrt{2}} \equiv \frac{1}{2v_{SM}^2} = \frac{1}{2v^2} \left[ 1 + \frac{Lm_W^2}{2M_{KK}^2} \mathcal{I}_{RS} + \dots \right], \quad (2.221)$$

$$\mathcal{I}_{mm} = 1, \quad \mathcal{I}_{mmbH} = \frac{2(1+\beta)^2}{(2+\beta)(3+2\beta)}, \quad \mathcal{I}_{cm} = \frac{1}{c_W^2},$$

which stem from the leading terms of the five-dimensional propagator functions. The remaining  $t$ -dependent terms in the propagator functions give suppressed contributions, if convoluted with the profile functions of the light zero-mode fermions, and are therefore neglected. In a similar manner, the parameter  $\rho_*$ , stemming from the effective four-fermion Lagrangian  $\mathcal{L}_{\text{eff}} = -\frac{4G_F}{\sqrt{2}} [J_\mu^+ J^{-\mu} + \rho_*(J_3^\mu - s_*^2 J_Q^\mu)^2]$ , is determined by the leading terms of the W and Z boson propagators [154], where one can get

$$\rho_{*,mm} = 1 + \frac{L(m_Z^2 - m_W^2)}{2M_{KK}^2} + \dots, \quad (2.222)$$

$$\rho_{*,mmbH} = 1 + \frac{(m_Z^2 - m_W^2)}{2M_{KK}^2} \frac{2L(1+\beta)^2}{(2+\beta)(3+2\beta)} + \dots,$$

$$\rho_{*,cm} = 1 + \dots$$

In the custodial model, the leading terms in the W and Z boson propagator functions both scale with the same mass parameter  $m_A^2$ , where  $\frac{\tilde{m}_W^2}{c_W^2} = \frac{\tilde{m}_Z^2}{c_Z^2} = m_A^2$ . These terms cancel each other out in the calculation of the  $\rho_*$  and  $T$  parameters [151], which is the custodial protection mechanism. The parameter  $s_*^2$  in the weak neutral current coincides with the definitions of the weak mixing angle  $s_w^2$  in the different scenarios [154]

$$s_{*,mm}^2 = \frac{g'^2}{g^2 + g'^2}, \quad s_{*,mmbH}^2 = \frac{g_5'^2}{g_5^2 + g_5'^2}, \quad s_{*,cm}^2 = \frac{g_Y^2}{g_L^2 + g_Y^2}. \quad (2.223)$$

Furthermore, there is a second definition, employing the ratio of the electroweak gauge boson masses as [82]

$$\tilde{s}_W^2 \equiv 1 - \frac{m_W^2}{m_Z^2}, \quad (2.224)$$

which reads in the different scenarios

$$\begin{aligned} \tilde{s}_{W,\text{mm}}^2 &= \frac{g'^2}{g^2 + g'^2} \left( 1 - \frac{m_W^2}{2M_{KK}^2} \left( L - 1 + \frac{1}{2L} \right) + \dots \right), \\ \tilde{s}_{W,\text{mmbH}}^2 &= \frac{g_5'^2}{g_5^2 + g_5'^2} \left( 1 - \frac{m_W^2}{2M_{KK}^2} \left[ \frac{2L(1+\beta)^2}{(2+\beta)(3+2\beta)} - 1 + \frac{1}{(2+\beta)^2} + \frac{1}{2L} \right] + \dots \right), \\ \tilde{s}_{W,\text{cm}}^2 &= \frac{g_Y^2}{g_L^2 + g_Y^2} \left( 1 - \frac{m_W^2}{2M_{KK}^2} \left[ -1 + \frac{1}{2L} \right] + \dots \right). \end{aligned} \quad (2.225)$$

A third definition relates the weak mixing angle to the precisely measured parameters  $G_F$ ,  $\alpha$  and  $m_Z$  by [82]

$$s_0^2 c_0^2 \equiv \frac{\pi\alpha}{\sqrt{2}G_F m_Z^2}, \quad (2.226)$$

where one has in the different scenarios

$$\begin{aligned} s_{0,\text{mm}}^2 &= \frac{g'^2}{(g^2 + g'^2)} \left( 1 + \frac{m_W^2}{2M_{KK}^2} \frac{1}{(\tilde{c}_W^2 - \tilde{s}_W^2)} \left[ s_W^2 L - 1 + \frac{1}{2L} \right] + \dots \right), \\ s_{0,\text{mmbH}}^2 &= \frac{g_5'^2}{g_5^2 + g_5'^2} \left( 1 + \frac{m_W^2}{2M_{KK}^2} \frac{1}{(\tilde{c}_W^2 - \tilde{s}_W^2)} \left[ \tilde{s}_W^2 \frac{2L(1+\beta)^2}{(2+\beta)(3+2\beta)} - 1 + \frac{1}{(2+\beta)^2} + \frac{1}{2L} \right] + \dots \right), \\ s_{0,\text{cm}}^2 &= \frac{g_Y^2}{g_L^2 + g_Y^2} \left( 1 - \frac{m_W^2}{2M_{KK}^2} \frac{1}{(\tilde{c}_W^2 - \tilde{s}_W^2)} \left[ 1 - \frac{1}{2L} \right] \dots \right) + \dots \end{aligned} \quad (2.227)$$

With this list of definitions, one can solve for the S,T,U parameters by using the first three relations of the equation (3.13) in [82], which are

$$\begin{aligned} \frac{m_W^2}{m_Z^2} - c_0^2 &= \frac{\alpha c_\star^2}{(c_\star^2 - s_\star^2)} \left( -\frac{1}{2} S + c_\star^2 T + \frac{(c_\star^2 - s_\star^2)}{4s_\star^2} U \right), \\ \rho_\star - 1 &= \alpha T, \\ s_\star^2 - s_0^2 &= \frac{\alpha}{(c_\star^2 - s_\star^2)} \left( \frac{1}{4} S - s_\star^2 c_\star^2 T \right). \end{aligned} \quad (2.228)$$

Then, the results in the different RS scenarios are

$$\begin{aligned} T_{\text{mm}} &= \frac{\pi v^2 L}{2M_{KK}^2 \tilde{c}_W^2}, & S_{\text{mm}} &= \frac{2\pi v^2}{M_{KK}^2} \left( 1 - \frac{1}{2L} \right), \\ T_{\text{mmbH}} &= \frac{\pi v^2}{\tilde{c}_W^2 M_{KK}^2} \frac{L(1+\beta)^2}{(2+\beta)(3+2\beta)}, & S_{\text{mmbH}} &= \frac{2\pi v^2}{M_{KK}^2} \left( 1 - \frac{1}{2L} - \frac{1}{(2+\beta)^2} \right), \\ T_{\text{cm}} &= 0, & S_{\text{cm}} &= \frac{2\pi v^2}{M_{KK}^2} \left( 1 - \frac{1}{2L} \right), \end{aligned} \quad (2.229)$$

whereas  $U = 0$  in all cases. These predictions can be compared to results that were derived from electroweak precision data in [86], which are

$$\begin{aligned} S_{\text{Ufree}} &= 0.05 \pm 0.11, & T_{\text{Ufree}} &= 0.09 \pm 0.13, & U &= 0.01 \pm 0.11, \\ S_{U=0} &= 0.06 \pm 0.09, & T_{U=0} &= 0.10 \pm 0.07. \end{aligned} \quad (2.230)$$

These experimental results were determined in two different manners, for a floating  $U$  parameter from a three parameter analysis, and for the constraint  $U = 0$ , respectively. The matrices with the correlation coefficients between the parameters are [86]

$$\rho_{\text{Ufree}} = \begin{pmatrix} 1 & 0.90 & -0.59 \\ 0.90 & 1 & -0.83 \\ -0.59 & -0.83 & 1 \end{pmatrix}, \quad \rho_{U=0} = \begin{pmatrix} 1 & 0.91 \\ 0.91 & 1 \end{pmatrix}. \quad (2.231)$$

The values  $m_{h,\text{ref}} = 125$  GeV and  $m_{t,\text{ref}} = 173$  GeV were taken for the SM reference point, see (1.52). The results were determined by a statistical maximum likelihood method to find the regions of maximal overlaps of the experimental results for the various electroweak precision observables. In this relation, the boundaries of the intervals that indicate a respective level of confidence for the results are defined by

$$\chi^2 = \vec{P}^T \rho^{-1} \vec{P}, \quad (2.232)$$

where

$$\begin{aligned} \vec{P}_{\text{Ufree}} &= \left( \frac{(S - S_{\text{central}})}{\Delta S}, \frac{(T - T_{\text{central}})}{\Delta T}, \frac{(U - U_{\text{central}})}{\Delta U} \right)^T, \\ \vec{P}_{U=0} &= \left( \frac{(S - S_{\text{central}})}{\Delta S}, \frac{(T - T_{\text{central}})}{\Delta T} \right)^T, \end{aligned} \quad (2.233)$$

and where the  $\chi^2$  is equal to 2.41 for 68%, to 5.99 for 95%, and to 9.21 for 99% CL, respectively. The regions of different CLs for the results are plotted in Figure 2.7, where for the case of a floating  $U$  parameter, we plot the two-dimensional projection on  $S$  and  $T$  of the three-parameter CL ellipse. The black lines mark the predictions from the different RS scenarios. By determining the points of the intersections between the RS predictions and the ellipses of CLs, we can determine the following exclusion bounds on the  $M_{KK}$  mass scale to 95% CL

$$M_{KK} > 4.4 \text{ TeV } (U \neq 0), \quad M_{KK} > 5.3 \text{ TeV } (U = 0) \quad (2.234)$$

for the minimal RS model,

$$\begin{aligned} M_{KK} &> 2.4 \text{ TeV for } \beta = 0, \quad M_{KK} > 3.1 \text{ TeV for } \beta = 1, \quad M_{KK} > 4.1 \text{ TeV for } \beta = 10 \text{ } (U \neq 0), \\ M_{KK} &> 2.9 \text{ TeV for } \beta = 0, \quad M_{KK} > 3.7 \text{ TeV for } \beta = 1, \quad M_{KK} > 4.9 \text{ TeV for } \beta = 10 \text{ } (U = 0) \end{aligned} \quad (2.235)$$

for the minimal model with a bulk Higgs field and

$$M_{KK} > 2.0 \text{ TeV } (U \neq 0), \quad M_{KK} > 4.7 \text{ TeV } (U = 0) \quad (2.236)$$

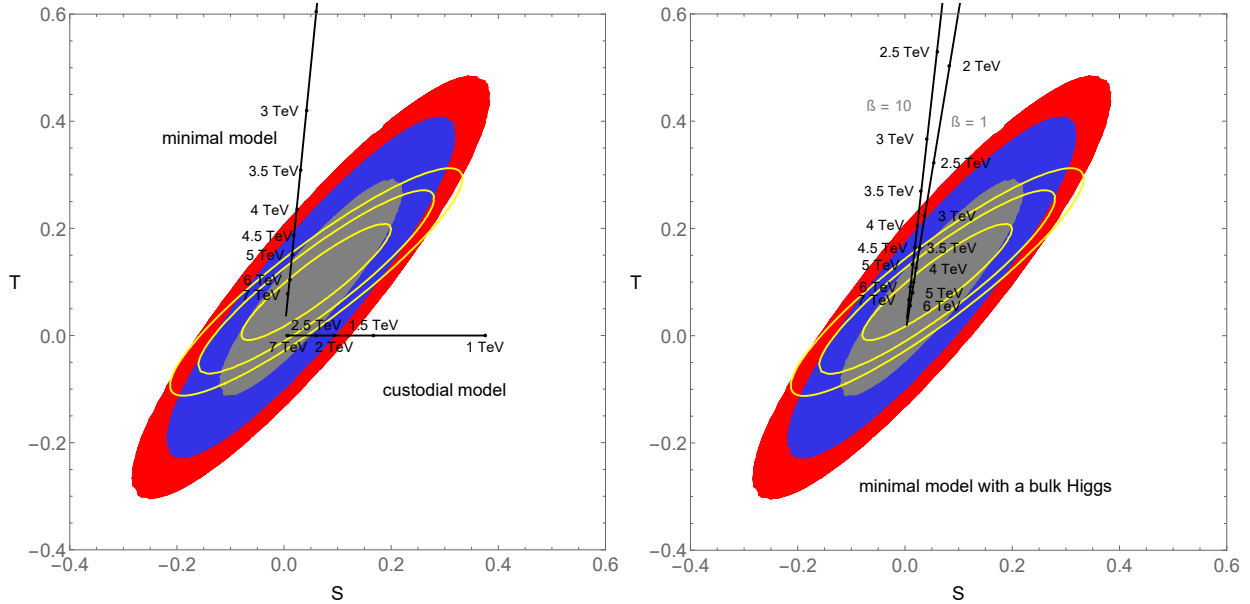


Figure 2.7: These graphics illustrate the ellipses of the 68%, 95% and 99% CL intervals for the experimental results for the parameters  $S$  and  $T$  from [86], together with the predictions for  $S$  and  $T$  in the different RS scenarios. Whereas the coloured ellipses correspond to the results with a floating  $U$  parameter, the yellow, line-shaped ellipses give the results for  $U = 0$ . By means of a comparison between the RS predictions and the ellipses of 95% CL, we have determined the bounds on the  $M_{KK}$  mass scale that are summarized in the text.

for the custodial model, respectively. We observe that the bounds, derived for a floating  $U$  parameter, are weaker than the bounds for  $U = 0$ .

The lightest KK mass state, the first KK resonance of the gluon, has a mass  $M_{g(1)} \approx 2.45 M_{KK}$ , as derived before [162, 169]. So, the lightest particle that is predicted in addition to the SM by the minimal RS model with a brane Higgs field has a mass of at least 10.8 TeV, whereas it can have a mass as low as 4.9 TeV in the custodial RS model, if optimistically assuming that  $U \neq 0$  due to higher order corrections. In the past, this established the custodial RS model to be very interesting for phenomenological searches. Nevertheless, it turned out that the parameter space of the custodial model can be constrained in a much stronger manner by investigations of Higgs processes, as *e.g.* by the  $h \rightarrow ZZ^*$  decay process, due to the presence of the enlarged particle structure, virtually contributing in loop processes [2–4]. In the RS model with a bulk Higgs field, masses for the lightest KK particles as low as  $M_{g(1)} > 5.9$  TeV, for  $\beta = 0$  and  $U \neq 0$ , are compatible to the Peskin-Takeuchi parameters. In this sense, the bulk-Higgs framework can nearly compete with the involved custodial model concerning the reduced exclusion bounds, compared to the minimal model with a brane Higgs [154]. Whereas the custodial model provides the enlarged particle structure, the bulk-Higgs scenario can be considered with a minimal bulk gauge group, instead. All the RS corrections, *i.e.* corrections in the effective four-dimensional vertex couplings and contributions from KK towers, are reduced for lower values of  $\beta$  and a stronger bulk-Higgs localization. Also, the corrections to the effective four-fermion interactions and the electroweak precision observables are reduced. A lower violation of the

custodial isospin symmetry occurs due to smaller couplings between the zero modes and KK states. For these reasons, the bulk-Higgs RS model can form a very interesting alternative to the complex custodial model. This bulk-Higgs model will be investigated in the main parts of the thesis.

# Chapter 3

## Five-Dimensional Propagator Functions

The scattering amplitudes of loop-induced production and decay processes involve the exchanges of virtual KK particle towers. As a consequence, the amplitudes depend on combinations of the four-dimensional propagators of KK particles, and the vertex functions that contain the KK profiles. Such combinations can be summed up by five-dimensional propagator functions in order to derive analytic expressions. The KK profile functions form complete sets of orthonormal functions on the orbifold, subject to appropriate boundary conditions. For that reason, it is possible to determine analytic expressions for the five-dimensional propagator functions. These can be obtained by solving the differential equations, which follow from the five-dimensional action that is bilinear in the particle fields. In this chapter, we derive the five-dimensional propagator functions for gauge bosons, physical scalars and fermions in the framework with a bulk-Higgs field. The differential equations for the propagator functions significantly complicate due to the inclusion of non-linear terms compared to brane-Higgs scenarios. The non-linear terms are caused by the Higgs vev that depends on the extra dimension. In this respect, we have to work with different kinds of approximations, according to the processes for which the respective five-dimensional propagator functions are used to sum up the KK particle towers, respectively.

### 3.1 Gauge boson propagator

The five-dimensional propagator function for the vector W bosons can be used to sum over the KK tower of W bosons in the amplitude of the Higgs decay into two photons. The differential equation for that function is defined by the terms of the Lagrangian that are bilinear in the vector W bosons. These terms result from the kinetic and gauge fixing parts, and also from the  $t$ -dependent mass term, which is induced by a coupling of the W bosons to the vev of the bulk-Higgs field, after spontaneous symmetry breaking. One finds the following expression

$$\mathcal{L}_{5D} \ni \frac{2\pi}{L} \int_{\epsilon}^1 \frac{dt}{t} W_{\mu}^{+} K_{\xi}^{\mu\nu} W_{\nu}^{-} + \text{terms of } W_t^{\pm} , \quad (3.1)$$

where

$$K_{\xi}^{\mu\nu} = \left( \partial^2 - M_{KK}^2 t \partial_t \frac{1}{t} \partial_t \right) \eta^{\mu\nu} - \left( 1 - \frac{1}{\xi} \right) \partial^{\mu} \partial^{\nu} + \frac{g_5^2}{4} k(1 + \beta) v^2 \eta^{\mu\nu} , \quad (3.2)$$

is the inverse Feynman propagator in the  $R_\xi$ -gauge for the vector part of the five-dimensional W boson propagator. By applying a Fourier-transformation of the four-coordinates, according to  $i\partial_\mu = p_\mu$ , one obtains the following defining differential equation for the five-dimensional propagator of the vector W bosons

$$\left[ \left( -\frac{p^2}{M_{KK}^2} - t\partial_t \frac{1}{t} \partial_t + \frac{g_5^2 k(1+\beta)v^2}{4M_{KK}^2} \right) \eta^{\mu\nu} + \left( 1 - \frac{1}{\xi} \right) \frac{p^\mu p^\nu}{M_{KK}^2} \right] D_{\nu\rho}^\xi(-p^2, t; t') = \frac{Lt'}{2\pi M_{KK}^2} \delta_\rho^\mu \delta(t-t'). \quad (3.3)$$

One can apply the following ansatz

$$\begin{aligned} D_{\nu\rho}^\xi(t, t'; -p^2) &= \sum_{n=0}^{\infty} \chi_n^W(t) \chi_n^W(t') \left[ \frac{i}{(m_n^{W2} - p^2)} \left( \eta_{\nu\rho} - \frac{p_\nu p_\rho}{p^2} \right) + \frac{i\xi}{(\xi m_n^{W2} - p^2)} \frac{p_\nu p_\rho}{p^2} \right] \\ &= B_W(t, t'; -p^2) \left( \eta_{\nu\rho} - \frac{p_\nu p_\rho}{p^2} \right) + A_\xi(t, t'; -p^2) \frac{p_\nu p_\rho}{p^2} \end{aligned} \quad (3.4)$$

for the propagator function in the equation before, where  $A_\xi(t, t'; -p^2) = B_W(t, t'; -p^2/\xi)$ . Therefore, the propagator in the Feynman-t'Hooft gauge for  $\xi = 1$  is defined by just the function  $B_W(t, t'; -p^2)$ , as [3]

$$D_{\nu\rho}^{\xi=1}(t, t'; -p^2) = \sum_{n=0}^{\infty} \frac{\chi_n^W(t) \chi_n^W(t')}{(m_n^{W2} - p^2)} i\eta_{\nu\rho} = B_W(t, t'; -p^2) i\eta_{\nu\rho}. \quad (3.5)$$

For this function, the following differential equation is derived [3], with  $\tilde{m}_W^2 = \frac{g_5^2 v^2}{8\pi r}$ ,

$$\left( t\partial_t \frac{1}{t} \partial_t + \frac{p^2}{M_{KK}^2} - 2\pi \frac{\tilde{m}_W^2}{M_{KK}^2} kr(1+\beta)t^{2+2\beta} \right) B_W(t, t'; -p^2) = -\frac{Lt}{2\pi M_{KK}^2} \delta(t-t'). \quad (3.6)$$

The boundary conditions at the branes are of Neuman-type,

$$\partial_t B_W(t, t'; -p^2) = 0 \quad \text{for } t = \epsilon, 1, \quad (3.7)$$

following from the boundary conditions for the gauge boson profiles.

The differential equation for the five-dimensional W boson propagator in the bulk-Higgs scenario contains a term that non-linearly depends on the coordinate  $t$ , which complicates the solving of the equation drastically. For  $p^2 = \mathcal{O}(m_h^2) \ll M_{KK}^2$ , much smaller than the KK mass scale, it is possible to calculate a result up to the order  $v^2/M_{KK}^2$ , by using a perturbative approach. In order to solve the homogeneous differential equation for  $t \neq t'$ , one can treat the last two terms on the left-hand side of the equation as a perturbation, along with the perturbation parameter

$$\rho = \frac{v^2}{M_{KK}^2}. \quad (3.8)$$

Then, one starts by considering two separate solutions for the cases  $t < t'$ , named  $B_W^<(t, t'; -p^2)$ , and for  $t > t'$ , named  $B_W^>(t, t'; -p^2)$ , respectively. These two solutions are matched together at the point  $t'$ , by fulfilling the continuity condition,

$$B_W^>(t', t', -p^2) \stackrel{!}{=} B_W^<(t', t', -p^2). \quad (3.9)$$



Further, a “jump condition” is obtained by integrating the differential equation over an infinitesimal interval around  $t = t'$ . The terms that do not contain derivatives cancel each other out when inserting the integration boundaries,

$$\begin{aligned} \int_{t_-}^{t_+} dt \left( t \partial_t \frac{1}{t} \partial_t \right) B_W(t, t'; -p^2) &= \int_{t_-}^{t_+} dt \partial_t^2 B_W(t, t'; -p^2) = \partial_t B_W(t, t'; -p^2) \Big|_{t=t_-}^{t=t_+} \\ &\stackrel{!}{=} \int_{t_-}^{t_+} dt \left( -\frac{Lt}{2\pi M_{KK}^2} \delta(t - t') \right) = -\frac{Lt'}{2\pi M_{KK}^2}, \end{aligned} \quad (3.10)$$

where  $t_{\pm} = t \pm \delta$ , and  $\lim \delta \rightarrow 0$ , resulting in the condition

$$\partial_t B_W^>(t, t'; -p^2) \Big|_{t=t'} - \partial_t B_W^<(t, t'; -p^2) \Big|_{t=t'} = -\frac{Lt'}{2\pi M_{KK}^2}. \quad (3.11)$$

The solutions for  $B_W^{(>,<)}(t, t'; -p^2)$  are expanded as series expansions in the parameter  $\rho$ . By retaining only the first three terms, one has

$$B_W^{(>,<)}(t, t'; -p^2) = B_{0,W}^{(>,<)}(t, t'; -p^2) + \rho B_{1,W}^{(>,<)}(t, t'; -p^2) + \rho^2 B_{2,W}^{(>,<)}(t, t'; -p^2) + \mathcal{O}(\rho^3). \quad (3.12)$$

Inserting this approach into the differential equation for the function  $B_W$  in (3.6), one gets three separate differential equations for the six functions  $B_{0,W}^{(>,<)}$ ,  $B_{1,W}^{(>,<)}$ ,  $B_{2,W}^{(>,<)}$ , which are proportional to  $\rho^0$ ,  $\rho^1$  and  $\rho^2$ , respectively,

$$\begin{aligned} \sim \rho^0 : \quad &\left( t \partial_t \frac{1}{t} \partial_t \right) B_{0,W}^{(>,<)}(t, t'; -p^2) = 0, \\ \sim \rho^1 : \quad &\left( t \partial_t \frac{1}{t} \partial_t \right) B_{1,W}^{(>,<)}(t, t'; -p^2) \\ &+ \left( \frac{p^2}{v^2} - 2\pi \frac{\tilde{m}_W^2}{v^2} kr(1 + \beta)t^{2+2\beta} \right) B_{0,W}^{(>,<)}(t, t'; -p^2) = -\frac{Lt'}{2\pi v^2} \delta(t - t'), \\ \sim \rho^2 : \quad &\left( t \partial_t \frac{1}{t} \partial_t \right) B_{2,W}^{(>,<)}(t, t'; -p^2) + \left( \frac{p^2}{v^2} - 2\pi \frac{\tilde{m}_W^2}{v^2} kr(1 + \beta)t^{2+2\beta} \right) B_{1,W}^{(>,<)}(t, t'; -p^2) = 0. \end{aligned} \quad (3.13)$$

The six solutions can be determined such that each one satisfies the boundary conditions together with the continuity and jump conditions. These conditions allow to determine the integration constants, where the right hand side of the jump condition holds only for  $B_{1,W}^{(>,<)}$ , and is 0 for the other four functions. First, one determines the constants in the functions  $B_{0,W}^{(>,<)}$ , and then in  $B_{1,W}^{(>,<)}$  and  $B_{2,W}^{(>,<)}$ , respectively. After that, an undetermined constant remains in the solutions for  $B_{2,W}^{(>,<)}$ , which is irrelevant, however, as we only keep the first four functions  $B_{0,W}^{(>,<)}$  and  $B_{1,W}^{(>,<)}$  in the result. Then, for the full gauge boson propagator, one finds

$$B_W^{(>,<)}(t, t'; -p^2) = \frac{1}{2\pi} \left[ \frac{c_1(t, t')}{m_W^2 - p^2} + \frac{c_2(t, t')}{2M_{KK}^2} + \mathcal{O} \left( \frac{v^2}{M_{KK}^4} \right) \right], \quad (3.14)$$

where

$$c_1(t, t') = 1 + \frac{m_W^2}{2M_{KK}^2} \left[ \frac{L(t^{4+2\beta} + t'^{4+2\beta})}{2 + \beta} + \frac{(1 + \beta)(3 + \beta)}{(2 + \beta)^2} - \frac{1}{L} - t^2 \left( L - \frac{1}{2} + \ln t \right) - t'^2 \left( L - \frac{1}{2} + \ln t' \right) \right] \quad (3.15)$$

and

$$c_2(t, t') = Lt_{<}^2 + \frac{1}{2L} + t^2 \left( \ln t - \frac{1}{2} \right) + t'^2 \left( \ln t' - \frac{1}{2} \right). \quad (3.16)$$

This solution holds for the two cases for  $t > t'$  and  $t < t'$ , where  $t_{<} = \min [t, t']$  and  $t_{>} = \max [t, t']$ . In an intermediate step of the calculation, the parametric W boson mass  $\tilde{m}_W$  was replaced by the physical W boson mass in the bulk-Higgs scenario, given in (2.88). Using this result, one can calculate the KK tower contributions in scattering processes up to the order  $v^2/M_{KK}^2$ .

In a scenario with a brane-localized Higgs field, the difference is that the mass term from the gauge-boson Lagrangian is included in the IR boundary conditions, and does not appear in the differential equation for the propagator function. This simplifies the differential equation for the function  $B_W(t, t'; -p^2)$  to [3]

$$\left( \frac{p^2}{M_{KK}^2} + t \partial_t \frac{1}{t} \partial_t \right) B_W(t, t'; -p^2) = -\frac{Lt}{2\pi M_{KK}^2} \delta(t - t'), \quad (3.17)$$

where the boundary conditions are

$$\partial_t B_W(t, t'; -p^2)|_{t=\epsilon} = 0, \quad B_W(t, t'; -p^2)|_{t=1^-} = -\frac{L\tilde{m}_W^2}{M_{KK}^2} B_W(1, t'; -p^2), \quad (3.18)$$

which include the mass term, and the jump condition

$$\partial_t B_W(t, t'; -p^2)|_{t=t'-0}^{t'+0} = -\frac{Lt'}{2\pi M_{KK}^2} \quad (3.19)$$

is derived as before. In this case, we have a linear differential equation, where it is possible to determine an exact solution to all orders of  $v^2/M_{KK}^2$ . The solution depends on the Bessel functions of the first and second kind, and was determined, *e.g.* in [3]. By means of an expansion including the order  $v^2/M_{KK}^2$ , we encounter a form similar to the solution in the bulk-Higgs case, given before in (3.14). Whereas  $c_2(t, t')$  remains equal, the expression  $c_1(t, t')$  reads in the brane-Higgs case

$$c_1(t, t') = 1 + \frac{m_W^2}{2M_{KK}^2} \left[ 1 - \frac{1}{L} - t^2 \left( L - \frac{1}{2} + \ln t \right) - t'^2 \left( L - \frac{1}{2} + \ln t' \right) \right], \quad (3.20)$$

which coincides with the limit  $\beta \rightarrow \infty$  of the bulk-Higgs result in (3.15).

### 3.1.1 Gauge-boson propagator for $p_4 \approx 0$

In Subsection 2.4, we have presented the calculations of the Peskin-Takeuchi parameters S, T, U in three different scenarios of the RS model. In this connection, the corrections to the Fermi

constant  $G_F$  and the parameter  $\rho_*$  could be extracted from the effective, four-dimensional Lagrangians that describe four-fermion interactions. In these interactions, the RS model corrections are induced by the virtual contributions of the zero-mode and KK-tower gauge bosons, which can be parametrized with the five-dimensional gauge boson propagator functions. Since the interactions are considered at lower energies, it is sufficient to work with the leading contributions of the approximate propagator functions, derived for  $p_4 \approx 0$ . In the minimal RS model with a bulk Higgs field, the W boson propagator function reads in this approximation, up to the order  $v^2/M_{KK}^2$  [154]

$$B_W(t, t'; 0) = \frac{1}{2\pi\tilde{m}_W^2} \left[ 1 + \frac{Lm_W^2}{2M_{KK}^2} \left( \frac{2(1+\beta)^2}{(2+\beta)(3+2\beta)} - t_{>}^2 + \frac{t^{4+2\beta} + t'^{(4+2\beta)}}{(2+\beta)} \right) \right], \quad (3.21)$$

and in the minimal RS model with a brane Higgs field, it reads

$$B_W(t, t'; 0) = \frac{1}{2\pi\tilde{m}_W^2} \left[ 1 + \frac{Lm_W^2}{2M_{KK}^2} (1 - t_{>}^2) \right]. \quad (3.22)$$

In these expressions, the parametric masses  $\tilde{m}_W^2$  are kept instead of the physical mass of the W boson, which has been convenient for the calculations of the corrections to the Peskin-Takeuchi parameters. For the Z boson propagator functions, one would have to replace  $\tilde{m}_W \rightarrow \tilde{m}_Z$ , accordingly.

In the custodial RS model, by using the vector notation from (2.186), rotated to the UV basis, where the L and R gauge bosons, and the Z and Z' gauge bosons are combined into vectors, one encounters a  $2 \times 2$  matrix expression for the five-dimensional gauge boson propagator function. The KK decomposed W boson propagator reads [3]

$$\mathbf{B}_W^{UV}(t, t'; -p^2) = \sum_{n=0}^{\infty} \frac{\vec{\chi}_n^W(t) \vec{\chi}_n^W(t')^T}{m_n^{W^2} - p^2}, \quad (3.23)$$

and the Z boson propagator has a similar form, including the Z boson profiles. In this vector notation, one derives the differential equation for the gauge boson propagator in a way similar to the minimal model, giving

$$\left( \frac{p^2}{M_{KK}^2} + t \partial_t \frac{1}{t} \partial_t \right) \mathbf{B}_W^{UV}(t, t'; -p^2) = -\frac{Lt}{2\pi M_{KK}^2} \mathbf{1} \cdot \delta(t - t'). \quad (3.24)$$

According to the boundary conditions that the gauge bosons fulfil at the branes, the boundary conditions for the propagator function read

$$\begin{aligned} (\mathbf{P}_+ \partial_t + \mathbf{P}_-) \mathbf{B}_W^{UV}(t, t'; -p^2) \Big|_{t=\epsilon} &= \mathbf{0}, \\ \mathbf{R}_A \partial_t \mathbf{B}_W^{UV}(t, t'; -p^2) \Big|_{t=1^-} &= -\frac{Lm_A^2}{M_{KK}^2} \mathbf{P}_+ \mathbf{R}_A \mathbf{B}_W^{UV}(1, t'; -p^2), \end{aligned} \quad (3.25)$$

where  $m_A^2 = M_A^2/(2\pi r)$ . One can solve the equation in a way similar to the minimal model by applying two solutions for the cases  $t < t'$  and  $t > t'$ , respectively, that have to fulfil the continuity and jump conditions and the boundary conditions at the branes. Again, the general

solution is a combination of Bessel functions, given *e.g.* in [3]. In the approximation  $p_4 \approx 0$ , and to the order  $v^2/M_{KK}^2$ , one finds for the W boson propagator function

$$\mathbf{B}_W^{UV}(t, t'; -p^2) = \frac{1}{2\pi\tilde{m}_W^2} \begin{pmatrix} 1 + \frac{Lm_W^2}{2M_{KK}^2} \left( \frac{1}{c_W^2} - t^2 \right) & \frac{Lm_W^2 s_W t'^2}{2c_W M_{KK}^2} \\ \frac{Lm_W^2 s_W t^2}{2c_W M_{KK}^2} & \frac{Lm_W^2 t'^2}{2M_{KK}^2} \end{pmatrix}, \quad (3.26)$$

where  $t_{>,<} = [\max, \min](t, t')$ . The parametric mass  $\tilde{m}_W^2$  is kept instead of the physical mass of the W boson. Here,  $c_W$  denotes the cosine of the angle that determines the transformation between the UV and IR basis sets of fields, as given in (2.185). The Z boson propagator is obtained by setting  $\tilde{m}_W \rightarrow \tilde{m}_Z$ , and equally  $m_W \rightarrow m_Z$ , and  $\theta_W \rightarrow \theta_Z$ . Note that in the custodial model both the W and Z boson propagators are governed by the same mass parameter  $\tilde{m}_{\tilde{A}} = \tilde{m}_W^2/c_W^2 = \tilde{m}_Z^2/c_Z^2$  [151], which is crucial for the custodial protection mechanism of the  $\rho_*$  and T parameters.

## 3.2 Scalar propagator

In the bulk-Higgs scenario, combinations of the fifth component of the gauge bosons and the pseudo NG bosons of the decomposed Higgs field remain physical, since they get some gauge-independent mass terms in the Lagrangian, as we have explained in 2.2.1. When these physical, scalar KK particles virtually contribute in interactions, the amplitudes depend on scalar KK towers. Similar to the case of the gauge bosons, these towers can be parametrized in terms of five-dimensional scalar propagator functions. In a KK decomposed form, for the case of the charged scalars,  $\phi^\pm$ , the propagator is defined by

$$D_{\phi^\pm}(p, t, t') = - \sum_{n=1}^{\infty} \frac{\chi_n^{\phi^\pm}(t)\chi_n^{\phi^\pm}(t')}{p^2 - m_n^{(\phi^\pm)^2}}. \quad (3.27)$$

In analogy to the case of the gauge boson propagator, presented before, the defining differential equation for the scalar propagator arises from the terms of the Lagrangian that are bilinear in the physical scalars. Those terms have predicted the equation of motion for the scalars, given in (2.99). For that reason, we insert the KK decompositions for the scalars in the equation of motion, and perform a Fourier transformation to the four-dimensional momentum space by replacing  $\square_4 = -p^2$ . In this way, we can derive the differential equation for the scalar propagator function, for  $t \neq t'$ , as

$$\left( \frac{p^2}{M_{KK}^2} + \partial_t^2 - \frac{1}{t}\partial_t - \frac{1}{t^2}(2 + \beta)\beta - \frac{2\tilde{m}_W^2}{M_{KK}^2}L(1 + \beta)t^{2+2\beta} \right) D_{\phi^\pm}(p, t, t') = 0. \quad (3.28)$$

This is similar to the derivation of the equation of motion for the scalar profiles, given in (2.101). In order to find the differential equation for a general  $t$ , we use (2.101) and the completeness

relation for the scalar profiles,  $\sum_{n=1}^{\infty} \chi_n^{\phi^\pm}(t) \chi_n^{\phi^\pm}(t') = \frac{Lt}{2\pi} \delta(t-t')$ , to derive

$$\begin{aligned}
& \left( \frac{p^2}{M_{KK}^2} + \partial_t^2 - \frac{1}{t} \partial_t - \frac{1}{t^2} (2 + \beta) \beta - \frac{2\tilde{m}_W^2}{M_{KK}^2} L(1 + \beta) t^{2+2\beta} \right) \cdot \sum_{n=1}^{\infty} -\frac{\chi_n^{\phi^\pm}(t) \chi_n^{\phi^\pm}(t')}{p^2 - m_n^{(\phi^\pm)^2}} \\
&= - \sum_{n=1}^{\infty} \frac{\chi_n^{\phi^\pm}(t')}{(p^2 - m_n^{(\phi^\pm)^2})} \cdot \left( \frac{p^2}{M_{KK}^2} + \partial_t^2 - \frac{1}{t} \partial_t - \frac{1}{t^2} (2 + \beta) \beta - \frac{2\tilde{m}_W^2}{M_{KK}^2} L(1 + \beta) t^{2+2\beta} \right) \chi_n^{\phi^\pm}(t) \\
&= - \sum_{n=1}^{\infty} \frac{\chi_n^{\phi^\pm}(t')}{p^2 - m_n^{(\phi^\pm)^2}} \cdot \left( \frac{p^2}{M_{KK}^2} - \frac{m_n^{(\phi^\pm)^2}}{M_{KK}^2} \right) \chi_n^{\phi^\pm}(t) = - \sum_{n=1}^{\infty} \frac{\chi_n^{\phi^\pm}(t') \chi_n^{\phi^\pm}(t)}{M_{KK}^2} = -\frac{Lt}{2\pi M_{KK}^2} \delta(t-t') .
\end{aligned} \tag{3.29}$$

In this way, we have determined the right-hand side of the general differential equation,

$$\left( \frac{p^2}{M_{KK}^2} + \partial_t^2 - \frac{1}{t} \partial_t - \frac{1}{t^2} (2 + \beta) \beta - \frac{2\tilde{m}_W^2}{M_{KK}^2} L(1 + \beta) t^{2+2\beta} \right) D_{\phi^\pm}(p, t, t') = \frac{-Lt}{2\pi M_{KK}^2} \delta(t-t') . \tag{3.30}$$

The scalar profiles fulfil vanishing boundary conditions at both branes, according to the  $Z_2$ -odd parity. Similarly, the boundary conditions for the propagator function read

$$D_{\phi^\pm}(p, \epsilon, t') = 0 , \quad D_{\phi^\pm}(p, 1^-, t') = 0 . \tag{3.31}$$

Again, the differential equation has a difficult non-linear behaviour, due to the last term scaling with  $t^{2+2\beta}$ . It can be approximately solved up to the order  $v^4/M_{KK}^4$ , where the four-momentum  $p^2 = \mathcal{O}(m_h^2)$  is assumed to be much smaller than the KK mass scale. For  $t \neq t'$ , one determines the two solutions for the cases  $t > t'$  and  $t < t'$ , respectively. The two solutions have to obey the continuity condition

$$D_{\phi^\pm}(p, t_+, t') = D_{\phi^\pm}(p, t_-, t') , \tag{3.32}$$

with  $t_\pm = t' \pm \delta$ , and the boundary conditions in (3.31). Further, a jump condition is obtained, similar to the case of the gauge-boson propagator, by integrating the differential equation over a small interval around  $t'$ . The terms that do not contain derivatives cancel each other out, so that one obtains

$$\begin{aligned}
\int_{t_-}^{t_+} dt \left( \partial_t^2 - \frac{1}{t} \partial_t \right) D_{\phi^\pm}(p, t, t') &= \int_{t_-}^{t_+} dt \partial_t^2 D_{\phi^\pm}(p, t, t') = \partial_t D_{\phi^\pm}(p, t, t') \Big|_{t_-}^{t_+} \\
&\stackrel{!}{=} \int_{t_-}^{t_+} dt \frac{-Lt}{2\pi M_{KK}^2} \delta(t-t') = -\frac{Lt'}{2\pi M_{KK}^2} ,
\end{aligned} \tag{3.33}$$

where a limiting procedure  $\lim_{\delta \rightarrow 0}$  holds. From the differential equation and the conditions presented before, one obtains the following result for the five-dimensional scalar propagator

function

$$\begin{aligned}
D_{\phi^\pm}^{>,<}(t, t'; -p^2) &= -\frac{Lt_{<}^{2+\beta} (t_{>}^{2+\beta} - t_{>}^{-\beta})}{4\pi M_{KK}^2(1+\beta)} - \frac{Lt_{>}^{-\beta} t_{<}^{2+\beta}}{16\pi\beta M_{KK}^4(1+\beta)(2+\beta)(3+2\beta)} \times \\
&\left[ 2L\tilde{m}_W^2\beta(1+\beta) \left[ -t_{<}^{4+2\beta} + t_{>}^{2+2\beta} \left( 2 - 3t_{>}^2 + t_{>}^{4+2\beta} - 2\beta(-1+t_{>}^2) + t_{<}^{4+2\beta} \right) \right] \right. \\
&\left. - p^2(3+2\beta) \left[ 2t_{>}^2 + \beta t_{>}^2 - \beta t_{<}^2 + t_{>}^{2+2\beta} (-2 + \beta(-2 + t_{>}^2 + t_{<}^2)) \right] \right] + \dots .
\end{aligned} \tag{3.34}$$

Terms of the order of  $\epsilon^2$  and smaller are neglected. The solution describes the two cases for  $t > t'$  and  $t < t'$ , since  $t_{<} = \min[t, t']$  and  $t_{>} = \max[t, t']$ .

For smaller values of the four-momentum  $p$ , the KK-decomposed propagator can be approximated as

$$D_{\phi^\pm}(p, t, t') \approx \sum_{n=1}^{\infty} \chi_n^{\phi^\pm}(t) \chi_n^{\phi^\pm}(t') \cdot \left[ \frac{1}{m_n^{(\phi^\pm)_2}} + \frac{p^2}{m_n^{(\phi^\pm)_4}} + \mathcal{O}(p^3) \right], \tag{3.35}$$

which will later be used in our calculations. In the result for the analytic propagator function in (3.34), the first two rows give the result for the first term  $\sum_{n=1}^{\infty} \chi_n^{\phi^\pm}(t) \chi_n^{\phi^\pm}(t') \frac{1}{m_n^{(\phi^\pm)_2}}$ , whereas the last row gives the result for the second term  $\sum_{n=1}^{\infty} \chi_n^{\phi^\pm}(t) \chi_n^{\phi^\pm}(t') \frac{p^2}{m_n^{(\phi^\pm)_4}}$ . The physical scalars are defined in the bulk-Higgs scenario only, and do not appear in brane-localized Higgs scenarios.

## 3.3 Fermion propagator

### 3.3.1 Fermion propagator for $p_4 \approx 0$

Using the 6-component spinor notation for the fermions, defined in (2.105), the  $6 \times 6$  propagator reads in the mixed momentum-position representation [5, 188, 189]

$$\begin{aligned}
i\mathbf{S}^f(t, t'; p) &= \int d^4x e^{ip \cdot x} \langle 0 | \mathbf{T} (\mathcal{F}_L(t, x) + \mathcal{F}_R(t, x)) (\bar{\mathcal{F}}_L(t', 0) + \bar{\mathcal{F}}_R(t', 0)) | 0 \rangle \\
&= \sum_{n=1}^{\infty} \left[ \mathcal{F}_L^{(n)}(t) \frac{1-\gamma_5}{2} + \mathcal{F}_R^{(n)}(t) \frac{1+\gamma_5}{2} \right] \frac{i}{\not{p} - m_{f_n}} \left[ \mathcal{F}_L^{(n)\dagger}(t') \frac{1+\gamma_5}{2} + \mathcal{F}_R^{(n)\dagger}(t') \frac{1-\gamma_5}{2} \right],
\end{aligned} \tag{3.36}$$

where  $\mathbf{T}$  denotes the time ordering. In this notation, the Dirac operator has the form [2, 5]

$$\mathcal{D}_f = \not{p} - M_{KK}\gamma_5 \frac{\partial}{\partial t} - M_{KK}\mathcal{M}_f(t), \tag{3.37}$$

where the generalized mass matrix has been defined in (2.110). Using the bulk equations of motion in (2.109) and the completeness relation for the fermion profiles,  $\sum_{n=1}^{\infty} \mathcal{F}_A^{(n)}(t) \mathcal{F}_A^{(n)\dagger}(t') = \delta(t - t')$ , one can show that the generalized Dirac equation

$$\mathcal{D}_f \mathbf{S}^f(t, t'; p) = \delta(t - t') \tag{3.38}$$

is fulfilled [2, 5]. Since massless fermions do not exist, one can study the special limit  $p^\mu \rightarrow 0$  without complications, and the propagator does not exhibit a singularity at  $p^2 = 0$  [5]. In this limit, the expression in (3.36) reads

$$\mathbf{S}^f(t, t'; 0) = - \left[ \Delta_{RL}^f(t, t') \frac{1 + \gamma_5}{2} + \Delta_{LR}^f(t, t') \frac{1 - \gamma_5}{2} \right], \quad (3.39)$$

including the functions

$$\Delta_{RL}^f(t, t') = \sum_{n=1}^{\infty} \frac{1}{m_{f_n}} \mathcal{F}_R^{(n)}(t) \mathcal{F}_L^{\dagger(n)}(t'), \quad \Delta_{LR}^f(t, t') = \Delta_{RL}^{f\dagger}(t', t). \quad (3.40)$$

In the following, we present the derivation of the function  $\Delta_{RL}^f(t, t')$  in the bulk-Higgs RS model for a vanishing four-momentum  $p^\mu \rightarrow 0$  [5]. One can start with the Dirac equation in (3.38), which implies the following differential equation for the function  $\Delta_{RL}^f(t, t')$

$$\left[ \frac{\partial}{\partial t} + \mathcal{M}_f(t) \right] \Delta_{RL}^f(t, t') = \frac{\mathbf{1}}{M_{KK}} \delta(t - t'), \quad (3.41)$$

along with the boundary conditions at the UV brane and the IR brane,

$$(\mathbf{1} \quad \mathbf{0}) \Delta_{RL}^f(t_i, t') = (\mathbf{0} \quad \mathbf{0}) \quad \text{for } t_i = \epsilon, 1. \quad (3.42)$$

Further, the jump condition

$$\Delta_{RL}^f(t' + 0, t') - \Delta_{RL}^f(t' - 0, t') = \frac{\mathbf{1}}{M_{KK}} \quad (3.43)$$

is obtained by integrating the equation of motion over an infinitesimal interval around  $t = t'$ , similar to the derivations of the jump conditions, presented before. The general solution to the differential equation in (3.41), for  $t \neq t'$ , is an ordered exponential [5],

$$\Delta_{RL}^f(t, t') = \mathbf{T} \exp \left[ - \int_1^t ds \mathcal{M}_f(s) \right] \Delta_{RL}^f(1, t'). \quad (3.44)$$

Due to the time-ordered prescription, it is not possible to get a solution in a closed form for the function  $\Delta_{RL}^f$ . However, one can calculate an approximate expression, by setting up a perturbative expansion in powers of

$$\rho = \frac{v}{\sqrt{2} M_{KK}} \ll 1. \quad (3.45)$$

In this regard, one can define the ‘‘time-evolution operator’’

$$\mathbf{U}(t, t_0) = \mathbf{T} \exp \left[ - \int_{t_0}^t ds \mathcal{M}_f(s) \right], \quad (3.46)$$

with the operator of the ‘‘unperturbed system’’, corresponding to  $\rho = 0$ , as

$$\mathbf{U}_0(t, t_0) = \mathbf{T} \exp \left[ - \int_{t_0}^t ds \frac{1}{s} \begin{pmatrix} \mathbf{c}_F & \mathbf{0} \\ \mathbf{0} & -\mathbf{c}_f \end{pmatrix} \right] = \begin{pmatrix} (t/t_0)^{-\mathbf{c}_F} & \mathbf{0} \\ \mathbf{0} & (t/t_0)^{\mathbf{c}_f} \end{pmatrix}. \quad (3.47)$$

The operator of the ‘‘perturbation’’ reads

$$\mathbf{H}_I(\tau) = (2 + \beta)\tau^{1+\beta} \begin{pmatrix} \mathbf{0} & \mathbf{Y}_f \\ \mathbf{Y}_f^\dagger & \mathbf{0} \end{pmatrix}. \quad (3.48)$$

The full operator can be constructed as a series expansion

$$\begin{aligned} \mathbf{U}(t, t_0) &= \mathbf{U}_0(t, t_0) - \rho \int_{t_0}^t d\tau \mathbf{U}_0(t, \tau) \mathbf{H}_I(\tau) \mathbf{U}_0(\tau, t_0) \\ &+ \frac{\rho^2}{2} \int_{t_0}^t \int_{t_0}^{\tau_1} d\tau_1 d\tau_2 \mathbf{U}_0(t, \tau_1) \mathbf{H}_I(\tau_1) \mathbf{U}_0(\tau_1, \tau_2) \mathbf{H}_I(\tau_2) \mathbf{U}_0(\tau_2, t_0) + \mathcal{O}(\rho^3). \end{aligned} \quad (3.49)$$

Written in form of components, one can get

$$\mathbf{U}(t, 1) = \mathbf{U}_0(t, 1) - \rho \mathbf{U}_1(t, 1) + \frac{\rho^2}{2} \mathbf{U}_2(t, 1) + \mathcal{O}(\rho^3), \quad (3.50)$$

with

$$\begin{aligned} \mathbf{U}_1(t, 1) &= \begin{pmatrix} \mathbf{0} & \mathbf{Y}^A(t) \\ \mathbf{Y}^{B^\dagger}(t) & \mathbf{0} \end{pmatrix}, \\ (Y^A)_{ij}(t) &= \frac{(2 + \beta)(Y_f)_{ij}}{p_2(c_{F_i} + c_{F_j})} \left[ t^{2+\beta+c_{F_j}} - t^{-c_{F_i}} \right], \\ (Y^{B^\dagger})_{ij}(t) &= \frac{(2 + \beta)(Y_f^\dagger)_{ij}}{p_2(-c_{F_i} - c_{F_j})} \left[ t^{2+\beta-c_{F_j}} - t^{c_{F_i}} \right], \end{aligned} \quad (3.51)$$

and

$$\begin{aligned} \mathbf{U}_2(t, 1) &= \begin{pmatrix} -\mathbf{Y}^A(t) \mathbf{Y}^{C^\dagger} + \mathbf{Y}^D(t) & \mathbf{0} \\ \mathbf{0} & -\mathbf{Y}^{B^\dagger}(t) \mathbf{Y}^E + \mathbf{Y}^{F^\dagger}(t) \end{pmatrix}, \\ (Y^{C^\dagger})_{kj} &= \frac{(2 + \beta)(Y_f^\dagger)_{kj}}{p_2(-c_{F_k} - c_{F_j})}, \quad (Y^D)_{ij}(t) = \frac{(2 + \beta)^2(Y_f)_{ik}(Y_f^\dagger)_{kj}}{p_2(-c_{F_k} - c_{F_j})} \left[ \frac{t^{4+2\beta-c_{F_j}} - t^{-c_{F_i}}}{q_4(c_{F_i} - c_{F_j})} \right], \\ (Y^E)_{kj} &= \frac{(2 + \beta)(Y_f)_{kj}}{p_2(c_{F_k} + c_{F_j})}, \quad (Y^{F^\dagger})_{ij} = \frac{(2 + \beta)^2(Y_f^\dagger)_{ik}(Y_f)_{kj}}{p_2(c_{F_k} + c_{F_j})} \left[ \frac{t^{4+2\beta+c_{F_j}} - t^{c_{F_i}}}{q_4(-c_{F_i} + c_{F_j})} \right]. \end{aligned} \quad (3.52)$$

Here, we introduce the new abbreviations  $\mathbf{Y}^A(t)$ ,  $\mathbf{Y}^{B^\dagger}(t)$ ,  $\mathbf{Y}^{C^\dagger}$ ,  $\mathbf{Y}^D(t)$ ,  $\mathbf{Y}^E$ , and  $\mathbf{Y}^{F^\dagger}(t)$ , which are  $3 \times 3$  matrices, according to the  $3 \times 3$  matrices  $\mathbf{Y}_f$  and  $\mathbf{c}_{(F,f)}$  in generation space. The full solution in (3.44) is a  $6 \times 6$  matrix, and reads

$$\begin{aligned} \Delta_{\mathbf{RL}}^{\mathbf{f}}(t, t') &= \mathbf{U}(t, 1) \cdot \Delta_{\mathbf{RL}}^{\mathbf{f}}(1, t'), \\ &= \begin{pmatrix} t^{-c_F} + \frac{v^2}{4M_{KK}^2} \left[ -\mathbf{Y}^A(t) \mathbf{Y}^{C^\dagger} + \mathbf{Y}^D(t) \right] & -\frac{v}{\sqrt{2}M_{KK}} \mathbf{Y}^A(t) \\ -\frac{v}{\sqrt{2}M_{KK}} \mathbf{Y}^{B^\dagger}(t) & t^{c_f} + \frac{v^2}{4M_{KK}^2} \left[ -\mathbf{Y}^{B^\dagger}(t) \mathbf{Y}^E + \mathbf{Y}^{F^\dagger}(t) \right] \end{pmatrix} \\ &\cdot \begin{pmatrix} \mathbf{C}_1^{>, <} & \mathbf{C}_2^{>, <} \\ \mathbf{C}_3^{>, <} & \mathbf{C}_4^{>, <} \end{pmatrix}, \end{aligned} \quad (3.53)$$



for  $t > t'$  ( $>$ ),  $t < t'$  ( $<$ ). The constants  $\mathbf{C}_i^{(>,<)}$  can be determined by solving the system of boundary conditions in (3.42) and (3.43). From the UV boundary conditions, one obtains

$$\left[ \epsilon^{-c_F} + \frac{v^2}{4M_{KK}^2} (-\mathbf{Y}^{\mathbf{A}}(\epsilon) \mathbf{Y}^{\mathbf{C}\dagger} + \mathbf{Y}^{\mathbf{D}}(\epsilon)) \right] \cdot \mathbf{C}_1^< - \frac{v}{\sqrt{2}M_{KK}} \mathbf{Y}^{\mathbf{A}}(\epsilon) \cdot \mathbf{C}_3^< = \mathbf{0}, \quad (3.54)$$

together with a similar equation, where  $\mathbf{C}_1^<$  is replaced by  $\mathbf{C}_2^<$ , and  $\mathbf{C}_3^<$  by  $\mathbf{C}_4^<$ . The following two relations are easy to verify,

$$\begin{aligned} \Rightarrow (\mathbf{Y}^{\mathbf{A}})^{-1}(\epsilon) \cdot \epsilon^{-c_F} &\approx -(\mathbf{Y}^{\mathbf{E}})^{-1}, \\ \Rightarrow (\mathbf{Y}^{\mathbf{A}})^{-1}(\epsilon) \cdot \mathbf{Y}^{\mathbf{D}}(\epsilon) &\approx (\mathbf{Y}^{\mathbf{E}})^{-1} \cdot \mathbf{Y}^{\mathbf{G}}, \quad Y_{ij}^{\mathbf{G}} \equiv \frac{(2+\beta)}{q_4(c_{F_i} - c_{F_j})} Y_{f,ik} Y_{kj}^{\mathbf{C}\dagger}, \end{aligned} \quad (3.55)$$

and by using these, one obtains

$$\mathbf{C}_3^< = \frac{\sqrt{2}M_{KK}}{v} \left[ -(\mathbf{Y}^{\mathbf{E}})^{-1} + \frac{v^2}{4M_{KK}^2} (-\mathbf{Y}^{\mathbf{C}\dagger} + (\mathbf{Y}^{\mathbf{E}})^{-1} \mathbf{Y}^{\mathbf{G}}) \right] \cdot \mathbf{C}_1^<, \quad (3.56)$$

as well as a similar relation for  $\mathbf{C}_4^<$  in dependence of  $\mathbf{C}_2^<$ . Checking the definitions in (3.51) and (3.52), one can clearly see that

$$\mathbf{Y}^{\mathbf{A}}(1) = \mathbf{Y}^{\mathbf{D}}(1) = \mathbf{0}, \quad (3.57)$$

and for that reason, the IR boundary conditions define  $\mathbf{C}_1^>$  and  $\mathbf{C}_2^>$  to be zero,

$$\mathbf{C}_1^> = \mathbf{C}_2^> = \mathbf{0}. \quad (3.58)$$

The jump conditions offer the following relations

$$\begin{aligned} \left[ t'^{-c_F} + \frac{v^2}{4M_{KK}^2} (-\mathbf{Y}^{\mathbf{A}}(t') \mathbf{Y}^{\mathbf{C}\dagger} + \mathbf{Y}^{\mathbf{D}}(t')) \right] (-\mathbf{C}_1^<) - \frac{v}{\sqrt{2}M_{KK}} \mathbf{Y}^{\mathbf{A}}(t') [\mathbf{C}_3^> - \mathbf{C}_3^<] &= \frac{\mathbf{1}}{M_{KK}}, \\ \left[ t'^{-c_F} + \frac{v^2}{4M_{KK}^2} (-\mathbf{Y}^{\mathbf{A}}(t') \mathbf{Y}^{\mathbf{C}\dagger} + \mathbf{Y}^{\mathbf{D}}(t')) \right] (-\mathbf{C}_2^<) - \frac{v}{\sqrt{2}M_{KK}} \mathbf{Y}^{\mathbf{A}}(t') [\mathbf{C}_4^> - \mathbf{C}_4^<] &= \mathbf{0}, \end{aligned} \quad (3.59)$$

$$\begin{aligned} \Leftrightarrow -\mathbf{C}_1^< &= t'^{c_F} \cdot \left[ \frac{\mathbf{1}}{M_{KK}} + \frac{v}{\sqrt{2}M_{KK}} \mathbf{Y}^{\mathbf{A}}(t') (\mathbf{C}_3^> - \mathbf{C}_3^<) \right] + \mathcal{O}\left(\frac{v^3}{M_{KK}^3}\right), \\ -\mathbf{C}_2^< &= \frac{v}{\sqrt{2}M_{KK}} t'^{c_F} \cdot \mathbf{Y}^{\mathbf{A}}(t') (\mathbf{C}_4^> - \mathbf{C}_4^<) + \mathcal{O}\left(\frac{v^3}{M_{KK}^3}\right), \end{aligned} \quad (3.60)$$

where terms of the order of  $v^3/M_{KK}^2$  and higher are skipped, and equally one can obtain

$$\begin{aligned} \mathbf{C}_3^> &= \mathbf{C}_3^< - \frac{v}{\sqrt{2}M_{KK}} t'^{-c_f} \mathbf{Y}^{\mathbf{B}\dagger}(t') \cdot \mathbf{C}_1^< + \mathcal{O}\left(\frac{v^3}{M_{KK}^3}\right) \\ \mathbf{C}_4^> &= \mathbf{C}_4^< - \frac{v}{\sqrt{2}M_{KK}} t'^{-c_f} \mathbf{Y}^{\mathbf{B}\dagger}(t') \cdot \mathbf{C}_2^< + \frac{t'^{-c_f}}{M_{KK}} + \mathcal{O}\left(\frac{v^3}{M_{KK}^3}\right). \end{aligned} \quad (3.61)$$

The solving of the system of equations is presented in Appendix B.1. The results are

$$\begin{aligned} \mathbf{C}_3^> &= (\mathbf{Y}^E)^{-1} t'^{\mathbf{c}_F} \frac{\sqrt{2}}{v} + \frac{v^2}{2M_{KK}^2} \frac{\sqrt{2}}{v} \left[ \left( \mathbf{1} + (\mathbf{Y}^E)^{-1} t'^{\mathbf{c}_F} \mathbf{Y}^A(t') \right) t'^{-\mathbf{c}_f} \mathbf{Y}^{B\dagger}(t') t'^{\mathbf{c}_F} \right. \\ &\quad \left. + \frac{1}{2} (\mathbf{Y}^{C\dagger} - (\mathbf{Y}^E)^{-1} \mathbf{Y}^G) t'^{\mathbf{c}_F} \right], \\ \mathbf{C}_4^> &= \left[ \mathbf{1} + (\mathbf{Y}^E)^{-1} t'^{\mathbf{c}_F} \mathbf{Y}^A(t') \right] \frac{t'^{-\mathbf{c}_f}}{M_{KK}}, \end{aligned} \quad (3.62)$$

and

$$\begin{aligned} \mathbf{C}_1^< &= -\frac{t'^{\mathbf{c}_F}}{M_{KK}}, \\ \mathbf{C}_2^< &= -\frac{v}{\sqrt{2}M_{KK}^2} t'^{\mathbf{c}_F} \mathbf{Y}^A(t') t'^{-\mathbf{c}_f}, \\ \mathbf{C}_3^< &= (\mathbf{Y}^E)^{-1} t'^{\mathbf{c}_F} \frac{\sqrt{2}}{v} + \frac{v^2}{2M_{KK}^2} \frac{\sqrt{2}}{v} \left[ (\mathbf{Y}^E)^{-1} t'^{\mathbf{c}_F} \mathbf{Y}^A(t') t'^{-\mathbf{c}_f} \mathbf{Y}^{B\dagger}(t') t'^{\mathbf{c}_F} + \frac{1}{2} (\mathbf{Y}^{C\dagger} - (\mathbf{Y}^E)^{-1} \mathbf{Y}^G) t'^{\mathbf{c}_F} \right], \\ \mathbf{C}_4^< &= \frac{1}{M_{KK}} (\mathbf{Y}^E)^{-1} t'^{\mathbf{c}_F} \mathbf{Y}^A(t') t'^{-\mathbf{c}_f}. \end{aligned} \quad (3.63)$$

Altogether, we obtain the following results for the propagator function, for the two cases  $t < t'$  and  $t > t'$ ,

$$\begin{aligned} \Delta_{RL}^<(t, t'; 0) &= \\ &\left( \begin{array}{cc} -\frac{1}{M_{KK}} \left[ \left( \frac{t'}{t} \right)^{\mathbf{c}_F} + \mathbf{Y}^A(t) (\mathbf{Y}^E)^{-1} t'^{\mathbf{c}_F} \right] & -\frac{v}{\sqrt{2}M_{KK}^2} \left[ \left( \frac{t'}{t} \right)^{\mathbf{c}_F} + \mathbf{Y}^A(t) (\mathbf{Y}^E)^{-1} t'^{\mathbf{c}_F} \right] \mathbf{Y}^A(t') t'^{-\mathbf{c}_f} \\ t^{\mathbf{c}_f} (\mathbf{Y}^E)^{-1} t'^{\mathbf{c}_F} \frac{\sqrt{2}}{v} + \frac{v}{\sqrt{2}M_{KK}^2} \left[ \mathbf{Y}^{B\dagger}(t) t'^{\mathbf{c}_F} \right. \\ \left. + \frac{1}{2} (-\mathbf{Y}^{B\dagger}(t) \mathbf{Y}^E + \mathbf{Y}^{F\dagger}(t)) (\mathbf{Y}^E)^{-1} t'^{\mathbf{c}_F} \right. \\ \left. + t^{\mathbf{c}_f} (\mathbf{Y}^E)^{-1} t'^{\mathbf{c}_F} \mathbf{Y}^A(t') t'^{-\mathbf{c}_f} \mathbf{Y}^{B\dagger}(t') t'^{\mathbf{c}_F} \right. \\ \left. + \frac{1}{2} t^{\mathbf{c}_f} (\mathbf{Y}^{C\dagger} - (\mathbf{Y}^E)^{-1} \mathbf{Y}^G) t'^{\mathbf{c}_F} \right] & \frac{1}{M_{KK}} t^{\mathbf{c}_f} (\mathbf{Y}^E)^{-1} t'^{\mathbf{c}_F} \mathbf{Y}^A(t') t'^{-\mathbf{c}_f} \end{array} \right) \end{aligned} \quad (3.64)$$

and

$$\begin{aligned} \Delta_{RL}^>(t, t'; 0) &= \\ &\left( \begin{array}{cc} -\frac{1}{M_{KK}} \mathbf{Y}^A(t) (\mathbf{Y}^E)^{-1} t'^{\mathbf{c}_F} & -\frac{v}{\sqrt{2}M_{KK}^2} \mathbf{Y}^A(t) \left[ \mathbf{1} + (\mathbf{Y}^E)^{-1} t'^{\mathbf{c}_F} \mathbf{Y}^A(t') \right] t'^{-\mathbf{c}_f} \\ t^{\mathbf{c}_f} (\mathbf{Y}^E)^{-1} t'^{\mathbf{c}_F} \frac{\sqrt{2}}{v} \\ + \frac{v}{\sqrt{2}M_{KK}^2} \left[ \frac{1}{2} (-\mathbf{Y}^{B\dagger}(t) \mathbf{Y}^E + \mathbf{Y}^{F\dagger}(t)) (\mathbf{Y}^E)^{-1} t'^{\mathbf{c}_F} \right. \\ \left. + \frac{t^{\mathbf{c}_f}}{2} (\mathbf{Y}^{C\dagger} - (\mathbf{Y}^E)^{-1} \mathbf{Y}^G) t'^{\mathbf{c}_F} \right. \\ \left. t^{\mathbf{c}_f} \left( \mathbf{1} + (\mathbf{Y}^E)^{-1} t'^{\mathbf{c}_F} \mathbf{Y}^A(t') \right) t'^{-\mathbf{c}_f} \mathbf{Y}^{B\dagger}(t') t'^{\mathbf{c}_F} \right] & \frac{1}{M_{KK}} \left[ \left( \frac{t}{t'} \right)^{\mathbf{c}_f} + t^{\mathbf{c}_f} (\mathbf{Y}^E)^{-1} t'^{\mathbf{c}_F} \mathbf{Y}^A(t') t'^{-\mathbf{c}_f} \right] \end{array} \right). \end{aligned} \quad (3.65)$$

With the help of these results, one can analytically sum up the KK tower contributions of fermions in the amplitudes of loop-induced Higgs processes, which will be presented later.

### 3.3.2 Fermion propagator for $v \approx 0$

In the following, we consider the five-dimensional fermion propagator for general momenta,  $p_4 \neq 0$  [2],

$$i\mathbf{S}^f(t, t'; p) = \left[ \Delta_{LL}^f(t, t'; -p^2) \not{p} + \Delta_{RL}^f(t, t'; -p^2) \right] \mathbf{P}_R + (L \leftrightarrow R) , \quad (3.66)$$

where  $i\mathbf{S}^f(t, t'; p)$  has been defined in (3.36), and  $\mathbf{P}_{R,L} = \frac{1}{2}(\mathbf{1} \pm \gamma_5)$ . Now, the KK decomposed propagator functions are [2]

$$\begin{aligned} \Delta_{LL}^f(t, t'; -p^2) &= \sum_n \frac{1}{p^2 - m_{f_n}^2} \mathcal{F}_L^{(n)}(t) \mathcal{F}_L^{(n)\dagger}(t') , \\ \Delta_{RL}^f(t, t'; -p^2) &= \sum_n \frac{m_{f_n}}{p^2 - m_{f_n}^2} \mathcal{F}_R^{(n)}(t) \mathcal{F}_L^{(n)\dagger}(t') , \end{aligned} \quad (3.67)$$

that are similar to the functions from before, except of a sign change, according to

$$\Delta_{RL}^f(t, t'; 0) \equiv -\Delta_{RL}^f(t, t') , \quad \Delta_{LR}^f(t, t'; 0) \equiv -\Delta_{LR}^f(t, t') , \quad (3.68)$$

where  $\Delta_{RL}^f(t, t')$  and  $\Delta_{LR}^f(t, t')$  are the functions used in the previous subsection. For the present case, the generalized Dirac equation in (3.38) implies the coupled system of equations [2]

$$\begin{aligned} p^2 \Delta_{LL}^f(t, t'; -p^2) - M_{KK} \left( \frac{\partial}{\partial t} \mathbf{1} + \mathcal{M}_f(t) \right) \Delta_{RL}^f(t, t'; -p^2) &= \mathbf{1} \cdot \delta(t - t') , \\ \Delta_{RL}^f(t, t'; -p^2) - M_{KK} \left( -\frac{\partial}{\partial t} \mathbf{1} + \mathcal{M}_f(t) \right) \Delta_{LL}^f(t, t'; -p^2) &= \mathbf{0} . \end{aligned} \quad (3.69)$$

By integrating these equations over an infinitesimal interval  $t \in [t' - 0, t' + 0]$  around a fixed  $t'$ , one can get the jump and continuity conditions [2]

$$\begin{aligned} \Delta_{RL}^f(t' + 0, t'; -p^2) - \Delta_{RL}^f(t' - 0, t'; -p^2) &= -\frac{\mathbf{1}}{M_{KK}} , \\ \Delta_{LL}^f(t' + 0, t'; -p^2) - \Delta_{LL}^f(t' - 0, t'; -p^2) &= \mathbf{0} . \end{aligned} \quad (3.70)$$

The boundary conditions at the UV and IR branes are

$$(\mathbf{0} \quad \mathbf{1}) \cdot \Delta_{LL}^f(t_i, t'; -p^2) = (\mathbf{1} \quad \mathbf{0}) \cdot \Delta_{RL}^f(t_i, t'; -p^2) = \mathbf{0} , \quad t_i = \epsilon, 1 . \quad (3.71)$$

These conditions state that the  $Z_2$ -odd fermion profiles obey to Dirichlet boundary conditions at the two branes, respectively.

In calculating the contributions of the KK fermion tower to the production and decay processes of a new, heavy bulk scalar  $S$ , with a mass  $m_S \sim 750$  GeV, one can neglect the Yukawa interactions, scaling with  $v \approx 246$  GeV  $\ll m_S$ , and skip the respective terms in the differential

equation of the propagator. In this sense, one can consider the limit  $v \approx 0$  in the mass matrix  $\mathcal{M}_f(t)$ , given in (2.110), and in this limit, the Higgs localization in the bulk does not play a role. In order to solve the coupled system of equations in (3.69), one combines the two equations to a second-order equation for the function  $\Delta_{LL}^f$  [2],

$$\left[ \mathbf{1} \frac{\partial^2}{\partial t^2} - \frac{1}{t^2} \begin{pmatrix} \mathbf{c}_F^2 & 0 \\ 0 & -\mathbf{c}_f^2 \end{pmatrix} + \frac{1}{t^2} \begin{pmatrix} \mathbf{c}_F & 0 \\ 0 & -\mathbf{c}_f \end{pmatrix} - \mathbf{1} \hat{p}_E^2 \right] \Delta_{LL}^f(t, t'; -p^2) = \frac{\mathbf{1}}{M_{KK}^2} \delta(t - t'), \quad (3.72)$$

where  $\hat{p}_E^2 \equiv -p^2/M_{KK}^2$ . Then, the second equation in (3.69) determines the function  $\Delta_{RL}^f$ . By solving the second order equation for  $t \neq t'$ , one finds the general solutions

$$\begin{aligned} \Delta_{LL}^{f(>,<)}(t, t', -p^2) &= \sqrt{t} \begin{pmatrix} I_{\mathbf{c}_F - \frac{1}{2}}(\hat{p}_E t) & 0 \\ 0 & I_{\mathbf{c}_f + \frac{1}{2}}(\hat{p}_E t) \end{pmatrix} \begin{pmatrix} \mathbf{C}_1^{(>,<)}(t') & \mathbf{C}_2^{(>,<)}(t') \\ \mathbf{C}_3^{(>,<)}(t') & \mathbf{C}_4^{(>,<)}(t') \end{pmatrix} \\ &+ \sqrt{t} \begin{pmatrix} I_{-\mathbf{c}_F + \frac{1}{2}}(\hat{p}_E t) & 0 \\ 0 & I_{-\mathbf{c}_f - \frac{1}{2}}(\hat{p}_E t) \end{pmatrix} \begin{pmatrix} \mathbf{C}_5^{(>,<)}(t') & \mathbf{C}_6^{(>,<)}(t') \\ \mathbf{C}_7^{(>,<)}(t') & \mathbf{C}_8^{(>,<)}(t') \end{pmatrix} \end{aligned} \quad (3.73)$$

and

$$\begin{aligned} \Delta_{RL}^{f(>,<)}(t, t', -p^2) &= -p_E \sqrt{t} \begin{pmatrix} I_{\mathbf{c}_F + \frac{1}{2}}(\hat{p}_E t) & 0 \\ 0 & I_{\mathbf{c}_f - \frac{1}{2}}(\hat{p}_E t) \end{pmatrix} \begin{pmatrix} \mathbf{C}_1^{(>,<)}(t') & \mathbf{C}_2^{(>,<)}(t') \\ \mathbf{C}_3^{(>,<)}(t') & \mathbf{C}_4^{(>,<)}(t') \end{pmatrix} \\ &- p_E \sqrt{t} \begin{pmatrix} I_{-\mathbf{c}_F - \frac{1}{2}}(\hat{p}_E t) & 0 \\ 0 & I_{-\mathbf{c}_f + \frac{1}{2}}(\hat{p}_E t) \end{pmatrix} \begin{pmatrix} \mathbf{C}_5^{(>,<)}(t') & \mathbf{C}_6^{(>,<)}(t') \\ \mathbf{C}_7^{(>,<)}(t') & \mathbf{C}_8^{(>,<)}(t') \end{pmatrix}. \end{aligned} \quad (3.74)$$

This is in correspondence with the calculation presented in [2]. The sixteen constant matrices  $\mathbf{C}_i^{(>,<)}(t')$  are defined by the 4 continuity and 4 jump conditions, together with the 8 boundary conditions at the branes. These conditions allow to determine the final result for the function  $\Delta_{RL}^f$  as

$$\begin{aligned} \Delta_{RL}^{f>}(t, t'; -p^2) &= \frac{p_E \pi \sqrt{tt'}}{2M_{KK}^2} \begin{pmatrix} \frac{D_2(\mathbf{c}_F, 1, t, \hat{p}_E) D_1(\mathbf{c}_F, \epsilon, t', \hat{p}_E)}{D_2(\mathbf{c}_F, \epsilon, 1, \hat{p}_E) \cos(\mathbf{c}_F \pi)} & 0 \\ 0 & \frac{D_1(\mathbf{c}_f, 1, t, \hat{p}_E) D_2(\mathbf{c}_f, \epsilon, t', \hat{p}_E)}{D_2(\mathbf{c}_f, \epsilon, 1, \hat{p}_E) \cos(\mathbf{c}_f \pi)} \end{pmatrix}, \\ \Delta_{RL}^{f<}(t, t'; -p^2) &= \frac{p_E \pi \sqrt{tt'}}{2M_{KK}^2} \begin{pmatrix} \frac{D_1(\mathbf{c}_F, 1, t', \hat{p}_E) D_2(\mathbf{c}_F, \epsilon, t, \hat{p}_E)}{D_2(\mathbf{c}_F, \epsilon, 1, \hat{p}_E) \cos(\mathbf{c}_F \pi)} & 0 \\ 0 & \frac{D_2(\mathbf{c}_f, t', 1, \hat{p}_E) D_1(\mathbf{c}_f, \epsilon, t, \hat{p}_E)}{D_2(\mathbf{c}_f, \epsilon, 1, \hat{p}_E) \cos(\mathbf{c}_f \pi)} \end{pmatrix}, \end{aligned} \quad (3.75)$$

whereas the function  $\Delta_{LL}^f$  reads

$$\begin{aligned} \Delta_{LL}^{f>}(t, t'; -p^2) &= \frac{\pi \sqrt{tt'}}{2M_{KK}^2} \begin{pmatrix} \frac{D_1(\mathbf{c}_F, 1, t, \hat{p}_E) D_1(\mathbf{c}_F, \epsilon, t', \hat{p}_E)}{D_2(\mathbf{c}_F, \epsilon, 1, \hat{p}_E) \cos(\mathbf{c}_F \pi)} & 0 \\ 0 & \frac{D_2(\mathbf{c}_f, 1, t, \hat{p}_E) D_2(\mathbf{c}_f, \epsilon, t', \hat{p}_E)}{D_2(\mathbf{c}_f, \epsilon, 1, \hat{p}_E) \cos(\mathbf{c}_f \pi)} \end{pmatrix}, \\ \Delta_{LL}^{f<}(t, t'; -p^2) &= \frac{\pi \sqrt{tt'}}{2M_{KK}^2} \begin{pmatrix} \frac{D_1(\mathbf{c}_F, 1, t', \hat{p}_E) D_1(\mathbf{c}_F, \epsilon, t, \hat{p}_E)}{D_2(\mathbf{c}_F, \epsilon, 1, \hat{p}_E) \cos(\mathbf{c}_F \pi)} & 0 \\ 0 & \frac{D_2(\mathbf{c}_f, 1, t', \hat{p}_E) D_2(\mathbf{c}_f, \epsilon, t, \hat{p}_E)}{D_2(\mathbf{c}_f, \epsilon, 1, \hat{p}_E) \cos(\mathbf{c}_f \pi)} \end{pmatrix}, \end{aligned} \quad (3.76)$$

and we introduce

$$\begin{aligned} D_1(\mathbf{c}, a, t) &= I_{-\mathbf{c}-\frac{1}{2}}(a\hat{p}_E)I_{\mathbf{c}-\frac{1}{2}}(t\hat{p}_E) - I_{\mathbf{c}+\frac{1}{2}}(a\hat{p}_E)I_{-\mathbf{c}+\frac{1}{2}}(t\hat{p}_E) , \\ D_2(\mathbf{c}, a, t) &= I_{-\mathbf{c}-\frac{1}{2}}(a\hat{p}_E)I_{\mathbf{c}+\frac{1}{2}}(t\hat{p}_E) - I_{\mathbf{c}+\frac{1}{2}}(a\hat{p}_E)I_{-\mathbf{c}-\frac{1}{2}}(t\hat{p}_E) . \end{aligned} \quad (3.77)$$

The functions  $I$  are Bessel functions of the second kind. It should be noticed that the following relations apply

$$\begin{aligned} D_1(\mathbf{c}, a, a) &= \frac{2\cos(\mathbf{c}\pi)M_{KK}}{\pi a p_E} , \\ D_2(-\mathbf{c}, \epsilon, t)D_2(\mathbf{c}, 1, t) - D_1(-\mathbf{c}, \epsilon, t)D_1(\mathbf{c}, 1, t) &= \frac{-2\cos(\mathbf{c}\pi)M_{KK}D_1(\mathbf{c}, 1, \epsilon)}{\pi t p_E} . \end{aligned} \quad (3.78)$$

The amplitudes of the loop-induced production and decay processes of the new scalar  $S$ , presented later, will depend on the following expressions [7]

$$\frac{\Delta_{LR}^f(t, t; p_E^2) + \Delta_{RL}^f(t, t; p_E^2)}{2} = \frac{1}{2M_{KK}^2} \begin{pmatrix} d^{(+)}(\mathbf{c}_Q, p_E, t) & 0 \\ 0 & -d^{(+)}(\mathbf{c}_q, p_E, t) \end{pmatrix} , \quad (3.79)$$

where

$$d^{(+)}(\mathbf{c}, p_E, t) = \frac{D_2(\mathbf{c}, \epsilon, t)D_1(\mathbf{c}, 1, t) + D_1(\mathbf{c}, \epsilon, t)D_2(\mathbf{c}, 1, t)}{D_2(\mathbf{c}, \epsilon, t)D_1(\mathbf{c}, 1, t) - D_1(\mathbf{c}, \epsilon, t)D_2(\mathbf{c}, 1, t)} . \quad (3.80)$$

Later, in Chapter 5, we will also calculate the production and decay processes of  $S$  in the enlarged RS model with a custodial bulk gauge symmetry. For that case, the differential equation for the propagator function can be generalized as follows

$$\left[ \mathbf{1} \frac{\partial^2}{\partial t^2} - \frac{1}{t^2} \begin{pmatrix} \mathbf{c}_{\bar{F}}^2 & 0 \\ 0 & -\mathbf{c}_{\bar{f}}^2 \end{pmatrix} + \frac{1}{t^2} \begin{pmatrix} \mathbf{c}_{\bar{F}} & 0 \\ 0 & -\mathbf{c}_{\bar{f}} \end{pmatrix} - \mathbf{1} \hat{p}_E^2 \right] \Delta_{LL}^f(t, t'; -p^2) = \frac{\mathbf{1}}{M_{KK}^2} \delta(t - t') , \quad (3.81)$$

where the bulk mass matrices have been given in (2.202). The following boundary conditions apply for the respective functions

$$\begin{aligned} (\mathbf{0} \ \mathbf{1} \ \mathbf{0} \ \mathbf{0} \ \mathbf{0}) \Delta_{LL}^U(\epsilon) &= (\mathbf{0} \ \mathbf{0} \ \mathbf{0} \ \mathbf{0} \ \mathbf{0}) , & (\mathbf{0} \ \mathbf{0} \ \mathbf{1} \ \mathbf{0} \ \mathbf{0}) \Delta_{LL}^U(\epsilon) &= (\mathbf{0} \ \mathbf{0} \ \mathbf{0} \ \mathbf{0} \ \mathbf{0}) , \\ (\mathbf{1} \ \mathbf{0} \ \mathbf{0} \ \mathbf{0} \ \mathbf{0}) \Delta_{RL}^U(\epsilon) &= (\mathbf{0} \ \mathbf{0} \ \mathbf{0} \ \mathbf{0} \ \mathbf{0}) , & (\mathbf{0} \ \mathbf{0} \ \mathbf{0} \ \mathbf{1} \ \mathbf{0}) \Delta_{RL}^U(\epsilon) &= (\mathbf{0} \ \mathbf{0} \ \mathbf{0} \ \mathbf{0} \ \mathbf{0}) , \\ (\mathbf{0} \ \mathbf{0} \ \mathbf{0} \ \mathbf{0} \ \mathbf{1}) \Delta_{RL}^U(\epsilon) &= (\mathbf{0} \ \mathbf{0} \ \mathbf{0} \ \mathbf{0} \ \mathbf{0}) , \end{aligned} \quad (3.82)$$

$$\begin{aligned} (\mathbf{0} \ \mathbf{0} \ \mathbf{1} \ \mathbf{0} \ \mathbf{0}) \Delta_{LL}^U(1) &= (\mathbf{0} \ \mathbf{0} \ \mathbf{0} \ \mathbf{0} \ \mathbf{0}) , & (\mathbf{0} \ \mathbf{0} \ \mathbf{0} \ \mathbf{1} \ \mathbf{0}) \Delta_{LL}^U(1) &= (\mathbf{0} \ \mathbf{0} \ \mathbf{0} \ \mathbf{0} \ \mathbf{0}) , \\ (\mathbf{0} \ \mathbf{0} \ \mathbf{0} \ \mathbf{0} \ \mathbf{1}) \Delta_{LL}^U(1) &= (\mathbf{0} \ \mathbf{0} \ \mathbf{0} \ \mathbf{0} \ \mathbf{0}) , & (\mathbf{1} \ \mathbf{0} \ \mathbf{0} \ \mathbf{0} \ \mathbf{0}) \Delta_{RL}^U(1) &= (\mathbf{0} \ \mathbf{0} \ \mathbf{0} \ \mathbf{0} \ \mathbf{0}) , \\ (\mathbf{0} \ \mathbf{1} \ \mathbf{0} \ \mathbf{0} \ \mathbf{0}) \Delta_{RL}^U(1) &= (\mathbf{0} \ \mathbf{0} \ \mathbf{0} \ \mathbf{0} \ \mathbf{0}) , \end{aligned} \quad (3.83)$$

$$\begin{aligned} (\mathbf{0} \ \mathbf{1} \ \mathbf{0}) \Delta_{LL}^D(\epsilon) &= (\mathbf{0} \ \mathbf{0} \ \mathbf{0}) , & (\mathbf{1} \ \mathbf{0} \ \mathbf{0}) \Delta_{RL}^D(\epsilon) &= (\mathbf{0} \ \mathbf{0} \ \mathbf{0}) , & (\mathbf{0} \ \mathbf{0} \ \mathbf{1}) \Delta_{RL}^D(\epsilon) &= (\mathbf{0} \ \mathbf{0} \ \mathbf{0}) \\ (\mathbf{0} \ \mathbf{1} \ \mathbf{0}) \Delta_{LL}^D(1) &= (\mathbf{0} \ \mathbf{0} \ \mathbf{0}) , & (\mathbf{0} \ \mathbf{0} \ \mathbf{1}) \Delta_{LL}^D(1) &= (\mathbf{0} \ \mathbf{0} \ \mathbf{0}) , & (\mathbf{1} \ \mathbf{0} \ \mathbf{0}) \Delta_{RL}^D(1) &= (\mathbf{0} \ \mathbf{0} \ \mathbf{0}) , \\ (\mathbf{0} \ \mathbf{1} \ \mathbf{0}) \Delta_{LL}^{\Lambda}(\epsilon) &= (\mathbf{0} \ \mathbf{0} \ \mathbf{0}) , & (\mathbf{1} \ \mathbf{0} \ \mathbf{0}) \Delta_{RL}^{\Lambda}(\epsilon) &= (\mathbf{0} \ \mathbf{0} \ \mathbf{0}) , & (\mathbf{0} \ \mathbf{0} \ \mathbf{1}) \Delta_{RL}^{\Lambda}(\epsilon) &= (\mathbf{0} \ \mathbf{0} \ \mathbf{0}) \\ (\mathbf{0} \ \mathbf{1} \ \mathbf{0}) \Delta_{LL}^{\Lambda}(1) &= (\mathbf{0} \ \mathbf{0} \ \mathbf{0}) , & (\mathbf{0} \ \mathbf{0} \ \mathbf{1}) \Delta_{LL}^{\Lambda}(1) &= (\mathbf{0} \ \mathbf{0} \ \mathbf{0}) , & (\mathbf{1} \ \mathbf{0} \ \mathbf{0}) \Delta_{RL}^{\Lambda}(1) &= (\mathbf{0} \ \mathbf{0} \ \mathbf{0}) , \end{aligned} \quad (3.84)$$

following from the conditions that  $\mathbf{S}_n^{(+)}(\epsilon) = \mathbf{0}$ , and  $\mathbf{C}_n^{(-)}(\epsilon) = \mathbf{0}$ , as well as  $\mathbf{S}_n^{\pm}(1) = \mathbf{0}$  [151]. Despite the extended matrix expressions for the propagator functions in the custodial model, it turns out that, analogously to (3.79), the expressions contained in the amplitudes can be determined as

$$\begin{aligned} \frac{\Delta_{LR}^u(t, t; p_E^2) + \Delta_{RL}^u(t, t; p_E^2)}{2} &= \frac{1}{2M_{KK}^2} \\ &\begin{pmatrix} d^{(+)}(\mathbf{c}_Q, p_E, t) & 0 & 0 & 0 & 0 \\ 0 & d^{(-)}(\mathbf{c}_Q, p_E, t) & 0 & 0 & 0 \\ 0 & 0 & -d^{(+)}(\mathbf{c}_{uc}, p_E, t) & 0 & 0 \\ 0 & 0 & 0 & -d^{(-)}(\mathbf{c}_{\tau_1}, p_E, t) & 0 \\ 0 & 0 & 0 & 0 & -d^{(-)}(\mathbf{c}_{\tau_2}, p_E, t) \end{pmatrix}, \\ \frac{\Delta_{LR}^d(t, t; p_E^2) + \Delta_{RL}^d(t, t; p_E^2)}{2} &= \frac{1}{2M_{KK}^2} \begin{pmatrix} d^{(+)}(\mathbf{c}_Q, p_E, t) & 0 & 0 \\ 0 & -d^{(+)}(\mathbf{c}_{\tau_2}, p_E, t) & 0 \\ 0 & 0 & -d^{(-)}(\mathbf{c}_{\tau_1}, p_E, t) \end{pmatrix}, \\ \frac{\Delta_{LR}^\lambda(t, t; p_E^2) + \Delta_{RL}^\lambda(t, t; p_E^2)}{2} &= \frac{1}{2M_{KK}^2} \begin{pmatrix} d^{(-)}(\mathbf{c}_Q, p_E, t) & 0 & 0 \\ 0 & -d^{(-)}(\mathbf{c}_{\tau_1}, p_E, t) & 0 \\ 0 & 0 & -d^{(-)}(\mathbf{c}_{\tau_2}, p_E, t) \end{pmatrix}, \end{aligned} \quad (3.85)$$

depending on  $d^{(+)}(\mathbf{c}, p_E, t)$ , defined in (3.80), and further on [7]

$$d^{(-)}(\mathbf{c}, p_E, t) = \frac{D_1(-\mathbf{c}, \epsilon, t)D_1(\mathbf{c}, 1, t) + D_2(-\mathbf{c}, \epsilon, t)D_2(\mathbf{c}, 1, t)}{D_1(-\mathbf{c}, \epsilon, t)D_1(\mathbf{c}, 1, t) - D_2(-\mathbf{c}, \epsilon, t)D_2(\mathbf{c}, 1, t)}, \quad (3.86)$$

where  $D_1$  and  $D_2$  are given before in (3.78). Note that the results in the minimal RS model are obtained by simply skipping all the  $d^{(-)}(\mathbf{c}, p_E, t)$ -entries.

# Chapter 4

## Higgs Productions and Decays

After the Higgs boson could experimentally be confirmed at the LHC in 2012 [67, 68], a solution to the gauge hierarchy problem, *i.e.* the question why the Higgs bosons mass is stabilized at the electroweak scale, has been demanded more than ever. Precisely measuring the Higgs couplings to the SM particles can help to discover new-physics approaches and to distinguish between different ones. The RS model was introduced as one of the most promising new-physics approaches that can solve the gauge hierarchy problem, as presented in the second chapter of this thesis. The clearest signals predicted by the RS model are the direct detections of KK resonances, inevitably occurring in the model as series of heavy copies of the SM particles. But, none of these KK particles has been observed yet, and precision tests of the Peskin-Takeuchi observables suggest that their masses could be too heavy for a direct detection at present collider experiments. However, KK particles induce significant, virtual loop-contributions in particle processes, even in lower energy scattering processes. The loop-induced Higgs production process through gluon fusion and the Higgs decay into two photons, for example, are very interesting candidates to test the predictions of the RS model and to search for the warped extra dimension in an indirect way. Furthermore, tree-level processes such as the vector boson fusion and Higgsstrahlung productions, and the Higgs decays into a pair of a virtual and a real gauge boson, or into a pair of fermions such as tau leptons, can be of interest to probe the direct Higgs couplings to SM particles. The direct Higgs couplings can receive sizeable new-physics contributions in the RS model compared to the SM. Technically, these deviations are caused by the overlap integrals, appearing in the effective four-dimensional Feynman vertices of the RS model. So, in total, precise experimental results for the Higgs couplings, presently investigated at the LHC experiments, and possibly in the near future at new International Linear Collider (ILC) experiments, constitute to be a suitable data set to search for the existence of a warped extra dimension.

Higgs production and decay rates were numerously investigated in RS scenarios, *e.g.* in [2, 3, 5, 151, 152, 171, 190–193], where the Higgs field was strictly localized on, or very close to, the IR brane. These brane-Higgs or very narrow bulk-Higgs scenarios are strongly constrained by tests of the Peskin-Takeuchi observables [82], as we have shown in the second chapter of the thesis. A bound on the KK mass scale is implied as  $M_{KK} > 4.4$  TeV to 95% CL [177]. Accordingly, the lightest KK state is predicted to have a mass of at least  $M_{g(1)} > 10.8$  TeV. This is a strong disadvantage of these scenarios, since higher KK mass scales reduce the ability of the model to mediate the gauge hierarchy problem, and give less interesting outcomes for present particle experiments. Also, we have presented the custodial RS model with a more involved

particle structure of fermions and gauge bosons [2, 151, 174–176], in which the bound from the electroweak observable tests can be softened to  $M_{KK} > 2.0$  TeV (where  $M_{g(1)} > 4.9$  TeV). In this model, the bulk gauge group is extended in such a way that there is no stronger violation of the custodial symmetry in the Higgs sector, compared with the SM. But, apart from the complex particle structure, also the custodial model is strongly constrained at the present level, as *e.g.* by the Higgs decay into a pair of a virtual and a real Z boson [2, 4]. For that reason, we have presented, in most parts of Chapter 2, the Higgs scenario of the RS model in which also the Higgs field extends into the extra dimension, with a maximal localization at the IR brane, the bulk-Higgs RS scenario. This framework has many advantages compared to other Higgs scenarios. The Higgs field does no longer have a special status as the only brane-localized field. From that point of view, this framework seems to be the most natural version of the RS model. The fermion mass hierarchy can be addressed in the bulk-Higgs scenario as well, and moreover, it can give some explanations for the small scale of neutrino masses [157, 194, 195]. In Section 2.4, we have explained that the bound stemming from the electroweak precision tests can be relaxed down to  $M_{KK} > 2.4$  TeV ( $M_{g(1)} > 5.6$  TeV) to 95 % CL in the bulk-Higgs scenario (for  $\beta = 0$ ) [154]. Consistently, the scenario seems to form a promising alternative to the strongly constrained brane-Higgs scenarios, without and even with a custodial bulk gauge symmetry.

The bulk-Higgs framework has the prejudice that the integrations over the profile functions of KK particles, performed in deriving the effective four-dimensional Feynman rules, depend in a complicated way on the shape of the Higgs profile, localized in the extra dimension. Instead, in the brane-localized Higgs scenarios, the Higgs profile is described by a simple delta-distribution, which significantly simplifies the integrations. In this relation, all the results for couplings and amplitudes in the bulk-Higgs RS model give much longer expressions in dependence of the parameter space of the model. We don't feel intimidated by this fact. The Higgs processes that we will investigate in the following have already been explored in the narrow bulk-Higgs scenario, *e.g.* in the references [2–4], which coincides with the benchmark case of the limit  $\beta \rightarrow \infty$  in the bulk-Higgs scenario. By taking these results as reference values for our investigations, we expect that the results for couplings and processes in the bulk-Higgs scenario should lie closer to the SM predictions, compared to the other Higgs scenarios. In fact, we will find that the results lie the closer to the SM predictions, the stronger the Higgs field is located in the extra dimension, and the more natural the considered setting is, actually. This is a very interesting outcome, which possibly establishes the bulk-Higgs scenario to be the most interesting incarnation of the RS model.

In this chapter, we present the calculations and evaluations of the various Higgs production and decay processes in the bulk-Higgs RS scenario. The infinite summations over all contributing KK states in the amplitudes will be related to five-dimensional propagator functions in the mixed momentum-position representations [188, 189, 196–199]. This is done in contrast to reference [154], where the same Higgs production and decay processes were calculated in a similar framework. The calculations of the propagator functions have been presented in the previous chapter. In our approach, we will be able to derive analytic formulas for all the different Higgs production and decay processes, in the end. The chapter will be structured as follows. At first, we will present the calculation of the W boson contribution to the loop-induced Higgs decay into two photons. In this context, we will also discuss the Higgs decay rate into a pair of a virtual and a real gauge boson. After that, we present the contribution of the physical scalars to the Higgs decay into two photons. After this, the most demanding part will follow, with the calculation of



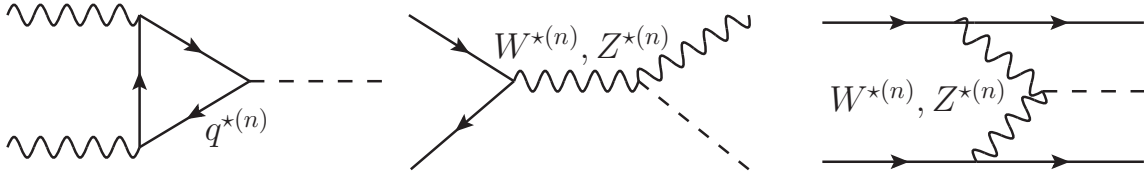


Figure 4.1: Feynman diagrams for the dominant Higgs production processes at the LHC, the loop-induced gluon fusion production mediated by quark fields (left), the production in association with a gauge boson named as Higgsstrahlung (middle), and the vector boson fusion (right) [4].

the fermion contribution to the loop-induced Higgs production process through gluon fusion and the Higgs decay into two photons. In this relation, at first we will sum over the full KK fermion tower in the amplitudes, and then we will consider the contributions of the zero-mode fermions in a separate manner. The summation over the full KK fermion tower will be related to the five-dimensional fermion propagator function, and the zero-mode contributions can be computed with the help of the approximate zero-mode fermion profiles. The zero-mode contributions will allow to derive the various tree-level Higgs couplings to a pair of fermions. In all cases, the first significant contributions by new-physics to the respective processes in the SM are given in powers of  $v^2/M_{KK}^2$ . All the results depend on the significant, open parameters of the bulk-Higgs RS scenario. These are the KK mass scale, the five-dimensional Yukawa matrices and the bulk-Higgs localization parameter  $\beta$ . After the presentation of the calculations, we will numerically evaluate our results with the help of diced parameter sets that give input values for the open parameters of the model. At first, we will evaluate the single Higgs couplings to particles, and then, we will discuss the different Higgs cross sections and decay rates, in order to illustrate the dependences on the RS model parameter space. Also, the new-physics corrections to the total Higgs decay width of the SM will be derived in this evaluation. To compare our results with the relevant results from the ATLAS and CMS experiments at the LHC [6, 200–202], we will further investigate the signal rates of a Higgs production at the LHC and a subsequent decay into the final states  $\gamma\gamma$ ,  $WW^*$ ,  $ZZ^*$ ,  $b\bar{b}$  and  $\tau\bar{\tau}$ , respectively. These signal rates are given by the cross sections of the Higgs production processes at the LHC, multiplied by the Higgs decay rate into the respective final states, corrected by the normalized total Higgs decay width in the RS model. However, in the bulk-Higgs scenario, there are only very moderate new-physics deviations from the SM. As a consequence, we will not be able to derive any new, significant exclusion bounds on the parameter space of the model, by comparing the predicted signal rates with the experimental results. As an outlook, we will consider the possible experimental capabilities of new ILC experiments on the precision measurements of Higgs couplings. We will compare our predictions in the RS model with these new, possible capabilities by assuming SM-like measurements. In this way, we can test up to which amount the parameter space of the bulk-Higgs RS model can possibly be explored at next-generation experiments. Altogether, this chapter is pivotal for the thesis, and will comprise its main results.

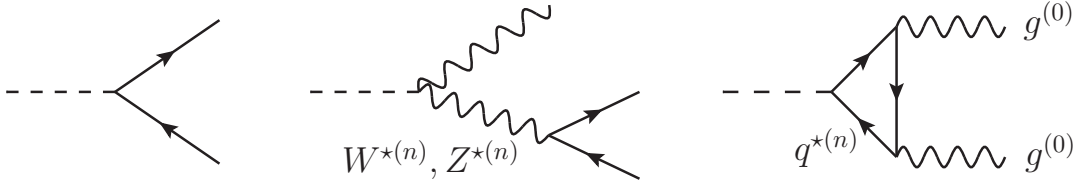


Figure 4.2: Feynman diagrams for the Higgs decays into a pair of fermions such as  $b$  quarks or  $\tau$  leptons (left), a pair of a virtual and a real gauge boson where the virtual gauge boson decays further into a fermion pair (middle), and into two gluons mediated by quark fields (right).

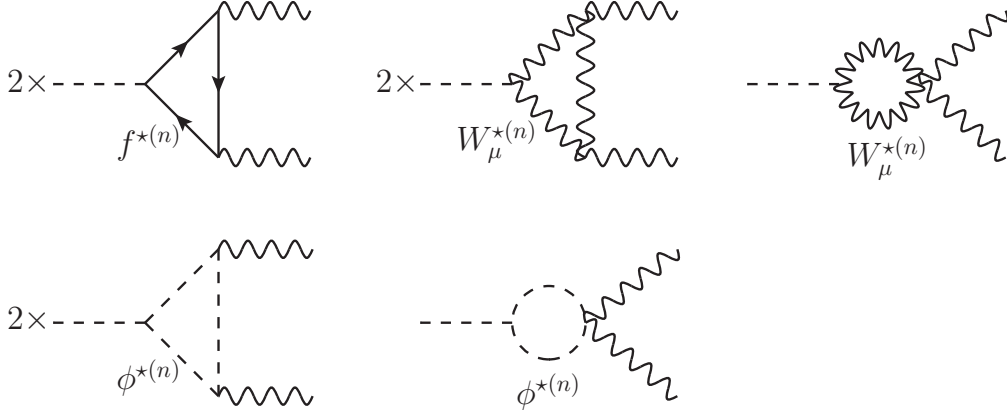


Figure 4.3: Feynman diagrams for the Higgs decay into two photons in the unitary gauge. The loops are mediated by KK fermions, KK  $W$  bosons, and the physical KK scalars of the bulk-Higgs model.

## 4.1 Calculations

The dominant Higgs production process at the LHC is the gluon fusion production. Moreover, the Higgs boson can be produced in association with a  $W$  or a  $Z$  boson via the Higgsstrahlung's production process, by the vector boson fusion, or together with a  $t\bar{t}$ -pair. In this connection, the different portions of the production processes are (for  $m_h = 125.1$  GeV and  $\sqrt{s} = 8$  TeV) [203]

$$\begin{aligned} \sigma(pp \rightarrow h) &= 0.872 \sigma(gg \rightarrow h) + 0.072 \sigma(q\bar{q} \rightarrow q\bar{q}V^*V^* \rightarrow q\bar{q}h) \\ &+ 0.032 \sigma(q\bar{q} \rightarrow Wh) + 0.019 \sigma(q\bar{q} \rightarrow Zh) + 0.006 \sigma(gg \rightarrow t\bar{t}h), \end{aligned} \quad (4.1)$$

where the vector boson fusion can be transmitted by both  $V = W, Z$  bosons. The Feynman diagrams for the first three processes are given in Figure 4.1, and will be calculated in the following in the bulk-Higgs framework. Shortly after its production, the Higgs boson decays, according to the different branching fractions [203],

$$\begin{aligned} \Gamma_{\text{tot}} &= 0.56 \Gamma(h \rightarrow b\bar{b}) + 0.23 \Gamma(h \rightarrow WW^*) + 0.03 \Gamma(h \rightarrow ZZ^*) \\ &+ 0.09 \Gamma(h \rightarrow gg) + 0.06 \Gamma(h \rightarrow \tau\bar{\tau}) + 0.03, \end{aligned} \quad (4.2)$$

with a total Higgs decay width of  $\Gamma_{\text{tot}} = 4.21 \text{ MeV}$ , for  $m_h = 126 \text{ GeV}$ .<sup>1</sup> The Feynman diagrams for the Higgs decays into a pair of fermions, gauge bosons and gluons are given in Figure 4.2. The corrections to the remaining Higgs decay modes, such as  $h \rightarrow c\bar{c}, Z\gamma, \dots$ , will have less significant effects on the total Higgs decay width in the RS model. We will summarize these effects by their combined branching fraction in the SM, which is 3%. However, the Higgs decay into two photons provides a clear, experimentally measurable channel despite its small branching fraction. Moreover, it is of special interest for new-physics searches due to its loop-induced transmission. The Feynman diagrams for this process are summarized in Figure 4.3, and the calculations of the single contributions will be presented in the following sections. The various tree-level and loop-induced Higgs couplings to SM particles can be described in terms of an effective Lagrangian, defined at the electroweak scale  $\mu \approx v$  [4, 5],

$$\begin{aligned} \mathcal{L}_{\text{eff}} = & C_W \frac{2m_W^2}{v_{SM}} h W_\mu^+ W^{-\mu} + C_Z \frac{m_Z^2}{v_{SM}} h Z_\mu Z^\mu - \sum_{f=t,b,\tau} \frac{m_f}{v_{SM}} h \bar{f} (C_f + C_{f5} i\gamma_5) f \\ & + C_g \frac{\alpha_s}{12\pi v_{SM}} h G_{\mu\nu}^a G^{a,\mu\nu} - C_{g5} \frac{\alpha_s}{8\pi v_{SM}} h G_{\mu\nu}^a \tilde{G}^{a,\mu\nu} \\ & + C_\gamma \frac{\alpha}{6\pi v_{SM}} h F_{\mu\nu} F^{\mu\nu} - C_{\gamma5} \frac{\alpha}{4\pi v_{SM}} h F_{\mu\nu} \tilde{F}^{\mu\nu} + \dots, \end{aligned} \quad (4.3)$$

with  $\tilde{F}^{\mu\nu} = -\frac{1}{2}\epsilon^{\mu\nu\alpha\beta} F_{\alpha\beta}$ ,  $\tilde{G}^{\mu\nu} = -\frac{1}{2}\epsilon^{\mu\nu\alpha\beta} G_{\alpha\beta}$  and  $\epsilon^{0123} = -1$ . In principle, effects from a renormalization-group running from the scale  $\mu \approx M_{KK}$  down to the electroweak scale would have to be taken into account, leading to insignificant deviations, however [5]. Also, there are Higgs self-couplings, or  $hZ_\mu \bar{f} \gamma^\mu f$ -couplings etc., where the RS corrections are of minor importance and will not be investigated in the thesis. The couplings  $C_i$  write the contributions from processes that are even under the CP transformations, whereas the couplings  $C_{i5}$  write the contributions that are odd under CP transformations, which are new compared to the SM. For that reason, we have  $C_W = C_Z = C_f = 1$ , and  $C_{f5} = C_g = C_{g5} = C_\gamma = C_{\gamma5} = 0$ , in the SM. With the help of the couplings, one can easily write the Higgs production cross sections and decay rates, normalized on the respective SM rates, as [2–5, 154]

$$\frac{\sigma(pp \rightarrow h)_{i,RS}}{\sigma(pp \rightarrow h)_{i,SM}} = C_i^{(\text{eff}),2} + C_{i5}^{(\text{eff}),2}, \quad \frac{\Gamma(h \rightarrow ii)_{RS}}{\Gamma(h \rightarrow ii)_{SM}} = C_i^{(\text{eff}),2} + C_{i5}^{(\text{eff}),2}. \quad (4.4)$$

For the loop-induced Higgs processes, the heavy SM particles  $t$ ,  $W$  and  $Z$  can be integrated out, resulting in additional contributions at the one-loop order, which are included in the effective couplings  $C_{[i,i5]}^{\text{eff}}$ . These effective couplings include the loop-induced couplings with the contributions from KK particles  $C_{[g,\gamma]}$ ,  $C_{[g,\gamma]5}$ , and the modified SM contributions from fermions in the case of the gluon fusion process [3–5],

$$C_g^{\text{eff}} = C_g + \sum_f C_f A(\tau_f), \quad C_{g5}^{\text{eff}} = C_{g5} + \sum_f C_{f5} B(\tau_f), \quad (4.5)$$

<sup>1</sup>The current result for the Higgs bosons mass is  $m_h = 125.09 \pm 0.21 \pm 0.11 \text{ GeV}$  (with statistical and systematic uncertainties), resulting from a combined analysis of ATLAS and CMS [204].

where  $\tau_f = 4m_f^2/m_h^2$ , and from fermions and W bosons in the case of the Higgs decay into two photons [4],

$$C_\gamma^{\text{eff}} = C_\gamma + \sum_f N_{cf} Q_f^2 C_f A(\tau_f) - \frac{21}{4} C_W A_W(\tau_W), \quad C_{\gamma 5}^{\text{eff}} = C_{\gamma 5} + \sum_f N_{cf} Q_f^2 C_{f5} B(\tau_f). \quad (4.6)$$

Here,  $N_{cf}$  is the color factor, which is 1 for leptons and 3 for quarks, and  $Q_f$  are the fermion charges. In this regard, the amplitudes of loop-induced processes will be parametrized in terms of the following parametrization<sup>2</sup> [2, 3, 5]

$$\begin{aligned} \mathcal{M}_{\text{ges}}(gg \rightarrow h) &= C_g^{\text{eff}} \frac{\alpha_s}{12\pi v} \langle 0 | G_{\mu\nu}^a G^{\mu\nu,a} | gg \rangle - C_{g5}^{\text{eff}} \frac{\alpha_s}{8\pi v} \langle 0 | G_{\mu\nu}^a \tilde{G}^{\mu\nu,a} | gg \rangle, \\ \mathcal{M}_{\text{ges}}(h \rightarrow \gamma\gamma) &= C_\gamma^{\text{eff}} \frac{\alpha}{6\pi v} \langle \gamma\gamma | F_{\mu\nu} F^{\mu\nu} | 0 \rangle - C_{5\gamma}^{\text{eff}} \frac{\alpha}{4\pi v} \langle \gamma\gamma | F_{\mu\nu} \tilde{F}^{\mu\nu} | 0 \rangle. \end{aligned} \quad (4.7)$$

In the SM, the corresponding, effective couplings read  $C_{g,SM} = \sum_f A(\tau_f)$ , and  $C_{\gamma,SM} = \sum_f N_{cf} Q_f^2 A(\tau_f) - \frac{21}{4} A_W(\tau_W)$ . The loop contributions that are induced by KK particles consist of fermionic parts in the case of the gluon fusion process,  $C_g = \sum_f \nu_f$ ,  $C_{g5} = \sum_f \nu_{f5}$ , whereas there are also contributions from KK W bosons and KK scalars in the Higgs decay into two photons [4, 154],

$$C_\gamma = \sum_f N_{cf} Q_f^2 \nu_f + \nu_W + \nu_\phi, \quad C_{\gamma 5} = \sum_f N_{cf} Q_f^2 \nu_{f5} + \nu_{W5} + \nu_{\phi 5}. \quad (4.8)$$

Our calculations will be performed in the unitary gauge, so that the loops in the production and decay processes are mediated by physical particles, exclusively. Goldstone bosons and ghost particles are absent in our calculations. The calculations and results for the individual contributions will be presented in the course of this chapter. We will especially focus on the contributions to the loop-induced Higgs decay rate into two photons, given by fermions, gauge bosons and scalars. The results for the fermion contributions will give the formulas for the tree-level Higgs couplings to fermions, forming the direct Higgs decay rates into a pair of fermions, such as b quarks or  $\tau$  leptons. Moreover, the results are equal to the gluon fusion production rate, apart from charge and color factors. The tree-level Higgs couplings to gauge bosons can be derived from the W boson contribution to the Higgs decay into two photons. In addition, we will explicitly determine the formulas for the Higgs decay rates into a pair of a virtual and a real gauge boson, normalized on the SM predictions, which only a bit differ from the squared of the Higgs to W bosons coupling. We will end up with a compendium of comprehensive formulas to describe the various Higgs decay rates into two particle states, which can numerically be evaluated in dependence of the parameter space of the bulk-Higgs RS model. By this, we will be able to determine the signal rates for a Higgs production at the LHC and a subsequent decay into a final state of two particles, which can be compared to the respective experimental results. In the following, we begin with a list of Feynman rules that are needed to calculate the amplitudes.

Vertex	Feynman rule
$hW_\mu^{+(m)}W_\nu^{-(n)}$	$i2\pi g_4 \tilde{m}_W \frac{2\pi}{L} \int_\epsilon^1 \frac{dt}{t} \frac{v(t)}{v} \chi_0^h(t) \chi_m^W(t) \chi_n^W(t) \eta_{\mu\nu}$
$A_\sigma^{(0)} W_\mu^{+(m)} W_\nu^{-(n)}$	$ie\delta_{mn} [(p_{W^+} - p_{W^-})_\sigma \eta_{\mu\nu} + (p_A - p_{W^+})_\nu \eta_{\sigma\mu} + (p_{W^-} - p_A)_\mu \eta_{\nu\sigma}]$
$A_\rho^{(0)} A_\sigma^{(0)} W_\mu^{+(m)} W_\nu^{-(n)}$	$ie^2 \delta_{mn} [\eta_{\rho\nu} \eta_{\sigma\mu} + \eta_{\sigma\nu} \eta_{\rho\mu} - 2\eta_{\rho\sigma} \eta_{\mu\nu}]$
$h\phi^{+(m)}\phi^{-(n)}$	$-i \int_\epsilon^1 dt \frac{2\pi}{Lt} \left( \frac{v(t)}{v} \chi_0^h(t) \frac{g}{2r} M_W \left( \frac{m_m^{\phi^\pm}}{m_n^{\phi^\pm}} + \frac{m_n^{\phi^\pm}}{m_m^{\phi^\pm}} \right) \chi_m^{\phi^-}(t) \chi_n^{\phi^+}(t) \right.$ $+ \frac{g}{2r} \frac{M_{KK}^2}{m_m^{\phi^\pm} m_n^{\phi^\pm}} \frac{v(t)}{v} M_W t \partial_t (t^{-1-\beta} \chi_0^h(t))$ $\times \left[ \chi_m^{\phi^+}(t) \cdot \partial_t (t^\beta \chi_n^{\phi^-}(t)) + \chi_n^{\phi^-}(t) \cdot \partial_t (t^\beta \chi_m^{\phi^+}(t)) \right]$ $+ \lambda \frac{4\pi}{L} \frac{M_{KK}^2}{m_m^{\phi^\pm} m_n^{\phi^\pm}} v(1) \chi_0^h(1) \partial_t (t^\beta \chi_m^{\phi^-}(t)) \partial_t (t^\beta \chi_n^{\phi^+}(t)) \Big _{t=1}$
$A_\mu^{(0)} \phi^{+(m)} \phi^{-(n)}$	$ie\delta_{mn} (p_{\phi^-} - p_{\phi^+})_\mu$
$A_\mu^{(0)} A_\nu^{(0)} \phi^{+(m)} \phi^{-(n)}$	$i2e^2 \delta_{mn} \eta_{\mu\nu}$
$\mathcal{G}_{\mu,\alpha}^{(0)} \bar{q}^{(m)} q^{(n)}$	$-ig_s \delta_{mn} \gamma_\mu t_a$
$A_\mu^{(0)} \bar{f}^{(m)} f^{(n)}$	$-ieQ_\Psi \delta_{mn} \gamma_\mu$
$h\bar{f}^{(n)} f^{(n)}$	$-i \left( \text{Re}(g_{nn}^{h\Psi_n\Psi_n}) + i\gamma_5 \text{Im}(g_{nn}^{h\Psi_n\Psi_n}) \right) ,$ $g_{nn}^{h\Psi_n\Psi_n} = \frac{(2+\beta)}{\sqrt{2}} \int_\epsilon^1 dt \sqrt{\frac{\pi}{L(1+\beta)}} \chi_0^h(t) \bar{\mathcal{F}}_L^{(n)\dagger}(t) \begin{pmatrix} \mathbf{0} & \mathbf{Y}_f \\ \mathbf{Y}_f^\dagger & \mathbf{0} \end{pmatrix} \mathcal{F}_R^{(n)}(t)$

Table 4.1: Feynman rules in the bulk-Higgs RS model, derived in the effective four-dimensional theory, which are used throughout the calculations.

### 4.1.1 Feynman rules

In this section, we list all the Feynman rules for three- and four-particle vertices that are used in the subsequent analyses. We use the four-dimensional, effective theory that can be derived from the five-dimensional action by integrating out the extra dimension, and using the KK decompositions and explicit profile functions for the relevant particle fields. In general, the integrations over the extra dimension reappear in the Feynman rules for the interaction vertices, containing overlap integrals over the profile functions of the interacting fields. In Table 4.1, the

<sup>2</sup>The expectation values  $\langle \gamma\gamma | F_{\mu\nu} F^{\mu\nu} | 0 \rangle = -4(k_1 \cdot k_2 \eta^{\mu\nu} - k_1^\nu k_2^\mu) \epsilon_\mu^*(k_1) \epsilon_\nu^*(k_2)$  and  $\langle \gamma\gamma | F_{\mu\nu} \tilde{F}^{\mu\nu} | 0 \rangle = 4\epsilon^{\mu\nu\alpha\beta} k_{1\alpha} k_{2\beta} \epsilon_\mu^*(k_1) \epsilon_\nu^*(k_2)$  parametrize the Lorentz structures of the external momenta of the loop amplitudes with the polarization vectors.

Feynman rules are listed, and we discuss several of these rules in the following.

Generally, the vertices of the couplings between zero-mode photons and KK particles are diagonal in the KK number, expressed by the Kronecker delta  $\delta_{mn}$ . These exclusively allow for couplings between KK particles of the same mode. In these vertices, the overlap integrals over the extra dimension can be traced back to the orthonormality conditions that the particles' profiles fulfil, in effect resulting in the Kronecker-delta expressions. This results from the fact that the zero-mode photon has a flat profile due to  $U(1)_{\text{em}}$ -gauge invariance, which is given in (2.86) [162]. On the contrary, note that the higher KK modes of the photons have non-flat profiles, and couple to KK fermions of different modes. This is also true for the case of the gluon, since KK gluons and photons have similar profile functions. In general, the Higgs couplings with two fermions, two charged gauge bosons or two scalars allow for couplings between KK particles of different modes. Furthermore, the couplings of the zero-mode Higgs boson with fermions are off-diagonal in flavor. The zero-mode Higgs profile  $\chi_0^{(h)}(t)$  is different from the Higgs vev  $v(t)$  by  $\mathcal{O}(v^2/M_{KK}^2)$ -corrections, and the five-dimensional Dirac fermion mass terms do not contribute, since these are not induced by Higgs couplings. Such effects are included in the couplings that can be fragmented into

$$g_{mn}^{(hf^m f^n)} = \frac{m_{f_n}}{v} \delta_{mn} - \frac{m_{f_n}}{v} \Phi_{ff,mn} - \frac{m_{f_m}}{v} \Phi_{FF,mn} + \frac{m_{f_n}}{v} \Delta \tilde{g}_{mn}^h - \frac{m_h^2}{4M_{KK}^2} \frac{m_{f_n}}{v} \Phi_{mn}^h . \quad (4.9)$$

In the subsequent section, we explain some steps of the derivations of these couplings, and give the definitions of the new mixing matrices  $\Delta \tilde{g}_{mn}^h$  and  $\Phi_{h,mn}$ , by deriving the explicit forms for the case of zero-mode fermions.

In the derivations of the vertex couplings between zero-mode photons and KK scalars, one has to include the equations of motion for the scalar profiles (2.101), in order to write the integrals over the extra dimension by the normalization conditions for the profiles [3, 154]. As an example, we shortly present the derivation of the vertex coupling between the zero-mode photon and two physical KK scalars. Starting with the terms from the Lagrangian that define the couplings between the five-dimensional photon field and the five-dimensional scalar fields  $\varphi^\pm$  and  $W_t^\pm$ ,

$$\begin{aligned} \frac{2\pi r}{L} \int_\epsilon^1 \frac{dt}{t} \frac{\epsilon^4}{t^4} (\mathcal{L}_{\text{Higgs}} + \mathcal{L}_{\text{gauge}}) \ni \frac{2\pi}{L} \int_\epsilon^1 \frac{dt}{t} \left( [-ie_5(\partial_\mu \varphi^-) \varphi^+ A^\mu + ie_5 \varphi^- (\partial_\mu \varphi^+) A^\mu] \right. \\ \left. + ie_5 r M_{KK}^2 A_\mu [\partial^\mu (W_t^+) W_t^- - \partial^\mu (W_t^-) W_t^+] \right) , \end{aligned} \quad (4.10)$$

one can insert the parts of the KK decompositions for the fields  $\varphi^\pm$  and  $W_t^\pm$  from (2.104) that contain the  $\phi^{(n)}$ -dependencies, and one has to consider one KK mode for every field, respectively. One has to change from spatial to momentum space for the four-dimensional coordinates by replacing  $\partial_\mu \phi^{(n)}(x) \rightarrow i(p_{\phi^{(n)}})_\mu \phi^{(n)}(p)$  and obtains

$$\begin{aligned} \frac{2\pi r}{L} \int_\epsilon^1 \frac{dt}{t} \frac{\epsilon^4}{t^4} (\mathcal{L}_{\text{Higgs}} + \mathcal{L}_{\text{gauge}}) \ni \frac{2\pi}{L} \int_\epsilon^1 \frac{dt}{t} \frac{e}{m_m^\pm m_n^\pm} (p_{\phi^-} - p_{\phi^+})_\mu \phi^{-(m)}(p) \phi^{+(n)}(p) A^{\mu(0)}(p) \\ \left( M_{KK}^2 t^{-2\beta} \partial_t \left( t^\beta \chi_m^{\phi^-}(t) \right) \partial_t \left( t^\beta \chi_n^{\phi^+}(t) \right) + M_W^2 \frac{v(t)^2}{v^{2r}} \chi_m^{\phi^-}(t) \chi_n^{\phi^+}(t) \right) . \end{aligned} \quad (4.11)$$

In these steps, the relation between the five-dimensional and the four-dimensional coupling constants,  $e_5 = \sqrt{2\pi r}e$ , and the constant zero-mode photon profile, given in (2.86), have been used. A partial integration of the first term on the right-hand side of (4.11) can be performed, while using the boundary conditions for the scalar profiles in (2.102). After that, one can insert the equations of motion for the scalar profiles in (2.101), finding

$$\frac{2\pi r}{L} \int_{\epsilon}^1 \frac{dt}{t} \frac{\epsilon^4}{t^4} (\mathcal{L}_{\text{Higgs}} + \mathcal{L}_{\text{gauge}}) \ni \phi^{-(m)}(p) \phi^{+(n)}(p) A^{\mu(0)}(p) e \frac{2\pi}{L} \int_{\epsilon}^1 \frac{dt}{t} \chi_m^{\phi^-}(t) \chi_n^{\phi^+}(t) (p_{\phi^-} - p_{\phi^+})_{\mu} . \quad (4.12)$$

Now, we recognize that the remaining integral over the extra dimension corresponds to the normalization condition for the scalar profiles, given in (2.103). With this result, one derives the vertex expression for the coupling of the zero-mode photon to KK scalars, which is given in Table 4.1.

The effective, four-dimensional propagators of the KK fermions, KK bosons and scalar KK particles are equal to the fermion, boson or scalar propagators of the SM, except of the inclusion of the respective KK masses,

$$\begin{aligned} D_{f^{(n)}}(p) &= \frac{i(\not{p} + m_{f_n})}{p^2 - m_{f_n}^2 + i\epsilon} , \\ D_{W^{(n)}}^{\xi, \mu\nu}(p) &= \frac{-i}{p^2 - m_{W^{(n)}}^2} \left( \eta^{\mu\nu} - (1 - \xi) \frac{p^{\mu} p^{\nu}}{p^2 - \xi m_{W^{(n)}}^2} \right) \\ &= \frac{-i}{p^2 - m_{W^{(n)}}^2} \left( \eta^{\mu\nu} - \frac{p^{\mu} p^{\nu}}{m_{W^{(n)}}^2} \right) + \frac{-i}{p^2 - \xi m_{W^{(n)}}^2} \frac{p^{\mu} p^{\nu}}{m_{W^{(n)}}^2} , \\ D_{\phi^{\pm(n)}}(p) &= \frac{i}{p^2 - m_n^{\phi^{\pm(n)2}} + i\epsilon} . \end{aligned} \quad (4.13)$$

Induced by the KK-diagonal vertex couplings to zero-mode photons, there are also KK-diagonal vertex couplings to the Higgs boson in the loop-induced Higgs production and decay processes, which will be calculated in the following. For that reason, every loop in the processes, to the lowest order in perturbation theory, is mediated by KK particles of the same mode, and any mixing between the different KK modes is forbidden. One single summation over the contributing states remains in every loop-amplitude, which will allow to derive finite results [3, 154]. On the contrary, for several summations in the amplitudes, this important property would not be guaranteed. The infinite summations are the largest technical differences in the calculations, compared to the SM. In this connection, parametrizations will be used in terms of five-dimensional propagator functions of the respective particle fields. Now, this will be outlined in the upcoming sections.

### 4.1.2 W boson contribution to the Higgs decay into two photons

To begin with the computational part of the thesis, we start with the presentation of the W boson contribution to the Higgs decay into two photons. In a general  $R_{\xi}$ -gauge, one would have to include a large amount of Feynman diagrams into the calculation that are mediated by unphysical particles, as Goldstone bosons and ghost particles. The corresponding calculation

in the SM was performed in [205], where it was explained that all diagrams with "unphysical" particles cancel out when summing over all contributions. Actually, this must happen because the physical result cannot depend on a gauge parameter  $\xi$ . The contributing diagrams are solely formed by loops of physical particles. These are the two diagrams given in Figure 4.3, corresponding to the diagrams that contribute in the unitary gauge for  $\xi \rightarrow \infty$ .

For the RS model with a brane-localized Higgs field and a very narrow bulk-Higgs field, the calculation of the W boson contribution to the Higgs decay to two photons was presented in detail in [3]. By using an effective, four-dimensional description, the amplitude for every bosonic diagram could be expressed in dependence of the respective SM amplitude, according to

$$\mathcal{M}_{RS,i}^W(h \rightarrow \gamma\gamma) = 2\pi \frac{\tilde{m}_W^2}{v} \sum_{n=0}^{\infty} \int_{\epsilon}^1 dt \delta^\eta(t-1) [\chi_n^W(t)]^2 \left[ \frac{v_{SM}}{m_W^2} \mathcal{M}_{SM,i}^W(h \rightarrow \gamma\gamma) \right]_{m_W \rightarrow m_n^W}. \quad (4.14)$$

Here,  $\delta^\eta(t-1)$ , with  $\eta \ll 1$ , denotes the profile of a very narrow bulk-Higgs field [2, 3], as explained in Subsection 2.2.3. In addition to the SM amplitudes, the amplitudes in the RS model contain one KK sum, which runs over the integral over the extra dimension that stems from the vertices of the zero-mode Higgs boson couplings to KK particles, and some factors accounting for the differences between the coupling constants. One can conclude that all diagrams with "unphysical" particles will cancel out to zero, by summing over the contributions for every single KK mode, because this is true for the SM, as confirmed in [205].

In the bulk-Higgs framework, one has to make the replacement in the amplitudes for the Higgs profile

$$\delta^\eta(t-1) \rightarrow \frac{2\pi v(t)}{Lt v} \chi_0^h(t) = 2(1+\beta)t^{1+2\beta} \left( 1 + \frac{m_h^2}{4M_{KK}^2} \left[ \frac{1}{(2+\beta)} - \frac{t^2}{(1+\beta)} \right] \right). \quad (4.15)$$

Then, the full amplitude of the W boson contribution to the Higgs decay into two photons can be obtained from the expression (4.14) by inserting the SM amplitude [205]

$$\begin{aligned} \mathcal{M}_{SM}^W(h \rightarrow \gamma\gamma) &= \frac{e^2 g}{(4\pi)^2 m_h^2 m_W} \left( m_h^2 + 6m_W^2 - 6m_W^2(m_h^2 - 2m_W^2) \times \int_0^1 dx \int_0^{1-x} dy \frac{1}{m_h^2 xy - m_W^2} \right) \\ &\quad \times (m_h^2 \eta^{\mu\nu} - 2k_2^\mu k_1^\nu) \epsilon_\mu^*(k_1) \epsilon_\nu^*(k_2), \end{aligned} \quad (4.16)$$

which depends on two Feynman parameter integrals over  $x$  and  $y$ ,

$$\begin{aligned} \mathcal{M}_{RS}^W(h \rightarrow \gamma\gamma) &= -3\pi \tilde{m}_W^2 \frac{2\pi}{L} \int_{\epsilon}^1 \frac{dt}{t} \frac{v(t)}{v} \chi_0^h(t) [\chi_n^W(t)]^2 \left( \frac{\alpha}{6\pi v} \right) \langle \gamma\gamma | F_{\mu\nu} F^{\mu\nu} | 0 \rangle \times \\ &\quad \left[ \frac{1}{m_n^{W2}} + \frac{6}{m_h^2} - 6 \left( 1 - 2 \frac{m_n^{W2}}{m_h^2} \right) \int_0^1 dx \int_0^{1-x} dy \frac{1}{m_h^2 xy - m_n^{W2}} \right]. \end{aligned} \quad (4.17)$$

One can use the relation

$$6 + 12 m_n^{W2} \int_0^1 dx \int_0^{1-x} dy \frac{1}{m_h^2 xy - m_n^{W2}} = 12 \int_0^1 dx \int_0^{1-x} dy \frac{m_h^2 xy}{m_h^2 xy - m_n^{W2}}, \quad (4.18)$$



where  $6 = 12 \int_0^1 dx \int_0^{1-x} dy [-m_h^2 xy + m_n^{W2}]^{-1}$ , together with the KK decomposed, five-dimensional W boson propagator function for  $\xi = 1$ , given in (3.5), in order to handle the infinite sum over the squared W boson profiles  $\chi_n^W(t)$  in the amplitude. By using the parametrization, given in the equation (4.7), we derive the complete W boson contribution to the effective CP-even Higgs coupling to two photons  $C_\gamma^{\text{eff}}$ ,

$$-\frac{21}{4}C_W A(\tau_W) + \nu_W = -3\pi \frac{\tilde{m}_W^2}{\kappa_v} \frac{2\pi}{L} \int_\epsilon^1 \frac{dt}{t} \frac{v(t)}{v} \chi_0^h(t) \times \left[ B_W(t, t; 0) + 6 \int_0^1 dx \int_0^{1-x} dy (1 - 2xy) B_W(t, t; -xym_h^2) \right]. \quad (4.19)$$

There is no CP-odd W boson contribution to  $C_{5\gamma}^{\text{eff}}$ . A division through the vev-shift  $\kappa_v$  is included, since the couplings are matched onto an effective Lagrangian in (4.3) that contains the SM vev. One can insert the analytic function for the W boson propagator, in order to derive an analytic result, and obtains

$$-\frac{21}{4}C_W A(\tau_W) + \nu_W = -3 \frac{\tilde{m}_W^2}{\kappa_v} \frac{\pi}{L} \int_\epsilon^1 \frac{dt}{t} \frac{v(t)}{v} \chi_0^h(t) \times \left( \frac{c_1(t, t)}{m_W^2} + \frac{c_2(t, t)}{2M_{KK}^2} + 6 \int_0^1 dx \int_0^{1-x} dy (1 - 2xy) \left[ \frac{c_1(t, t)}{m_W^2 - xym_h^2} + \frac{c_2(t, t)}{2M_{KK}^2} \right] \right), \quad (4.20)$$

where  $c_1(t, t')$  and  $c_2(t, t')$  are part of the analytic boson propagator function, defined in (3.14). With the help of the following two integral expressions

$$\int_0^1 dx \int_0^{1-x} dy f(xy) = \frac{1}{2} \int_0^1 dx \int_0^1 dy f(xy(1-y)), \quad (4.21)$$

$$\int_0^1 dx \int_0^1 dy f(4xy(1-y)) = \int_0^1 dz \operatorname{arctanh}(\sqrt{1-z}) f(z),$$

one finds, then,

$$-\frac{21}{4}C_W A(\tau_W) + \nu_W = -3 \frac{\tilde{m}_W^2}{\kappa_v} \frac{\pi}{L} \int_\epsilon^1 \frac{dt}{t} \frac{v(t)}{v} \chi_0^h(t) \times \left( \frac{c_1(t, t)}{m_W^2} + \frac{c_2(t, t)}{2M_{KK}^2} + 3 \int_0^1 dz \operatorname{arctanh}(\sqrt{1-z}) \left(1 - \frac{z}{2}\right) \cdot \left[ \frac{\tau_W c_1(t, t)}{m_W^2(\tau_W - z)} + \frac{c_2(t, t)}{2M_{KK}^2} \right] \right). \quad (4.22)$$

One can perform the following two integrals, by using the integration described in Appendix C.1,

$$\int_0^1 dz \operatorname{arctanh}(\sqrt{1-z}) \left(1 - \frac{z}{2}\right) = \frac{5}{6}, \quad (4.23)$$

$$\int_0^1 dz \operatorname{arctanh}(\sqrt{1-z}) \frac{(1 - \frac{z}{2})}{(\tau_W - z)} = \frac{1}{2} + \left(1 - \frac{\tau_W}{2}\right) f(\tau_W),$$

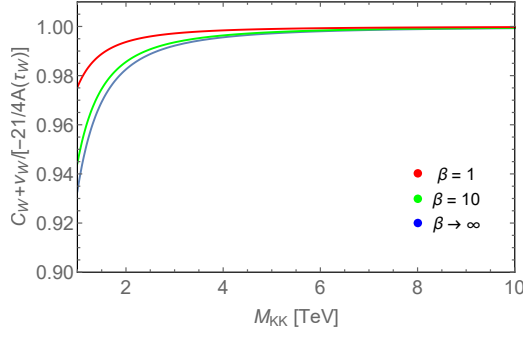


Figure 4.4: Here, the W boson contribution,  $-\frac{21}{4}C_W A(\tau_W) + \nu_W$ , normalized on the SM contribution,  $-\frac{21}{4}A(\tau_W)$ , is plotted in dependence of the KK mass scale and for three different choices for the parameter  $\beta$ . A tendency to suppressed values can be observed for smaller values of  $M_{KK}$ , and larger values of  $\beta$ .

and gets

$$\begin{aligned}
& -\frac{21}{4}C_W A(\tau_W) + \nu_W \\
&= -3 \frac{\tilde{m}_W^2}{\kappa_v} \frac{\pi}{L} \int_{\epsilon}^1 \frac{dt}{t} \frac{v(t)}{v} \chi_0^h(t) \cdot \left( \frac{c_1(t, t)}{m_W^2} + \frac{c_2(t, t)}{2M_{KK}^2} + [7A_W(\tau_W) - 2] \frac{c_1(t, t)}{2m_W^2} + \frac{5}{4} \frac{c_2(t, t)}{M_{KK}^2} \right) \quad (4.24) \\
&= -3\tilde{m}_W^2 \frac{\pi}{L} \int_{\epsilon}^1 \frac{dt}{t} \frac{v(t)}{v} \chi_0^h(t) \cdot \frac{7}{2} \left( \frac{c_1(t, t)}{m_W^2} A_W(\tau_W) + \frac{c_2(t, t)}{2M_{KK}^2} \right),
\end{aligned}$$

which depends on one remaining integral over the  $t$ -coordinate. Moreover, one has to include the mass relation between the parametric mass and the physical mass of the W boson from (2.88). Then, one derives the final result for the W boson contribution to the Higgs decay into two photons,

$$-\frac{21}{4}C_W A(\tau_W) + \nu_W + \mathcal{O}\left(\frac{v^4}{M_{KK}^4}\right). \quad (4.25)$$

Here, one can identify the zero-mode W boson contribution,  $-\frac{21}{4}C_W A(\tau_W)$ , and the loop contributions of KK W bosons,  $\nu_W$  [3], reading

$$\begin{aligned}
C_W &= 1 - \frac{m_W^2}{2M_{KK}^2} \left( \frac{3L(1+\beta)^2}{(2+\beta)(3+2\beta)} - \frac{(1+\beta)(3+\beta)}{(2+\beta)^2} + \frac{1}{2L} \right), \\
\nu_W &= -\frac{21}{4} \frac{m_W^2}{2M_{KK}^2} \left( \frac{L(1+\beta)}{(2+\beta)} - \frac{(1+\beta)(3+\beta)}{(2+\beta)^2} + \frac{1}{2L} \right),
\end{aligned} \quad (4.26)$$

where  $\tau_W = 4m_W^2/m_h^2$ . The function  $A_W(\tau_W) = \frac{1}{7} [2 + 3\tau_W + 3\tau_W(2 - \tau_W) \arctan^2(1/\sqrt{\tau_W - 1})]$  is normalized in such a way that it approaches 1 in the asymptotic limit  $\tau_W \rightarrow \infty$ , see Appendix C.1. In the SM, the W boson contribution to the Higgs decay into two photons, parametrized in terms of the coefficients in (4.7), is given by  $-\frac{21}{4}A(\tau_W)$ . In the RS model, the contribution of the zero-mode W bosons corresponds to the SM W boson contribution, apart from a modified

coupling  $C_W$ . In addition, the whole KK tower of W bosons,  $\nu_W$ , contributes, which is absent in the SM. In Figure 4.4, the W boson contribution to the Higgs decay into two photons is plotted in the RS model, normalized on the SM W boson contribution, in dependence of the KK mass scale, and for three different values of  $\beta$ . The contribution is negative in the SM, and we observe that in the RS model it is suppressed even stronger, at least for smaller values of the KK mass scale and higher values of  $\beta$ . In the limit  $\beta \rightarrow \infty$  (4.26), the result smoothly interpolates into the result derived in the very narrow bulk-Higgs scenario of the RS model [3], reading

$$-\frac{21}{4}C_W^{\text{nbH}}A(\tau_W) + \nu_W^{\text{nbH}} = -\frac{21}{4} \left[ \left( 1 - \frac{m_W^2}{2M_{KK}^2} \left( \frac{3}{2}L - 1 + \frac{1}{2L} \right) \right) A_W(\tau_W) + \frac{m_W^2}{2M_{KK}^2} \left( L - 1 + \frac{1}{2L} \right) \right] + \mathcal{O} \left( \frac{v^4}{M_{KK}^4} \right). \quad (4.27)$$

Also, this result equals the result in a strict brane-Higgs scenario.

### 4.1.3 Higgs decay rates into vector bosons

The Higgs boson can directly decay into a pair of W or Z bosons, which consists of a virtual and a real particle, according to the relations  $m_h < 2m_W$  and  $m_h < 2m_Z$ , where the virtual gauge boson decays further into a pair of fermions. Also, the description of such tree-level processes involves exchanges of virtual gauge bosons, as it can be observed from the Feynman diagram in Figure 4.2. In the RS model, this implies the exchange of the full KK tower of virtual gauge bosons. In the following, we will present the significant calculative steps of these decay rates, by using a calculation presented in [4]. In this reference, the decay rates were computed for the brane-localized Higgs scenario of the RS model. The authors have expressed their results in dependence of the SM decay rates that are rescaled by certain correction factors. The calculative steps presented there are similarly valid for the calculation in the bulk-Higgs scenario, with the exception that the rescaling factors accordingly differ, and have to be determined anew. In this subsection, we calculate these factors, while referencing on the previous work to a large amount [4]. Later, a numerical evaluation will be performed, exclusively with the new results derived for the bulk-Higgs RS scenario.

We start with the calculation of  $h \rightarrow WW^*$ , by following [4], and thus consider the process  $h \rightarrow W^-W^{+*} \rightarrow W^-f_i\bar{f}'_j$ , where  $f_i$  and  $\bar{f}'_j$  denote a pair of light fermions with the generation indices  $i, j$ . The corresponding differential decay rate in the SM reads [4, 206],

$$\frac{d\Gamma}{ds} = \frac{1}{16\pi^2 m_h^3} \frac{\Gamma(W^+ \rightarrow f_i\bar{f}'_j)}{m_W} \frac{m_W^2}{v^2} \frac{\lambda^{1/2}(m_h^2, m_W^2, s)}{(m_W^2 - s)^2} [(m_h^2 - m_W^2)^2 + 2s(5m_W^2 - m_h^2) + s^2], \quad (4.28)$$

where  $s$  is the squared invariant mass of the fermion pair, and  $\lambda(x, y, z) = (x - y - z)^2 - 4yz$ . The result includes the on-shell decay rate for the process  $W^+ \rightarrow f_i\bar{f}'_j$  [4],

$$\Gamma(W^+ \rightarrow f_i\bar{f}'_j) = N_c^f m_W \frac{g^2}{24\pi} |g_{ij,L}|^2, \quad (4.29)$$

where  $g$  denotes the  $SU(2)_L$  gauge coupling, and  $N_c^f$  is the color factor, equalling 1 for leptons and 3 for quarks. Furthermore, there is  $g_{ij,L} = \delta_{ij}/\sqrt{2}$  for leptons and  $g_{ij,L} = V_{ij}^{CKM}/\sqrt{2}$  for quarks.

After having performed the remaining integration over  $s$  in the interval  $0 \leq s \leq (m_h - m_W)^2$ , one can derive [4]

$$\Gamma(h \rightarrow W^- W^{*\pm} \rightarrow W^- f_i \bar{f}'_j) = \frac{m_h^3}{32\pi v^2} \frac{\Gamma(W^+ \rightarrow f_i \bar{f}'_j)}{\pi m_W} g\left(\frac{m_W^2}{m_h^2}\right), \quad (4.30)$$

where fermion-mass effects are neglected. The first factor is one half of the would-be on-shell  $h \rightarrow WW$  decay width in the limit  $m_h \gg m_W$ , and the second factor accounts for the suppression, arising because one of the  $W$  bosons is produced off-shell. The function  $g(x)$  gives the result stemming from the phase-space [4], which reads

$$g(x) = \frac{6x(1 - 8x + 20x^2)}{\sqrt{4x - 1}} \arccos\left(\frac{3x - 1}{2x^{3/2}}\right) - 3x(1 - 6x + 4x^2) \ln x - (1 - x)(2 - 13x + 47x^2). \quad (4.31)$$

It is a common practice in the literature to define the off-shell  $h \rightarrow WW^*$  decay rate by [4]

$$\Gamma(h \rightarrow WW^*) \equiv 2 \sum_{f_i, f'_j} \Gamma(h \rightarrow W^+ f_i \bar{f}'_j), \quad (4.32)$$

where the sum includes all fermion pairs with a total mass lighter than  $m_W$ . The factor 2 results from the inclusion of the charge-conjugated decays  $h \rightarrow W^- \bar{f}_i f'_j$ . In the SM, the partial decay rate  $\Gamma(W^+ \rightarrow f_i \bar{f}'_j)$  would be replaced by twice the total decay width  $\Gamma_W$  of the  $W$  boson.

Analogous formulas hold for the decays of the Higgs boson into a pair of a virtual and a real  $Z$  boson. In this connection, one must replace  $W \rightarrow Z$  everywhere, and use [4]

$$\Gamma(Z \rightarrow f \bar{f}) = N_c^f m_Z \frac{g^2}{24\pi c_w^2} (g_{f,L}^2 + g_{f,R}^2), \quad (4.33)$$

for the partial decay rates of the  $Z$  boson in the SM. Here,  $g_{f,L} = T_3^f - s_w^2 Q_f$  and  $g_{f,R} = -s_w^2 Q_f$  are the left-handed and right-handed couplings of the various fermion species, and  $s_w = \sin \theta_w$  and  $c_w = \cos \theta_w$  denote the sine and cosine of the weak mixing angle. In this case, the total off-shell decay rate reads [4]

$$\Gamma(h \rightarrow ZZ^*) \equiv \sum_f \Gamma(h \rightarrow Z f \bar{f}), \quad (4.34)$$

where the sum runs over all fermions with a mass lighter than  $m_Z/2$ . So far, we have summarized just the derivations from [4].

Apart from the RS corrections to the decay rates that are caused by the exchanges of the full KK towers of gauge bosons, also the electroweak gauge couplings, entering the partial decay rates in (4.29) and (4.33), get modified, as well as the Higgs couplings to vector bosons. The Feynman rule for the  $W_\mu^{+(0)} W_\nu^{-(n)} h$ -vertex coupling reads in the bulk-Higgs RS model

$$2\pi i \frac{2\tilde{m}_W^2}{v} \frac{2\pi}{L} \int_\epsilon^1 \frac{dt}{t} \frac{v(t)}{v} \chi_0^h(t) \chi_n^W(t) \chi_0^W(t) \eta_{\mu\nu}, \quad (4.35)$$

as given in Table 4.1. For the zero modes, one encounters the correction factor  $C_W$ , rescaling this vertex compared to the SM, which has been derived just before in (4.26). A second correction

factor stems from the Feynman rule of the  $W_\mu^{+(n)} \bar{u}_A^{(i)} d_A^{(j)}$ -vertex, where  $A = L, R$  is a chirality label and  $i, j$  label the flavours of the SM quarks. It was explained in [150] that this vertex is given in the RS model, in good approximation, by [4]

$$\frac{i}{\sqrt{2}} \frac{g_5}{\sqrt{2\pi r}} \sqrt{2\pi} \chi_n^W(\epsilon) V_{ij}^{\text{CKM}} \gamma^\mu P_L, \quad (4.36)$$

which is also valid in the bulk-Higgs scenario, since the Higgs field is not involved in this coupling. Further contributions, including the couplings to right-handed fermions, are strongly chirality-suppressed. For the zero mode, one encounters a correction factor relative to the SM <sup>3</sup>

$$C_{\Gamma_W}^{1/2} \equiv \frac{g_5}{\sqrt{2\pi r g}} \sqrt{2\pi} \chi_0^W(\epsilon) \approx 1 - \frac{m_W^2}{2M_{KK}^2} \frac{1}{4L}, \quad (4.38)$$

which affects all the amplitudes of the W boson decays into light fermions. It follows that, relative to the SM, one must perform the following replacements in the SM decay amplitude of the process  $h \rightarrow W^- W^{*+} \rightarrow W^- u_i \bar{d}_j$ ,

$$\begin{aligned} \frac{1}{m_W^2 - s} &\rightarrow \frac{v_{SM}}{v} \frac{\tilde{m}_W^2}{m_W^2} \frac{g_5}{\sqrt{2\pi r g}} \frac{2\pi}{L} \int_\epsilon^1 \frac{dt}{t} \frac{v(t)}{v} \chi_0^h(t) \sqrt{2\pi} \chi_0^W(t) 2\pi B_W(t, \epsilon, -s) \\ &\approx C_{\Gamma_W}^{1/2} C_W \left[ \frac{1}{m_W^2 - s} - \frac{1}{4M_{KK}^2} \left( \frac{(1+\beta)(3+\beta)}{(2+\beta)^2} - \frac{1}{L} \right) \right], \end{aligned} \quad (4.39)$$

where  $B_W(t, t'; -p^2)$  is the W boson propagator function, defined in (3.5). This result has an intuitive form. The factor  $C_{\Gamma_W}^{1/2}$  rescales the W boson decay amplitudes of the SM, whereas the factor  $C_W$  rescales the Higgs boson coupling to a  $W^+ W^-$ -pair, and the last term denotes the contributions from the KK resonances, encoded in the W boson propagator function [4]. Then, by substituting the expression into (4.28), and by performing the integration over  $s$ , one derives the result

$$\Gamma(h \rightarrow WW^*) \approx \frac{m_h^3}{16\pi v_{SM}^2} \frac{C_{\Gamma_W} \Gamma_W^{SM}}{\pi m_W} C_W^2 \left[ g \left( \frac{m_W^2}{m_h^2} \right) - \frac{m_h^2}{2M_{KK}^2} \left( \frac{(1+\beta)(3+\beta)}{(2+\beta)^2} - \frac{1}{L} \right) h \left( \frac{m_W^2}{m_h^2} \right) \right], \quad (4.40)$$

where [4]

$$\begin{aligned} h(x) &= - (1 - 4x + 12x^2) \sqrt{4x - 1} \arccos \left( \frac{3x - 1}{2x^{3/2}} \right) \\ &\quad - \frac{1}{2} (1 - 6x + 36x^2) \ln x + \frac{1}{6} (1 - x) (11 - 61x + 38x^2). \end{aligned} \quad (4.41)$$

<sup>3</sup>The first-order corrections to the relation between the five-dimensional gauge coupling  $g_5$  and the gauge coupling in the SM read

$$\frac{g_5}{\sqrt{2\pi r g}} = \frac{\tilde{m}_W}{m_W \kappa_v} \approx 1 - \frac{m_W^2}{4M_{KK}^2} \left[ \frac{(1+\beta)(3+\beta)}{(2+\beta)^2} - \frac{1}{2L} \right]. \quad (4.37)$$

In the subsequent numerical evaluation, we will encounter the ratio of the decay rate in the RS model divided by the decay rate in the SM, which is accordingly

$$\frac{\Gamma(h \rightarrow WW^*)_{RS}}{\Gamma(h \rightarrow WW^*)_{SM}} \approx C_{\Gamma_W} C_W^2 \left[ 1 - \frac{m_h^2}{2M_{KK}^2} \left( \frac{(1+\beta)(3+\beta)}{(2+\beta)^2} - \frac{1}{L} \right) h \left( \frac{m_W^2}{m_h^2} \right) / g \left( \frac{m_W^2}{m_h^2} \right) \right]. \quad (4.42)$$

The analysis of the  $h \rightarrow ZZ^*$ -decay rate proceeds in an analogous way. The correction factor for the  $hZZ$ -coupling of the zero-mode particles reads

$$\begin{aligned} C_Z &= \frac{v_{SM}}{v} \frac{\tilde{m}_Z^2}{m_Z^2} \frac{2\pi}{L} \int_\epsilon^1 \frac{dt}{t} \frac{v(t)}{v} \chi_0^h(t) 2\pi [\chi_0^Z(t)]^2 \\ &\approx 1 - \frac{m_Z^2}{2M_{KK}^2} \left( \frac{2L(1+\beta)^2}{(2+\beta)(3+2\beta)} - \frac{(1+\beta)(3+\beta)}{(2+\beta)^2} + \frac{1}{2L} \right) - \frac{m_W^2}{2M_{KK}^2} \frac{L(1+\beta)^2}{(2+\beta)(3+2\beta)}, \end{aligned} \quad (4.43)$$

where the last term stems from the correction of the vev-shift  $\kappa_v$ . Moreover, the  $Zf\bar{f}$ -couplings in the RS model, which enter the partial rates in (4.33), underlie the replacement [4]

$$\frac{g}{c_w} g_{f,A}(s_w^2) \rightarrow \frac{g_5}{\sqrt{2\pi r c_w}} \sqrt{2\pi} \chi_0^Z(\epsilon) g_{f,A}(s_w^2). \quad (4.44)$$

If the weak mixing angle is defined via the structure of the couplings  $g_{f,A}(s_w^2)$ , one finds the following correction factor for the Z boson decay amplitude [4]

$$C_{\Gamma_Z}^{1/2} = \frac{g_5}{\sqrt{2\pi r g}} \sqrt{2\pi} \chi_0^Z(\epsilon) \approx 1 + \frac{m_Z^2 - m_W^2}{4M_{KK}^2} \left( \frac{(1+\beta)(3+\beta)}{(2+\beta)^2} - \frac{1}{L} \right) - \frac{m_W^2}{4M_{KK}^2} \frac{1}{2L}. \quad (4.45)$$

For the Z boson decay width, normalized on the decay width in the SM, one can use the result from (4.42) by inserting the correction factors for the Z boson decay, and one has to replace  $m_W$  by  $m_Z$  in the functions  $g(x)$  and  $h(x)$ , accordingly. Numerically, the two results for the Higgs decay into a pair of W or Z bosons are very similar, where the small differences are induced by the difference between the W and Z boson masses.

#### 4.1.4 Higgs production through Higgsstrahlung and vector boson fusion

In a manner similar to the one just presented for the Higgs decay rates into vector bosons, the Higgs production processes through Higgsstrahlung and vector boson fusion can be parametrized, as discussed in [4] for the RS model with a brane-localized Higgs field. The Feynman diagram for the Higgsstrahlung's production process is similar to the twisted diagram of the Higgs boson decay into a pair of gauge bosons, see Figures 4.1 and 4.2. The two incoming fermions decay into a pair of a Higgs boson and a gauge boson, mediated by a gauge boson propagator. Therefore, at the quark level, the amplitude of Higgsstrahlung gets the same corrections as the amplitude of the Higgs decay into a pair of gauge bosons [4]. With  $s$  as the invariant mass squared of the  $hV$ -pair in the final state, the differential cross section for the Higgsstrahlung's process reads

$$\frac{d\sigma(pp \rightarrow hV)}{ds} = C_{\Gamma_V} C_V^2 \left[ 1 + \frac{s - m_V^2}{2M_{KK}^2} \left( \frac{(1+\beta)(3+\beta)}{(2+\beta)^2} - \frac{1}{L} \right) + \dots \right] \frac{d\sigma(pp \rightarrow hV)_{SM}}{ds}, \quad (4.46)$$

where the correction terms stem from the contributions of the KK resonances, forming the corrections to the gauge boson propagator, similar to (4.42). However, it is not possible to derive a simple analytic formula for the Higgsstrahlung's cross section, because the SM cross section and therefore the  $s$ -dependence is related in a complicated way to the shapes of parton distribution functions. But, the leading  $L$ -enhanced correction terms stemming from  $C_V^2$  are independent of  $s$ . Keeping only these terms, one can approximate [4]

$$\sigma(pp \rightarrow hV)_{RS} \approx C_V^2 \cdot \sigma(pp \rightarrow hV)_{SM} . \quad (4.47)$$

In a similar manner, one can approximate the corrections to the cross section of the vector-boson fusion. This process is mediated by two virtual gauge bosons, as illustrated in Figure 4.1. Two gauge boson propagators account for the respective corrections in the bulk-Higgs RS model, so that one has to replace

$$\begin{aligned} \frac{1}{(m_V^2 - p_1^2)(m_V^2 - p_2^2)} &\rightarrow \frac{v_{SM}}{v} \frac{\tilde{m}_V^2}{m_V^2} \left( \frac{g_5}{\sqrt{2\pi r g}} \right)^2 \frac{2\pi}{L} \int_\epsilon^1 \frac{dt}{t} \frac{v(t)}{v} \chi_0^h(t) (2\pi)^2 B_V(t, \epsilon; -p_1^2) B_V(t, \epsilon; -p_2^2) \\ &= \frac{C_{\Gamma_V} C_V}{(m_V^2 - p_1^2)(m_V^2 - p_2^2)} \left( 1 - \frac{2m_V^2 - p_1^2 - p_2^2}{4M_{KK}^2} \left( \frac{(1+\beta)(3+\beta)}{(2+\beta)^2} - \frac{1}{L} \right) + \dots \right) , \end{aligned} \quad (4.48)$$

in an amplitude expression. Again, the integrations over  $s$  involve complicated convolutions with parton distribution functions. The leading  $L$ -enhanced corrections are included in  $C_V^2$ , and are independent of  $s$ , so that the approximation

$$\sigma(pp \rightarrow hqq')_{RS} \approx C_V^2 \sigma(pp \rightarrow hqq')_{SM} \quad (4.49)$$

can be used for the Higgs production through vector boson fusion, as well [4].

#### 4.1.5 Scalar contribution to the Higgs decay into two photons

In the following, we present the calculation of the scalar contribution to the Higgs decay into two photons. The physical scalars are a special feature of the bulk-Higgs RS model, as presented in the second chapter of the thesis. Most easily, one can express the amplitudes of the two contributing diagrams, which are given in Figure 4.3, in dependence of the following Passarino-Veltman (PV) loop-integrals [207–209]

$$\begin{aligned} B^0(a, b) &= \frac{1}{i\pi^{d/2}} \int d^d p \frac{1}{[(p-a)^2 - m^2][(p-b)^2 - m^2]} , \\ C^0(0, k_1, k_1 + k_2) &= \frac{1}{i\pi^{d/2}} \int d^d p \frac{1}{[p^2 - m^2][(p-k_1)^2 - m^2][(p-k_1-k_2)^2 - m^2]} , \\ C^\mu(0, k_1, k_1 + k_2) &= \frac{1}{i\pi^{d/2}} \int d^d p \frac{p^\mu}{[p^2 - m^2][(p-k_1)^2 - m^2][(p-k_1-k_2)^2 - m^2]} , \\ C^{\mu\nu}(0, k_1, k_1 + k_2) &= \frac{1}{i\pi^{d/2}} \int d^d p \frac{p^\mu p^\nu}{[p^2 - m^2][(p-k_1)^2 - m^2][(p-k_1-k_2)^2 - m^2]} . \end{aligned} \quad (4.50)$$

In these expressions, it has been already applied that the masses of the virtual loop-particles are equal, where there is in our case  $m = m_n^\phi$ . In this notation, the amplitudes of the two contributing diagrams read

$$\begin{aligned}\mathcal{M}_1 &= \sum_{n=1}^{\infty} 2 \times 2^{2-d} \pi^{d/2} e^2 g_{nn}^{h\phi\phi} (C^{\mu\nu}(0, k_1, k_1 + k_2) - C^\mu(0, k_1, k_1 + k_2) k_1^\nu) \epsilon_\mu^*(k_1) \epsilon_\nu^*(k_2) , \\ \mathcal{M}_2 &= \sum_{n=1}^{\infty} -2^{1-d} \pi^{-d/2} e^2 g_{nn}^{h\phi\phi} \eta^{\mu\nu} B^0(0, k_1 + k_2) \epsilon_\mu^*(k_1) \epsilon_\nu^*(k_2) ,\end{aligned}\tag{4.51}$$

given as a sum over all the virtual KK states that propagate in the loops. It has been used that  $k_1^\mu \epsilon_\mu^*(k_1) = k_2^\nu \epsilon_\nu^*(k_2) = 0$ , according to the polarization of the external photon states. Using the PV integrals, it is convenient to reduce the tensor and vector PV integrals to the scalar PV integrals [209],

$$\begin{aligned}C^\mu(0, k_1, k_1 + k_2) &= -\frac{k_2^\mu}{m_h^2} [B^0(0, k_1 + k_2) - B^0(k_1, k_1 + k_2)] , \\ C^{\mu\nu}(0, k_1, k_1 + k_2) &= \frac{\eta^{\mu\nu}}{2} \times \left[ m_n^{\phi^2} C^0(0, k_1, k_1 + k_2) + \frac{1}{2} B^0(0, k_1 + k_2) + \frac{1}{2} \right] \\ &\quad + \frac{k_2^\mu k_1^\nu}{m_h^2} \times \left[ -B^0(0, k_1 + k_2) + B^0(k_1, k_1 + k_2) - m_n^{\phi^2} C^0(0, k_1, k_1 + k_2) - \frac{1}{2} \right] .\end{aligned}\tag{4.52}$$

In these expressions, a dimensional regularization has been already performed, so that there is  $d \rightarrow 4$  now. In addition, the relation  $2k_1 k_2 = m_h^2$  has been applied, following from momentum conservation. With the help of these steps, one derives the full amplitude of the scalar contribution to the Higgs decay into two photons as

$$\mathcal{M}_{\text{ges}} = \sum_{n=1}^{\infty} \frac{e^2 g_{nn}^{h\phi\phi}}{2\pi^2 m_h^2} \left( m_n^{\phi^2} C^0(0, k_1, k_1 + k_2) + \frac{1}{2} \right) \left[ \frac{m_h^2}{2} \eta^{\mu\nu} - k_2^\mu k_1^\nu \right] \epsilon_\mu^*(k_1) \epsilon_\nu^*(k_2) .\tag{4.53}$$

The remaining PV integral  $C^0$  is the same as the Feynman parameter integral in the amplitude of the W boson contribution to the Higgs decay into two photons, presented before,

$$\begin{aligned}C^0(0, k_1, k_1 + k_2) &\stackrel{d=4}{=} \frac{1}{i\pi^2} \int d^4 p [(p^2 - m_n^{\phi^2}) ((p - k_1)^2 - m_n^{\phi^2}) ((p - k_1 - k_2)^2 - m_n^{\phi^2})]^{-1} \\ &= \frac{1}{i\pi^2} \int d^4 p 2 \int_0^1 dx dy dz \frac{\delta(x + y + z - 1)}{\left[ p^2 - m_n^{\phi^2} - 2pk_1 y - 2p(k_1 + k_2)z + m_h^2 z \right]^3} \\ &= \frac{2}{i\pi^2} \int d^4 \tilde{p} \int_0^1 dx \int_0^{1-x} dz [\tilde{p}^2 + m_h^2 xz - m_n^{\phi^2}]^{-3} \\ &= - \int_0^1 dx \int_0^{1-x} dz [-m_h^2 xz + m_n^{\phi^2}]^{-1} = -\frac{2}{m_h^2} \arctan^2 \left( \frac{1}{\sqrt{\tau_{\phi_n} - 1}} \right) ,\end{aligned}\tag{4.54}$$



where  $\tilde{p} = p - [k_1 y + (k_1 + k_2) z]$ , and  $\tau_{\phi_n} = 4m_n^{(\phi^\pm)^2}/m_h^2$ . In the second to last step, the momentum integral over  $\tilde{p}$  has been performed [79]. The calculation of the Feynman parameter integral is presented in Appendix C.1. One derives the CP-even loop contribution of the scalars to the coupling  $C_\gamma^{\text{eff}}$  as follows

$$\nu_\phi = \sum_{n=1}^{\infty} \frac{v g_{nn}^{h\phi\phi}}{8m_n^{(\phi^\pm)^2}} A_\phi(\tau_{\phi_n}), \quad (4.55)$$

with the function  $A_\phi(\tau_{\phi_n}) = -3\tau_{\phi_n} [1 - \tau_{\phi_n} \arctan^2(1/\sqrt{\tau_{\phi_n} - 1})]$ , using the parametrization in (4.7) and (4.8). A scalar, CP-odd loop contribution does not arise. The scalars do not have zero modes, so that their masses are much heavier than the mass of the zero-mode Higgs boson. Therefore, one can approximate  $\tau_{\phi_n}$  to have high values, for which the function  $A(\tau_{\phi_n})$  approaches to 1, as  $\lim_{\tau_{\phi_n} \rightarrow \infty} A_\phi(\tau_{\phi_n}) = 1$ , see Appendix C.1. The coupling expression

$$\begin{aligned} g_{mn}^{h\phi\phi} = & \int_\epsilon^1 dt \frac{2\pi}{Lt} \left( \frac{v(t)}{v} \chi_0^h(t) \frac{g}{2r} M_W \left( \frac{m_m^{\phi^\pm}}{m_n^{\phi^\pm}} + \frac{m_n^{\phi^\pm}}{m_m^{\phi^\pm}} \right) \chi_m^{\phi^-}(t) \chi_n^{\phi^+}(t) \right. \\ & + \frac{g}{2r} \frac{M_{KK}^2}{m_m^{\phi^\pm} m_n^{\phi^\pm}} \frac{v(t)}{v} M_W t \partial_t (t^{-1-\beta} \chi_0^h(t)) \times \left[ \chi_m^{\phi^+}(t) \cdot \partial_t (t^\beta \chi_n^{\phi^-}(t)) + \chi_n^{\phi^-}(t) \cdot \partial_t (t^\beta \chi_m^{\phi^+}(t)) \right] \\ & \left. + \lambda \frac{4\pi}{L} \frac{M_{KK}^2}{m_m^{\phi^\pm} m_n^{\phi^\pm}} v(1) \chi_0^h(1) \partial_t (t^\beta \chi_m^{\phi^-}(t)) \partial_t (t^\beta \chi_n^{\phi^+}(t)) \right|_{t=1}, \end{aligned} \quad (4.56)$$

contains an integral over the Higgs' vev and profile, and the scalar KK profiles. By including the infinite sum over the KK states into the integral, one can express the result in dependence of the five-dimensional scalar propagator, by using the approximate KK-decomposed scalar propagator, given in (3.35). Then, up to the order  $v^2/M_{KK}^2$ , one can give the scalar loop contribution in the form

$$\begin{aligned} \nu_\phi = \sum_{n=1}^{\infty} \frac{v g_{nn}^{h\phi\phi}}{8m_n^{(\phi^\pm)^2}} = \frac{v}{8} \int_\epsilon^1 dt \frac{2\pi g}{Lt r} \chi_0^h(t) \frac{v(t)}{v} M_W D_{\phi^\pm}(0, t, t) \\ + \frac{v\pi}{2L} \lambda M_{KK}^2 v(1) \chi_0^h(1) \frac{\partial}{\partial t} \frac{\partial}{\partial t'} \frac{\partial}{\partial p^2} D_{\phi^\pm}(p, t, t') \Big|_{t'=t=1}. \end{aligned} \quad (4.57)$$

The following two expressions

$$D_{\phi^\pm}(0, t, t) = \frac{L(t^2 - t^{4+2\beta})}{4\pi M_{KK}^2(1 + \beta)}, \quad \frac{\partial}{\partial t} \frac{\partial}{\partial t'} \frac{\partial}{\partial p^2} D_{\phi^\pm}(p, t, t') \Big|_{t'=t=1} = \frac{L}{4\pi M_{KK}^4(2 + \beta)}, \quad (4.58)$$

can be determined from the analytic five-dimensional propagator function of the scalars, derived in (3.34). Furthermore, the relation  $\lambda = m_h^2 \pi / [32v^2 L(1 + \beta)^2]$ , and the dependence between the five-dimensional mass parameter  $M_W$  and the four-dimensional mass parameter  $\tilde{m}_W$  of the W boson, equalling the physical mass of the W boson  $m_W$  to the leading order,  $M_W = \sqrt{2\pi r} \tilde{m}_W$ ,

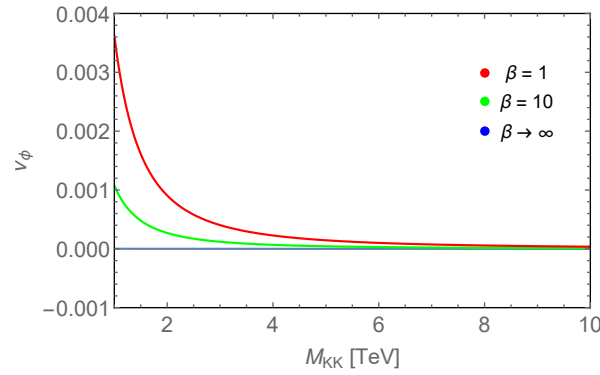


Figure 4.5: In this graphic, the loop-contributions of the physical KK scalars of the bulk-Higgs RS model to the Higgs decay into two photons are plotted, in dependence of the KK mass scale and for three choices of the parameter  $\beta$ . The contributions are the smaller, the higher the value of  $\beta$  is, and completely vanish in the limit  $\beta \rightarrow \infty$ , since the scalars decouple in the limit of a brane-localized Higgs field.

have to be taken into account. Then, one obtains the result for the scalar contribution to the Higgs decay into two photons as follows

$$\nu_\phi = \frac{Lm_W^2}{8M_{KK}^2} \left( \frac{1}{(2+\beta)} - \frac{1}{(3+2\beta)} \right) + \frac{m_h^2}{128 M_{KK}^2 (1+\beta)(2+\beta)} + \mathcal{O} \left( \frac{v^3}{M_{KK}^3} \right). \quad (4.59)$$

In Figure 4.5, the result is plotted in dependence of the KK mass scale and for three choices of the parameter  $\beta$ . Altogether, the scalars only give a sub-leading effect to the Higgs decay rate. One observes that the contributions are the smaller the higher the value of  $\beta$  is, and completely vanish in the limit  $\beta \rightarrow \infty$ , corresponding to the result in an RS scenario with a very narrow bulk-Higgs field. In fact, the physical scalars are an exclusive feature of the bulk-Higgs RS model, and decouple in the limit of a brane-Higgs localization.

#### 4.1.6 Fermion contribution to the Higgs decay into two photons

Figure 4.6 recapitulates the two Feynman diagrams that describe the fermion contribution to the Higgs decay into two photons. The loops are formed by all the different KK states of the fermions. Similar diagrams hold for the gluon fusion production process, except that they are reversed with incoming gluons, and only quarks can contribute in the loops. With the help of the Feynman rules, summarized in Table 4.1, one can write the full amplitude for the fermion contribution to the Higgs decay into two photons as follows

$$\begin{aligned} \mathcal{M}_{h \rightarrow \gamma\gamma}^f = & -i \sum_{f=u,d,e} \sum_{n=1}^{\infty} (-ieQ_f)^2 i^3 N_{c,f} (-1) \epsilon_\mu^*(k_1) \epsilon_\nu^*(k_2) \int \frac{d^d p}{(2\pi)^d} \frac{1}{d_1 d_2 d_3} \\ & - i (\text{Re}(g_{nn}^f) \text{Tr}[A_{Tr}] + i \text{Im}(g_{nn}^f) \text{Tr}[\gamma_5 A_{Tr}]) , \end{aligned} \quad (4.60)$$

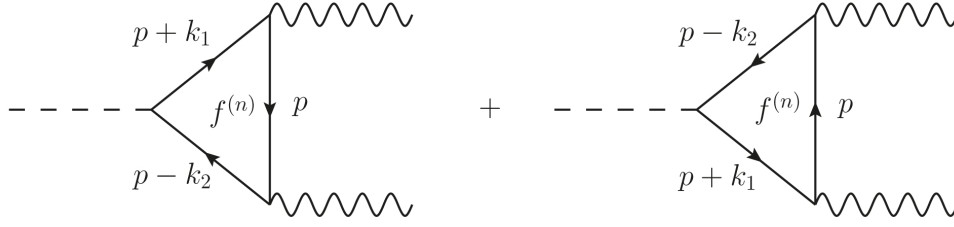


Figure 4.6: In this graphic, the two Feynman diagrams are displayed that parametrize the fermion contribution to the Higgs decay into two photons. The diagrams for the Higgs production process through gluon fusion are similar, but in a reversed form, with incoming gluon states. The outgoing photons are replaced by each other in the second diagram.

including

$$\begin{aligned}
 A_{Tr} = & (\not{p} - k_2 + m_n^f) \gamma^\nu (\not{p} + m_n^f) \gamma^\mu (\not{p} + k_1 + m_n^f) \\
 & + (-\not{p} - k_1 + m_n^f) \gamma^\mu (-\not{p} + m_n^f) \gamma^\nu (-\not{p} + k_2 + m_n^f) ,
 \end{aligned} \tag{4.61}$$

and

$$d_1 = (p^2 - m_{f_n}^2) , \quad d_2 = ([p + k_1]^2 - m_{f_n}^2) , \quad d_3 = ([p - k_2]^2 - m_{f_n}^2) . \tag{4.62}$$

In this expression, the Kronecker deltas from the fermion to photon vertices are evaluated already. The amplitude depends on one single summation over all contributing KK fermion states, with  $n = 1, \dots, \infty$ . The first sum runs over the fermions  $f = u, d, e$ , where each of which are three component vectors in generation space. Besides,  $N_{c,f}$  denotes the color factor, which is  $N_{c,q} = 3$  for quarks, to account for the fact that quarks of all three colors as quantum numbers can mediate the loop, whereas  $N_{c,e} = 1$  for leptons. To derive the amplitude of the gluon fusion production process, one has to replace  $e^2 Q_f^2 N_{c,f} \rightarrow g_s^2$ , include  $\text{Tr}[t_a t_b] = \delta_{ab}/2$ , with the color indices a and b, skip the lepton contribution, and consider the polarization vectors of incoming gluons. The first terms in (4.60), proportional to  $\text{Re}(g_{nn}^f)$ , give the CP-even contributions to the amplitude, as can be recognized from (2.124). For one respective term of the sum over the KK states, the calculation of the CP-even contribution is similar to the corresponding calculation in the SM.<sup>4</sup> By using the result from [210], one determines the result for the loop form factors of the CP-even contributions. In addition, we compute the loop form factors of the CP-odd contributions, given by the second terms in (4.60) proportional to  $\text{Im}(g_{nn}^f)$ , whereof the calculation is presented in Appendix C.2. In total, one determines the following two expressions for the CP-even and -odd contributions to the couplings  $C_\gamma^{\text{eff}}$  and  $C_{5\gamma}^{\text{eff}}$  from (4.6) and (4.8), by using the parametrization in (4.7),

$$\begin{aligned}
 \sum_{f=u,d,e} Q_f^2 N_{c,f} [C_f A(\tau_f) + \nu_f] &= \frac{1}{\kappa_v} \sum_{f=u,d,e} Q_f^2 N_{c,f} \sum_{n=1}^{\infty} \frac{v \text{Re}(g_{nn}^f)}{m_{f_n}} A(\tau_{f_n}) , \\
 \sum_{f=u,d,e} Q_f^2 N_{c,f} [C_{f5} B(\tau_f) + \nu_{f5}] &= \frac{1}{\kappa_v} \sum_{f=u,d,e} Q_f^2 N_{c,f} \sum_{n=1}^{\infty} \frac{v \text{Im}(g_{nn}^f)}{m_{f_n}} B(\tau_{f_n}) .
 \end{aligned} \tag{4.63}$$

<sup>4</sup>The gluon fusion production process in the SM was calculated, and presented in very detail, *e.g.* in [210].

The summations run over the Yukawa couplings  $g_{nn}^f$  between the zero-mode Higgs boson and KK fermions, times the constant vev parameter  $v$ , divided through the masses of the KK fermions  $m_{f_n}$ . Furthermore, they are multiplied with the loop-form factors  $A(\tau_{f_n})$  and  $B(\tau_{f_n})$ , which parametrize the results in dependence of  $\tau_{f_n} = 4m_{f_n}^2/m_h^2$ , and read [211]

$$A(\tau_{f_n}) = \frac{3\tau_{f_n}}{2} \left[ 1 + (1 - \tau_{f_n}) \arctan^2 \frac{1}{\sqrt{\tau_{f_n} - 1}} \right], \quad B(\tau_{f_n}) = \tau_{f_n} \arctan^2 \frac{1}{\sqrt{\tau_{f_n} - 1}}. \quad (4.64)$$

If one considers KK fermions of the modes  $n = 4, \dots$ , having much heavier masses than the zero-mode Higgs boson  $m_h$ , one can approximate the form factors by their asymptotic values,  $\lim_{\tau_{f_n} \rightarrow \infty} A(\tau_{f_n}) = \lim_{\tau_{f_n} \rightarrow \infty} B(\tau_{f_n}) = 1$ , see Appendix C.1. Instead, for the light zero-mode fermions with  $n = 1, 2, 3$ , the form factors  $A(\tau_{f_n})$  and  $B(\tau_{f_n})$  cannot be neglected. For that reason, one first has to subtract the first three contributions for  $n = 1, 2, 3$  in the calculation, and then adds them again multiplied with the exact form factors, according to [5]

$$\begin{aligned} & \sum_{f=u,d,e} Q_f^2 N_{c,f} [C_f A(\tau_{f_n}) + \nu_f] \\ &= \frac{1}{\kappa_v} \sum_{f=u,d,e} Q_f^2 N_{c,f} \left[ \sum_{n=1}^{\infty} \frac{v \operatorname{Re}(g_{nn}^f)}{m_{f_n}} + \sum_{n=1}^3 \frac{v \operatorname{Re}(g_{nn}^f)}{m_{f_n}} [-1 + A(\tau_{f_n})] \right], \\ & \sum_{f=u,d,e} Q_f^2 N_{c,f} [C_{f5} B(\tau_{f_n}) + \nu_{f5}] \\ &= \frac{1}{\kappa_v} \sum_{f=u,d,e} Q_f^2 N_{c,f} \left[ \sum_{n=1}^{\infty} \frac{v \operatorname{Im}(g_{nn}^f)}{m_{f_n}} + \sum_{n=1}^3 \frac{v \operatorname{Im}(g_{nn}^f)}{m_{f_n}} [-1 + B(\tau_{f_n})] \right]. \end{aligned} \quad (4.65)$$

In the following, we present the separate calculations of the contributions from the zero modes and the KK fermion towers. The KK tower contributions, given by the infinite summations over all KK fermion states, can be related to the five-dimensional fermion propagator function, to find a closed, analytic expression [5]. This procedure will be presented a bit later. The zero-mode fermion contributions have to be explicitly computed by performing the integral over the zero-mode fermion profiles contained in  $g_{nn}^f$ . For that purpose, one uses the approximate zero-mode fermion profiles, derived in (2.114). After having independently calculated the two different contributions, we will further set all the fermion bulk mass parameters  $c$  to the value  $-1/2$ , in order to decrease the large parameter space on which the results depend on. In this way, we will derive a concise and clear expression for the fermion contributions to the loop-induced Higgs processes, in the end.

### Zero-mode fermion contribution

We start with the calculation of the contribution of the zero-mode fermions to the loop-induced Higgs couplings, given by the separate sum over the first three KK states,  $n = 1, 2, 3$  in (4.65). To derive an expression for this sum, one can start with the equations of motion in (2.109) and consider the KK decompositions from (2.106). In this connection, one has to take the conjugate-transpose of the equation of motion of  $\mathbf{C}_m^F(t) \hat{a}_m^F$ , and multiply it with  $\mathbf{S}_n^F(t) \hat{a}_n^F$ . Equally, one has

to multiply  $\hat{a}_m^{F\dagger} \mathbf{C}_m^{F\dagger}(t)$  with the equation of motion of  $\mathbf{S}_n^F(t) \hat{a}_n^F$ , yielding [151]

$$\begin{aligned}
-\frac{d}{dt} \left( \hat{a}_m^{F\dagger} \mathbf{C}_m^{F\dagger}(t) \mathbf{S}_n^F(t) \hat{a}_n^F \right) &= x_n \hat{a}_m^{F\dagger} \mathbf{S}_m^{F\dagger}(t) \mathbf{S}_n^F(t) \hat{a}_n^F - \hat{a}_m^{F\dagger} \mathbf{C}_m^{F\dagger}(t) \mathbf{C}_n^F(t) \hat{a}_n^F x_m \\
&\quad - \frac{v(2+\beta)}{\sqrt{2}M_{KK}} t^{1+\beta} \left( \hat{a}_m^{f\dagger} \mathbf{S}_m^{f\dagger}(t) \mathbf{Y}_f^\dagger \mathbf{S}_n^F(t) \hat{a}_n^F - \hat{a}_m^{F\dagger} \mathbf{C}_m^{F\dagger}(t) \mathbf{Y}_f \mathbf{C}_n^f(t) \hat{a}_n^f \right).
\end{aligned} \tag{4.66}$$

When this relation is integrated over the whole orbifold, the total derivative on the left-hand side of the equation does not contribute, because the  $S$ -profiles obey to declining, odd boundary conditions at the branes,  $\mathbf{S}_n^F(0) = \mathbf{S}_n^F(1) = 0$ . Using further the normalization condition for the profile functions from (2.107), one derives the following expression

$$\begin{aligned}
\frac{(2+\beta)\sqrt{2\pi}}{L\epsilon} \int_\epsilon^1 dt t^{1+\beta} \hat{a}_m^{F\dagger} \mathbf{C}_m^{F\dagger}(t) \mathbf{Y}_f \mathbf{C}_n^f \hat{a}_n^f &= \frac{(2+\beta)\sqrt{2\pi}}{L\epsilon} \int_\epsilon^1 dt t^{1+\beta} \hat{a}_m^{f\dagger} \mathbf{S}_m^{f\dagger}(t) \mathbf{Y}_f^\dagger \mathbf{S}_n^F(t) \hat{a}_n^F \\
+ \frac{m_{f_m} \delta_{mn}}{v} - \frac{m_{f_n} 2\pi}{v L\epsilon} \int_\epsilon^1 dt \hat{a}_m^{f\dagger} \mathbf{S}_m^{f\dagger}(t) \mathbf{S}_n^f(t) \hat{a}_n^f &- \frac{m_{f_m} 2\pi}{v L\epsilon} \int_\epsilon^1 dt \hat{a}_m^{F\dagger} \mathbf{S}_m^{F\dagger}(t) \mathbf{S}_n^F(t) \hat{a}_n^F.
\end{aligned} \tag{4.67}$$

With the help of this expression, one can determine the sum over the first three KK states in the fermion contribution. The Yukawa couplings  $g_{nn}^f$  from (2.123) contain an integral over the profile functions of the fermions and the Higgs boson, and one includes the sum over the three KK states into the integral. Then, the expression can be split up into the different terms, by using (4.67),

$$\sum_{n=1}^3 \frac{v g_{nn}^f}{m_{f_n}} = 3 - \text{Tr}(\Phi_{ff} + \Phi_{FF}) + \text{Tr}(\Delta \tilde{g}_{nn}^h) - \frac{m_h^2}{4M_{KK}^2} \text{Tr}(\Phi^h) + \mathcal{O}\left(\frac{v^3}{M_{KK}^3}\right), \tag{4.68}$$

where

$$\begin{aligned}
\Phi_{ff,mn} &\equiv \frac{2\pi}{L\epsilon} \int_\epsilon^1 dt \hat{a}_m^{f\dagger} \mathbf{S}_m^{f\dagger}(t) \mathbf{S}_n^f(t) \hat{a}_n^f \\
\Phi_{FF,mn} &\equiv \frac{2\pi}{L\epsilon} \int_\epsilon^1 dt \hat{a}_m^{F\dagger} \mathbf{S}_m^{F\dagger}(t) \mathbf{S}_n^F(t) \hat{a}_n^F \\
\Delta \tilde{g}_{mn}^h &\equiv \frac{v}{m_{f_n}} \sqrt{2} (2+\beta) \frac{2\pi}{L\epsilon} \int_\epsilon^1 dt t^{1+\beta} \hat{a}_m^{f\dagger} \mathbf{S}_m^{f\dagger}(t) \mathbf{Y}_f^\dagger \mathbf{S}_n^F(t) \hat{a}_n^F, \\
\Phi_{mn}^h &\equiv \frac{v}{m_{f_n}} \frac{(2+\beta) 2\pi}{\sqrt{2} L\epsilon} \int_\epsilon^1 dt t^{1+\beta} \left( \frac{t^2}{1+\beta} - \frac{1}{2+\beta} \right) \hat{a}_m^{F\dagger} \mathbf{C}_m^{F\dagger}(t) \mathbf{Y}_f \mathbf{C}_n^f(t) \hat{a}_n^f.
\end{aligned} \tag{4.69}$$

This is in correspondence with the vertex of the general Higgs couplings to fermions, given in (4.9). With the help of the approximate zero-mode fermion profiles in (2.114), one computes

the single matrix expressions, and derives

$$\begin{aligned}
\Phi_{ff,mn} = & \frac{v^2}{M_{\text{KK}}^2} \left[ \frac{m_{f_m}}{v} \sum_i W_{f,mi}^\dagger \frac{1}{1-2c_{f_i}} \left( \frac{1}{F(c_{f_i})^2} - 1 + \frac{F(c_{f_i})^2}{2c_{f_i}+3} \right) W_{f,in} \frac{m_{f_n}}{v} \right. \\
& + \frac{m_{f_m}}{\sqrt{2}v} \sum_{i,j} W_{f,mi}^\dagger \left( \frac{1}{p_4(c_{f_i}+c_{f_j})} - \frac{1}{F(c_{f_i})^2} \right) \frac{\tilde{\mathbf{Y}}_{f,ij}^{\dagger\text{eff}}}{p_3(-c_{f_i}+c_{f_j})} U_{f,jn} \\
& + \frac{m_{f_n}}{\sqrt{2}v} \sum_{i,j} U_{f,mj}^\dagger \left( \frac{1}{p_4(c_{f_i}+c_{f_j})} - \frac{1}{F(c_{f_i})^2} \right) \frac{\tilde{\mathbf{Y}}_{f,ji}^{\text{eff}}}{p_3(-c_{f_i}+c_{f_j})} W_{f,in} \\
& \left. + \frac{1}{2} \sum_{i,j,k} U_{f,mj}^\dagger \frac{\tilde{\mathbf{Y}}_{f,ji}^{\text{eff}} \tilde{\mathbf{Y}}_{f,ik}^{\dagger\text{eff}}}{F(c_{f_i})^2 q_5(c_{f_j}+c_{f_k})} U_{f,kn} \right], \tag{4.70}
\end{aligned}$$

$$\begin{aligned}
\Phi_{FF,mn} = & \frac{v^2}{M_{\text{KK}}^2} \left[ \frac{m_{f_m}}{v} \sum_i U_{f,mi}^\dagger \frac{1}{1-2c_{F_i}} \left( \frac{1}{F(c_{F_i})^2} - 1 + \frac{F(c_{F_i})^2}{2c_{F_i}+3} \right) U_{f,in} \frac{m_{f_n}}{v} \right. \\
& + \frac{m_{f_m}}{\sqrt{2}v} \sum_{i,j} U_{f,mi}^\dagger \left( \frac{1}{p_4(c_{F_i}+c_{f_j})} - \frac{1}{F(c_{F_i})^2} \right) \frac{\tilde{\mathbf{Y}}_{f,ij}^{\text{eff}}}{p_3(-c_{F_i}+c_{f_j})} W_{f,jn} \\
& + \frac{m_{f_n}}{\sqrt{2}v} \sum_{i,j} W_{f,mj}^\dagger \left( \frac{1}{p_4(c_{F_i}+c_{f_j})} - \frac{1}{F(c_{F_i})^2} \right) \frac{\tilde{\mathbf{Y}}_{f,ji}^{\dagger\text{eff}}}{p_3(-c_{F_i}+c_{f_j})} U_{f,in} \\
& \left. + \frac{1}{2} \sum_{i,j,k} W_{f,mj}^\dagger \frac{\tilde{\mathbf{Y}}_{f,ji}^{\dagger\text{eff}} \tilde{\mathbf{Y}}_{f,ik}^{\text{eff}}}{F(c_{F_i})^2 q_5(c_{f_j}+c_{f_k})} W_{f,kn} \right], \tag{4.71}
\end{aligned}$$

$$\begin{aligned}
\Delta \tilde{g}_{mn}^h = & -\frac{v}{m_{f_n}} \frac{v^2}{M_{\text{KK}}^2} \left[ \frac{\sqrt{2}m_{f_m}}{v} \sum_{i,j} W_{mi}^\dagger \tilde{\mathbf{Y}}_{f,ij}^{\dagger\text{eff}} U_{jn} \frac{m_{f_n}}{v_4} \frac{p_2(c_{f_i}+c_{f_j})}{p_2(-c_{f_i}-c_{f_j})} \right. \\
& \times \left( \frac{-2(1+c_{f_i}+c_{f_j})}{p_4(c_{f_i}+c_{f_j})(1+2c_{f_i})(1+2c_{f_j})} + \frac{1}{F(c_{f_i})^2 F(c_{f_j})^2} \right. \\
& \left. \left. + \frac{[(1+2c_{f_i})^{-1} - F(c_{f_i})^{-2}]}{p_3(-c_{f_i}+c_{f_j})} + \frac{[(1+2c_{f_j})^{-1} - F(c_{f_j})^{-2}]}{p_3(c_{f_i}-c_{f_j})} \right) \right. \\
& + \frac{m_{f_m}}{v} \sum_{k,i,l} W_{mk}^\dagger \left( \frac{1}{q_5(c_{f_k}+c_{f_l})} - \frac{1}{F(c_{f_k})^2} \right) \frac{p_2(c_{f_k}+c_{f_l})}{q_4(-c_{f_k}+c_{f_l})} \frac{\tilde{\mathbf{Y}}_{f,ki}^{\dagger\text{eff}} \tilde{\mathbf{Y}}_{f,il}^{\text{eff}}}{F(c_{f_i})^2} W_{ln} \\
& + \frac{m_{f_n}}{v} \sum_{k,i,l} U_{mk}^\dagger \left( \frac{1}{q_5(c_{F_k}+c_{F_l})} - \frac{1}{F(c_{F_l})^2} \right) \frac{\tilde{\mathbf{Y}}_{f,ki}^{\text{eff}} \tilde{\mathbf{Y}}_{f,il}^{\dagger\text{eff}}}{q_4(c_{F_k}-c_{F_l})} \frac{p_2(c_{f_i}+c_{F_l})}{F(c_{f_i})^2} U_{ln} \\
& \left. + \frac{1}{\sqrt{2}} \sum_{i,j,k,p} U_{mi}^\dagger \frac{\tilde{\mathbf{Y}}_{f,ij}^{\text{eff}} \tilde{\mathbf{Y}}_{f,jk}^{\dagger\text{eff}} \tilde{\mathbf{Y}}_{f,kp}^{\text{eff}}}{F(c_{f_j})^2 r_6(c_{F_i}+c_{f_p})} \frac{p_2(c_{f_j}+c_{F_k})}{F(c_{F_k})^2} W_{pn} \right], \tag{4.72}
\end{aligned}$$

$$\Phi_{mn}^h = \frac{v}{m_{f_n}} \sum_{i,j} U_{mi}^\dagger \frac{\tilde{\mathbf{Y}}_{f,ij}^{\text{eff}}}{\sqrt{2}} \frac{p_2(c_{F_i} + c_{f_j})}{p_4(c_{F_i} + c_{f_j})(1 + \beta)} W_{jn} - \frac{\delta_{mn}}{2 + \beta} . \quad (4.73)$$

The matrices  $\mathbf{U}_f$ ,  $\mathbf{W}_f$  and  $\tilde{\mathbf{Y}}_f$  have been defined in (2.120), and  $F(c)$  is the zero-mode fermion profile, given in (2.115). In addition, we have introduced the abbreviations [154]

$$p_k(c) = (k + c + \beta) , \quad q_k(c) = (k + c + 2\beta) , \quad r_k(c) = (k + c + 3\beta) . \quad (4.74)$$

One can compare the result with previous findings, derived in the very narrow bulk-Higgs scenario of the RS model, corresponding to the limit  $\beta \rightarrow \infty$  performed in the results of the bulk-Higgs scenario. In this limit, the different matrix expressions read

$$\begin{aligned} \Phi_{ff,mn} &\stackrel{\lim_{\beta \rightarrow \infty}}{=} \frac{m_{f_m} m_{f_n}}{M_{\text{KK}}^2} \sum_i W_{f,mi}^\dagger \frac{1}{1 - 2c_{f_i}} \left( \frac{1}{F(c_{f_i})^2} - 1 + \frac{F(c_{f_i})^2}{2c_{f_i} + 3} \right) W_{f,in} , \\ \Phi_{FF,mn} &\stackrel{\lim_{\beta \rightarrow \infty}}{=} \frac{m_{f_m} m_{f_n}}{M_{\text{KK}}^2} \sum_i U_{f,mi}^\dagger \frac{1}{1 - 2c_{F_i}} \left( \frac{1}{F(c_{F_i})^2} - 1 + \frac{F(c_{F_i})^2}{2c_{F_i} + 3} \right) U_{f,in} , \\ \Delta \tilde{g}_{mn}^h &\stackrel{\lim_{\beta \rightarrow \infty}}{=} -\frac{1}{3} \sum_{i,j,k} \frac{v^2}{M_{\text{KK}}^2} U_{mi}^\dagger F(c_{F_i}) Y_{f,ij} Y_{f,jk}^\dagger F(c_{F_k})^{-1} U_{kn} , \\ \Phi_{mn}^h &\stackrel{\lim_{\beta \rightarrow \infty}}{=} 0 . \end{aligned} \quad (4.75)$$

To find the results, one has to use the eigenvalue equations

$$m_{f_n} \mathbf{W} = \frac{v}{\sqrt{2}} \mathbf{Y}_f^\dagger \mathbf{U} , \quad m_{f_n} \mathbf{U} = \frac{v}{\sqrt{2}} \mathbf{Y}_f^{\text{eff}} \mathbf{W} , \quad (4.76)$$

resulting from (2.153). These outcomes coincide with the results determined in the references, *e.g.* in [2, 5, 151].

### Contribution of the full KK fermion tower

The infinite summation over the Yukawa couplings  $g_{nn}^f$ , times the vev, divided through the KK fermion masses in (4.65), can be computed in a closed form by relating it to the five-dimensional fermion propagator function [2, 5]. Using the KK decomposed propagator functions, given in (3.40), one can write the summation over the KK fermion states in the fermion contribution as [5]

$$\sum_{n=1}^{\infty} \frac{v g_{nn}^f}{m_{f_n}} = \int_{\epsilon}^1 dt \sqrt{\frac{\pi}{L}} \frac{\chi_0^h(t)}{\sqrt{1 + \beta}} T_{RL}^f(t, t) , \quad (4.77)$$

where

$$T_{RL}^f(t, t') = \frac{v(2 + \beta)}{\sqrt{2}} \text{Tr} \left[ \begin{pmatrix} \mathbf{0} & \mathbf{Y}_f \\ \mathbf{Y}_f^\dagger & \mathbf{0} \end{pmatrix} \Delta_{RL}^f(t, t') \right] \quad (4.78)$$

depends on the propagator function  $\Delta_{RL}^f(t, t')$ . Notice that only the off-diagonal blocks of the propagator function enter into the result. In Section 3.3.1, we have presented the calculation

and result for the propagator function  $\Delta_{RL}(t, t')$ , depending on the two  $3 \times 3$  matrix expressions  $\mathbf{C}_3^>$  and  $\mathbf{C}_4^>$ , given in (3.62). Including these results, the expression in (4.78) is determined as

$$\begin{aligned}
T_{RL}^f(t, t) &= \frac{v(2+\beta)}{\sqrt{2}} \text{Tr} \left[ \mathbf{Y}_f \left( t^{\mathbf{c}_f} + \frac{v^2}{4M_{KK}^2} (-\mathbf{Y}^{B\dagger}(t) \mathbf{Y}^E + \mathbf{Y}^{F\dagger}(t)) \right) \mathbf{C}_3^> \right. \\
&\quad \left. + \mathbf{Y}_f^\dagger \left( -\frac{v}{\sqrt{2}M_{KK}} \mathbf{Y}^A(t) \right) \mathbf{C}_4^> \right] \\
&= (2+\beta) \text{Tr} \left[ \mathbf{Y}_f t^{\mathbf{c}_f} \left( (\mathbf{Y}^E)^{-1} t^{\mathbf{c}_F} + \frac{v^2}{2M_{KK}^2} \left[ (\mathbf{1} + (\mathbf{Y}^E)^{-1} t^{\mathbf{c}_F} \mathbf{Y}^A(t)) t^{-\mathbf{c}_f} \mathbf{Y}^{B\dagger}(t) t^{\mathbf{c}_F} \right. \right. \right. \\
&\quad \left. \left. + \frac{1}{2} (\mathbf{Y}^{C\dagger} - (\mathbf{Y}^E)^{-1} \mathbf{Y}^G) t^{\mathbf{c}_F} \right) \right] + \frac{v^2}{4M_{KK}^2} \mathbf{Y}_f (-\mathbf{Y}^{B\dagger}(t) \mathbf{Y}^E + \mathbf{Y}^{F\dagger}(t)) (\mathbf{Y}^E)^{-1} t^{\mathbf{c}_F} \\
&\quad \left. - \frac{v^2}{2M_{KK}^2} \mathbf{Y}_f^\dagger \mathbf{Y}^A(t) (\mathbf{1} + (\mathbf{Y}^E)^{-1} t^{\mathbf{c}_F} \mathbf{Y}^A(t)) t^{-\mathbf{c}_f} \right]. \tag{4.79}
\end{aligned}$$

After having performed the remaining integral over the function  $T_{RL}^f(t, t)$  and the Higgs profile in (4.77), one obtains the following result

$$\begin{aligned}
&\sum_{n=1}^{\infty} \frac{v(g_{nn}^f)}{m_{f_n}} \\
&= \sum_{i,j} \left( \frac{2+\beta}{p_2(c_{f_j} + c_{F_i})} + \frac{m_h^2}{4M_{KK}^2} \left[ \frac{1}{p_2(c_{f_j} + c_{F_i})} - \frac{2+\beta}{(1+\beta)p_4(c_{f_j} + c_{F_i})} \right] \right) \cdot [\mathbf{Y}_{f,ij} (\mathbf{Y}^E)_{ji}^{-1}] \\
&+ \frac{v^2}{2M_{KK}^2} \left[ \sum_{i,j} \left( \frac{2+\beta}{p_2(c_{f_j} + c_{F_i})} - \frac{1}{4} \right) [\mathbf{Y}_{f,ij} \mathbf{Y}_{ji}^{C\dagger}] \right. \\
&- \frac{1}{2} \sum_{i,j,k,l} \frac{(2+\beta)^2}{p_2(c_{f_j} + c_{F_i}) q_4(c_{F_k} - c_{F_i})} [\mathbf{Y}_{f,ij} (\mathbf{Y}^E)_{jk}^{-1} \mathbf{Y}_{f,kl} \mathbf{Y}_{li}^{C\dagger}] \\
&+ \sum_{i,j,k,l} \left( \frac{2+\beta}{r_6(c_{f_j} + c_{F_k})} - \frac{2+\beta}{q_4(c_{f_j} + c_{F_k} + c_{f_l} + c_{F_i})} \right) \cdot [\mathbf{Y}_{f,ij} (\mathbf{Y}^E)_{jk}^{-1} \mathbf{Y}_{kl}^E \mathbf{Y}_{li}^{C\dagger}] \\
&+ \frac{1}{2} \sum_{i,j} [\mathbf{Y}_{f,ij}^\dagger \mathbf{Y}_{ji}^E] - \sum_{i,j,k,l} \frac{2+\beta}{r_6(c_{f_k} + c_{F_l})} \cdot [\mathbf{Y}_{f,ij}^\dagger \mathbf{Y}_{jk}^E (\mathbf{Y}^E)_{kl}^{-1} \mathbf{Y}_{li}^E] \\
&+ \frac{1}{2} \sum_{i,j,k,l} \frac{2+\beta}{q_4(-c_{f_j} + c_{f_l})} \left( \frac{2+\beta}{r_6(c_{f_l} + c_{F_i})} - \frac{2+\beta}{p_2(c_{f_j} + c_{F_i})} \right) \cdot [\mathbf{Y}_{f,ij} (\mathbf{Y}^\dagger)_{f,jk} \mathbf{Y}_{kl}^E (\mathbf{Y}^E)_{li}^{-1}] \Big], \tag{4.80}
\end{aligned}$$

by skipping terms of  $\mathcal{O}(\epsilon^2)$  and smaller. The abbreviations containing the Yukawa matrices  $\mathbf{Y}^A(t)$ ,  $\mathbf{Y}^{B\dagger}(t)$ ,  $\mathbf{Y}^{C\dagger}$ ,  $\mathbf{Y}^E$ ,  $\mathbf{Y}^{F\dagger}(t)$ ,  $\mathbf{Y}^G$  have been defined in Subsection 3.3.1. In the limit of a very narrow bulk-Higgs field, corresponding to  $\beta \rightarrow \infty$ , the result in (4.80) gives

$$\lim_{\beta \rightarrow \infty} \left( \sum_{n=1}^{\infty} \frac{v(g_{nn}^f)}{m_{f_n}} \right) = \mathbf{1} + \frac{v^2}{2M_{KK}^2} \frac{1}{3} \text{Tr} \left( \mathbf{Y}_f \mathbf{Y}_f^\dagger \right) + \dots \tag{4.81}$$



This is in correspondence with previous findings, derived in the very narrow-bulk Higgs scenario of the RS model, *e.g.* in [5].

### Complete result for the fermion contribution

In the previous subsections, we have separately presented the calculations of the zero-mode fermion contributions, and the contributions from the full KK fermion tower. The results are given by extensive formulas, which depend, in a complicated way, on the different fermion bulk mass parameters  $c_{[F,f]_i}$ , for example. In the subsequent part of the thesis, we want to numerically evaluate and graphically present the results for the various Higgs decay rates into two particle states, in dependence of the RS model parameter space. In this regard, the significant and interesting parameters are the KK mass scale, the five-dimensional Yukawa matrices and the bulk-Higgs localization parameter  $\beta$ . For this purpose, we want to minimize the large parameter space of our system, and to obtain a more concise expression for the complete fermion contribution. The bulk mass parameters, except of the one for the top quark, are all situated near the value  $-1/2$  in order to derive the accurate zero-mode fermion masses in the RS model [150, 154]. For that reason, one can approximate the extended formulas for the fermion contribution by setting all the various fermion bulk mass parameters  $c$  to be of value  $-1/2$ . Then, for example, one can obtain reductions as

$$\frac{(2 + \beta)}{p_2(c_{A_i} + c_{B_j})} \rightarrow \frac{(2 + \beta)}{(1 + \beta)}, \quad (4.82)$$

where  $c_{A_i}$  and  $c_{B_j}$  are arbitrary fermion bulk mass parameters. Then, using the eigenvalue equations from (2.116), one can derive the following results for the expressions  $\Phi_{ff,nn}$  and  $\Phi_{FF,nn}$ , appearing in the sum over the KK-diagonal zero-mode fermion contributions,

$$\begin{aligned} \Phi_{ff,nn} \stackrel{c_i \rightarrow -1/2}{=} \Phi_{FF,nn} \stackrel{c_i \rightarrow -1/2}{=} \sum_n \frac{m_{f_n}^2}{2M_{KK}^2} \left( L \left[ 1 - \frac{(5 + 3\beta)}{(2 + \beta)(3 + \beta)} \right] - 1 + \frac{1}{2L} \right), \\ \Phi_{nn}^h \stackrel{c_i \rightarrow -1/2}{=} - \sum_n \frac{\delta_{nn}}{(2 + \beta)(3 + \beta)}. \end{aligned} \quad (4.83)$$

These expressions are suppressed by the square of the zero-mode fermion masses over the square of the KK mass scale. For that reason, they play a less significant role in the subsequent numerical evaluation [2, 150, 151]. In the complete result for the fermion contribution, given in (4.65), the sum over the first three KK states is subtracted, and is again added, multiplied with the exact form factors  $A(\tau_{f_i})$  and  $B(\tau_{f_i})$ . These functions adopt significant values only for the cases of the third generation fermions, for  $m_f = m_\tau, m_b, m_t$ . For the last entry of the matrix expression  $\Delta \tilde{\mathbf{g}}^h$ , giving the contribution of the third generation fermions, one can derive the following formula in the limit  $c_i \rightarrow -1/2$ ,

$$\begin{aligned} \Delta \tilde{g}_{33}^h \stackrel{c_i \rightarrow -1/2}{=} \frac{v^2}{M_{KK}^2} \left[ \bar{U}_{3i} Y_{f,ij} Y_{f,jk}^\dagger \bar{U}_{k3} \left( -\frac{4(2 + \beta)^3}{(1 + \beta)(3 + \beta)(5 + 3\beta)} + \frac{(2 + \beta)}{2(1 + \beta)} \right) \right. \\ \left. + \bar{W}_{3i} Y_{f,ij}^\dagger Y_{f,jk} \bar{W}_{k3} \frac{(2 + \beta)}{2(1 + \beta)} \right] \approx -\frac{v^2}{M_{KK}^2} \frac{(1 + \beta)(2 + \beta)}{(3 + \beta)(5 + 3\beta)} \frac{(\mathbf{Y}_f \mathbf{Y}_f^\dagger \mathbf{Y}_f)_{33}}{(\mathbf{Y}_f)_{33}}, \end{aligned} \quad (4.84)$$

where here the unitary matrices in the limit  $c_i \rightarrow -1/2$  are labelled by  $\bar{\mathbf{U}}$  and  $\bar{\mathbf{W}}$ . For the sum over the full KK fermion tower, one obtains further

$$\sum_{n=1}^{\infty} \frac{v g_{nn}^f}{m_{f_n}} \stackrel{c \rightarrow -1/2}{=} \sum_{n,k} \left[ 1 + \frac{m_h^2}{4M_{KK}^2} \frac{1}{(2+\beta)(3+\beta)} \right] \delta_{nn} + \frac{v^2}{2M_{KK}^2} \frac{(2+\beta)}{(5+3\beta)} Y_{f,nk} Y_{f,kn}^\dagger. \quad (4.85)$$

Now, after having computed the limit for the individual parts of the fermion contribution, one can determine the complete result, according to the formula (4.65). In this connection, one can distinguish between the results for the tree-level Higgs couplings to the fermions of the third generation, and the loop-contributions of the KK fermion tower, as

$$\begin{aligned} C_f + iC_{f5} &= 1 - \varepsilon_f + \frac{m_h^2}{4M_{KK}^2} \frac{1}{(2+\beta)(3+\beta)} - \frac{v^2}{M_{KK}^2} \frac{(1+\beta)(2+\beta)}{(3+\beta)(5+3\beta)} \frac{(\mathbf{Y}_f \mathbf{Y}_f^\dagger \mathbf{Y}_f)_{33}}{(\mathbf{Y}_f)_{33}} \\ &\quad - \frac{Lm_W^2}{2M_{KK}^2} \frac{(1+\beta)^2}{(2+\beta)(3+2\beta)}, \quad (4.86) \\ \nu_f + i\nu_{f5} &= \frac{v^2}{2M_{KK}^2} \frac{(2+\beta)}{(3+\beta)} \text{Tr} \left[ \mathbf{Y}_f \mathbf{Y}_f^\dagger \right]. \end{aligned}$$

The indices  $f$  of the couplings  $C_f + iC_{f5}$  are written as  $f = t, b, \tau$ . We neglect the zero-mode contributions of the lighter fermions, since the corresponding form factors  $A(\tau_{f_i})$  and  $B(\tau_{f_i})$  have insignificantly small values. On the contrary, for  $\nu_f + i\nu_{f5}$  and the Yukawa matrices  $\mathbf{Y}_f$  the indices  $f$  mean  $f = u, d, e$ , classifying between up-type quarks, down-type quarks and leptons. In the numerical evaluation, we will neglect further the contributions  $\varepsilon_f$  that are

$$\varepsilon_f = (\Phi_{ff})_{33} + (\Phi_{FF})_{33}, \quad (4.87)$$

given in the first row of (4.83), which are suppressed by  $m_{f_n}^2/M_{KK}^2$  [2, 150, 151]. The traces of the hermitian matrix  $\mathbf{Y}_f \mathbf{Y}_f^\dagger$  are real, so that the CP-odd loop contributions of the KK towers vanish completely,  $\nu_{f5} = 0$  [2, 3]. By now, the present result does no longer depend on the 15 different fermion bulk mass parameters. Therefore, the phenomenological impact of the KK mass scale  $M_{KK}$ , the Yukawa matrices  $\mathbf{Y}_f$  and the parameter  $\beta$  of the Higgs can be investigated much better.

Taking the concise expressions in (4.86), one can perform the limit  $\beta \rightarrow \infty$ , in which the results smoothly merge into the result derived in the very narrow bulk-Higgs scenario, reading

$$\begin{aligned} C_f^{\text{nbH}} + iC_{f5}^{\text{nbH}} &\approx 1 - \varepsilon_f^{\text{nbH}} - \frac{v^2}{M_{KK}^2} \frac{1}{3} \frac{(\mathbf{Y}_u \mathbf{Y}_u^\dagger \mathbf{Y}_u)_{33}}{(\mathbf{Y}_u)_{33}} - \frac{Lm_W^2}{4M_{KK}^2}, \quad (4.88) \\ \nu_f^{\text{nbH}} + i\nu_{f5}^{\text{nbH}} &\approx \frac{v^2}{2M_{KK}^2} \text{Tr} \left[ \mathbf{Y}_f \mathbf{Y}_f^\dagger \right], \end{aligned}$$

These outcomes coincide with the results calculated *e.g.* in [2, 5]. In references [2, 3], the profile function of a very narrow bulk-Higgs field was taken to be a regularized distribution  $\delta^\eta(t-1)$  of width  $\eta \ll 1$ , as mentioned in Subsection 2.2.3. The bulk-Higgs profile  $\chi_0^h(t)$ , given in (2.74), behaves similarly to this distribution in the limit  $\beta \rightarrow \infty$ . It should be noticed that the results for

the fermion contributions in loop-induced Higgs processes do not smoothly interpolate between a very narrow bulk-Higgs scenario and a real brane-Higgs scenario [2, 5, 151, 152, 171, 212]. The difference is due to a “resonance effect” in the very narrow bulk-Higgs scenario, where very heavy KK modes with masses of the order of the inverse Higgs width  $\Delta_h = v/\eta$  give an unsuppressed contribution to loop amplitudes [2, 172]. As a result, the effective field theory description breaks down in the intermediate region between the two scenarios. This has been briefly discussed in Subsection 2.2.3. The result for the loop-contributions of fermions to the gluon fusion in a brane-Higgs scenario is of opposite sign compared to the result in the very narrow bulk-Higgs scenario, and reads [2, 5]

$$\nu_f^{\text{bH}} + i\nu_{f5}^{\text{bH}} \approx -\frac{v^2}{2M_{KK}^2} \text{Tr} \left[ \mathbf{Y}_f \mathbf{Y}_f^\dagger \right]. \quad (4.89)$$

For that reason, the predictions for the Higgs decay into two photons and the gluon fusion production process significantly differ between the two Higgs scenarios, although these might consider a similar Higgs localization, from a naive point of view. But actually, the brane-Higgs scenario and the very narrow bulk-Higgs scenario really form two different incarnations of the RS model.

In the following, the analytic results, derived for the various Higgs couplings and processes presented in the previous subsections, will numerically be evaluated, in the following, in dependence of the significant, open parameters of the RS model. For the bulk-Higgs localization parameter, a value 1 is chosen for a scenario with a real bulk-Higgs field, and a value 10 is chosen for a scenario with a narrow bulk-Higgs field. For the numerical input of the evaluations, three parameter sets have been dived with 5000 points for the Yukawa matrices  $\mathbf{Y}_f$  and the KK mass scale  $M_{KK}$ , where each set respects a different maximally allowed entry of the Yukawa matrices  $y_\star$ , with  $y_\star = 1, 2, 3$ . For a given value of  $M_{KK}$ , a  $\chi^2$ -minimization has been performed, by starting from a random point, with anarchic, random, complex entries for  $(Y_f)_{ij}$  that obey to the upper bound  $y_\star$ . All points have been rejected that deviate by more than  $1\sigma$  from the Wolfenstein parameters and the masses of the zero-mode quarks [150]. During the dicing process, appropriate bulk mass parameters  $c_i$  were used for the fermions to reproduce the correct quark masses. Details on the dicing process are presented in Appendix C.3.

In Figure 4.7, the CP-even Higgs couplings to top quarks  $C_t$  are plotted, for  $\beta = 1$  on the left-hand side and  $\beta = 10$  on the right-hand side, and for three different maximally allowed entries of the Yukawa matrices  $y_\star = 1, 2, 3$ . One observes that the deviations from the SM are stronger for lower values of the KK mass scale, higher values of  $\beta$ , and higher maximally allowed entries of the Yukawa matrices  $y_\star$ , respectively. Similarly, the CP-odd Higgs couplings to top quarks  $C_{5t}$  are plotted in Figure 4.8 for the same choices of parameters. The results scatter around zero, with larger magnitudes for higher maximally allowed entries of the Yukawa matrices  $y_\star$ , smaller values for the KK mass scale and higher values for  $\beta$ . Both the CP-even and -odd Higgs couplings to top quarks are mainly determined by the Yukawa matrices, entering through the expressions  $\frac{(\mathbf{Y}_f \mathbf{Y}_f^\dagger \mathbf{Y}_f)_{33}}{(\mathbf{Y}_f)_{33}}$ . These expressions can be averaged, by following the assumption that the entries of the Yukawa matrices are distributed with a Gaussian shape around its central value, for a large enough set of scattered points. Then, it follows that [2]

$$\left\langle \frac{(\mathbf{Y}_f \mathbf{Y}_f^\dagger \mathbf{Y}_f)_{33}}{(\mathbf{Y}_f)_{33}} \right\rangle \approx (2N_g - 1) \frac{y_\star^2}{2}, \quad (4.90)$$

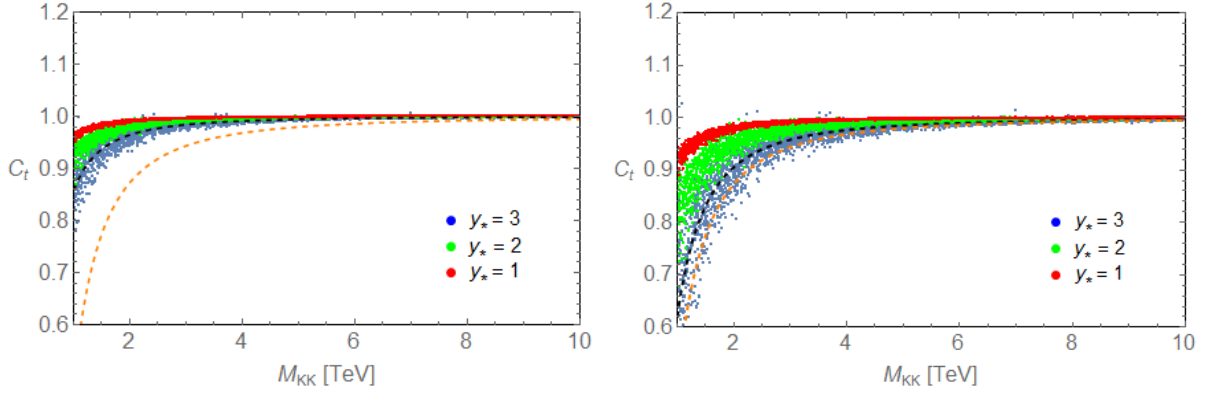


Figure 4.7: The CP-even Higgs couplings  $C_t$  to a pair of  $t$  quarks are plotted in dependence of the KK mass scale, for  $\beta = 1$  on the left-hand side and  $\beta = 10$  on the right-hand side, for the three different maximally allowed entries of the Yukawa matrices,  $y_\star = 1, 2, 3$ , respectively.

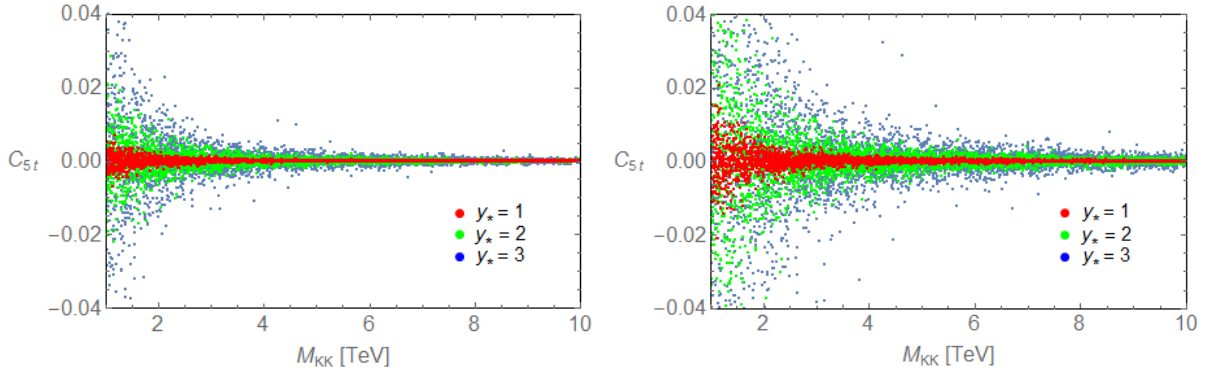


Figure 4.8: The CP-odd Higgs couplings  $C_{5t}$  to a pair of  $t$  quarks are plotted in dependence of the KK mass scale, for  $\beta = 1$  on the left-hand side and  $\beta = 10$  on the right-hand side, for the three different maximally allowed entries of the Yukawa matrices,  $y_\star = 1, 2, 3$ , respectively.

where  $N_g = 3$  is the number of fermion generations.<sup>5</sup> Using this average, one can find for the Higgs couplings to quark fields,

$$C_q \approx 1 - \frac{v^2}{M_{KK}^2} \left( \begin{matrix} 3.75 \\ 10.97 \\ 15.00 \end{matrix} \times \left(\frac{y_\star}{3}\right)^2 + \begin{matrix} 0.95 \\ 1.57 \\ 1.78 \end{matrix} \right), \quad (4.91)$$

for  $\beta = 1$  (upper numbers),  $\beta = 10$  (numbers in the middle) and  $\beta \rightarrow \infty$  (lower numbers). Instead, for the Higgs couplings to lepton fields, one can find

$$C_l \approx 1 - \frac{v^2}{2M_{KK}^2} \left( \begin{matrix} 8.44 \\ 13.06 \end{matrix} \times \left(\frac{y_\star}{3}\right)^2 + \begin{matrix} 0.94 \\ 1.57 \end{matrix} \right), \quad (4.92)$$

<sup>5</sup>For the matrices  $\tilde{\mathbf{Y}}_f$  in the bulk-Higgs RS model, it follows further that  $\langle \frac{(\tilde{\mathbf{Y}}_f \tilde{\mathbf{Y}}_f^\dagger \tilde{\mathbf{Y}}_f)_{33}}{(\tilde{\mathbf{Y}}_f)_{33}} \rangle \approx \frac{(1+\beta)^2}{(2+\beta)^2} (2N_g - 1) \frac{y_\star^2}{2}$ .

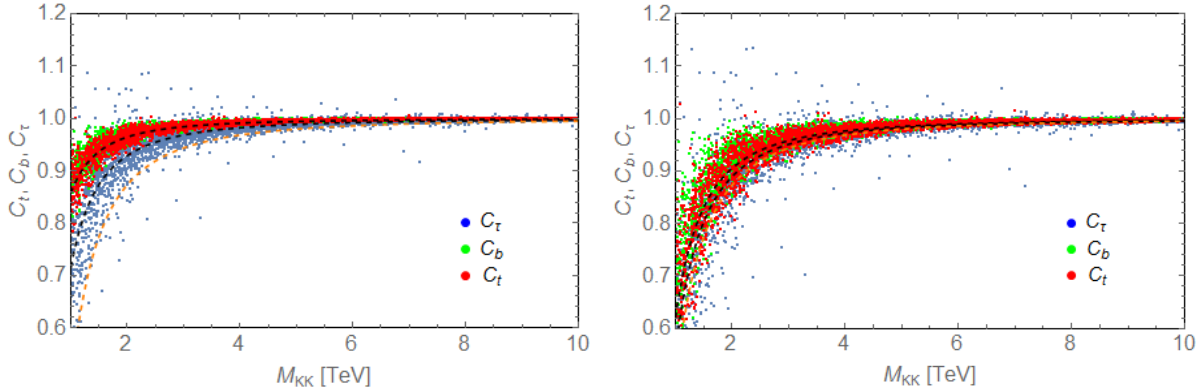


Figure 4.9: The CP-even Higgs couplings to a pair of t quarks, b quarks and  $\tau$  leptons,  $C_t, C_b, C_\tau$ , are plotted, for  $y_\star = 3$ , in dependence of the KK mass scale, for  $\beta = 1$  on the left-hand side and  $\beta = 10$  on the right-hand side, respectively.

for  $\beta = 1$  (upper numbers) and  $\beta = 10$  (lower numbers), whereas the result for the limit  $\beta \rightarrow \infty$  is equal to the quark case. The last values denote the corrections from the vev-shift of the Higgs  $\kappa_v$  in the RS model. So, the scattered results for the CP-even Higgs couplings to fermions are rather insensitive to the individual entries of the Yukawa matrices, but form broad bands that scale with  $y_\star^2$ , as plotted in Figure 4.7. For higher values of the KK mass scale  $M_{KK}$ , all the rates approach to the SM expectations, since the new-physics effects scale with  $v^2/(2M_{KK}^2)$ . The differences between the quark and lepton results stem from the factors  $(1 + \beta)^2/(2 + \beta)^2$ , which are only included in the quark case. The matrices  $\tilde{\mathbf{Y}}_q$  from (2.115) were diced subject to the constraints that these have to reproduce the correct quark masses and the CKM mixing matrix. On the contrary and for simplicity, the matrices for the leptons  $\mathbf{Y}_l$  were diced without implementing such constraints. This may have created the small differences in the numerical Higgs couplings. The averaged curves for the couplings  $C_f$ , for  $y_\star = 3$ , are indicated by the black and dashed lines in the plots in Figure 4.7. The results obtained in the limit  $\beta \rightarrow \infty$  are given by the orange and dashed curves. The curve for  $\beta = 10$  already strongly approaches to the orange curve of the benchmark case. The CP-odd couplings average to 0, and one observes a broad scattering of the results around this central value in the plots in Figure 4.8, with larger amounts for larger values of  $y_\star$  and smaller values for the KK mass scale.

In Figure 4.9, the CP-even Higgs couplings to a pair of t quarks, b quarks and  $\tau$  leptons are illustrated, for  $\beta = 1$  on the left-hand side and  $\beta = 10$  on the right-hand side, and a maximally allowed entry  $y_\star = 3$  of the Yukawa matrices. In Figure 4.10, the CP-odd Higgs couplings to t and b quarks and  $\tau$  leptons,  $C_{5t}, C_{5b}$  and  $C_{5\tau}$ , are plotted, for  $\beta = 10$ , and  $y_\star = 3$ , on the left-hand side. On the right-hand side, the correlation of the CP-odd Higgs couplings to a pair of t and b quarks,  $C_{5t}$  and  $C_{5b}$ , is indicated for  $\beta = 10$  and three different maximally allowed entries of the Yukawa matrices. The different behaviours of the curves result from the different kinds of matrices  $\mathbf{Y}_u, \mathbf{Y}_d$  and  $\mathbf{Y}_l$  that enter the expressions  $\frac{(\mathbf{Y}_f \mathbf{Y}_f^\dagger \mathbf{Y}_f)_{33}}{(\mathbf{Y}_f)_{33}}$ , which determine the Higgs couplings to the fermions. It can be observed from the plots that there is only a moderate dependence on the different types of Yukawa matrices, especially for the CP-even couplings for  $\beta = 10$ . For  $\beta = 1$ , the lepton couplings  $C_\tau$  slightly differ from the quark couplings  $C_b$  and  $C_t$

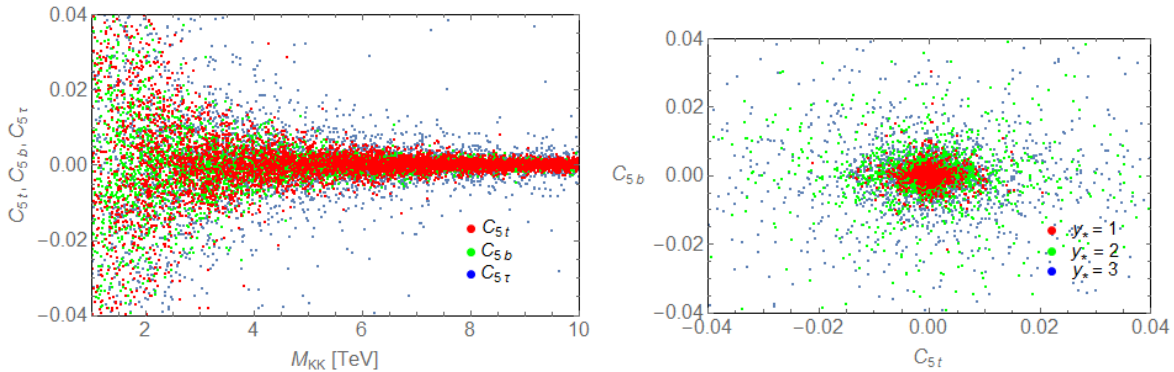


Figure 4.10: The CP-odd Higgs couplings to t and b quarks and  $\tau$  leptons,  $C_{5t}$ ,  $C_{5b}$  and  $C_{5\tau}$ , are plotted for  $\beta = 10$  and  $y_* = 3$ , on the left-hand side, respectively. On the right-hand side, the correlation of the CP-odd Higgs couplings to a pair of t and b quarks,  $C_{5t}$ ,  $C_{5b}$ , is indicated, for  $\beta = 10$ , and three different maximally allowed entries of the Yukawa matrices.

in the range of lower KK masses, as predicted by the averaged expressions in (4.91) and (4.92). For the CP-odd Higgs couplings, the behaviour of the Higgs couplings to t and b quarks seems to be nearly symmetric in the right plot of Figure 4.10. On the left-hand side, the CP-odd Higgs couplings to leptons seem to scatter with slightly larger magnitudes, compared to the couplings to t and b quarks. One can conclude that the flavor-specific constraints, applied in the dicing processes of  $\mathbf{Y}_u$  and  $\mathbf{Y}_d$ , seem to have quite insignificant effects, according to the similar magnitudes of the new-physics effects in the Higgs couplings. The lepton Yukawa matrices  $\mathbf{Y}_l$ , diced with the absence of flavor-specific constraints, cause slightly larger new-physics effects in the CP-even Higgs couplings, and a broader scattering of the CP-odd Higgs couplings, compared to the quark cases.

After having discussed the behaviour of the single Higgs couplings to fermions, in dependence of the parameters of the bulk-Higgs RS model, one can evaluate, in the next step, the new-physics effects on the various Higgs production and decay rates, which are easily calculated by means of the different Higgs couplings.

## 4.2 Higgs cross sections and decay rates, and the total Higgs decay width

### 4.2.1 Tree-level Higgs decay rates

In the following, several Higgs production cross sections and decay rates are numerically evaluated in dependence of the RS model's parameter space. We start with an analysis of the tree-level Higgs production cross sections through W boson fusion and Higgsstrahlung, produced in association with a W boson, which are given to good approximation by  $C_W^2$  from (4.26), according to the formulas (4.49) and (4.47). The results for these processes in connection with a Z boson are very similar, so that we restrain on the W boson case in the following. The results are plotted in Figure 4.11 on the left-hand side, in dependence of the KK mass scale and three different choices

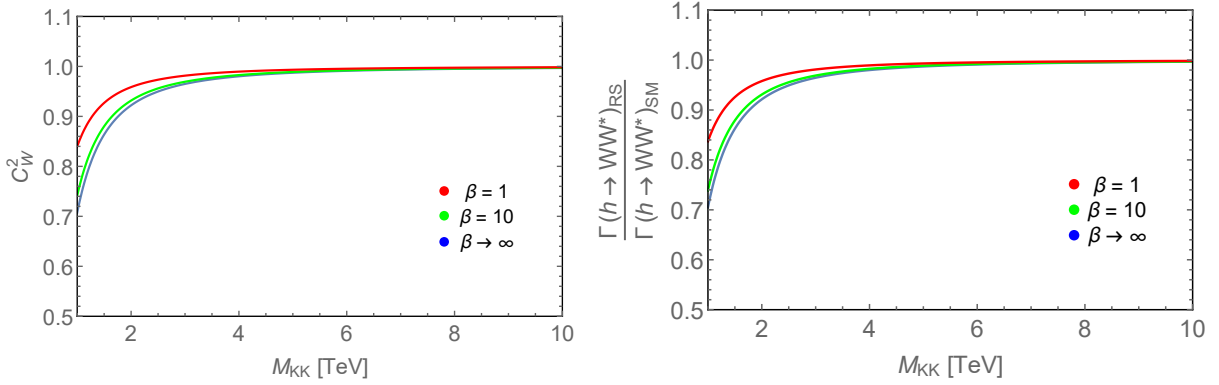


Figure 4.11: The cross sections for Higgs productions via W boson fusion, and Higgsstrahlung, given by  $C_W^2$  in good approximation, are plotted on the left-hand side, and the Higgs decay rates into a pair of heavy W bosons are plotted on the right-hand side, normalized on the SM predictions, respectively. Very similar curves could be derived for the processes in connection with a Z boson.

for the parameter  $\beta$ . Smaller new-physics deviations from the SM can be observed that are only important for very low KK masses  $< 3$  TeV, and one can find a less significant dependence on the parameter  $\beta$ , as well. On the right-hand side of Figure 4.11, the Higgs decay rates into states of a virtual and a real W boson are plotted, where the virtual W boson is decaying further into a state of two fermions. Again, the decay into two Z bosons would give very similar results that are skipped here. The rates in the plot are normalized on the SM values, and are plotted in dependence of the KK mass scale for three parameter choices of  $\beta$ , respectively. One can observe that the curves strongly resemble the curves of the Higgs production cross sections, given in Figure on the left-hand side. The formula for the normalized decay rates in (4.42) is similar to the formula for the normalized Higgs cross sections, given by  $C_W^2$  that gets corrected by the factor  $C_{\Gamma_W}$ , arising from the gauge boson to fermions couplings, and the contributions from the KK gauge boson tower that are exchanged in the process, as well. Similarly, the dependences on the Higgs localization parameter  $\beta$  are of minor importance, as the new-physics corrections are, in total, of a moderate magnitude.

In Figure 4.12, the Higgs decay rates into a pair of b quarks and  $\tau$  leptons are plotted, for  $y_* = 3$ , and  $\beta = 1$  on the left-hand side and  $\beta = 10$  on the right-hand side, where the blue points give the results for a Higgs decaying into a pair of  $\tau$  leptons, and the green points give the results for a Higgs decaying into a pair of b quarks. The single Higgs couplings to fermions have been investigated before, and the decay rates consist of the sum of the square of the CP-even and -odd Higgs couplings, as given in (4.4). The new-physics effects in the two different decay rates get amplified now, compared to the effects arising in the single Higgs couplings that have been discussed before. Again, the small differences between the two decay rates into  $\tau\tau$  and  $bb$  final states stem from the expressions that contain the different Yukawa matrices  $\tilde{\mathbf{Y}}_d$  and  $\tilde{\mathbf{Y}}_l$ . The results for the decays into  $\tau$  leptons scatter in a bit broader manner. It has been discussed that these differences do not necessarily result from a physical reason, but merely from the dicing procedure of the Yukawa matrices. Also, the contributions of the CP-odd Higgs couplings that scatter around zero may cause a slightly broader scattering of the curves of the decay rates,

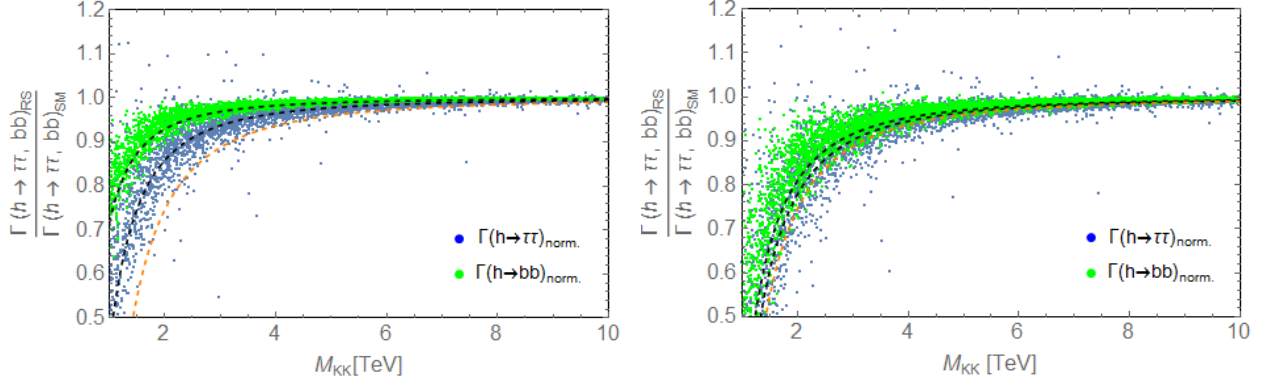


Figure 4.12: Here, the Higgs decay rates into a pair of  $\tau$  leptons and  $b$  quarks, normalized on the SM decay rates, are plotted for  $y_* = 3$ , and  $\beta = 1$  on the left-hand side and  $\beta = 10$  on the right-hand side. The black, dashed lines give the averaged results, obtained from (4.91) and (4.92), for  $\beta = 1$  and  $\beta = 10$ , whereas the orange, dashed lines give the averages for  $\beta \rightarrow \infty$ .

compared to the curves of the single, CP-even Higgs couplings. All in all, stronger new-physics effects can be found in the Higgs decay rates to fermions in Figure (4.12), compared to the Higgs decay rates to  $W$  bosons in Figure 4.11. In this sense, also the dependence on the Higgs localization parameter  $\beta$  is more severe.

### 4.2.2 Loop-induced Higgs processes

As a next step, the loop-induced Higgs production process through gluon fusion and the Higgs decay rate into two photons, normalized on the SM predictions, are evaluated. These Higgs production and decay rates include both the RS models modifications of the tree-level Higgs couplings to fermions and gauge bosons, as well as the loop-contributions induced by KK fermions, KK gauge bosons and KK scalars. For that reason, these rates can be of special importance in the context of new-physics searches. The results, derived with the diced sets of parameters, are displayed in Figure 4.13, for  $\beta = 1$  on the left-hand side and  $\beta = 10$  on the right-hand side, respectively. The fermion loop-contributions, given by the traces of Yukawa matrices, can be averaged for a large enough set of scattered points as [4]

$$\langle \text{Tr} \left( \mathbf{Y}_f \mathbf{Y}_f^\dagger \right) \rangle \approx N_g^2 \frac{y_*^2}{2}, \quad (4.93)$$

assuming that the entries of the Yukawa matrices are distributed with a Gaussian shape around its central value, and  $N_g = 3$  is the number of fermion generations, similar as before. With the help of the averaged expressions, and  $L = 33.5$ ,  $A(\tau_W) \approx 1.19$ ,  $A(\tau_t) \approx 1$ ,  $A(\tau_b) \approx 0$ , and therefore  $C_\gamma^{SM} \approx -4.91$ , and  $C_g^{SM} \approx 1$ , one determines the following averages to the lowest order

$$\frac{\sigma_{[gg \rightarrow h]}^{RS}}{\sigma_{[gg \rightarrow h]}^{SM}} \approx 1 + \frac{v^2}{2M_{KK}^2} \begin{cases} (-7.5 + 54.0) \cdot \left(\frac{y_*}{3}\right)^2 - 1.9 \\ (-21.9 + 125.7) \cdot \left(\frac{y_*}{3}\right)^2 - 3.1 \\ (-30 + 162) \cdot \left(\frac{y_*}{3}\right)^2 - 3.6 \end{cases}, \quad (4.94)$$



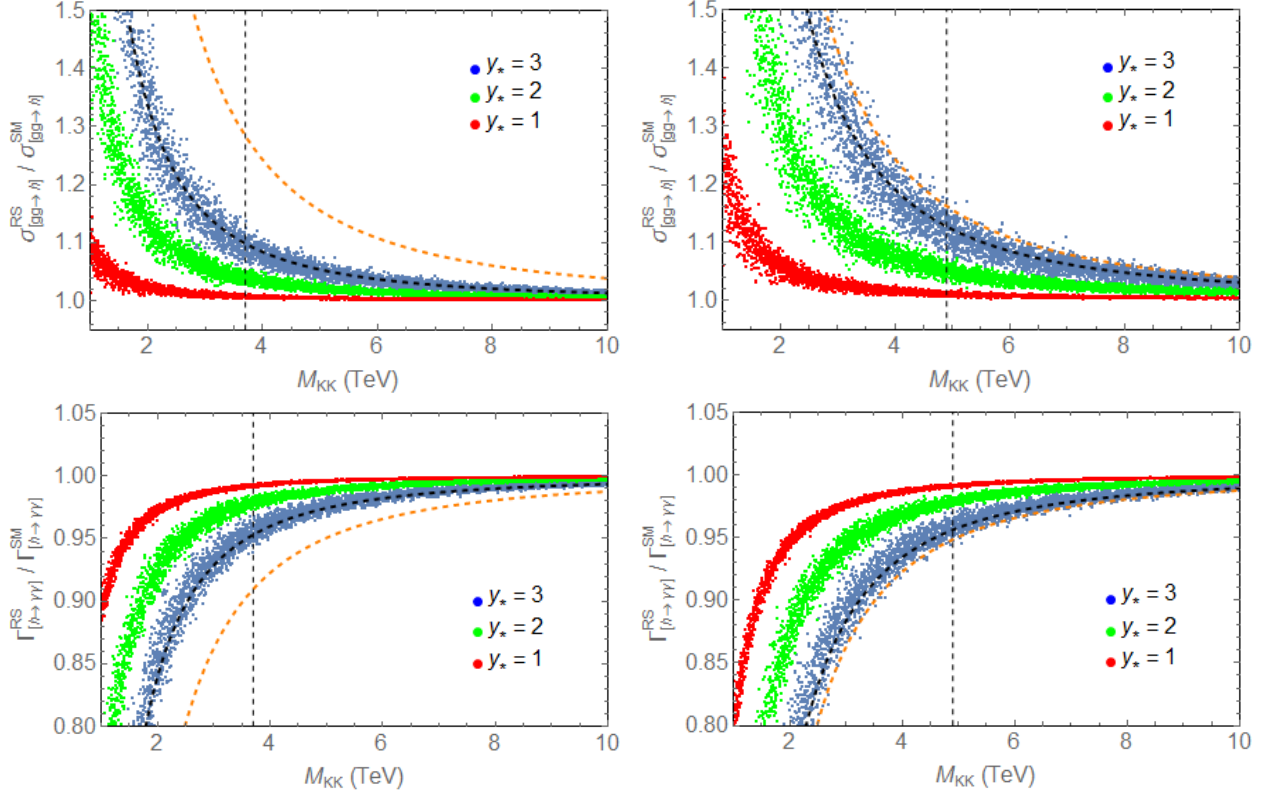


Figure 4.13: Numerical results for the cross sections of the Higgs boson production through gluon fusion (upper plots), and the Higgs decay rates into two photons (lower plots), normalized on the corresponding SM predictions. The dependencies on the KK mass scale  $M_{KK}$  and the maximally allowed entry of the Yukawa matrices  $y_*$  are illustrated. The left plots correspond to the scenario with a real bulk-Higgs field, for  $\beta=1$ , and the right plots correspond to the scenario with a narrow bulk-Higgs field, for  $\beta=10$ . The vertical, black and dashed lines express the constraints that are implied by tests of the Peskin-Takeuchi observables in the respective bulk-Higgs scenarios [82].

and

$$\frac{\Gamma_{[h \rightarrow \gamma\gamma]}^{RS}}{\Gamma_{[h \rightarrow \gamma\gamma]}^{SM}} \approx 1 - \frac{v^2}{2M_{KK}^2} \left( \frac{1}{4.9} \begin{pmatrix} 0.2 - 1.4 + 95.8 \cdot \left(\frac{y_*}{3}\right)^2 \\ 0.1 + 4.6 + 150.2 \cdot \left(\frac{y_*}{3}\right)^2 \\ 0 + 6.9 + 176 \cdot \left(\frac{y_*}{3}\right)^2 \end{pmatrix} + \begin{pmatrix} 1.9 \\ 3.1 \\ 3.6 \end{pmatrix} \right). \quad (4.95)$$

The numbers in the upper rows correspond to the real bulk-Higgs case ( $\beta = 1$ ), the numbers in the middle rows correspond to the narrow bulk-Higgs case ( $\beta = 10$ ), whereas the numbers in the lower rows give the results in the limit  $\beta \rightarrow \infty$ . Similar to the tree-level Higgs couplings to fermions, the new-physics effects in these rates, scaling with  $v^2/(2M_{KK}^2)$ , strongly depend on the parameter  $y_*$ . The averages from (4.94) and (4.95) are plotted in Figure 4.13 by the black and dashed curves. From (4.94), one can find that the fermion contributions, solely determining the gluon fusion process, contain two different and contrary new-physics effects, given by the two different terms proportional to  $(y_*/3)^2$ . At first, the top quark zero mode mixes with the tower

of KK resonances, resulting in a suppression of the top quark Yukawa coupling to the Higgs boson, which are the first, negative values. Then, the full KK tower of fermions contributes in the loop, which are the second, positive values that elevate the whole result [154]. The last values denote the corrections from the vev-shift of the Higgs  $\kappa_v$  in the RS model. The suppression of the zero-mode top quark Yukawa coupling is of smaller magnitude, compared to the elevation caused by the KK tower contributions, so that the results for the gluon fusion cross section are increased compared to the SM. For the averaged, normalized Higgs decay rates into two photons in (4.95), one can notice that all contributions, except of the vev shift, are divided through the SM prediction, which is dominated by the W boson contribution [3]. The first, very small values in (4.95) write the loop-contributions from the physical KK scalars that do not arise in the SM, and vanish for  $\beta \rightarrow \infty$ . The second values correspond to the W boson contributions, and the third values are the combined fermion contributions. In contrast to the SM, one can observe that the fermion loop-contributions dominate the Higgs decay rate into two photons in the RS model, in correspondence with findings, *e.g.* from [2, 3, 5, 151, 152, 154, 171, 193]. Again, the last values denote the corrections from the vev-shift  $\kappa_v$ . Altogether, the new-physics effects in the Higgs decay rates to two photons, which are suppressed compared to the SM, are smaller compared to the effects to the gluon fusion productions. This is because an interference effect arises between the negative W boson contribution of the SM prediction and the positive contribution from the KK fermions. The exclusion bounds implied by the Peskin-Takeuchi observable tests on the KK mass scale, derived in (2.235), are indicated by the black and dashed lines in the plots. Here, we take the bounds derived for  $U = 0$  as predicted by the RS model. Above the bounds, significantly smaller deviations from the SM expectations can be observed. Respecting the lowest, allowed KK masses for the case of  $y_\star = 3$ , the gluon fusion production rates can be enhanced by 12.7 % for  $\beta=1$  and by 15.1 % for  $\beta=10$ , compared to the SM prediction. The curves of the normalized Higgs decay rate for  $y_\star = 3$  can be reduced by 5.4 % for  $\beta=1$ , and by 6.1 % for  $\beta=10$ . The results in a scenario with a very narrow bulk-Higgs field, corresponding to the limit  $\beta \rightarrow \infty$ , for the case of  $y_\star = 3$ , are given by the lowest rows of the averages in (4.94) and (4.95), and are illustrated in the plots by the orange, dashed curves. One can see that for higher values of  $\beta$ , the yellow curves approach to the orange curves, where the curves for  $\beta = 10$  lie already very close to these curves. So, again, it is explicitly shown that the new-physics effects have a more profound impact, the higher the value of  $\beta$  is, and the less the bulk-Higgs localization is realized.

In Figure 4.14, the correlated new-physics corrections to the gluon fusion production process and the Higgs decay rate into two photons are displayed, for  $\beta = 1$  on the left-hand side and  $\beta = 10$  on the right-hand side, and for three different choices for the maximally allowed entry of the Yukawa matrices  $y_\star$ , respectively. The anti-correlation of the corrections to the two processes can be observed, and also, that the magnitudes of the new-physics effects to the gluon fusion productions are larger than for the Higgs decay rates. The black points depict the results that respect the exclusion bounds from the Peskin-Takeuchi observables in the respective bulk-Higgs scenarios, for all three cases of  $y_\star = 1, 2, 3$ . In comparison with the coloured points, these black points visualize the very slight deviations from the SM predictions in the parameter ranges that are compatible to the bounds. For that reason, one can suspect that it might not be possible to derive significantly stronger exclusion bounds on the parameter space of the bulk-Higgs RS model by comparing the predictions with experimental results, as it will be presented subsequently.

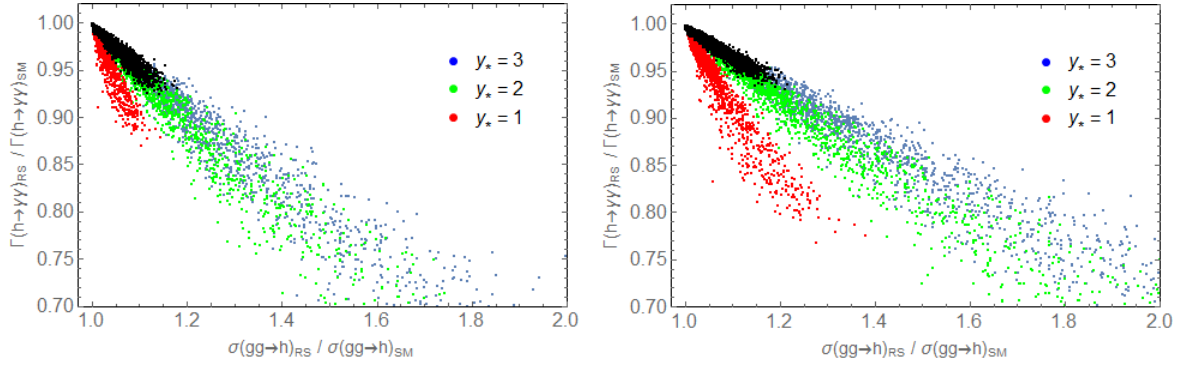


Figure 4.14: Here, the correlated new-physics effects to the Higgs production cross sections of gluon fusion, and the Higgs decay rates into two photons are plotted, for  $\beta = 1$  on the left-hand side and  $\beta = 10$  on the right-hand side. The black points depict the results that respect the bounds implied by the Peskin-Takeuchi observable tests for all three choices of  $y_*$ .

### 4.2.3 Total Higgs decay width

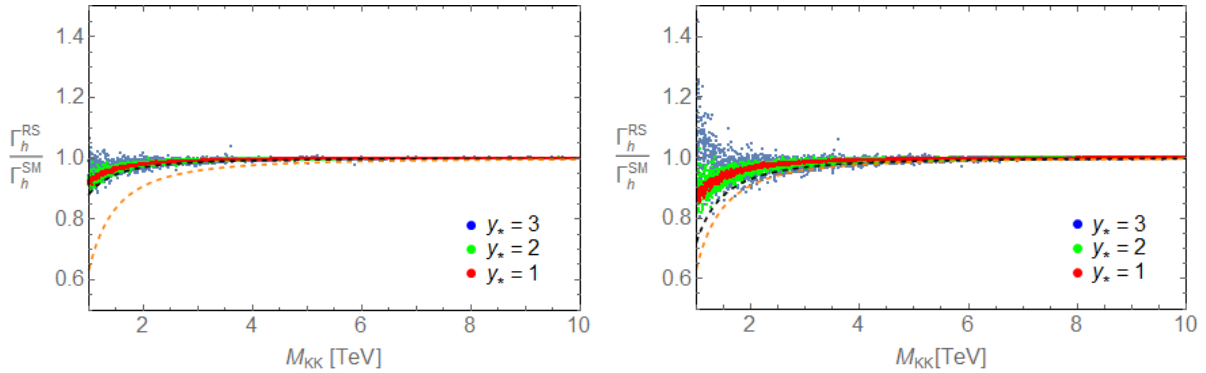


Figure 4.15: Predictions for the total Higgs decay width in the RS model, for  $\beta = 1$  on the left-hand side, and  $\beta = 10$  on the right-hand side, and for three choices for the parameter  $y_*$ , respectively.

Altogether, the new-physics corrections to the various Higgs decay rates, defined via the couplings in (4.4), affect the total Higgs decay width from (4.2). So, if assuming the branching fractions from the SM, one can account for the RS corrections to the total Higgs decay width  $\Gamma_h^{SM} = 4.21$  MeV (for  $m_h = 126$  GeV) via the formula [203]

$$\kappa_h \approx 0.56 (|C_b|^2 + |C_{b5}|^2) + 0.23 C_W^2 + 0.03 C_Z^2 + 0.09 (|C_g|^2 + |C_{g5}|^2) + 0.06 (|C_\tau|^2 + |C_{\tau5}|^2) + 0.03. \quad (4.96)$$

The results are plotted in Figure 4.15, for  $\beta = 1$  and  $\beta = 10$ , and  $y_* = 1, 2, 3$ . Higher maximally allowed entries of the Yukawa matrices  $y_*$  do not significantly alter the magnitude of the RS corrections, but rather cause a broader scattering of the results, as it can be observed from the blue points in the plots. The new-physics corrections to all the different decay rates, except

of the decay rate to two gluons, cause a suppression of the predictions compared to the SM. However, the Higgs decay rate to two gluons receives the strongest new-physics corrections in the RS model, as can be observed from the augmented predictions for the gluon fusion cross sections in Figure 4.13, which are calculated by means of the equal formula. Although having a branching fraction of only 9% of the total Higgs decay width, the new-physics corrections to this rate significantly counteract with the remaining Higgs decay rates, which are reduced compared to the SM.

The normalized total Higgs decay width will enter all the predictions for the signal strengths of the various Higgs decay processes at the LHC that will be evaluated in the upcoming section. Since the signal strengths involve a division through the normalized Higgs decay width, they are accordingly enhanced in the regions of lower KK masses. Using the previously given averages for the Higgs couplings and decay rates, one can determine the averages for the normalized total Higgs decay width as

$$\kappa_h \approx 1 - \frac{v^2}{2M_{KK}^2} \left( \begin{pmatrix} 1.03 \\ 4.51 \\ 6.72 \end{pmatrix} \times \left(\frac{y_\star}{3}\right)^2 + \begin{pmatrix} 2.86 \\ 4.72 \\ 5.38 \end{pmatrix} \right), \quad (4.97)$$

for  $\beta = 1$  (upper numbers),  $\beta = 10$  (middle numbers) and  $\beta \rightarrow \infty$  (lower numbers). These curves are indicated in the plots by the black and dashed lines for  $\beta = 1$  and 10, whereas the orange, dashed lines correspond to  $\beta \rightarrow \infty$ . One can see that the averaged curves deviate from the scattered points, which may occur due to the contributions from the CP odd couplings, which average to 0 but scatter in a broader manner. However, these differences turn out to be less significant when calculating the averages for the signal strengths of the Higgs decay rates in the next section.

### 4.3 Signal strengths for the Higgs decays at the LHC

With the help of the diced sets of parameters, one can numerically calculate the signal strengths  $R_{ii}$  for the combined rates of a Higgs production at the LHC and a subsequent decay into the final states  $ii = \gamma\gamma, ZZ^\star, WW^\star, b\bar{b}, \tau\bar{\tau}$ . In contrast to the single Higgs couplings, or the individual Higgs production and decay rates, measurements of the signal strengths are directly experimentally accessible. The predictions are normalized on the respective SM predictions to investigate the effects that solely arise from new physics. The formulas for the signal strengths include the cross sections for the Higgs boson productions, by accounting for the different branching fractions, where the gluon fusion productions are considered with a fraction of  $\approx 90\%$ , and the Higgsstrahlung and vector boson fusion productions are considered with a fraction of  $\approx 10\%$ . For simplicity, it is also assumed that the latter processes are always mediated by W bosons, which is a sufficient approximation for the numerical evaluations. In the formulas for the signal strengths, the sum of the cross sections is multiplied with the branching ratio of the respective Higgs decay rates under consideration. The corrections to the total Higgs decay width are included. Altogether, the new-physics effects to the signal strengths can become manifest in the three individual quantities, which have been separately evaluated in the previous subsections.

	$R_{\gamma\gamma}$	$R_{WW}$	$R_{ZZ}$	$R_{\tau\tau}$	$R_{bb}$
ATLAS	$1.14^{+0.27}_{-0.25}$	$1.22^{+0.23}_{-0.21}$	$1.52^{+0.40}_{-0.34}$	$1.41^{+0.40}_{-0.36}$	$0.62^{+0.37}_{-0.37}$
CMS	$1.11^{+0.25}_{-0.23}$	$0.90^{+0.23}_{-0.21}$	$1.04^{+0.32}_{-0.26}$	$0.88^{+0.30}_{-0.28}$	$0.81^{+0.45}_{-0.43}$
av.:	$1.14^{+0.19}_{-0.18}$	$1.09^{+0.18}_{-0.16}$	$1.29^{+0.26}_{-0.23}$	$1.11^{+0.24}_{-0.22}$	$0.70^{+0.29}_{-0.27}$

Table 4.2: Experimental results and their total uncertainties for the signal strengths  $R_{ii}$  of the various Higgs decay rates, from combined data collected at the LHC at Runs with center of mass energies  $\sqrt{s} = 7$  and 8 TeV [6].

The following formulas apply for the rates

$$\begin{aligned}
R_{\gamma\gamma} &= \frac{(\sigma \cdot BR)(pp \rightarrow h \rightarrow \gamma\gamma)_{RS}}{(\sigma \cdot BR)(pp \rightarrow h \rightarrow \gamma\gamma)_{SM}} = \frac{1}{\kappa_h} [ (|C_g^{\text{eff}}|^2 + |C_{g5}^{\text{eff}}|^2) \cdot 0.9 + C_W^2 \cdot 0.1 ] \cdot (|C_\gamma^{\text{eff}}|^2 + |C_{\gamma5}^{\text{eff}}|^2) , \\
R_{VV} &= \frac{(\sigma \cdot BR)(pp \rightarrow h \rightarrow VV^*)_{RS}}{(\sigma \cdot BR)(pp \rightarrow h \rightarrow VV^*)_{SM}} = \frac{1}{\kappa_h} [ (|C_g^{\text{eff}}|^2 + |C_{g5}^{\text{eff}}|^2) \cdot 0.9 + C_W^2 \cdot 0.1 ] \\
&\cdot \frac{\Gamma(h \rightarrow VV^*)_{RS}}{\Gamma(h \rightarrow VV^*)_{SM}} , \quad V = W, Z , \\
R_{\tau\tau} &= \frac{(\sigma \cdot BR)(pp \rightarrow h \rightarrow \tau\tau)_{RS}}{(\sigma \cdot BR)(pp \rightarrow h \rightarrow \tau\tau)_{SM}} = \frac{1}{\kappa_h} [ (|C_g^{\text{eff}}|^2 + |C_{g5}^{\text{eff}}|^2) \cdot 0.9 + C_W^2 \cdot 0.1 ] \cdot (|C_\tau|^2 + |C_{\tau5}|^2) , \\
R_{bb} &= \frac{(\sigma \cdot BR)(pp \rightarrow h \rightarrow bb)_{RS}}{(\sigma \cdot BR)(pp \rightarrow h \rightarrow bb)_{SM}} = \frac{1}{\kappa_h} C_W^2 \cdot (|C_b|^2 + |C_{b5}|^2) .
\end{aligned} \tag{4.98}$$

The formula for the corrections to the total Higgs decay width  $\kappa_h$  has been presented in (4.97), and the formula for the decay rates into the gauge boson final states  $WW^*$  and  $ZZ^*$  has been derived in (4.42). The Higgs production process through gluon fusion, and the Higgs decay rates into  $\gamma\gamma, \tau\bar{\tau}, b\bar{b}$ , are computed by the sum of the square of the CP-even and -odd Higgs couplings, as given in (4.4). For the signal strengths of the Higgs decay into a pair of b quarks, the Higgsstrahlung's production process is an experimentally more feasible Higgs production channel at the LHC than the gluon fusion production, which suffers from an overwhelming QCD background [213]. For that reason, only this channel is considered in the formula in (4.98) [4]. In the following, the numeric results for the individual signal strengths are presented, as predicted by the bulk-Higgs RS model. Furthermore, the results are compared to the results reported by the ATLAS and CMS collaborations from the LHC, given in [6]. The experimental results are summarized in Table 4.2, and we will compare our predictions with the naive averages that are given in the lowest row, built by the results for a specific rate from the two collaborations, respectively.

We begin with an evaluation of the signal strengths for the loop-induced Higgs decay rate into two photons. The numeric results for this rate, normalized on the SM prediction, are displayed in Figure 4.16. The left plot gives the results for  $\beta=1$  in a scenario with a real bulk-Higgs

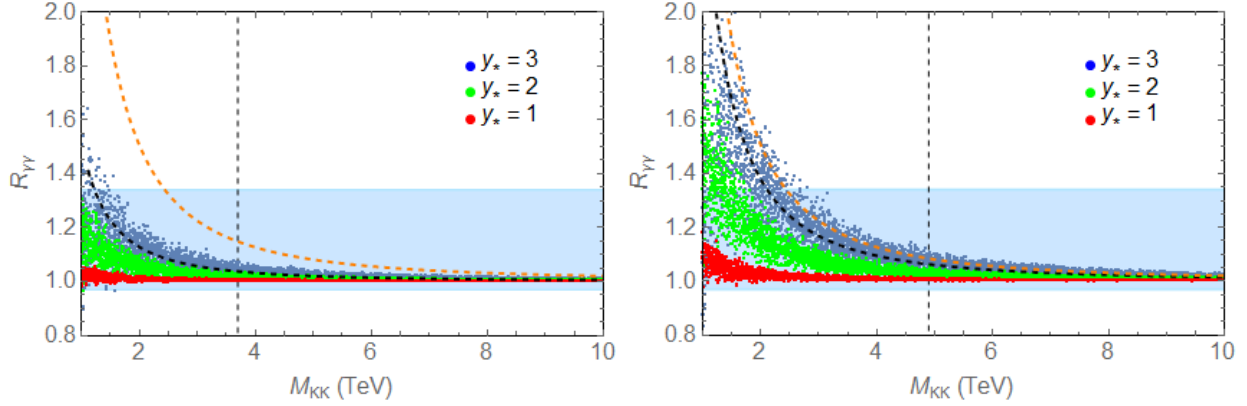


Figure 4.16: Numerical results for the signal strengths for the Higgs decay into two photons, normalized on the SM prediction, for three different maximally allowed entries of the Yukawa matrices  $y_*$ . The left plot corresponds to a scenario with a real bulk-Higgs field ( $\beta=1$ ), and the right plot corresponds to a scenario with a narrow bulk-Higgs field ( $\beta=10$ ). The light blue band shows the averaged  $1\sigma$  error region from the experimental results by ATLAS and CMS [6]. The dashed lines indicate the exclusion bounds implied by tests of the Peskin-Takeuchi observables from (2.235).

field, and the right plot gives the results for  $\beta=10$  in a scenario with a narrow bulk-Higgs field. The results are elevated compared to the SM. Using the previously given averages for the cross sections and decay rates, one can determine the signal strengths for the Higgs decay into two photons, normalized on the SM prediction, to the lowest order as

$$R_{\gamma\gamma} \approx 1 + \frac{v^2}{2M_{KK}^2} \begin{cases} 46.5 \cdot 0.9 \cdot \left(\frac{y_*}{3}\right)^2 - 3.6 \cdot 0.1 + 0.2 - 19.5 \cdot \left(\frac{y_*}{3}\right)^2 - 5.3 \\ 103.7 \cdot 0.9 \cdot \left(\frac{y_*}{3}\right)^2 - 6.0 \cdot 0.1 - 0.9 - 30.6 \cdot \left(\frac{y_*}{3}\right)^2 - 11.1 \\ 132.0 \cdot 0.9 \cdot \left(\frac{y_*}{3}\right)^2 - 6.9 \cdot 0.1 - 1.4 - 35.8 \cdot \left(\frac{y_*}{3}\right)^2 - 13.9 \end{cases} . \quad (4.99)$$

The values in the upper row correspond to  $\beta = 1$ , the values in the middle row correspond to  $\beta = 10$ , and the last row gives the result for  $\beta \rightarrow \infty$ . The averages are illustrated in the plots, for  $y_* = 3$ , by the black and dashed curves. It can be observed that the new-physics effects to the gluon fusion production cross sections, given by the first positive values in the averages, and the Higgs decay rates into two photons, given by the third and fourth values, interfere with each other [3]. The elevations from the gluon fusions dominate, and the results for the signal strengths are elevated compared to the SM, accordingly. The suppression effect of the Higgs decay rate into two photons is of moderate size, due to the interplay between the fermion contributions and the SM W boson contributions in that decay rate, as has been discussed before. The second values in (4.99) are related to the fraction of the Higgs boson production through vector boson fusion and Higgsstrahlung, and the last values denote the combined corrections from the vev-shift  $\kappa_v$  and the total Higgs decay width  $\kappa_h$ . In the plots, the orange, dashed curves illustrate the results in a scenario with a very narrow bulk-Higgs field, corresponding to  $\beta \rightarrow \infty$ , for  $y_* = 3$ , which are given by the last row in the averages in (4.99). For a certain choice of  $v^2/(2M_{KK}^2)$  and  $y_* = 3$ , one can find that the new-physics effects for  $\beta = 1$  are about 25 %, and for  $\beta = 10$  are about 75 % of

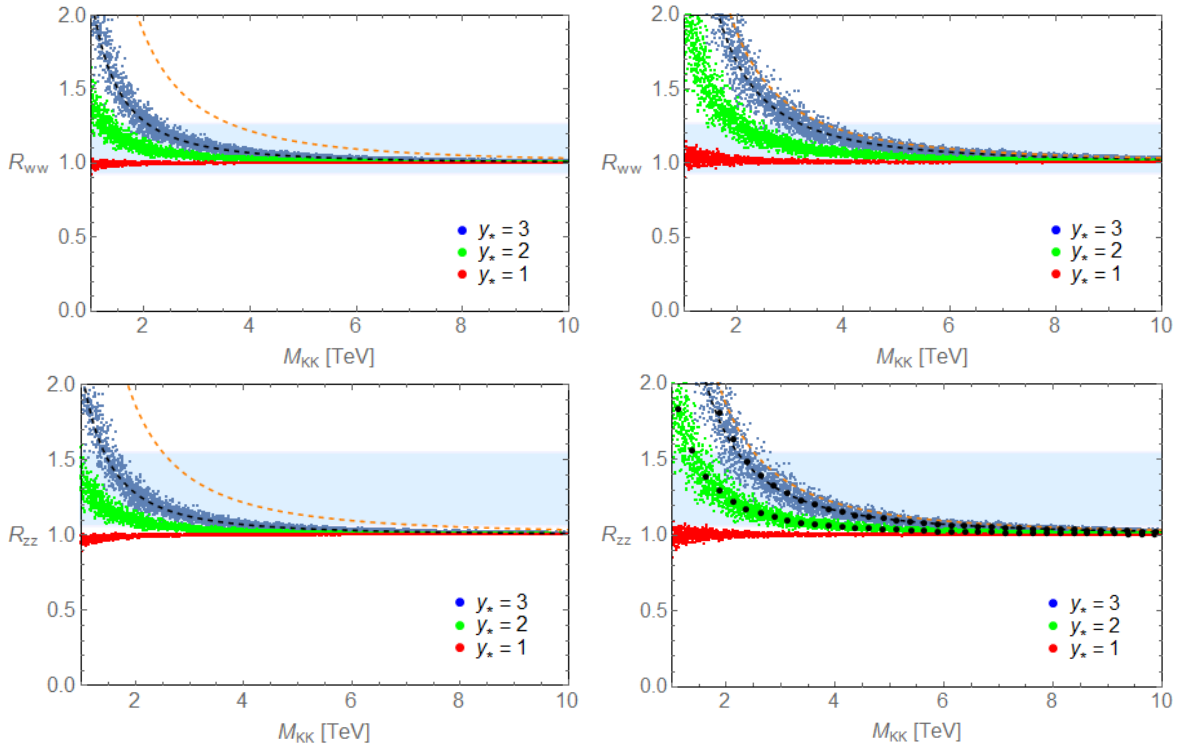


Figure 4.17: Numerical results for the signal strengths for the Higgs decays into pairs of gauge bosons ( $WW^*$ ,  $ZZ^*$ ) at the LHC. The plots on the left-hand side give the results for  $\beta = 1$ , whereas the plots on the right-hand side give the results for  $\beta = 10$ , for three choices of  $y_*$ , respectively. The light blue band gives the averages of the experimental results from ATLAS and CMS [6]. The black points in the lower right plot indicate the scatter points, binned in a range of 250 GeV, that are used for the determination of the exclusion bounds, which are summarized in Table 4.21.

the effects that are obtained in the benchmark case for  $\beta \rightarrow \infty$ . The average of the experimental results from ATLAS and CMS, given in Table 4.2, is displayed by the corresponding  $1\sigma$  error region by the light blue band in the plots in Figure 4.16. Points that lie outside of this band can be excluded to 68 % CL. The bulk-Higgs results for  $\beta = 1$  are nearly completely covered by this band, and the results for a narrow bulk Higgs for  $\beta = 10$  are situated in the  $1\sigma$  band in most of the parameter ranges. The dashed lines indicate the exclusion bounds derived from the Peskin Takeuchi parameters, given in (2.235). Above these bounds, only very slight deviations from the SM can be observed.

All in all, the enhanced Higgs production cross sections through gluon fusion determine largely the results for all the signal strengths, except of the  $R_{bb}$ -rate, and cause augmented predictions compared to the SM. These get attenuated by the suppressed contributions from the other Higgs production cross sections, given by  $\approx C_W^2$ , displayed in the Figure 4.11, and the respective Higgs decay rates, which are illustrated in Figures 4.11 and 4.12. The signal rates for the Higgs decays into  $WW^*$  and  $ZZ^*$  states  $R_{WW}$  and  $R_{ZZ}$  are plotted in Figure 4.17, for  $\beta = 1$  on the left-hand side and  $\beta = 10$  on the right-hand side, and the three different maximally allowed entries of the Yukawa matrices. Very similar trends can be observed for the curves of the

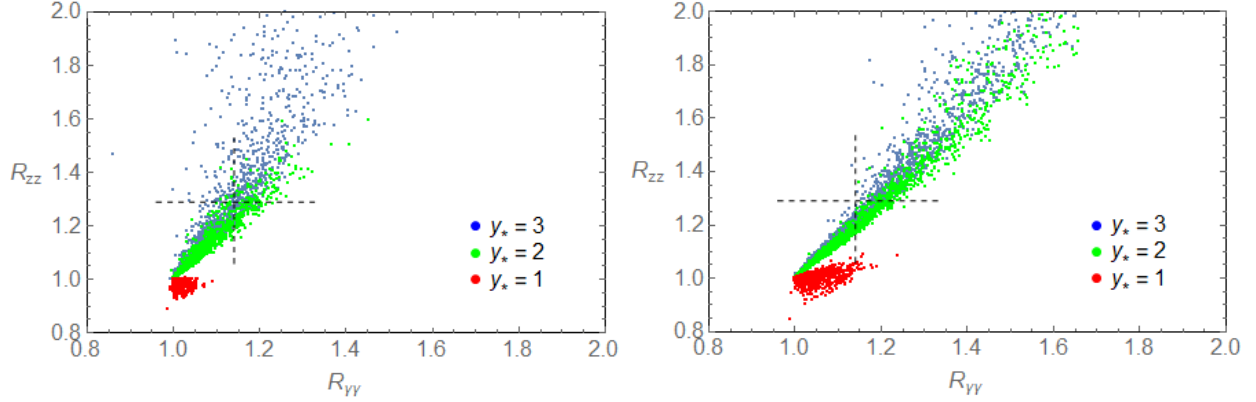


Figure 4.18: Plots of the correlations between the signal strengths  $R_{\gamma\gamma}$  and  $R_{ZZ}$ , for  $\beta = 1$  on the left-hand side and  $\beta = 10$  on the right-hand side, and for three choices of  $y_*$ , respectively. The gray, dashed crosses indicate the results and uncertainties from the averages of the ATLAS and CMS results [6].

two processes. By using the previously given averages, one can average the signal rates  $R_{WW}$  and  $R_{ZZ}$ , normalized on the SM predictions, by

$$\begin{aligned}
 R_{WW} &\approx 1 + \frac{v^2}{2M_{KK}^2} \left( \begin{pmatrix} 42.88 \\ 97.93 \\ 125.52 \end{pmatrix} \times \left(\frac{y_*}{3}\right)^2 - \begin{pmatrix} 5.12 \\ 8.39 \\ 9.63 \end{pmatrix} \right), \\
 R_{ZZ} &\approx 1 + \frac{v^2}{2M_{KK}^2} \left( \begin{pmatrix} 42.88 \\ 97.93 \\ 125.52 \end{pmatrix} \times \left(\frac{y_*}{3}\right)^2 - \begin{pmatrix} 6.15 \\ 10.12 \\ 11.61 \end{pmatrix} \right).
 \end{aligned} \tag{4.100}$$

These averages are given in the plots by the black and dashed curves for  $\beta = 1$  and  $\beta = 10$ , and the orange, dashed curves for the limit  $\beta \rightarrow \infty$ , respectively. One can observe that there are stronger new-physics corrections to  $R_{WW}$  and  $R_{ZZ}$  in comparison to the results for  $R_{\gamma\gamma}$ , given in Figure 4.16. In all the cases, the largest contributions stem from the loop-contributions of KK fermions that determine the gluon fusion production rate, entering  $R_{WW}$ ,  $R_{ZZ}$  and  $R_{\gamma\gamma}$ . Then, in the rate  $R_{\gamma\gamma}$ , the extenuated fermion loop-contributions to the Higgs decay rates lead to a stronger compensation effect, compared to the effects by the tree-level decay rates  $h \rightarrow WW^*$ ,  $h \rightarrow ZZ^*$  in  $R_{WW}$  and  $R_{ZZ}$ . In Figure 4.18, the results for  $R_{\gamma\gamma}$  and  $R_{ZZ}$  are plotted in a combination for  $\beta = 1$  on the left-hand side and  $\beta = 10$  on the right-hand side. All the results are correlatively enhanced compared to the SM predictions, which correspond to just the ratios 1. As before, one can observe that the new-physics corrections to  $R_{ZZ}$  are larger, compared to the corrections to  $R_{\gamma\gamma}$ . The gray, dashed crosses indicate the averages and  $1\sigma$  uncertainties from the experimental results of ATLAS and CMS [6]. One can see that for larger values of  $y_*$ , the scattered points are passing the regions that are marked by the crosses to a large amount.

Similar to the evaluations before, the results for the signal strengths for the Higgs decays into tau leptons are plotted in Figure 4.19, for  $\beta = 1$  and  $\beta = 10$ , and three different maximally



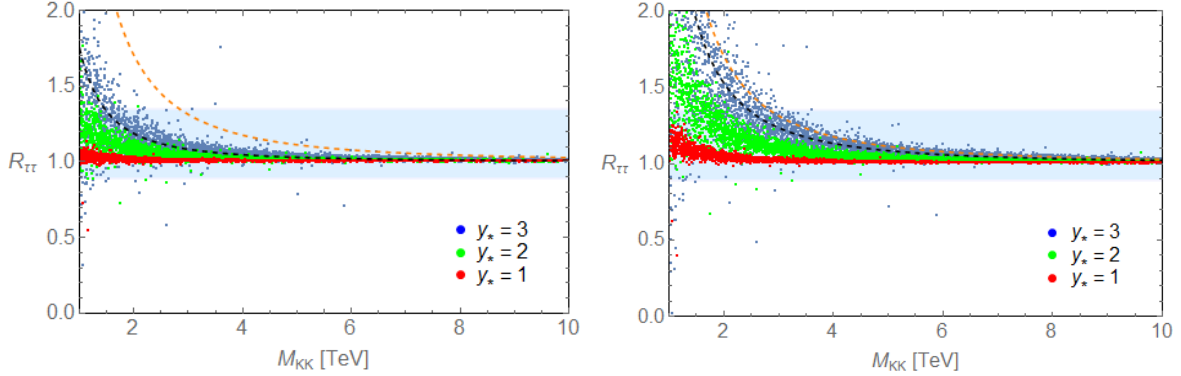


Figure 4.19: Plots of the signal strengths for the Higgs decay into a pair of tau leptons. The plot on the left-hand side corresponds to a value  $\beta = 1$ , and the plot on the right-hand side to a value  $\beta = 10$ . The light blue bands mark the average of the experimental results from ATLAS and CMS [6].

allowed entries of the Yukawa matrices. Whereas the curves resemble the curves for  $R_{\gamma\gamma}$ , plotted in Figure 4.16, the magnitudes of the new-physics corrections are, in fact, a bit larger, compared to the effects to  $R_{\gamma\gamma}$ . Again, a partial compensation arises in the rates  $R_{\tau\tau}$  between the enhanced gluon fusion cross sections and the suppressed decay rates into tau leptons. But, the decay rates into tau leptons, plotted in Figure 4.12, are mediated at the tree level compared to the loop-induced decay rates into two photons that receive contributions from the full KK fermion tower. For that reason, there is a weaker compensation effect in  $R_{\tau\tau}$  compared to  $R_{\gamma\gamma}$ , and the new-physics corrections are a bit larger. The averaged signal strengths read

$$R_{\tau\tau} \approx 1 + \frac{v^2}{2M_{KK}^2} \left( \begin{array}{c} 26.0 \\ 71.81 \\ 95.52 \end{array} \times \left(\frac{y_\star}{3}\right)^2 - \begin{array}{c} 1.28 \\ 2.13 \\ 2.47 \end{array} \right), \quad (4.101)$$

given by the black ( $\beta = 1, 10$ ) and orange, dashed curves ( $\beta \rightarrow \infty$ ) in the plots in Figure 4.19.

Solely the predictions for the signal strengths for the Higgs decay into a pair of b quarks are suppressed compared to the SM, as it can be observed from Figure 4.20. The only production channel included here is the Higgsstrahlung's production, given by  $\approx C_W^2$ , which is suppressed compared to the SM, as plotted in Figure 4.11. It is multiplied with the suppressed Higgs decay rate into b quarks, evaluated in Figure 4.12. Using the previously given averages, one can approximate the signal strengths for the Higgs decays into a pair of b quarks by

$$R_{bb} \approx 1 - \frac{v^2}{2M_{KK}^2} \left( \begin{array}{c} 6.47 \\ 17.43 \\ 23.28 \end{array} \times \left(\frac{y_\star}{3}\right)^2 + \begin{array}{c} 4.56 \\ 7.62 \\ 8.68 \end{array} \right), \quad (4.102)$$

which are plotted in Figure 4.20 by the black ( $\beta = 1, 10$ ) and orange, dashed lines ( $\beta \rightarrow \infty$ ).

The  $1\sigma$  uncertainty regions of the averages of the experimental results from ATLAS and CMS, collected in Table 4.2, are marked in all the plots by the light blue areas, respectively.

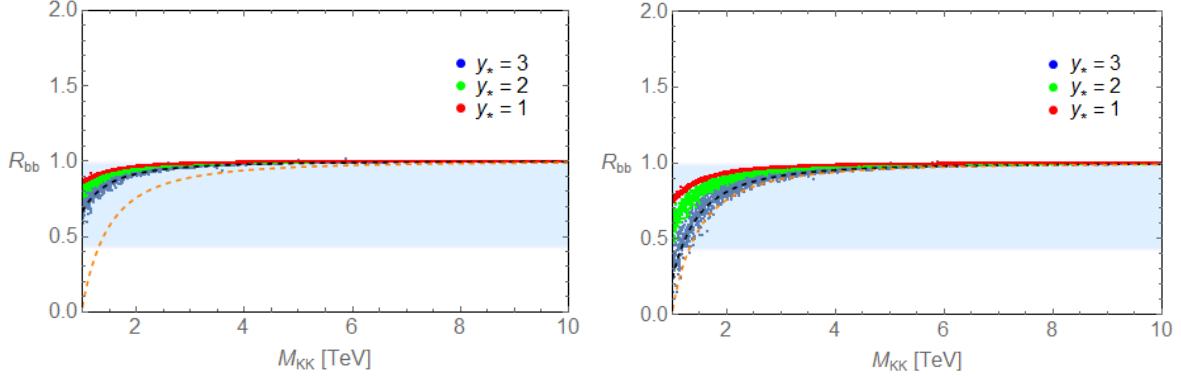


Figure 4.20: Plots of the signal strengths for the Higgs decay into a pair of b quarks. The plot on the left-hand side corresponds to a value  $\beta = 1$  and the plot on the right-hand side to a value  $\beta = 10$ . The light blue bands mark the average of the experimental results from ATLAS and CMS [6].

Interestingly, the tendencies of these results to enhanced or suppressed values compared to the SM predictions are in agreement with the predictions in the bulk-Higgs RS model. There are enhanced results for the rates  $R_{\gamma\gamma}$ ,  $R_{WW}$ ,  $R_{ZZ}$  and  $R_{\tau\tau}$ , whereas the results for  $R_{bb}$  are suppressed. For the rates  $R_{\gamma\gamma}$  and  $R_{ZZ}$ , both the results from ATLAS and CMS are enhanced compared to the SM, whereas for  $R_{WW}$  and  $R_{\tau\tau}$ , the results from CMS are suppressed, actually. For the rate  $R_{bb}$ , the results from the two collaborations are both suppressed compared to the SM. So, the predictions in the bulk-Higgs RS model are in a good agreement with the experimental results. But, the experimental results are also compatible to the SM predictions within the uncertainties. As a consequence, since the RS model with a bulk-Higgs localization gives predictions much closer to the SM, compared to the brane-Higgs scenarios of the RS model, the predictions are also better compatible to the experimental results that prove more or less the SM predictions.

For that reason, we had low expectations for deriving any significant, new exclusion bounds on the parameter space of the bulk-Higgs RS model, by comparing the experimental results with the numerical predictions for the signal strengths of the Higgs processes. Nevertheless, in order to perform such comparisons, the scattered points for each of the signal strengths have been binned within a range of 250 GeV, as is indicated by the black points in the lower right plot of Figure 4.17, as an example. Then, one could determine the parameter value for  $M_{KK}$ , at which the binned results for the rates  $R_{ii}$ , divided through the respective experimental result  $R_{ii,\text{exp}}$ , deviate by more than  $1\sigma$  or  $2\sigma$  from the ratio 1, according to the formula

$$z = \frac{R_{ii,\text{bin}}}{R_{ii,\text{exp}}} \Rightarrow |1 - z| > \begin{cases} 1\sigma(z) & \Rightarrow 68\% \\ 2\sigma(z) & \Rightarrow 95\% \end{cases} \quad \text{excluded ,} \quad (4.103)$$

$$\sigma(z) = \sqrt{\left(\frac{\Delta R_{ii,\text{th}}}{R_{ii,\text{exp}}}\right)^2 + \left(\frac{\Delta R_{ii,\text{exp}} \cdot R_{ii,\text{th}}}{R_{ii,\text{exp}}^2}\right)^2} .$$

This evaluation has been performed for all the scattered curves, for  $y_* = 3$  and  $y_* = 2$ , and both values of  $\beta = 1$  and 10, respectively. In the experiments, the scattering events for the signal

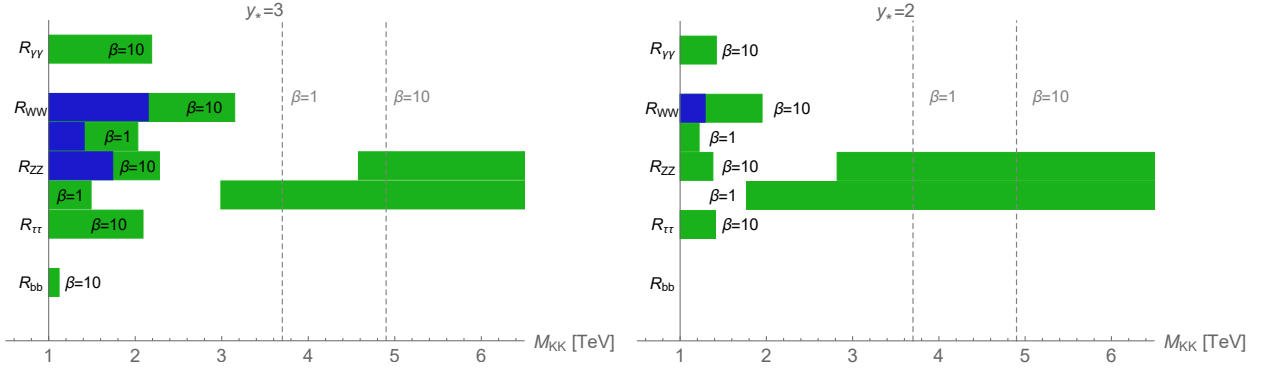


Figure 4.21: Parameter regions for the KK mass scale that can be excluded to 68% or 95% CL, given by the green and blue areas, which were derived by means of comparisons between the predicted signal strengths in the bulk-Higgs RS model and the experimental results from ATLAS and CMS. The left plot gives the results for  $y_* = 3$ , and the right plot gives the results for  $y_* = 2$ . The parameter values for  $\beta$  are indicated. The gray, dashed lines indicate the upper bounds of the regions that are excluded by the Peskin-Takeuchi parameters to 95% CL. In this sense, evaluations of the signal strengths for the Higgs decay rates cannot provide any stronger constraints on the parameter space.

strength of a considered process follow a statistical procedure. In a Gaussian normal distribution, 68% or 95% of all the values of the distribution can be found in the intervals of  $\pm 1\sigma$  or  $\pm 2\sigma$  around the mean value, respectively. Accordingly, one can consider  $R_{ii,\text{bin}}/R_{ii,\text{exp}} = 1$  as the mean value, and the mentioned percentile fractions of a measurement, divided by the experimental results as a prediction  $R_{ii,\text{exp}}$ , can be found in the  $\sigma$ -intervals around the mean value. Here,  $\sigma$  is calculated according to the evolution of errors with the formula in (4.103), where the standard deviations of the points in the bins are considered as the theoretical errors. In this sense, a range of points in the  $M_{KK} - R_{ii}$ -planes, for which the ratio  $R_{ii}/R_{ii,\text{exp}}$  deviates by more than  $1\sigma$  or  $2\sigma$  from 1, is not included in 68% or 95% of all the experimental data, and can be excluded by the respective CLs.

The results from this evaluation are summarized in the graphics of Figure 4.21. The comparisons were performed for  $y_* = 3$  (left plot) and  $y_* = 2$  (right plot), and for  $\beta = 1$  and  $\beta = 10$ , as specified. The green areas indicate the regions that are excluded to 68% CL according to the described evaluation, and the blue areas indicate the regions that are excluded to 95% CL. The results resemble those of the before mentioned discussions for the various signal strengths for the Higgs processes in the RS model. The strongest exclusion bounds stem from the rates  $R_{WW}$  and  $R_{ZZ}$ , since the strongest new-physics effects arise there. Only for  $R_{WW}$  and  $R_{ZZ}$ , exclusion bounds could be determined to 95% CL. The results for  $R_{ZZ}$ , to 68% CL, apparently exclude a large range of higher KK masses. This is a consequence of the fact that the  $1\sigma$  region of the average of the experimental results for  $R_{ZZ}$  ends above the ratio 1. This might, however, be related to an insufficient experimental precision, connected with the present results, and the statement is given to 68% CL, only. All the other results exclude certain parameter regions of lower KK masses. The signal strengths for the Higgs decay into two photons and tau leptons give smaller excluded regions, and the predictions for the signal strengths of the Higgs decay into

$C_W$	$C_Z$	$C_g$	$C_\gamma$
(-0.004,0)	(-0.006,0)	(-0.014,0.014)	(-0.032, 0.035)
$C_t$	$C_b$	$C_\tau$	
(-0.044,0.035)	(-0.003,0.011)	(-0.013,0.017)	

Table 4.3: Experimental capabilities for the precision measurements at a future ILC [214–217], for  $\sqrt{s} = 1$  TeV and  $1000 \text{ fb}^{-1}$ , demonstrated by the  $1\sigma$  confidence intervals that have been derived in [218].

b quarks have been found to lie in the experimental  $1\sigma$  regions in most of the parameter ranges. The gray, dashed lines indicate the bounds that are implied by the Peskin-Takeuchi parameters in the respective bulk-Higgs RS scenarios, to 95% CL. As suspected before, the results we have been able to derive with our evaluations give only very weak exclusion bounds on the parameter space of the model, which are much below the exclusion bounds from the Peskin-Takeuchi parameters.

This is in contrast to the evaluations performed in other Higgs scenarios of the RS model, *e.g.* in [2–4]. For the brane-Higgs scenario, the predictions for the cross sections of the gluon fusion production rate are suppressed compared to the SM, and as an effect, the signal strengths  $R_{\gamma\gamma}$ ,  $R_{WW}$ ,  $R_{ZZ}$  and  $R_{\tau\tau}$  are suppressed compared to the SM, as well. In principle, brane-Higgs scenarios with a minimal particle content are less significant for phenomenological searches, since they suffer from the strong exclusion bounds, implied by the Peskin-Takeuchi parameters. But, in realizations of the RS model with a custodial bulk gauge symmetry and a brane-Higgs, as presented in Section 2.3 of the thesis, the enlarged KK fermion content causes negative and much stronger new-physics contributions to the Higgs processes. In these scenarios, the evaluations of the signal strengths for Higgs processes were performed *e.g.* in [2–4], and resulted in very strong exclusion bounds on the parameter space of the custodial RS model, exceeding the bounds from the Peskin-Takeuchi parameters to a large amount. To 95% CL, the most stringent, derived constraints are  $M_{KK} > 8.12$  TeV for a brane Higgs, and  $M_{KK} > 6.08$  TeV for a narrow bulk Higgs ( $\beta \rightarrow \infty$ ), both for  $y_\star = 3$  [4]. In this regard, the masses of the lightest KK particles must lie above  $M_{g(1)} > 19.89$  TeV and  $M_{g(1)} > 14.90$  TeV, accordingly. Nevertheless, the bounds can be weaker for lower values of  $y_\star$ . But, in total, also the custodial RS model is very strongly constrained at the present level by means of the various Higgs processes. On the contrary, the evaluations presented in this chapter of the thesis can demonstrate that the predictions for the Higgs processes in the bulk-Higgs RS model are, in principle, well compatible to the SM. Furthermore, they are in a good agreement with the experimental results of the LHC. From these outcomes, one can conclude that the existence of a small and warped extra dimension in connection with a bulk-Higgs field might still be conceivable.

### 4.3.1 Outlook on the precision measurements of Higgs couplings

In the previous section, the signal strengths for the various Higgs decay processes at the LHC have been evaluated, and have been compared to the experimental results from ATLAS and CMS. It was not possible to derive any new, significant constraints on the parameter space of the bulk-Higgs RS model by means of these comparisons. So, it proves to be quite difficult to

test the predictions of the bulk-Higgs RS model using the current precision measurements in the Higgs sector. Future, more advanced experiments with stronger sensitivities are demanded in order to perform enough precise measurements. In this context, the ILC is one proposed, future collider project [214–223], where the sensitivity on measuring the Higgs rates can be enormously improved compared to the LHC.<sup>6</sup> The possible, experimental capabilities of an upgraded version of the ILC, on testing the Higgs couplings in a model-independent way, were derived in [218], expressed by  $1\sigma$  confidence intervals for the uncertainties. The results are summarized in Table 4.3, and can be compared to the Higgs couplings predicted by the bulk-Higgs RS model [4]. In this way, the ability of the upgraded ILC on deriving constraints on the parameter space of the model can be tested [4]. Such a comparison was performed in [4] for the predictions in a brane-localized Higgs scenario with a custodial bulk gauge symmetry. In this relation, one can assume SM like Higgs couplings for the experimental results  $C_i^{\text{exp}} = 1$ , while taking the  $1\sigma$  uncertainties from Table 4.3 [218]. Then, a similar evaluation can be performed, as done before for the Higgs signal strengths. The deviations for  $z = C_i/C_i^{\text{exp}}$ , according to (4.103), can be computed to determine the excluded parameter regions to certain CLs. The results are displayed in the graphics in 4.22, for  $y_\star = 3$  on the left and  $y_\star = 2$  on the right, and for  $\beta = 1$  and  $\beta = 10$ , as indicated. Again, the green areas mark the regions that can be excluded to 68% CL, whereas the blue areas mark the regions that can be excluded to 95% CL. The exclusion bounds derived

---

<sup>6</sup>The ILC will be a linear collider experiment with a length of  $\approx 34$  km, reaching a center of mass energy of  $\sqrt{s} = 500$  GeV, or 1 TeV in a possible upgrading level, and will operate with colliding electron and positron beams. A possible location for this project could be in Japan, according to the ILC Design Report from 2013 [222, 223]. In this experiment, the center of mass energy will enormously be increased compared to preceding lepton collider experiments. In principle, at lepton colliders it is possible to test particle interactions at much higher precisions compared to hadron colliders like the LHC. The full center of mass energy is available in the interactions to produce new particles, and the energies and momenta of the initial particles in the collisions are well known. This allows to apply a reconstruction method for the detection of “hidden” particles that do not leave any traces in the detectors, as neutrinos, or possible dark matter and light supersymmetric particles. In this way, it might be conceivable that new particles will be detected at the ILC in lower energy ranges, whose signals might have been too inconspicuous for a detection at the LHC. Whereas in the LHC collisions, much higher center of mass energies are reached, in principle, the colliding protons consist of a substructure of quarks, carrying an unknown fraction of the total center of mass energy. The interactions are carried out by some of the sub-particles, and it is possible to search after new particles in a large energy region. The disadvantage is that large rates of highly-energetic jets of particles are produced in the interactions of quarks and gluons that cause a strong background pollution in the measurements. At lepton colliders, the background pollution is significantly reduced, compared to hadron colliders. Therefore, they are suitable to test for rare particle processes, and processes with less precise signatures. Altogether, the lepton colliders are especially helpful to test processes that are mediated by the electroweak interaction, whereas hadron colliders allow to better explore the theories of the strong interaction. So, it will be of special interest to extend the precision measurements of the electroweak interactions in the new ILC experiments. The top quark physics will be better explored, because the center of mass energy will be sufficient to produce a pair of top quarks at a lepton collider, for the first time. In this relation, the asymmetric coupling of the top quarks to Z bosons can be investigated, for example. Furthermore, the properties of the Higgs boson, *e.g.* its mass, spin and its interaction strengths with the SM particles, will be studied thoroughly. In this way, it will be possible to test a large range of new-physics theories by indirect means. We have just presented an evaluation in the context of the bulk-Higgs RS model of the various Higgs couplings to particles. These could be compared with precise experimental measurements, in order to constrain the parameters space of the model, or to “detect” even some possible hints for the existence of an extra dimension. In total, the ILC will offer a complementary experimental facility to the LHC, to significantly advance the researches in the field of particle physics.

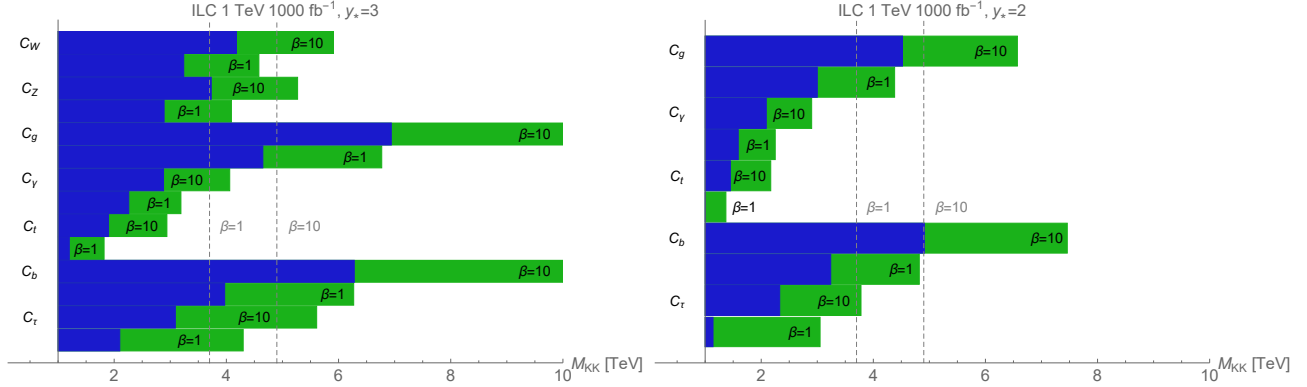


Figure 4.22: Plot of the excluded parameter regions, derived by means of a comparison between the Higgs couplings predicted by the bulk-Higgs RS model and the experimental capabilities of a possible, future ILC. It is assumed that the results reproduce the SM predictions, by  $C_i^{\text{exp}} = 1$ , together with the  $1\sigma$  uncertainties derived in [218], given in Table 4.3. The green fields mark the excluded regions to 68% CL, and the blue fields mark the excluded regions to 95% CL. The gray, dashed lines indicate the exclusion bounds derived from tests of the Peskin-Takeuchi observables to 95% CL.

from the couplings  $C_g$  and  $C_b$  to 95% CL, for  $y_\star = 3$ ,

$$\begin{aligned}
 C_g : \quad & M_{KK} > 4.7 \text{ TeV} \quad (\beta = 1), \quad M_{KK} > 7.0 \text{ TeV} \quad (\beta = 10), \\
 C_b : \quad & M_{KK} > 4.0 \text{ TeV} \quad (\beta = 1), \quad M_{KK} > 6.3 \text{ TeV} \quad (\beta = 10),
 \end{aligned}
 \tag{4.104}$$

are stronger than the dashed lines, which indicate the bounds from the Peskin-Takeuchi observable tests, to 95 % CL. These results could possibly exclude masses for the lightest KK particle, the KK gluon, up to  $M_{g(1)} < 11.5$  TeV for  $\beta = 1$ , and up to  $M_{g(1)} < 17.2$  TeV for  $\beta = 10$ , respectively. Weaker constraints would apply for lower maximally allowed entries of the Yukawa matrices  $y_\star$ , as it can be observed from the plot on the right-hand side of 4.22. All the other exclusion bounds lie still below the bounds from the Peskin-Takeuchi parameters, actually.

### 4.3.2 Intermediate summary

In this chapter, the various direct Higgs couplings to the SM particles, and the loop-induced Higgs couplings to gluons and photons, have been computed in the RS model with a minimal bulk gauge group similar to the SM and a bulk-Higgs field. It has been possible to express the summations, arising in the loop-induced Higgs couplings to gluons and photons, in dependence of five-dimensional propagator functions in mixed momentum-position representations, as discussed in [188, 189, 196–199]. Furthermore, the tree-level Higgs decay rates to two W or Z boson or fermion final states have been computed. Analytical results have been derived for all the different processes, valid to the first order in  $v^2/M_{KK}^2$ , which visualise the first, significant corrections in the bulk-Higgs RS model compared to the SM. For the bulk-Higgs localization parameter, it has been able to smoothly perform the limit  $\beta \rightarrow \infty$ , offering the results calculated before in a scenario with a very narrow bulk-Higgs field, *e.g.* in [2–5, 171, 172, 212]. A numerical and

graphical evaluation has been performed for the various Higgs couplings, and Higgs production and decay rates, in dependence of the KK mass scale  $M_{KK}$ , the Yukawa matrices  $\mathbf{Y}_f$  and the characteristic parameter of the bulk-Higgs scenario  $\beta$ . For the parameter  $\beta$ , a value 1 has been taken for a real bulk-Higgs field, and a value 10 has been taken for a narrow bulk-Higgs field.

Enhancements have been observed for the predictions of the gluon fusion cross section, normalized on the SM prediction. On the contrary, all the normalized Higgs decay rates into the final states  $ii = WW^*, ZZ^*, \gamma\gamma, b\bar{b}, \tau\bar{\tau}$  are suppressed compared to the SM. From the production and decay rates, we have been able to determine the new-physics corrections to the signal strengths for a Higgs production and decay into the different final states  $ii$  at the LHC, according to  $pp \rightarrow h \rightarrow ii$ , where  $ii = \gamma\gamma, b\bar{b}, \tau\bar{\tau}, WW^*, ZZ^*$ . In the loop-induced rates, the largest contributions are given by the contributions of KK fermions, in agreement with findings derived in [2, 3, 5, 151, 152, 154, 171, 193]. Via the gluon fusion cross section, these contributions dominate the various signal strengths for the Higgs decay rates at the LHC, giving enhanced predictions compared to the SM. Consistently, the predictions lie the closer to the SM predictions, the lower the value of  $\beta$  is and the stronger the Higgs field is located in the extra dimension. Already for  $\beta = 10$ , the results approach strongly to the results of the very narrow bulk-Higgs scenario, corresponding to  $\beta \rightarrow \infty$ . Altogether, the new-physics effects have a stronger impact on the signal strengths of the direct Higgs decays, compared to the signal strength of the Higgs decay into photons that is mediated by loops of virtual particles. In the latter process, an interference effect arises between the KK tower contributions by the fermions in the gluon fusion cross section and the KK tower contributions by fermions and W bosons in the Higgs decay rate into two photons, causing a partial decompensation of the new-physics effects, as a consequence. Remarkably, the averages of experimental results from ATLAS and CMS for all the signal strengths, given in [6], are in quite good coherence with the predictions in the bulk-Higgs RS model. The predictions have been compared with the experimental results in order to determine exclusion bounds on the parameter space of the model. However, all the determined bounds are weaker than the exclusion bounds that follow from the Peskin-Takeuchi parameters. Also, with a future and possible upgraded ILC experiment, it might be very challenging to determine any significant exclusion bounds on the parameter space of the bulk-Higgs RS model, even if all measurements of the Higgs couplings would prove the SM predictions.

So, we have consistently proven that in the bulk-Higgs RS model, besides the reduced exclusion bounds from the Peskin-Takeuchi parameters, also the Higgs production and decay processes lie significantly closer to the SM predictions. For these reasons, the bulk-Higgs RS model can be considered to be an interesting alternative to the RS scenario with a custodial protection mechanism. Whereas the custodial model provides the lowest predictions and therefore the best agreements for the Peskin-Takeuchi parameters, it significantly suffers from the enlarged KK particle content of fermions and gauge bosons, which can induce strong new-physics contributions in Higgs processes [2–4]. In the bulk-Higgs RS model, it is not necessary to implement an enlarged bulk gauge group and particle content to provide good agreements for the Peskin-Takeuchi parameters and the Higgs processes. It will be interesting to test whether the good agreements of the bulk-Higgs RS model persist in phenomenological evaluations of other particle processes. Currently, the model appears to be a promising theoretical framework to address gauge and flavour hierarchy problems of the SM.





# Chapter 5

## A New, Heavy Bulk Scalar in the RS Model

### 5.1 Di-photon resonance from a warped extra dimension

#### 5.1.1 Some introductory remarks

Run 2 of the LHC experiments has operated with the highest center of mass energies that were ever reached in collider experiments. There were big expectations that new particle states, *e.g.* predicted by theories with extra dimensions, or SUSY, could be discovered, providing hints at the existence of new physics beyond the SM. Whereas the Higgs boson was successfully detected at the LHC [67, 68], discoveries of any new particles have been lacking, however. Then, an observation of an anomaly in the di-photon mass spectrum of first 13 TeV data from Run 2 of the LHC was finally reported in December 2015. Interestingly, the anomaly, peaked as an excess of recorded data at an invariant mass of 750 GeV, was independently observed by both the ATLAS and CMS collaborations [8, 9, 224, 225]. At last, such an anomaly could be the observation of a new particle state that was produced in pp collisions and subsequently decayed into a state of two photons. Other decay channels of the presumably new particle were absent. The decay width of the observed resonance could have a narrow or a broad shape, with a value fitted to the data between 0 and 100 GeV. The best fit result for ATLAS was obtained for a broad width of  $\Gamma_{\text{tot}} \sim 45 \text{ GeV} \sim 0.06 \cdot m_S$  [9], whereas CMS favoured a narrow width of  $\Gamma_{\text{tot}} = 1.4 \cdot 10^{-4} \cdot m_S$  [226]. An independent analysis in reference [227] concluded that the large-width scenario was disfavoured by a combination of the ATLAS and CMS analyses, considering the  $\sqrt{s}=13 \text{ TeV}$  data, and was slightly preferred if including the data recorded at  $\sqrt{s}=8 \text{ TeV}$ . For example, the total decay rates were summarized in [228] for a width narrower or a width broader than the experimental resolution of 6 – 10 GeV, by using the results reported from ATLAS and CMS in [224, 225].

In collider experiments, the scatterings of beam particles, comprised in bunches, are performed repeatedly, while recording the data obtained in the detectors around the collision point. This process is performed over a long period of time, at which the detected signals are summed up. In this context, the luminosity is a quantity that describes the number of particle scatter-

ings in an experiment.<sup>1</sup> The first results from ATLAS and CMS were reported for integrated luminosities of  $3.2 \text{ fb}^{-1}$  [9], and  $2.6 \text{ fb}^{-1}$  [8], respectively. The detections of particle signals in scattering experiments follow statistical rules. For smaller data sets, fluctuations from the expected amount of background signals may arise at any point in the invariant mass range. So, for a resonance detected above the background signals a certain statistical significance has to be determined to quantify whether it is the result of a particles decay, rather than just a fluctuation of the background. A possibility to get an expression for the statistical significance is to calculate the p-value, which is the probability that the background-only-hypothesis is true and the observed excess was created by just a fluctuation. The lower this probability is, the more convenient is it to reject the background-only-hypothesis and to claim for the alternative hypothesis, which confirms the detection of a new resonance. The p-value can also be formulated as a number of standard-deviations of a statistical distribution, giving a value for the extremeness of a would-be fluctuation. In this connection, a local statistical significance of  $5\sigma$  is usually set as the threshold for a discovery in high-energy physics. For such a fluctuation, the p-value lies around  $2.7 \cdot 10^{-7}$ , which is 270 in a billion. For a resonance with such a small p-value, one can make the conditional statement that the background-only-hypothesis seems to be very unlikely, at least. The according conclusion is that the resonance was very probably created by the decay of a new particle, which had induced the signals above the background at the particular region in the mass plot. The Higgs boson could be discovered in the year 2012 with a statistical significance above  $5\sigma$  [67, 68], for example.

Several variables of the measurements have to be accounted for in the determination of the statistical significance, such as specific detector uncertainties, or the fact that data from several experiments is combined in the evaluations. These factors create a certain model-dependence for the calculation, which can hardly be avoided. The results for the di-photon anomaly were reported for local statistical significances of  $3.9\sigma$  for ATLAS favouring a broad width for the resonance, and  $3.4\sigma$  for CMS favouring a narrow width in this case [9, 226]. Actually, no excess was observed in the results of previous Runs of the LHC that were performed at  $\sqrt{s} = 7 \text{ TeV}$  and  $\sqrt{s} = 8 \text{ TeV}$ . However, the results from these Runs were compatible in most ranges with the theoretical assumption of a new, heavy scalar particle with a mass of  $750 \text{ GeV}$  [224, 225]. By a naive combination of the data, collected at Run 1 at  $\sqrt{s} = 8 \text{ TeV}$  and Run 2 at  $\sqrt{s} = 13 \text{ TeV}$ , the anomalous excess could reach a local statistical significance of about  $4\sigma$  [228], corresponding

---

<sup>1</sup>The luminosity is a quantity to describe the number of particle scattering events in an experiment per units of time and surface,

$$L = \frac{n \cdot N_1 \cdot N_2 \cdot f}{4\pi\sigma_x\sigma_y}, \quad \dot{N} = \sigma_p \cdot L. \quad (5.1)$$

Here,  $\dot{N}$  is the number of the expected events per units of time, in a detector placed around the collision point, and  $\sigma_p$  is the cross section of the considered process, whereas  $N_1$  and  $N_2$  are the particles in the colliding bunches. In addition,  $n$  is the number of the bunches that collide with the frequency  $f$ , and the beam density usually follows a Gaussian shape with the widths  $\sigma_x$  and  $\sigma_y$  [229]. The luminosity characterizes the ability of a certain particle scattering experiment to accomplish results with a high statistical significance. In this sense, the integrated luminosity is the integral of the luminosity with respect to time [230],

$$L_{\text{int}} = \int L dt. \quad (5.2)$$

The higher the integrated luminosity is, the more data is available to analyse, and the more precise are the experimental results.

to a probability of 1 in a 50000 of just being created by a background fluctuation.

But, in fact, the local statistical significance only forms a reliable quantity to determine whether a resonance has a physical origin, if the measurements are restricted to a specific range where a resonance is expected to be found. This was not the case for the diphoton anomaly, which could have been materialised equally in  $\sim 10^2$  other places within the same data-set [228]. If measuring processes that follow statistical principles over a large range of energy intervals, also statistically unlikely fluctuations may appear at some point in the observation range. Since so many different experiments have been performed at the LHC, outcomes, which seem to be unlikely, are expected to be observed in a small fraction of them, caused by fluctuations that disappear if measuring for a longer time. This is the so-called “Look-elsewhere effect”, which may dilute the local statistical significance. It is accounted for in the **global** statistical significance, in which the whole mass range is taken into account over which an observation is performed. In the case of the di-photon anomaly, ATLAS reported a global statistical significance of  $2.3\sigma$  whereas CMS reported a global statistical significance of  $1.6\sigma$  [9, 226].

So, despite the apparently strong indications for an observation, the di-photon anomaly did not pass the  $5\sigma$ -threshold for the local statistical significance. For that reason, it had never been called a discovery. In fact, it turned out that the high  $5\sigma$ -threshold is mandatory in order to guarantee a high discovery standard in the field of high energy physics. Subsequent investigations of the di-photon anomaly have proven that the matter of statistics has seriously to be taken in particle scattering experiments, and, in fact, the anomaly turned out to be a manifestation of the “Look-elsewhere effect”. Very probably, it was created by a random fluctuation of the background at the particular energy. With much more of recorded data,  $15.4 \text{ fb}^{-1}$  for ATLAS and  $12.9 \text{ fb}^{-1}$  for CMS, both collaborations announced in the summer of 2016 that the excess had disappeared in the updated invariant mass spectrum [231, 232]. Instead, the data was conform with the expected background signals at the one standard-deviation level [231, 232]. Unfortunately, such disturbances can happen in statistical processes.

Shortly after the announcement of the excess in December 2015, a reaction, maybe disproportionate, was caused by the field of theoretical physics [233]. Over 500 publications were released that offered very plausible explanations for the excess. After having waited for tens of years, the hope was enormous that the anomaly would have been verified with more data, so that a first discovery of new physics beyond the SM would have been manifested, finally. And, although the excess had not passed the  $5\sigma$ -discovery threshold, further compelling reasons contributed to the big excitement about this excess. As a very important point, the excess was **independently** observed by both the ATLAS and CMS collaborations at the same point in the mass range of di-photons! This could have been a clear indication for a possible physical origin of the excess by the decay of a new particle. Furthermore, the observation was made in a very clear observation channel, the di-photon invariant mass plot. The two produced photons in this channel constitute to be a clean measurable final state, and the background rates to this process can be determined to a high precision. Only the di-lepton and four-lepton final states are even cleaner observables. Probably, more attention is paid to anomalies observed in the di-photon channel than to anomalies found in final states that suffer from a strong background pollution. Moreover, the di-photon channel was one of the discovery channels of the Higgs boson [67, 68].

On the other hand, maybe it was necessary to present something new, besides the Higgs boson, after so much money had been spent on the construction of the LHC experiments. The search for new phenomena beyond the SM formed one of the main incentives for the development

of the LHC. But, theoretical particle physicists have the duty to give explanations for newly observed phenomena, which also applied to the case of the di-photon anomaly. So far, there is no experimental evidence for the existence of any new physics beyond the SM, although there are many well-motivated theories. Theoretical physicists have to speculate and have to elaborate hypothetical frameworks to explain specific problems of the existing theory, and they must postulate experimental signals that would allow to confirm new theories. After the falsification of the di-photon anomaly in the summer 2016, all the new, theoretical explanations remain. These provide interesting approaches to theoretical phenomena, and give fruitful impulses to the field of particle physics, which, in this sense, have certainly their own values.

### 5.1.2 Inclusion of a singlet bulk scalar to the RS model

After these short, introductory remarks, I would like to outline in the next sections our work from [7], which gives a consistent and natural explanation for the di-photon anomaly in the framework of the RS model. In this context, I focus on the values of the excess reported in December 2015 and spring 2016, given in the publications [8, 9, 224, 226]. The signal strength for a narrow-width, scalar particle produced via gluon fusion was determined in [234] as a combination of ATLAS and CMS data from measurements performed at  $\sqrt{s} = 8$  TeV and  $\sqrt{s} = 13$  TeV, as

$$\sigma(pp \rightarrow S \rightarrow \gamma\gamma) = (4.6 \pm 1.2) \text{ fb} . \quad (5.3)$$

In the subsequently presented evaluations, we fit our analysis to this value. Very interestingly, this signal could not be reproduced by a minimal extension of the SM with just one single new scalar  $S$ , or by a large set of theoretically well-motivated, UV-completed theories (e.g. [235]). The reason was that additional new particles, with either a large multiplicity or sizeable couplings to  $S$ , had to enter the loop in the gluon-fusion or  $b\bar{b}$ -initiated production processes [236]. A production of the resonance from other quark-initiated states would have caused a tension with 8 TeV data, whereas photon-induced production would have required non-perturbatively large couplings [237, 238]. Moreover, the minimal super-symmetric UV completion of the SM would have been ruled out by the resonance. This was due to the fact that the theory lacks a neutral scalar candidate with appropriate couplings, although the additional degrees of freedom, needed in the loop-induced production process, would have been motivated well [239]. As a consequence, one had to resort to models with a low SUSY breaking scale, giving an sgoldstino explanation [240], or  $R$ -parity violating scenarios in which a sneutrino had large enough couplings to explain the excess [241, 242]. In principle, a large di-photon branching ratio could be obtained from several composite resonances, like neutral composite scalars in non-minimal composite Higgs models [243–246]. Also, a dilaton or radion could have been considered as a possible candidate in extra dimensional models, which required either a fine-tuned Higgs-radion mixing [247, 248] or a small radius of the extra dimension [249]. In all cases, unwanted consequences were obtained for the scale of the UV completion. Also, several non-minimal extensions of the SM were proposed, explaining the di-photon excess along with other anomalies observed in the flavor sector and the anomalous magnetic moment of the muon [239, 250–256].

Fortunately, the RS model, and especially the enlarged RS model with a custodial symmetry, could offer very natural explanations for the observed excess [7]. Here, only one single bulk scalar singlet had to be included to the traditional framework of the RS model. The only renormalizable interactions of that bulk scalar were the couplings to the bilinears of vector-like

bulk fermions, present in the RS model, with the exception of possible Higgs “portal”-couplings. For coupling parameters of this new bulk scalar to fermions of  $\mathcal{O}(1)$ , the di-photon excess could be explained with KK masses in the multi-TeV range, compatible to electroweak precision tests and constraints from flavor physics and Higgs phenomenology. The results are largely insensitive to the parameters of the RS model, such as the five-dimensional masses of the fermions and their Yukawa couplings to the Higgs field. In good approximation, the loop-induced couplings of the new resonance to di-boson states just count the number of the degrees of freedom that propagate in the loop, times group-theory factors. For that reason, the enlarged custodial RS model with the extended degrees of freedom for fermions and gauge bosons was particularly suitable to explain the excess. Moreover, all the calculated decay rates  $S \rightarrow \gamma\gamma, WW, ZZ, Z\gamma, gg, t\bar{t}$  and  $t\bar{t}h$  were compatible to the experimental results from  $\sqrt{s} = 8$  TeV measurements at the LHC. And furthermore, a similar scenario with the inclusion of a new bulk scalar to the RS model can offer intriguing possibilities in the context of flavor physics, by generating the  $Z_2$ -odd bulk fermion mass terms via a spontaneous symmetry breaking induced by the vacuum expectation value of a similar scalar [257, 258]. Some features of this possibility will be explored in the last section of this chapter.

Besides, similar extra-dimensional frameworks were considered in the context of the di-photon excess. For example, the new resonance was identified with the lowest spin-2 KK graviton in a warped extra dimensional model in [259–261]. In [262, 263], flat extra dimensional scenarios were investigated that cannot address the gauge hierarchy problem of the Higgs and the new scalar. The authors from [262] took the assumption that the new scalar could exclusively couple to heavy, vector-like leptons by placing only the SM lepton fields in the bulk. They had to introduce a cut-off for overlap integrals by hand, which was motivated by stringy arguments. Furthermore, a very similar framework to that of ours was published in [264], shortly after the release of our paper. Our framework certainly has the advantage that the explanations could be found on a very natural way without further complicated model building.

We identified the di-photon resonance with the lightest KK excitation of a new bulk scalar field  $S(x, \phi)$  in the RS model, forming a singlet under the bulk gauge group. In the RS model, there is a four-component vector-like, five-dimensional fermion field for every Weyl fermion of the SM [150]. For the zero-mode fermions, the chirality parts, not compatible to the SM, are projected out by means of the  $Z_2$ -symmetry, which is determined by the boundary conditions at the branes. There are two towers of KK excitations for the two chirality parts of the fermion fields. The new scalar field  $S$  couples to the scalar density of vector-like fermions,  $\bar{f}f = \bar{f}_L f_R + \bar{f}_R f_L$ , which combines fermions of even and odd chiralities, and therefore fermions of opposite  $Z_2$ -parities, in each of the terms. Accordingly, the field  $S(x, \phi)$  must own an odd  $Z_2$ -parity,  $S(x, -\phi) = -S(x, \phi)$ , to maintain the symmetry invariance of the coupling terms. The five-dimensional Lagrangian, comprising the kinetic and mass terms of the new scalar  $S$  and its coupling terms to fermions, reads

$$\int_{-\pi}^{\pi} d\phi \, r e^{-4\sigma(\phi)} \left[ \frac{g^{MN}}{2} (\partial_M S) (\partial_N S) - \frac{\mu_S^2}{2} S^2 - \sum_f (\text{sgn}(\phi) \bar{f} \mathbf{M}_f f + S \bar{f} \mathbf{G}_f f) \right], \quad (5.4)$$

where the sum runs over all the five-dimensional fermion multiplets  $f$ . In the custodial RS model, additional exotic fermion fields are included in the sum. The bulk mass and coupling matrices  $\mathbf{M}_f$  and  $\mathbf{G}_f$  are hermitian matrices in generation space. By means of field redefinitions,

one can arrange that the matrices  $\mathbf{M}_f$  are real and diagonal [150]. Furthermore, it is sensible to assume similar structures for the two matrices  $\mathbf{M}_f$  and  $\mathbf{G}_f$ , assuming a “hidden” framework in which the fermion bulk mass matrices are induced via a spontaneous  $Z_2$ -symmetry breaking by coupling the fermions to the vev of an odd bulk scalar. Conventionally, the matrices with the dimensionless bulk mass parameters are defined by  $\mathbf{c}_f = \pm \mathbf{M}_f/k$ , where the plus (minus) signs hold for fermions whose left-handed (right-handed) components have even profile functions under the  $Z_2$ -symmetry. With the same sign conventions, one can further define the dimensionless coupling matrices  $\mathbf{g}_f$  via

$$\mathbf{g}_f = \pm \frac{\sqrt{k(1 + \beta_S)}}{(2 + \beta_S)} \mathbf{G}_f , \quad (5.5)$$

where  $\beta_S^2 = 4 + \mu_S^2/k^2$ . The definition is in analogy to the definition of the dimensionless Yukawa matrices in the bulk-Higgs RS model. The terms with the  $\beta_S$ -dependence ensure that the dimensionless couplings behave well in the limit  $\beta_S \rightarrow \infty$ , describing an IR brane-localized scalar field similar to the Higgs case. In the subsequent phenomenological analysis, it will be assumed that the entries of the matrices  $\mathbf{g}_f$  have the same signs and similar magnitudes, with a possible exception of  $g_t \equiv (\mathbf{g}_u)_{33}$ . This is well grounded by the fact that all fermion bulk mass parameters  $\mathbf{c}_f$  cluster near or below the value  $-1/2$ , below which the zero-mode fermion profile is localized near the UV brane. The only exception can be the parameter of the right-handed top quark that is positive to realize a localization for the zero-mode profile close to the IR brane. Besides the couplings to fermions given in (5.4), the scalar can possibly couple to the Higgs field. Such a coupling is inevitably induced at the one-loop order, as will be discussed later. Other direct couplings to SM particles are not allowed due to the demand of gauge invariance.

The KK decomposition for the five-dimensional scalar field  $S$  can be chosen as follows

$$S(x, \phi) = \frac{e^{\sigma(\phi)}}{\sqrt{r}} \sum_n S_n(x) \chi_n^S(t) , \quad (5.6)$$

including a switch-over from the  $\phi$ - to the  $t$ -coordinate. From the five-dimensional action, the following equation of motion follows for the profiles in order to obtain the correct four-dimensional mass terms for the KK scalars,

$$(t^2 \partial_t^2 + t \partial_t - \beta_S^2 + t^2 x_n^2) \frac{\chi_n^S(t)}{t} = 0 , \quad (5.7)$$

with  $x_n = m_n^S/M_{KK}$ . In order to obtain appropriate kinetic terms for the KK scalars, the normalization condition,

$$\frac{2\pi}{L} \int_\epsilon^1 \frac{dt}{t} \chi_m^S(t) \chi_n^S(t) = \delta_{mn} , \quad (5.8)$$

has to be fulfilled, as well. Due to the  $Z_2$ -odd parity of the field  $S$ , the Dirichlet boundary condition,  $\chi_n^S(\epsilon) = 0$ , is required to be fulfilled at the UV brane. From these conditions, the general solution for the profiles can be determined as

$$\chi_n^S(t) = N_n t [J_{\beta_S}(x_n t) - r_n J_{-\beta_S}(x_n t)] , \quad r_n = \frac{J_{\beta_S}(\epsilon x_n)}{J_{-\beta_S}(\epsilon x_n)} \approx \frac{\Gamma(1 - \beta_S)}{1 + \beta_S} \left( \frac{\epsilon x_n}{2} \right)^{2\beta_S} , \quad (5.9)$$

including the expression  $r_n$ , and  $N_n$  is a normalization constant. In order to adapt the mass for the first KK resonance to the reported mass of 750 GeV, which is quite light in comparison to the KK mass scale, one has to impose a mixed boundary condition,

$$\chi_n^S(1) = \xi \chi_n^{S'}(1) , \quad (5.10)$$

at the IR brane. It can be engineered by adding brane-localized terms to the action. In the limits  $\xi \rightarrow 0$ , and  $\xi \rightarrow \infty$ , the special cases of Dirichlet and Neumann boundary conditions are recovered. In general, the subsequent relation follows from the IR boundary condition

$$[1 - \xi(1 - \beta_S)] J_{\beta_S}(x_n) - \xi x_n J_{\beta_S-1}(x_n) = r_n \{ [1 - \xi(1 + \beta_S)] J_{-\beta_S}(x_n) - \xi x_n J_{-\beta_S-1}(x_n) \} . \quad (5.11)$$

Due to the smallness of the quantity  $r_n \propto \epsilon^{2\beta_S}$ , given in (5.9), the whole right-hand side of (5.11) can be set to zero, in good approximation. Then, one can derive for the mass of the lightest KK resonance

$$x_1^2 \approx \frac{4(1 + \beta_S) [1 - \xi(1 + \beta_S)]}{1 - \xi(3 + \beta_S)} . \quad (5.12)$$

For a value  $m_1^S \approx 750$  GeV, a moderate, justifiable tuning of parameters is necessary. With  $M_{KK} = 2$  TeV, for example, one would need  $\xi \approx 0.69$  for  $\beta_S = 0.5$ ,  $\xi \approx 0.51$  for  $\beta_S = 1$ ,  $\xi \approx 0.17$  for  $\beta_S = 5$ , and  $\xi \approx 0.09$  for  $\beta_S = 10$ . In this way, the hierarchy problem, associated with the mass of the new scalar, can be solved in the RS framework, similar to the case of the Higgs boson. For such a lighter mass, one can expand the profile of the first KK resonance in powers of  $x_1^2$ , as follows

$$\chi_1^S(t) = \sqrt{\frac{L(1 + \beta_S)}{\pi}} t^{1+\beta_S} \left( 1 - \frac{x_1^2}{4} \left[ \frac{t^2}{(1 + \beta_S)} - \frac{1}{(2 + \beta_S)} \right] + \mathcal{O}(x_1^4) \right) . \quad (5.13)$$

This is equal to the profile of the zero-mode bulk-Higgs field, derived in (2.74). Similar to the bulk-Higgs scenario, it is assumed that  $\beta_S > 0$  (i.e.,  $\mu_S^2 > -4k^2$ ) following the Breitenlohner-Freedman bound [160]. Also, the parameter  $\beta_S$  controls the localization of the bulk scalar. For  $\beta_S = \mathcal{O}(1)$ , the scalar profile extends through the extra dimension, whereas for  $\beta_S \gg 1$ , it is localized close to the IR brane, according to

$$\chi_1^S(t) \stackrel{\beta \rightarrow \infty}{\approx} \sqrt{\frac{L(1 + \beta_S)}{\pi}} \frac{1}{(2 + \beta_S)} \delta(t - 1) . \quad (5.14)$$

In analogy to the Higgs case, there is no particular reason why the scalar  $S$  should be localized close to the IR brane. But again, the results take a particularly simple form in this limit.

### 5.1.3 S couplings to particles

The direct couplings of the scalar  $S$  to the scalar density of vector-like fermions are included in equation (5.4). Then, transmitted by loops of KK fermions, the scalar can couple to gauge bosons at the one-loop order. Since the masses of the lightest KK fermions lie in the multi-TeV range, these are much heavier than the mass of the 750 GeV di-photon resonance. For that reason, one can integrate out the tower of heavy KK fermion modes in computing the  $S$  decays

to di-boson final states. We can define the following effective Lagrangian, which is valid below the KK mass scale,

$$\begin{aligned} \mathcal{L}_{\text{eff}} = & c_{gg} \frac{\alpha_s}{4\pi} S G_{\mu\nu}^a G^{\mu\nu,a} + c_{WW} \frac{\alpha}{4\pi s_w^2} S W_{\mu\nu}^a W^{\mu\nu,a} + c_{BB} \frac{\alpha}{4\pi c_w^2} B_{\mu\nu} B^{\mu\nu} \\ & - \left[ S \bar{Q}_L \hat{Y}_u \tilde{\Phi} u_R + S \bar{Q}_L \hat{Y}_d \Phi d_R + S \bar{L}_L \hat{Y}_e \Phi e_R + \text{h.c.} \right] . \end{aligned} \quad (5.15)$$

The mass of the scalar  $S$  lies much above the electroweak scale. For that reason, the effective Lagrangian is considered in the electroweak symmetric phase. In the first row, the loop-induced couplings of  $S$  to gauge bosons are given, where the RS model effects are summarized into the Wilson coefficients  $c_{gg}$ ,  $c_{WW}$  and  $c_{BB}$ . In the second row, there are the direct couplings to fermions that are governed by the couplings matrices  $\hat{Y}_f$ . Here,  $G_{\mu\nu}^a$ ,  $W_{\mu\nu}^a$  and  $B_{\mu\nu}$  are the field strength tensors of the groups  $SU(3)_c$ ,  $SU(2)_L$  and  $U(1)_Y$ , respectively,  $\Phi$  is the scalar Higgs doublet, and  $s_w = \sin\theta_w$  and  $c_w = \cos\theta_w$ . After electroweak symmetry breaking, the resulting couplings to  $\gamma\gamma$ ,  $WW$  and  $ZZ$  states can be deduced as

$$\mathcal{L}_{\text{eff}} = c_{\gamma\gamma} \frac{\alpha}{4\pi} S F_{\mu\nu} F^{\mu\nu} + c_{Z\gamma} \frac{\alpha}{4\pi} S Z_{\mu\nu} F^{\mu\nu} + c_{ZZ} \frac{\alpha}{4\pi} S Z_{\mu\nu} Z^{\mu\nu} , \quad (5.16)$$

where

$$c_{\gamma\gamma} = c_{WW} + c_{BB} , \quad c_{Z\gamma} = \frac{c_W}{s_W} c_{WW} - \frac{s_W}{c_W} c_{BB} , \quad c_{ZZ} = \frac{c_W^2}{s_W^2} c_{WW} + \frac{s_W^2}{c_W^2} c_{BB} . \quad (5.17)$$

The second line in (5.15) writes the  $S$  couplings to the Higgs field and a pair of fermions. The  $S$  couplings to fermions have a hierarchical structure in the model, where the largest coupling, by far, is the  $S$  coupling to top quarks. After a transformation to the mass basis, one can rewrite  $\text{Re}[(\hat{Y})_{33}] = c_{tt} y_t$ , with the top-quark Yukawa coupling  $y_t = \sqrt{2} m_t / v$ , giving

$$\mathcal{L}_{\text{eff}} \ni -c_{tt} m_t \left( 1 + \frac{h}{v} \right) S \bar{t} t + \dots . \quad (5.18)$$

In the effective Lagrangian, the results for the Wilson coefficients are suppressed by the mass scale of the new physics, as  $c_{ii} \propto 1/M_{KK}$ .

Further, the coefficients are supposed to hold at the matching scale  $\Lambda_{KK} = \text{few} \times M_{KK}$ , which is the mass scale of the low-lying KK modes that give the dominant contributions in the loops of the processes. The two-gluon operator has a non-trivial QCD evolution for altering energies [265, 266], and it mixes with the operator in (5.18) under renormalization [267]. If the strong coupling  $\alpha_s$  and the Yukawa coupling  $y_t$  are factored out from the definitions of  $c_{gg}$  and  $c_{tt}$ , as it is in the present case, then, the evolution effects from the high matching scale  $\Lambda_{KK}$  down to the scale  $\mu = m_S$  arise only at the next-to-leading order in renormalization-group improved perturbation theory. The following relations apply [7]

$$\begin{aligned} c_{gg}(\mu) &= \left[ 1 + \frac{\beta_1}{4\beta_0} \frac{\alpha_s(\mu) - \alpha_s(\Lambda_{KK})}{\pi} \right] c_{gg}(\Lambda_{KK}) , \\ c_{tt}(\mu) &= c_{tt}(\Lambda_{KK}) + \frac{3C_F}{\beta_0} \frac{\alpha_s(\mu) - \alpha_s(\Lambda_{KK})}{\pi} c_{gg}(\Lambda_{KK}) , \end{aligned} \quad (5.19)$$



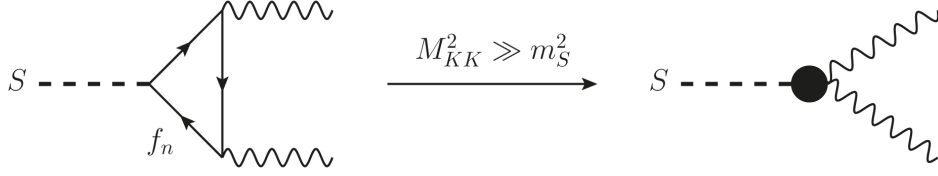


Figure 5.1: Loop-diagrams, which are transmitted by exchanges of heavy KK fermions, can be described at lower energies by effective local interactions that couple  $S$  to diboson final states.

where  $\beta_0 = 7$ ,  $\beta_1 = 26$  and  $C_F = 4/3$ . The coefficients  $c_{WW}$  and  $c_{BB}$  remain invariant under the QCD evolution. From these relations, it follows that the  $S$  to top quarks coupling is inevitably induced to a small amount by a renormalization group evolution, even if it is absent at the high matching scale. For  $\Lambda_{KK} = 5$  TeV, and  $\mu = 750$  GeV, one can determine

$$c_{tt}(\mu) \approx c_{tt}(\Lambda_{KK}) + 0.0028c_{gg}(\Lambda_{KK}) , \quad c_{gg}(\mu) \approx 1.0045c_{gg}(\Lambda_{KK}) . \quad (5.20)$$

Higher-order QCD corrections to the Wilson coefficients at the high matching scale are likely to have a stronger impact [268, 269], but, to be conservative, such enhancement factors are not included in the present analysis.

In order to calculate the RS model effects to the loop-induced  $S$  couplings, transmitted by KK fermions, one has to consider one-loop diagrams as the one plotted in Figure 5.1. The calculations are similar to the calculations of the loop-induced Higgs processes, presented in the previous chapter of this thesis. One can parametrize each of the couplings in terms of an integral over a single, five-dimensional fermion propagator function to sum over the transmitted KK fermion states. Starting from the Lagrangian in (5.4), one can employ the KK decompositions for the fermion fields, and finds for the  $S$  couplings to fermions

$$\begin{aligned} \mathcal{L}_{\text{ferm}} = & - \sum_f \sum_{l,m,n} \sqrt{\frac{\pi}{L(1+\beta_S)}} (2 + \beta_S) \int_{\epsilon}^1 dt S_l(x) \left[ \bar{f}_L^{(m)}(x) f_R^{(n)}(x) \right. \\ & \left. \times \chi_l^S(t) \mathcal{F}_L^{\dagger(m)}(t) \begin{pmatrix} \mathbf{g}_F & 0 \\ 0 & -\mathbf{g}_f \end{pmatrix} \mathcal{F}_R^{(n)}(t) + \text{h.c.} \right] , \end{aligned} \quad (5.21)$$

which is very similar to the couplings of the bulk Higgs to fermions. According to the calculation, presented in [2], one can derive the  $S$  couplings to di-boson states as

$$\begin{aligned} c_{gg} &= - \sum_{f=q} \frac{d_f}{2} \int_0^1 dx \int_0^1 dy (1 - 4xy\bar{y}) \mathcal{T}_f [-xy\bar{y}m_S^2 - i0] , \\ c_{WW} &= - \sum_{f=q,l} N_c^f T_f \int_0^1 dx \int_0^1 dy (1 - 4xy\bar{y}) \mathcal{T}_f [-xy\bar{y}m_S^2 - i0] , \\ c_{BB} &= - \sum_{f=q,l} N_c^f d_f Y_f^2 \int_0^1 dx \int_0^1 dy (1 - 4xy\bar{y}) \mathcal{T}_f [-xy\bar{y}m_S^2 - i0] . \end{aligned} \quad (5.22)$$

The sum in the result for  $c_{gg}$  is running over quark states, only, whereas for  $c_{WW}$  and  $c_{BB}$ , one has to sum over all states of quarks and leptons. These expressions only differ in the group-theory factors. Here,  $d_f$  is the dimension of the  $SU(2)$  multiplet,  $T_f$  is the Dynkin index of

$SU(2)$ , where there is  $T_f = 1/2$  for doublets,  $T_f = 2$  for triplets and  $T_f = 0$  for singlets,  $Y_f$  is the hypercharge of the multiplet, and the color factor  $N_c^f$  equals 3 for quarks and 1 for leptons. In addition, two Feynman parameter integrals over  $x$  and  $y$  are included, where  $\bar{y} = 1 - y$ . The product of the mixed-chirality components of the five-dimensional fermion propagator, and the profile of the scalar  $S$ , are included in the expression  $\mathcal{T}_f(p_E^2)$ . For Euclidean momenta  $p_E^2 = -p^2$ , it reads

$$\mathcal{T}_f(p_E^2) = \sqrt{\frac{\pi}{L}} \frac{(2 + \beta_S)}{\sqrt{1 + \beta_S}} \int_\epsilon^1 dt \chi_1^S(t) \text{Tr} \left[ (\pm \mathbf{g}_f) \frac{1}{2} \left( \Delta_{LR}^f(t, t; p_E^2) + \Delta_{RL}^f(t, t; p_E^2) \right) \right], \quad (5.23)$$

where the trace is performed over  $3 \times 3$  matrices in the generation space. The relations hold under the assumptions that  $\mathcal{T}_f(p_E^2)$  vanishes for  $p_E \rightarrow \infty$ , and that  $p_E \frac{d\mathcal{T}_f}{dp_E}$  vanishes for  $p_E = 0$  and  $p_E \rightarrow \infty$  [2], which are satisfied in the present model. The KK decomposed representation of the fermion propagator function has been derived in Chapter 3, given in (3.67). Moreover, it is assumed that the Higgs vev  $v$  is negligibly small, compared to the energy scale of the considered processes, by neglecting tiny corrections of the order of  $v^2/M_{KK}^2$ , compared to  $m_S^2/M_{KK}^2$ . It follows that the zero-mode particles are approximately massless, and do not contribute to the leading order. The calculation of the analytic, five-dimensional fermion propagator function, for  $v \approx 0$ , in the minimal and the custodial RS models has been presented in Section 3.3.2 of the thesis. With the help of the results for the propagator function, one can compute the expressions

$$\begin{aligned} \frac{\Delta_{LR}^f(t, t; p_E^2) + \Delta_{RL}^f(t, t; p_E^2)}{2} &= \pm \frac{1}{2M_{KK}^2} d^{(\pm)}(\mathbf{c}_f, p_E, t) \\ &= \pm \frac{1}{2M_{KK}^2} \left( k_0^{(\pm)}(\mathbf{c}_f, t) + \hat{p}_E^2 k_2^{(\pm)}(\mathbf{c}_f, t) + \mathcal{O}(\hat{p}_E^4) \right), \end{aligned} \quad (5.24)$$

which are diagonal matrices, with a dimension according to the specific fermion content of the model (minimal or custodial model). The functions  $d^{(\pm)}(\mathbf{c}_f, p_E, t)$  are given in (3.80) and (3.86), respectively. Here, the overall  $\pm$ -signs correspond to fermions whose left-handed (right-handed) components have even profile functions under the  $Z_2$ -symmetry, whereas the superscripts  $(\pm)$  refer to the boundary conditions (normal or twisted) that are obeyed by the fermion multiplet  $f$  at the branes. It is justified to expand the results in a power series in  $\hat{p}_E^2$ , as it is done in (5.24), because interactions are considered at an energy scale much below the KK mass scale,  $\hat{p}_E^2 \sim (m_S/M_{KK})^2 \ll 1$ . Then, the expressions  $k_0^{(\pm)}(\mathbf{c}_f, t)$  and  $k_2^{(\pm)}(\mathbf{c}_f, t)$  read

$$\begin{aligned} k_0^{(+)}(\mathbf{c}_f, t) &= 1 + \frac{2F^2(\mathbf{c}_f)}{1 + 2\mathbf{c}_f} (t^{1+2\mathbf{c}_f} - 1), & k_0^{(-)}(\mathbf{c}_f, t) &= 1, \\ k_2^{(+)}(\mathbf{c}_f, t) &= \frac{2t^2(1 - t^{-1-2\mathbf{c}_f})}{1 - 4\mathbf{c}_f^2} + 2(1 - \epsilon^2)F^4(\mathbf{c}_f) \frac{t^{1+2\mathbf{c}_f} - 1}{(1 - 4\mathbf{c}_f^2)(3 + 2\mathbf{c}_f)} \\ &\quad - 2F^2(\mathbf{c}_f) \left( \frac{t^2(2 - t^{-1-2\mathbf{c}_f})}{(1 - 2\mathbf{c}_f)(1 + 2\mathbf{c}_f)^2} - \frac{2(1 + \mathbf{c}_f)t^{3+2\mathbf{c}_f}}{(1 + 2\mathbf{c}_f)^2(3 + 2\mathbf{c}_f)} - \frac{1 + \epsilon^2(t^{1+2\mathbf{c}_f} - 1)}{(1 - 2\mathbf{c}_f)(3 + 2\mathbf{c}_f)} \right), \\ k_2^{(-)}(\mathbf{c}_f, t) &= \frac{2t^2(1 - t^{-1-2\mathbf{c}_f})}{1 - 4\mathbf{c}_f^2} \left( 1 - \left( \frac{\epsilon}{t} \right)^{1-2\mathbf{c}_f} \right). \end{aligned} \quad (5.25)$$

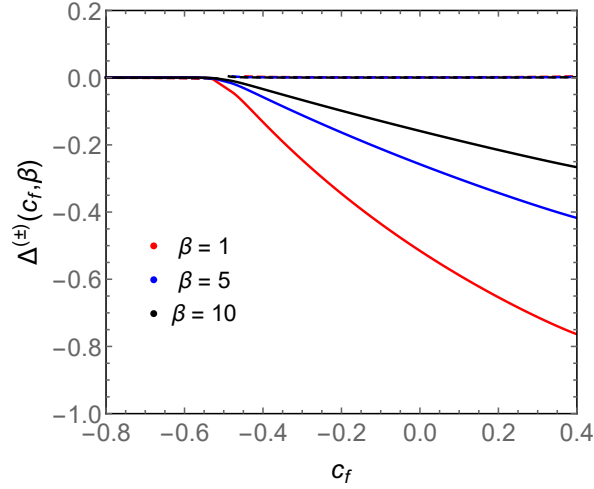


Figure 5.2: Results for the corrections  $\Delta^{(+)}(c_f, \beta)$  (solid curves) and  $\Delta^{(-)}(c_f, \beta)$  (dashed curves), for  $m_S = 750$  GeV and  $M_{KK} = 2$  TeV, according to the formulas given in Appendix D.1.

Here, the zero-mode fermion profile  $F(\mathbf{c})$  is included, which is exponentially small for all the fermions, except of the right-handed top quark. Considering the limit  $\epsilon \rightarrow 0$  wherever possible, one can derive

$$\begin{aligned}
c_{gg} &= -\frac{1}{3M_{KK}} \sum_{f=q} \frac{d_f}{2} \int_0^1 dt (2 + \beta_S) t^{1+\beta_S} \left( 1 - \frac{m_S^2}{4M_{KK}^2} \left[ \frac{t^2}{1 + \beta_S} - \frac{1}{2 + \beta_S} \right] + \dots \right) \\
&\times \text{Tr} \left[ \mathbf{g}_f \left( k_0^{(\pm)}(\mathbf{c}_f, t) - \frac{7m_S^2}{120M_{KK}^2} k_2^{(\pm)}(\mathbf{c}_f, t) + \dots \right) \right] \\
&\equiv -\frac{1}{3M_{KK}} \sum_{f=q} \frac{d_f}{2} \text{Tr} \left[ \mathbf{g}_f (1 + \Delta^{(\pm)}(\mathbf{c}_f, \beta_S)) \right], \tag{5.26}
\end{aligned}$$

with

$$\Delta^{(+)}(\mathbf{c}_f, \beta_S) = -\frac{2F^2(\mathbf{c}_f)}{3 + \beta_S + 2\mathbf{c}_f} + \mathcal{O}\left(\frac{m_S^2}{M_{KK}^2}\right), \quad \Delta^{(-)}(\mathbf{c}_f, \beta_S) = \mathcal{O}\left(\frac{m_S^2}{M_{KK}^2}\right). \tag{5.27}$$

The expressions for  $c_{WW}$  and  $c_{BB}$  are derived similarly. Also, these can be obtained by replacing  $d_f/2$  with  $N_c^f T_f$  or  $N_c^f d_f Y_f^2$  in (5.26), and including the lepton fields, according to the formulas (5.22). The corrections to  $\Delta^{(\pm)}(\mathbf{c}_f, \beta_S)$  of  $\mathcal{O}(m_S^2/M_{KK}^2)$  are given in Appendix D.1. Even for  $M_{KK}$  masses as low as 2 TeV, one can find that these corrections are very small and can be neglected. Note that in the limit  $\beta_S \rightarrow \infty$ , there is  $\Delta^{(\pm)}(\mathbf{c}_f, \beta_S) \rightarrow 0$ . In Figure 5.2, the full expressions  $\Delta^{(\pm)}(c_f, \beta)$  are plotted as functions of the bulk mass parameters  $c_f$  for different choices of the parameter  $\beta$ . One can also neglect the exponentially small quantities  $F^2(\mathbf{c}_f)$ , except for the case of the right-handed top quark, for which there is  $F^2(c_t) \approx 1 + 2c_t$ . In this approximation, the Wilson coefficients simply count the numbers of the fermionic degrees of freedom that are predicted by the respective RS scenarios. For the custodial model I, one can

find

$$\begin{aligned}
c_{gg} &= -\frac{1}{3M_{KK}} \text{Tr} \left( 2\mathbf{g}_Q + \frac{1}{2}\mathbf{g}_u + \frac{3}{2}\mathbf{g}_d + \frac{3}{2}\mathbf{g}_{\mathcal{T}_1} \right) \approx -\frac{16g_{\text{eff}}}{3M_{KK}} - \frac{(1 + \beta_S - 2c_t)}{(3 + \beta_S + 2c_t)} \frac{g_t}{6M_{KK}}, \\
c_{WW} &= -\frac{1}{3M_{KK}} \text{Tr} (3\mathbf{g}_Q + 6\mathbf{g}_{\mathcal{T}_1} + \mathbf{g}_L + 2\mathbf{g}_{\mathcal{T}_3}) \approx -\frac{12g_{\text{eff}}}{M_{KK}}, \\
c_{BB} &= -\frac{1}{3M_{KK}} \text{Tr} \left( \frac{25}{3}\mathbf{g}_Q + \frac{4}{3}\mathbf{g}_u + 10\mathbf{g}_d + 4\mathbf{g}_{\mathcal{T}_1} + \mathbf{g}_L + 2\mathbf{g}_e \right) \\
&\approx -\frac{236g_{\text{eff}}}{9M_{KK}} - \frac{(1 + \beta_S - 2c_t)}{(3 + \beta_S + 2c_t)} \frac{4g_t}{9M_{KK}},
\end{aligned} \tag{5.28}$$

whereas for the custodial model II, the results are

$$\begin{aligned}
c_{WW} &= -\frac{1}{3M_{KK}} \text{Tr} \left( 3\mathbf{g}_Q + 6\mathbf{g}_{\mathcal{T}_1} + \frac{1}{2}\mathbf{g}_L \right) \approx -\frac{19g_{\text{eff}}}{2M_{KK}}, \\
c_{BB} &= -\frac{1}{3M_{KK}} \text{Tr} \left( \frac{25}{3}\mathbf{g}_Q + \frac{4}{3}\mathbf{g}_u + 10\mathbf{g}_d + 4\mathbf{g}_{\mathcal{T}_1} + \frac{1}{2}\mathbf{g}_L + \mathbf{g}_e \right) \\
&\approx -\frac{445g_{\text{eff}}}{18M_{KK}} - \frac{(1 + \beta_S - 2c_t)}{(3 + \beta_S + 2c_t)} \frac{4g_t}{9M_{KK}},
\end{aligned} \tag{5.29}$$

and  $c_{gg}$  is unchanged. In the minimal RS model, one can derive

$$\begin{aligned}
c_{gg} &= -\frac{1}{3M_{KK}} \text{Tr} \left( \mathbf{g}_Q + \frac{1}{2}\mathbf{g}_u + \frac{1}{2}\mathbf{g}_d \right) \approx -\frac{11g_{\text{eff}}}{6M_{KK}} - \frac{(1 + \beta_S - 2c_t)}{(3 + \beta_S + 2c_t)} \frac{g_t}{6M_{KK}}, \\
c_{WW} &= -\frac{1}{3M_{KK}} \text{Tr} \left( \frac{3}{2}\mathbf{g}_Q + \frac{1}{2}\mathbf{g}_L \right) \approx -\frac{2g_{\text{eff}}}{M_{KK}}, \\
c_{BB} &= -\frac{1}{3M_{KK}} \text{Tr} \left( \frac{1}{6}\mathbf{g}_Q + \frac{4}{3}\mathbf{g}_u + \frac{1}{3}\mathbf{g}_d + \frac{1}{2}\mathbf{g}_L + \mathbf{g}_e \right) \approx -\frac{26g_{\text{eff}}}{9M_{KK}} - \frac{(1 + \beta_S - 2c_t)}{(3 + \beta_S + 2c_t)} \frac{4g_t}{9M_{KK}}.
\end{aligned} \tag{5.30}$$

It is assumed that the diagonal entries of all the matrices  $\mathbf{g}_f$  are equal to a universal value  $g_{\text{eff}}$ , except of the value  $g_t$ , which corresponds to the right-handed top quark. This is in correspondence with the behaviour of the  $c_f$ -parameters that lie very close to each other, except of the value  $c_t$ . Note that the bulk localization parameter  $\beta_S$  appears only in these correction terms scaling with  $g_t$ .

In the tree-level  $S$  couplings to zero-mode fermions, as the zero-mode top quarks, one has to consider an integral over the extra dimension. In this integral, the zero-mode fermion profiles and the  $S$  profile are included. Neglecting terms of the order of  $m_h^2/M_{KK}^2$ , the Lagrangian of

$\sqrt{s}$	MSTW2008 [270]	NNPDF30 [271]	PDF4LHC15 [272]	HERA20 [273]	MMHT2014 [274]
8 TeV	$44.9_{-2.4}^{+1.6}$ fb	$45.8_{-2.5}^{+1.6}$ fb	$46.7_{-2.5}^{+1.7}$ fb	$42.2_{-2.2}^{+1.4}$ fb	$46.7_{-2.5}^{+1.6}$ fb
13 TeV	$203_{-10}^{+6}$ fb	$207_{-10}^{+7}$ fb	$208_{-10}^{+7}$ fb	$197_{-9}^{+6}$ fb	$208_{-10}^{+7}$ fb

Table 5.1: NNLO predictions for the production cross sections of  $S$  through gluon fusion in units of  $(c_{gg}/\text{TeV})^2$ . The different columns correspond to different sets of PDFs, used in the derivations, and the quoted errors are estimated from scale variations [7, 275].

the  $S$  to up quarks couplings reads

$$\begin{aligned}
\mathcal{L}_{\text{ferm}} = & - \sum_{m,n} S(x) \bar{u}_L^{(m)}(x) u_R^{(n)}(x) (2 + \beta_S) \int_0^1 dt t^{1+\beta_S} \\
& \times \left[ x_n \hat{a}_m^{(U)\dagger} F(\mathbf{c}_Q) t^{\mathbf{c}_Q} \mathbf{g}_Q F(\mathbf{c}_Q) \frac{t^{1+\mathbf{c}_Q} - \epsilon^{1+2\mathbf{c}_Q} t^{-\mathbf{c}_Q}}{1 + 2\mathbf{c}_Q} \hat{a}_n^{(U)} \right. \\
& \left. + x_m \hat{a}_m^{(u)\dagger} F(\mathbf{c}_u) \frac{t^{1+\mathbf{c}_u} - \epsilon^{1+2\mathbf{c}_u} t^{-\mathbf{c}_u}}{1 + 2\mathbf{c}_u} \mathbf{g}_u F(\mathbf{c}_u) t^{\mathbf{c}_u} \hat{a}_n^{(u)} \right] + \text{h.c.} ,
\end{aligned} \tag{5.31}$$

where  $x_n = m_n/M_{KK}$ , and  $n = 1, 2, 3$ , label the three lowest-lying states that are  $u$ ,  $c$  and  $t$ . Here, a  $Z_2$ -even profile is combined with a  $Z_2$ -odd profile, where the  $Z_2$ -odd profile arises after electroweak symmetry breaking, induced by a mixing between the zero modes and their KK excitations. For that reason, the expressions scale with the masses  $m_n^f$  of the zero-mode fermions. The vectors  $\hat{a}_n^{(U)}$  and  $\hat{a}_n^{(u)}$  describe the fermion mixings in the flavor space, whose entries are strongly hierarchical, having the largest entry at the position  $n$ . For the  $S$  coupling to a pair of top quarks, one can, then, find in a good approximation

$$\begin{aligned}
c_{tt} & \approx \frac{1}{M_{KK}} \left[ \mathbf{g}_Q \left( 1 - \frac{F^2(\mathbf{c}_Q)}{3 + \beta_S + 2\mathbf{c}_Q} \right) + \mathbf{g}_u \left( 1 - \frac{F^2(\mathbf{c}_u)}{3 + \beta_S + 2\mathbf{c}_u} \right) \right]_{33} \\
& \approx \frac{1}{M_{KK}} \left[ (\mathbf{g}_Q)_{33} + \frac{2 + \beta_S}{3 + \beta_S + 2c_t} g_t \right] ,
\end{aligned} \tag{5.32}$$

which applies for both the minimal and the custodial RS models.

#### 5.1.4 Phenomenological evaluations of the various S decay rates

In the following, the cross section for the S boson production at the LHC, and the various S decay rates into SM particle states, parametrized in terms of the Wilson coefficients from the effective Lagrangian in (5.15), are summarized. The general formulas are valid for many new-physics models, where the couplings of  $S$  to SM particles are induced by exchanges of heavy new particles. With the previously derived results for the Wilson coefficients in the different RS scenarios, one can perform explicit evaluations in dependence of the RS model parameter space. The cross section for the  $S$  boson production through gluon fusion at the LHC is given, at the

Born level, by

$$\sigma(pp \rightarrow S) = \frac{\alpha_s^2(\mu)m_S^2}{64\pi s} c_{gg}^2(\mu) \int_{m_S^2/s}^1 \frac{dx}{x} f_{g/p}[x, \mu] f_{g/p} \left[ \frac{m_S^2}{sx}, \mu \right], \quad (5.33)$$

depending on a gluon-gluon luminosity function  $f_{g/p}$ . The factorization and renormalization scales are set to  $\mu \sim m_S$ . It is known well from the calculation of the analogous Higgs production cross section that higher-order QCD corrections may have an enormous impact. In this sense, we have been very grateful to Daniel Wilhelm for having used his adaptation of the code `CuTe` [276], developed in [277, 278], to calculate the  $pp \rightarrow S$  cross section at the NNLO, including resummation effects. The results are displayed in Table 5.1, corresponding to the ratio  $\sigma(pp \rightarrow S)/c_{gg}^2(\mu)$  for different sets of parton distribution functions (PDFs) quoted, and the default scale choice  $\mu = m_S$ . With the MSTW2008-PDF, one can find

$$\begin{aligned} \sigma_{\text{NNLO}}^{8 \text{ TeV}}(pp \rightarrow S) &= (44.9_{-2.4-2.7}^{+1.6+1.8}) \text{ fb} \times \left( \frac{c_{gg}(m_S)}{\text{TeV}} \right)^2, \\ \sigma_{\text{NNLO}}^{13 \text{ TeV}}(pp \rightarrow S) &= (203_{-10-6}^{+6+5}) \text{ fb} \times \left( \frac{c_{gg}(m_S)}{\text{TeV}} \right)^2. \end{aligned} \quad (5.34)$$

The errors refer to scale variations and the variation of the PDFs. Also, the program `CuTe` predicts the  $p_T$ -distribution of the produced  $S$  bosons, and it has been found that this distribution peaks around 22 GeV. The higher-order corrections enhance the cross section by more than a factor 2 compared to the Born cross section, given in (5.33).

According to the general formula for the partial decay rate with a final state of two particles<sup>2</sup>, one can determine the  $S$  decay rates into  $\gamma\gamma$ ,  $WW$ ,  $ZZ$  and  $Z\gamma$  final states, and into hadronic final states, such as  $gg$  and  $t\bar{t}$ , in dependence of the Wilson coefficients computed before for the

---

<sup>2</sup>The general formula for the partial decay rate of a particle's decay,  $A \rightarrow B, C$ , accounting for the summation over the phase space, reads [279]

$$\Gamma(A \rightarrow B + C) = \frac{N}{16\pi} \frac{\lambda^{1/2}(m_A^2, m_B^2, m_C^2)}{m_A^2} \sum_{\text{d.o.f.}} |\mathcal{M}|^2, \quad (5.35)$$

where

$$\lambda(x, y, z) = x^2 + y^2 + z^2 - 2xy - 2xz - 2yz. \quad (5.36)$$

The formula depends on a sum over the internal degrees of freedom (d.o.f.) of the particles, such as spins, polarizations and colors. For the decay rate into a final state of equal particles, with  $B = C$ , one has to consider  $N = \frac{1}{2}$  to avoid an over-counting of the d.o.f.s.

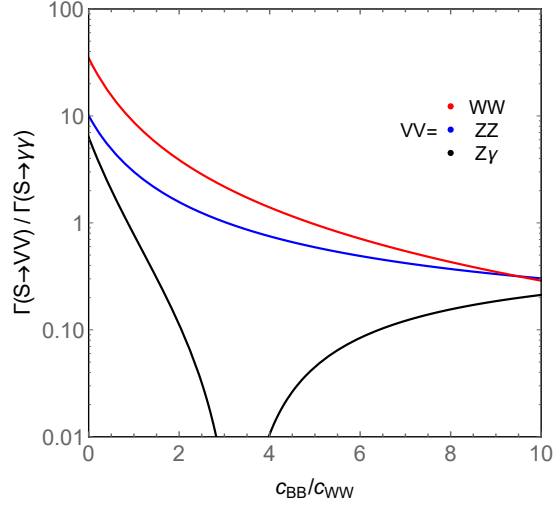


Figure 5.3: Dependence on the ratio  $c_{BB}/c_{WW}$  of the  $S$  decay rates into  $WW$ ,  $ZZ$  and  $Z\gamma$  final states, divided through the  $S$  decay rate into the  $\gamma\gamma$  final state.

different RS scenarios. The results are

$$\begin{aligned}
 \Gamma(S \rightarrow \gamma\gamma) &= \frac{\alpha^2 m_S^3}{64\pi^3} (c_{WW} + c_{BB})^2, \\
 \Gamma(S \rightarrow WW) &= \frac{\alpha^2 m_S^3}{32\pi^3} \frac{c_{WW}^2}{s_w^4} (1 - 4x_W + 6x_W^2) (1 - 4x_W)^{1/2}, \\
 \Gamma(S \rightarrow ZZ) &= \frac{\alpha^2 m_S^3}{64\pi^3} \left[ \frac{c_w^2}{s_w^2} c_{WW} + \frac{s_w^2}{c_w^2} c_{BB} \right]^2 (1 - 4x_Z + 6x_Z^2) (1 - 4x_Z)^{1/2}, \\
 \Gamma(S \rightarrow Z\gamma) &= \frac{\alpha^2 m_S^3}{32\pi^3} \left[ \frac{c_w}{s_w} c_{WW} - \frac{s_w}{c_w} c_{BB} \right]^2 (1 - x_Z)^3,
 \end{aligned} \tag{5.37}$$

where  $x_{[W,Z]} = m_{[W,Z]}^2/m_S^2$ . The Wilson coefficients are evaluated at the scale  $\mu = m_S$ . Instead, the gauge couplings and the Weinberg angle are evaluated at the appropriate scale for the final-state bosons, so that  $\alpha(m_Z) = 1/127.94$  for the  $Z$  and  $W$  bosons,  $\alpha = 1/137.04$  for photon final states, and  $s_W^2 = 0.2313$ . All the rates are entirely determined by the Wilson coefficients  $c_{WW}$  and  $c_{BB}$ . In this regard, any ratio of two rates is a function of the ratio  $c_{BB}/c_{WW}$ , which is an important quantity that characterizes the specific model under consideration. The dependencies on this quantity for the ratio of two rates are illustrated in Figure 5.3. For the different scenarios, assuming  $-2 < g_t/g_{\text{eff}} < 1$ , one encounters  $2.11 < c_{BB}/c_{WW} < 2.23$  in the custodial model I,  $2.50 < c_{BB}/c_{WW} < 2.65$  in the custodial model II, and  $1.00 < c_{BB}/c_{WW} < 1.66$  in the minimal model. Especially the  $S \rightarrow Z\gamma$  decay rate has a large dependence on the ratio  $c_{BB}/c_{WW}$ , and is strongly suppressed for the three RS scenarios that are considered.

For the  $S$  decay rates into gluon and top quark final states, one can determine the following

$jj$ [280]	$WW$ [281]	$ZZ$ [282]	$Z\gamma$ [283]	$t\bar{t}$ [284]	$hh$ [285]
$< 2.5$ pb	$< 40$ fb	$< 12$ fb	$< 4$ fb	$< 700$ fb	$< 50$ fb

Table 5.2: Bounds on the production cross sections  $pp \rightarrow S \rightarrow XX$  to 95% CL, obtained in dijet, diboson and  $t\bar{t}$  resonance searches performed at Run 1 at  $\sqrt{s} = 8$  TeV of the LHC.

results

$$\begin{aligned}\Gamma(S \rightarrow gg) &= \frac{\alpha_s^2(\mu)m_S^3}{8\pi^3} K_{gg}(\mu)c_{gg}^2(\mu) , \\ \Gamma(S \rightarrow t\bar{t}) &= \frac{3m_t^2(\mu)m_S}{8\pi} c_{tt}^2(\mu)(1 - 4x_t)^{3/2} ,\end{aligned}\tag{5.38}$$

where all the running quantities are considered at  $\mu \approx m_S$ . Here,  $m_t(\mu)$  is the running top-quark mass, for which it is used  $m_t(m_S) = 146.8$  GeV, whereas the top-quark pole mass  $m_t = 173.34$  GeV is entering the phase space factors via  $x_t = m_t^2/m_S^2$ . For most of the parameter choices in the RS model, the  $S \rightarrow gg$  decay mode is the dominant decay channel, and forms the most important part of the total decay width in the calculation of the branching fractions. By using calculations of the Higgs boson decay rate into two gluons, up to the order of  $\mathcal{O}(\alpha_s^5)$ , in the heavy top-quark limit [286, 287], authors from [7] were able to derive the  $S \rightarrow gg$  decay rate to the same accuracy. The impact of radiative corrections is significantly smaller than in the Higgs case, and the perturbative series at  $\mu = m_S$  exhibits a very good convergence. The result was determined to be  $K_{gg}^{N^3LO} \approx 1.348$  [7].

In the following, the experimental results for the di-photon rate from equation (5.3) are reproduced in the parameter spaces of the different RS scenarios. Furthermore, by including the predictions for the various S decay rates, computed before, one can compare the theoretically reproduced di-photon rates in dependence of the RS model parameters with results obtained from dijet, diboson and  $t\bar{t}$  resonance searches, performed at Run 1 of the LHC, which are summarized in Table 5.2. To compare the results with the di-photon measurements at  $\sqrt{s} = 13$  TeV, the numbers in Table 5.2 have to be multiplied with the boost factor 4.52, which is obtained from the ratio of the production cross sections in (5.34). In this way, exclusion bounds for the RS model parameter spaces can be obtained that are implied by Run 1 searches. In Figure 5.4, the results are displayed in the  $M_{KK}/g_{\text{eff}} - g_t/g_{\text{eff}}$ -parameter plane, where the  $1\sigma$  and  $2\sigma$  fit regions correspond to the green and blue marked areas. The gray areas indicate the excluded regions that follow from Run 1 searches, with the boundaries drawn in red (dijet searches), purple ( $t\bar{t}$  searches), blue ( $WW$  searches), orange ( $ZZ$  searches) and green ( $Z\gamma$  searches). For the contribution of the right-handed zero-mode top quark, the input parameters  $\beta_S = 1$  and  $c_t = 0.4$  were used. The central fit results for  $\beta_S = 1$  (black, dashed),  $\beta_S = 10$  (green, dashed) and  $\beta_S \rightarrow \infty$  (red) are illustrated in the plot in the lower right corner, and one can observe that varying the parameter  $\beta_S$  does not substantially alter the course of the central fit curves. Similarly, this can be concluded for variations of the parameter  $c_t$ .

One can find that in the two enlarged custodial models, the di-photon rate can be reproduced over a wide range of parameters, without any fine tuning necessary, or conflict caused with Run 1 exclusion bounds. By varying the parameter choice for  $g_t/g_{\text{eff}}$ , one gets values for  $M_{KK}/g_{\text{eff}}$



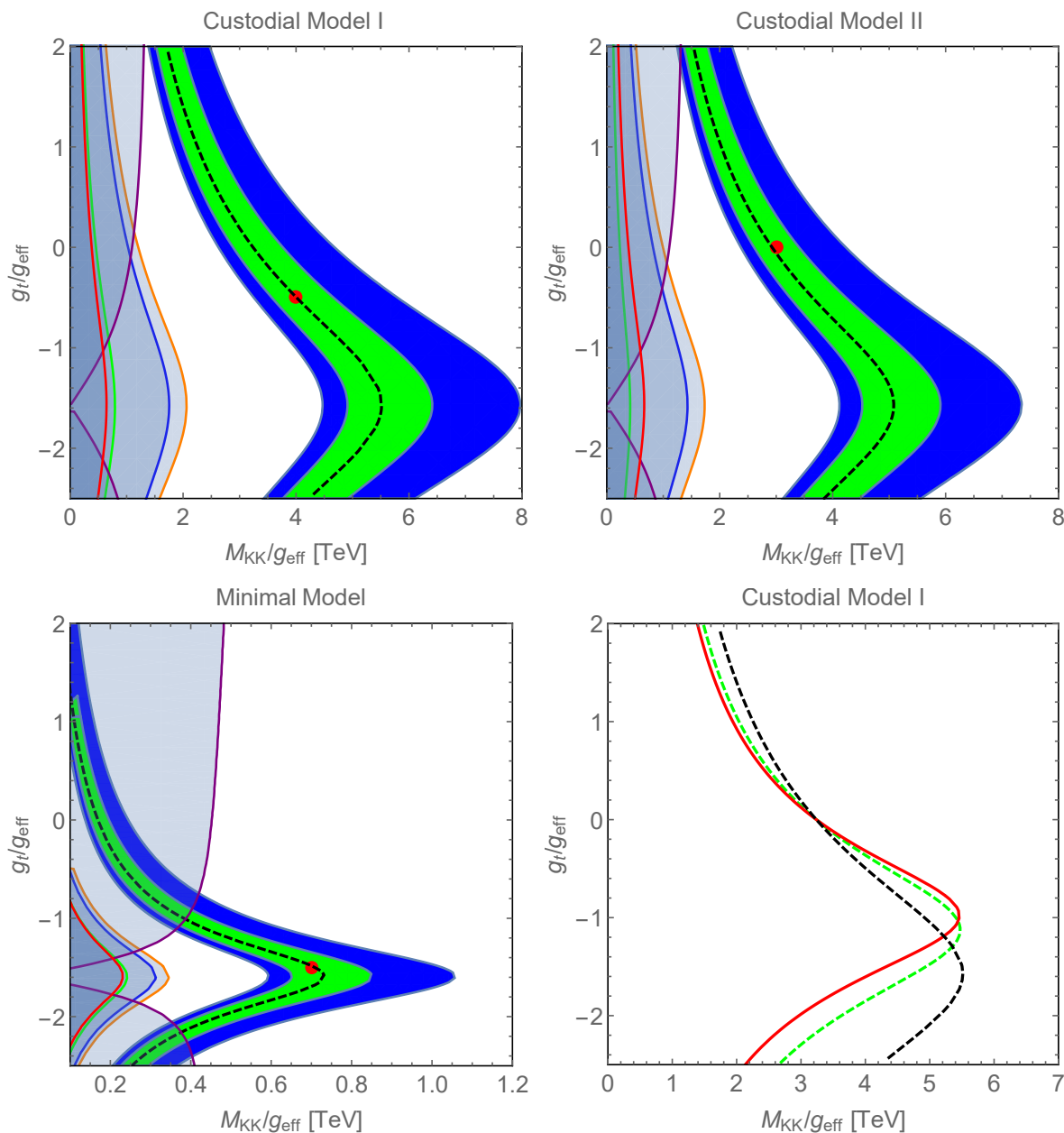


Figure 5.4: Regions in the parameter spaces of the different RS scenarios, where the di-photon signal is reproduced at  $1\sigma$  (green area) and  $2\sigma$  (blue area). The black, dashed lines correspond to the fit to the central result, given in (5.3). The exclusion bounds from Run 1 resonance searches at 95% CL, given in Table 5.2, are indicated by the gray regions with the boundaries drawn in red (dijets), purple ( $t\bar{t}$ ), blue (WW), orange (ZZ), and green ( $Z\gamma$ ). The results hold for  $\beta_S = 1$  and  $c_t = 0.4$ . In the lower right plot, a variation of the central fit result is illustrated, for  $\beta_S = 1$  (black dashed),  $\beta_S = 10$  (green dashed) and  $\beta_S \rightarrow \infty$  (red).

ranging from 2 to 8 TeV. For a KK mass scale  $M_{KK}$  close to the lowest allowed value by electroweak precision tests, the coupling  $g_{\text{eff}}$  ranges from 0.25 to 1, which is well inside the

$\text{Br}(S \rightarrow XX)$	$gg$	$\gamma\gamma$	$WW$	$ZZ$	$Z\gamma$	$t\bar{t}$	$hh$	$t\bar{t}h$	$\Gamma_{\text{tot}}$ [GeV]
custodial I	43.56	1.28	5.08	2.11	0.10	47.39	0	0.49	0.08
custodial II	28.84	0.68	2.09	0.92	0.02	66.76	0	0.69	0.22
minimal	89.45	0.36	2.61	0.95	0.16	6.41	0	0.07	0.14
custodial I	32.73	0.97	9.79	4.56	0.08	48.18	3.11	0.59	0.11
custodial II	24.49	0.58	4.28	2.04	0.01	66.56	1.30	0.76	0.26
minimal	78.38	0.32	6.21	2.78	0.14	9.99	2.05	0.14	0.16
custodial I	21.90	0.65	17.93	8.66	0.05	41.91	8.31	0.59	0.16
custodial II	19.53	0.46	9.09	4.42	0.01	61.59	4.13	0.76	0.32
minimal	60.94	0.25	13.55	6.45	0.11	12.14	6.37	0.20	0.21

Table 5.3: Branching ratios in % for the various  $S$  decay modes in the three RS scenarios under consideration, for the benchmark parameter points given in the text. The values in the center and lower portions give the results for small Higgs portal couplings,  $\lambda_1 = 0.02$  and  $0.04$ , whereas  $\lambda_2$  is set to zero in all cases.

perturbative region. In this case, the masses for the lightest KK particles could be as low as a bit more than 4 TeV. But, also for  $M_{KK} \approx 5$  TeV, and  $g_{\text{eff}} \sim 1$ , *i.e.* for KK particles as light as 12 TeV, the di-photon signal could be reproduced for very natural choices of parameters.

In contrast, the parameter space of the minimal RS model is much more constrained. Respecting the bound implied by electroweak precision tests, allowing for ratios as  $M_{KK}/g_{\text{eff}} \sim 0.4 - 1$ , the resulting coupling values,  $g_{\text{eff}} \sim 5 - 12$ , lie close to the perturbativity limit. Also, only negative ratios are allowed for  $g_t/g_{\text{eff}}$ , respecting the strong constraint from the  $t\bar{t}$  resonance searches, which is indicated by the purple line in the plot.<sup>3</sup>

In the following, the individual branching fractions for the various  $S$  decay modes are studied, by choosing the following benchmark points for the RS model parameters in the three scenarios:

	custodial model I	custodial model II	minimal model
$M_{KK}/g_{\text{eff}}$	4.0 TeV	3.0 TeV	0.7 TeV
$g_t/g_{\text{eff}}$	-0.5	0	-1.5

These parameter choices are indicated in the plots by the red points. For these benchmark points, the branching ratios for the various  $S$  decay rates are summarized in Table 5.3. The  $S \rightarrow t\bar{t}$  decay rate has been calculated to the lowest order, only, and it might be afflicted with some uncertainty due to neglected QCD corrections. The corresponding branching ratio is quite sensitive to the choice for  $g_t/g_{\text{eff}}$ , in contrast to the remaining branching ratios that depend on it only mildly. The results in the different scenarios for the total decay widths of  $S$  are written

<sup>3</sup>However, it might be conceivable that the exclusion bound from the  $t\bar{t}$  searches is considerably weaker, due to interference effects not considered in the experimental analyses [288–290].

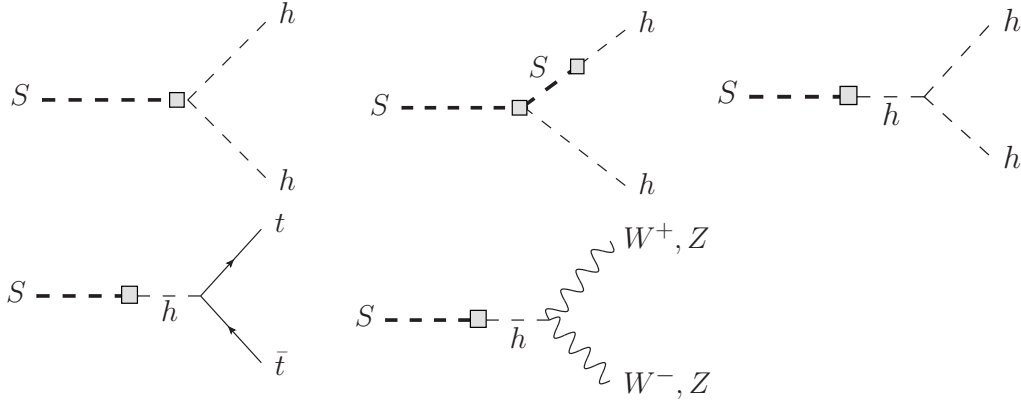


Figure 5.5: Diagrams of the  $S$  decays mediated by Higgs “portal” couplings.

in the last column of Table 5.3. All in all, these give narrow widths in the range of

$$\frac{\Gamma_{\text{tot}}}{m_S} \approx (1.1 - 4.3) \cdot 10^{-4} . \quad (5.39)$$

Originally, ATLAS had reported a result with a large width, such as  $\Gamma_{\text{tot}}/m_S \approx 0.06$  [9]. However, this was only slightly preferred against a result with a narrow width, leading to an improvement of the fit by  $0.3\sigma$ . Instead, CMS had reported a result with a narrow width, as  $\Gamma_{\text{tot}}/m_S = 1.4 \cdot 10^{-4}$ , as the outcome from a combined analysis of 8 TeV and 13 TeV data [226]. In [227], it was concluded that the large-width scenario is disfavoured by a combination of the 13 TeV data from ATLAS and CMS, and is slightly preferred if including the 8 TeV data, because it is easier to absorb the signal of a broad resonance into the background model. The local statistical significance was changing by at most of  $0.5\sigma$  between these two options [7].

To summarize, in the different RS scenarios, any of the three chosen benchmark points could reproduce the reported di-photon signal, and was consistent with the exclusion bounds derived from Run 1 data of the LHC. Strongly differing results were observed in particular for the  $S \rightarrow gg$  and  $S \rightarrow t\bar{t}$  decay modes, whereas the  $S \rightarrow Z\gamma$  decay mode turned out to be very small in all the considered scenarios.

### 5.1.5 Higgs “portal” couplings

In principle, the Higgs field can couple to the new scalar  $S$  in a direct way, following the demands from gauge invariance and renormalizability. In this sense, the Higgs field can form a “portal” to the new-physics sector, which in the present case is the framework with the new scalar field  $S$ . Such a Lagrangian with the Higgs portal couplings reads [236, 239, 291, 292]

$$\delta\mathcal{L}_{\text{eff}} = -\lambda_1 m_S S |\Phi|^2 - \frac{\lambda_2}{2} S^2 |\Phi|^2 \in -\frac{\lambda_1}{2} m_S S (v+h)^2 - \frac{\lambda_2}{4} S^2 (v+h)^2 . \quad (5.40)$$

In any case<sup>4</sup>, the Higgs portal couplings were inevitably induced at the one loop order, by diagrams similar to those in Figure 5.1, where the external gauge fields would be replaced by

<sup>4</sup>In the RS model with a brane-localized Higgs sector, one could implement an odd bulk scalar  $S$ , which completely vanishes on the IR brane. In such a scenario, direct Higgs portal interactions would be avoided. In

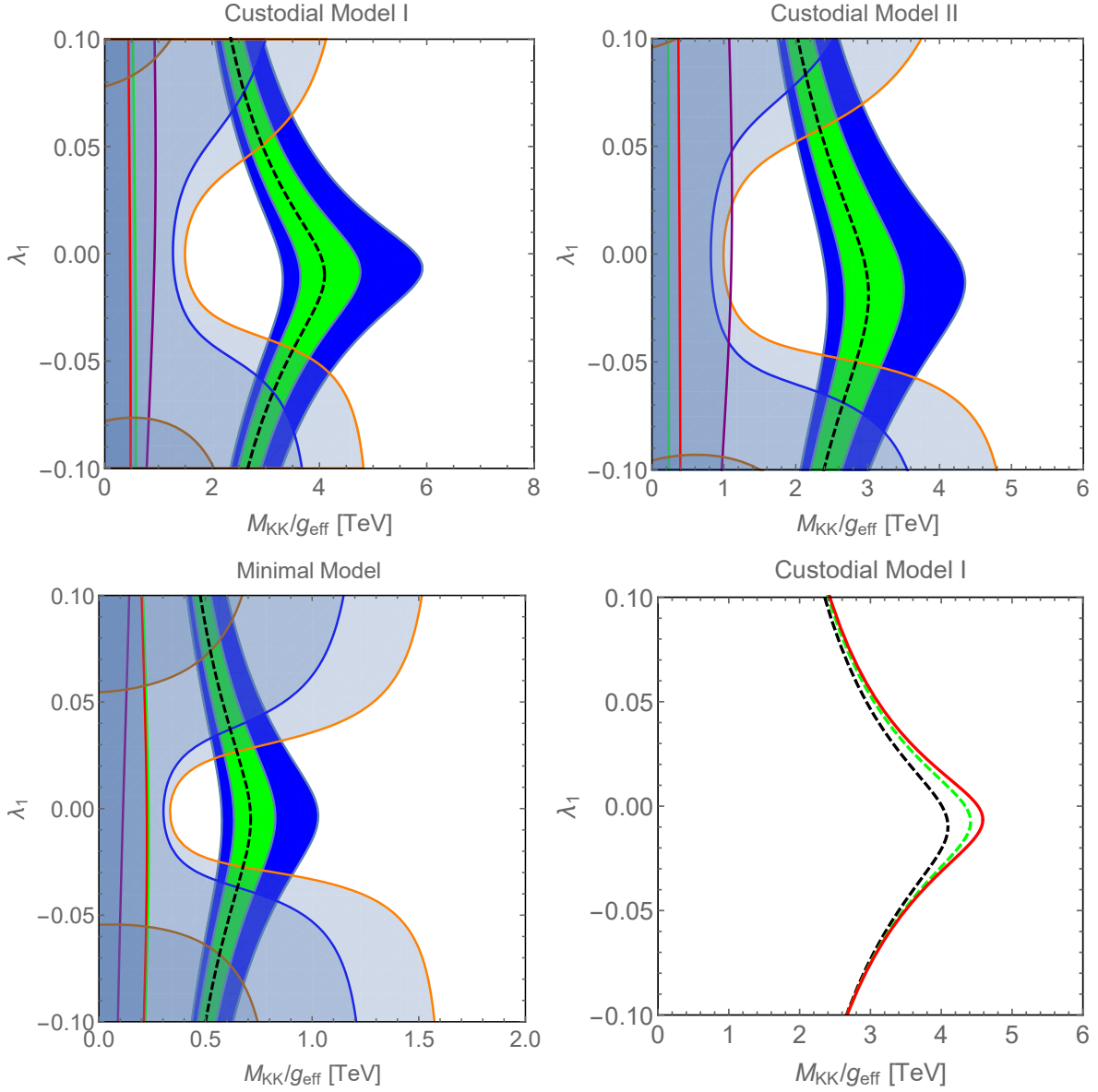


Figure 5.6: Regions in the parameter spaces of the different RS scenarios, where the di-photon signal is reproduced at  $1\sigma$  (green area) and  $2\sigma$  (blue area), with the inclusion of Higgs portal couplings. The meaning of the colors is the same as in Figure 5.4. It is used  $g_t/g_{\text{eff}} = -1.5$  for the custodial model I,  $g_t/g_{\text{eff}} = 0$  for the custodial model II, and  $g_t/g_{\text{eff}} = -1.5$  for the minimal model, together with  $\beta_S = 1$  and  $c_t = 0.4$ . In the lower right plot, a variation of the central fit values is illustrated, for  $\beta_S = 1$  (black dashed),  $\beta_S = 10$  (green dashed) and  $\beta_S \rightarrow \infty$  (red), respectively.

principle, such a scenario would be more natural, because a  $Z_2$ -odd bulk scalar  $S$  would naturally vanish on both branes to avoid a non-continuous behaviour at the boundaries, in contrast to the present scenario, where it was necessary to implement mixed-typed IR boundary conditions in order to get a mass for  $S$  below the KK mass scale,  $m_S \approx 750$  GeV, as presented before.

Higgs bosons. Also, an effective Lagrangian from the type considered in (5.15) induces a portal coupling  $\lambda_1$  proportional to  $c_{tt}$ , from top-quark loop graphs below the electroweak scale. In this sense, Higgs portal couplings in the RS model cannot be omitted completely.

In the following, the interactions are computed that are induced by the Higgs portal couplings, given in (5.40). The first portal coupling can induce three different and interesting effects. The presence of a tadpole demands for a shift of the physical field  $S$ , such as  $S \rightarrow S - (\lambda_1 v^2)/(2m_S)$ . If performing this shift in (5.15), the SM Yukawa couplings receive corrections, and wave-function corrections are induced to the gauge fields. Furthermore, there is a direct decay mode of  $S$  into two Higgs particles, as illustrated in the upper three diagrams of Figure 5.5. To the leading order in the portal coupling  $\lambda_1$ , this decay rate can be computed as

$$\Gamma(S \rightarrow hh) = \frac{m_S}{32\pi} \lambda_1^2 \left( 1 + \frac{3m_h^2 - 2\lambda_2 v^2}{m_S^2 - m_h^2} \right)^2 \sqrt{1 - 4x_h}. \quad (5.41)$$

Also, there is a mixing between the scalar  $S$  and the Higgs boson, which modifies the results for the tree-level decay modes  $S \rightarrow t\bar{t}, WW, ZZ$ , via the diagrams that are given in the lower row of Figure 5.5. The modified  $S \rightarrow t\bar{t}$  and  $S \rightarrow WW$  decay rates read

$$\begin{aligned} \Gamma(S \rightarrow t\bar{t}) &= \frac{3m_t^2}{8\pi m_S} (1 - 4x_t)^{3/2} \left( m_S c_{tt} + \frac{\lambda_1}{1 - x_h} \right)^2, \\ \Gamma(S \rightarrow WW) &= \frac{m_S}{16\pi} \sqrt{1 - 4x_W} \left[ \frac{m_S^2 c_{WW}^2}{2} \left( \frac{\alpha}{\pi s_W^2} \right)^2 (1 - 4x_W + 6x_W^2) \right. \\ &\quad \left. + \left( \frac{\lambda_1}{1 - x_h} \right)^2 (1 - 4x_W + 12x_W^2) - 6m_S c_{WW} \frac{\alpha}{\pi s_W^2} \frac{\lambda_1}{1 - x_h} x_W (1 - 2x_W) \right], \end{aligned} \quad (5.42)$$

and a similar decay rate can be found for  $S \rightarrow ZZ$ . And further, the mixing between the field  $S$  and the Higgs has an impact on the properties of the Higgs boson. In this case, the physical Higgs boson is given by a combination  $(\cos \theta h - \sin \theta S)$ , with  $\sin 2\theta = 2\lambda_1 m_S v / (m_S^2 - m_h^2) \approx 0.67\lambda_1$ , where  $m_S$  and  $m_h$  are referred to after the field redefinitions. Measurements of the Higgs branching fractions constrain  $\cos \theta$  to be larger than 0.86, to 95% CL [293, 294], which implies  $|\lambda_1| < 1.3$  as a rather weak constraint.

The  $S$  decay mode into two Higgs bosons, and the contributions to the  $S$  decays into  $WW$  and  $ZZ$  states, have a strong impact on the phenomenological analysis of the di-photon signal in the RS scenarios. Similar to the evaluations before, in Figure 5.6, the  $1\sigma$  and  $2\sigma$  fit regions to the di-photon signal from (5.3) are presented in dependence of the portal coupling  $\lambda_1$ . The values for  $g_t/g_{\text{eff}}$  are fixed to those of the benchmark points, given before, and also, the meaning of the colors of the various curves is the same as before. In the case of Higgs portal couplings, the exclusion bounds from the  $S \rightarrow ZZ$  decay rate from Run 1 of the LHC provide the strongest constraints, and exclude portal couplings as  $|\lambda_1| \geq 0.06$  (0.07) in the custodial RS model I (II), respectively. In Table 5.3, the results for the branching fractions of the various  $S$  decay modes, and the total  $S$  decay widths, for  $\lambda_1 = 0.02$ , and  $\lambda_1 = 0.04$ , are included. Even for such small portal couplings, the  $S \rightarrow hh$  branching fraction can have a sizeable portion of the decay modes, and the branching fractions of the  $S \rightarrow WW, ZZ$  decays can be enhanced significantly. The parameter space of the minimal model suffers from the strongest exclusion bounds, similar

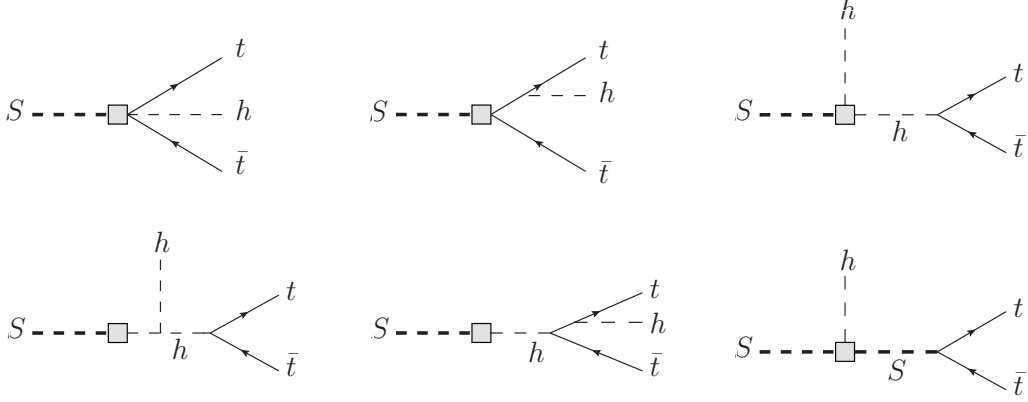


Figure 5.7: Diagrams that describe the three-body decay mode  $S \rightarrow t\bar{t}h$ .

to the evaluations before. However, for small Higgs portal couplings, as  $|\lambda_1| \leq 0.03$ , natural parameter choices are possible for  $M_{KK}/g_{\text{eff}}$ . The lower right plot gives the dependence of the fits on the central values for  $\beta_S = 1$  (black dashed line),  $\beta_S = 5$  (green dashed) and  $\beta_S \rightarrow \infty$  (red), indicating a minor dependence on the bulk localization parameter  $\beta_S$ , as before.

### 5.1.6 Three-body decay rate $S \rightarrow t\bar{t}h$

The LHC experiments measured results for the  $t\bar{t}h$  production rate that are enhanced compared to the SM prediction [295, 296]. The framework, considered here, includes a coupling of the new field  $S$  to a  $t\bar{t}$  pair and a Higgs boson at the tree level. In this regard, it was interesting to see whether the hypothetical scalar  $S$  might also has contributed to the enhanced  $t\bar{t}h$ -rate. The diagrams that describe the  $S \rightarrow t\bar{t}h$  decay mode are illustrated in Figure 5.7. The two Higgs portal couplings, governed by  $\lambda_1$  and  $\lambda_2$ , contribute in this case. The kinematics of a three body decay can be described in a Dalitz distribution by means of two variables, which are the squares of the invariant masses of two pairs of the decay products, for example [279]. In the present case, one can derive the following result in dependence on the dimensionless variables  $z = m_{t\bar{t}}^2/m_S^2$  and  $w = m_{th}^2/m_S^2$  [7],

$$\frac{d^2\Gamma(S \rightarrow t\bar{t}h)}{dwdz} = \frac{3y_t^2 m_S^3}{256\pi^3} c_{tt}^2 \left[ A^2(z - 4x_t) - 2ABx_t(1 - 2w - z + 2x_t + x_h) \right. \\ \left. + B^2x_t((1 - w + x_t)(w - x_t - x_h) - z(w - x_t)) \right], \quad (5.43)$$

with

$$A = 1 + \left( \frac{2x_t}{1 - w - z + x_t + x_h} + \frac{2x_t}{w - x_t} \right) \left( 1 + \frac{1}{m_{Sc_{tt}}} \frac{\lambda_1}{1 - x_h} \right) \\ + \frac{1}{m_{Sc_{tt}}} \frac{\lambda_1}{z - x_h} \left( 1 + \frac{3x_h}{1 - x_h} \right) - \frac{v^2}{m_S^2} \frac{\lambda_2}{1 - z}, \quad (5.44)$$

$$B = \left( \frac{1}{1 - w - z + x_t + x_h} - \frac{1}{w - x_t} \right) \left( 1 + \frac{1}{m_{Sc_{tt}}} \frac{\lambda_1}{1 - x_h} \right).$$

$\lambda_1$	Custodial I	Custodial II	Minimal
0	$3.92244 \times 10^{-4}$	$1.49561 \times 10^{-3}$	$9.37345 \times 10^{-5}$
0.02	$6.33963 \times 10^{-4}$	$1.93907 \times 10^{-3}$	$2.27213 \times 10^{-4}$
0.04	$9.35606 \times 10^{-4}$	$2.44245 \times 10^{-3}$	$4.20614 \times 10^{-4}$

Table 5.4: Results for the decay rates  $S \rightarrow t\bar{t}h$  in [GeV], obtained by numerical integrations over the Dalitz plot in the different RS scenarios, for three different and small choices for  $\lambda_1$ , and  $\lambda_2 = 0$ . The resulting branching fractions are given in the previous to last column of Table 5.3, respectively.

The phase space for the variables  $w$  and  $z$  is bounded by [7]

$$w_{\min}(z) \leq w \leq w_{\max}(z) , \quad 4x_t \leq z \leq (1 - \sqrt{x_h})^2 , \quad (5.45)$$

with

$$w_{\max/\min}(z) = \frac{(1 - x_h)^2}{4z} - \frac{1}{4z} \left( \sqrt{z(z - 4x_t)} \mp \sqrt{(1 - z - x_h)^2 - 4zx_h} \right)^2 . \quad (5.46)$$

The results for the decay rates in [GeV], obtained from numeric integrations over the Dalitz distribution, are summarized in Table 5.4. The predicted signal strengths,  $\sigma(pp \rightarrow S) \times BR(S \rightarrow t\bar{t}h)$ , do not exceed 5 fb in the considered RS scenarios. The results for the  $S \rightarrow t\bar{t}h$  branching ratio are given in the previous to last column of Table 5.3. Typically, these are two orders of magnitude smaller than the  $S \rightarrow t\bar{t}$  branching ratios. Nevertheless, all the results were too small to explain the enhanced Higgs production rate in association with a  $t\bar{t}$ -pair.

### 5.1.7 Intermediate summary

The anomalous excess of photon pairs, detected by both the experiments from ATLAS and CMS at 750 GeV in the invariant mass spectrum from first 13 TeV data, had raised enormous hopes on finally having detected a hint on new physics beyond the SM. Unfortunately, the excess was not verified by future analyses, leading to the conclusion that the presumed resonance was, in fact, a statistical fluctuation. Alternatively, the resonance would most likely have been created by the decay of a new, scalar boson with a mass of 750 GeV, produced by gluon fusion. It was remarkable that the simple addition of a single new scalar to the SM, as well as several, well motivated UV completions, including the MSSM, had failed to explain the resonance. We argued that the diphoton signal could straightforwardly be reproduced from an extension of the RS model, by identifying the resonance with the lightest KK excitation of an additional bulk scalar field [7]. In the RS model, the gluon fusion production rate of a scalar, and the decay rate of the scalar into two photons, can have large magnitudes, due to the large multiplicity of vector-like KK fermion states that contribute in the virtual loops. By summing up the KK tower of fermions with the help of the five-dimensional fermion propagator function, we were able to derive remarkably simple, analytic expressions for the effective  $S$  couplings to gluons and photons. In good approximation, these simply count the number of the fermionic degrees of freedom in the loops, weighted by group-theory factors. In this regard, the RS framework

with a custodial bulk gauge symmetry, featuring a larger number of fermion states compared to the minimal model, was particularly suitable to explain the excess. It was found that, with  $\mathcal{O}(1)$ -couplings of the resonance to fermions, and KK masses in the multi-TeV range, one could explain the di-photon signal, without violating any of Run 1 exclusion bounds from the resonance searches in various di-boson and di-jet channels. By working with an effective Lagrangian of local interactions to subsume the RS corrections into Wilson coefficients, the findings can be adapted to any model that considers a similar resonance. In the case of a possible, but unlike, reappearance of the di-photon signal, or of a new and similar signal, our findings could open the door to detailed studies of the parameter spaces of the RS models.

## 5.2 Localization mechanism of fermions by an $Z_2$ -odd bulk scalar

A scenario similar to the one considered in the last section can form a particularly interesting framework to describe a localization mechanism for fermions in the extra dimension. This localization mechanism is a crucial ingredient of the RS model, grounded on the  $Z_2$ -odd bulk fermion masses that determine the fermion profiles along the extra dimension. The odd bulk fermion masses have to be generated via couplings of the fermions to the vev of an odd bulk scalar. The different fermion localizations in the extra dimension can account for the mass splitting of the four-dimensional zero-mode fermions in a natural way, as has been explained in the end of Section 2.2.3.

Considering a five-dimensional Dirac fermion  $f$  with a mass  $M_f$  of the order of the fundamental scale  $M$ , which propagates in a five-dimensional space with RS metric, one can write its most general action as follows

$$S = \int d^4x \int_{-\pi}^{\pi} d\phi \sqrt{G} \{ \bar{f} (i\Gamma^M \nabla_M - \text{sgn}(\phi) \mathbf{M}_f) f - \mathcal{L}_{\text{Yuk}} \} . \quad (5.47)$$

The odd Dirac bulk fermion mass terms include the scalar density of the vector-like fermions

$$\text{sgn}(\phi) \mathbf{M}_f (\bar{f} f) = \text{sgn}(\phi) \mathbf{M}_f (\bar{F}_L F_R + \bar{F}_R F_L + \bar{f}_L f_R + \bar{f}_R f_L) , \quad (5.48)$$

where  $Z_2$ -even fermion fields are combined with  $Z_2$ -odd fermion fields, where  $F$  denote  $SU(2)$  doublets and  $f$  are singlets. The left-handed doublets and right-handed singlets are  $Z_2$ -even, and their counterparts of opposite chiralities are  $Z_2$ -odd. To ensure the  $SU(2)$ -invariance, two doublet and two singlet fermions are combined in the mass terms, respectively. In order to maintain the  $Z_2$ -invariance of the action, the five-dimensional fermion mass terms have to transform with an odd behaviour under the  $Z_2$ -symmetry, obeying to a sign change under  $\phi \rightarrow -\phi$ , as it is provided by the  $\text{sgn}\phi$ . The  $Z_2$ -odd bulk mass terms can be induced by a **spontaneous** breaking of the  $Z_2$ -symmetry, which origin has to be described by an underlying mechanism.

For such a framework, one can consider the implementation of a new scalar field  $S_L$ , just as before, with the Lagrangian

$$\int_{-\pi}^{\pi} d\phi r e^{-4\sigma(\phi)} \left[ \frac{g^{MN}}{2} (\partial_M S_L) (\partial_N S_L) + \frac{\mu_L^2}{2} S_L^2 - \frac{\lambda_L}{2} S_L^4 - \sum_f (S_L \bar{f} \mathbf{G}_f f) \right] , \quad (5.49)$$



including now a quartic self-coupling term that scales with  $\lambda_L$ . The fermion bulk mass terms will be induced by the last terms, which couple the scalar to the scalar density of vector-like fermions, with the coupling-strength matrices  $\mathbf{G}_f$ . For  $\mu_L > 0$  and  $\lambda_L > 0$ , the potential of the scalar will exhibit a Mexican-hat behaviour in the five-dimensional space, similar to the Higgs case, with a region of degenerate, non-zero minima.<sup>5</sup> With one particular of these minima, the couplings to the fermions induce a spontaneous symmetry breaking of the  $Z_2$ -symmetry. One can write the vev of the scalar, induced by the potential, as follows

$$\langle S_L(x, t) \rangle = \frac{w_L(t)}{\sqrt{r\epsilon}}, \quad (5.50)$$

which depends on the extra dimensional coordinate, similar to the case of the bulk-Higgs vev. Here, a factor  $1/(\sqrt{r\epsilon})$  is extracted so that the vev  $w_L(t)$  and the field  $\bar{S}_L(x, t)$  have the dimension of energy. The scalar field can be expanded around that vev by

$$S_L(x, t) = \frac{1}{\sqrt{r\epsilon}} [w_L(t) + \bar{S}_L(x, t)]. \quad (5.51)$$

With this expansion, and by using the redefinition of the fermions in (2.105), one rewrites the scalar Lagrangian as

$$\begin{aligned} & \frac{2\pi}{L} \int_{\epsilon}^1 \frac{dt}{t} \left[ \frac{\eta^{\mu\nu}}{2t^2} [\partial_{\mu} \bar{S}_L(x, t)] [\partial_{\nu} \bar{S}_L(x, t)] - \frac{M_{KK}^2}{2t^2} (\partial_t [w_L(t) + \bar{S}_L(x, t)])^2 \right. \\ & + \frac{\mu_L^2 \epsilon^2}{2t^4} [w_L(t) + \bar{S}_L(x, t)]^2 - \frac{\lambda_L}{2rt^4} [w_L(t) + \bar{S}_L(x, t)]^4 \\ & \left. - \sum_f \frac{[w_L(t) + \bar{S}_L(x, t)]}{\sqrt{r\epsilon}} \left( \bar{\mathcal{F}}_L(x, t) \begin{pmatrix} \mathbf{G}_F & 0 \\ 0 & \mathbf{G}_f \end{pmatrix} \mathcal{F}_R(x, t) + \text{h.c.} \right) \right]. \end{aligned} \quad (5.52)$$

The KK expansion for the field  $\bar{S}_L(x, t)$  is chosen as

$$\bar{S}_L(x, t) = \sum_{n=1}^{\infty} \chi_n^{S_L}(t) \bar{S}_L^{(n)}(x), \quad (5.53)$$

and the equation of motion for the scalar profiles reads

$$\left( \partial_t^2 - \frac{3}{t} \partial_t + \frac{\mu_L^2}{k^2 t^2} - \frac{3\xi}{t^2} w_L^2(t) + \frac{m_n^{S^2}}{M_{KK}^2} \right) \chi_n^{S_L}(t) = 0, \quad (5.54)$$

where  $\xi = \frac{2\lambda_L}{M_{KK}^2 r}$ . The term scaling with  $\xi$  is new, compared to the equation of motion for the Higgs profiles. The function  $w_L(t)$  of the vev is the value of  $s(t)$  that minimizes [258]

$$\frac{2\pi}{L} \int_{\epsilon}^1 \frac{dt}{t} \left[ -\frac{M_{KK}^2}{2t^2} (\partial_t s(t))^2 + \frac{\mu_L^2 \epsilon^2}{2t^4} (s(t))^2 - \frac{\lambda_L}{2rt^4} (s(t))^4 \right], \quad (5.55)$$

<sup>5</sup>For convenience, in the case of the Higgs field, considered in this thesis, the electroweak symmetry breaking is maintained on the IR brane, even for a bulk-Higgs localization. For that reason, a quartic coupling term is solely included on the IR brane, rather than in the bulk.

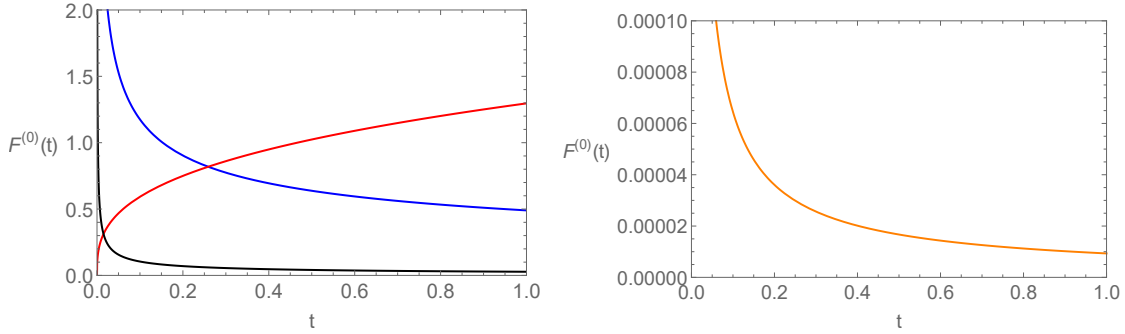


Figure 5.8: Plots of the zero-mode fermion profiles in the conventional RS model, for bulk mass parameters as  $c = -0.38$  (blue curve),  $c = -0.58$  (black curve),  $c = +0.34$  (red curve), and  $c = -0.84$  (orange curve). It can be observed that for  $\mathcal{O}(1)$ -differences between the fermion bulk mass parameters, the profiles considerably differ in the magnitudes. This behaviour is crucial for explaining the mass differences between the four-dimensional zero-mode fermion particles in a natural way.

subject to the boundary conditions

$$s(\epsilon) = s(1) = 0 . \quad (5.56)$$

Due to the  $Z_2$ -odd behaviour, the boundary conditions demand the function to vanish on the branes. By means of a variational principle with respect to  $w_L(t)$ , one derives the equation of motion for the vev as follows

$$t^2 w_L''(t) - 3t w_L'(t) + \frac{\mu_L^2}{k^2} w_L(t) - \xi w_L^3(t) = 0 . \quad (5.57)$$

There is a tension between the boundary conditions and the potential that determines a non-zero vev in the bulk. It is only possible to solve the differential equation in (5.57), while fulfilling the boundary conditions to a good approximation. The mass matrix expression  $\mathcal{M}_f(t)$ , determining the equations of motion for the fermion profiles, is modified in the present framework and contains the coupling to the vev  $w_L(t)$ , as

$$\mathcal{M}_f^w(t) = \frac{w_L(t)}{t} \sqrt{\frac{\pi}{L}} \begin{pmatrix} \mathbf{g}_F & 0 \\ 0 & -\mathbf{g}_f \end{pmatrix} + \frac{v(2+\beta)}{\sqrt{2}M_{KK}} t^{1+\beta} \begin{pmatrix} 0 & \mathbf{Y}_f \\ \mathbf{Y}_f^\dagger & 0 \end{pmatrix} , \quad (5.58)$$

where the dimensionless coupling matrices are defined by

$$\mathbf{g}_{F,f} = \pm \sqrt{k} \mathbf{G}_{F,f} . \quad (5.59)$$

To the lowest order in  $v/M_{KK}$ , the equations of motion for the zero-mode fermion profiles read

$$\begin{aligned} \partial_t \mathcal{F}_L^{(0)}(t) &= \frac{w_L(t)}{t} \sqrt{\frac{\pi}{L}} \begin{pmatrix} \mathbf{g}_F & 0 \\ 0 & -\mathbf{g}_f \end{pmatrix} \mathcal{F}_L^{(0)}(t) , \\ -\partial_t \mathcal{F}_R^{(0)}(t) &= \frac{w_L(t)}{t} \sqrt{\frac{\pi}{L}} \begin{pmatrix} \mathbf{g}_F & 0 \\ 0 & -\mathbf{g}_f \end{pmatrix} \mathcal{F}_R^{(0)}(t) . \end{aligned} \quad (5.60)$$

In the case of the conventional RS model with constant fermion bulk masses  $c_f$ , as has been described in Section 2.2.3, the fermion profiles read to the lowest order

$$\mathcal{F}_L^{(0)}(t) = (F(\mathbf{c}_F)t^{c_F} \ 0)^T, \quad \mathcal{F}_R^{(0)}(t) = (0 \ F(\mathbf{c}_f)t^{c_f})^T, \quad (5.61)$$

where  $F(c)$  is the “zero-mode fermion profile” from (2.115), and  $\mathbf{c}$  are the diagonal  $3 \times 3$  bulk mass matrices. For the following choices of bulk mass parameters  $c = -0.38, -0.58, +0.34$ , and  $-0.84$ , the individual zero-mode fermion profiles in the conventional framework are plotted in Figure 5.8. It is essential in deriving the natural explanation mechanism for the four-dimensional fermion mass hierarchies that the magnitudes of these various fermion profiles show a strong hierarchical behaviour for  $\mathcal{O}(1)$ -differences between the bulk mass parameters  $c$ . In this connection, the small profile for  $c = -0.88$  accounts for a light lepton mass, whereas the profile for  $c = -0.38$  gives a mass for a quark of the second generation, and the IR-localized profile for  $c = +0.34$  can explain the heavy top quark mass. The explicit mechanism to derive the zero-mode fermion masses in the conventional RS model has been summarized in Subsection 2.2.3.

### 5.2.1 Framework with a flat extra dimension

For the case of a flat extra dimension, as discussed in Subsection 2.1.2 in the context of models with universal extra dimensions, the localizer mechanism was worked out in [257, 258]. In this case, the differential equation for the vev considerably simplifies, to [258]

$$\partial_{x_5} w(x_5) = -\lambda v^2 w(x_5) + \lambda w(x_5)^3, \quad (5.62)$$

with the boundary conditions,  $w(0) = w(L) = 0$ , where  $L$  is the size of the extra dimension. A solution for the limiting case  $L = \infty$  is given by a single kink,

$$w(x_5) = v \tanh \sqrt{\frac{\lambda}{2}} v x_5, \quad (5.63)$$

whereas for large, finite  $L^2 \gg \frac{1}{\lambda v^2}$ , it was possible to construct an approximate solution by a series of well-separated kinks [257, 258], as

$$w(x_5) \approx v \tanh \sqrt{\frac{\lambda}{2}} v (-L - x_5) \tanh \sqrt{\frac{\lambda}{2}} v x_5 \tanh \sqrt{\frac{\lambda}{2}} v (L - x_5). \quad (5.64)$$

This result for the vev has an odd behaviour at the boundaries of the extra dimension, as can be observed from Figure 5.9. Furthermore, the function can be approximated by a step function, assuming  $\lambda v^2 L \gg 1$  [257],

$$w(x_5) = u \epsilon(x_5), \quad \epsilon(x_5) = \begin{cases} +1 & 0 < x_5 < L \\ -1 & -L < x_5 < 0 \end{cases}. \quad (5.65)$$

In this way, the  $Z_2$ -odd, approximately constant bulk fermion mass terms of the conventional model are reproduced via the couplings of the fermions to the bulk vev.

In the case of a warped extra dimension, the differential equation complicates due to the warp factor in the kinetic terms of the scalar action, as given in (5.57).

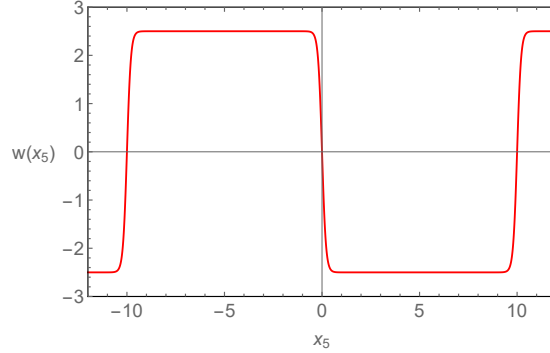


Figure 5.9: Plot of the approximate solution  $w(x_5)$ , derived in [257, 258], and given in (5.64), for  $v = 2.5$ ,  $L = 10$  and  $\lambda = 8$ , in a framework with a flat extra dimension.

### 5.2.2 Analytic solutions for $w_L(t)$

By fixing the parameters

$$\frac{\mu_L^2}{k^2} = \frac{32}{9}, \quad (5.66)$$

one can analytically solve the differential equation for the bulk vev in (5.57), where the solution reads

$$w_L(t) = \frac{2}{3} \sqrt{\frac{2}{\xi}} \left[ \tanh \left( \frac{2}{3} \ln(\alpha \cdot t) \right) + 1 \right] = \frac{4}{3} \sqrt{\frac{2}{\xi}} \cdot \frac{1}{1 + (\alpha t)^{-\frac{4}{3}}}. \quad (5.67)$$

The solution adopts the following values at the branes

$$w_L(\epsilon) = \frac{4}{3} \sqrt{\frac{2}{\xi}} \cdot \frac{(\alpha \epsilon)^{\frac{4}{3}}}{1 + (\alpha \epsilon)^{\frac{4}{3}}}, \quad w_L(1) = \frac{4}{3} \sqrt{\frac{2}{\xi}} \cdot \frac{(\alpha)^{\frac{4}{3}}}{1 + (\alpha)^{\frac{4}{3}}}. \quad (5.68)$$

Obviously, these are in contradiction with the boundary conditions in (5.56). In the  $\phi$ -coordinate, the equation of motion for the vev reads

$$\frac{1}{r^2} w_L''(\phi) - \frac{4k}{r} \operatorname{sgn}(\phi) w_L'(\phi) + \mu_L^2 w_L(\phi) - \frac{2\lambda_L}{r} e^{2kr\pi} w_L(\phi)^3 = 0, \quad (5.69)$$

which is fulfilled by the following solution (for the special case of  $\mu_L^2 = \frac{32}{9}k^2$ ),

$$w(\phi) = \frac{4}{3} k e^{-kr\pi} \sqrt{\frac{r}{\lambda_L}} \frac{\operatorname{sgn}(\phi)}{1 + \alpha^{-4/3} e^{\frac{4kr}{3}(\pi - |\phi|)}}. \quad (5.70)$$

The solution depends on the parameter  $\alpha$ , which is in principle arbitrary, but determines the shape of the solution. For the three parameter choices  $\alpha = 1, 1000, 10^{10}$ , the solutions are plotted in Figure 5.10. For these cases, the UV boundary condition is approximately fulfilled, whereas the functions remain constant on the IR brane.<sup>6</sup> For higher values of  $\alpha$ , a kink-like behaviour is observed. However, it is not possible to construct a series of well-separated kinks, repeatedly for

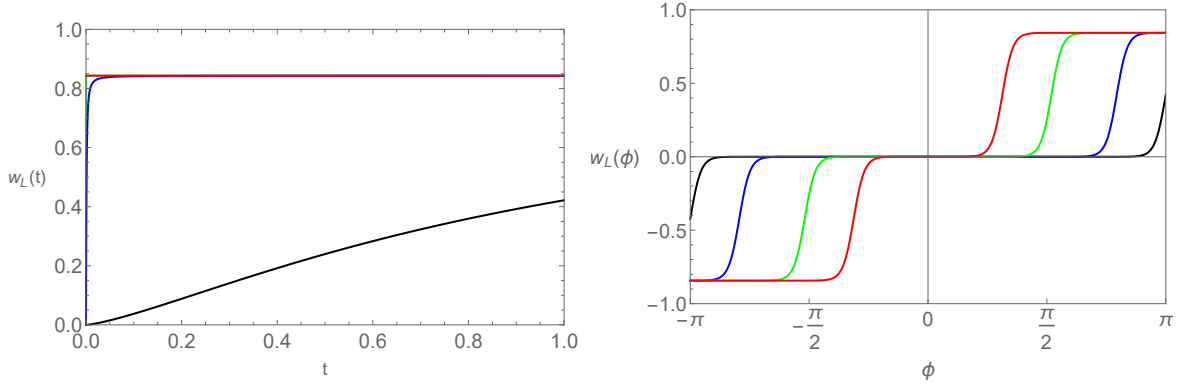


Figure 5.10: Plots of the analytic solutions for the vev  $w_L$ , in the  $t$ -coordinate on the left-hand side, and the  $\phi$ -coordinate on the right-hand side, for  $\xi = 5$ , and  $\alpha = 1$  (black curves),  $\alpha = 1000$  (blue curves),  $\alpha = 10^7$  (green curves), and  $\alpha = 10^{10}$  (red curves), respectively. The solutions decline to zero at the UV boundary in good approximation, whereas they remain constant at the IR boundary.

every half of the extra dimension, as has been shown before for the case of a flat extra dimension.

From the equations of motion in (5.60), one determines the following zero-mode fermion profiles to the lowest order, which are induced by the analytic solutions for the vev,

$$\mathcal{F}_L^{(0)}(t) = \begin{pmatrix} \left[1 + (\alpha t)^{\frac{4}{3}}\right]^{\mathbf{g}_F \sqrt{\frac{2\pi}{L\xi}}} \mathcal{N}_F \hat{a}_F \\ 0 \end{pmatrix}, \quad \mathcal{F}_R^{(0)}(t) = \begin{pmatrix} 0 \\ \left[1 + (\alpha t)^{\frac{4}{3}}\right]^{\mathbf{g}_f \sqrt{\frac{2\pi}{L\xi}}} \mathcal{N}_f \hat{a}_f \end{pmatrix}. \quad (5.71)$$

These profiles respect the boundary conditions for the fermions at the branes. Furthermore, the normalization condition for the fermion profiles gives

$$\mathcal{N}_{F,f} = \frac{1}{\sqrt{\int_{\epsilon}^1 dt \left[1 + (\alpha t)^{\frac{4}{3}}\right]^{2\mathbf{g}_{F,f} \sqrt{\frac{2\pi}{L\xi}}}}}. \quad (5.72)$$

The question is whether it is possible to reproduce hierarchical zero-mode fermion profiles in this framework, similar to the conventional model. For  $\alpha = 10^7$ ,  $\xi = 5$ , and the coupling choices  $g = -5, -2.5, -1, +1$ , the results derived for the zero-mode fermion profiles are plotted in Figure 5.11. Intriguingly, these results look very similar to the profiles of the conventional model with the constant bulk fermion masses, plotted in Figure 5.8, which provide a hierarchical behaviour in the magnitudes. All coupling choices for  $g$  are of the same order of magnitude, although one order of magnitude larger than for the case of the conventional profiles. Solely, the parameter  $\alpha$  is chosen to have a high value. It turns out that for smaller values of  $\alpha$ , it is not possible to

<sup>6</sup>It should be noticed that the Dirac fermion mass terms,  $m\bar{\psi}\psi = m(\bar{F}F + \bar{f}f) = m(\bar{F}_L F_R + \bar{F}_R F_L + \bar{f}_L f_R + \bar{f}_R f_L)$ , inevitably vanish on both branes, following from the fermion boundary conditions that are chosen such that  $F_R(t_i) = f_L(t_i) = 0$  for  $t_i = \epsilon, 1$ , as presented before.

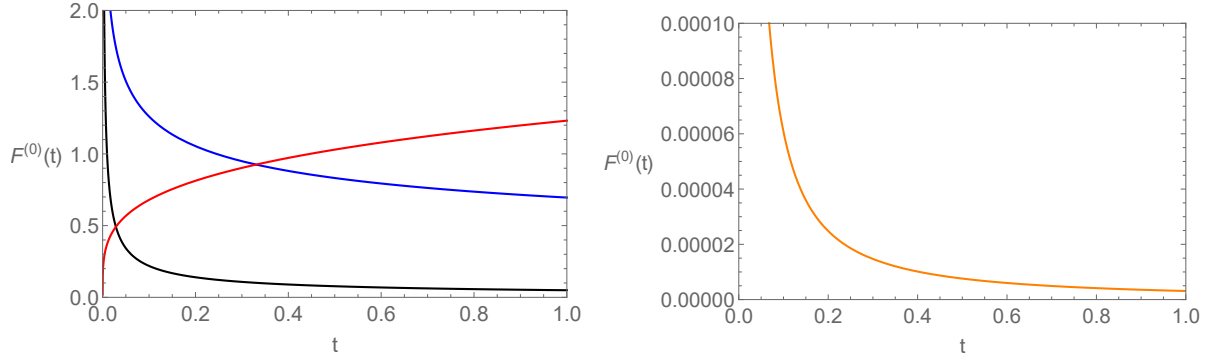


Figure 5.11: Zero-mode fermion profiles implied by the analytic solutions for the vev in (5.67), for  $\alpha = 10^7$ ,  $\xi = 5$ , and  $g = -5$  (orange curve),  $-2.5$  (black curve),  $-1$  (blue curve), and  $+1$  (red curve), respectively. For these parameter choices, a hierarchical behaviour for the profiles can be observed.

derive hierarchical zero-mode fermion profiles. In Appendix D.2, the zero-mode fermion profiles are plotted for  $\alpha = 1000$  and  $\alpha = 1$  for the same coupling choices as used in Figure 5.11. In principle, it can be observed that the magnitudes of the fermion profiles are less hierarchical for a lower value of the parameter  $\alpha$ .

Moreover, by fixing the input parameter values, one can also determine numeric solutions for the bulk vev  $w_L(t)$ . Some numeric solutions are shown in Appendix D.2.

### 5.2.3 Intermediate summary

The origin of the  $Z_2$ -odd bulk fermion masses can possibly be explained by couplings of the fermions to the vev of an odd bulk scalar. The bulk fermion masses are a crucial ingredient of the RS model to explain the mass splitting of the zero-mode fermions, as has been shown in the last paragraph of Section 2.2.3. However, the defining differential equation for the bulk scalar vev has a complicated non-linear behaviour, making it challenging to determine solutions compatible to the boundary conditions for a  $Z_2$ -odd field. For the special parameter choice  $\mu_L^2/k^2 = 32/9$ , we have been able to determine analytic solutions that approximately vanish at the UV boundary. The solutions depend on an arbitrary parameter  $\alpha$ , which has to be large  $\sim 10^7$  to derive zero-mode fermion profiles with a hierarchical behaviour, which is necessary to explain the mass splitting of the fermions. In addition, it is possible to solve the differential equation for the vev numerically, where it has turned out that the solution must reproduce a kink-like behaviour in the  $t$ -coordinate in order to have hierarchical zero-mode fermion profiles. For other choices of parameters, the resulting zero-mode fermion profiles cannot reproduce the necessary hierarchical behaviour.

Therefore, most parts of this intriguing, but challenging project of finding the “localizer” mechanism for the bulk fermions of the RS model, by means of an odd bulk scalar, has to remain for future work.

# Chapter 6

## Summary and Conclusions

The discovery of the Higgs boson at the LHC in summer 2012 finally proved the existence of the last missing element of the SM of particle physics [67, 68]. Indeed, the couplings of this new particle are close to those predicted by the SM [200–202]. As a consequence, an explanation for the gauge hierarchy problem, inevitably arising in scalar sectors in or additionally included to the SM, is demanded more than ever. The precise determinations and experimental measurements of Higgs interaction strengths with SM particles provide important tools to test different new-physics approaches to the gauge hierarchy problem and to distinguish between different ones. In this thesis, concepts and implications of scalar sectors have been investigated in a framework of new physics beyond the SM with a small and warped extra dimension: the RS model.

In the first chapter of the thesis, the main features of the SM have been dealt with. The most pressing open questions have been discussed, such as the gauge hierarchy problem, as well as two approaches to this problem, provided by theories of new physics. Furthermore, in the second chapter, theories with extra dimensions and the main features of the minimal RS model with a bulk-Higgs localization have been dealt with. In this context, the bulk-Higgs field, as considered in this thesis, has a profile function that depends on the extra dimensional coordinate  $t = \epsilon e^{k|x_5|}$  with a power of  $(1 + \beta)$  [2, 154, 157]. The sectors of the gauge fields and the spontaneous symmetry breaking mechanism have been illustrated, and it has been shown that, in the bulk-Higgs RS model, the gauge hierarchy problem is mitigated to a very small amount of fine-tuning that is still necessary to compute the correct Higgs mass. The sector of physical scalar fields, exclusively present in the bulk-Higgs RS model, and the realization of the fermion sector have been displayed. In addition, a scenario has been discussed where the Higgs sector is implemented on, or very close to, the IR brane. After that, the main characteristics of the RS model with a custodial bulk gauge symmetry have been presented. In this context, the S, T, U parameters by Peskin and Takeuchi [82] have been derived at the tree level in the different RS scenarios, and the excluded parameter regions implied on the KK mass scale  $M_{KK}$ , which is the scale of the lightest additional particles predicted by the RS model, have been summarized.

Then, in Chapter 3 of the thesis, a set of five-dimensional propagator functions has been presented in the mixed momentum-position representation [188, 189, 196–199]. With the help of these propagator functions, one has been able to compute the various Higgs production and decay processes in the RS model with a minimal bulk gauge group similar to the SM and a bulk-Higgs field. The computations have been done and explained in detail in Chapter 4. In an extra-dimensional model, modifications of the effective, four-dimensional Feynman rules arise

due to integrals over the particles profiles in the extra dimension, which modify the tree-level Higgs couplings to fermions and gauge bosons. The Higgs couplings to gluons and photons are induced at the one-loop order, where the largest technical differences, compared to the SM, are infinite summations over virtual KK particle states contributing in loops. These summations can be related to the five-dimensional propagator functions. A concise and clear result has been obtained for the tree-level Higgs couplings to fermions and the loop contributions of KK fermions, after having approximated the 15 different fermion bulk-mass parameters  $c_f$  by the value  $-1/2$ , respectively. For the bulk-Higgs localization parameter, the limit  $\beta \rightarrow \infty$  could be smoothly performed, giving results computed in a narrow bulk-Higgs scenario, *e.g.* in [2,3,5,171,172,212]. In these references, the narrow bulk-Higgs state was described by a normalized distribution  $\delta^\eta(t-1)$  of width  $\eta \ll 1$ , in contrast to the bulk-Higgs profile used in this thesis. Furthermore, the contributions of W bosons and scalars to the Higgs decay into two photons have been computed in the bulk-Higgs RS model, as well as the corrections to the decay rates  $h \rightarrow WW^*$  and  $h \rightarrow ZZ^*$ . All Higgs couplings to gauge bosons and fermions, which form the Higgs production rates of gluon fusion, vector boson fusion and Higgsstrahlung, and the Higgs decay rates into  $\gamma\gamma$ ,  $WW^*$ ,  $ZZ^*$ ,  $b\bar{b}$  and  $\tau\bar{\tau}$  final states, have been determined. Analytic results, valid to the first order of  $v^2/M_{KK}^2$ , could be derived for all the different Higgs processes, which visualise the first, significant corrections in the RS model compared to the SM.

The results for the various Higgs processes have been numerically and graphically evaluated in dependence of the KK mass scale  $M_{KK}$ , the Yukawa matrices  $\mathbf{Y}_f$ , and the bulk-Higgs localization parameter  $\beta$ . In this connection, enhanced predictions, compared to the SM prediction, have been observed for the gluon fusion cross sections. On the contrary, the other Higgs production rates and all the decay rates are suppressed compared to the SM. The largest contributions to the processes are caused by virtual KK fermions, in correspondence with [2,3,5,151,152,154,171,193]. The physical KK scalars of the bulk Higgs RS model only give very small contributions to the Higgs decay into two photons. Also, the contributions from W bosons to this process have a small effect compared to the SM. Consistently, it has been detected that the predictions for all the Higgs processes lie the closer to the SM predictions the lower the value of  $\beta$  is and the stronger the bulk-Higgs field is located in the extra dimension. Besides, the results for  $\beta = 10$  lie already very close to the results for the very narrow bulk-Higgs scenario, corresponding to  $\beta \rightarrow \infty$ .

The predictions for the LHC signal strengths of the Higgs decays into two photon, gauge boson or tau lepton states are consistently augmented compared to the respective SM predictions. The augmentations result from the dominant, augmented contributions of the gluon fusion cross sections, which are extenuated by the negative contributions stemming from the other Higgs productions, the Higgs decay rates, and the corrections to the total Higgs decay width. For the signal strengths of the Higgs decays into a pair of b quarks, only the Higgsstrahlung's production process that causes suppressed predictions compared to the SM has been included. Remarkably, the experimental results, reported by ATLAS and CMS [6], agree with the tendencies of the RS predictions to enhanced or suppressed rates compared to the SM. For that reason, it has not been possible to constrain the parameter space of the bulk-Higgs RS model in any significant manner by means of the evaluations, comparing the RS predictions with the experimental results.

As an outlook, the various Higgs couplings in the bulk-Higgs RS model have been compared to the possible experimental capabilities of a future, upgraded ILC facility [214–218]. Even in this case, it might be very challenging to constrain the parameter space of the bulk-Higgs RS



model in a significant way, also if all measurements would prove the SM's predictions.

In contrast to these outcomes of the bulk-Higgs RS scenario, previous investigations of Higgs processes in a brane-Higgs scenario of the RS model gave suppressed predictions for the cross sections of the gluon fusion, which dominate the signal strengths of the various Higgs decay rates. As a consequence, even the parameter space of the custodial RS model can be constrained very strongly, as proven in [2–4]. Accordingly, one may conclude that, as well as having the most natural Higgs setting and predicting reduced exclusion bounds by the Peskin-Takeuchi parameters, also the examinations of the Higgs processes favour the bulk-Higgs scenario of the RS model. This framework provides a compelling alternative to the complex RS model with a custodial protection mechanism [151, 174–176], and in fact might appear to be the most plausible and interesting scenario of the RS model.

In a second part of the thesis, the analyses have been enlarged to explain the temporarily reported di-photon anomaly, seen in first data from Run 2 of the LHC, performed at  $\sqrt{s} = 13$  TeV [8, 9, 224, 226]. Unfortunately, the excess did not pass future verifications, indicating that it resulted from a statistical fluctuation [231, 232]. Alternatively, and most likely, it could have been created by the decay of a new scalar boson with a mass of 750 GeV. For this reason, the framework of the RS model has been extended by a single, new scalar field, and the anomaly has been identified with the decay of its first KK resonance [7]. It has been able to especially well explain the di-photon signal in the framework of the custodial RS model [151, 174–176], for  $\mathcal{O}(1)$ -couplings and KK masses compatible to electroweak precision tests. But, also the framework with a minimal bulk gauge group has been suitable for explaining the excess. The Higgs localization in the extra dimension has been irrelevant in these evaluations since the processes have been considered for  $v \ll m_S^2$ , where the significant effects have been scaling with  $m_S^2/M_{KK}^2$ . The various  $S$  decay rates into  $gg, \gamma\gamma, WW, ZZ, Z\gamma, t\bar{t}, hh$  and  $t\bar{t}h$  final states have been computed, and the exclusion bounds implied by Run 1 measurements of the LHC have been derived, and have been taken into account in the evaluations. In addition, the effects of possible Higgs portal couplings on the production and decay rates of the new scalar  $S$  have been determined. In this case, the excluded parameter regions, following from Run 1 searches, have been detected to be more significant.

Furthermore, a mechanism can be found to explain the origin of the mass differences of the SM fermions by coupling the fermions to the vev of a similar, new bulk scalar field, as considered for the di-photon excess [257, 258]. Such a framework has to some extent been explored in the last section of Chapter 5, but there remain many more features to be investigated in future analyses.

Altogether, calculations of scalar production and decay processes, to be tested at present-day experiments, are important tools to investigate new approaches of physics to the gauge hierarchy problem. In this context, the RS model with a small and warped extra dimension forms one of the most suitable frameworks of research in this field, and the thesis, too, would like to contribute to this task by its computations and analysis.



# Appendix A

## The Randall-Sundrum Model

### A.1 Notations for the extradimensional coordinate

In the following, a short compendium of relations between the original five-dimensional coordinate  $x_5 = r\phi$  and the dimensionless coordinate  $t = \epsilon e^{kr|\phi|}$  [155], which is used throughout this thesis, is given. The  $t$  coordinate reflects the orbifold compactification of the extra dimension, where the UV boundary at  $x_5 = 0$  transforms to  $\epsilon = e^{-kr\pi}$ , and the IR boundary at  $x_5 = \pm r\pi$  transforms to  $t = e^{-kr\pi} e^{kr\pi} = 1$ . The non-linear correlation between the  $x_5$  or  $\phi$  coordinates and the  $t$  coordinate is plotted in Figure A.1. The  $t$  coordinate effectively maps the inverse warping of the space along the extra dimension, getting a sizeable amount only in the last region of the orbifold, close to the IR brane. Partial derivatives transform according to

$$\frac{\partial}{\partial x_5} \rightarrow \frac{1}{r} \frac{\partial}{\partial \phi} \rightarrow \text{sgn}(\phi) kt \frac{\partial}{\partial t}, \quad (\text{A.1})$$

between the coordinates. For the integration over the  $x_5$ -coordinate, there is [150]

$$\int_{-r\pi}^{r\pi} dx_5 = \int_{-r\pi}^0 dx_5 + \int_0^{r\pi} dx_5 = -\frac{\pi r}{L} \int_1^\epsilon \frac{dt}{t} + \frac{\pi r}{L} \int_\epsilon^1 \frac{dt}{t} = \frac{2\pi r}{L} \int_\epsilon^1 \frac{dt}{t}, \quad (\text{A.2})$$

since  $\frac{dt}{dx_5} = \text{sgn}(x_5) \cdot kt$ . The metric reads in the two notations

$$ds^2 = G_{MN} dx^M dx^N = e^{-2kr|\phi|} \eta_{\mu\nu} dx^\mu dx^\nu - r^2 d\phi^2 = \frac{\epsilon^2}{t^2} \left( \eta_{\mu\nu} dx^\mu dx^\nu - \frac{1}{M_{KK}^2} dt^2 \right), \quad (\text{A.3})$$

such that the matrix notation for the metric is

$$G_{MN} = \begin{pmatrix} e^{-2kr|\phi|} \eta_{\mu\nu} & 0 \\ 0 & -r^2 \end{pmatrix}, \quad G^{MN} = \begin{pmatrix} e^{2kr|\phi|} \eta^{\mu\nu} & 0 \\ 0 & -\frac{1}{r^2} \end{pmatrix}, \quad \sqrt{|G|} = e^{-4kr|\phi|} r, \quad (\text{A.4})$$

in the  $\phi$  coordinate, and

$$G_{MN} = \begin{pmatrix} \frac{\epsilon^2}{t^2} \eta_{\mu\nu} & 0 \\ 0 & -\frac{1}{k^2 t^2} \end{pmatrix}, \quad G^{MN} = \begin{pmatrix} \frac{t^2}{\epsilon^2} \eta^{\mu\nu} & 0 \\ 0 & -k^2 t^2 \end{pmatrix}, \quad \sqrt{|G|} = \frac{\epsilon^4 \pi r}{t^5 L} \quad (\text{A.5})$$

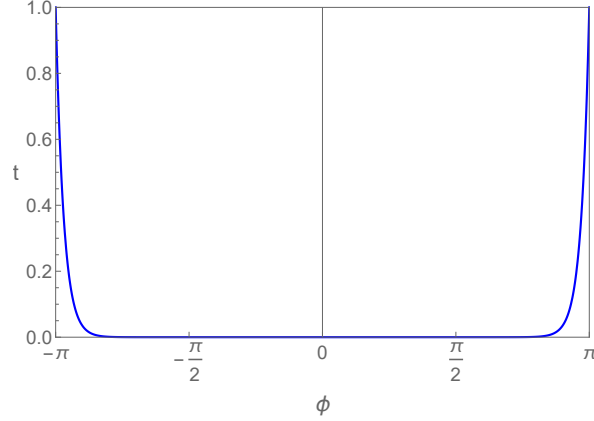


Figure A.1: A sketch of the relation between the  $\phi = \frac{x_5}{r}$  and the  $t = \epsilon e^{k|x_5|}$  coordinates. The  $t$  coordinate effectively maps the inverse warping of the space along the extra dimension, compactified on an orbifold, in this way getting a sizeable amount only in the last region of the orbifold, close to the IR brane.

in the  $t$  coordinate. Considering the brane-localized potentials  $V_{UV}$  and  $V_{IR}$  with the original Lagrangian

$$\mathcal{L}_{\text{branes}} = \int_{-r\pi}^{r\pi} dx_5 e^{-4\sigma(\phi)} [-V_{UV}\delta(x_5) - V_{IR}\delta(|x_5| - r\pi)] , \quad (\text{A.6})$$

the  $\delta$ -functions can be transformed according to

$$\delta(x_5) \rightarrow k\epsilon\delta(t - \epsilon) , \quad \delta(|x_5| - r\pi) \rightarrow k\delta(t - 1) . \quad (\text{A.7})$$

However, a symmetric integration interval is needed for the integration over the  $\delta$ -function. For that reason, the full transformation reads

$$\mathcal{L}_{\text{branes}} = \frac{\pi r}{L} \int_{\epsilon}^1 \frac{dt}{t} \frac{\epsilon^4}{t^4} [-M_{KK}\delta(t - \epsilon)V_{UV} - k\delta(t - 1)V_{IR}] , \quad (\text{A.8})$$

where there is no factor 2 compared to the transformation shown in (A.2) before.

# Appendix B

## Five-Dimensional Propagator Functions

### B.1 System of equations involved in the calculation of the fermion propagator

Here, the determination of the coefficient matrices  $\mathbf{C}_i^{>,<}$  of the five-dimensional fermion propagator function, derived in Section 3.3.1, is presented. These coefficient matrices are defined by a system of equations resulting from the boundary conditions at the branes and the jump condition for the propagator function, given in (3.56), (3.60) and (3.61). In the following, we name *•equation I*:

$$-\mathbf{C}_1^< = t'^{c_F} \cdot \left[ \frac{\mathbf{1}}{M_{KK}} + \frac{v}{\sqrt{2}M_{KK}} \mathbf{Y}^A(t') \cdot (\mathbf{C}_3^> - \mathbf{C}_3^<) \right], \quad (\text{B.1})$$

*•equation II*:

$$\mathbf{C}_3^> = \mathbf{C}_3^< - \frac{v}{\sqrt{2}M_{KK}} t'^{-c_f} \mathbf{Y}^{B\dagger}(t') \cdot \mathbf{C}_1^<, \quad (\text{B.2})$$

and *•equation III*:

$$\mathbf{C}_3^< = \frac{\sqrt{2}M_{KK}}{v} \cdot \left[ -(\mathbf{Y}^E)^{-1} + \frac{v^2}{4M_{KK}^2} (-\mathbf{Y}^{C\dagger} + (\mathbf{Y}^E)^{-1} \mathbf{Y}^G) \right] \cdot \mathbf{C}_1^<. \quad (\text{B.3})$$

By inserting *equation I* into *equation II*, one gets:

$$\begin{aligned} \mathbf{C}_3^> &= \mathbf{C}_3^< + \frac{v}{\sqrt{2}M_{KK}} t'^{-c_f} \mathbf{Y}^{B\dagger}(t') t'^{c_F} \cdot \left[ \frac{\mathbf{1}}{M_{KK}} + \frac{v}{\sqrt{2}M_{KK}} \mathbf{Y}^A(t') \cdot (\mathbf{C}_3^> - \mathbf{C}_3^<) \right], \\ \Leftrightarrow \left[ \mathbf{1} - \frac{v^2}{2M_{KK}^2} t'^{-c_f} \mathbf{Y}^{B\dagger}(t') t'^{c_F} \mathbf{Y}^A(t') \right] \cdot \mathbf{C}_3^> &= \left[ \mathbf{1} - \frac{v^2}{2M_{KK}^2} t'^{-c_f} \mathbf{Y}^{B\dagger}(t') t'^{c_F} \mathbf{Y}^A(t') \right] \cdot \mathbf{C}_3^< \\ &+ \frac{v}{\sqrt{2}M_{KK}^2} t'^{-c_f} \mathbf{Y}^{B\dagger}(t') t'^{c_F}, \\ \Leftrightarrow \mathbf{C}_3^< &= \mathbf{C}_3^> - \frac{v}{\sqrt{2}M_{KK}^2} t'^{-c_f} \mathbf{Y}^{B\dagger}(t') t'^{c_F}. \end{aligned} \quad (\text{B.4})$$

And by setting *equation I* into *equation III*, one derives:

$$\begin{aligned}
\mathbf{C}_3^{\leq} &= \frac{\sqrt{2}M_{KK}}{v} \left[ -(\mathbf{Y}^E)^{-1} + \frac{v^2}{4M_{KK}^2} (-\mathbf{Y}^{C\dagger} + (\mathbf{Y}^E)^{-1}\mathbf{Y}^G) \right] \cdot \mathbf{C}_1^{\leq} \\
&\stackrel{eq.I}{=} \left[ (\mathbf{Y}^E)^{-1} + \frac{v^2}{4M_{KK}^2} (\mathbf{Y}^{C\dagger} - (\mathbf{Y}^E)^{-1}\mathbf{Y}^G) \right] t'^{c_F} \cdot \left[ \frac{\sqrt{2}}{v} \mathbf{1} + \mathbf{Y}^A(t') (\mathbf{C}_3^{\geq} - \mathbf{C}_3^{\leq}) \right] \\
&= (\mathbf{Y}^E)^{-1} t'^{c_F} \frac{\sqrt{2}}{v} + \frac{v^2}{4M_{KK}^2} [\mathbf{Y}^{C\dagger} - (\mathbf{Y}^E)^{-1}\mathbf{Y}^G] t'^{c_F} \frac{\sqrt{2}}{v} \\
&+ \left[ (\mathbf{Y}^E)^{-1} t'^{c_F} \mathbf{Y}^A(t') + \frac{v^2}{4M_{KK}^2} (\mathbf{Y}^{C\dagger} - (\mathbf{Y}^E)^{-1}\mathbf{Y}^G) t'^{c_F} \mathbf{Y}^A(t') \right] \cdot \mathbf{C}_3^{\geq} \\
&- \left[ (\mathbf{Y}^E)^{-1} t'^{c_F} \mathbf{Y}^A(t') + \frac{v^2}{4M_{KK}^2} (\mathbf{Y}^{C\dagger} - (\mathbf{Y}^E)^{-1}\mathbf{Y}^G) t'^{c_F} \mathbf{Y}^A(t') \right] \cdot \mathbf{C}_3^{\leq} .
\end{aligned} \tag{B.5}$$

By combining the upper two results, one finds:

$$\begin{aligned}
\mathbf{C}_3^{\geq} - \frac{v}{\sqrt{2}M_{KK}^2} t'^{-c_f} \mathbf{Y}^{B\dagger}(t') t'^{c_F} &= (\mathbf{Y}^E)^{-1} t'^{c_F} \frac{\sqrt{2}}{v} + \frac{v^2}{4M_{KK}^2} [\mathbf{Y}^{C\dagger} - (\mathbf{Y}^E)^{-1}\mathbf{Y}^G] t'^{c_F} \frac{\sqrt{2}}{v} \\
&+ \left[ (\mathbf{Y}^E)^{-1} t'^{c_F} \mathbf{Y}^A(t') + \frac{v^2}{4M_{KK}^2} (\mathbf{Y}^{C\dagger} - (\mathbf{Y}^E)^{-1}\mathbf{Y}^G) t'^{c_F} \mathbf{Y}^A(t') \right] \cdot \mathbf{C}_3^{\geq} \\
&- \left[ (\mathbf{Y}^E)^{-1} t'^{c_F} \mathbf{Y}^A(t') + \frac{v^2}{4M_{KK}^2} (\mathbf{Y}^{C\dagger} - (\mathbf{Y}^E)^{-1}\mathbf{Y}^G) t'^{c_F} \mathbf{Y}^A(t') \right] \cdot \left[ \mathbf{C}_3^{\geq} - \frac{v}{\sqrt{2}M_{KK}^2} t'^{-c_f} \mathbf{Y}^{B\dagger}(t') t'^{c_F} \right] , \\
&\Leftrightarrow \\
\mathbf{C}_3^{\geq} &= (\mathbf{Y}^E)^{-1} t'^{c_F} \frac{\sqrt{2}}{v} + \frac{v^2}{2M_{KK}^2} \frac{\sqrt{2}}{v} t'^{-c_f} \mathbf{Y}^{B\dagger}(t') t'^{c_F} \\
&+ \frac{v^2}{4M_{KK}^2} [\mathbf{Y}^{C\dagger} - (\mathbf{Y}^E)^{-1}\mathbf{Y}^G] t'^{c_F} \frac{\sqrt{2}}{v} + \frac{v^2}{2M_{KK}^2} \frac{\sqrt{2}}{v} (\mathbf{Y}^E)^{-1} t'^{c_F} \mathbf{Y}^A(t') t'^{-c_f} \mathbf{Y}^{B\dagger}(t') t'^{c_F} \\
&= (\mathbf{Y}^E)^{-1} t'^{c_F} \frac{\sqrt{2}}{v} + \frac{v^2}{2M_{KK}^2} \frac{\sqrt{2}}{v} \left[ \left( \mathbf{1} + (\mathbf{Y}^E)^{-1} t'^{c_F} \mathbf{Y}^A(t') \right) t'^{-c_f} \mathbf{Y}^{B\dagger}(t') t'^{c_F} \right. \\
&\left. + \frac{1}{2} (\mathbf{Y}^{C\dagger} - (\mathbf{Y}^E)^{-1}\mathbf{Y}^G) t'^{c_F} \right] .
\end{aligned} \tag{B.6}$$

In a similar manner, we name *equation I'*:

$$\mathbf{C}_4^{\leq} = \frac{\sqrt{2}M_{KK}}{v} \cdot \left[ -(\mathbf{Y}^E)^{-1} + \frac{v^2}{4M_{KK}^2} (-\mathbf{Y}^{C\dagger} + (\mathbf{Y}^E)^{-1}\mathbf{Y}^G) \right] \cdot \mathbf{C}_2^{\leq} , \tag{B.7}$$

and *equation II'*:

$$-\mathbf{C}_2^{\leq} = \frac{v}{\sqrt{2}M_{KK}} t'^{c_F} \mathbf{Y}^A(t') \cdot (\mathbf{C}_4^{\geq} - \mathbf{C}_4^{\leq}) , \tag{B.8}$$

as well as  $\bullet$ equation III':

$$\mathbf{C}_4^> = \mathbf{C}_4^< - \frac{v}{\sqrt{2}M_{KK}} t'^{-\mathbf{c}_f} \mathbf{Y}^{B\dagger}(t') \cdot \mathbf{C}_2^< + \frac{t'^{-\mathbf{c}_f}}{M_{KK}} . \quad (\text{B.9})$$

One can put *equation II'* into *equation I'* and obtains:

$$\mathbf{C}_4^< = (\mathbf{Y}^E)^{-1} t'^{\mathbf{c}_F} \mathbf{Y}^A(t') \cdot (\mathbf{C}_4^> - \mathbf{C}_4^<) , \Leftrightarrow \left( \mathbf{1} + (\mathbf{Y}^E)^{-1} t'^{\mathbf{c}_F} \mathbf{Y}^A(t') \right) \cdot \mathbf{C}_4^< = (\mathbf{Y}^E)^{-1} t'^{\mathbf{c}_F} \mathbf{Y}^A(t') \cdot \mathbf{C}_4^> . \quad (\text{B.10})$$

By combining this result with *equation III'*, one finds up to  $\mathcal{O}\left(\frac{v}{M_{KK}}\right)$ :

$$\mathbf{C}_4^> = \mathbf{C}_4^< + \frac{t'^{-\mathbf{c}_f}}{M_{KK}} , \Leftrightarrow \mathbf{C}_4^> = \left[ \mathbf{1} + (\mathbf{Y}^E)^{-1} t'^{\mathbf{c}_F} \mathbf{Y}^A(t') \right] \frac{t'^{-\mathbf{c}_f}}{M_{KK}} . \quad (\text{B.11})$$

By inserting *equation II'* into *equation III'*, one obtains

$$\mathbf{C}_4^> = \mathbf{C}_4^< + \frac{v^2}{2M_{KK}^2} t'^{-\mathbf{c}_f} \mathbf{Y}^{B\dagger}(t') t'^{\mathbf{c}_F} \mathbf{Y}^A(t') (\mathbf{C}_4^> - \mathbf{C}_4^<) + \frac{t'^{-\mathbf{c}_f}}{M_{KK}} , \quad (\text{B.12})$$

and by using the result for  $\mathbf{C}_4^>$  in (B.11), one gets

$$\mathbf{C}_4^< = \frac{1}{M_{KK}} (\mathbf{Y}^E)^{-1} t'^{\mathbf{c}_F} \mathbf{Y}^A(t') t'^{-\mathbf{c}_f} . \quad (\text{B.13})$$

Then, by using *equation II'*, one obtains

$$\mathbf{C}_2^< = -\frac{v}{\sqrt{2}M_{KK}^2} t'^{\mathbf{c}_F} \mathbf{Y}^A(t') t'^{-\mathbf{c}_f} . \quad (\text{B.14})$$

Again, by inserting *equation I* into *equation II*, one finds

$$\begin{aligned} \mathbf{C}_3^> &= \mathbf{C}_3^< + \frac{v^2}{2M_{KK}^2} t'^{-\mathbf{c}_f} \mathbf{Y}^{B\dagger}(t') t'^{\mathbf{c}_F} \left[ \frac{\sqrt{2}}{v} \mathbf{Y}^A(t') (\mathbf{C}_3^> - \mathbf{C}_3^<) \right] , \quad \Leftrightarrow \\ \mathbf{C}_3^< &= \mathbf{C}_3^> - \frac{v^2}{2M_{KK}^2} \frac{\sqrt{2}}{v} t'^{-\mathbf{c}_f} \mathbf{Y}^{B\dagger}(t') t'^{\mathbf{c}_F} \\ &= (\mathbf{Y}^E)^{-1} t'^{\mathbf{c}_F} \frac{\sqrt{2}}{v} + \frac{v^2}{2M_{KK}^2} \frac{\sqrt{2}}{v} \left[ (\mathbf{Y}^E)^{-1} t'^{\mathbf{c}_F} \mathbf{Y}^A(t') t'^{-\mathbf{c}_f} \mathbf{Y}^{B\dagger}(t') t'^{\mathbf{c}_F} + \frac{1}{2} (\mathbf{Y}^{C\dagger} - (\mathbf{Y}^E)^{-1} \mathbf{Y}^G) t'^{\mathbf{c}_F} \right] , \end{aligned} \quad (\text{B.15})$$

and from *equation I*, one derives

$$\mathbf{C}_1^< = -\frac{t'^{\mathbf{c}_F}}{M_{KK}} + \dots . \quad (\text{B.16})$$

Altogether, the two solutions  $\Delta_{RL}^<(t, t'; 0)$  and  $\Delta_{RL}^>(t, t'; 0)$  read up to the order  $\mathcal{O}\left(\frac{v^3}{M_{KK}^3}\right)$ :

$$\begin{aligned} \Delta_{RL}^<(t, t'; 0) = & \left( \begin{array}{cc} -\frac{1}{M_{KK}} \left[ \left(\frac{t'}{t}\right)^{\mathbf{c}_F} + \mathbf{Y}^A(t)(\mathbf{Y}^E)^{-1}t'^{\mathbf{c}_F} \right] & -\frac{v}{\sqrt{2}M_{KK}^2} \left[ \left(\frac{t'}{t}\right)^{\mathbf{c}_F} + \mathbf{Y}^A(t)(\mathbf{Y}^E)^{-1}t'^{\mathbf{c}_F} \right] \mathbf{Y}^A(t')t'^{-\mathbf{c}_f} \\ t^{\mathbf{c}_f}(\mathbf{Y}^E)^{-1}t'^{\mathbf{c}_F} \frac{\sqrt{2}}{v} + \frac{v}{\sqrt{2}M_{KK}^2} [\mathbf{Y}^{B\dagger}(t)t'^{\mathbf{c}_F} \\ + \frac{1}{2}(-\mathbf{Y}^{B\dagger}(t)\mathbf{Y}^E + \mathbf{Y}^{F\dagger}(t))(\mathbf{Y}^E)^{-1}t'^{\mathbf{c}_F} \\ + t^{\mathbf{c}_f}(\mathbf{Y}^E)^{-1}t'^{\mathbf{c}_F}\mathbf{Y}^A(t')t'^{-\mathbf{c}_f}\mathbf{Y}^{B\dagger}(t')t'^{\mathbf{c}_F} \\ + \frac{1}{2}t^{\mathbf{c}_f}(\mathbf{Y}^{C\dagger} - (\mathbf{Y}^E)^{-1}\mathbf{Y}^G)t'^{\mathbf{c}_F}] & \frac{1}{M_{KK}} t^{\mathbf{c}_f}(\mathbf{Y}^E)^{-1}t'^{\mathbf{c}_F}\mathbf{Y}^A(t')t'^{-\mathbf{c}_f} \end{array} \right), \\ \Delta_{RL}^>(t, t'; 0) = & \left( \begin{array}{cc} -\frac{1}{M_{KK}} \mathbf{Y}^A(t)(\mathbf{Y}^E)^{-1}t'^{\mathbf{c}_F} & -\frac{v}{\sqrt{2}M_{KK}^2} \mathbf{Y}^A(t) [\mathbf{1} + (\mathbf{Y}^E)^{-1}t'^{\mathbf{c}_F}\mathbf{Y}^A(t')] t'^{-\mathbf{c}_f} \\ t^{\mathbf{c}_f}(\mathbf{Y}^E)^{-1}t'^{\mathbf{c}_F} \frac{\sqrt{2}}{v} \\ + \frac{v}{\sqrt{2}M_{KK}^2} \left[ \frac{1}{2}(-\mathbf{Y}^{B\dagger}(t)\mathbf{Y}^E + \mathbf{Y}^{F\dagger}(t))(\mathbf{Y}^E)^{-1}t'^{\mathbf{c}_F} \right. \\ \left. + \frac{t^{\mathbf{c}_f}}{2}(\mathbf{Y}^{C\dagger} - (\mathbf{Y}^E)^{-1}\mathbf{Y}^G)t'^{\mathbf{c}_F} \right. \\ \left. t^{\mathbf{c}_f}(\mathbf{1} + (\mathbf{Y}^E)^{-1}t'^{\mathbf{c}_F}\mathbf{Y}^A(t'))t'^{-\mathbf{c}_f}\mathbf{Y}^{B\dagger}(t')t'^{\mathbf{c}_F} \right] & \frac{1}{M_{KK}} \left[ \left(\frac{t'}{t}\right)^{\mathbf{c}_f} + t^{\mathbf{c}_f}(\mathbf{Y}^E)^{-1}t'^{\mathbf{c}_F}\mathbf{Y}^A(t')t'^{-\mathbf{c}_f} \right] \end{array} \right). \end{aligned} \tag{B.17}$$

With the help of these results, analytic expressions can be determined for the sum over the KK fermion tower in the calculations of the loop-induced Higgs production and decay processes, as presented in Chapter 3 of this thesis.



# Appendix C

## Higgs Productions and Decays

### C.1 Feynman parameter integral, and loop form factors of Higgs couplings

In the calculation of the W boson contribution to the Higgs decay into two photons, presented in 4.1.2, the following Feynman parameter integral appears

$$\begin{aligned} \int_0^1 dz \operatorname{arctanh}(\sqrt{1-z}) \frac{1 - \frac{z}{2}}{\tau_W - z} &= \int_0^1 dz \operatorname{arctanh}(\sqrt{1-z}) \left( \frac{1 - \frac{\tau_W}{2}}{\tau_W - z} + \frac{1}{2} \right) \\ &= \left( 1 - \frac{\tau_W}{2} \right) \int_0^1 dz \frac{\operatorname{arctanh}(\sqrt{1-z})}{\tau_W - z} + \frac{1}{2}, \end{aligned} \quad (\text{C.1})$$

containing the remaining integral

$$\begin{aligned} \int_0^1 dz \frac{\operatorname{arctanh}(\sqrt{1-z})}{\tau_W - z} &= -\frac{1}{2} \int_0^1 dx \int_0^{1-x} dy \frac{-1}{-xy + \frac{m_W^2}{m_h^2}} \\ &= -\frac{1}{2} \int_0^1 dx \frac{1}{x} \ln \left[ 1 - \frac{m_h^2}{m_W^2} x(1-x) \right] \equiv -\frac{1}{2} J(\xi), \end{aligned} \quad (\text{C.2})$$

where  $\xi \equiv \frac{m_h^2}{m_W^2}$ . Here, the integral is retyped according to the relations in (4.21). The integral  $J(\xi)$  is the most difficult part to determine. Luckily, its calculation is presented in great detail in [297]. The argument of the logarithm is positive in  $0 \leq x \leq 1$  for  $\xi < 4$ , and touches the x-axis for  $\xi = 4$ . For  $\xi > 4$ , the argument has two roots, and after an integration by parts, the integral  $J(\xi)$  can be written as

$$J(\xi) = \xi \int_0^1 dx \frac{(1-2x) \ln x}{1-x(1-x)\xi}. \quad (\text{C.3})$$

The denominator vanishes at the two roots in the integration range, and one splits the integral into the principal part and the contributions of the poles, by using the rule

$$\int \frac{dx'}{x' - x \mp i\epsilon} = P \int \frac{dx'}{x' - x} \pm i\pi \delta(x' - x). \quad (\text{C.4})$$

One uses the condition

$$\delta(1 - x\xi + x^2\xi) = \xi^{-1}\beta^{-1} \left[ \delta\left(x - \frac{1}{2}(1 + \beta)\right) + \delta\left(x - \frac{1}{2}(1 - \beta)\right) \right], \quad (\text{C.5})$$

with the abbreviation  $\beta = \sqrt{1 - 4\xi^{-1}}$ , to determine the imaginary part of  $J(\xi)$ . If  $\xi > 4$  holds, the parameter  $\beta$  is real, and one obtains

$$\text{Im } J(\xi) = -\pi \ln \frac{1 + \beta}{1 - \beta}. \quad (\text{C.6})$$

To calculate the real part of the integral, one differentiates the definition of  $J(\xi)$  in (C.2) with respect to  $\xi$ , yielding

$$\frac{dJ}{d\xi} = - \int_0^1 dx \frac{1 - x}{1 - x(1 - x)\xi}. \quad (\text{C.7})$$

One substitutes  $x = \frac{1}{2}(1 + u)$ , and obtains

$$\frac{dJ}{d\xi} = - \int_{-1}^1 \frac{du}{4 - \xi + \xi u^2}, \quad (\text{C.8})$$

after dropping an antisymmetric term in the integrand. For positive  $\beta$  values, resulting from  $\xi > 4$  or  $\xi < 0$ , one obtains

$$\frac{dJ}{d\xi} = \frac{1}{2\beta\xi} \int_{-1}^1 du \left( \frac{1}{u + \beta} - \frac{1}{u - \beta} \right) = \frac{1}{\beta\xi} \ln \left| \frac{1 + \beta}{1 - \beta} \right|. \quad (\text{C.9})$$

For the case of  $0 < \xi < 4$ , one obtains

$$\begin{aligned} \frac{dJ}{d\xi} &= \frac{-1}{\sqrt{\xi(4 - \xi)}} \arctan \left( u \sqrt{\frac{\xi}{4 - \xi}} \right) \Big|_{-1}^1 \\ &= \frac{-2}{\sqrt{\xi(4 - \xi)}} \arctan \sqrt{\frac{\xi}{4 - \xi}} = \frac{-2}{\sqrt{\xi(4 - \xi)}} \arcsin \sqrt{\frac{1}{4}\xi}. \end{aligned} \quad (\text{C.10})$$

One can integrate (C.9) and (C.10) over  $\xi$  and derives

$$\begin{aligned} J(\xi) &= -2 \left( \arcsin \sqrt{\frac{1}{4}\xi} \right)^2 + \text{const.}, \quad (0 < \xi < 4), \\ \text{Re}[J(\xi)] &= \frac{1}{2} \ln^2 \left| \frac{1 + \beta}{1 - \beta} \right| + \text{const.}, \quad (\xi > 4, \xi < 0). \end{aligned} \quad (\text{C.11})$$

One concludes that the constants are zero for the case of  $\xi < 4$ , because  $J(\xi)$  vanishes at  $\xi = 0$ . A comparison between the solutions in (C.11) at the point  $\xi = 4$  shows that one has to include a constant  $-\frac{1}{2}\pi^2$  for the case of  $\xi > 4$ . Then, the solutions for  $J(\xi)$  read

$$J(\xi) = \begin{cases} \frac{1}{2} \ln^2 \frac{\beta+1}{\beta-1} & (\xi < 0) \\ -2 \left( \arcsin \sqrt{\frac{1}{4}\xi} \right)^2 & (0 < \xi < 4) \\ \frac{1}{2} \ln^2 \frac{1+\beta}{1-\beta} - \frac{1}{2}\pi^2 - i\pi \ln \frac{1+\beta}{1-\beta} & (\xi \geq 4) \end{cases}. \quad (\text{C.12})$$

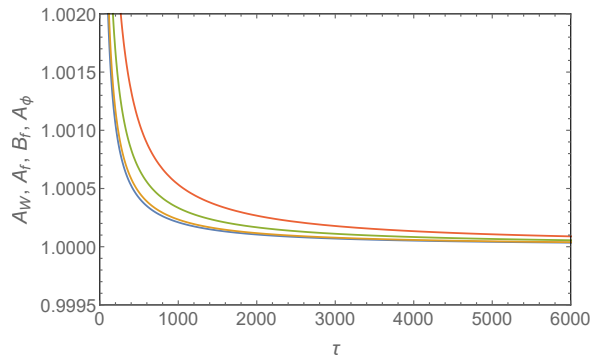


Figure C.1: The behaviour of the form factors  $A_W(\tau)$  (blue),  $A_f(\tau)$  (yellow),  $B_f(\tau)$  (green) and  $A_\phi(\tau)$  (orange) for large arguments is indicated. They are all normalized in such a way that they approach to 1 in the asymptotic limit.

The case of  $\xi = \frac{m_h^2}{m_W^2} < 0$  is not possible in the present considerations. The solutions for the other cases can be rewritten as  $J(\xi) = J(4/\tau_W) = -2f(\tau_W)$  [205], by writing  $\tau_W = 4m_W^2/m_h^2$ , and with

$$f(\tau_W) = \begin{cases} \arctan^2 \frac{1}{\sqrt{\tau_W-1}} & (\tau_W > 1) \\ -\frac{1}{4} \left[ \ln \frac{1+\sqrt{1-\tau_W}}{1-\sqrt{1-\tau_W}} - i\pi \right]^2 & (\tau_W \leq 1) \end{cases} . \quad (\text{C.13})$$

This result appears in the loop-form factors, describing the KK contributions of W bosons, fermions and scalars in the loop-induced Higgs production and decay processes. One has

$$\begin{aligned} A_W(\tau) &= \frac{1}{7} [2 + 3\tau + 3\tau(2 - \tau)f(\tau)] , & A_\phi(\tau) &= -3\tau [1 - \tau f(\tau)] , \\ A_f(\tau) &= \frac{3\tau}{2} [1 + (1 - \tau)f(\tau)] , & B_f(\tau) &= \tau f(\tau) . \end{aligned} \quad (\text{C.14})$$

They are normalized in such a way that they converge to 1 in the asymptotic limit  $\tau \rightarrow \infty$ , as it can be observed from Figure C.1.

## C.2 CP-odd loop-contribution of fermions to Higgs processes

Here, the significant steps of the calculation of the CP-odd part of the fermion contribution to the loop-induced Higgs processes are presented shortly. Starting from equation (4.60), the CP-odd part of the amplitude for the fermion contribution to the Higgs decay into two photons is

$$\mathcal{M}_{h \rightarrow \gamma\gamma}^{f, \text{CP odd}} = - \sum_{f=u,d,e} \sum_{n=1}^{\infty} (eQ_f)^2 N_{c,f} \text{Im}(g_{nn}^f) \epsilon_\mu^*(k_1) \epsilon_\nu^*(k_2) \int \frac{d^d p}{(2\pi)^d} \frac{\text{Tr}[\gamma_5 A_{Tr}]}{d_1 d_2 d_3}, \quad (\text{C.15})$$

with

$$\begin{aligned} A_{Tr} &= (\not{p} - k_{\not{2}} + m_n^f) \gamma^\nu (\not{p} + m_n^f) \gamma^\mu (\not{p} + k_{\not{1}} + m_n^f) \\ &\quad + (-\not{p} - k_{\not{1}} + m_n^f) \gamma^\mu (-\not{p} + m_n^f) \gamma^\nu (-\not{p} + k_{\not{2}} + m_n^f), \\ d_1 &= (p^2 - m_{f_n}^2), \quad d_2 = ([p + k_1]^2 - m_{f_n}^2), \quad d_3 = ([p - k_2]^2 - m_{f_n}^2). \end{aligned} \quad (\text{C.16})$$

Using the relations

$$\text{Tr}[\text{any odd n. of } \gamma' s] = 0, \quad \text{Tr}[\gamma_5 \gamma^\mu \gamma^\nu] = 0, \quad \text{Tr}[\gamma_5 \gamma^\mu \gamma^\nu \gamma^\rho \gamma^\sigma] = -4i \epsilon^{\mu\nu\rho\sigma}, \quad (\text{C.17})$$

one can determine

$$\begin{aligned} \text{Tr}[\gamma_5 A_{Tr}] &= \text{Tr}[\gamma_5 ((\not{p} - k_{\not{2}} + m_n^f) \gamma^\nu (\not{p} + m_n^f) \gamma^\mu (\not{p} + k_{\not{1}} + m_n^f) \\ &\quad + (-\not{p} - k_{\not{1}} + m_n^f) \gamma^\mu (-\not{p} + m_n^f) \gamma^\nu (-\not{p} + k_{\not{2}} + m_n^f))] \\ &= -4im_n^f (\epsilon^{\rho\nu\sigma\mu} \cdot [p_\rho p_\sigma - k_{2\rho} p_\sigma] + \epsilon^{\rho\nu\mu\sigma} \cdot [p_\rho p_\sigma + p_\rho k_{1\sigma}] + \epsilon^{\rho\nu\mu\sigma} \cdot [-k_{2\rho} p_\sigma - k_{2\rho} k_{1\sigma}] \\ &\quad + \epsilon^{\nu\rho\mu\sigma} \cdot [p_\rho p_\sigma + p_\rho k_{1\sigma}] + \epsilon^{\rho\mu\sigma\nu} \cdot [p_\rho p_\sigma + k_{1\rho} p_\sigma] + \epsilon^{\rho\mu\nu\sigma} \cdot [p_\rho p_\sigma - p_\rho k_{2\sigma}] \\ &\quad + \epsilon^{\rho\mu\nu\sigma} \cdot [k_{1\rho} p_\sigma - k_{1\rho} k_{2\sigma}] + \epsilon^{\mu\rho\nu\sigma} \cdot [p_\rho p_\sigma - p_\rho k_{2\sigma}]) \\ &= \dots = 8im_n^f \epsilon^{\mu\nu\sigma\rho} k_{1\sigma} k_{2\rho}. \end{aligned} \quad (\text{C.18})$$

Here, the anti-cyclic behaviour of the tensor  $\epsilon^{\mu\nu\sigma\rho}$  under the exchange of two indices in juxtaposition with each other has been used. So, the result is

$$\begin{aligned} \mathcal{M}_{h \rightarrow \gamma\gamma}^{f, \text{CP odd}} &= - \sum_{f=u,d,e} \sum_{n=1}^{\infty} (eQ_f)^2 N_{c,f} \text{Im}(g_{nn}^f) 8im_n^f \epsilon^{\mu\nu\sigma\rho} k_{1\sigma} k_{2\rho} \epsilon_\mu^*(k_1) \epsilon_\nu^*(k_2) \int \frac{d^d p}{(2\pi)^d} \frac{1}{d_1 d_2 d_3}, \\ &= -i \sum_{f=u,d,e} \sum_{n=1}^{\infty} Q_f^2 N_{c,f} \text{Im}(g_{nn}^f) \frac{\alpha}{4\pi v} (4\pi)^2 2vm_n^f \int \frac{d^d p}{(2\pi)^d} \frac{1}{d_1 d_2 d_3} \langle \gamma\gamma | F_{\mu\nu} \tilde{F}^{\mu\nu} | 0 \rangle, \\ \Leftrightarrow C_5^f &= i \sum_{f=u,d,e} \sum_{n=1}^{\infty} Q_f^2 N_{c,f} \text{Im}(g_{nn}^f) (4\pi)^2 2vm_n^f \int \frac{d^d p}{(2\pi)^d} \frac{1}{d_1 d_2 d_3}. \end{aligned} \quad (\text{C.19})$$

The parametrization in (4.7) has been applied. The momentum integral can be expressed in dependence of Feynman parameters, and one finds

$$\begin{aligned}
& \int \frac{d^d p}{(2\pi)^d} \frac{1}{(p^2 - m_n^{f2})((p + k_1)^2 - m_n^{f2})((p - k_2)^2 - m_n^{f2})} \\
&= 2 \int \frac{d^d p}{(2\pi)^d} \int_0^1 dx \int_0^{1-x} dy \frac{1}{(p^2 - m_n^{f2} + 2p(k_1 x - k_2 y))^3} \\
&= 2 \int \frac{d^d \tilde{p}}{(2\pi)^d} \int_0^1 dx \int_0^{1-x} dy \frac{1}{(\tilde{p}^2 - m_n^{f2} + m_h^2 xy)^3} = -\frac{2i}{(4\pi)^2} \int_0^1 dx \int_0^{1-x} dy \frac{1}{m_n^{f2} - m_h^2 xy} \\
&= -\frac{2i}{(4\pi)^2} \frac{-1}{2m_h^2} J(\xi) = -\frac{2i}{(4\pi)^2 m_h^2} f(\tau_{f_n}) ,
\end{aligned} \tag{C.20}$$

where the momentum shift  $\tilde{p} = p + k_1 x - k_2 y$  is performed, and  $k_1^2 = k_2^2 = 0$  and  $2k_1 k_2 = m_h^2$  has been used. The calculation of the Feynman parameter integral  $J(\xi)$  has been presented before in Section C.1. The full result can be determined as

$$C_5^f = \sum_{f=u,d,e} Q_f^2 N_{c,f} \sum_{n=1}^{\infty} \frac{\text{Im}(g_{nn}^f) v}{m_n^f} B(\tau_{f_n}) , \tag{C.21}$$

where  $B(\tau) = \tau f(\tau)$  has been defined in the section before in Appendix C.1.

### C.3 Dicing of the RS model parameter sets

For the input parameters of the numerical evaluations, performed in Chapter 3 of the thesis, three sets have been diced for the Yukawa matrices  $\mathbf{Y}_u$  and  $\mathbf{Y}_d$ , whose entries are bounded in magnitude by  $|(\mathbf{Y}_f)_{ij}| \leq y_*$ , with  $y_* = 1, 2, 3$ , in dependence of the KK mass scale in the range of  $M_{KK} \in [1, 10]$  TeV. The diced Yukawa matrices can reproduce the correct zero-mode fermion masses and Wolfenstein parameters, according to the formulas (2.154) and (2.164). In the dicing process, the correct zero-mode fermion profiles have been used, which can be expressed in terms of the quark masses, Yukawa matrices and Wolfenstein parameters, together with one chosen profile, as for example  $F(c_{u_3})$  [150],

$$\begin{aligned}
|F(c_{Q_1})| &= \frac{\sqrt{2}m_t}{v} \frac{A\lambda^3}{\left| \frac{(M_d)_{21}}{(M_d)_{21}} - \frac{(M_u)_{21}}{(M_u)_{21}} \right| |(Y_u)_{33}| \left| \frac{(Y_d)_{23}}{(Y_d)_{33}} - \frac{(Y_u)_{23}}{(Y_u)_{33}} \right|} \frac{1}{|F(c_{u_3})|} , \\
|F(c_{Q_2})| &= \frac{\sqrt{2}m_t}{v} \frac{A\lambda^2}{|(Y_u)_{33}| \left| \frac{(Y_d)_{23}}{(Y_d)_{33}} - \frac{(Y_u)_{23}}{(Y_u)_{33}} \right|} \frac{1}{|F(c_{u_3})|} , \\
|F(c_{Q_3})| &= \frac{\sqrt{2}m_t}{v} \frac{\left| \frac{(Y_d)_{23}}{(Y_d)_{33}} - \frac{(Y_u)_{23}}{(Y_u)_{33}} \right|}{|(Y_u)_{33}| \left| \frac{(Y_d)_{23}}{(Y_d)_{33}} - \frac{(Y_u)_{23}}{(Y_u)_{33}} \right|} \frac{1}{|F(c_{u_3})|} , \\
|F(c_{u_1})| &= \frac{m_u}{m_t} \frac{|(M_u)_{11}| \left| \frac{(M_d)_{21}}{(M_d)_{11}} - \frac{(M_u)_{21}}{(M_u)_{11}} \right| |(Y_u)_{33}| \left| \frac{(Y_d)_{23}}{(Y_d)_{33}} - \frac{(Y_u)_{23}}{(Y_u)_{33}} \right|}{A\lambda^3 |\det(\mathbf{Y}_u)|} |F(c_{u_3})| , \\
|F(c_{u_2})| &= \frac{m_c}{m_t} \frac{|(Y_u)_{33}|^2 \left| \frac{(Y_d)_{23}}{(Y_d)_{33}} - \frac{(Y_u)_{23}}{(Y_u)_{33}} \right|}{A\lambda^2 |(M_u)_{11}|} |F(c_{u_3})| , \\
|F(c_{d_1})| &= \frac{m_d}{m_t} \frac{|(M_d)_{11}| \left| \frac{(M_u)_{21}}{(M_u)_{11}} - \frac{(M_d)_{21}}{(M_d)_{11}} \right| |(Y_u)_{33}| \left| \frac{(Y_d)_{23}}{(Y_d)_{33}} - \frac{(Y_u)_{23}}{(Y_u)_{33}} \right|}{A\lambda^3 |\det(\mathbf{Y}_d)|} |F(c_{u_3})| , \\
|F(c_{d_2})| &= \frac{m_s}{m_t} \frac{|(Y_d)_{33}| |(Y_u)_{33}| \left| \frac{(Y_d)_{23}}{(Y_d)_{33}} - \frac{(Y_u)_{23}}{(Y_u)_{33}} \right|}{A\lambda^2 |(M_d)_{11}|} |F(c_{u_3})| , \\
|F(c_{d_3})| &= \frac{m_b}{m_t} \frac{|(Y_u)_{33}|}{|(Y_d)_{33}|} |F(c_{u_3})| .
\end{aligned} \tag{C.22}$$

The dicing process has been performed with a program written for *Mathematica* by U. Haisch *et al.*. The entries of the quark Yukawa matrices  $\mathbf{Y}_u$  and  $\mathbf{Y}_d$  have been diced as random complex numbers, following a flat distribution, according to the formula

$$(\mathbf{Y}_f)_{ij} = \sqrt{y_* \cdot |(\mathbf{Y}_f)_{ij}|} e^{i\phi} , \quad (\mathbf{Y}_f)_{ij} \in [0, y_*] , \quad \phi \in [0, 2\pi] , \tag{C.23}$$

so that every number within the allowed range  $0 \leq |(\mathbf{Y}_q)_{ij}| \leq y_*$ , has been diced with an equal probability. The two Wolfenstein parameters  $\bar{\rho}$  and  $\bar{\eta}$  have been calculated for the diced Yukawa

matrices, and the quantity

$$\chi^2[X_i] = \sum_i \left( \frac{X_i - X_{i,\text{exp}}}{\sigma(X_{i,\text{exp}})} \right)^2, \quad (\text{C.24})$$

with  $X_i = (\bar{\eta}, \bar{\rho})$ , has been demanded to fulfil a *FindMinimum* condition of *Mathematica*, otherwise the calculated matrices have been rejected. Then, the zero-mode profiles for the quark fields have been determined, according to the formulas presented above, for a randomly chosen  $|F(c_{u_3})| \in [0, \sqrt{3}]$ . Using the formulas (2.154) and (2.164), a ten parameter set has been determined for the quark masses and Wolfenstein parameters, as  $X_i = (m_u, m_c, m_t, m_d, m_s, m_b, A, \lambda, \bar{\rho}, \bar{\eta})$ . For this set, the  $\chi^2$  has been computed, according to (C.24), with the experimentally determined quark masses, Wolfenstein parameters and the  $1\sigma$  error values as inputs. It has been demanded that  $\chi^2 < 10$  according to the degrees of freedom, and that  $\max|F(c_{(Q_i, q_i)})| < \sqrt{2}$  (except of  $|F(c_{u_3})|$ ), otherwise the calculated parameter points have been rejected. In this vein, the data-sets for  $\mathbf{Y}_u, \mathbf{Y}_d$  could be derived in dependence of  $M_{KK}$  that reproduce the physical fermion masses and the Wolfenstein parameters. A simplification has been used for the dicing of the lepton Yukawa matrices  $\mathbf{Y}_l$ , which have been determined according to the formula (C.23), without imposing further chi-square minimizations adapting to lepton masses.

The experimental input values for the quark masses in GeV, and Wolfenstein parameters, with corresponding  $1\sigma$  errors, used in the dicing program, have been

$$\begin{aligned} m_u &= 0.0015 & m_c &= 0.55 & m_t &= 140 & m_d &= 0.003 & m_s &= 0.05 & m_b &= 2.2 \\ \sigma[m_u] &= 0.001 & \sigma[m_c] &= 0.05 & \sigma[m_t] &= 10. & \sigma[m_d] &= 0.002 & \sigma[m_s] &= 0.03 & \sigma[m_b] &= 0.1 \\ \lambda &= 0.2265 & A &= 0.807 & \bar{\rho} &= 0.147 & \bar{\eta} &= 0.343 \\ \sigma[\lambda] &= 0.0008 & \sigma[A] &= 0.018 & \sigma[\bar{\rho}] &= 0.023 & \sigma[\bar{\eta}] &= 0.016 \end{aligned}$$

These values might slightly deviate from the latest experimental results, which we expect to be numerically insignificant for the evaluations. Besides, the dicing program was written for the minimal RS scenario with a brane-localized Higgs field. The relations for the fermion mass eigenvalues and Wolfenstein parameters in the bulk-Higgs RS scenario involve the matrices  $\tilde{\mathbf{Y}}_f$ , defined in (2.115), rather than the matrices  $\mathbf{Y}_f$ , see equation (2.119). For that reason, the diced sets from the program have been used for  $\tilde{\mathbf{Y}}_u$  and  $\tilde{\mathbf{Y}}_d$  in the formulas. In the end, it was set  $c_{f_i} \rightarrow -1/2$ , and the results have been rewritten in dependence of the matrices  $\mathbf{Y}_f$ , as in (4.86), for example. Accordingly, rescaling factors  $\frac{(1+\beta)}{(2+\beta)} \tilde{\mathbf{Y}}_q = \mathbf{Y}_q$  have been included in the calculation of the scatter plots. For the leptons, such rescaling factors have not been included, and the simply diced sets have been taken for  $\mathbf{Y}_l$ .





# Appendix D

## A New, Heavy Bulk Scalar in the RS Model

### D.1 Corrections to the expressions $\Delta^{(\pm)}(c_f, \beta)$

Here, the expressions from (5.27) are displayed up to  $\mathcal{O}(\frac{m_S^4}{M_{KK}^4})$ -corrections,

$$\begin{aligned}
\Delta^{(+)}(c_f, \beta) &= -\frac{2F^2(c_f)}{(3 + \beta + 2c_f)} \\
&\quad - \frac{m_S^2}{60M_{KK}^2} \left[ -\frac{(2 + \beta)}{(1 - 2c_f)(4 + \beta)(3 + \beta - 2c_f)} - \frac{(1 - \epsilon^2)F^4(c_f)}{(1 - 2c_f)(3 + 2c_f)(3 + \beta + 2c_f)} \right. \\
&\quad - \frac{F^2(c_f)(2 + \beta)(2 + \beta - 4c_f)}{(1 - 2c_f)(1 + 2c_f)^2(4 + \beta)(3 + \beta - 2c_f)} + \frac{2F^2(c_f)(1 + c_f)(2 + \beta)}{(1 + 2c_f)^2(3 + 2c_f)(5 + \beta + 2c_f)} \\
&\quad \left. + \frac{F^2(c_f)}{(1 - 2c_f)(3 + 2c_f)} \left( 1 - \epsilon^2 \frac{(1 + 2c_f)}{(3 + \beta + 2c_f)} \right) \right] + \frac{m_S^2}{4M_{KK}^2} \left[ \frac{\beta}{(1 + \beta)(2 + \beta)(4 + \beta)} \right. \\
&\quad \left. + \frac{4c_f F^2(c_f)(2 + \beta)}{(1 + \beta)(1 + 2c_f)(4 + \beta + 2c_f)(4 + \beta)} - \frac{2F^2(c_f)}{(3 + \beta + 2c_f)} \right] + \mathcal{O}\left(\frac{m_S^4}{M_{KK}^4}\right), \\
\Delta^{(-)}(c_f, \beta) &= -\frac{m_S^2}{60M_{KK}^2} \frac{1}{(1 - 2c_f)} \left[ -\frac{(2 + \beta)}{(4 + \beta)(3 + \beta - 2c_f)} + \frac{\epsilon^{1-2c_f}}{(3 + \beta + 2c_f)} \right] \\
&\quad + \frac{m_S^2}{4M_{KK}^2} \frac{\beta}{(1 + \beta)(2 + \beta)(4 + \beta)} + \mathcal{O}\left(\frac{m_S^4}{M_{KK}^4}\right),
\end{aligned} \tag{D.1}$$

which have been plotted in Figure 5.2.

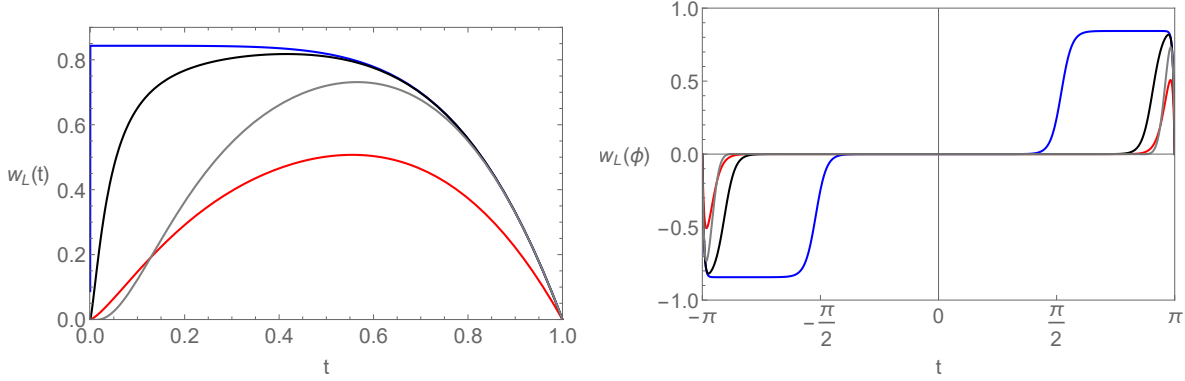


Figure D.1: Numeric solutions for  $w_L(t)$ , derived for  $\mu_L^2/k^2 = 32/9, \xi = 5, w'(1) = -3.8651104855284$  (blue curve),  $\mu_L^2/k^2 = 32/9, \xi = 4.7, w'(1) = -3.8651104855284$  (black curve),  $\mu_L^2/k^2 = 32/9 + 1.5, \xi = 5, w'(1) = -3.8651104855284$  (gray curve),  $\mu_L^2/k^2 = 32/9, \xi = 5, w'(1) = -2.6$  (green curve).

## D.2 Solutions for the odd bulk scalar vev $w_L(t)$

In Section 5.2, approximate, analytic solutions have been determined for the bulk scalar vev, which could possibly form the origin of the  $Z_2$ -odd bulk fermion masses of the RS model. The odd bulk masses determine the localizations of the fermions along the extra dimension, which have to show a hierarchic behaviour in order to explain the mass splitting of the zero-mode fermions. For suitable choices of parameters, it has been possible to derive hierarchic zero-mode fermion profiles, which have been plotted in Figure 5.11.

By further fixing the parameter values for  $\mu_L^2/k^2$  and  $\xi$ , one can numerically solve the differential equation for the vev  $w_L(t)$ , given in (5.57). In Figure D.1, the numeric results, derived for the vev, are plotted for:

$$\begin{array}{llll}
 \mu_L^2/k^2 = 32/9 & \xi = 5 & w'(1) = -3.8651104855284 & \text{(blue curve)} \\
 \mu_L^2/k^2 = 32/9 & \xi = 4.7 & w'(1) = -3.8651104855284 & \text{(black curve)} \\
 \mu_L^2/k^2 = 32/9 + 1.5 & \xi = 5 & w'(1) = -3.8651104855284 & \text{(gray curve)} \\
 \mu_L^2/k^2 = 32/9 & \xi = 5 & w'(1) = -2.6 & \text{(red curve)}
 \end{array}$$

Again, due to the non-linear relation between the  $\phi$  and the  $t$  coordinates, the shapes of the solutions differ in the two coordinates. For the first of these results, which is the blue curve in the plot that reproduces a kink-like behaviour over half of the extra dimension, the resulting zero-mode fermion profiles have been determined numerically, according to (5.60). The results are plotted in Figure D.2, for  $\mu_L^2/k^2 = 32/9, \xi = 5, w'(1) = -3.8651104855284$  and  $g = -5$  (orange curve),  $-2.5$  (black curve),  $-1$  (blue curve) and  $+1$  (red curve). The solutions fulfil the normalization condition for the fermion profiles, and the IR boundary values are chosen as  $F^{(0)}(1) = 0.1$ , which are arbitrary, in principle. Taking similar input parameter values as before, one determines very similar shapes for the solutions, showing a hierarchic behaviour. Moreover, the vev fulfils the two boundary conditions in good approximation, and there is no big parameter value needed, as for the parameter  $\alpha$  in the analytic solutions shown before. For the other parame-

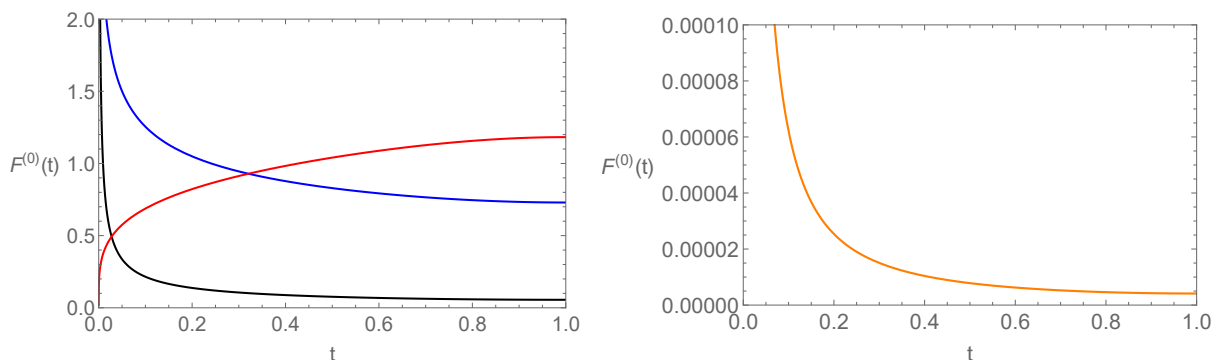


Figure D.2: Zero-mode fermion profiles from the numerically calculated vev, for  $\mu_L^2/k^2 = 32/9$ ,  $\xi = 5$ ,  $w'(1) = -3.8651104855284$ , and  $g = -5$  (orange curve),  $-2.5$  (black curve),  $-1$  (blue curve) and  $+1$  (red curve), taking  $F^{(0)}(1) = 0.1$ .

ter choices, indicated by the black, gray and red curves in Figure D.1, the resulting zero-mode fermion profiles are given in Figures D.4 and D.5. For these cases, it is not possible to derive hierarchical zero-mode fermion profiles.

Similarly, in Figures D.3 and D.4, solutions are given for the zero-mode fermion profiles to the lowest order, derived from the analytic vev for  $\alpha = 1000$  and  $\alpha = 1$ , for which the solutions for the vev are plotted in Figure 5.10.

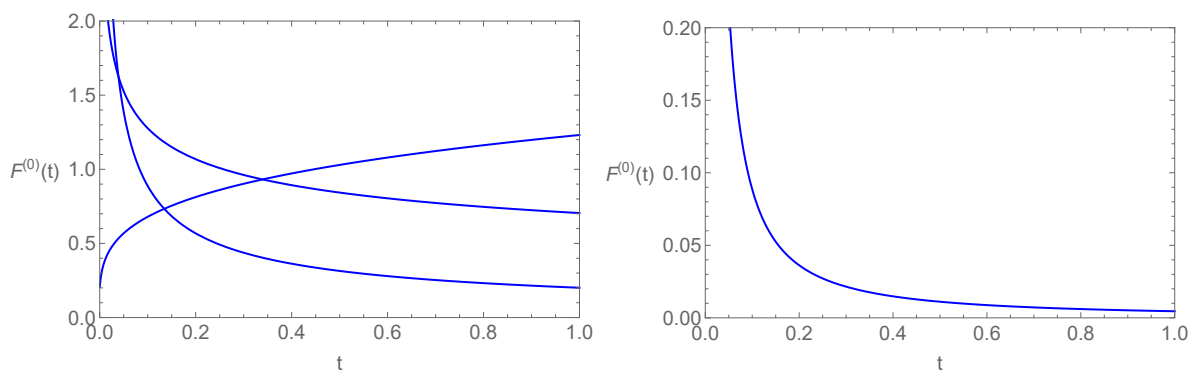


Figure D.3: Here, the zero-mode fermion profiles, implied by the solution for the vev in (5.67), are plotted for  $\alpha = 1000$  and  $\mu_L^2/k^2 = 32/9$  and  $\xi = 5$ , whereat  $g = +1, -1, -2.5$  (left-hand side) and  $g = -5$  (right-hand side).

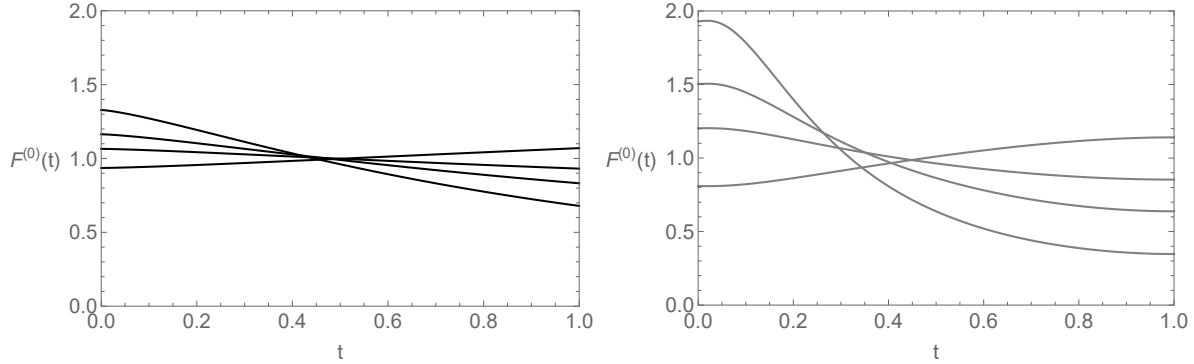


Figure D.4: Here, the zero-mode fermion profiles are plotted for  $g = +1, -1, -2.5, -5$ , respectively, implied by the solution for the vev in (5.67) for  $\mu_L^2/k^2 = 32/9$ ,  $\xi = 5$ , and  $\alpha = 1$  on the left-hand side, and implied by the numerically determined vev for  $\mu_L^2/k^2 = 32/9 + 1.5$ ,  $\xi = 5$  and  $w'(1) = -3.8651104855284$  on the right-hand side.

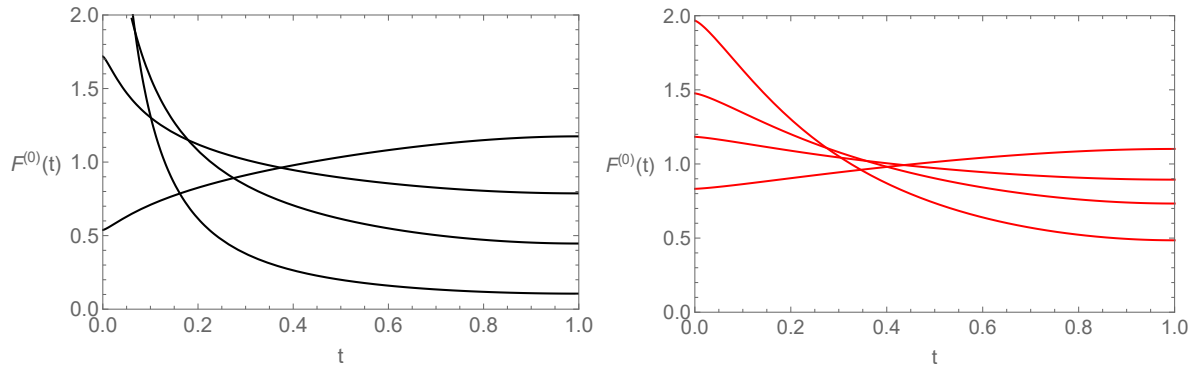


Figure D.5: Here, the zero-mode fermion profiles implied by the numerically determined vev for  $g = +1, -1, -2.5, -5$  are plotted on the left-hand side for  $\mu_L^2/k^2 = 32/9 + 1.5$ ,  $\xi = 4.7$  and  $w'(1) = -3.8651104855284$ , and are plotted on the right-hand side for  $\mu_L^2/k^2 = 32/9 + 1.5$ ,  $\xi = 5$  and  $w'(1) = -2.6$ .

# Bibliography

- [1] Randall, Lisa and Sundrum, Raman, A Large mass hierarchy from a small extra dimension, Phys. Rev. Lett., vol. **83**, p. 3370-3373, (1999), arXiv:hep-ph/9905221
- [2] Malm, Raoul and Neubert, Matthias and Novotny, Kristiane and Schmell, Christoph, 5D Perspective on Higgs Production at the Boundary of a Warped Extra Dimension, JHEP, vol. **01**, p. 173, (2014), arXiv:hep-ph/1303.5702
- [3] Hahn, Juliane and Hörner, Clara and Malm, Raoul and Neubert, Matthias and Novotny, Kristiane and Schmell, Christoph, Higgs Decay into Two Photons at the Boundary of a Warped Extra Dimension, Eur. Phys. J., vol. **C74**, p. 2857, (2014), arXiv:hep-ph/1312.5731
- [4] Malm, Raoul and Neubert, Matthias and Schmell, Christoph, Higgs Couplings and Phenomenology in a Warped Extra Dimension, JHEP, vol. **02**, p. 008, (2015), arXiv:hep-ph/1408.4456
- [5] Carena, Marcela and Casagrande, Sandro and Goertz, Florian and Haisch, Ulrich and Neubert, Matthias, Higgs Production in a Warped Extra Dimension, JHEP, vol. **08**, p. 156, (2012), arXiv:hep-ph/1204.0008
- [6] Aad, Georges and others, Measurements of the Higgs boson production and decay rates and constraints on its couplings from a combined ATLAS and CMS analysis of the LHC pp collision data at  $\sqrt{s} = 7$  and 8 TeV, JHEP, vol. **08**, p. 045, (2016), arXiv:hep-ex/1606.02266
- [7] Bauer, Martin and Hörner, Clara and Neubert, Matthias, Diphoton Resonance from a Warped Extra Dimension, JHEP, vol. **07**, p. 094, (2016), arXiv:hep-ph/1603.05978
- [8] CMS Collaboration, Search for new physics in high mass diphoton events in proton-proton collisions at 13TeV, [CMS-PAS-EXO-15-004] (2015)
- [9] The ATLAS collaboration, Search for resonances decaying to photon pairs in 3.2 fb<sup>-1</sup> of pp collisions at  $\sqrt{s} = 13$  TeV with the ATLAS detector, [ATLAS-CONF-2015-081] (2015)
- [10] Ramond, Pierre, Journeys beyond the standard model, Front. Phys., vol. **101**, p. 1-390, (1999)
- [11] Schrödinger, E., Quantisierung als Eigenwertproblem, Annalen Phys., vol. **384**, p. 489-527, (1926)
- [12] Schrödinger, E., Quantisierung als Eigenwertproblem, Annalen Phys., vol. **384**, p. 361-376, (1926)

- [13] Born, M. and Jordan, P., Zur Quantenmechanik, Z. Phys., vol. **34**, p. 858-888, (1925)
- [14] Heisenberg, W., A quantum-theoretical reinterpretation of kinematic and mechanical relations, Z. Phys., vol. **33**, p. 879-893, (1925)
- [15] Einstein, A., Cosmological Considerations in the General Theory of Relativity, Sitzungsber. Preuss. Akad. Wiss. Berlin (Math. Phys.), vol. **1917**, p. 142-152, (1917)
- [16] Einstein, A., Zur Quantentheorie der Strahlung, Phys. Z., vol. **18**, p. 121-128, (1917)
- [17] Einstein, A., The Foundation of the General Theory of Relativity, Annalen Phys., vol. **49**, p. 769-822, (1916)
- [18] Einstein, A., On The influence of gravitation on the propagation of light, Annalen Phys., vol. **35**, p. 898-908, (1911)
- [19] Dirac, Paul A. M., Quantized Singularities in the Electromagnetic Field, Proc. Roy. Soc. Lond., vol. **A133**, p. 60-72, (1931)
- [20] Dirac, P. A. M., The Quantum theory of electron. 2., Proc. Roy. Soc. Lond., vol. **A118**, p. 351, (1928)
- [21] Dirac, Paul A. M., The quantum theory of the electron, Proc. Roy. Soc. Lond., vol. **A117**, p. 610-624, (1928)
- [22] Dirac, Paul A. M., On the Theory of quantum mechanics, Proc. Roy. Soc. Lond., vol. **A112**, p. 661-677, (1926)
- [23] Fermi, E., An attempt of a theory of beta radiation. 1., Z. Phys., vol. **88**, p. 161-177, (1934)
- [24] Yukawa, Hideki, On the Interaction of Elementary Particles I, Proc. Phys. Math. Soc. Jap., vol. **17**, p. 48-57, (1935)
- [25] Klein, O., On the Theory of Charged Fields, Surveys High Energ. Phys., vol. **5**, p. 269-285, (1986)
- [26] Tomonaga, S., On a relativistically invariant formulation of the quantum theory of wave fields, Prog. Theor. Phys., vol. **1**, p. 27-42, (1946)
- [27] Feynman, R. P., Relativistic cutoff for quantum electrodynamics, Phys. Rev., vol. **74**, p. 1430-1438, (1948)
- [28] Feynman, R. P., A Relativistic cut-off for classical electrodynamics, Phys. Rev., vol. **74**, p. 939-946, (1948)
- [29] Feynman, R. P., Space-time approach to non-relativistic quantum mechanics, Rev. Mod. Phys., vol. **20**, p. 367-387, (1948)
- [30] Schwinger, Julian S., Quantum electrodynamics. III: The electromagnetic properties of the electron: Radiative corrections to scattering, Phys. Rev., vol. **76**, p. 790-817, (1949)

- [31] Schwinger, Julian S., Quantum electrodynamics. 2. Vacuum polarization and self-energy, *Phys. Rev.*, vol. **75**, p. 651, (1948)
- [32] Schwinger, Julian S., Quantum electrodynamics. I A covariant formulation, *Phys. Rev.*, vol. **74**, p. 1439, (1948)
- [33] Schwinger, Julian S., On Quantum electrodynamics and the magnetic moment of the electron, *Phys. Rev.*, vol. **73**, p. 416-417, (1948)
- [34] Tomonaga, Sin-Itiro and Oppenheimer, J. R., On Infinite Field Reactions in Quantum Field Theory, *Phys. Rev.*, vol. **74**, p. 224-225, (1948)
- [35] Koba, Zirô and Tati, Takao and Tomonaga, Shin ichirô, On a Relativistically Invariant Formulation of the Quantum Theory of Wave Fields. II: Case of Interacting Electromagnetic and Electron Fields, *Prog. Theor. Phys.*, vol. **2**, p. 101-116, (1947)
- [36] Bargmann, V. and Michel, L. and Telegdi, V., Precession of the polarization of particles moving in a homogeneous electromagnetic field, *Phys. Rev. Lett.*, vol. **2**, p. 435-436, (1959)
- [37] Lee, T. and Yang, C., Question of Parity Conservation in Weak Interactions, *Phys. Rev.*, vol. **104**, p. 254-258, (1956)
- [38] Wu, C. S. and Ambler, E. and Hayward, R. W. and Hoppes, D. D. and Hudson, R. P., Experimental Test of Parity Conservation in Beta Decay, *Phys. Rev.*, vol. **105**, p. 1413-1414, (1957)
- [39] Yang, C. and Mills, R., Conservation of Isotopic Spin and Isotopic Gauge Invariance, *Phys. Rev.*, vol. **96**, p. 191-195, (1954)
- [40] Gell-Mann, M. and Zachariasen, F., Broken Symmetries and Bare Coupling Constants, *Phys. Rev.*, vol. **123**, p. 1065-1071, (1961)
- [41] Gell-Mann, M., The Eightfold Way: A Theory of strong interaction symmetry, (1961) [CTSL-20, TID-12608]
- [42] Ne'eman, Y., Derivation of strong interactions from a gauge invariance, *Nucl. Phys.*, vol. **26**, p. 222-229, (1961)
- [43] Zweig, G., An  $SU(3)$  model for strong interaction symmetry and its breaking. Version 2, Developments in the Quark Theory of Hadrons, Volume 1. Edited by D. Lichtenberg and S. Rosen. pp. 22-101, p. 22-101, (1964)
- [44] Zweig, G., An  $SU(3)$  model for strong interaction symmetry and its breaking. Version 1, (1964) [CERN-TH-401]
- [45] Freund, G. and Nambu, Y., Broken  $SU(3) \times SU(3) \times SU(3) \times SU(3)$  symmetry of strong interactions, Proceedings, 12th International Conference on High Energy Physics (ICHEP 1964): Dubna, vol. **1**, p. 811-813, (1964)

- [46] Salam, A. and Ward, J., Electromagnetic and weak interactions, Phys. Lett., vol. **13**, p. 168-171, (1964)
- [47] Glashow, S. and Weinberg, S., Breaking chiral symmetry, Phys. Rev. Lett., vol. **20**, p. 224-227, (1968)
- [48] Weinberg, S., A Model of Leptons, Phys. Rev. Lett., vol. **19**, p. 1264-1266, (1967)
- [49] Glashow, S., Model of Weak Interactions with CP Violation, Phys. Rev. Lett., vol. **14**, p. 35-38, (1965)
- [50] Goldstone, J., Field Theories with Superconductor Solutions, Nuovo Cim., vol. **19**, p. 154-164, (1961)
- [51] Nambu, Y. and Jona-Lasinio, G., Dynamical Model of Elementary Particles based on an Analogy with Superconductivity. 2., Phys. Rev., vol. **124**, p. 246-254, (1961)
- [52] Nambu, Y. and Jona-Lasinio, G., Dynamical Model of Elementary Particles Based on an Analogy with Superconductivity. 1., Phys. Rev., vol. **122**, p. 345-358, (1961)
- [53] Guralnik, G. and Hagen, C. and Kibble, T., Global Conservation Laws and Massless Particles, Phys. Rev. Lett., vol. **13**, p. 585-587, (1964)
- [54] Englert, F. and Brout, R., Broken Symmetry and the Mass of Gauge Vector Mesons, Phys. Rev. Lett., vol. **113**, p. 321-323, (1964)
- [55] Higgs, P., Broken Symmetries and the Masses of Gauge Bosons, Phys. Rev. Lett., vol. **13**, p. 508-509, (1964)
- [56] Glashow, S. and Iliopoulos, J. and Maiani, L., Weak Interactions with Lepton-Hadron Symmetry, Phys. Rev., vol. **D2**, p. 1285-1292, (1970)
- [57] 't Hooft, G., Renormalization of Massless Yang-Mills Fields, Nucl. Phys., vol. **B33**, p. 173-199, (1971)
- [58] 't Hooft, G., Renormalizable Lagrangians for Massive Yang-Mills Fields, Nucl. Phys., vol. **B35**, p. 167-188, (1971)
- [59] Fritzsche, H. and Gell-Mann, M. and Leutwyler, H., Advantages of the Color Octet Gluon Picture, Phys. Lett., vol. **47B**, p. 365-368, (1973)
- [60] Perl, M., The Discovery of The Tau Lepton, NATO Sci. Ser. B, vol. **352**, p. 277-302, (1996)
- [61] Hasert, F. and others, Observation of Neutrino Like Interactions Without Muon Or Electron in the Gargamelle Neutrino Experiment, Phys. Lett., vol. **46B**, p. 138-140, (1973)
- [62] Hasert, F. and others, Search for Elastic  $\nu_\mu$  Electron Scattering, Phys. Lett., vol. **46B**, p. 121-124, (1973)
- [63] Arnison, G. and others, Experimental Observation of Lepton Pairs of Invariant Mass Around  $95 \text{ GeV}/c^2$  at the CERN SPS Collider, Phys. Lett., vol. **126B**, p. 398-410, (1983)



- [64] Arnison, G. and others, Further Evidence for Charged Intermediate Vector Bosons at the SPS Collider, *Phys. Lett.*, vol. **129B**, p. 273-282, (1983)
- [65] Banner, M. and others, Observation of Single Isolated Electrons of High Transverse Momentum in Events with Missing Transverse Energy at the CERN  $\bar{p}p$  Collider, *Phys. Lett.*, vol. **122B**, p. 476-485, (1983)
- [66] Bagnaia, P. and others, Evidence for  $Z^0 \rightarrow e^+e^-$  at the CERN  $\bar{p}p$  Collider, *Phys. Lett.*, vol. **129B**, p. 130-140, (1983)
- [67] Aad, Georges and others, Observation of a new particle in the search for the Standard Model Higgs boson with the ATLAS detector at the LHC, *Phys. Lett.*, vol. **B716**, p. 1-29, (2012), arXiv:hep-ex/1207.7214
- [68] Chatrchyan, Serguei and others, Observation of a new boson at a mass of 125 GeV with the CMS experiment at the LHC, *Phys. Lett.*, vol. **B716**, p. 30-61, (2012), arXiv:hep-ex/1207.7235
- [69] Ahmad, Q. and others, Measurement of the rate of  $\nu_e + d \rightarrow p + p + e^-$  interactions produced by  $^8B$  solar neutrinos at the Sudbury Neutrino Observatory, *Phys. Rev. Lett.*, vol. **87**, p. 071301, (2001), arXiv:nucl-ex/0106015
- [70] Fukuda, Y. and others, Evidence for oscillation of atmospheric neutrinos, *Phys. Rev. Lett.*, vol. **81**, p. 1562-1567, (1998), arXiv:hep-ex/9807003
- [71] Canetti, L. and Drewes, M. and Shaposhnikov, M., Matter and Antimatter in the Universe, *New J. Phys.*, vol. **14**, p. 095012, (2012), arXiv:hep-ph/1204.4186
- [72] Perlmutter, S. and others, Measurements of Omega and Lambda from 42 high redshift supernovae, *Astrophys. J.*, vol. **517**, p. 565-586, (1999), arXiv:astro-ph/9812133
- [73] Riess, A. and others, Observational evidence from supernovae for an accelerating universe and a cosmological constant, *Astron. J.*, vol. **116**, p. 1009-1038, (1998), arXiv:astro-ph/9805201
- [74] Jarosik, N. and others, Seven-Year Wilkinson Microwave Anisotropy Probe (WMAP) Observations: Sky Maps, Systematic Errors, and Basic Results, *Astrophys. J. Suppl.*, vol. **192**, p. 14, (2011), arXiv:astro-ph/1001.4744
- [75] Ade, P. and others, Planck 2013 results. I. Overview of products and scientific results, *Astron. Astrophys.*, vol. **571**, p. A1, (2014), arXiv:astro-ph/1303.5062
- [76] Weinberg, S., *The Quantum theory of fields. Vol. 1: Foundations*, (2005), Cambridge University Press, (2005)
- [77] Mandl, F. and Shaw, G., *Quantum Field Theory*, Chichester, Uk: Wiley (1984) 354 p. (A Wiley-interscience Publication)
- [78] Cheng, T. and Li, L., *Gauge Theory of Elementary Particle Physics*, Oxford, Uk: Clarendon (1984) 536 P. (Oxford Science Publications)

- [79] Peskin, M. and Schroeder, D., *An Introduction to quantum field theory*, Reading, USA: Addison-Wesley (1995) 842 p.
- [80] Chau, Ling-Lie and Keung, Wai-Yee, *Comments on the Parametrization of the Kobayashi-Maskawa Matrix*, *Phys. Rev. Lett.*, vol. **53**, p. 1802, (1984)
- [81] Wolfenstein, Lincoln, *Parametrization of the Kobayashi-Maskawa Matrix*, *Phys. Rev. Lett.*, vol. **51**, p. 1945, (1983)
- [82] Peskin, Michael E. and Takeuchi, Tatsu, *Estimation of oblique electroweak corrections*, *Phys. Rev.*, vol. **D46**, p. 381-409, (1992)
- [83] Kuroda, M. and Moutaka, G. and Schildknecht, D., *Direct one loop renormalization of  $SU(2)_L \times U(1)_Y$  four fermion processes and running coupling constants*, *Nucl. Phys.*, vol. **B350**, p. 25-72, (1991)
- [84] Kennedy, D. and Lynn, B., *Electroweak Radiative Corrections with an Effective Lagrangian: Four Fermion Processes*, *Nucl. Phys.*, vol. **B322**, p. 1-54, (1989)
- [85] Peskin, M. and Takeuchi, T., *A New constraint on a strongly interacting Higgs sector*, *Phys. Rev. Lett.*, vol. **65**, p. 964-967, (1990)
- [86] Baak, M. and Cúth, J. and Haller, J. and Hoecker, A. and Kogler, R. and Mönig, K. and Schott, M. and Stelzer, J., *The global electroweak fit at NNLO and prospects for the LHC and ILC - Gfitter Group*, *Eur. Phys. J.*, vol. **C74**, p. 3046, (2014), arXiv:hep-ph/1407.3792
- [87] Diaz, Rodolfo A. and Martinez, R., *The Custodial symmetry*, *Rev. Mex. Fis.*, vol. **47**, p. 489-492, (2001), arXiv:hep-ph/0302058
- [88] Neubert, M., *Effective field theory and heavy quark physics*, *Physics in  $D \geq 4$ . Proceedings, Theoretical Advanced Study Institute in elementary particle physics, TASI 2004, Boulder, USA, June 6-July 2, 2004*, arXiv:hep-ph/0512222
- [89] Polchinski, J., *Effective field theory and the Fermi surface*, *Theoretical Advanced Study Institute (TASI 92): From Black Holes and Strings to Particles Boulder, Colorado, June 3-28, 1992*, arXiv:hep-th/9210046
- [90] Ecker, G., *Effective field theories*, arXiv:hep-ph/0507056
- [91] Dirac, P., *New basis for cosmology*, *Proc. Roy. Soc. Lond.*, vol. **A165**, p. 199-208, (1938)
- [92] Dirac, P., *The Cosmological constants*, *Nature*, vol. **139**, p. 323, (1937)
- [93] 't Hooft, G., *Naturalness, chiral symmetry, and spontaneous chiral symmetry breaking*, *NATO Sci. Ser. B*, vol. **59**, p. 135-157, (1980)
- [94] Giudice, G., *Naturally Speaking: The Naturalness Criterion and Physics at the LHC*, *Perspectives on LHC Physics*, p. 155-178, (2008), arXiv:hep-ph/0801.2562

- [95] Barbieri, R. and Strumia, A., The 'LEP paradox', 4th Rencontres du Vietnam: Physics at Extreme Energies (Particle Physics and Astrophysics) Hanoi, Vietnam, July 19-25, (2000), arXiv:hep-ph/0007265
- [96] Pontecorvo, B., Inverse beta processes and nonconservation of lepton charge, *Sov. Phys. JETP*, vol. **7**, p. 172-173, (1958)
- [97] Maki, Z. and Nakagawa, M. and Sakata, S., Remarks on the unified model of elementary particles, *Prog. Theor. Phys.*, vol. **28**, p. 870-880, (1962)
- [98] Friedmann, A., On the Possibility of a world with constant negative curvature of space, *Z. Phys.*, vol. **21**, p. 326-332, (1924)
- [99] Barvinsky, A., Nonlocal action for long distance modifications of gravity theory, *Phys. Lett.*, vol. **B572**, p. 109-116, (2003), arXiv:hep-th/0304229
- [100] Dvali, G. and Hofmann, S. and Khoury, J., Degravitation of the cosmological constant and graviton width, *Phys. Rev.*, vol. **D76**, p. 084006, (2007), arXiv:hep-th/0703027
- [101] Arkani-Hamed, N. and Dimopoulos, S. and Dvali, G. and Gabadadze, G., Nonlocal modification of gravity and the cosmological constant problem, arXiv:hep-th/0209227
- [102] Dirkes, A., Degravitation, Orbital Dynamics and the Effective Barycentre, arXiv:gr-qc/1607.04123
- [103] Dirkes, A., The relaxed Einstein equations in the context of a mixed UV-IR modified theory of gravity, *Class. Quant. Grav.*, vol. **34**, p. 065008, (2017)
- [104] Georgi, H. and Glashow, S., Unity of All Elementary Particle Forces, *Phys. Rev. Lett.*, vol. **32**, p. 438-441, (1974)
- [105] Georgi, H. and Quinn, H. and Weinberg, S., Hierarchy of Interactions in Unified Gauge Theories, *Phys. Rev. Lett.*, vol. **33**, p. 451-454, (1974)
- [106] Pati, J., Discovery of proton decay: A Must for theory, a challenge for experiment, *AIP Conf. Proc.*, vol. **533**, p. 37-53, (2000), arXiv:hep-ph/0005095
- [107] Baez, J. and Huerta, J., The Algebra of Grand Unified Theories, *Bull. Am. Math. Soc.*, vol. **47**, p. 483-552, (2010), arXiv:hep-th/0904.1556
- [108] Corbelli, E. and Salucci, P., The Extended Rotation Curve and the Dark Matter Halo of M33, *Mon. Not. Roy. Astron. Soc.*, vol. **311**, p. 441-447, (2000), arXiv:astro-ph/9909252
- [109] Markevitch, M. and Gonzalez, A. and Clowe, D. and Vikhlinin, A. and David, L. and Forman, W. and Jones, C. and Murray, S. and Tucker, W., Direct constraints on the dark matter self-interaction cross-section from the merging galaxy cluster 1E0657-56, *Astrophys. J.*, vol. **606**, p. 819-824, (2004), arXiv:astro-ph/0309303

- [110] Clowe, D. and Gonzalez, A. and Markevitch, Weak lensing mass reconstruction of the interacting cluster 1E0657-558: Direct evidence for the existence of dark matter, *Astrophys. J.*, vol. **604**, p. 596-603, (2004), arXiv:astro-ph/0312273
- [111] Faber, S. and Jackson, R., Velocity dispersions and mass to light ratios for elliptical galaxies, *Astrophys. J.*, vol. **204**, p. 668, (1976)
- [112] Ade, P. and others, Planck 2015 results. XIII. Cosmological parameters, *Astron. Astrophys.* vol. **594**, p. A13, (2016), arXiv:astro-ph/1502.01589
- [113] Springel, V. and others, Simulating the joint evolution of quasars, galaxies and their large-scale distribution, *Nature*, vol. **435**, p. 629-636, (2005), arXiv:astro-ph/0504097
- [114] Aprile, E. and others, The XENON100 Dark Matter Experiment, *Astroparticle Physics* vol. **35**, Iss. **9**, p. 573-590, (2012), arXiv:astro-ph/1107.2155
- [115] Aad, G. and others, Search for dark matter candidates and large extra dimensions in events with a photon and missing transverse momentum in  $pp$  collision data at  $\sqrt{s} = 7$  TeV with the ATLAS detector, *Phys. Rev. Lett.* **110**, p. 011802, (2013), arXiv:hep-ex/1209.4625
- [116] Baker, M. and others, The Coannihilation Codex, *JHEP* vol. **12**, p. 120, (2015), arXiv:hep-ph/1510.03434
- [117] Buschmann, M. and El Hedri, S. and Kaminska, A. and Liu, J. and de Vries, M. and Wang, X. and Yu, F. and Zurita, J., Hunting for dark matter coannihilation by mixing dijet resonances and missing transverse energy, *JHEP* vol. **09**, p. 033, (2016), arXiv:hep-ph/1605.08056
- [118] Wess, J. and Zumino, B., A Lagrangian Model Invariant Under Supergauge Transformations, *Phys. Lett.* vol. **49B**, p. 52, (1974)
- [119] Wess, J. and Zumino, B., Supergauge Transformations in Four-Dimensions, *Nucl. Phys.*, vol. **B70**, p. 39-50, (1974)
- [120] Neveu, A. and Schwarz, J., Factorizable dual model of pions, *Nucl. Phys.*, vol. **B31**, p. 86-112, (1971),
- [121] Ramond, P., Dual Theory for Free Fermions, *Phys. Rev.*, vol. **D3**, p. 2415-2418, (1971)
- [122] Volkov, D. and Akulov, V., Possible universal neutrino interaction, Supersymmetry and quantum field theory. Proceedings, D. Volkov Memorial Seminar, Kharkov, Ukraine, January 5-7, 1997, *JETP Lett.*, vol. **16**, p. 438-440, (1972)
- [123] Golfand, A. and Likhtman, E., Extension of the Algebra of Poincare Group Generators and Violation of  $p$  Invariance, *JETP Lett.*, vol. **13**, p. 323-326, (1971)
- [124] Gervais, J. and Sakita, B., Field Theory Interpretation of Supergauges in Dual Models, *Nucl. Phys.*, vol. **B34**, p. 632-639, (1971)
- [125] Spiesberger, H., LHC Physics - Lecture at Mainz University in the context of the Graduate School in summer term (2016)

- [126] Fayet, P., Spontaneously Broken Supersymmetric Theories of Weak, Electromagnetic and Strong Interactions, *Phys. Lett.*, vol. **69B**, p. 489, (1977)
- [127] Fayet, P. and Ferrara, S., Supersymmetry, *Phys. Rept.*, vol. **32**, p. 249-334, (1977)
- [128] Martin, S., A Supersymmetry primer, [Adv. Ser. Direct. High Energy Phys. 18, 1 (1998)], arXiv:hep-ph/9709356
- [129] 't Hooft, G., A Planar Diagram Theory for Strong Interactions, *Nucl. Phys.*, vol. **B72**, p. 461, (1974)
- [130] 't Hooft, G., A Two-Dimensional Model for Mesons, *Nucl. Phys.*, vol. **B75**, p. 461-470, (1974)
- [131] Agashe, K. and Contino, R. and Pomarol, A., The Minimal composite Higgs model, *Nucl. Phys.*, vol. **B719**, p. 165-187, (2005), arXiv:hep-ph/0412089
- [132] Contino, R. and Da Rold, L. and Pomarol, A., Light custodians in natural composite Higgs models, *Phys. Rev.*, vol. **D75**, p. 055014, (2007), arXiv:hep-ph/0612048
- [133] Coleman, S. and Weinberg, E., Radiative Corrections as the Origin of Spontaneous Symmetry Breaking, *Phys. Rev.*, vol. **D7**, p. 1888-1910, (1973)
- [134] Contino, R., The Higgs as a Composite Nambu-Goldstone Boson, Physics of the large and the small, TASI 09, proceedings of the Theoretical Advanced Study Institute in Elementary Particle Physics, Boulder, Colorado, USA, 1-26 June 2009, (2011), arXiv:hep-ph/1005.4269
- [135] Gripaos, B. and Pomarol, A. and Riva, F. and Serra, J., Beyond the Minimal Composite Higgs Model, *JHEP*, vol. **04**, p. 070, (2009), arXiv:hep-ph/0902.1483
- [136] Nordström, G., Über die Möglichkeit, das elektromagnetische Feld und das Gravitationsfeld zu vereinigen, *Physik Zeitschrift* vol. **XV** p. 504-506 (1914), arXiv:physics/0702221 translated by F. Borg
- [137] Kaluza, T., Zum Unitätsproblem der Physik, International School of Cosmology and Gravitation: 8th Course: Unified Field Theories of More than Four Dimensions, Including Exact Solutions Erice, Italy, May 20-June 1, 1982, Sitzungsberichte der Königlich Preußischen Akademie der Wissenschaften Berlin (Math. Phys.), vol. **1921**, p. 966-972, (1921)
- [138] Klein, O., Quantentheorie und fünfdimensionale Relativitätstheorie, *Zeitschrift für Physik* **37**, p. 895-906, (1926)
- [139] Arkani-Hamed, Nima and Dimopoulos, Savas and Dvali, G., The Hierarchy problem and new dimensions at a millimeter, *Phys. Lett.*, vol. **B429**, p. 263-272, (1998), arXiv:hep-ph/9803315
- [140] Kapner, D. J. and Cook, T. S. and Adelberger, E. G. and Gundlach, J. H. and Heckel, Blayne R. and Hoyle, C. D. and Swanson, H. E., Tests of the gravitational inverse-square law below the dark-energy length scale, *Phys. Rev. Lett.*, vol. **98**, p. 021101, (2007), arXiv:hep-ph/0611184

- [141] Arkani-Hamed, N. and Dimopoulos, S. and Dvali, G., Phenomenology, astrophysics and cosmology of theories with submillimeter dimensions and TeV scale quantum gravity, *Phys. Rev.* **D59**, p. 086004, (1999), arXiv:hep-ph/9807344
- [142] Dimopoulos, Savas and Landsberg, Greg L., Black holes at the LHC, *Phys. Rev. Lett.*, vol. **87**, p. 161602, (2001), arXiv:hep-ph/0106295
- [143] Hannestad, Steen and Raffelt, Georg G., Stringent neutron star limits on large extra dimensions, *Phys. Rev. Lett.*, vol. **88**, p. 071301, (2002), arXiv:hep-ph/0110067
- [144] Appelquist, Thomas and Cheng, Hsin-Chia and Dobrescu, Bogdan A., Bounds on universal extra dimensions, *Phys. Rev.*, vol. **D64**, p. 035002, (2001), arXiv:hep-ph/0012100
- [145] Agashe, K., Extra dimensions, Proceedings of Theoretical Advanced Study Institute in Elementary Particle Physics: Exploring New Frontiers Using Colliders and Neutrinos, p. 1-48, **TASI 2006**: Boulder, Colorado, June 4-30, (2006)
- [146] Rizzo, Thomas G., Probes of universal extra dimensions at colliders, *Phys. Rev.*, vol. **D64**, p. 095010, (2001), arXiv:hep-ph/0106336
- [147] Maccesanu, C. and McMullen, C. D. and Nandi, S., Collider implications of universal extra dimensions, *Phys. Rev.*, vol. **D66**, p. 015009, (2002), arXiv:hep-ph/0201300
- [148] Goldberger, Walter D. and Wise, Mark B., Modulus stabilization with bulk fields, *Phys. Rev. Lett.*, vol. **83**, p. 4922-4925, (1999), arXiv:hep-ph/9907447
- [149] Goldberger, Walter D. and Wise, Mark B., Phenomenology of a stabilized modulus, *Phys. Lett.*, vol. **B475**, p. 275-279, (2000), arXiv:hep-ph/9911457
- [150] Casagrande, S. and Goertz, F. and Haisch, U. and Neubert, M. and Pfoh, T., Flavor Physics in the Randall-Sundrum Model: I. Theoretical Setup and Electroweak Precision Tests, *JHEP*, vol. **10**, p. 094, (2008), arXiv:hep-ph/0807.4937
- [151] Casagrande, Sandro and Goertz, Florian and Haisch, Uli and Neubert, Matthias and Pfoh, Torsten, The Custodial Randall-Sundrum Model: From Precision Tests to Higgs Physics, *JHEP*, vol. **09**, p. 014, (2010), arXiv:hep-ph/1005.4315
- [152] Goertz, Florian and Haisch, Ulrich and Neubert, Matthias, Bounds on Warped Extra Dimensions from a Standard Model-like Higgs Boson, *Phys. Lett.*, vol. **B713**, p. 23-28, (2012), arXiv:hep-ph/1112.5099
- [153] Csaki, Csaba and Falkowski, Adam and Weiler, Andreas, The Flavor of the Composite Pseudo-Goldstone Higgs, *JHEP*, vol. **09**, p. 008, (2008), arXiv:hep-ph/0804.1954
- [154] Archer, Paul R. and Carena, Marcela and Carmona, Adrian and Neubert, Matthias, Higgs Production and Decay in Models of a Warped Extra Dimension with a Bulk Higgs, *JHEP*, vol. **01**, p. 060, (2015), arXiv:hep-ph/1408.5406
- [155] Grossman, Yuval and Neubert, Matthias, Neutrino masses and mixings in non-factorizable geometry, *Phys. Lett.*, vol. **B474**, p. 361-371, (2000), arXiv:hep-ph/9912408

- [156] Gherghetta, Tony and Pomarol, Alex, Bulk fields and supersymmetry in a slice of AdS, Nucl. Phys., vol. **B586**, p. 141-162, (2000), arXiv:hep-ph/0003129
- [157] Archer, Paul R., The Fermion Mass Hierarchy in Models with Warped Extra Dimensions and a Bulk Higgs, JHEP, vol. **09**, p. 095, (2012), arXiv:hep-ph/1204.4730
- [158] Cabrer, Joan A. and von Gersdorff, Gero and Quiros, Mariano, Suppressing Electroweak Precision Observables in 5D Warped Models, JHEP, vol. **05**, p. 083, (2011), arXiv:hep-ph/1103.1388
- [159] Cacciapaglia, Giacomo and Csaki, Csaba and Marandella, Guido and Terning, John, The Gaugephobic Higgs, JHEP, vol. **02**, p. 036, (2007), arXiv:hep-ph/0611358
- [160] Breitenlohner, Peter and Freedman, Daniel Z., Stability in Gauged Extended Supergravity, Annals Phys., vol. **144**, p. 249, (1982)
- [161] Luty, Markus A. and Okui, Takemichi, Conformal technicolor, JHEP, vol. **09**, p. 070, (2006), arXiv:hep-ph/0409274
- [162] Davoudiasl, H. and Hewett, J. L. and Rizzo, T. G., Bulk gauge fields in the Randall-Sundrum model, Phys. Lett., vol. **B473**, p. 43-49, (2000), arXiv:hep-ph/9911262
- [163] Falkowski, Adam and Perez-Victoria, Manuel, Electroweak Breaking on a Soft Wall, JHEP, vol. **12**, p. 107, (2008), arXiv:hep-ph/0806.1737
- [164] Csaki, Csaba and Grojean, Christophe and Murayama, Hitoshi and Pilo, Luigi and Terning, John, Gauge theories on an interval: Unitarity without a Higgs, Phys. Rev., vol. **D69**, p. 055006, (2004), arXiv:hep-ph/0305237
- [165] Agashe, Kaustubh and Perez, Gilad and Soni, Amarjit, Flavor structure of warped extra dimension models, Phys. Rev., vol. **D71**, p. 016002, (2005), arXiv:hep-ph/0408134
- [166] Blanke, Monika and Buras, Andrzej J. and Duling, Bjoern and Gori, Stefania and Weiler, Andreas,  $\Delta F=2$  Observables and Fine-Tuning in a Warped Extra Dimension with Custodial Protection, JHEP, vol. **03**, p. 001, (2009), arXiv:hep-ph/0809.1073
- [167] Huber, Stephan J., Flavor violation and warped geometry, Nucl. Phys., vol. **B666**, p. 269-288, (2003), arXiv:hep-ph/0303183
- [168] Huber, Stephan J. and Shafi, Qaisar, Fermion masses, mixings and proton decay in a Randall-Sundrum model, Phys. Lett., vol. **B498**, p. 256-262, (2001), arXiv:hep-ph/0010195
- [169] Pomarol, Alex, Gauge bosons in a five-dimensional theory with localized gravity, Phys. Lett., vol. **B486**, p. 153-157, (2000), arXiv:hep-ph/9911294
- [170] Azatov, Aleksandr and Toharia, Manuel and Zhu, Lijun, Higgs Mediated FCNC's in Warped Extra Dimensions, Phys. Rev., vol. **D80**, p. 035016, (2009), arXiv:hep-ph/0906.1990
- [171] Azatov, Aleksandr and Toharia, Manuel and Zhu, Lijun, Higgs Production from Gluon Fusion in Warped Extra Dimensions, Phys. Rev., vol. **D82**, p. 056004, (2010), arXiv:hep-ph/1006.5939

- [172] Delaunay, Cedric and Kamenik, Jernej F. and Perez, Gilad and Randall, Lisa, **Charming CP Violation and Dipole Operators from RS Flavor Anarchy**, JHEP, vol. **01**, p. 027, (2013), arXiv:hep-ph/1207.0474
- [173] Froggatt, C. D. and Nielsen, Holger Bech, **Hierarchy of Quark Masses, Cabibbo Angles and CP Violation**, Nucl. Phys., vol. **B147**, p. 277-298, (1979)
- [174] Agashe, Kaustubh and Delgado, Antonio and May, Michael J. and Sundrum, Raman, **RS1, custodial isospin and precision tests**, JHEP, vol. **08**, p. 050, (2003), arXiv:hep-ph/0308036
- [175] Csaki, Csaba and Grojean, Christophe and Pilo, Luigi and Terning, John, **Towards a realistic model of Higgsless electroweak symmetry breaking**, Phys. Rev. Lett., vol. **92**, p. 101802, (2004), arXiv:hep-ph/0308038
- [176] Agashe, Kaustubh and Contino, Roberto and Da Rold, Leandro and Pomarol, Alex, **A Custodial symmetry for  $Zb\bar{b}$** , Phys. Lett., vol. **B641**, p. 62-66, (2006), arXiv:hep-ph/0605341
- [177] Carena, Marcela and Delgado, Antonio and Ponton, Eduardo and Tait, Timothy M. P. and Wagner, C. E. M., **Precision electroweak data and unification of couplings in warped extra dimensions**, Phys. Rev., vol. **D68**, p. 035010, (2003), arXiv:hep-ph/0305188
- [178] Albrecht, Michaela E. and Blanke, Monika and Buras, Andrzej J. and Duling, Bjorn and Gemmler, Katrin, **Electroweak and Flavour Structure of a Warped Extra Dimension with Custodial Protection**, JHEP, vol. **09**, p. 064, (2009), arXiv:hep-ph/0903.2415
- [179] Bagger, Jonathan A. and Feruglio, Ferruccio and Zwirner, Fabio, **Generalized symmetry breaking on orbifolds**, Phys. Rev. Lett., vol. **88**, p. 101601, (2002), arXiv:hep-th/0107128
- [180] Agashe, Kaustubh and Perez, Gilad and Soni, Amarjit, **B-factory signals for a warped extra dimension**, Phys. Rev. Lett., vol. **93**, p. 201804, (2004), arXiv:hep-ph/0406101
- [181] Blanke, Monika and Buras, Andrzej J. and Duling, Bjorn and Gemmler, Katrin and Gori, Stefania, **Rare K and B Decays in a Warped Extra Dimension with Custodial Protection**, JHEP, vol. **03**, p. 108, (2009), arXiv:hep-ph/0812.3803
- [182] Bauer, M. and Casagrande, S. and Haisch, U. and Neubert, M., **Flavor Physics in the Randall-Sundrum Model: II. Tree-Level Weak-Interaction Processes**, JHEP, vol. **09**, p. 017, (2010), arXiv:hep-ph/0912.1625
- [183] Carmona, Adrian and Ponton, Eduardo and Santiago, Jose, **Phenomenology of Non-Custodial Warped Models**, JHEP, vol. **10**, p. 137, (2011), arXiv:hep-ph/1107.1500
- [184] Agashe, Kaustubh and Azatov, Aleksandr and Zhu, Lijun, **Flavor Violation Tests of Warped/Composite SM in the Two-Site Approach**, Phys. Rev., vol. **D79**, p. 056006, (2009), arXiv:hep-ph/0810.1016
- [185] Archer, Paul R. and Huber, Stephan J. and Jager, Sebastian, **Flavour Physics in the Soft Wall Model**, JHEP, vol. **12**, p. 101, (2011), arXiv:hep-ph/1108.1433



- [186] Cabrer, Joan A. and von Gersdorff, Gero and Quiros, Mariano, Flavor Phenomenology in General 5D Warped Spaces, JHEP, vol. **01**, p. 033, (2012), arXiv:hep-ph/1110.3324
- [187] Cabrer, Joan A. and von Gersdorff, Gero and Quiros, Mariano, Improving Naturalness in Warped Models with a Heavy Bulk Higgs Boson, Phys. Rev., vol. **D84**, p. 035024, (2011), arXiv:hep-ph/1104.3149
- [188] Puchwein, Martin and Kunszt, Zoltan, Radiative corrections with 5D mixed position - momentum space propagators, Annals Phys., vol. **311**, p. 288-313, (2004), arXiv:hep-th/0309069
- [189] Carena, Marcela and Delgado, Antonio and Ponton, Eduardo and Tait, Timothy M. P. and Wagner, C. E. M., Warped fermions and precision tests, Phys. Rev., vol. **D71**, p. 015010, (2005), arXiv:hep-ph/0410344
- [190] Cacciapaglia, Giacomo and Deandrea, Aldo and Llodra-Perez, Jeremie, Higgs  $\rightarrow$  Gamma Gamma beyond the Standard Model, JHEP, vol. **06**, p. 054, (2009), arXiv:hep-ph/0901.0927
- [191] Bhattacharyya, Gautam and Ray, Tirtha Sankar, Probing warped extra dimension via  $gg \rightarrow h$  and  $h \rightarrow \gamma\gamma$  at LHC, Phys. Lett., vol. **B675**, p. 222-225, (2009), arXiv:hep-ph/0902.1893
- [192] Bouchart, Charles and Moreau, Gregory, Higgs boson phenomenology and VEV shift in the RS scenario, Phys. Rev., vol. **D80**, p. 095022, (2009), arXiv:hep-ph/0909.4812
- [193] Azatov, Aleksandr and Galloway, Jamison, Light Custodians and Higgs Physics in Composite Models, Phys. Rev., vol. **D85**, p. 055013, (2012), arXiv:hep-ph/1110.5646
- [194] Agashe, Kaustubh and Okui, Takemichi and Sundrum, Raman, A Common Origin for Neutrino Anarchy and Charged Hierarchies, Phys. Rev. Lett., vol. **102**, p. 101801, (2009), arXiv:hep-ph/0810.1277
- [195] von Gersdorff, Gero and Quiros, Mariano and Wiechers, Michael, Neutrino Mixing from Wilson Lines in Warped Space, JHEP, vol. **02**, p. 079, (2013), arXiv:hep-ph/1208.4300
- [196] Randall, Lisa and Schwartz, Matthew D., Quantum field theory and unification in AdS5, JHEP, vol. **11**, p. 003, (2001), arXiv:hep-th/0108114
- [197] Contino, Roberto and Pomarol, Alex, Holography for fermions, JHEP, vol. **11**, p. 058, (2004), arXiv:hep-th/0406257
- [198] Csaki, Csaba and Grossman, Yuval and Tanedo, Philip and Tsai, Yuhsin, Warped penguin diagrams, Phys. Rev., vol. **D83**, p. 073002, (2011), arXiv:hep-ph/1004.2037
- [199] Blanke, Monika and Shakya, Bibhushan and Tanedo, Philip and Tsai, Yuhsin, The Birds and the Bs in RS: The  $b \rightarrow s\gamma$  penguin in a warped extra dimension, JHEP, vol. **08**, p. 038, (2012), arXiv:hep-ph/1203.6650
- [200] The ATLAS collaboration, Measurements of the Higgs boson production and decay rates and coupling strengths using pp collision data at  $\sqrt{s} = 7$  and 8 TeV in the ATLAS experiment, [ATLAS-CONF-2015-007] (2015)

- [201] Khachatryan, Vardan and others, Observation of the diphoton decay of the Higgs boson and measurement of its properties, *Eur. Phys. J.*, vol. **C74**, p. 3076, (2014), arXiv:hep-ex/1407.0558
- [202] Khachatryan, Vardan and others, Precise determination of the mass of the Higgs boson and tests of compatibility of its couplings with the standard model predictions using proton collisions at 7 and 8 TeV, *Eur. Phys. J.*, vol. **C75**, p. 212, (2015), arXiv:hep-ex/1412.8662
- [203] Andersen, J. and others, Handbook of LHC Higgs Cross Sections: 3. Higgs Properties - LHC Higgs Cross Section Working Group, (2013), arXiv:hep-ph/1307.1347
- [204] Aad, Georges and others, Combined Measurement of the Higgs Boson Mass in  $pp$  Collisions at  $\sqrt{s} = 7$  and 8 TeV with the ATLAS and CMS Experiments, *Phys. Rev. Lett.*, vol. **114**, p. 191803, (2015), arXiv:hep-ex/1503.07589
- [205] Marciano, William J. and Zhang, Cen and Willenbrock, Scott, Higgs Decay to Two Photons, *Phys. Rev.*, vol. **D85**, p. 013002, (2012), arXiv:hep-ph/1109.5304
- [206] Keung, Wai-Yee and Marciano, William J., Higgs Scalar Decays:  $H \rightarrow W^\pm X$ , *Phys. Rev.*, vol. **D30**, p. 248, (1984)
- [207] 't Hooft, Gerard and Veltman, M. J. G., Scalar One Loop Integrals, *Nucl. Phys.*, vol. **B153**, p. 365-401, (1979)
- [208] Passarino, G. and Veltman, M. J. G., One Loop Corrections for  $e^+e^-$  Annihilation Into  $\mu^+\mu^-$  in the Weinberg Model, *Nucl. Phys.*, vol. **B160**, p. 151-207, (1979)
- [209] Ellis, R. Keith and Kunszt, Zoltan and Melnikov, Kirill and Zanderighi, Giulia, One-loop calculations in quantum field theory: from Feynman diagrams to unitarity cuts, *Phys. Rept.*, vol. **518**, p. 141-250, (2012), arXiv:hep-ph/1105.4319
- [210] Bentvelsen, S. and Laenen, E. and Motylinski, P., Higgs production through gluon fusion at leading order - NIKHEF 007, (2005)
- [211] Gunion, John F. and Haber, Howard E. and Kane, Gordon L. and Dawson, Sally, The Higgs Hunter's Guide, *Front. Phys.*, vol. **80**, p. 1-404, (2000)
- [212] Frank, Mariana and Pourtolami, Nima and Toharia, Manuel, Higgs Bosons in Warped Space, from the Bulk to the Brane, *Phys. Rev.*, vol. **D87**, p. 096003, (2013), arXiv:hep-ph/1301.7692
- [213] The ATLAS collaboration, Search for the  $bb$  decay of the Standard Model Higgs boson in associated  $W/ZH$  production with the ATLAS detector, [ATLAS-CONF-2013-079] (2013)
- [214] Baer, Howard and Barklow, Tim and Fujii, Keisuke and Gao, Yuanning and Hoang, Andre and Kanemura, Shinya and List, Jenny and Logan, Heather E. and Nomerotski, Andrei and Perelstein, Maxim and others, The International Linear Collider Technical Design Report - Volume 2: Physics, (2013), arXiv:hep-ph/1306.6352

- [215] Tian, Junping and Fujii, Keisuke, *Measurement of Higgs couplings and self-coupling at the ILC*, Proceedings, 2013 European Physical Society Conference on High Energy Physics (EPS-HEP 2013): Stockholm, Sweden, July 18-24, 2013, vol. **EPS-HEP2013**, p. 316, (2013), arXiv:hep-ph/1311.6528
- [216] Asner, D. M. and others, *ILC Higgs White Paper*, Proceedings, 2013 Community Summer Study on the Future of U.S. Particle Physics: Snowmass on the Mississippi (CSS2013): Minneapolis, MN, USA, July 29-August 6, 2013, (2013), arXiv:hep-ph/1310.0763
- [217] Klute, Markus and Lafaye, R. and Plehn, Tilman and Rauch, Michael and Zerwas, Dirk, *Measuring Higgs Couplings at a Linear Collider*, Europhys. Lett., vol. **101**, p. 51001, (2013), arXiv:hep-ph/1301.1322
- [218] Peskin, Michael E., *Comparison of LHC and ILC Capabilities for Higgs Boson Coupling Measurements*, (2012), arXiv:hep-ph/1207.2516
- [219] Behnke, Ties and Brau, James E. and Foster, Brian and Fuster, Juan and Harrison, Mike and Paterson, James McEwan and Peskin, Michael and Stanitzki, Marcel and Walker, Nicholas and Yamamoto, Hitoshi, *The International Linear Collider Technical Design Report - Volume 1: Executive Summary*, (2013), arXiv:acc-ph/1306.6327
- [220] Adolphsen, Chris and Barone, Maura and Barish, Barry and Buesser, Karsten and Burrows, Philip and Carwardine, John and Clark, Jeffrey and Mainaud Durand, H el ene and Dugan, Gerry and Elsen, Eckhard and others, *The International Linear Collider Technical Design Report - Volume 3.II: Accelerator Baseline Design*, (2013), arXiv:acc-ph/1306.6328
- [221] Abramowicz, Halina and others, *The International Linear Collider Technical Design Report - Volume 4: Detectors*, (2013), arXiv:ins-det/1306.6329
- [222] *Website of the Linear Collider Collaboration*, retrieved on 2017-06-27
- [223] Rika Takahashi, *ILC candidate site in Japan announced*, (2013), retrieved on 2017-06-27
- [224] Aaboud, Morad and others, *Search for resonances in diphoton events at  $\sqrt{s}=13$  TeV with the ATLAS detector*, JHEP, vol. **09**, p. 001 (2016), arXiv:hep-ex/1606.03833
- [225] Khachatryan, Vardan and others, *Search for Resonant Production of High-Mass Photon Pairs in Proton-Proton Collisions at  $\sqrt{s}=8$  and 13 TeV*, Phys. Rev. Lett., vol. **117**, p. 051802, (2016), arXiv:hep-ex/1606.04093
- [226] CMS Collaboration, *Search for new physics in high mass diphoton events in  $3.3 \text{ fb}^{-1}$  of proton-proton collisions at  $\sqrt{s}=13$  TeV and combined interpretation of searches at 8 TeV and 13 TeV*, [CMS-PAS-EXO-16-018] (2016)
- [227] Buckley, Matthew R., *Wide or narrow? The phenomenology of 750 GeV diphotons*, Eur. Phys. J., vol. **C76**, p. 345, (2016), arXiv:hep-ph/1601.04751
- [228] Strumia, Alessandro, *Interpreting the 750 GeV digamma excess: a review*, Proceedings, 51st Rencontres de Moriond on Electroweak Interactions and Unified Theories: La Thuile, Italy, March 12-19, 2016, **ARISF**, p. 407-426, (2016), arXiv:hep-ph/1605.09401

- [229] D.A. Edwards, M.J. Syphers, Accelerator physics of colliders - Particle Data Group (2011), retrieved on 2017-06-29
- [230] Herr, W. and Muratori, B., Concept of luminosity, Intermediate accelerator physics. Proceedings, CERN Accelerator School, Zeuthen, Germany, September 15-26, 2003, p. 361-377, (2003)
- [231] The ATLAS collaboration, Search for scalar diphoton resonances with  $15.4 \text{ fb}^{-1}$  of data collected at  $\sqrt{s}=13 \text{ TeV}$  in 2015 and 2016 with the ATLAS detector, [ATLAS-CONF-2016-059] (2016)
- [232] CMS Collaboration, Search for resonant production of high mass photon pairs using  $12.9 \text{ fb}^{-1}$  of proton-proton collisions at  $\sqrt{s} = 13 \text{ TeV}$  and combined interpretation of searches at 8 and 13 TeV, [CMS-PAS-EXO-16-027] (2016)
- [233] "After the hangover" - Particle Physics Blog, retrieved on 2017-06-29
- [234] Buttazzo, Dario and Greljo, Admir and Marzocca, David, Knocking on new physics' door with a scalar resonance, Eur. Phys. J., vol. **C76**, p. 116, (2016), arXiv:hep-ph/1512.04929
- [235] Staub, Florian and others, Precision tools and models to narrow in on the 750 GeV diphoton resonance, Eur. Phys. J., vol. **C76**, p. 516, (2016), arXiv:1602.05581
- [236] Franceschini, Roberto and Giudice, Gian F. and Kamenik, Jernej F. and McCullough, Matthew and Pomarol, Alex and Rattazzi, Riccardo and Redi, Michele and Riva, Francesco and Strumia, Alessandro and Torre, Riccardo, What is the  $\gamma\gamma$  resonance at 750 GeV?, JHEP, vol. **03**, p. 144, (2016), arXiv:1512.04933
- [237] Fichet, Sylvain and von Gersdorff, Gero and Royon, Christophe, Scattering light by light at 750 GeV at the LHC, Phys. Rev., vol. **D93**, p. 075031, (2016), arXiv:hep-ph/1512.05751
- [238] Csáki, Csaba and Hubisz, Jay and Terning, John, Minimal model of a diphoton resonance: Production without gluon couplings, Phys. Rev., vol. **D93**, p. 035002, (2016), arXiv:hep-ph/1512.05776
- [239] Gupta, Rick S. and Jäger, Sebastian and Kats, Yevgeny and Perez, Gilad and Stamou, Emmanuel, Interpreting a 750 GeV Diphoton Resonance, JHEP, vol. **07**, p. 145, (2016), arXiv:hep-ph/1512.05332
- [240] Petersson, Christoffer and Torre, Riccardo", 750 GeV Diphoton Excess from the Goldstino Superpartner, Phys. Rev. Lett., vol. **116**, p. 151804, (2016), arXiv:hep-ph/1512.05333
- [241] Ding, Ran and Huang, Li and Li, Tianjun and Zhu, Bin, Interpreting 750 GeV diphoton excess with R -parity violating supersymmetry, Int. J. Mod. Phys., vol. **A32**, p. 1750014, (2017), arXiv:hep-ph/1512.06560
- [242] Allanach, B. C. and Dev, P. S. Bhupal and Renner, S. A. and Sakurai, Kazuki, 750 GeV diphoton excess explained by a resonant sneutrino in R-parity violating supersymmetry, Phys. Rev., vol. **D93**, p. 115022, (2016), arXiv:hep-ph/1512.07645

- [243] Harigaya, Keisuke and Nomura, Yasunori, A Composite Model for the 750 GeV Diphoton Excess, JHEP, vol. **03**, p. 091, (2016), arXiv:hep-ph/1602.01092
- [244] Son, Minho and Urbano, Alfredo, A new scalar resonance at 750 GeV: Towards a proof of concept in favor of strongly interacting theories, JHEP, vol. **05**, p. 181, (2016), arXiv:hep-ph/1512.08307
- [245] Belyaev, Alexander and Cacciapaglia, Giacomo and Cai, Haiying and Flacke, Thomas and Parolini, Alberto and Serôdio, Hugo, Singlets in composite Higgs models in light of the LHC 750 GeV diphoton excess, Phys. Rev., vol. **D94**, p. 015004, (2016), arXiv:hep-ph/1512.07242
- [246] Harigaya, Keisuke and Nomura, Yasunori, Composite Models for the 750 GeV Diphoton Excess, Phys. Lett., vol. **B754**, p. 151-156, (2016), arXiv:hep-ph/1512.04850
- [247] Bardhan, Debjyoti and Bhatia, Disha and Chakraborty, Amit and Maitra, Ushoshi and Raychaudhuri, Sreerup and Samui, Tousik, Radion Candidate for the LHC Diphoton Resonance, arXiv:hep-ph/1512.06674
- [248] Ahmed, Aqeel and Dillon, Barry M. and Grzadkowski, Bohdan and Gunion, John F. and Jiang, Yun, Implications of the absence of high-mass radion signals, Phys. Rev., vol. **D95**, p. 095019, (2017), arXiv:hep-ph/1512.05771
- [249] Cox, Peter and Medina, Anibal D. and Ray, Tirtha Sankar and Spray, Andrew, Implications of diphoton searches for a Radion in the Bulk-Higgs Scenario, Int. J. Mod. Phys., vol. **A32**, p. 1750020, (2017), arXiv:hep-ph/1512.05618
- [250] Bélanger, Geneviève and Delaunay, Cédric, A Dark Sector for  $g_\mu - 2$ ,  $R_K$  and a Diphoton Resonance, Phys. Rev., vol. **D94**, p. 075019, (2016), arXiv:hep-ph/1603.03333
- [251] Cárcamo Hernández, A. E., A novel and economical explanation for SM fermion masses and mixings, Eur. Phys. J., vol. **C76**, p. 503, (2016), arXiv:hep-ph/1512.09092
- [252] Dev, P. S. Bhupal and Mohapatra, Rabindra N. and Zhang, Yongchao, Quark Seesaw, Vectorlike Fermions and Diphoton Excess, JHEP, vol. **02**, p. 186, (2016), arXiv:hep-ph/1512.08507
- [253] Goertz, Florian and Kamenik, Jernej F. and Katz, Andrey and Nardecchia, Marco, Indirect Constraints on the Scalar Di-Photon Resonance at the LHC, JHEP, vol. **05**, p. 187, (2016), arXiv:hep-ph/1512.08500
- [254] Murphy, Christopher W., Vector Leptoquarks and the 750 GeV Diphoton Resonance at the LHC, Phys. Lett., vol. **B757**, p. 192-198, (2016), arXiv:hep-ph/1512.06976
- [255] Bauer, Martin and Neubert, Matthias, Flavor anomalies, the 750 GeV diphoton excess, and a dark matter candidate, Phys. Rev., vol. **D93**, p. 115030, (2016), arXiv:hep-ph/1512.06828
- [256] Aloni, Daniel and Blum, Kfir and Dery, Avital and Efrati, Aielet and Nir, Yosef, On a possible large width 750 GeV diphoton resonance at ATLAS and CMS, JHEP, vol. **08**, p. 017, (2016), arXiv:hep-ph/1512.05778

- [257] Kaplan, David Elazzar and Tait, Timothy M. P., New tools for fermion masses from extra dimensions, *JHEP*, vol. **11**, p. 051, (2001), arXiv:hep-ph/0110126
- [258] Georgi, Howard and Grant, Aaron K. and Hailu, Girma", Chiral fermions, orbifolds, scalars and fat branes, *Phys. Rev.*, vol. **D63**, p. 064027, (2001), arXiv:hep-ph/0007350
- [259] Giddings, Steven B. and Zhang, Hao, Kaluza-Klein graviton phenomenology for warped compactifications, and the 750 GeV diphoton excess, *Phys. Rev.*, vol. **D93**, p. 115002, (2016), arXiv:hep-ph/1602.02793
- [260] Geng, Chao-Qiang and Huang, Da, Note on spin-2 particle interpretation of the 750 GeV diphoton excess, *Phys. Rev.*, vol. **D93**, p. 115032, (2016), arXiv:hep-ph/1601.07385
- [261] Arun, Mathew Thomas and Saha, Pratishruti, Gravitons in multiply warped scenarios - at 750 GeV and beyond, *Pramana*, vol. **88**, p. 93, (2017), arXiv:hep-ph/1512.06335
- [262] Abel, Steven and Khoze, Valentin V., Photo-production of a 750 GeV di-photon resonance mediated by Kaluza-Klein leptons in the loop, *JHEP*, vol. **05**, p. 063, (2016), arXiv:hep-ph/1601.07167
- [263] Cai, Chengfeng and Yu, Zhao-Huan and Zhang, Hong-Hao, 750 GeV diphoton resonance as a singlet scalar in an extra dimensional model, *Phys. Rev.*, vol. **D93**, p. 075033, (2016), arXiv:hep-ph/1512.08440
- [264] Csaki, Csaba and Randall, Lisa, A Diphoton Resonance from Bulk RS, *JHEP*, vol. **07**, p. 061, (2016), arXiv:hep-ph/1603.07303
- [265] Inami, Takeo and Kubota, Takahiro and Okada, Yasuhiro, Effective Gauge Theory and the Effect of Heavy Quarks in Higgs Boson Decays, *Z. Phys.*, vol. **C18**, p. 69, (1983)
- [266] Grinstein, Benjamin and Randall, Lisa, The Renormalization of  $g^2$ , *Phys. Lett.*, vol. **B217**, p. 335-340, (1989)
- [267] Collins, John C. and Duncan, Anthony and Joglekar, Satish D., Trace and Dilatation Anomalies in Gauge Theories, *Phys. Rev.*, vol. **D16**, p. 438-449, (1977)
- [268] Schroder, Y. and Steinhauser, M., Four-loop decoupling relations for the strong coupling, *JHEP*, vol. **01**, p. 051, (2006), arXiv:hep-ph/0512058
- [269] Chetyrkin, K. G. and Kuhn, Johann H. and Sturm, Christian, QCD decoupling at four loops, *Nucl. Phys.*, vol. **B744**, p. 121-135, (2006), arXiv:hep-ph/0512060
- [270] Martin, A. D. and Stirling, W. J. and Thorne, R. S. and Watt, G., Parton distributions for the LHC, *Eur. Phys. J.*, vol. **C63**, p. 189-285, (2009), arXiv:hep-ph/0901.0002
- [271] Ball, Richard D. and others, Parton distributions for the LHC Run II, *JHEP*, vol. **04**, p. 040, (2015), arXiv:hep-ph/1410.8849
- [272] Butterworth, Jon and others, PDF4LHC recommendations for LHC Run II, *J. Phys.*, vol. **G43**, p. 023001, (2016), arXiv:hep-ph/1510.03865

- [273] Cooper-Sarkar, A. M., HERA Collider Results, Proceedings, 23rd International Workshop on Deep-Inelastic Scattering and Related Subjects (DIS 2015): Dallas, Texas, USA, April 27-May 01, (2015), arXiv:hep-ph/1507.03849
- [274] Harland-Lang, L. A. and Martin, A. D. and Motylinski, P. and Thorne, R. S., Parton distributions in the LHC era: MMHT 2014 PDFs, Eur. Phys. J., vol. **C75**, p. 204, (2015), arXiv:hep-ph/1412.3989
- [275] Special thanks goes to D. Wilhelm for adapting the CuTe program to the calculation of the  $pp \rightarrow S$  cross section.
- [276] The program CuTe and a manual are available under: <https://cute.hepforge.org>
- [277] Becher, Thomas and Neubert, Matthias and Wilhelm, Daniel, Higgs-Boson Production at Small Transverse Momentum, JHEP, vol. **05**, p. 110, (2013), arXiv:hep-ph/1212.2621
- [278] Becher, Thomas and Neubert, Matthias and Wilhelm, Daniel, Electroweak Gauge-Boson Production at Small  $q_T$ : Infrared Safety from the Collinear Anomaly, JHEP, vol. **02**, p. 124, (2012), arXiv:hep-ph/1109.6027
- [279] de Wit, B., Utrecht University, Ch. 03: Cross sections and decay rates, Script, (2011)
- [280] CMS Collaboration, Search for Resonances Decaying to Dijet Final States at  $\sqrt{s} = 8$  TeV with Scouting Data, CMS-PAS-EXO-14-005, (2015)
- [281] Aad, Georges and others, Search for a high-mass Higgs boson decaying to a  $W$  boson pair in  $pp$  collisions at  $\sqrt{s} = 8$  TeV with the ATLAS detector, JHEP, vol. **01**, p. 032, (2016), arXiv:hep-ex/1509.00389
- [282] Aad, Georges and others, Search for an additional, heavy Higgs boson in the  $H \rightarrow ZZ$  decay channel at  $\sqrt{s} = 8$  TeV in  $pp$  collision data with the ATLAS detector, Eur. Phys. J., vol. **C76**, p. 45, (2016), arXiv:hep-ex/1507.05930
- [283] Aad, Georges and others, Search for new resonances in  $W\gamma$  and  $Z\gamma$  final states in  $pp$  collisions at  $\sqrt{s} = 8$  TeV with the ATLAS detector, Phys. Lett., vol. **B738**, p. 428-447, (2014), arXiv:hep-ex/1407.8150
- [284] Aad, Georges and others, A search for  $t\bar{t}$  resonances using lepton-plus-jets events in proton-proton collisions at  $\sqrt{s} = 8$  TeV with the ATLAS detector, JHEP, vol. **08**, p. 148, (2015), arXiv:hep-ex/1505.07018
- [285] CMS Collaboration, Search for di-Higgs resonances decaying to 4 bottom quarks, CMS-PAS-HIG-14-013, (2014)
- [286] Baikov, P. A. and Chetyrkin, K. G., Top Quark Mediated Higgs Boson Decay into Hadrons to Order  $\alpha_s^5$ , Phys. Rev. Lett., vol. **97**, p. 061803, (2006), arXiv:hep-ph/0604194
- [287] Schreck, Marco and Steinhauser, Matthias, Higgs Decay to Gluons at NNLO, Phys. Lett., vol. **B655**, p. 148-155, (2007), arXiv:hep-ph/0708.0916

- [288] Dicus, D. and Stange, A. and Willenbrock, S., Higgs decay to top quarks at hadron colliders, Phys. Lett., vol. **B333**, p. 126-131, (1994), arXiv:hep-ph/9404359
- [289] Craig, Nathaniel and D'Eramo, Francesco and Draper, Patrick and Thomas, Scott and Zhang, Hao, The Hunt for the Rest of the Higgs Bosons, JHEP, vol. **06**, p. 137, (2015), arXiv:hep-ph/1504.04630
- [290] Gori, Stefania and Kim, Ian-Woo and Shah, Nausheen R. and Zurek, Kathryn M., Closing the Wedge: Search Strategies for Extended Higgs Sectors with Heavy Flavor Final States, Phys. Rev., vol. **D93**, p. 075038, (2016), arXiv:hep-ph/1602.02782
- [291] Cheung, Kingman and Ko, P. and Lee, Jae Sik and Park, Jubin and Tseng, Po-Yan, Higgs precision study of the 750 GeV diphoton resonance and the 125 GeV standard model Higgs boson with Higgs-singlet mixing, Phys. Rev., vol. **D94**, p. 033010, (2016), arXiv:hep-ph/1512.07853
- [292] D'Eramo, Francesco and de Vries, Jordy and Panci, Paolo, A 750 GeV Portal: LHC Phenomenology and Dark Matter Candidates, JHEP, vol. **05**, p. 089, (2016), arXiv:hep-ph/1601.01571
- [293] Carmi, Dean and Falkowski, Adam and Kuflik, Eric and Volansky, Tomer and Zupan, Jure, Higgs After the Discovery: A Status Report, JHEP, vol. **10**, p. 196, (2012), arXiv:hep-ph/1207.1718
- [294] Cheung, Kingman and Ko, P. and Lee, Jae Sik and Tseng, Po-Yan, Bounds on Higgs-Portal models from the LHC Higgs data, JHEP, vol. **10**, p. 057, (2015), arXiv:hep-ph/1507.06158
- [295] The ATLAS and CMS Collaborations, Measurements of the Higgs boson production and decay rates and constraints on its couplings from a combined ATLAS and CMS analysis of the LHC pp collision data at  $\sqrt{s} = 7$  and 8 TeV, ATLAS-CONF-2015-044, (2015)
- [296] CMS Collaboration, Measurements of the Higgs boson production and decay rates and constraints on its couplings from a combined ATLAS and CMS analysis of the LHC pp collision data at  $\sqrt{s} = 7$  and 8 TeV, CMS-PAS-HIG-15-002, (2015)
- [297] de Wit, B. and Smith, J., Field Theory in Particle Physics, Elsevier Science, (1986)





# Miscellaneous

## List of abbreviations

ADD	Arkani-Hamed-Dimopoulos-Dvali
AdS	Anti-de Sitter
ATLAS	A Toroidal LHC ApparatuS
CERN	European Organization for Nuclear Research
CKM	Cabibbo-Kobayashi-Maskawa
CL	confidence level
CMS	Compact Muon Solenoid
CP	charge and parity
em	electromagnetic
eV	electron Volt
GeV	Giga electron Volt
ILC	International Linear Collider
IR	infra-red
KK	Kaluza-Klein
$\Lambda$ -CDM	$\Lambda$ -Cold-Dark-Matter
LHC	Large Hadron Collider
m	meter
MeV	Mega electron Volt
NG	Nambu-Goldstone
PDF	parton distribution function
PV	Passarino-Veltman
QCD	quantum chromodynamics
QED	quantum electrodynamics
RS	Randall-Sundrum
SLAC	Stanford Linear Accelerator Center
SM	Standard Model
S-matrix	Scattering-matrix
SUSY	supersymmetry
TeV	Tera electron Volt
UV	ultra-violet
vev	vacuum expectation value
WIMP	weakly interacting massive particle
XD	X-dimensional

## Acknowledgements

In the course of writing this thesis, I have accumulated a number of obligations. First of all, I have an extensive debt to my Ph.D. advisor. I owe sincere and special thanks to him for affording me the opportunity to scientifically work in his field of science, and alongside to prepare for a Ph.D. degree. While working in his area, I deeply benefited from his profound knowledge of physics, and his helpful and pragmatic advise, as well as from inspiriting discussions and cooperations with members of his working group. Moreover, his financial support by granting me a position of an assistant was of great help, otherwise it would have been difficult to accomplish this thesis. Furthermore, I wish to thank the co-censor for accepting the co-censor's burden with my thesis.

It is also a pleasure to record my special thanks to the members of the Theoretical High Energy Physics (THEP) group. Their pleasant and inspiring working atmosphere, and the stimulating scientific environment by means of many seminars and discussions offered insights in current, new developments in physics, and in topics beyond one's own research.

## Curriculum Vitae

Name Clara Coletta Hörner

Date of birth 01.04.1990

Place of birth Wiesbaden

Nationality German

### Educational background

- 2014 - 2017** Ph.D. studies in physics  
*Johannes Gutenberg-University, Mainz*
- 2012 - 2014** Master of Science in physics  
*Johannes Gutenberg-University, Mainz*
- 2008 - 2012** Bachelor of Science in physics  
*Johannes Gutenberg-University, Mainz*
- 2005 - 2008** Abitur<sup>1</sup>, secondary school  
*Internatsschule Schloss Hansenberg, Geisenheim Johannisberg*
- 2000 - 2005** Secondary school  
*Gutenberg Gymnasium, Wiesbaden*
- 1996 - 2000** Primary school  
*Grundschule Wiesbaden-Igstadt*

1: Diploma from German secondary school qualifying for university entrance